N73-13783
NASA CR-120881
Bell 8636-950004

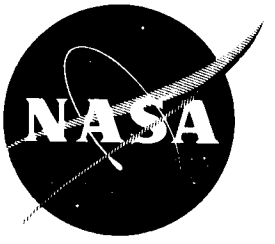

HIGH PRESSURE REVERSE FLOW APS ENGINE

by

J.M. Senneff, Project Manager

BELL AEROSPACE COMPANY
Division of Textron
Buffalo, New York 14240

prepared for

NATIONAL AERONAUTICS AND SPACE ADMINISTRATION

NASA Lewis Research Center
Contract NAS 3-14353
Stephen Cohen, Project Manager

NOTICE

This report was prepared as an account of Government-sponsored work. Neither the United States, nor the National Aeronautics and Space Administration (NASA), nor any person acting on behalf of NASA:

A.) Makes any warranty or representation, expressed or implied, with respect to the accuracy, completeness, or usefulness of the information contained in this report, or that the use of any information, apparatus, method, or process disclosed in this report may not infringe privately-owned rights; or

B.) Assumes any liabilities with respect to the use of, or for damages resulting from the use of, any information, apparatus, method or process disclosed in this report.

As used above, "person acting on behalf of NASA" includes any employee or contractor of NASA, or employee of such contractor, to the extent that such employee or contractor of NASA or employee of such contractor prepares, disseminates, or provides access to any information pursuant to his employment or contract with NASA, or his employment with such contractor.

1. Report No.	2. Government Accession No.	3. Recipient's Catalog No.
NASA CR-120881		

4. Title and Subtitle	5. Report Date
HIGH PRESSURE REVERSE FLOW APS ENGINE	Nov.1972
	6. Performing Organization Code

7. Author(s)	8. Performing Organization Report No.
J. M. Senneff	BELL 8636-950004
	10. Work Unit No.

9. Performing Organization Name and Address	11. Contract or Grant No.
Bell Aerospace Company Division of Textron Buffalo, New York 14240	NAS 3-14353
	13. Type of Report and Period Covered
12. Sponsoring Agency Name and Address	Contractor Report
National Aeronautics and Space Administration Washington, D. C. 20546	14. Sponsoring Agency Code

15. Supplementary Notes

Project Manager, Stephen M. Cohen, Chemical Propulsion Division, NASA Lewis Research Center, Cleveland, Ohio

16. Abstract

A design and test demonstration effort was undertaken (Contract NAS3-14353) to evaluate the concept of the reverse flow engine for the APS engine application. The 1500 lb (6672 N) thrust engine was designed to operate on gaseous hydrogen and gaseous oxygen propellants at a mixture ratio of 4 and to achieve the objective performance of 435 sec (4266 Nsec/kg) specific impulse. Superimposed durability requirements called for a million-cycle capability with 50 hours duration. The program was undertaken as a series of tasks including the initial preliminary design, design of critical test components and finally, the design and demonstration of an altitude engine which could be used interchangeably to examine operating parameters as well as to demonstrate the capability of the concept. The program results are reported with data to indicate that all of the program objectives were met or exceeded within the course of testing on the program. The analysis effort undertaken is also reported in detail and supplemented with test data in some cases where prior definitions could not be made. This document contains the results of these analyses as well as the test results conducted throughout the course of the program. Finally, the test data and analytical results were combined to allow recommendations for a flight weight design. This preliminary design effort is also detailed within the report.

17. Key Words (Suggested by Author(s))	18. Distribution Statement
Reverse Flow Engine Film Cooling Dump Cooling Gaseous Oxygen Gaseous Hydrogen	Unclassified - unlimited

19. Security Classif. (of this report)	20. Security Classif. (of this page)	21. No. of Pages	22. Price*
Unclassified	Unclassified	397	$6.00

* For sale by the National Technical Information Service, Springfield, Virginia 22151

FOREWORD

The purpose of this contract was to demonstrate the applicability of a 1500 pound (6672.3 N) thrust reverse-flow thrust chamber assembly for the Space Shuttle Auxiliary Propulsion System (APS). Significant objectives of the program included the demonstration of high performance [97% c* and 435 seconds (4266N sec/kg.) specific impulse] and rapid response at altitude conditions. Additional design goals included the capability of a 50 hour firing time over a 10 year period with a million starts and single firings of up to 1000 seconds.

The program consisted of analytical and test efforts to characterize and demonstrate the reverse-flow thrust chamber concept. The program progressed through initial phases of definition and analysis to sea-level firings with heat sink hardware, and into design and fabrication of hardware for long-duration firings and pulse testing at simulated altitude test conditions.

The sea-level firings have produced injection configurations which are considered to be acceptable in producing the altitude performance goals. The configurations of altitude test hardware permitted evaluation of several thrust chamber nozzle section and nozzle extension cooling schemes. The scheduled altitude test program included duration and pulse firings at "nominal" conditions of 540°R (300°K) propellant feed temperature and 300 psia (206.8N/cm^2) chamber pressure. A survey of thruster operation was also conducted at high and low propellant temperatures and chamber pressures. The combined efforts of test coordination, data evaluation and cooled chamber design required substantial contributions from the following individuals: Mr. N. Roth, Project Engineer; Messrs. N. Safeer and J. Panosian, Test Coordination and Data Evaluation; Messrs. R. Bryndle and J. Martino, Test Directors.

Finally, hardware designed to compensate for suspected low temperature performance decrease was tested to demonstrate the performance recovery at proper design condions. The accomplishment of these goals was made possible by the cooperation and significant contributions of specialists including Messrs. N. Roth, N. Safeer and J. Panosian in the thrust chamber design, Messrs. L. Baker and G. Sabak for detailed analyses, Messrs. M. Shorr and G. Le Blanc for components, Messrs. J. Martino, R. Bryndle and E. Oleksy in test and Mr. W. Sanscrainte for the project analysis.

CONTENTS

CONTENTS (CONT)

CONTENTS (CONT)

CONTENTS (CONT)

CONTENTS (CONT)

ILLUSTRATIONS

ILLUSTRATIONS (CONTD)

TABLES

TABLES (CONT)

I. SUMMARY

A program to evaluate the use of a gaseous-hydrogen and gaseous-oxygen-fueled reverse-flow engine for the APS application of the space shuttle was undertaken. Principal testing of the 1500 lb (6672N) thrust rocket engine was performed at simulated 100,000 ft (30,480M) altitude with a 40 to 1 area ratio nozzle. The prime objective of the program was to demonstrate 435 seconds (4266N sec/kg.) specific impulse in an engine configuration which would allow for a vehicle internal installation while withstanding a million starts.

The program was conducted in 10 segments which included component design, fabrication and test. Preliminary segments were scheduled to allow for combustion component demonstration and evaluation before fabrication of the altitude demonstration engine. This early test program, called injector testing, was successful in its purpose, allowing a combustor configuration to be selected which produced acceptable performance and heat rejection. The selection of the combustor configuration then allowed progression into the cooled thrust chamber fabrication and evaluation portions of the program.

The cooled thrust chamber tests demonstrated the capability of the engine to exceed the program objective of 435 seconds (4266N sec/kg.) specific impulse. If, as an example, a regeneratively cooled nozzle were accepted, a nominal performance of 440 seconds (4315M sec/kg.) specific impulse could have readily been exceeded at ambient propellant temperatures. Since interest waned for a regeneratively cooled nozzle divergent section as a result of vehicle studies, a more applicable dump-cooled columbium design was substituted and the cooling requirements examined. Testing demonstrated that the columbium unit could be adequately cooled. With a modest performance decrease for additional cooling, a stainless steel divergent nozzle section could be employed.

The evaluation of temperature effects on operation became important as vehicle studies indicated the probable use of less than ambient propellants. The program continuation took two forms; one of evaluation of ambient designs at cold temperatures; a second included an addition to the program of a unit designed for cold propellants. The cold propellant design incorporated changes that injected the cold propellants at the same velocity as the original ambient design.

The concern that cold propellants would result in decreased performance was confirmed in test. The expected propellant energy loss is nearly 2-1/2% where the ambient designs displayed an additional loss of some 7%, attributed to the decrease in injection velocity as the mass flow remained constant and the density increased. The injector designed to compensate for this difference was extremely successful in producing a 431 second (4227N sec/kg.) specific impulse at the decreased propellant temperature.

Prior to conducting the propellant temperature test series, duration test of the design in an insulated configuration was demonstrated. Preliminary tests set up the configuration to use about 7-1/2% of the fuel to "dump" cool the nozzle extension. Film cooling of the chamber was accomplished with the remaining injected fuel. The 500 second test conducted was without incident and could have been readily repeated if inclination or funding had so defined.

The remaining tests included the demonstration of pulsing operation. Sufficient testing was conducted to demonstrate rapid response operation in a variety of pulse on and off times. The condensed pulse program showed a very reasonable level of pulse performance achievement as well as the capability to achieve repetitive starts when valve timing and ignition were not an influencing factor. Both the valve and ignition operation were somewhat hampered throughout the program by the original limitation of "off the shelf hardware".

The final results of the program suggested that the objectives had been met. The scale-up of the reverse flow chamber to a 1500 lb (6672N) thrust level was demonstrated.

The achievement of performance objectives suggests not only that the feasibility of such an engine has been demonstrated but that design objectives have been incorporated. A section illustrating such a flight-weight design has been included in the later sections of this report.

II. INTRODUCTION

This report presents the analytical and experimental effort to investigate a "Reverse-Flow", gaseous hydrogen/gaseous oxygen, rocket engine for the auxiliary propulsion system of the Space Shuttle. The reverse-flow thrust chamber consists of a spherical combustion chamber and a conventional nozzle. The oxidizer is injected into the combustion chamber through a single swirl cup at the head end of the chamber. The fuel enters the engine in the divergent portion of the nozzle and the fuel circuit includes regenerative cooling passages from a low area ratio of the divergent nozzle through the throat to a station in the convergent nozzle section. The fuel is injected rearward through slots terminating the regenerative cooling passages. The fuel travels along the spherical combustion chamber wall and is then turned into the oxidizer at the outlet of the O_2 swirl cup.

Assessment of the reverse flow design indicated a number of potential advantages relative to conventional multielement injectors and regenerative or film cooled combustion chambers. The potential advantages which led to the award of contract NAS 3-14353 include:

1. The injection of fuel and oxidizer at separate locations and the single element oxidizer injector approach provides a significant simplification of propellant injection.

2. The fuel flow circuit provides regenerative cooling of the throat combustion section with all the H_2 flow (less any H_2 employed for film cooling of a nozzle extension). The chamber is film cooled in the reverse or counter flow direction, the effectiveness of the counter flow film cooling allowing the use of an insulated wall spherical combustion chamber fabricated from stainless steel.

3. The cooling of the spherical combustion chamber wall and the mixing of O_2 and H_2 flows allows direct spark plug ignition of the main propellant flows. The spark plug can be installed in any circumferential position toward the head end of the chamber. The direct ignition of main propellant flows eliminates the requirement for any auxiliary combustion chamber of alternate ignition methods. The direct ignition also eliminates requirement for any devices, such as valves, to sequence ignition flows and main propellant flows.

4. The method of propellant mixing incorporating a high level of eddy and vortex transport promotes the attainment of high combustion efficiency.

5. The simplicity of propellant injection and the effectiveness of chamber and nozzle cooling provides the potential of designing a compact lightweight thrust chamber with essentially an unlimited life cycle capability.

The analyses and test efforts reported show that the above advantages were maintained and/or demonstrated in the conduct of the Space Shuttle APS reverse flow engine program.

The reverse flow rocket engine concept was originally conceived at the Air Force Institute of Technology, Wright-Patterson Air Force Base and several analyses and test firings were made there and at the Institute of Technology, USAF Academy (References 1-6). BAC Company supported programs began in 1968 with 50 lb (222 N) thrust gaseous O_2/H_2 and gaseous F_2/H_2 thrust chambers. The results of those assemblies led to the exploration of the concept at 1,000 lb

(4448 N) and a chamber pressure of 250 psia (172.4 N/cm^2) (Figure 1). The 1,000 lb (4448 N) engine was test fired 188 times for a total accumulated run duration of 1265 seconds (Ref. 7). The company work resulted in programs of development of a 25 lb (111 N) F_2/H_2 engine for AFRPL, Figure 2, (Ref. 8) and the 1,500 lb (6672 N) O_2/H_2 engine described in this report.

The scope of the NAS 3-14353 program is indicated by a listing of the contract technical tasks:

Task I	–	Injector Analysis and Design
Task II	–	Injector Fabrication
Task III	–	Thrust Chamber Analysis and Design
Task IV	–	Thrust Chamber Fabrication
Task V	–	Ignition System Analysis and Design
Task VI	–	Ignition System Fabrication and Checkout
Task VII	–	Propellant Valves
Task VIII	–	Injector Tests
Task IX	–	Thrust Chamber Cooling Tests
Task X	–	Pulsing Tests
Task XI	–	Reporting Requirements

These tasks form most of the major subdivisions of the main text of this report. Company sponsored analyses and tests which were carried out to complement the definition and demonstration of the reverse-flow engine concept are included with the related contract effort description.

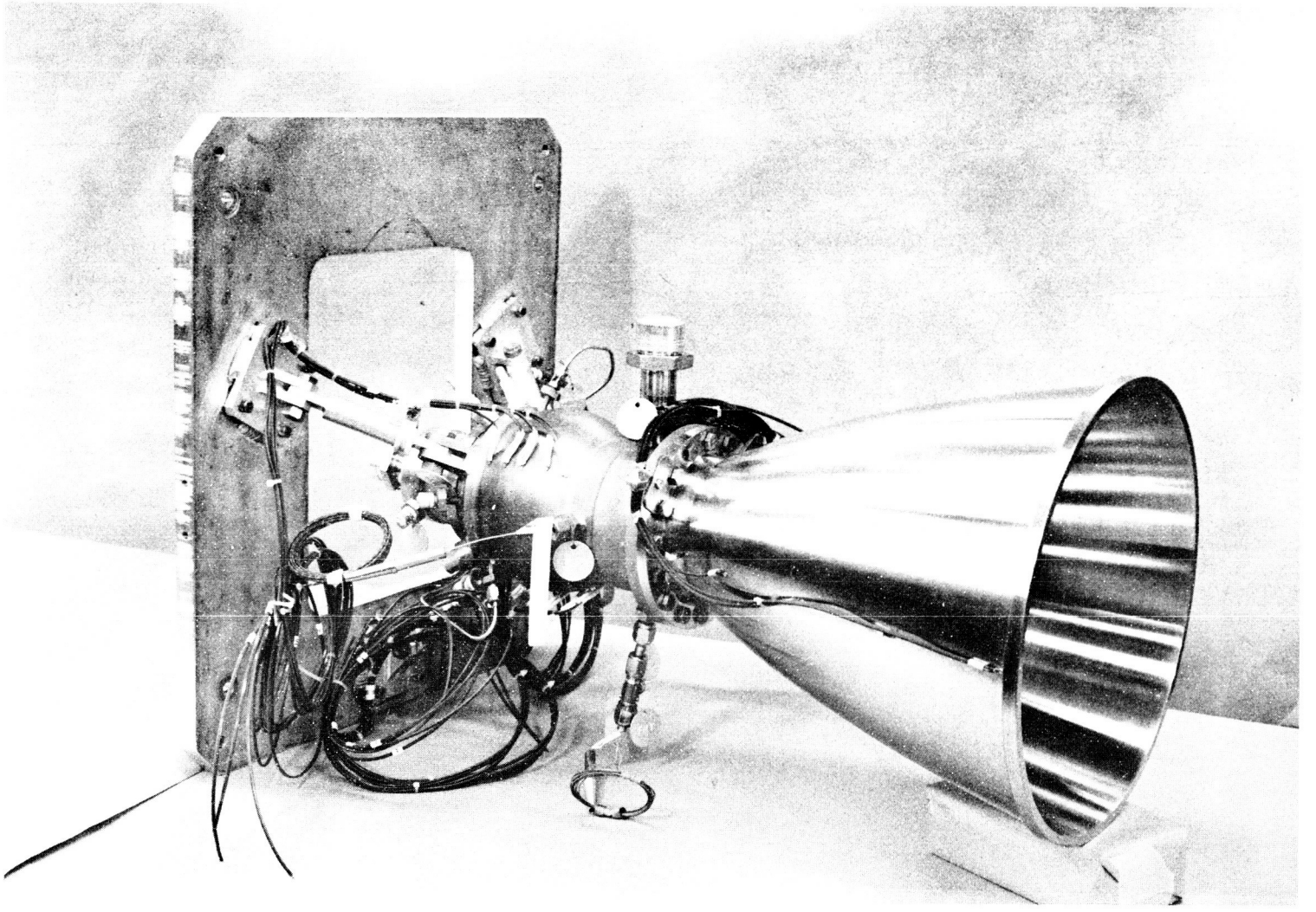

Figure 1. 1000 lb (4448N) Thrust Reverse Flow Engine

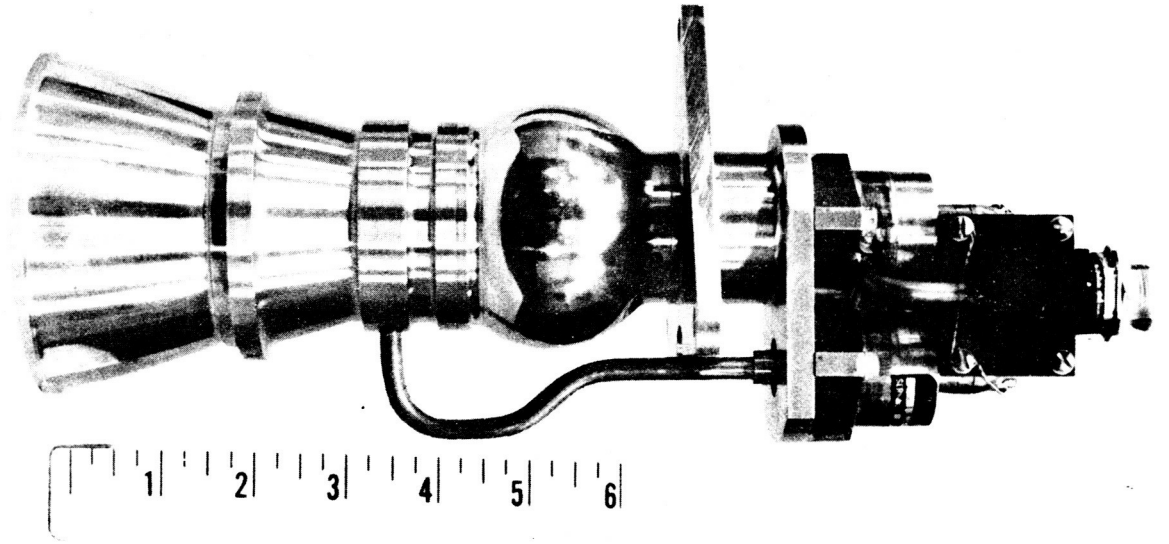

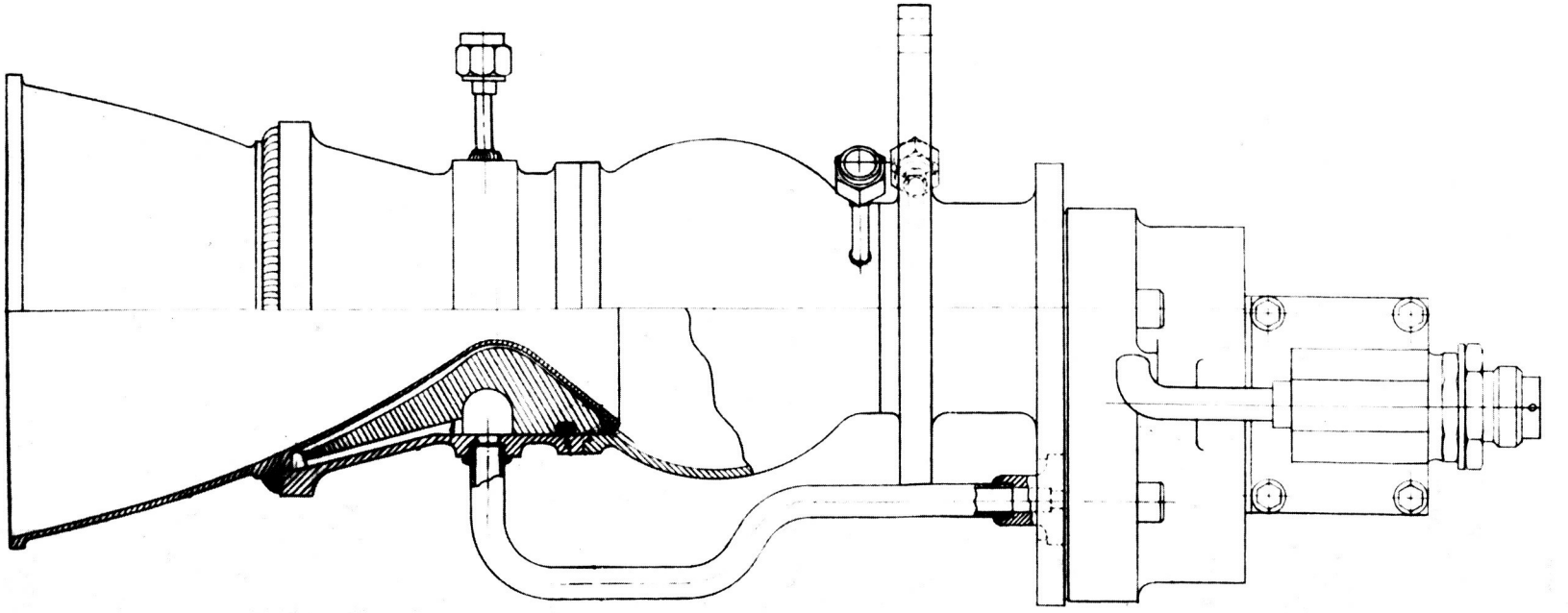

Figure 2. 25-lb (111N) Reverse Flow Thrust Chamber Assembly

III. CONTRACT REQUIREMENTS AND PROGRAM PLAN

The contract design point and operating ranges are summarized in Table I. The gaseous hydrogen and oxygen propellants met the requirements of MIL-P-27201 and MIL-P-25508A. The O_2 and H_2 feed pressures of 375 psia (258.5 N/cm^2) were defined at the engine valves inlets. The life cycle requirements were based on 10,000 pulses per mission for 100 missions during a 10-year period. Additional design and demonstration goals included 97% characteristic velocity efficiency; 435 seconds (4226 N sec/Kg) specific impulse; compatibility with propellants, test fluids, and cleaning fluids for 10 years; minimum servicing and refurbishment; and ease of service and maintenance when required. The maximum demonstration duration (Table I) was 500 seconds. This duration was considered to be representative of long firings although the specified design maximum was 1,000 seconds.

Tasks I, II and VIII of the contract work statement, Injector Analysis and Design, Injector Fabrication and Injector Test lead to the definition of injector configurations for altitude testing of complete thrust chamber assemblies. The Analysis and Design, Fabrication, and Testing of the thrust chamber assemblies comprise Tasks III, IV, IX and X.

Tasks I, II and IX, Injector Analysis and Design, Injector Fabrication, and Thrust Chamber Cooling Test, were amended in June 1971 to add the design and demonstration of a thrust chamber assembly with nominal propellant feed temperatures of 375°R (208°K) (O_2) and 250°R (139°K) (H_2). Performance loss due to reduced feed temperature was to be minimized in this design.

Tasks V, VI and VII included the effort to define, procure and check out spark ignition systems and engine test valves. The general time phasing of the major program tasks is depicted in Figure 3. The supporting programs effort consisted of company-sponsored analyses and testing which complemented the contracted tasks.

TABLE I
APS ENGINE REQUIREMENTS

Design Point	Contract NAS3-14353
Thrust	1500 lbf (6672 N)
Chamber Pressure	300 psia (206.8 N/cm^2)
Mixture Ratio	4.0
Feed Pressure (Valve Inlet)	375 psia (258.5 N/cm^2)
Area Ratio	40
H_2 Feed Temp	540 and 250°R (300 and 139°K)
O_2 Feed Temp	540 and 375°R (300 and 208°K)
Min Impulse Bit	50 lb sec (222.5 N sec)
Max Firing Duration	1000 sec
Life Cycle Pulses	9 x 10^5
Steady State	1 x 10^5
Cumulative	50 hr
Max External Temp	800°F (426°K)
Operating Range	
P_c	100 – 500 psia (68.95 –344.7 N/cm^2)
O/F	3 – 5
Feed Pressures	As Required
O_2 Feed Temp	Saturated Gas 250–800°R (139–444°K)
H_2 Feed Temp	200 – 800°R (111 – 444°K)
Duration (Demonstration)	500 sec
Goal	
Specific Impulse (I_{sp})	435 sec (4266 N sec/kg)

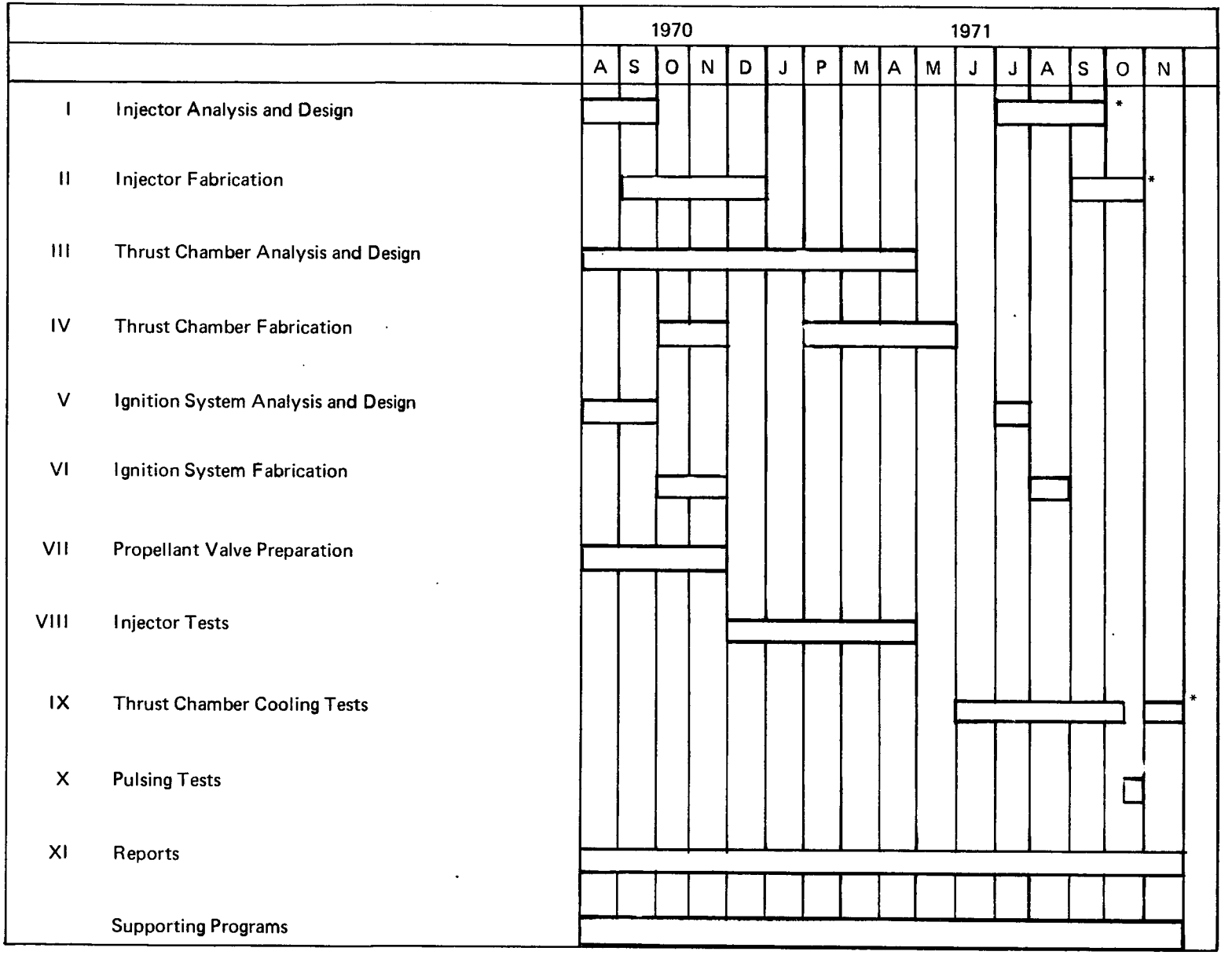

*Low Feed Temperature Design

Figure 3. Program Plan

IV. INJECTOR DESIGN AND ANALYSES

A. SELECTION OF TEST VARIABLES

1. Definition of Injector Variables

Figure 4 presents the components and general geometry of the reverse flow engine configuration employed for injector testing. Figure 5 shows an oxidizer cup and a fuel injector. The heat sink chamber assembly includes provisions for complete disassembly to evaluate several different oxidizer cups and fuel injectors.

The oxidizer and fuel injection design variables are shown in Figure 6. The O_2 swirl cup is defined primarily by the cup inside diameter, D_1, the outlet diameter, D_2, and the area of the swirl holes, A_S. The O_2 gas efflux angle a and the ratio of tangential and axial velocities of the diverging O_2 gas sheet are functions of the ratio of $\frac{D_1 D_2}{A_S}$. Those functional relationships will be discussed in more detail in subsection B, Flow Calculations. The oxidizer cup pressure drop is determined largely by A_S and D_2.

Part of the O_2 flow is injected through a central orifice in the cap of the oxidizer cup. The primary function of the O_2 center flow is the prevention of combustion product circulation into the oxidizer cup.

The oxidizer cup axial length, the converging geometry of the cup between the D_1 and D_2 diameters, the inlet geometry of the center flow hole and the swirl holes, the number of swirl holes, and the angle of the swirl hole centerline relative to the centerline of the cup complete the swirl cup design.

The fuel is injected tangential to the combustion chamber wall and includes the design variables of fuel injection station and the additional parameters shown in Figure 6; the slot width and height, spacing between slots and the turn angle B at the oxidizer cup outlet. The total number of fuel injection slots is based on the number of throat regenerative cooling passages; each passage terminates in an injection slot. The slot width and height is based on the injection velocity desired, the fuel injection station, the density of the H_2 at the point of injection and the allowance for C, the dimension between slots. A small C dimension insures complete film cooling of the chamber wall at the fuel injection station. The maximum fuel injection velocity is limited by the available engine H_2 feed pressure; most of the fuel circuit ΔP is associated with the H_2 injection velocity.

The basic configuration of the reverse flow thrust chamber with the oxidizer injected at the head end and the fuel in the convergent throat together with a spherical combustion chamber makes the chamber volume or characteristic length a primary injector variable. For given oxidizer and fuel injectors, the chamber L* defines the length of chamber film cooling path, the velocity of the H_2 at the point of O_2 injection and the overall mixing pattern of propellants within the combustion volume. In like manner, changes to the fuel injection station with other variables fixed including L* could be expected to change the combustion efficiency and heat rejection.

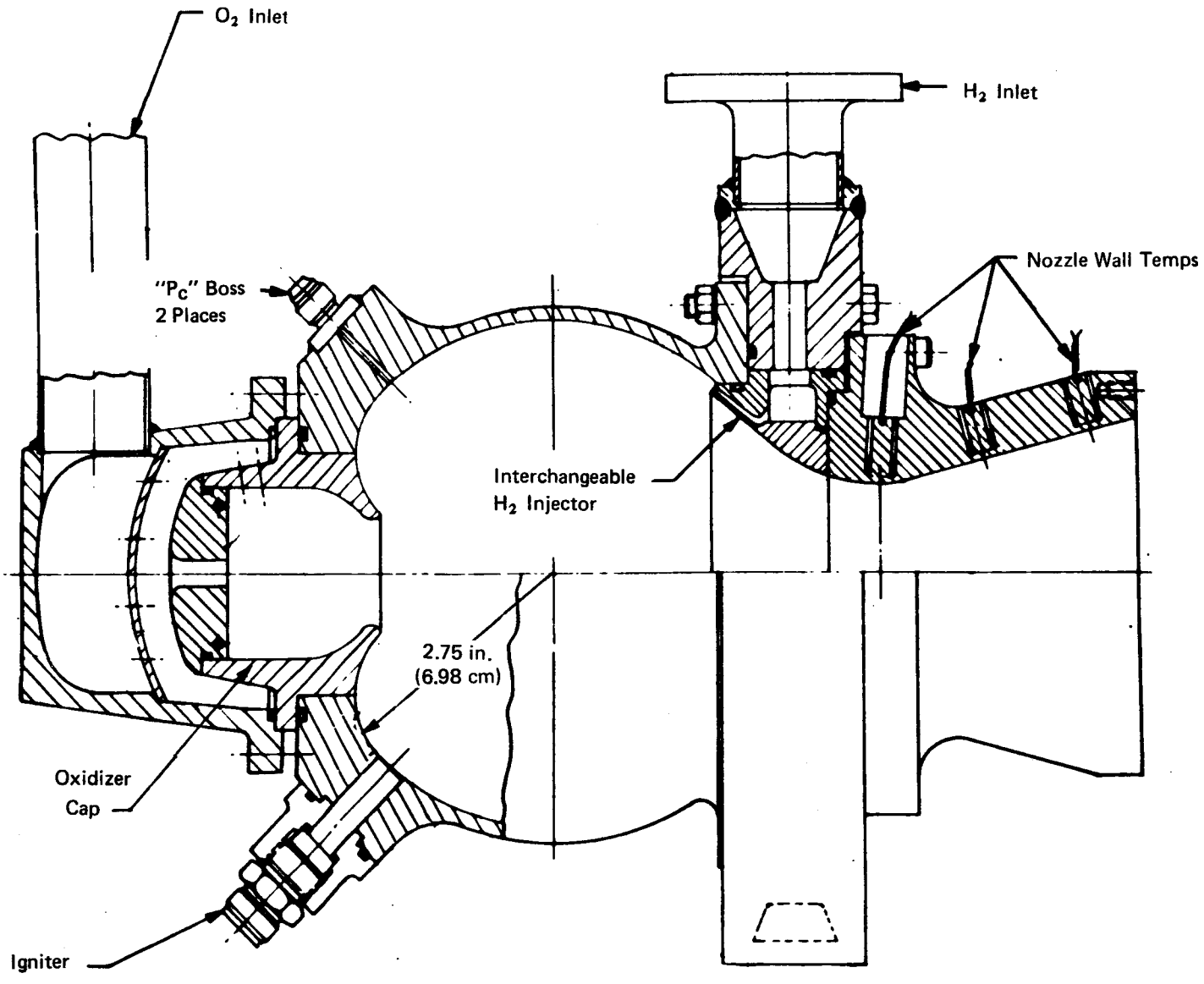

Figure 4. Heat Sink Thrust Chamber

Figure 5. Oxidizer Swirl Cup and Fuel Injector

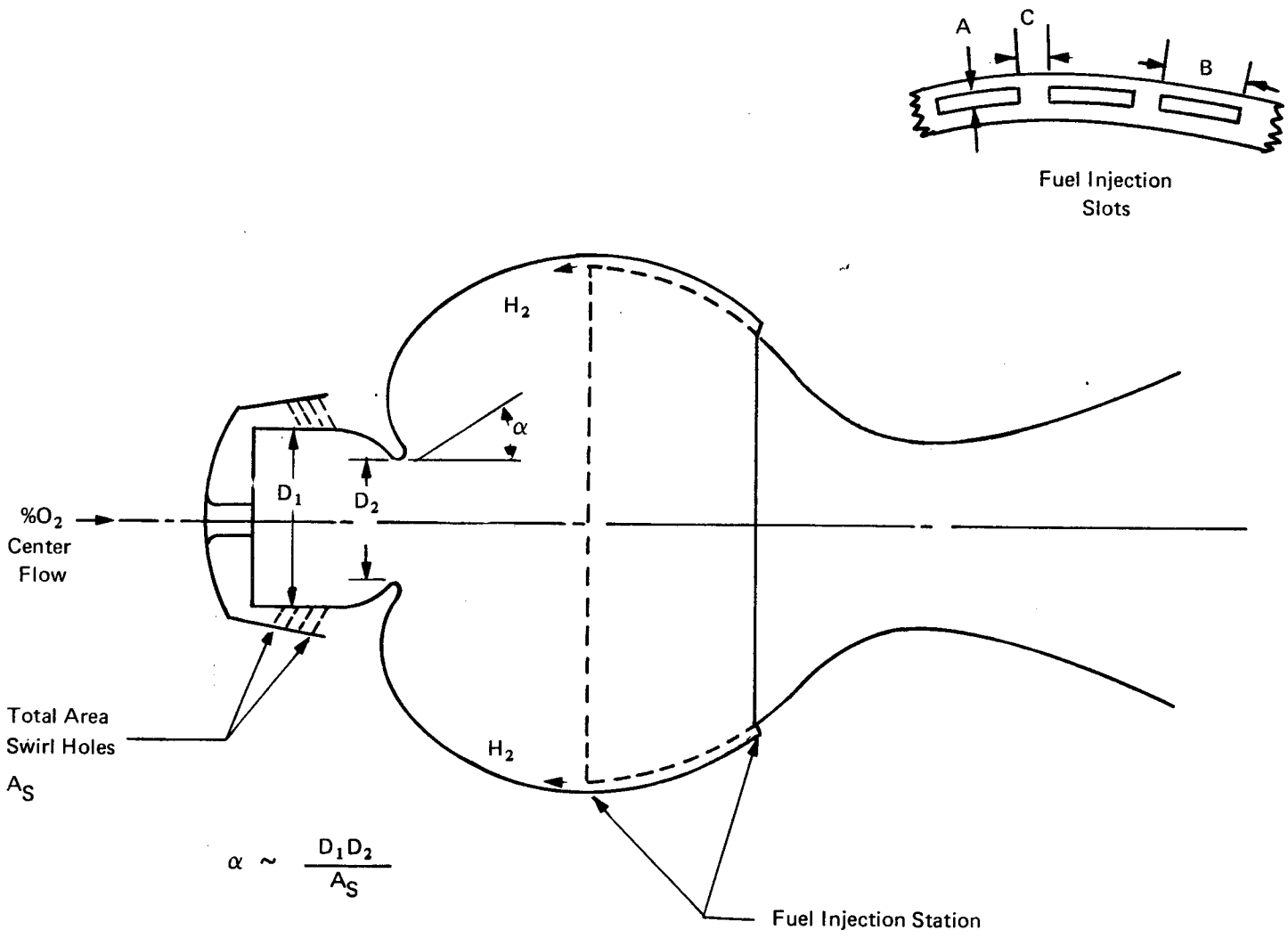

Figure 6. Injector Design Variables

2. 1000 lb (4448 N) Thrust Baseline Characteristics

The operating characteristics of the 1000 lb (4 448 N) reverse flow engine demonstrated before the start of the contract effort were close to the NAS 3-14353 goals for operation with ambient 540° R (300K) feed temperature propellants. The baseline injection characteristics of the 1K engine and the chamber L* were based on the earlier low P_C 50 lb (222 N) tests conducted at BAC, the data available in the literature (References 1-6), and a limited series of injector characterization test firings of the 1K engine. Figure 7 presents some of the details of the engine. The figure includes a line between the O_2 inlet and the combustion chamber to provide O_2 gas augmentation at the spark ignitor.

The 1K engine demonstrated a characteristic velocity efficiency of 95 to 96% at 250-psia (172.4 N/cm^2) chamber pressure, a mixture ratio range of two to four and a maximum regenerative cooled throat temperature of approximately 1000° F (811° K). The highest percentage of characteristic velocity was obtained at low O/F operation (Figure 8). The maximum combustion chamber wall temperature was 1200° F (922° K) for duration firings at an O/F of 4:1. The NAS 3-14353 contract goals of 97% c* and 1 x 10^6 cycle life required increase of the combustion efficiency and a reduction of the throat heat flux in addition to the scaling of thrust and chamber pressure to 1500 lbf (6672 N) and 300 psia (206.8 N/cm^2).

The 1000 lb (4 448 N) unit incorporated a chamber characteristic length of 32 in. (81.3 cm) and a fuel injection station at a contraction ratio of 4:1. The ratio of the maximum combustion chamber cross-sectional area to throat area was 9:1 for the 2.55-in. (6.47 cm) radius spherical combustion chamber and 1.70-in. (4.32 cm) throat diameter. The fuel injection slots were sized for an injection Mach No. of approximately 0.50.

The 1K engine oxidizer injector employed a cup I.D. of 1.594 in. (4.05 cm) a cup outlet diameter of 1.00 in. (2.54 cm) and 24 swirl holes of 0.140-in. (0.357 cm) diameter. The product of cup diameters divided by the area of the swirl holes was 4.27 giving an O_2 efflux cone angle of approximately 23 degrees to the centerline. The oxidizer cup pressure drop was 140 psi (96.5 N/cm^2) at P_C = 250 psia (172.4 N/cm^2) and O/F = 4, and 14% center flow.

3. Selected Variables

The initial NAS 3-14353 program effort was directed toward a combustion chamber with a propellant feed temperature design point of 540° R (300° K). Amendment 2 to the contract established a second design point for low feed temperature operation after experience was gained with operation of the 540° R (300° K) design hardware.

The preceding discussion of test variables and the results with the 1K thrust chamber indicate that a wide range of oxidizer injection could be investigated with minimum hardware cost by fixing the cup diameter D_1 and varying the outlet diameter D_2, the swirl hole area and the percent centerflow. One configuration of combustion chamber cup mounting would be required with D_1 fixed. The oxidizer injection angle, the cup ΔP and the total velocity of O_2 injection could be varied by changing the D_2 and swirl hole dimensions. Changes to the remaining cup design characteristics such as the contour between D_1 and D_2 and the number of swirl holes as defined by the 1K (4,448 N) engine were considered to be of secondary or negligible effect on the O_2 injection pattern.

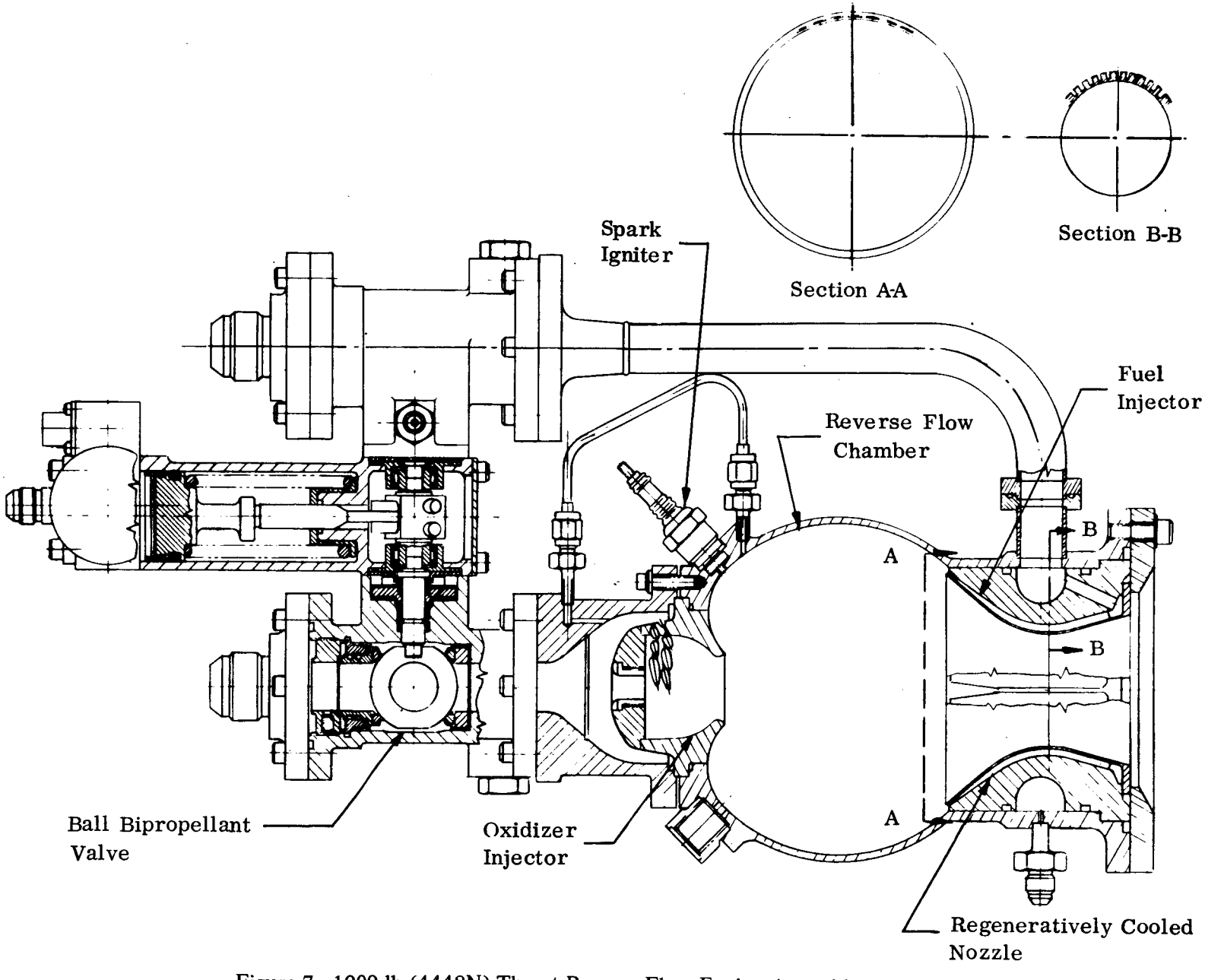

Figure 7. 1000-lb (4448N) Thrust Reverse Flow Engine Assembly

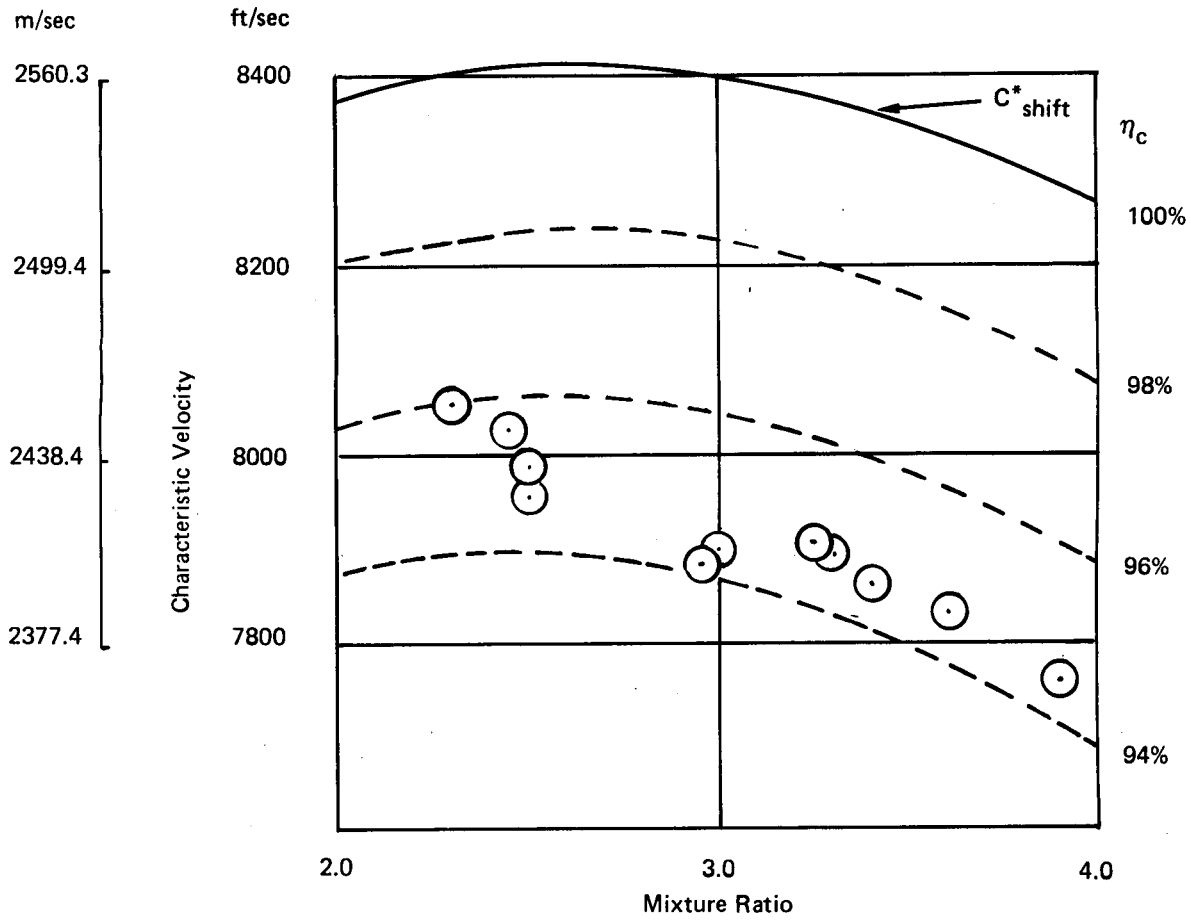

Figure 8. 1K (4448N) Reverse Flow O_2 - H_2 Gas Engine

The chamber L* was selected as a test variable for the 540° R (300° K) design to establish the relationship between combustion volume and the percentage of characteristic velocity achieved. An L* of 32 in. (81.3 cm) was established as the baseline, and 42 in. (107 cm) and 22 in. (55.8 cm) characteristic length/contours were defined as shown in Figure 9.

Fuel injection velocity was a logical choice of injector test variable in view of the increase of % c* observed with the 1K (4,448 N) unit with decreasing O/F. The higher relative flow rate of fuel at low O/F provided higher fuel injection velocity with the fixed-geometry 1K (4,448 N) hardware.

The additional variation of fuel injection station was not included in the initial injector characterization at 540° R (300° K). A partial evaluation of that variable would be achieved with tests at different L*. As shown by Figure 9, the relative distance between the planes of fuel and oxidizer injection increased with increasing L*. The number of pieces of injector test hardware and the number of tests would have been substantially increased beyond the program scope to include fuel injection velocity, L* and fuel injection station. The fuel turn angle at the oxidizer cup outlet was held constant equal to that of the 1K (4,448 N) engine for the same reasons.

The injector tests conducted with the 540° R (300° K) hardware resulted in the selection of 32 in. (81.3 cm) L* for continued 1500-lbf (6,672 N) engine testing. The highest fuel injection velocity consistent with the available fuel feed circuit pressure drop gave the highest combustion efficiency. The fuel injection velocity was observed to have more influence on performance than equivalent percentage changes of the O_2 injection velocity. An optimum oxidizer cup was also defined after thrust chamber firings at altitude based on a trade-off of pressure drop and engine I_{sp}. The fuel and oxidizer injectors exhibited nominal pressure drops approximately 10 psi (6.89 N/cm^2) and 25 psi (17.24 N/cm^2) respectively, above the contract goal of 75 psi (51.7 N/cm^2).

The selected 540° R (300° K) design configuration exhibited an I_{sp} fall-off of approximately 9% when operated with 250° R (139° K) fuel and 300° R (167° K) oxidizer. The performance reduction showed that the injection velocities played a dominant role in achieving high combustion efficiency. The design of the fuel and oxidizer injectors for the low-temperature hardware compensated for the increased density of the propellants. The design of the fuel and oxidizer injectors for the low temperature design hardware was based primarily in providing injection velocities equal to or approaching those exhibited by the 540° R (300° K) hardware. The low temperature design oxidizer cups incorporated similar angles of O_2 injection to preserve the fuel and oxidizer mixing pattern but with lower values of D_2 and A_s to increase O_2 injection velocity. The height of the fuel injector slots was reduced in the low temperature hardware design to provide an injection velocity approaching that of the ambient hardware.

The calculated pressure drop to match both the fuel and oxidizer velocities was above the contract goal. Consequently, additional oxidizer cups were designed with lower pressure drops at some expense in the injection velocities. The reduction of fuel ΔP and fuel injection velocity required some offsetting feature because of the observed strong dependence of % c* on the H_2 injection velocity. One additional change was available to counteract the anticipated combustion efficiency loss; the fuel injection station. Injection at a higher contraction ratio or closer to the plane of O_2 injection would provide a shorter fuel film flow path and would offset the lower H_2 injection velocity.

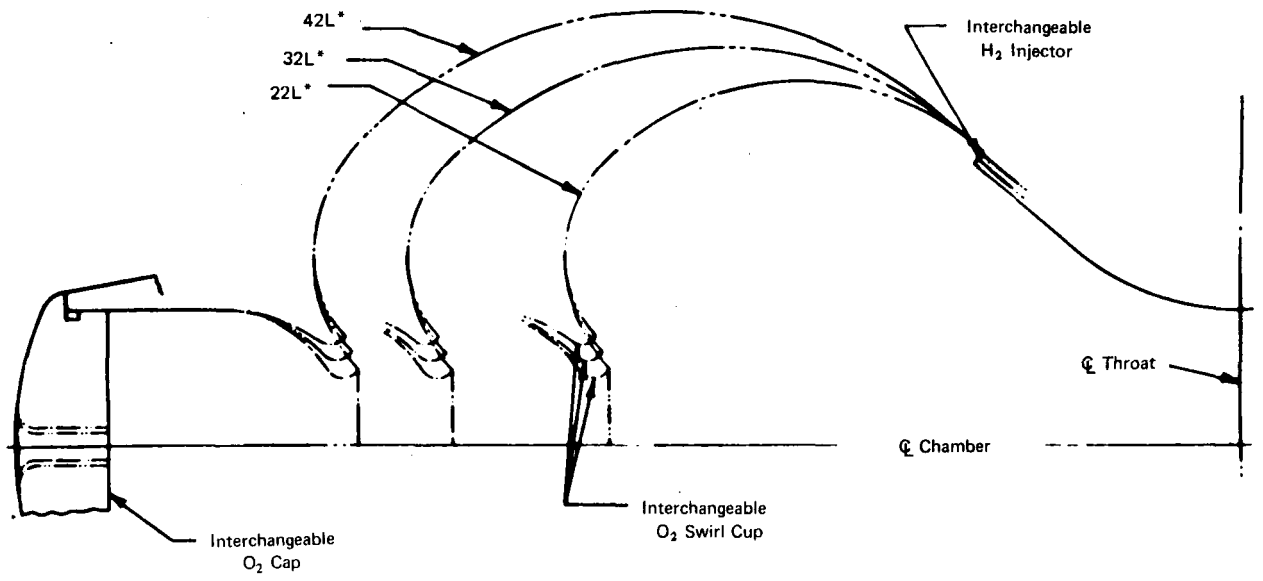

Figure 9. Configuration Variation

The following section of this report describes the analytical and test methods employed to establish the various injection parameters and presents the numerical values associated with the above general description of test variables.

B. FLOW CALCULATIONS

1. Oxidizer Cup

Early in the program the oxidizer cup injection angle was defined, using a simplified swirl atomizer correlation reported by E. Griffen.[9] In the analysis the efflux angle a of a cup is established as:

$$a = \frac{K\ D_1\ D_2}{A_S}$$

where:

K = constant determined empirically
D_1 = inside diameter of the cup
D_2 = the cup outlet diameter
A_S = total area of the tangential swirl holes

The value of K was established by cold-flow testing of both the 1000 lb (4,448 N) and 1500 lb (6,672 N) oxidizer cups with ambient air back pressure as described in Section XI A of this report The efflux angle was employed as a comparative description to identify different oxidizer cups designed for 540° R (300° K) operation. The efflux angle for injection into the combustion back pressure was not established by measurement. The efflux angle was observed to be largely independent of density and therefore not suited for extrapolation of 540° R (300° K) designs to the low feed temperature design requirement. The cup pressure drop calculations employed the gas flow-orifice equation, the A_S of the swirl holes and the empirically derived vortex flow crossection at D_2 for the ΔP between the inside of the cup and the combustion chamber.

The more detailed analytical approach taken to define the characteristics of the oxidizer swirl cup assumed a flowfield which is inviscid, axisymmetric and compressible. The effects of center-flow are accounted for only by decreasing tangential inlet flow. These assumptions result in the following system of differential equations for the steady-state flow field where a cylindrical coordinate

$$\rho \left\{ V_r \frac{\partial V_r}{\partial r} - \frac{V_\theta^2}{r} \right\} = - \frac{\partial P}{\partial r} \tag{1}$$

$$\rho \left\{ V_r \frac{\partial V_\theta}{\partial r} + \frac{V_r V_\theta}{r} \right\} = 0 \tag{2}$$

$$\frac{\partial}{\partial r} (\rho r V_r) = 0 \tag{3}$$

$$\left(\frac{\rho}{\rho_o} \right) = \left(\frac{P}{P_o} \right)^{1/\gamma} \tag{4}$$

Nomenclature

ρ	=	Density
V	=	Velocity
P	=	Pressure
r	=	Radius
γ	=	Specific heat ratio
M	=	Mach number
ϕ	=	$2 P_{Total}/P_{Static} = \frac{2 P_o}{P_s}$

Subscripts

r	=	Radial
θ	=	Tangential
o	=	Total
s	=	Static

system is used. The approach leads to a free vortex with radial components and is believed to be an accurate simulation of the flow field outside the core area.

Closed-form expressions for pressure drop and radial velocity cannot be obtained directly for the compressible case. However, a first order correction on the incompressible solution results in the following expression for nondimensionalized radial velocity:

$$V_r^* = \xi \left\{ 1 + \phi \gamma M^2 \left[\frac{1-r^{*2}}{r^{*2}} \right] \right\}^{1/2} \tag{5}$$

where V_r^* represents the radial velocity divided by the tangential inlet velocity and r* is a nondimensionalized radius($r^* = r/r_{cup}$), ξ is the value of V_r^* at the cup wall, and M is the injection Mach number. Use of this expression in the momentum equation shows that for practical design considerations the pressure ratio can be approximated by:

$$p^* = \left\{ 1 - \phi \left(\frac{\gamma-1}{2\gamma} \right) \left(\frac{1-r^{*2}}{r^{*2}} \right) \right\}^{\gamma/\gamma-1} \tag{6}$$

Here, ϕ represents twice the ratio of the injection dynamic to static pressure and p* is the pressure relative to the static pressure at the wall.

As the flow approaches the core region, it cannot retain its free vortex character. Viscous effects must come into play and the flow approaches that of a bound vortex. This conclusion has been empirically substantiated in numerous cases. In addition, axial flow components appear and begin to dominate the flow field. The simulation used in the core region therefore involves a bound vortex tangential velocity assumption and an isentropic one-dimensional axial flow model. The thickness of the annular core is established by requiring satisfaction of the continuity equation (mass flow in equals mass flow through annular area) and a pressure at the free surface equal to chamber pressure. The related equations are:

$$p^* = \left\{ 1 - \phi \left(\frac{\gamma-1}{2\gamma} \right) \left[1-r^{*2} \right] \right\}^{\frac{\gamma}{\gamma-1}} \tag{7}$$

for the bound vortex and:

$$\dot{W} = \int_{r_1}^{r_2} 2\pi r \left[\left(\frac{2\gamma}{\gamma-1} \right) P_\rho g \left(\frac{P_o}{P} \right)^{\frac{2}{\gamma}} \left[1-\left(\frac{P_o}{P} \right)^{\frac{\gamma-1}{\gamma}} \right] \right]^{1/2} dr \tag{8}$$

for axial flow and velocity.

These equations plus the additional assumption of isentropic expansion across the tangential swirl holes were programmed for computer solution. Several different cup geometries were calculated for O_2 flow at 540° R (300° K) and excellent agreement was achieved between the predicted and observed pressure drops as shown in Figure 10. Direct pilot measurement of the total velocity also showed good agreement with the calculated measurement. The pressure drop agreement lends

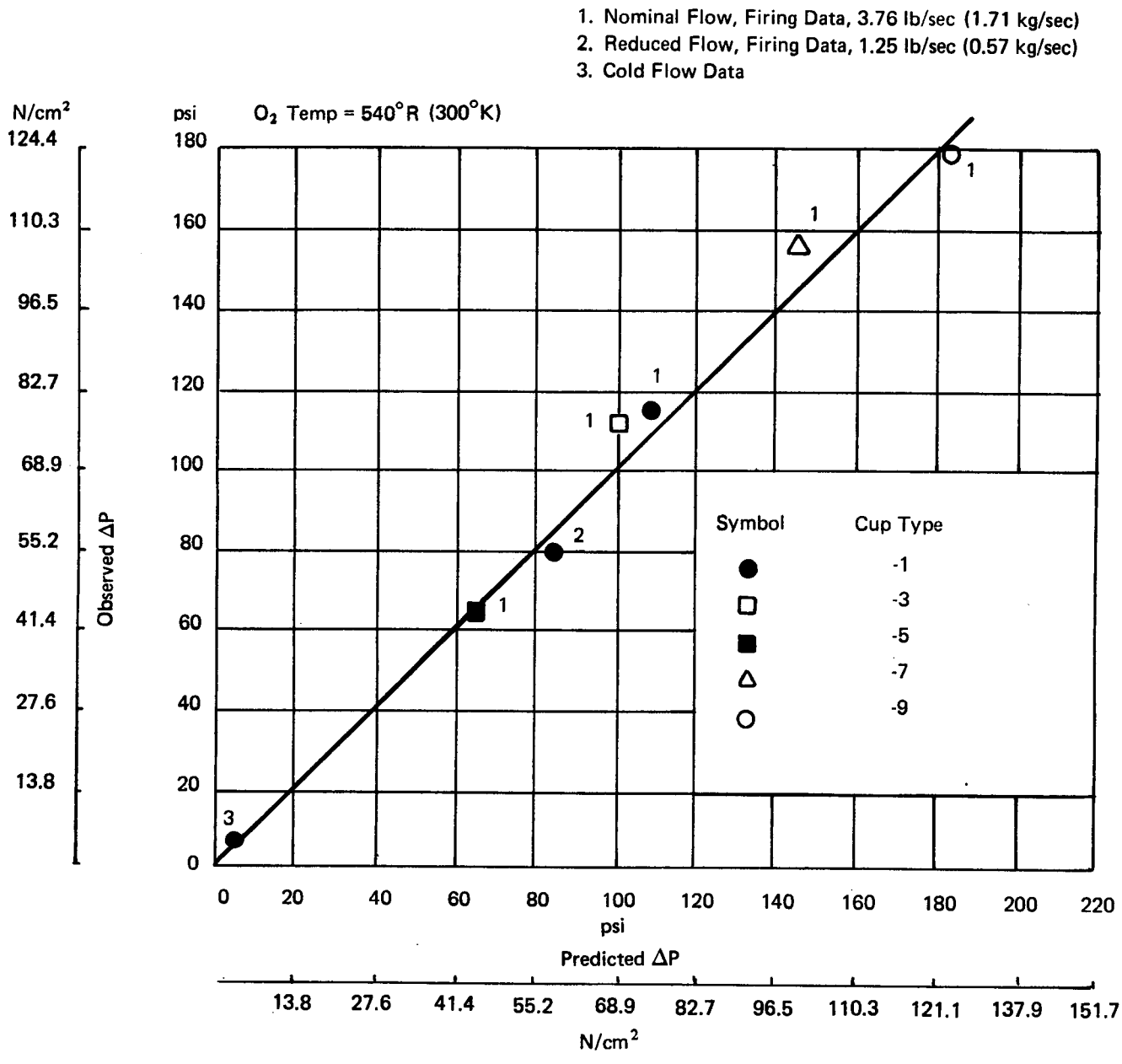

Figure 10. Predicted versus Observed Pressure Drops for Various Swirl Cup Injectors

credibility to the axial, tangential velocity and total velocity vector values which are part of the same solution, Table II.

A parametric study was conducted, using the more detailed oxidizer flow field equations to establish axial and tangential velocities, velocity ratios, and the vortex flow thickness at the cup outlet as a function of D_1, D_2 and A_S for operation at the low feed temperature design requirement of 375°R (208.3°K). Sample data from the study is given in Table III together with the calculated values for the one configuration oxidizer cup operating with 540°R (300°K) O_2. The selection of cup designs for the low temperature operation was made on the basis of the parametric study. The earlier approach of using the calculated ΔP and efflux angle was superseded by the more detailed calculations. Subsection D will describe the performance relationships established as a function of the oxidizer and fuel injection characteristics.

2. Fuel Injector

Isentropic compressible flow equations were used to define the fuel injection characteristics:

$$\frac{\dot{W}}{A} = \sqrt{\frac{\gamma}{R}\frac{P_O}{T_O}}\;\frac{M}{\left(1+\frac{\gamma-1}{2}M^2\right)^{\frac{\gamma+1}{2(\gamma-1)}}}$$

$$\frac{P_O}{P} = \left(1+\frac{\gamma-1}{2}M^2\right)^{\frac{\gamma}{\gamma-1}}$$

$$M = \frac{V_{H_2}}{\sqrt{\gamma R T g}}$$

where
- W = H_2 injection mass flow rate
- A = total injection area
- γ = ratio of specific heats
- R = gas constant
- P = pressure
- T = temperature
- M = injected H_2 Mach number
- V_{H_2} = injected H_2 velocity
- g = gravity

Subscripts: o = stagnation or total

The injection stagnation temperature, T_O, is a function of the thrust chamber hydrogen inlet temperature and the H_2 temperature rise associated with nozzle regenerative cooling up to the point of hydrogen injection.

The initial fuel injection calculations were made on the basis of assumed values of H_2 injection velocity at a T_O of 540°R (300°K) and nominal H_2 flow, which fixed the total fuel injection area for each velocity selected for evaluation.

TABLE II
CALCULATED O_2 INJECTOR CHARACTERISTICS

Dash No.	D_2 in.	D_2 cm	A_s in.^{2}	A_s cm^2	$\alpha \sim \frac{D_1 D_2}{A_s}$	α (°)	% C.F.	β	V_θ ft/sec	V_θ m/sec	V_Z ft/sec	V_Z m/sec	V_T ft/sec	V_T m/sec
-1	1.427	3.625	0.421	2.72	6.44	(28)		51.4	554	169	442	135	709	216
-3	1.189	3.025	0.519	3.35	4.35	(21)	5	44.5	543	165	553	168		
-5	1.427	3.625	0.519	3.35	5.22	(23)	5	49.0	498	152	431	131		
-7	1.66	4.216	0.295	1.90	10.73	(39)	5	57.3	725	221	465	142		
-9	1.427	3.625	0.295	1.90	9.18	(35)	5							
							10	53.9	784	239	572	174		
-3A	1.189	3.025	0.346	2.25	6.53	(28.4)	5	47.7	657	200	599	182		

TABLE III
OX SWIRL CUP PARAMETRIC STUDY

Case No. Parameter	1 (Nom.)	2	3	4	5	6	7	8
Ox Temp, °R (°K)	540 (300)	375 (208)	375 (208)	375 (208)	375 (208)	375 (208)	375 (208)	375 (208)
D_1, in. (cm)	1.9 (4.83)	1.9 (4.83)	1.9 (4.83)	1.9 (4.83)	1.9 (4.83)	1.9 (4.83)	1.9 (4.83)	1.9 (4.83)
D_2, in. (cm)	1.427 (3.625)	1.400 (3.55)	1.275 (3.24)	1.275 (3.24)	1.427 (3.625)	1.215 (3.086)	1.3835 (3.514)	1.2796 (3.25)
A_s, in.^{2}-(cm^2)	0.421 (2.72)	0.350 (2.26)	0.400 (2.58)	0.450 (2.90)	0.421 (2.72)	0.3065 (1.975)	0.4179 (2.695)	0.3899 (2.515)
ΔP, psi (N/cm^2)	103.4 (71.3)	103.7 (71.5)	101.1 (69.8)	86.1 (59.3)	76.8 (52.95)	158.1 (91.9)	81.7 (56.3)	103.4 (71.3)
$V\theta$, fps (m/s)	554.2 (169)	478.1 (145.5)	450.4 (137)	410.8 (125)	407.5 (124)	555.3 (169)	418.0 (127)	459.4 (140)
V_Z fps (m/s)	442.0 (134.7)	350.2 (106.7)	379.1 (115.3)	359.7 (109.5)	319.6 (97.3)	443.8 (135)	330.7 (100.5)	366.9 (111.7)
β,°	51.43	53.79	49.92	48.80	51.90	51.37	51.65	51.39
Sheet Thickn. t, in. (cm)	0.156 (0.396)	0.135 (0.343)	0.150 (0.381)	0.158 (0.401)	0.152 (0.386)	0.133 (0.338)	0.149 (0.378)	0.140 (0.355)
Characteristics	540°R/300°K Baseline	One Case Constant ΔP	Approx. Const. β	Const. t	540°R (300°K) Design at 375°R (208.3°K)	Const.β Same V_θ, V_Z	Const.β 20% Lower ΔP	Constant β Same ΔP as Case 1

V_θ = tangential velocity

β = $\arctan \frac{V_\theta}{V_Z}$

V_Z = axial velocity

t = calculated flow field thickness at cup outlet

The calculated injection ΔP is presented as a function of the H_2 injection velocity in Figure 11 for T_O = 540°R (300°K).

The injector testing established the nominal H_2 injection velocity for the subsequently designed cooled thrust chamber. The injectors of the cooled thrust chamber configuration were sized on the basis of injector test hardware results adjusted for hydrogen heating in the nozzle coolant passages. The fuel injection area of the film- and dump-cooled nozzles were adjusted to compensate for the bleed off of the H_2 coolant upstream of the injection orifices.

The operation of the thrust chamber designed for 540°R (300°K) propellant inlet temperatures at low propellant feed temperatures showed a loss of combustion efficiency. As predicted, the operation of the 540°R (300°K) design injector at the low propellant feed temperatures resulted in a reduction of V_{H_2} as a result of the increase of propellant density;

$$\frac{W_{H_2}}{A} = \text{constant for a given O/F and combustion efficiency at nominal thrust and chamber pressure.} = (\rho_1 V_1)_{540°R\ (300°K)} = (\rho_2 V_2)\ \text{low temperature.}$$

Consequently, the fuel injector of one of the low feed temperature designs was sized to increase the fuel injection velocity to that of 540°R (300°K) hardware.

The second low feed temperature design fuel injector incorporated a changed point of fuel injection and a lower injection velocity based on an overall reduction of H_2 feed circuit pressure drop of 20 psi (13.79 N/cm^2) as described in Section IV.A.3.

C. DESIGNS

1. Oxidizer Cups

The 1000 lb (4,448 N) reverse-flow engine oxidizer cup was scaled to the 1500 lb (6,672 N) level by matching the average velocity at the cup outlet, D_2, accepting the same ratio of inside diameter to outlet diameter, D_1/D_2, and employing the same ratio of diameters and swirl hole areas, $\frac{D_1 D_2}{A_S}$. The more exact analytical characterization of the oxidizer injection was not available for design purposes at the beginning of the program. This first approximation and two other variations were cold-flow tested (Section XI) to compare velocity profiles and gas efflux angle at the cup outlet relative to the highest performing 1K (4,448 N) cup.

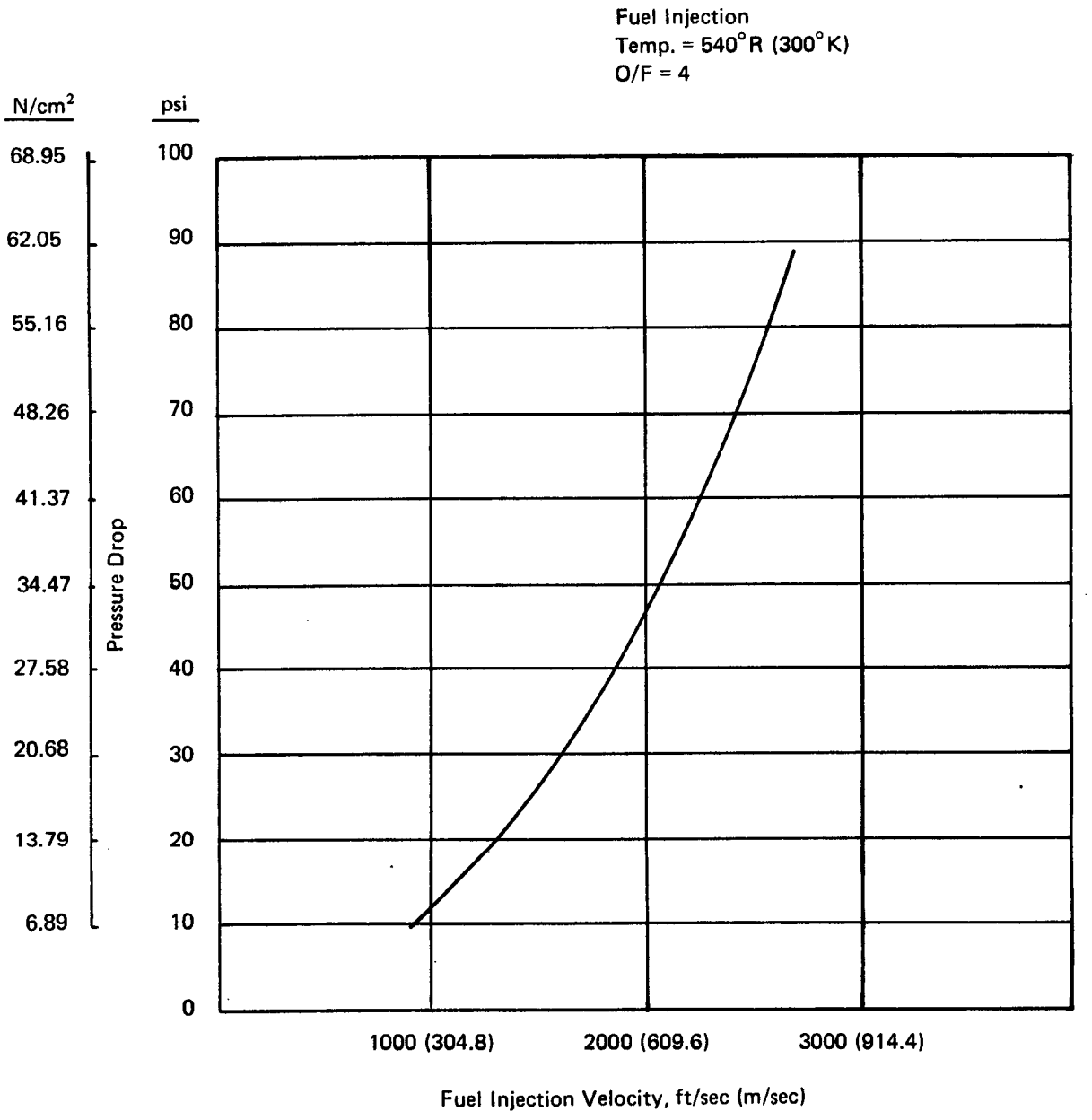

Figure 11. Fuel Injection Pressure Drop versus Fuel Injection Velocity

The 3 designs were as follows:

D_1 in.	D_1 cm	D_2 in.	D_2 cm	A_S sq. in.	A_S cm^2	$\frac{D_1 D_2}{A_S}$	α
1.90	4.83	1.189	3.02	0.520	3.35	4.35	23°
1.90	4.83	1.427	3.62	0.421	2.72	6.44	28°
1.90	4.83	1.427	3.62	0.520	3.35	5.22	25°

where α is the gas efflux angle.

Trends of increasing combustion efficiency were explored during injector test firings by extending the range of cup characteristics to encompass

D_2 = 1.189, 1.427, 1.660 in. (3.02, 3.62 and 4.22 cm)

A_S = 0.294 - 0.520 $in.^2$ (1.90 - 3.35 cm^2)

α = 23-39°

% Centerflow = 1.5-15

$\frac{D_1 D_2}{A_S}$ = 4.35-10.73

The general configuration of the oxidizer cup as shown in Figure 4 permitted interchangability of the various cup configurations. The percent centerflow changes were facilitated by the removable cup cap. Several of the changes to A_S were simply accomplished by installing metal pins in a number of the 24 swirl holes. A total of 12 variations of the ratio of $D_1 D_2 / A_S$ or the related gas efflux angle α and percent centerflow were evaluated for design operation at 540°R (300°K) feed temperature propellants.

The oxidizer cups defined for low O_2 feed temperature, 375°R (208.3°K), are described in Table III, numbers 6, 7 and 8. Configuration 6 from that table provided the same oxidizer axial and tangential swirl velocity as the principal 540°R (300°K) cup design. The principal cup designation here refers to the configuration which was selected from the injector test firings for most of the thrust chamber cooling tests carried out under simulated altitude test conditions. The matching of oxidizer velocities resulted in an increase of O_2 cup ΔP from 103 psi (71 N/cm^2) for the 540°R (300°K) design cup to 158 psi (108.9 N/cm^2) for configuration number 6 as shown in the table. Configuration number 8 was established on the basis of operation at 375°R (208.3°K) with the same cup ΔP as at 540°R (300°K) and with the same ratio of V_θ to V_z but with the reduced V_θ and V_z associated with the reduced pressure drop relative to the configuration number 6. The third low temperature design cup, number 7 of Table III, was defined on the basis of a pressure drop of approximately 82 psi (56.54 N/cm^2) to assess lower ΔP operation in conjunction with a changed station of fuel injection.

2. Fuel Injector

Three fuel injection velocities were selected for initial evaluation at the 1500 lbf (6,672 N) level. The successful operation of the 1000 lbf (4 448 N) unit with an injection velocity of 2100 ft/sec

(640 m/sec) provided the baseline design. Separate fuel injector rings were designed for the injector test hardware to evaluate 2100 ft/sec (640 m/sec) H_2 injection and injection at approximately 1700 ft/sec (518 m/sec) and 2400 ft/sec (731 m/sec). Each of the 3 injectors incorporated 40 fuel slots with a slot width of 0.292 (0.74 cm) inches and slot heights adjusted to give the desired velocity (Table IV). The results of the injector test hardware firings led to the selection of 2400 ft/sec (731 m/sec) as the nominal design condition for the cooled thrust chamber hardware.

Adjustments were made in the slot height of the regeneratively cooled nozzle sections for the increase of the adiabatic recovery temperature due to the regenerative cooling. Changes in slot height were also made for changes to the H_2 combustion flow for nozzle sections which evaluated H_2 bleed-off for nozzle extension and nozzle throat film cooling. The nomenclature of regenerative/film and regenerative/dump in Table IV distinguishes between H_2 bleed-off for throat and nozzle extension supplementary cooling respectively. The fuel injector of the nozzle section designed for low propellant feed temperature was reduced in height for the lower fuel injection temperature. The low-temperature design hardware included only nozzle extension dump cooling flow because the throat film coolant configuration showed little improvement of the throat temperatures and the recorded temperatures for nozzle extension operation indicated that auxilliary divergent nozzle cooling would be required to meet the eventual cycle-life requirements.

The second fuel injector/nozzle liner section designed for low-temperature operation included a wider slot width in keeping with the larger chamber diameter for the modified fuel injection location. The second nozzle section was also designed for 20 psi (13.79 N/cm^2) less fuel pressure drop to comply with the hypothesis that lesser velocity was needed as the injection position was moved forward on the chamber.

A change in the fuel injector made between the injector test hardware and the cooled thrust chamber hardware was in the land thickness or section between injection slots. The section thickness between slots was changed from approximately 0.020 to 0.040 in. (0.0508 to 0.1016 cm) to increase the fuel injector ruggedness for parts handling during chamber assembly. Long-duration firings (over 100 seconds) showed heat discoloration and some pitting of the chamber wall immediately downstream of this land area. The section (land area) was modified as shown in Figure 12 for the 500-second duration firing. The modification reduced the localized chamber heating.

D. THRUST CHAMBER PERFORMANCE AND INJECTOR VARIABLES

During the program the emphasis of the injector design was placed on engine I_{sp} or the percentage of theoretical c* together with the injector's pressure drop. Cooling of the combustion chamber for the life cycle requirements presented no problems, as all injector combinations tested provided compatible temperatures or heat fluxes in the combustion and throat sections. At nominal flow rates the observed maximum heat fluxes in the throat section indicated design margins of 1.4 to over 5 relative to the 1×10^6 cycle contract life requirement. The combustion chamber temperatures and regenerative cooled throat section temperatures provided a high life cycle margin over the entire range of operation (P_C, O/F, propellant feed temperatures). The thermal data and structural analyses are described in some detail in later sections of this report.

General trends of increasing combustion efficiency were noted during the injector test firings at sea level and those trends were pursued primarily with additional oxidizer cup configurations. The

TABLE IV
FUEL INJECTORS

	Injection Velocity*		Design 1 Temp.		Slot Width		Slot Height	
	fps	(m/s)	°R	°K	in.	cm	in.	cm
Injector Test	1700	(518)	540	(300)	0.292	(0.742)	0.048	0.122
	2100	(640)	540	(300)	0.292	(0.742)	0.038	0.097
	2400	(731)	540	(300)	0.292	(0.742)	0.034	0.086
Cooled Thrust Chamber								
Regen only	2400	(731)	540	(300)	0.274	(0.696)	0.042	0.107
Regen/Film	2400	(731)	540	(300)	0.274	(0.696)	0.038	0.097
Regen/Dump	2400	(731)	540	(300)	0.274	(0.696)	0.040	0.102
Cooled Thrust Chamber								
Regen/Dump	2400	(731)	250	139	0.274	0.696	0.023	(0.058)
Regen/Dump2	2150	(655)	250	139	0.359	0.911	0.019	(0.048)

*At nominal O/F and P_C
1 Propellant feed temp.
2 Changed point of fuel injection

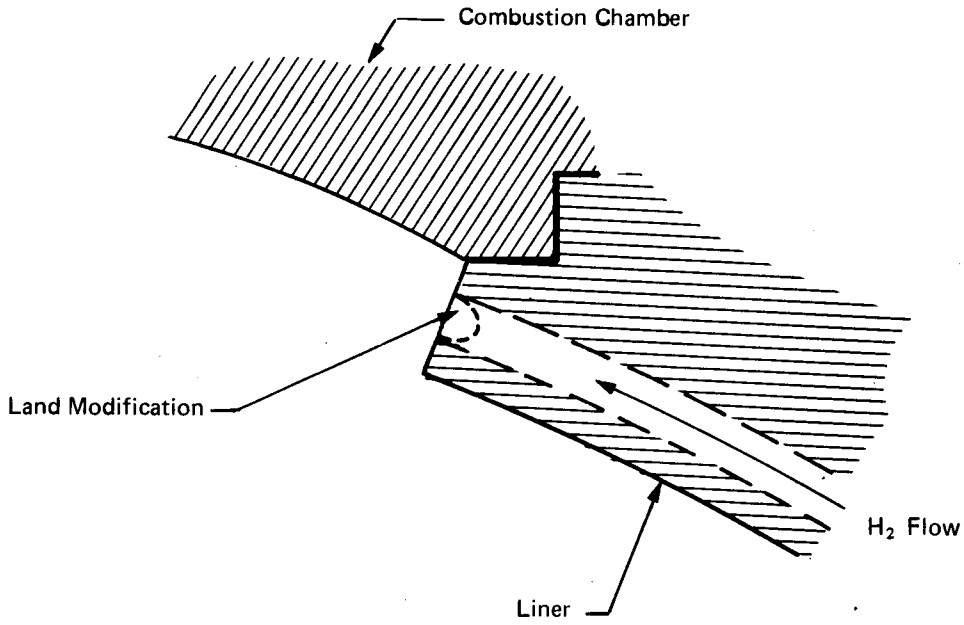

Figure 12. Fuel Injection Configuration 500 Second Firing

performance of selected injector configurations was confirmed during the thrust chamber cooling tests at altitude. Subsequently, the observed trends of operation were employed for the design of injectors for low propellant feed temperature operation. The high percentage of theoretical I_{sp} achieved with the low temperature design hardware and an observed I_{sp} in excess of the contract goal with the 540°R (300°K) design thrust chambers demonstrated successful exploitation of the injector test firing observations. The following paragraphs will discuss the observed trends of combustion efficiency with changes to the fuel and oxidizer injectors and the attempts made to qualitatively relate the trends with the hardware designs.

The trend of increased combustion efficiency was consistent with increased fuel injection velocity, with other variables fixed. The highest tolerable H_2 velocity injection with consideration of the fuel circuit pressure drop budget, was used for the cooled thrust chamber designs.

Peak c* performance was obtained with approximately 5% centerflow and the performance dropped on either side of this value. The heat rejection at the throat was reduced with increased O_2 cup centerflow but the largest reduction was between 1.5 and 5% centerflow.

The two highest performance O_2 cups had high O_2 velocities; one cup outlet diameter was 1.19 in. (3.02 cm) the other was 1.66 in. (4.22 cm). The intermediate cup outlet diameter, 1.43 in. (3.62 cm) did not achieve the same performance level even when the total velocity vector exceeded that of the two highest c* units. A hypothesis is readily formulated from this data in that the balance velocity vectors are of primary importance and not an either/or type relation found in shear mixing combustors. Further consideration would rationalize that shear forces in opposing gas streams are important, leading to the conclusion that the combination of oxidizer swirl and fuel velocities would optimize for a chamber of a given size.

The % c* with gas efflux angle or the related ratio of $D_1 D_2 / A_S$ generally increased with increased α, (where $\alpha = D_1 D_2 / A_S$), but as noted with the injection velocities, high performance was achieved at the lower and upper limits of D_2. The lower and upper limits of D_2 translated to intermediate and high values of α. The highest α tested, corresponding to 39°, showed a marked c* fall-off at an O/F above 4.0 when tested with a fuel injector designed for a lower injection velocity than the maximum of 2400 ft/sec (731.5 m/sec). The c* fall off with the 39° cup indicated that the limit of increasing α had been approached and the proper balance between oxidizer penetration (swirl) and fuel velocity had been exceeded. It may be noted that the actual oxidizer emittance angle (α) was not measured under operating conditions but was extrapolated from the initial cold-flow calibration results.

The percentage of theoretical c* for the thrust chamber cooling tests showed a fall-off of about 1% from an O/F of 3 to an O/F of 5. Operation of high (500 psia) (344.7 N/cm^2) and low (100 psia) (68.95 N/cm^2) chamber pressure, by increase and decrease of O_2 and H_2 mass flow rates with the fixed diameter throat sized for 300 psia (206.8 N/cm^2) operation, indicated little change of performance at nominal O/F. These observations are for fixed fuel and oxidizer injectors. The relative change of the fuel and oxidizer velocities with O/F for one injection combination is shown in Figure 13. The c* achieved was relatively insensitive to the large percentage changes of fuel and oxidizer velocities over the range of O/F. The same observation can be made for velocity ratios versus chamber pressure. The insensitivities appear to conflict with the performance change noted for changes of the design velocity of the fuel injector at an O/F of 4. The lack of a simple relationship between the O_2 injection velocity and performance is also apparent.

O_2 Component Velocity Ratios

	V_θ	V_Z
O/F = 3	0.94	0.93
O/F = 4	1.00	1.00
O/F = 5	1.05	1.06

P_C = 300 psia (206.8 N/cm^2)
540°R (300°K) Feed Temp.
Fuel Injector
2400 ft/sec (731.5 m/sec) at O/F = 4

Ox Injector
α = 28°
10% Center Flow
709 ft/sec (216.1 m/sec) Total Velocity at O/F = 4

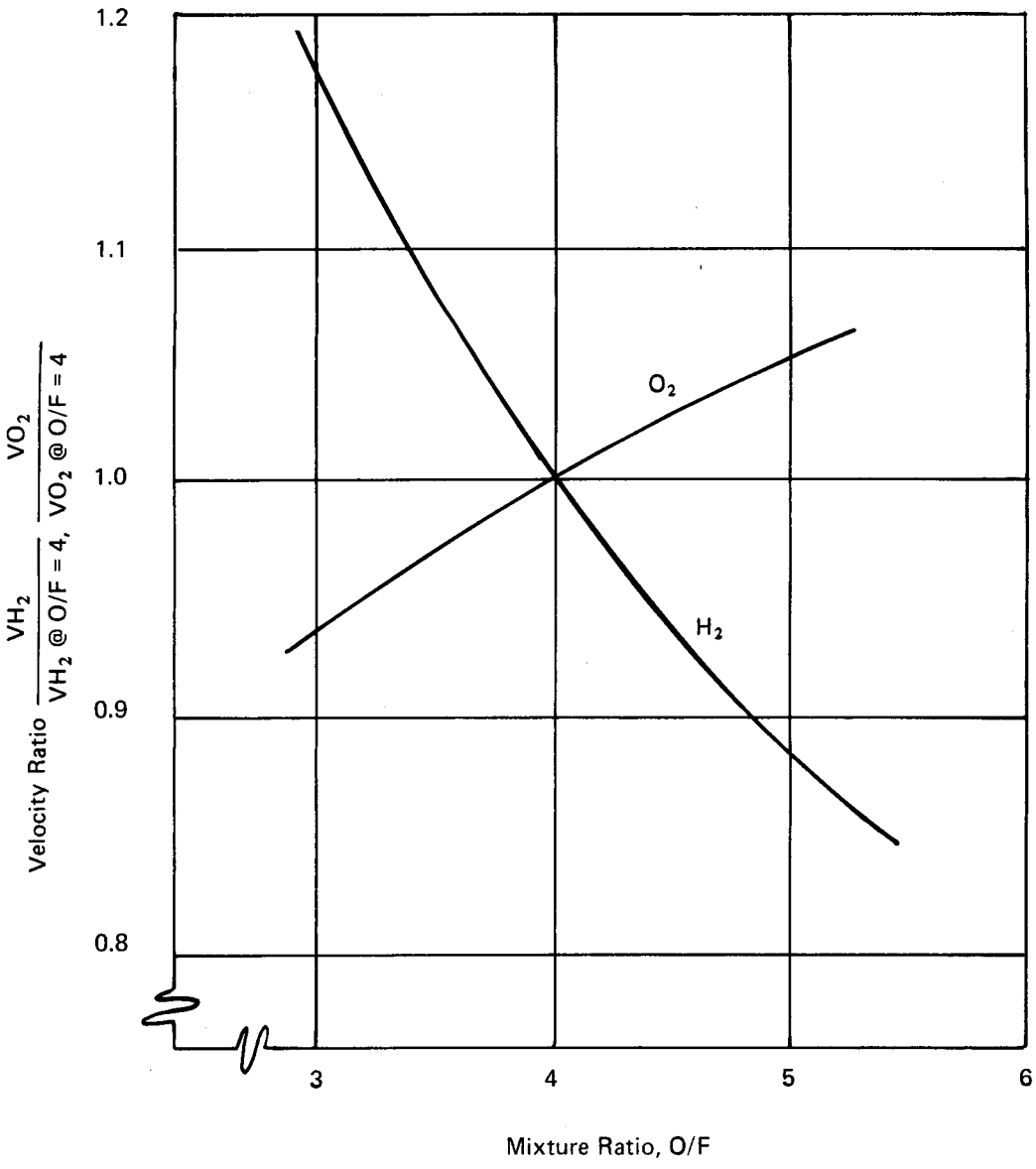

Figure 13. Velocity Ratio versus Mixture Ratio

An attempt was made to correlate the percentage of c* achieved with such parameters as injector velocities, gas efflux angle, cup outlet diameter, percent centerflow and the ratio of $D_1 D_2 / A_S$ of the oxidizer cup. The effort appears to be hampered by the inability to define the interaction of the oxidizer-cone-directed combustion zone and the fuel near the point of H_2 injection. The result showed that certain trends could be forecast, but that capability of mathematically describing a combustion mode fell short of its goal.

A parallel effort to analytically establish a complete mixing and combustion model, progressed to the point of partial agreement with the observed combustion chamber wall temperatures with one set of oxidizer and fuel injectors. That "Spalding Mixing Model" is described in Appendix A. The NAS 3-14353 program schedule and scope precluded the effort to complete the semiempiricalization of the more detailed combustion calculations. It was hypothesized that the completed model could also be employed to characterize the combustion as a function of the chamber diameter and length.

The subject of combustion modeling for the reverse flow engine is continued in Section XVI, "Recommended Follow-On Technology."

V. INJECTOR FABRICATION

A. GENERAL

Due to the unique propellant separation of the reverse flow engine the injector fabrication effort encompassed the two basic separate components to inject the oxygen and the hydrogen. The fabrication of the associated manifolding to supply the propellants to each of the injectors was also included in this task.

The three major elements in this task consisted of fabrication of the following:

(1) Oxidizer injector cold flow models
(2) Heat sink/sea level injector assemblies (oxidizer and fuel)
(3) Cooled injector assemblies (oxidizer and fuel)

Each of these major elements are discussed in detail in the following paragraphs.

B. OXIDIZER INJECTOR COLD FLOW MODELS

The oxidizer injector cold flow models were fabricated early in the program to allow characterization of "scaling" from the 1000 lb (4 448 N) thrust reverse flow chamber design to the 1500 lb (6672 N) thrust design. The cold flow models were designed and fabricated to duplicate the critical parameters of the actual "hot fire" hardware. These parameters included flow areas, injection orifices, manifold volumes, baffle configuration, inlet conditions and surface finish. The basic oxidizer injector cold flow model design was made flexible for ease of changeability of parts and all pieces were machined by conventional methods, e.g., lathe and jig bores, from 6061 Aluminum. The oxidizer injector cold flow model consisted of five basic parts.

A summary of these five basic parts, their function and the quantity of pieces fabricated is listed in Table V. A cross section of the oxidizer injector cold flow model is shown in Figure 14.

TABLE V
OXIDIZER COLD FLOW MODEL PARTS

Part Number	Part Name	Function
8636-473011	End Plate	Affects injector pressure drop and oxidizer angle
8636-473011-1		D_2 = 0.951 in (2.415 cm)
8636-473011-3		D_2 = 1.189 in (3.020 cm)
8636-473011-5		D_2 = 1.427 in (3.625 cm)
8636-473012	Swirl Cup	Affects area of tangential holes
8636-473012-1		A_S = 0.5192 sq in ($3.349\ cm^2$)
8636-473012-3		A_S = 0.4211 sq in ($2.716\ cm^2$)
8636-473013	Cap	Holds replaceable cap
8636-473014	Insert	Controls percent of center flow
8636-473014-1		D_c = 0
8636-473014-3		D_c = 5%
8636-473014-5		D_c = 10%
8636-473015	Baffle	Affects flow symmetry
8636-473016	Body	Ties other parts together
8636-473017	Cover	Oxidizer feed manifold

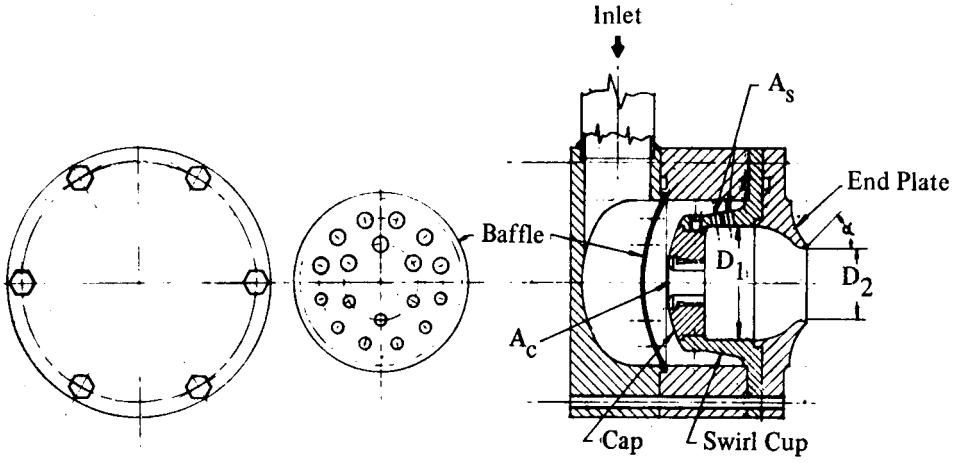

Figure 14. Oxidizer Injector Cold Flow Model

C. HEAT SINK/SEA LEVEL INJECTORS

The initial oxidizer and fuel injectors were fabricated for evaluation with the uncooled chamber/heat sink hardware early in the program. This hardware allowed characterization of the 1500 lb (6672 N) thrust design prior to the final design and fabrication of the cooled chamber configuration. These injectors were fire tested in Task VIII. The oxidizer and fuel injectors fabricated under this task follows:

1. Oxidizer Injector Assembly and Manifold Assembly

The basic oxidizer injector assembly consists of two parts, the injector swirl cup and the injector cap. The basic oxidizer manifold assembly consists of four parts, the manifold inlet tube, the manifold cover, the manifold baffle and the manifold inlet flange.

A summary of these parts and their function and the quantity of pieces fabricated is listed in Table VI. A cross section of the oxidizer injector assembly and manifold assembly is shown in Figure 15 and a photograph of this hardware is included in Figure 16.

The method of fabrication and assembly of these parts follows:

(a) Oxidizer Injector Assembly

(1) Swirl Cup - Machined from 304L SST bar with drilled tangential orifices

(2) Injector Cap - Machined from 304L SST bar with drilled center flow orifice

(3) Injector Assembly - Injector cap inserted in swirl cup and secured with SST spring pins or hardened steel pins. Viton "O" ring provides seal at cap to swirl cup joint. Spring pins were later changed to drill rod to facilitate cup/cap disassembly in the list cell.

TABLE VI
HEAT SINK/SEA LEVEL HARDWARE
INJECTOR ASSEMBLIES AND MANIFOLD ASSEMBLIES

Part Number	Part Name	Material	Qty	Function	Controlling Dimension Description	Significance
8636-473020	Oxidizer Injector Assembly			Provides Oxidizer Injection into Combustion Chamber		
8636-473018-1	Oxidizer Injector Swirl Cup	SST, 304L	1	Generates Gas Vortex	Number and diameter of tangential holes	Affects tangential velocity of gases
-3	Oxidizer Injector Swirl Cup	SST, 304L	1			
-5	Oxidizer Injector Swirl Cup	SST, 304L	1		Oxidizer cup exit diameter	Affects axial component of velocity
8636-473019-1	Oxidizer Injector Cap	SST, 304L	1	Controls percent centerflow	Hole size	Controls percent gas flow distribution in swirl cup
-3	Oxidizer Injector Cap	SST, 304L	1			
-7	Oxidizer Injector Cap	SST, 304L	1			
8636-473021-1	Oxidizer Manifold Assembly		1	Feeds oxidizer to injector		
-3	Oxidizer Manifold Inlet Tube	SST, 304	1	Feeds oxidizer from valve to manifold	Diameter	Affects entering ΔP
8636-473022-1	Oxidizer Manifold Cover	SST, 304L	1			
8636-473023-1	Oxidizer Manifold Baffle	SST, 304L	1	Provides symmetrical distribution of oxidizer flow to injector		
8636-473024-1	Oxidizer Manifold Inlet Flange	SST, 304L	1			
8636-470014-1	Fuel Injector Assembly -015-1 -016-1		1	Provides fuel injection into combustion chamber		
-5	Fuel Injector Assembly -015-5 -016-5		1			
-9	Fuel Injector Assembly -015-9 -016-9		1			
8636-470015-1	Fuel Injector Ring	OFHC Copper			Number of, height and width of injection slots	Control injection velocity
-5	Fuel Injector Ring	OFHC Copper				
-9	Fuel Injector Ring	OFHC Copper				
8636-470016-1	Fuel Injector Jacket	OFHC Copper		Covers slots and provides symmetrical distribution of fuel flow to injector ring		
8636-470030-1	Fuel Injector Assembly		1	Provides fuel injection into combustion chamber and fuel film cooling for nozzle		
8636-470031-1	Fuel Injector Ring	OFHC Copper			Number of, height and width of injection and film-cooling slots	Control fuel injection velocity and percent of fuel used for film cooling
8636-470032-5	Fuel Injector Jacket	OFHC Copper				
8636-470029-1	Fuel Injector/Nozzle	OFHC Copper	1	Combined fuel injector and nozzle	Number of, height and width of injection slots	Control injection velocity
8636-470011-1	Fuel Manifold Assembly		1	Feeds fuel to injector		
8636-470012-1	Fuel Manifold	SST, 304L	1			
8636-470013-1	Fuel Manifold Cover	SST, 304L	1			
8636-470018-1	Fuel Manifold Inlet Fitting	SST, 304L	1	Feeds fuel from valve to manifold	Diameter	Affects entering ΔP

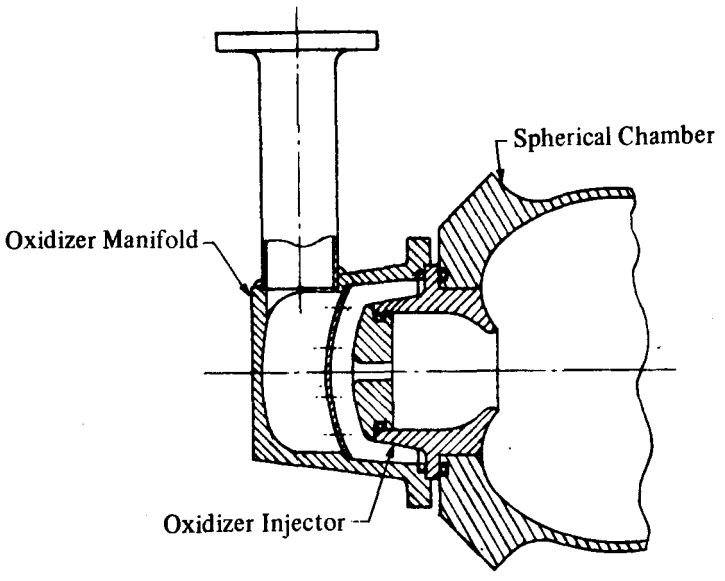

Figure 15. Oxidizer Injector Assembly and Manifold Assembly (Heat Sink/Sea Level Chamber)

(b) Oxidizer (Injector) Manifold Assembly

(1) Manifold Cover - Machined from 304L SST bar

(2) Baffle - Formed from 304L SST sheet with drilled distribution hole pattern

(3) Inlet Tube - Type 304 SST seamless tubing

(4) Inlet Flange (Valve Interface) - Machined from 304L SST bar

(5) Manifold Assembly - Baffle tack welded in manifold cover. Inlet tube TIG welded to cover and inlet flange TIG welded to inlet tube. Final machining including facing off flanges and "O" ring groove, done after all welds had been made.

2. Fuel Injector Assembly and Manifold Assembly

The basic fuel injector assembly consists of two parts, the injector ring and the injector jacket. A second configuration fuel system assembly consists of the injector ring and injector jacket integral with the nozzle. The basic fuel manifold assembly consists of three parts, the manifold, manifold cover and inlet fitting.

A summary of these parts and their function and the quantity of pieces fabricated is listed in Table VI. A cross section of the basic fuel injector assembly and manifold assembly is shown in Figure 17 and a photograph of this hardware is also included in Figure 16. A photograph of the integral injector/nozzle is given in Figure 18.

The method of fabrication and assembly of these parts follow:

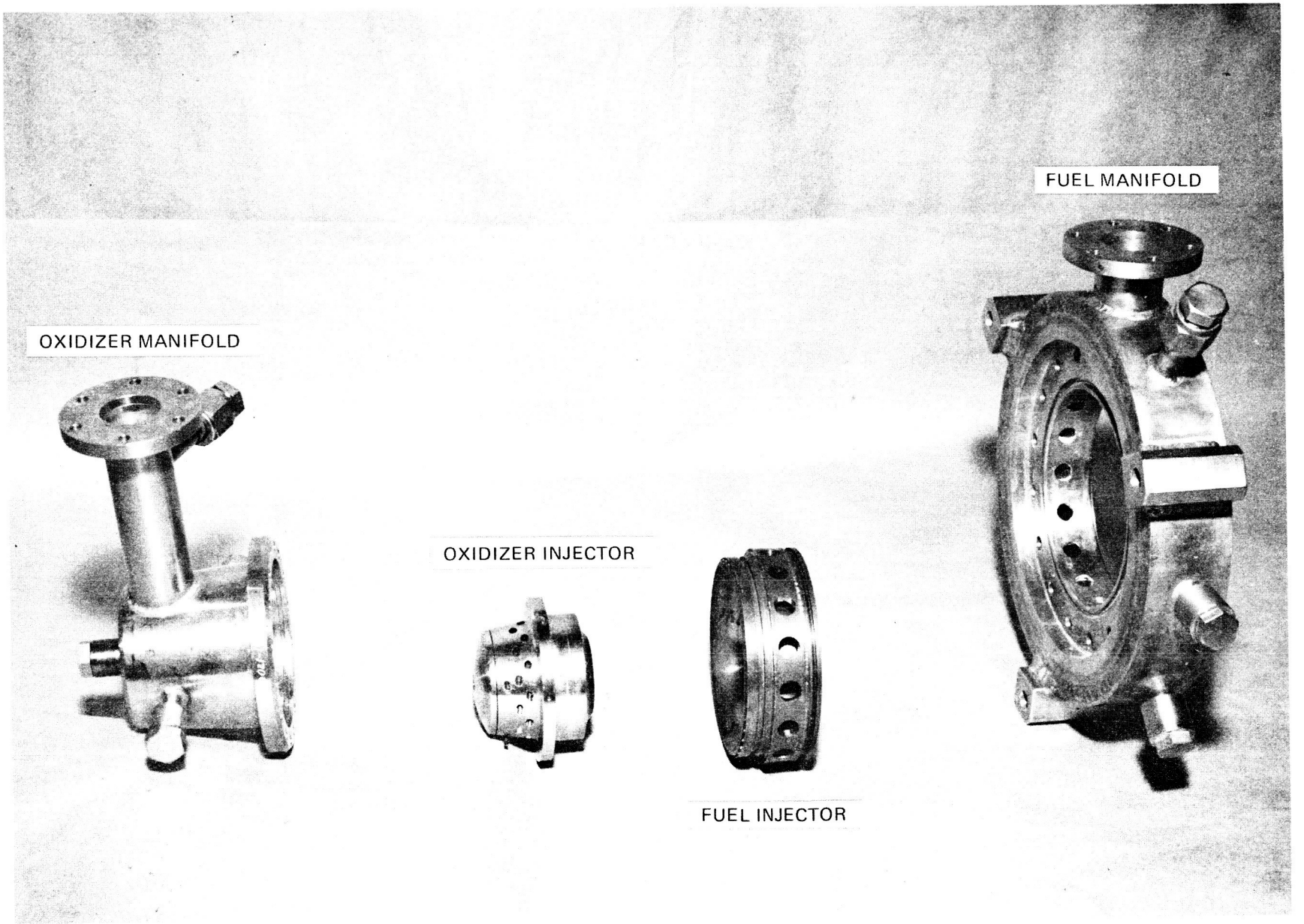

Figure 16. Heat Sink/Sea Level Oxidizer and Fuel Injector Assemblies

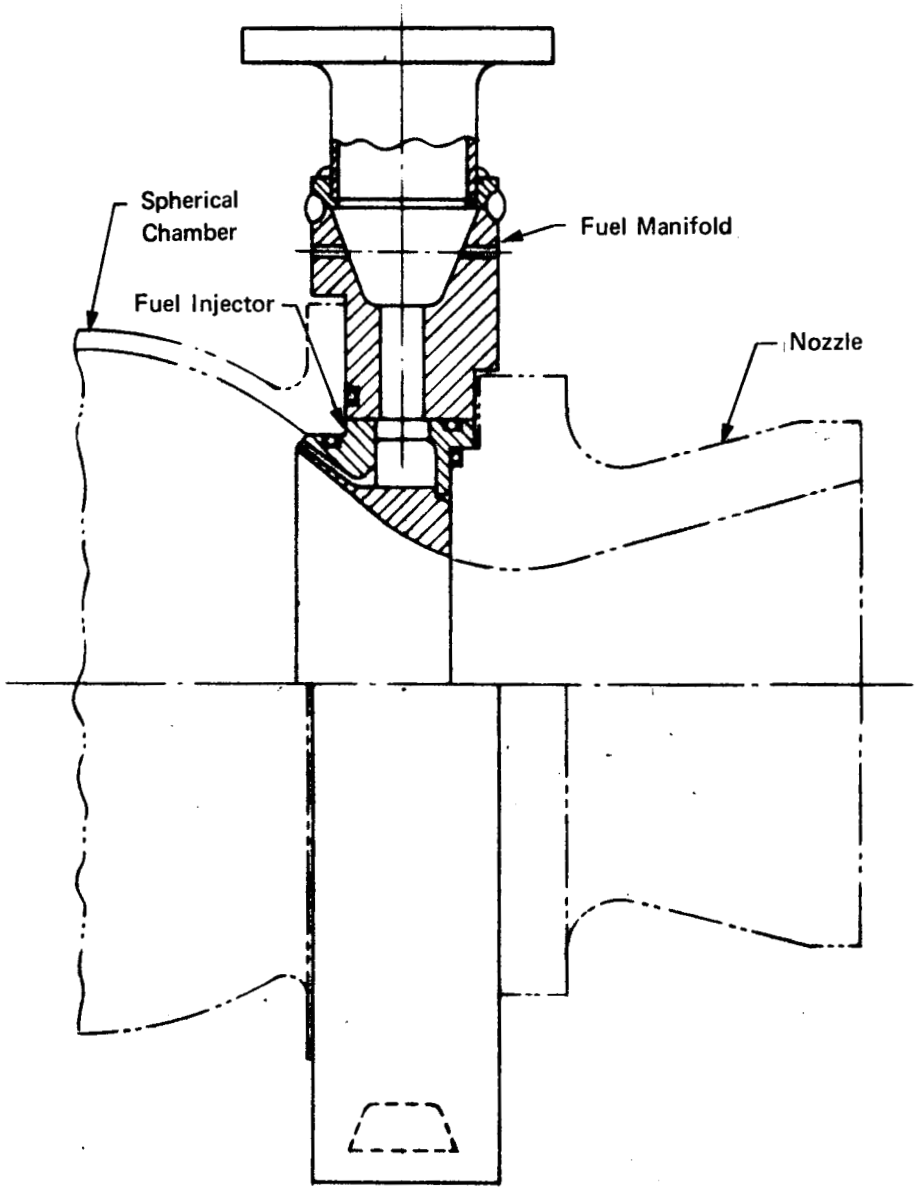

Figure 17. Fuel Injector Assembly and Fuel Manifold Assembly
(Heat Sink/Sea Level Chamber)

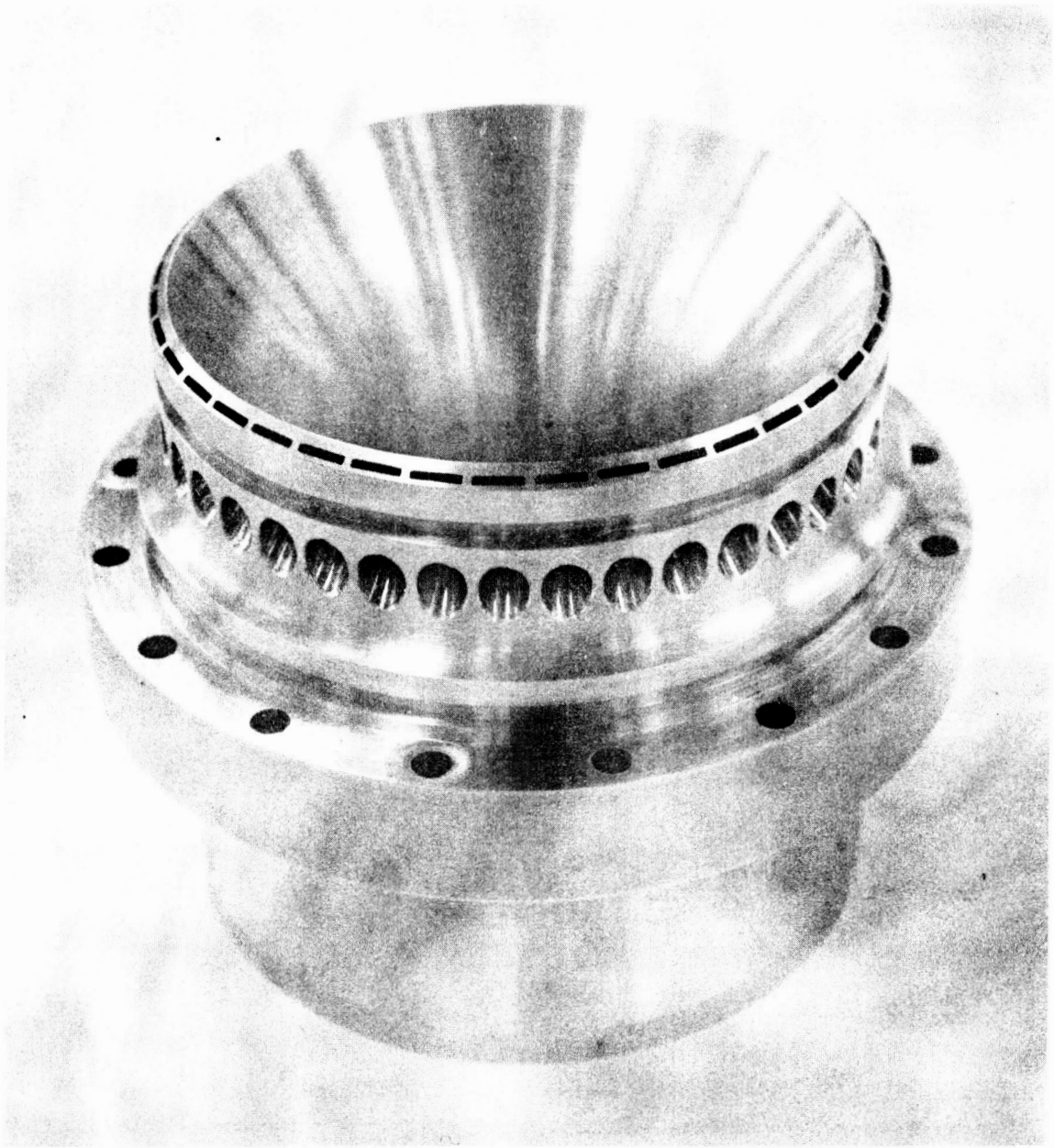

Figure 18. Integral Fuel Injector/Nozzle Configuration

*(a) Fuel Injector Assembly

(1) Injector Ring - Machined from oxygen free copper bar. Injection orifices were EDM'd rectangular slots. (EDM operation at BAC).

(2) Injector Jacket - Machined from oxygen free copper with drilled fuel distribution holes.

(3) Injector Assembly - Injector ring EB welded to jacket. Welded assembly when final machined.

(b) Fuel Manifold Assembly

(1) Manifold - Machined from 304L SST plate

(2) Manifold Cover - Machined from 304L SST plate

(3) Inlet Fitting - Machined from 304L SST bar

(4) Manifold Assembly - Manifold cover TIG welded to the cover. Final machining of assembly done after all welding completed.

D. COOLED INJECTORS

The same oxidizer injector design used for the uncooled/heat sink hardware was used with the cooled/altitude hardware. New fuel injector assembly designs were used for the cooled/altitude hardware that incorporated both the fuel injection orifices (rectangular slots) and the regeneratively cooled nozzle section.

This integral assembly, identified as a liner, contains rectangular channels for the regeneratively cooled passages. This hardware allowed for steady state, long duration testing during Task IX. The oxidizer and fuel injectors fabricated under this task follows:

1. Oxidizer Injector Assembly and Manifold Assembly

The oxidizer injector assemblies and manifold assembly that were used with the uncooled chamber were also used with the cooled/altitude chamber. Additional oxidizer injector assemblies were also fabricated for use with the cooled/altitude hardware. A summary of the additional parts fabricated is listed in Table VII. The method of fabrication is the same as for the heat sink/sea level hardware.

*In a second design the injector ring and the nozzle were machined as an integral part of oxygen free copper bar.

TABLE VII
COOLED/ALTITUDE HARDWARE
INJECTOR ASSEMBLIES AND MANIFOLD ASSEMBLIES

Part Number	Part Name	Material	Qty	Function	Controlling Dimension Description	Significance
8636-470020	Oxidizer Injector Assembly					
8636-473018-1W	Oxidizer Injector Swirl Cup (Welded Cup/Cap Assembly) (Reduced A_S)	SST, 304L	1			
-3A			1			
-7			1	Same as described for the heat sink/ sea level hardware		
-11			1			
-13			1			
-15			1			
8636-473019-1W	Oxidizer Injector Cap (Welded Cup/Cap Assembly)	SST, 304L	1			
-9			1	Same as described for the heat sink/ sea level hardware		
-11			1			
-13			1			
8636-473021-1	Oxidizer Manifold Assembly		1	Same manifold assembly as used for heat sink/sea level hardware		
8636-470044-1	Nozzle Liner	"AMZIRC" (Cu-0.15% Zr)	1	Combines fuel injector with regeneratively cooled nozzle	Number of, height and width of injection slots Height and width of coolant channels	Controls injection velocity Affects wall temperature
8636-470076-1	Nozzle Liner	"AMZIRC" (Cu-0.15% Zr)	1	Combines fuel injector with a regeneratively and film-cooled nozzle	Same as regeneratively cooled nozzle plus height and width of film cooling slots	Controls percent of fuel used for film cooling
8636-470077-1	Nozzle Liner	"AMZIRC" (Cu-0.15% Zr)	2	Combines fuel injector with regeneratively cooled nozzle with dump cooling slots for cooling nozzle extension	Same as regeneratively cooled nozzle plus height and width of dump cooling slots	Controls percent of fuel used for cooling nozzle extension
8636-470092-1	Nozzle Liner	"AMZIRC" (Cu-0.15% Zr)	1	Combines regeneratively cooled and dump cooled nozzle with high injection point fuel injector	Same as 8636-470071	Same as 8636-470077
8636-470045-1	Split Shroud	AL AL, 6061-T6	2	Covers coolant channels and provides symmetrical distribution of fuel to all nozzle liners except high injection point liner		
8636-470095-1	Split Shroud	AL AL, 6061-T6	1	Covers coolant channels and provides symmetrical distribution of fuel to high injection point nozzle liner		
8636-470046-1	Fuel Manifold Assembly		1	Feeds fuel to regeneratively cooled nozzle liners. Used with all nozzle liners except high injection point nozzle		
8636-470051-1	Manifold Blank	SST, 304L				
8636-470058-3	Fuel Manifold Inlet Fitting	SST, 304L		Feeds fuel from valve to fuel manifold	Diameter	Affects entering ΔP
8636-470094-1	Fuel Manifold Assembly		1	Feeds fuel to regeneratively cooled high injection point nozzle liner		
8636-470058-3	Fuel Manifold Inlet Fitting	SST, 304L				
8636-470096-1	Manifold Blank	SST, 304L				

2. Fuel Injector Assembly and Manifold Assembly

The basic fuel injector assembly consists of a one piece liner, incorporating the fuel injection orifices (slots) and rectangular channels for regenerative cooling to an area ratio of 10:1. Three types of liners were fabricated for ambient temperature evaluation; regeneratively cooled,regeneratively cooled with film cooling, and regeneratively cooled with dump cooling. Two additional regeneratively cooled liners with dump cooling were also fabricated for low temperature evaluation; the first with fuel injected at the standard injector station, the second with the higher fuel injection station (closer to the major diameter of the spherical chamber).

The rectangular channels of the liner were "closed out" with a shroud assembly that consisted of two "split" half sections. The shroud assembly also served as a H_2 distribution device and baffle as well as a "filler" to reduce the H_2 manifold volume. Two shroud assemblies were fabricated for use with the standard fuel injection station hardware (both ambient temperature hardware and low temperature hardware). One shroud assembly was fabricated for use with the high fuel injection station hardware (for low temperature).

The basic fuel manifold assembly consists of three parts; the manifold, the inlet fitting, and the mounting lugs.

A summary of these parts and their function and the quantity of pieces fabricated is listed in Table VII. A cross section of the regeneratively cooled fuel injector with dump cooling, the shroud assembly and the manifold assembly is given in Figure 19. A photograph is included in Figure 20.

The method of fabrication and assembly of these parts was as follows:

(a) Nozzle Liner - There were three types of nozzle liners fabricated and tested: regeneratively cooled, regeneratively cooled with film cooling, and regeneratively cooled with dump cooling. All liners were machined from forged "Amzirc" bar (Cu/0.15 Zr.). Cooling channels, injection slots, and film cooling and dump cooling slots were EDM'd. (EDM operation at EDM Exotics).

(b) Shroud Assembly - Machined in halves from 6061-T6 Al Al/Bar, with dowel pins to provide alignment of the halves on assembly. Slots were milled at the interface of the shroud halves to provide for attachment of thermocouple leads to the nozzle liner.

(c) Fuel Manifold Assembly

(1) Manifold - Machined from 304L SST bar.

(2) Inlet Fitting - Machined from 304L SST bar.

(3) Thrust Chamber Mounting Lugs - Machined from 304L SST plate.

(4) Manifold Assembly - Inlet fitting and mounting lugs were TIG welded to the manifold and the weldment was final machined.

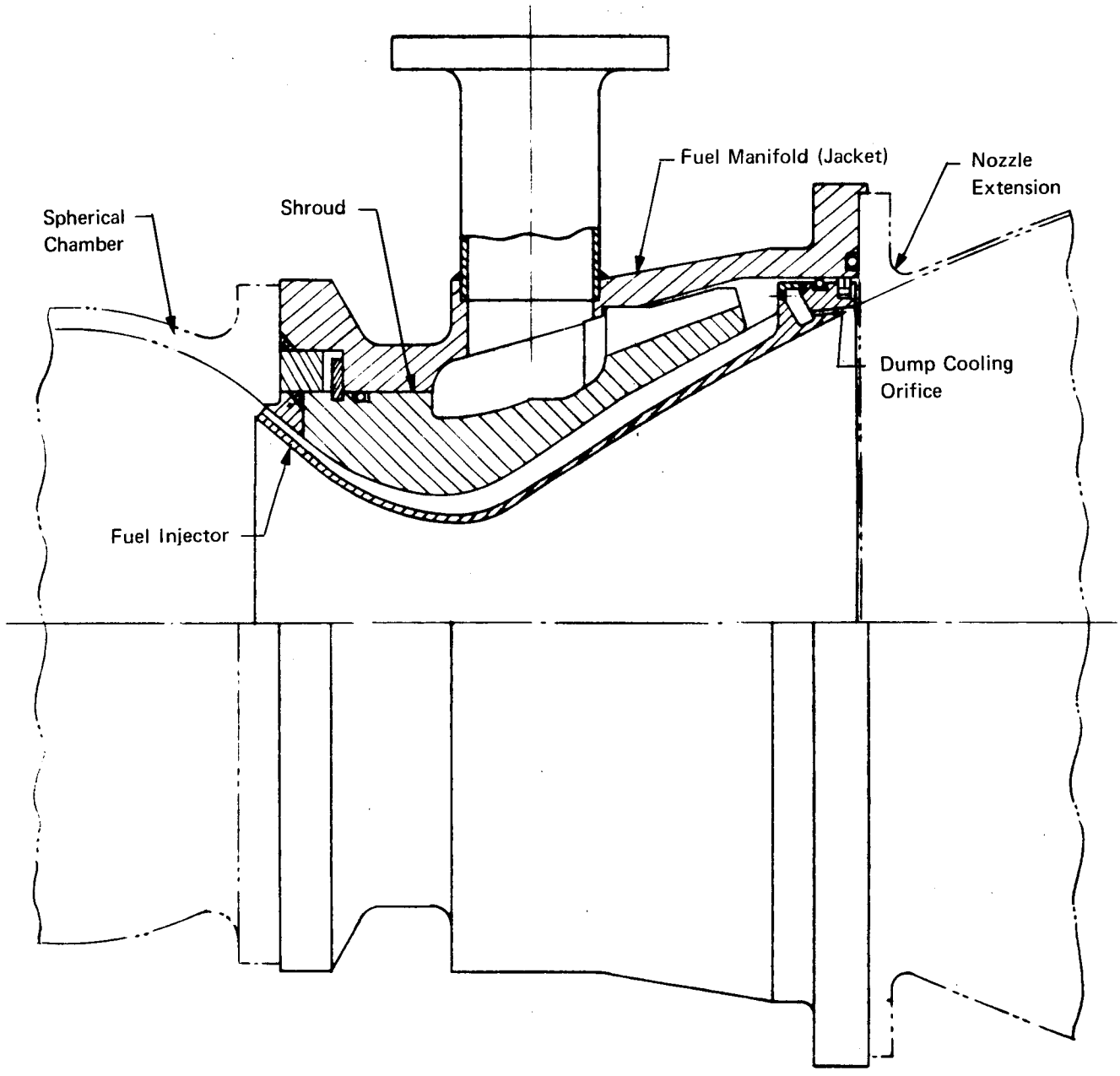

Figure 19. Regeneratively Cooled Fuel Injector, Shroud, and Manifold Assembly (Cooled/Altitude Chamber)

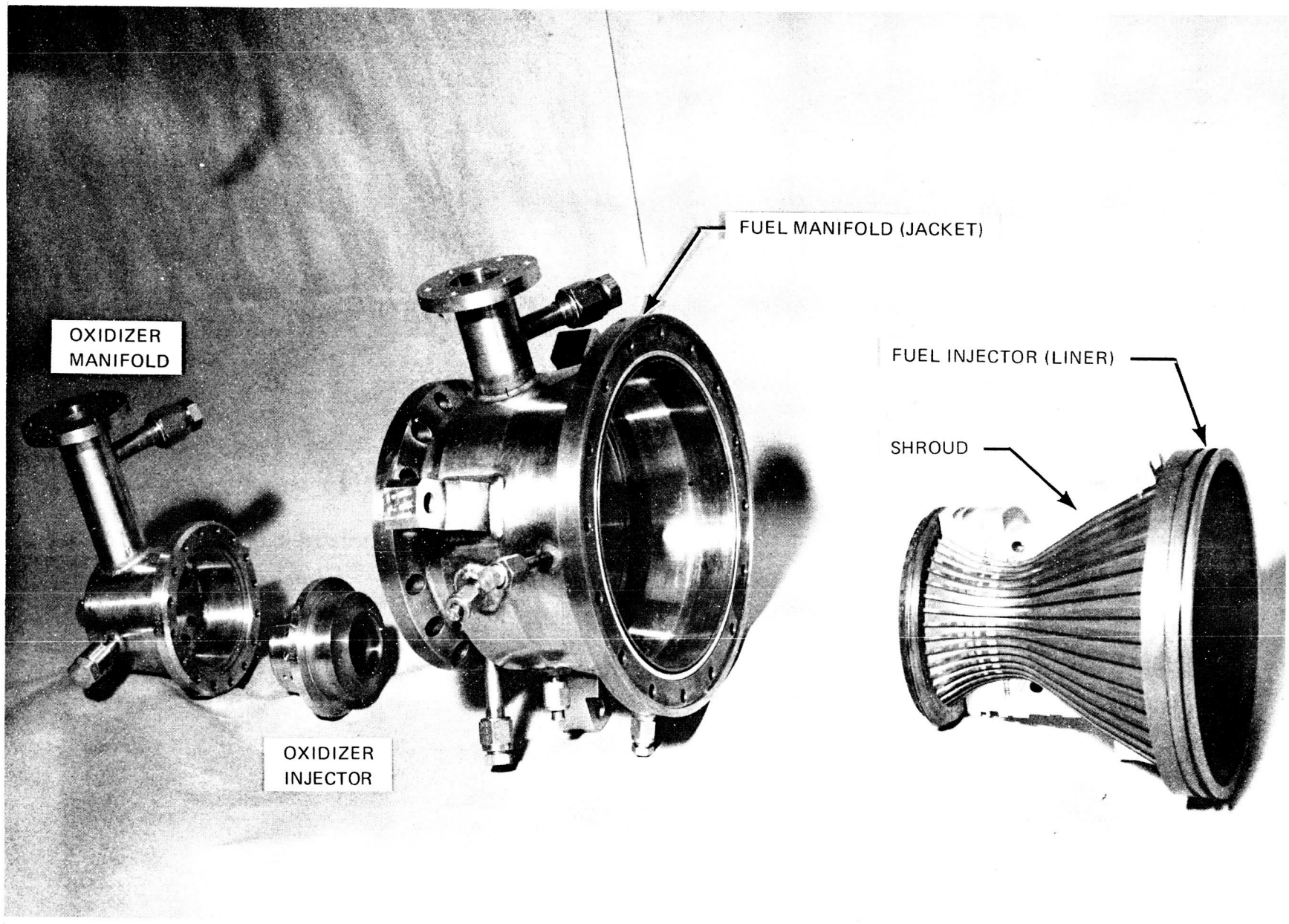

Figure 20. Regeneratively Cooled Fuel Injector, Oxidizer Injector and Manifold Assemblies (Cooled/Altitude Chamber)

VI. THRUST CHAMBER ANALYSIS AND DESIGN

The effort under Task III of the NAS3-14353 Contract required the analysis and design of thrust chamber assemblies for both injector testing at sea level and thrust chamber firings under simulated altitude test conditions. The injector test chamber configuration was defined as heat-sink hardware; the altitude assembly was to include the more exacting task of cooling necessary for firings of up to 500 seconds. The work statement required the examination of alternate cooling methods for the altitude chamber and that consideration be given to additional features such as firing cycle life and steady-state and pulse-mode performance.

This section describes the design of the injector test heat-sink hardware, the major design considerations of the cooled thrust chamber assembly for altitude testing, the analytical techniques employed for cooled thrust chamber preliminary designs, the selection of the configurations for hardware design and finally the detailed analyses associated with the selected cooled hardware designs. The section concludes with the analytical effort of a regenerative cooled nozzle section for sea-level testing and nozzle sections for low propellant feed temperature operation.

A. HEAT SINK THRUST CHAMBER

The contract work statement required that a heat-sink thrust chamber be used for injector tests at sea level. The fuel injection characteristics of the reverse-flow combustion chamber are such that the fuel injector is an integral part of the nozzle section and the spherical combustion chamber is film-cooled by the fuel. The injector test variables described in Section IV defined interchangeable oxidizer cups, fuel injectors, and combustion chambers to vary the critical combustor parameters. Therefore, the basic configuration of the heat-sink test hardware was established as interchangeable, spherical, film-cooled combustion chambers with provisions for bolt-on oxidizer cups and O_2 inlet assemblies, with replaceable fuel injector rings installed between the combustion chamber and a heat-sink nozzle section (Figure 21). The nozzle section expanded the exhaust to sea-level pressure.

A transient heat transfer analysis was made of the heat-sink nozzle section to select materials and define running time. Two candidate materials, copper and nickel, were analyzed at varying thicknesses to investigate the judicious time for length of run under nominal heat rejection conditions. The heating rate for the combustion process was the best estimate for the maximum heat flux area located immediately upstream of the throat. A driving temperature related to a combustion efficiency of 100% was assumed for the study without the benefit of film cooling. The analysis was made with the assumption of the one-dimensional flow of heat without radial heat conduction path growth. The calculated data are summarized in Figure 22.

The wall thickness of copper had a significant effect on the maximum gas-side wall temperature at any given time as shown in Figure 22; however, increasing the Nickel 200 wall thickness above 0.5 inch (1.27 cm) did not aid in reducing the maximum wall temperature at times of interest. Wall temperatures of copper are more dependent on thickness than Nickel 200 primarily because of its higher thermal conductivity. It was concluded that a wall constructed of copper should have walls thicker than 0.6 inch (1.524 cm) to allow a maximum firing test time exceeding 3 seconds without overheating.

The heat sink nozzles, were designed with trepanned posts for thermocouple installations to obtain (Figure 21) heat flux measurements. It was desirable to minimize the distance from the outer top surface of the posts so that a maximum temperature transient could be measured without jeopardizing the gas-side wall by excessively high temperatures. The design dimension of the top of the post from the gas surface was 0.73 inch (1.854 cm). Use of the temperatures measured at the top of the post to calculate the heat flux to the wall is explained in Appendix B.

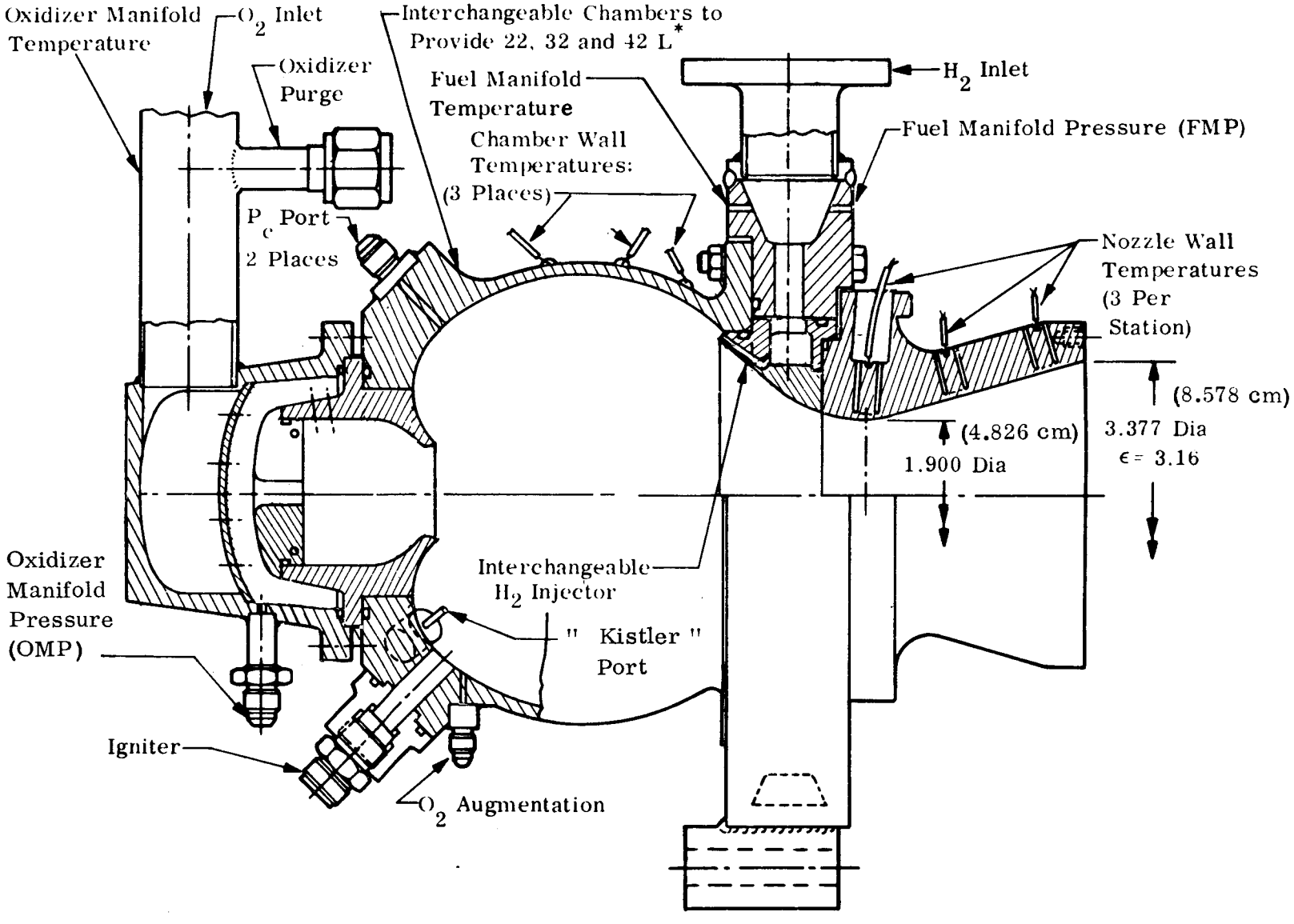

Figure 21. Heat Sink Thrust Chamber Assembly

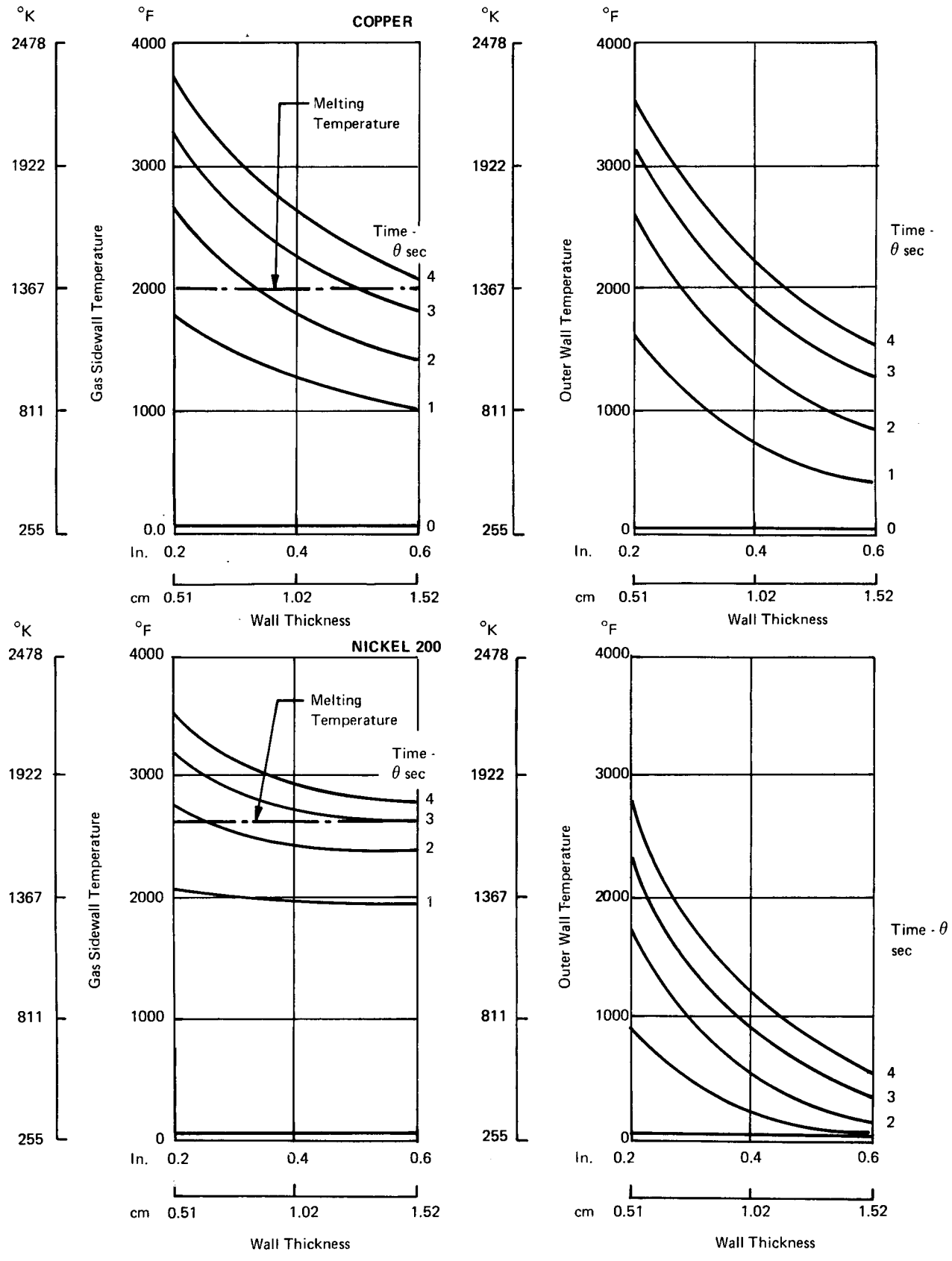

Figure 22. Wall Temperature Variation with Material Wall Thickness and Time

B. COOLED THRUST CHAMBER CONFIGURATION STUDIES

1. Major Design Considerations

The thrust chamber design task included tradeoff studies of the potential cooled thrust chamber configurations and initiation of detailed performance, thermal and structural analyses of the favored configurations. The work culminated in the recommended cooled chamber configurations for test firings at simulated altitude. This subsection will describe that effort through the configurations selection. Subsequent subsections will describe the detailed design of the selected test hardware.

Several thrust chamber configurations were considered, consisting of several cooling methods applicable to the reverse flow engine. The various configurations, shown in Table VIII, employ three basic cooling schemes:

Regenerative Cooling
Film Cooling
Dump Cooling (internal and external)

Because of the unique configuration of the reverse flow engine, the combustion chamber forms an integral part of the propellant injection system. Furthermore, as the fuel injection method affords excellent thermal protection of the spherical combustion chamber structure, the question of alternate thrust chamber cooling configurations applies only to the convergent and divergent nozzle sections. Thus, the "thrust chamber" terminology, used herein in reference to cooling, refers only to the convergent/divergent nozzle.

During the tradeoff evaluation of the various candidate designs the major parameters considered were:

(a) Performance
(b) Pressure Schedule
(c) Start and Shutdown Response
(d) Wall Temperature
(e) Material and Structural Cycle Life
(f) Fabrication Techniques
(g) Vehicle Interface/Installation
(h) Weight

A discussion of each of these considerations follows to complete their definition and importance relative to the NAS 3-14353 requirements.

a. Performance

For the initial performance assessment of the chamber configurations, a Rao optimance with 540°R (300°K) propellants was found to be 474.4 sec (4652N sec/kg) which, with the usual nozzle losses, results in a predicted delivered performance of 440.8 sec (4322N sec/kg) at 97% c* efficiency. That maximum performance level was based on an all-regeneratively cooled chamber with no supplemental film cooling. A performance penalty is incurred if film cooling of

TABLE VIII
REVERSE FLOW CHAMBER CONFIGURATIONS

Case	Type of Cooling		Performance Potential	Fuel Pressure Drop	Wall Temperature		Cycle Life Nozzle Section	Vehicle Installation Flexibility
					Nozzle Section	Nozzle Extension		
A.	• Fully Regenerative with • Optional Film Cooling	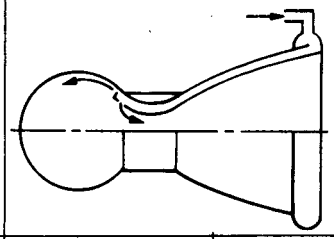	No Film Cooling High with Film Cooling Acceptable	Excessively High Low	Acceptable Low	Acceptable Acceptable	Acceptable High	Poor Poor
B.	• Partial Regenerative with • Internal Dump-Cooled Nozzle Extension	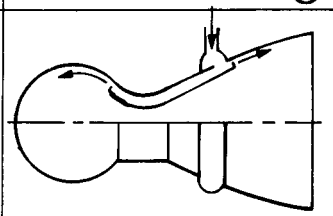	Acceptable	Acceptable	Acceptable	Acceptable	Acceptable	Acceptable
C.	• Partial Regenerative with • Supplemental Film-Cooled Throat and • Internal Dump-Cooled Nozzle Extension	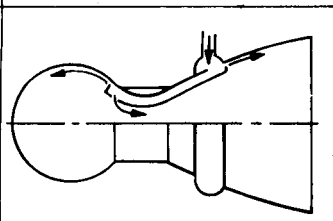	Acceptable	Low	Low	Acceptable	High	Acceptable
D.	• Partial Regenerative with • All Film-Cooled Throat and Nozzle Extension	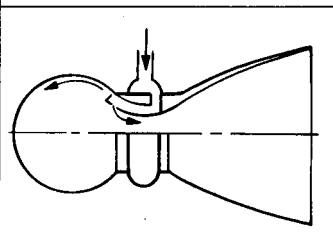	Unacceptable Marginal	Lowest	Low	Acceptable	High	Acceptable
E.	• Partial Regenerative with • External Dump-Cooled Nozzle Extension	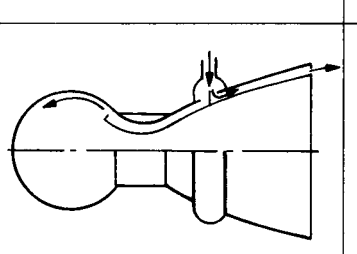	Acceptable	Acceptable	Acceptable	Acceptable	Acceptable	Acceptable
F.	• Partial Regenerative with • Supplemental Film-Cooled Throat and External Dump-Cooled Nozzle Extension	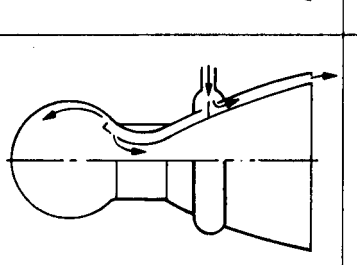	Acceptable	Low	Low	Acceptable	High	Acceptable

the throat is used to reduce local heat flux and/or reduce jacket pressure drop (Case A of Table VIII). The performance degradation is minimal because the film coolant need only afford protection of the throat region. Thus, optimization by appropriate selection of film injection station, coolant velocity and weight flow would provide nearly complete dissipation of coolant within the divergent nozzle with compatible wall temperatures to minimize flow and mixture ratio stratification across the nozzle exit.

The nozzle extension cooling options included partial regenerative cooling with what will be defined as internal dump cooling, Case B, Table VIII, and external dump cooling, Case E. The internal dump-cooled configuration would provide somewhat better performance than the external dump cooled approach since the external dump coolant specific impulse contribution is limited to a Mach 1 exit velocity. The internal dump-cooled divergent nozzle allows the coolant flow to expand to a higher Mach number with some mixing of the main stream gases, which improves the core off mixture ratio operation. Supplemental film cooling injected within the convergent nozzle would exhibit a small effect on performance, if used in conjunction with either dump cooling method and partial regenerative cooling of the throatm Cases C and F. Thus, considerable latitude was allowed with the partial regenerative/internal dump-cooled divergent nozzle cooling configurations. Coolant flow rate, injection velocity and injection station could be adjusted to obtain the desired nozzle wall temperature with small performance penalty.

Film cooling of the entire divergent nozzle, Case D of Table VIII, would have a greater effect on reducing performance since a greater amount of film coolant flow would be required to provide nozzle wall temperatures compatible with structural considerations.

Figure 23 summarizes the performance levels calculated for the basic thrust chamber cooling configurations. The figure shows that the chambers would exceed the design I_{sp} goal if the total film and/or dump cooling were limited to 6% of the total hydrogen flow. The difference in maximum performance is somewhat misleading as other considerations such as wall temperature (structural capability) and pressure schedule significantly change the amount of coolant required. The calculations suggested that one of the chamber cooling approaches,the all film cooled nozzle extension, would not meet the I_{sp} goal within the restraint of 97% C* because of the high probability of requiring substantially more than 6% film cooling.

b. Pressure Schedule

The candidate regenerative cooling nozzle sections included drilled copper and channel nickel configurations based on earlier work with reverse flow engines. Preliminary designs were established for each candidate to compare their fuel pressure drops at the contract design requirements (Figure 24). The comparison was made on the basis of a common injector Mach number of the hydrogen coolant of 0.50. The drilled copper configuration required a significantly higher coolant passage plus injection ΔP, 165 (113.8) versus 71 psia (48.9 N/cm^2). The pressure drop calculations included 56 psi (38.6 N/cm^2) for the H_2 fuel injection plus the pressure losses due to momentum and friction within the cooling passages plus the dynamic head losses due to sudden pressure changes.

The concept of the drilled throat section as shown in Figure 24 was improved by rounding entrances into the injection orifices and tapering the exits of the drilled coolant holes to increase the diffuser efficiency. The changes reduced the calculated pressure drop 28 psi to a 137 psia (19.3 to 94.5 N/cm^2) total. The modifications were insufficient to make the drilled copper pressure drop competitive with the channel nickel configuration.

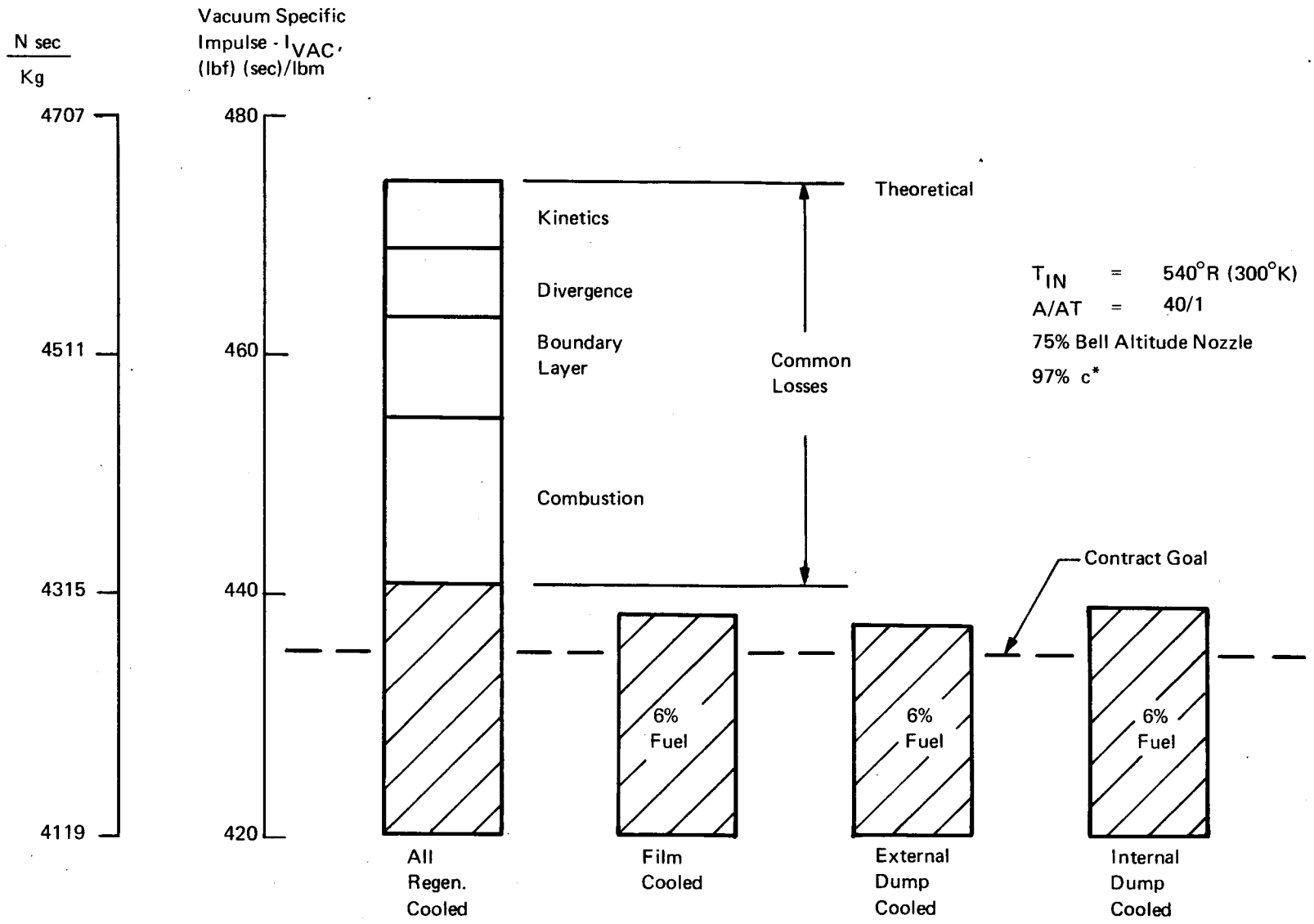

Figure 23. Performance Apportionment Cooled Designs

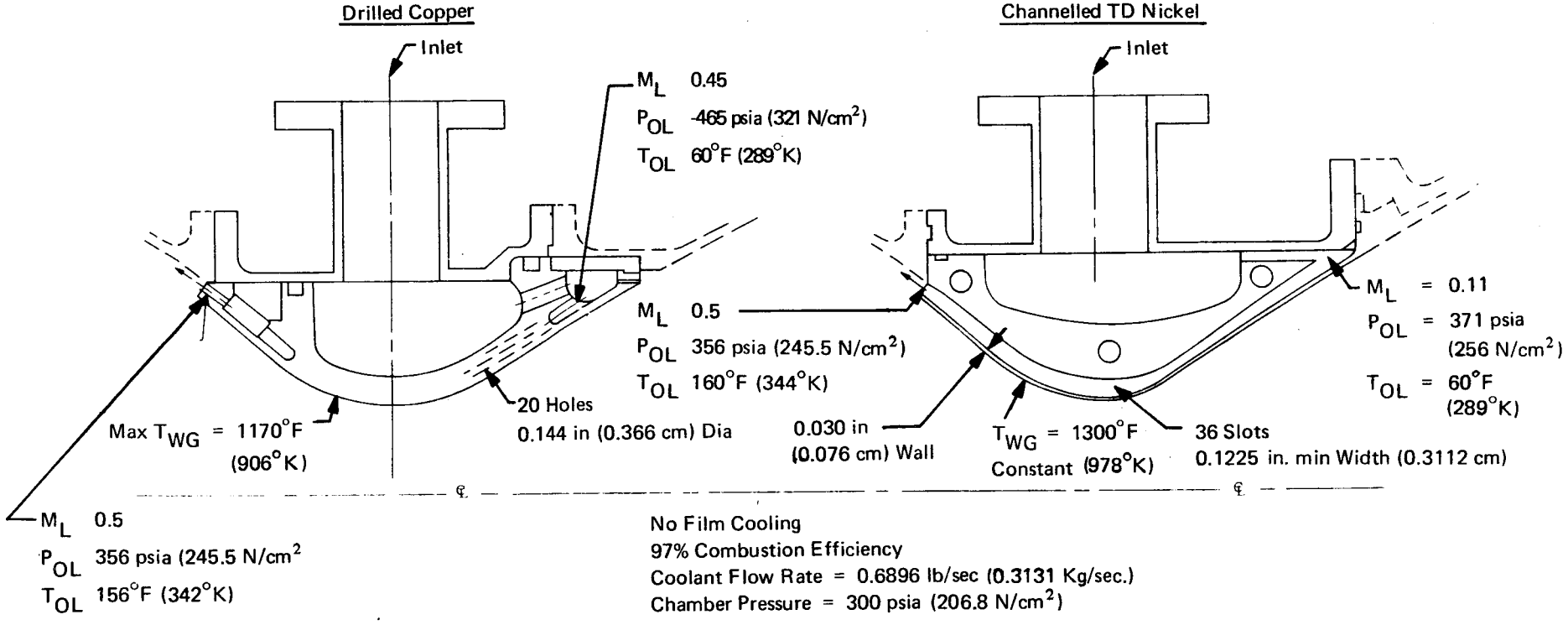

Figure 24. Drilled and Channeled Nozzle Configurations

A thermal analysis of the candidate drilled and channel designs indicated no significant advantages for either the drilled or channel designs relative to operating temperature. The comparison was made on the basis of equal driving gas temperatures and the gas side maximum temperatures included in Figure 24.

The pressure schedule requirements were then estimated for the various thrust chamber cooling configurations based on channel regenerative cooling passages. The fuel injector was sized to determine its nominal pressure drop based on injection at Mach 0.5 with the injection station at a convergent nozzle contraction ratio of 4. The nominal fuel-injector pressure drop was recalculated as 61 psi (42.1 N/cm^2) thus allowing 14 psi (9.66 N/cm^2) for the cooling passages.

The pressure schedule for the cooling configurations under consideration was highly important, since all but one of the designs employed some regenerative cooling. Since the pressure drop associated with regenerative cooling is directly related to the cooling passage geometry, nozzle construction techniques and wall material, an extensive examination of point designs was required. Structural integrity and lifetime were also dependent on these parameters. As a consequence, parametric analyses were conducted to evaluate various materials and thrust chamber fabrication techniques. In order to provide a baseline for a qualitative evaluation, it was necessary to preselect some reasonable maximum wall temperatures that would satisfy the high-cyclic-lifetime requirements using available fabrication techniques and materials. Typical cases were examined to determine the pressure drop attributed to all regenerative cooling, partial regenerative cooling and partial regenerative cooling with supplemental film. Pressure drop values for two configurations (which include fuel injector pressure drop) are presented in Table IX.

TABLE IX
THRUST CHAMBER-FUEL PRESSURE DROP

Cooling Scheme with Wall Temperature °F/°K	T.D. Nickel						Amzirc					
	1100°F	867°K	1300°K	978°K	1500°K	1089°K	600°K	589°K	700°F	644°K	800°F	700°K
	Pressure Drop						Pressure Drop					
	psi	N/m^2	psi	N/m^2	psi	N/m^2	psi	N/m^2	psi	N/m^2	psi	N/m^2
No Regenerative Cooling (Injector Only)	61	4.2×10^5	61	4.2×10^5	61	4.2×10^5	61	4.2×10^5	61	4.2×10^5	61	4.2×10^5
Partial Regenerative, $\epsilon = 10$	104	7.2×10^5	87	6.6×10^5	81	5.6×10^5	138	9.5×10^5	110	7.6×10^5	99	6.8×10^5
Partial Regenerative, + 10% Film	78	5.4×10^5	77	5.3×10^5	76	5.2×10^5	79	5.4×10^5	77	5.3×10^5	76	5.2×10^5
Full Regenerative, $\epsilon = 40$	112	7.7×10^5	89	6.1×10^5	82	5.6×10^5	190	1.3×10^6	130	9.0×10^5	105	7.2×10^5
Full Regenerative, $\epsilon = 40$ + 10% Film	79	5.4×10^5	78	5.4×10^5	77	5.3×10^5	81	5.6×10^5	78	5.4×10^5	77	5.3×10^5

Table IX indicates that the greatest portion of the regenerative section pressure drop occurs within a 10:1-area ratio thus resulting in negligible tradeoff as to ΔP versus inlet-area-ratio station. A much greater reduction in total drop was predicted with supplemental film cooling, which would reduce the throat heat flux and wall temperature, than with decreasing the length of the regenerative cooling circuit. From a pressure drop and performance viewpoint an all-regeneratively cooled thrust chamber with supplemental film cooling was indicated to be satisfactory if the wall temperature and fabrication techniques were compatible with cyclic life time. The findings are reflected in the "low" ΔP ratings of the film cooled configurations of Table VIII.

c. Start and Shutdown Response

The response characteristics of the APS engine were bound to be relatively insensitive to manifold volumes. The response of a fully regenerative nozzle (Volume 149 in.^{3} (2440 cm^3)) as compared to a partially regenerative configuration (Volume 70 in.^{3} (1145 cm^3)) is shown in Figure 25. The calculated response for large or small coolant volume is similar if the pressure drop of the units are similar.

d. Wall Temperature

For the preliminary evaluation of thrust chamber cooling configurations, wall temperature ranges were preselected based on material and structural capability and coolant flow rates adjusted to provide a valid performance assessment. The wall temperature was also considered in light of the effect of thermal expansion and gradients on both mechanical and welded-joint designs and nozzle fabrication techniques.

e. Material and Structural-Cycle-Life

The contract defined operational life of 50 hours of accumulated firing time made up of 1 x 10^6 firings and individual firings of up to 1000 seconds duration clearly indicated that life requirements were a governing factor in material selection. The complete material and firing life capability requirements are given in Table X. Specifically, creep and fatigue capability as well as thermal properties were primary design parameters for establishing material choices in the thrust chamber. Since the governing factor in material selection was based on stress considerations, a parametric study of representative materials was conducted. The material screening involved nickel, TD nickel, copper and copper alloys, aluminum, stainless steels, nickel-base and cobalt-base high temperature steels and refractory alloys.

TABLE X

MATERIAL SELECTION REQUIREMENTS

1. Environment	
(a) Compatibility	Compatible with propellants GH_2 and GO_2, test fluids and cleaning fluids for 10-year life
(b) Temperature	200°R to 800°R (111°K to 444°K)
2. Life Capability	
(a) Operational Life	50 hrs, with maintenance -based on 30-minutes life required/mission for 100 missions during a 10-year period.
(b) Pulse Life	1,000,000 pulses, with maintenance–based on 10,000 pulses per mission for 100 missions during a 10-year period.
(c) Max Single Firing	1000 seconds
(d) Duty Cycle Limit	None

Material selection included the cooled-nozzle-section liner geometry. Selection of either the integral channel wall or free-standing liner configuration revealed that to achieve the high cyclic life requirements a material of high conductivity and good fatigue strength was mandatory. The high conductivity assured a small thermal gradient through the inner wall and small thermal

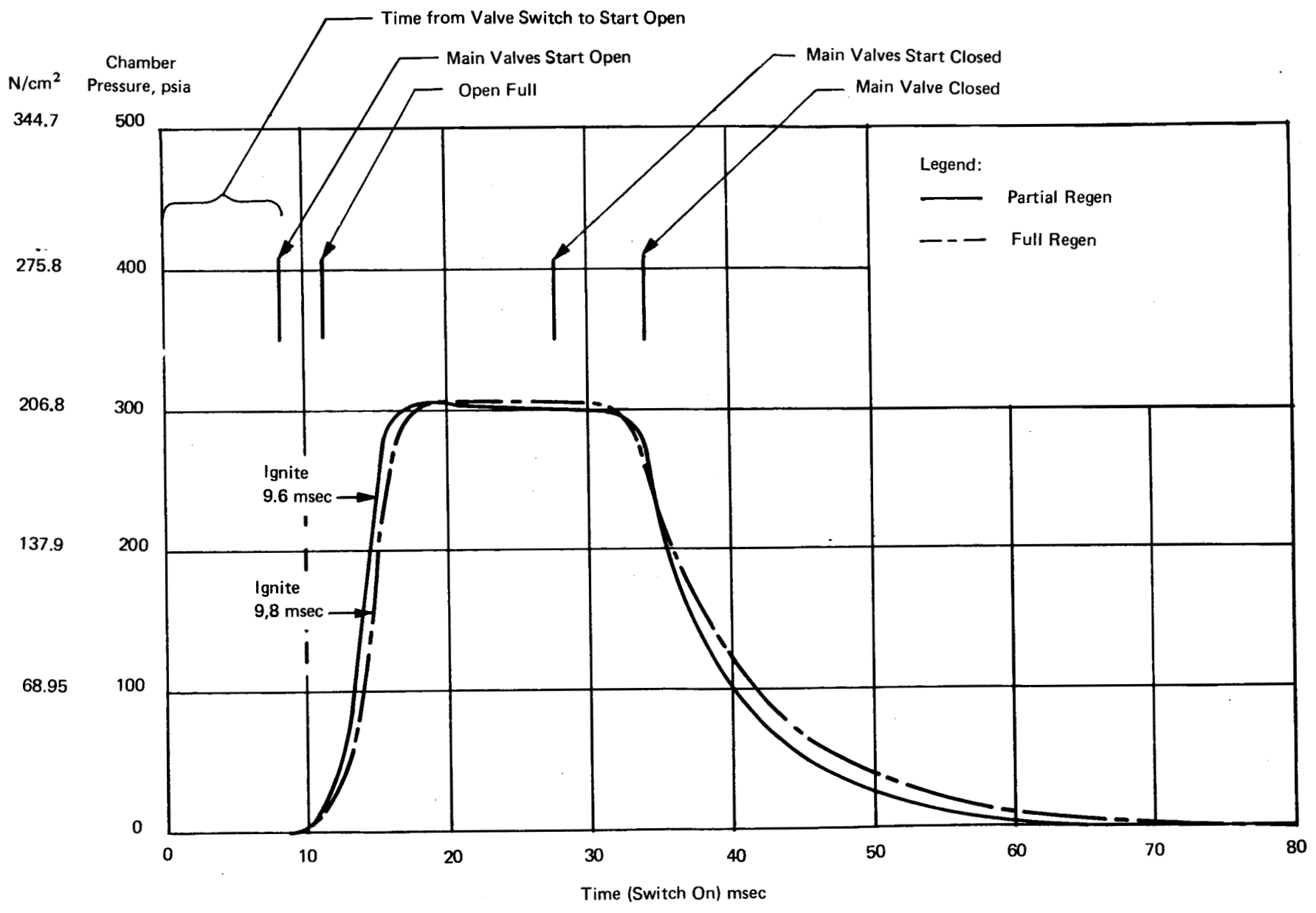

Figure 25. Transient Analysis - Partial and Fully-Regeneratively Cooled Chambers

strains (which were found to be the dominant strains) which increased fatigue life. The prime candidate materials resulting from the preliminary evaluation were OFHC copper, copper alloys, TD nickel and nickel 200 for the hot liner wall. For an integral wall configuration electroformed nickel or electroformed copper could be considered for the closeout of the liner regenerative cooling passages.

Candidate materials for the nozzle extension were stainless steel, high strength super-alloys and columbium alloys. With maximum wall temperatures up to 1900°F (1311°K), the 300 series stainless steels would be a proper choice since no oxidation coatings would be required. However, for temperatures above 2100 or 2200°F (1422 or 1478°K) use of columbium alloys would be required to avoid excessive creep. The columbium alloys would require an oxidation-protection coating which has an unknown effect on physical and mechanical properties for long-term exposure under cyclic stressing. From a purely oxidation-exposure environment, for 50-hours exposure at temperature, the temperature limit of columbium is set at 2500-2700°F (1644-1751°K). The high strength non-refractory alloys could be considered for the temperature range between stainless steel and columbium. Since stress levels would be low, regardless of material selection, nozzle-extension wall thicknesses would be established by fabrication limitations rather than by structural considerations.

One additional consideration employed in the final material selection was the hydrogen-embrittlement effect on fatigue life. A lack of positive information existed for some of the materials considered concerning the operating environment including temperatures and pressures. OFHC copper, most copper alloys and stabilized 300 series stainless had been reported to be unaffected by hydrogen, while the embrittlement of nickel, nickel alloys and TD nickel presented a potential problem.

The following tentative material selections were made for the reverse flow thrust chamber prior to completion of the preliminary structural cycle life analysis:

Integral-Channel Wall-Construction	
Main Chamber	300 Series Stainless Steel
Nozzle Section Integral-Channel Wall	
(a) Hot Wall	TD Nickel or Copper Alloy
(b) Closure Shell	Electrodeposited Nickel or Copper
Nozzle Extension	Stainless Steel or Columbium Alloys such as Cb-291, C-103, C-129.
Free-Standing Liner-Construction	
Main Chamber	300 Series Stainless Steel
Nozzle Section - Free Standing Liner	
(a) Hot Wall	TD Nickel or Copper Alloy
(b) Jacket	Aluminum or Stainless Steel
Nozzle Extension	Stainless Steel or Columbium Alloys such as Cb-291, C-103, C-129.

The nozzle section of the reverse flow design, which is regeneratively cooled, is the area of maximum heat flux and the most critical portion for cycle-life capability. Preliminary structural analyses of the nozzle section revealed that a free-standing Amzirc (zirconium copper alloy) inner liner would meet all the cycle-life requirements without the use of film cooling. An integral-wall construction for the nozzle section would not meet the cycle life without the use of film cooling. Detailed information on these analyses is included later in this section.

f. Fabrication Techniques

The contract defined the test hardware fabrications techniques as state of the art to minimize fabrication cost and risks.

g. Vehicle Interface/Installation

There were two considerations relative to the vehicle/engine interface. The problem of engine-wall temperature effect on vehicle structure could be readily resolved by either thermal shielding or insulation, with little impact upon engine configuration. However, the question of packaging (volume, length, cross section, etc.) could exhibit an overriding influence upon design selection. This pertains primarily to regenerative type designs wherein the regenerative nozzle inlet has to be held within the minimum-package vehicle limitation. The location of the coolant inlet manifold, and the maximum nozzle expansion ratio that can be regeneratively cooled, would be limited by packaging requirements. Therefore, the fully regeneratively cooled engine configuration was rated poor for vehicle installation flexibility in Table VIII.

h. Weight Considerations

The lowest thrust chamber weight was associated with the minimum of regeneratively cooled structure. Weight considerations favored the dump cooled nozzle extension configurations and the film cooled throat and extension approach, Cases B, D and F of Table VIII.

2. Principle Analytical Techniques

a. Performance Prediction

(1) General

The goal of the program was a delivered minimum vacuum specific impulse of 435 lbf sec/lbm (4260 N sec/kg), at an overall O/F mixture ratio of 4.0, a combustion chamber pressure of 300 psia (206.8 N/cm^2), propellant inlet temperatures of 540°R (300°K), and a nozzle expansion ratio of 40/1. The base performance was taken as that for the regeneratively cooled thrust chamber (Table XI) and decrements assigned to the others with non-uniform exhaust associated with film or dump cooling.

Thrust chamber performance of gaseous O_2/H_2 was compared to ideal one dimensional, isentropic shifting equilibrium. This reference represents the upper limit of theoretical performance as a consequence of losses inherent in the design. The losses considered in estimating deliverable performance were due to:

Combustion kinetics
Non-axial flow or nozzle divergence
Viscous boundary layer effects

Combustion efficiency
Mass addition effects, (film and dump cooling) where applicable.

The following paragraphs present the methods, basis of assumptions and data used to estimate the performance of the 40/1 altitude nozzle in addition to two conical nozzles used in sea level tests.

TABLE XI

PREDICTED VACUUM SPECIFIC IMPULSE
ALTITUDE THRUSTER

Thruster Configuration	Regenerative
Nozzle Area Ratio	40/1
Nozzle Length	75% Bell
Propellant Inlet Temp, °R	540 (300°K)
Overall Mixture Ratio (°/F)	4/1
Theoretical Vacuum Spec. Impulse	474.4 sec (4650 N sec/kg)
Losses, ΔI_{sp}	
Divergence	5.6 (54.8 N sec/kg)
Drag	8.0 (78.3 N sec/kg)
Boundary Layer Displacement	0.4 (3.9 N sec/kg)
Kinetics	5.7 (55.8 N sec/kg)
Energy Release (97% c*)	13.9 (136.2 N sec/kg)
Total	33.6 (329 N sec/kg)
Predicted Vacuum Specific Impulse	440.8 (4321 N sec/kg)

The delivered vacuum performance was calculated by the ICRPG simplified method where the losses are assumed independent of each other. In essence, the predicted performance ($I_{\infty, pred.}$) is calculated by multiplication of efficiencies due to losses times the theoretical ($I_{\infty, theo. S.E.}$). In addition to the ICRPG losses the detrimental effect of energy release on kinetic performance ($\eta_{CF(c^*)}$) was also included. Thus:

$$I_{\infty, pred.} = (\eta_{3D})\ (\eta_D)\ (\eta_{BL})\ (\eta_{Kin})\ (\eta_{CF(c^*)})\ (\eta_{ER})\ I_{\infty, theo., S.E.}$$

where

η_{3D} = 1 - divergence loss
η_D = 1 - drag loss
η_{BL} = 1 - boundary layer displacement loss
η_{Kin} = 1 - chemical expansion kinetics loss
$\eta_{CF(c^*)}$ = 1 - losses due to combustion kinetics
η_{ER} = combustion efficiency

(2) Divergence Loss

The supersonic nozzle like most rocket engine components is a compromise of various design tradeoffs. Increased nozzle length (and increased nozzle weight) results in a higher performance engine. The final configuration for the altitude nozzle was selected to provide high performance with a relatively short overall length, a 75% Bell length with a circular arc one-half of the throat diameter. The completely optimized flight configuration of the nozzle would require a detailed tradeoff of envelope, nozzle weight and engine specific impulse versus vehicle structure weight and the weight of the loaded propellant feed system. Performance variations as a function of supersonic nozzle geometry produce divergence losses depending partially on initial nozzle configuration ground rules. Tradeoffs in performance with geometry are described further in the section under detailed design of the nozzle extension contour.

Shifting equilibrium combustion gas, using the ICRPG ODE computer program, was used for the nozzle design.

The conical sea level nozzles were assigned a divergence loss of 1.73% for 15° semidivergent nozzles calculated by Malina in Reference 9.

(3) Boundary Layer

Viscous drag and boundary layer displacement were calculated using the ICRPG TBL computer program assuming 750°F (672°K) walls and a three-dimensional Mach number distribution on the 75% bell length altitude nozzle. The losses varied somewhat with mixture ratio as follows:

Mixture Ratio	Drag Thrust (lbf)	(N)	Area Ratio Corrected For Displacement Thickness
2	26.85	(119.43)	39.075
3	27.35	(121.66)	39.055
4	27.18	(120.90)	39.129
5	25.19	(112.05)	39.284

Of the total nozzle drag at the nominal mixture ratio, 9.7% is upstream of the throat. A one-dimensional Mach number distribution within the nozzle was used for calculations of the conical sea level nozzles.

Transport properties of the gas mixtures are presented in Appendix B of this report.

(4) Combustion Kinetics

A significant source of performance loss in the rocket nozzle arises from the fact that chemical reactions take a finite amount of time to be completed and therefore the products of combustion never reach equilibrium. Since most of the chemical reactions in the nozzle are recombination reactions which release energy, the failure to reach equilibrium results in less energy being released and hence less energy is converted to kinetic energy of the exhaust products. Therefore, the kinetically controlled performance is lower than the equilibrium performance, and the difference is considered a loss. Most of the loss occurs in the nozzle, although a small loss in c* is observed in chamber calculations due to non-equilibrium conditions occurring at the throat.

The one dimensional inviscid kinetic performance was computed at Bell Aerospace using the ICRPG ODK computer program originally developed by TRW Systems, and later modified for JANNAF by Dynamic Science Corporation. This program has been adopted by the JANNAF Performance Standardization Working Group for their standardized performance evaluation procedures. The kinetic reaction rate constants are input in the form $K = AT^{-XN} e^{-B/RT}$ where the terms A, XN and B are rate parameters determined experimentally for each reaction.

The following reactions and rate parameters were used in the analysis for the oxygen/hydrogen system, where M represents any third body. The rate parameters are equal to those adopted by JANNAF and listed in CPIA Publication 178, Reference 10.

Reaction	A	B	XN
$H_2O + M \rightleftarrows OH + H + M$	1.0×10^{19}	0	1.0
$H_2 + M \rightleftarrows H + H + M$	7.5×10^{18}	0	1.0
$OH + M \rightleftarrows O + H + M$	2.0×10^{18}	0	1.0
$O_2 + M \rightleftarrows O + O + M$	1.9×10^{16}	0	0.5
$H_2O + H \rightleftarrows H_2 + OH$	6.0×10^{11}	5.0	-0.5
$H_2O + O \rightleftarrows OH + OH$	1.0666×10^{13}	0.96671	0.0134
$H_2 + O \rightleftarrows OH + H$	1.4×10^{12}	5.19	0
$H_2 + O_2 \rightleftarrows OH + OH$	1.4127×10^{13}	49.2644	0.015
$O_2 + H \rightleftarrows OH + O$	3.2×10^{11}	0.10	-0.47

(5) Energy Release

The performance calculations were based on the contract combustion efficiency goal of 97% c*. It can be shown numerically that a reduced c* can result in a reduction in kinetic performance by more than the reduction in c* considered as it affects further the equilibrium level of the exhaust. This was included in the performance predictions by noting the loss in thrust coefficient with reduced (90% c*) combustion efficiency and linearly interpolating at 97%, 95%, and 93% of theoretical c*. This was done for the area ratio of 40/1 and in similar manner, interpolated between the area ratios of 1/1, 4/1 and 6/1 for the sea-level conical nozzles of 2.39/1 and 3.16/1 area ratios which were used on the program.

(6) Theoretical Shifting Specific Impulse

The theoretical specific impulse was calculated with the ICRPG ODE computer program at arrays of mixture ratio, inlet temperature and chamber pressure. Typical of these are the results of the computations at the nominal mixture ratio of 4/1 as shown in Figure 26.

(7) Predicted Vacuum Specific Impulse

The loss breakdown for the regeneratively cooled nozzle at nominal mixture ratio and ambient inlet temperature is listed in Table XI. Results of predicted impulse for the altitude nozzle and the two conical nozzles are listed on Table XII. Predictions of performance are plotted versus energy release of % c* for interpretation purposes on Figures 27, 28, 29, and 30.

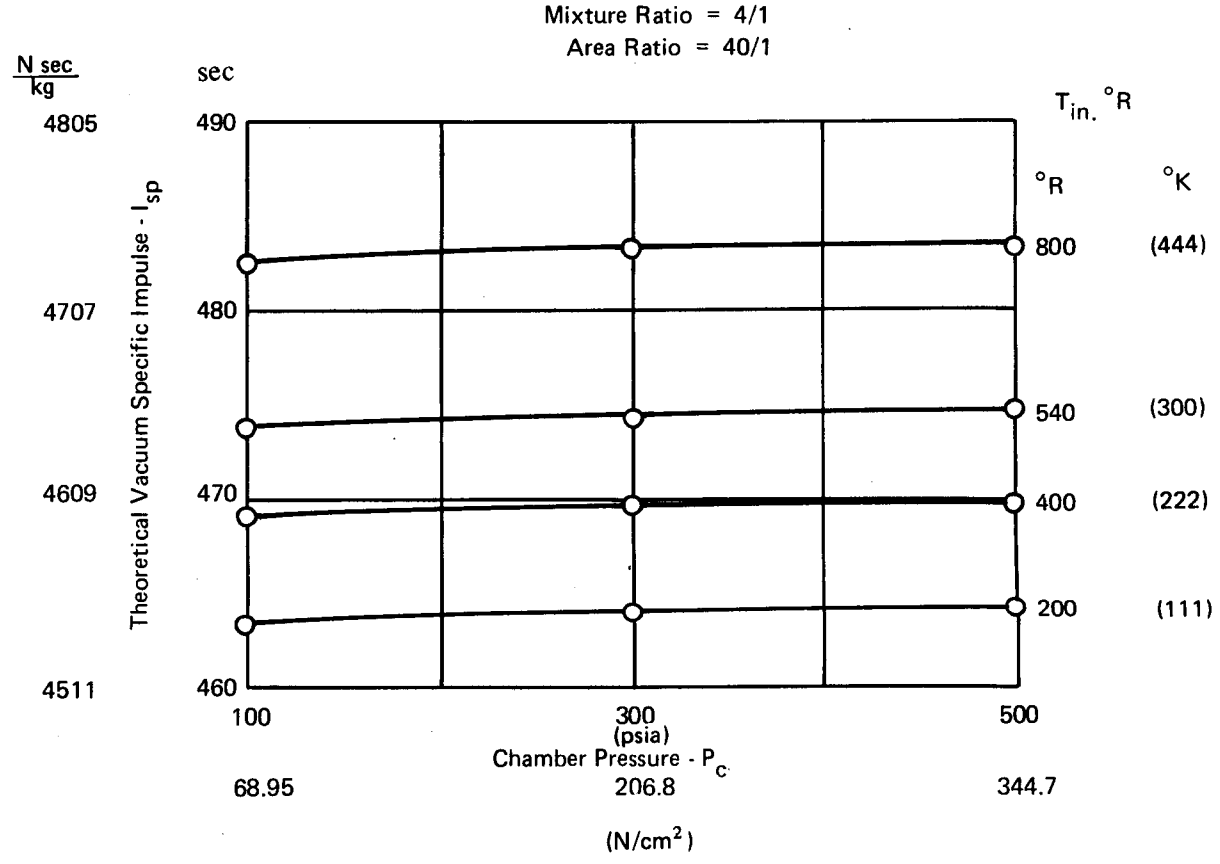

Figure 26. Theoretical Vacuum Specific Impulse versus Chamber Pressure

TABLE XII
PREDICTED PERFORMANCE SUMMARY

Mixture Ratio		3/1			4/1			5/1		
A/A_T		40	2.39	3.16	40	2.39	3.16	40	2.39	3.16
% Bell		75	100	100	75	100	100	75	100	100
Theo I_{vac}	$\frac{(lbf)(sec)}{lbm}$	472.1	390.7	404.4	474.4	384.6	399.1	471.2	373.7	389.0
	$\frac{N/sec}{kg}$	4629	3831	3966	4660	3771	3914	4610	3664	3814
$\frac{\eta_C^* = 0.97}{\eta_{oa}}$		0.934			0.929			0.925		
Pred I_{vac}	$\frac{(lbf)(sec)}{lbm}$	441.17			440.82			436.18		
	$\frac{N/sec}{kg}$	4326			4322			4270		
Pred I_{sl}	$\frac{(lbf)(sec)}{lbm}$		339.69	341.88		333.78	336.45		324.55	328.07
	$\frac{N/sec}{kg}$		3326	3352		3273	3299		3182	3217
Pred C_{F_∞}		1.7444			1.7787			1.8183		
Pred C_F, sl			1.3433	1.3518		1.3466	1.3575		1.3531	1.3675
$\frac{\eta_C^* = 0.95}{\eta_{oa}}$		0.913			0.907			0.902		
Pred I_{vac}	$\frac{(lbf)(sec)}{lbm}$	431.37			430.42			425.09		
	$\frac{N/sec}{kg}$	4230			4221			4169		
Pred I_{sl}	$\frac{(lbf)(sec)}{lbm}$		332.67	334.68		326.72	329.07		317.55	320.60
	$\frac{N/sec}{kg}$		3262	3281		3203	3227		3113	3143
Pred C_{F_∞}		1.7415			1.7733			1.8094		
Pred $C_{F,\ sl}$			1.3432	1.3512		1.3459	1.3557		1.3518	1.3645
$\frac{\eta_C^* = 0.93}{\eta_{oa}}$		0.893			0.885			0.878		
Pred I_{vac}	$\frac{(lbf)(sec)}{lbm}$	421.60			420.06			414.09		
	$\frac{N/sec}{kg}$	4134			4119			4061		
Pred I_{sl}	$\frac{(lbf)(sec)}{lbm}$		325.65	327.49		319.67	321.74		310.56	313.21
	$\frac{N/sec}{kg}$		3193	3213		3134	3154		3045	3071
Pred C_{F_∞}		1.7387			1.7679			1.8005		
Pred $C_{F,\ sl}$			1.3431	1.3506		1.3452	1.3540		1.3505	1.3617

P_c = 300 psi (206.8 N/cm²)
T_{in} = 540°R (300°K)

η_C^* = Assumed Combustion Efficiency
$\eta_{oa} = \frac{I_{sp_{Pred}}}{I_{sp_{S.E.}}}$
sl = sea level

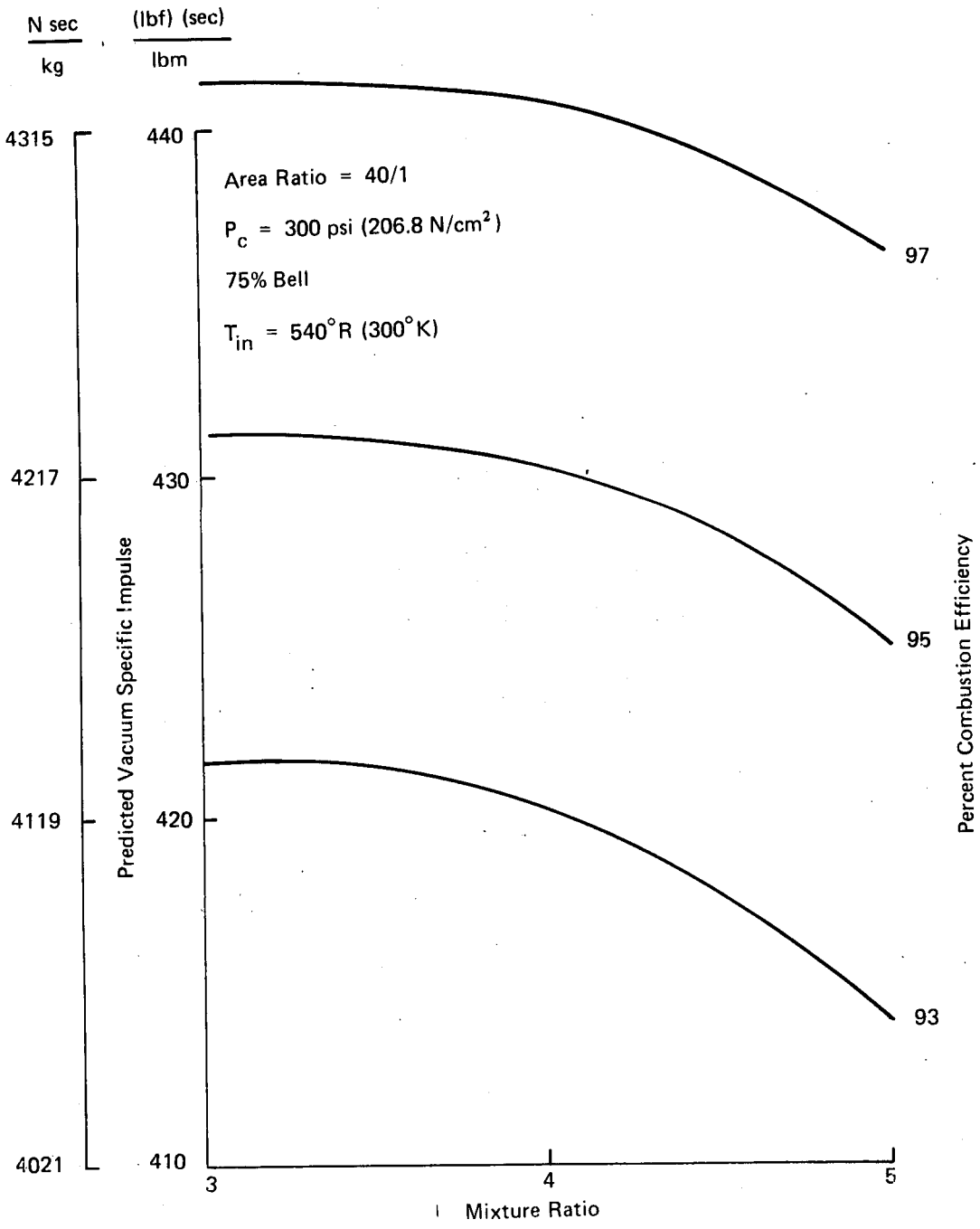

Figure 27. Predicted Vacuum Specific Impulse versus Mixture Ratio and Combustion Efficiency

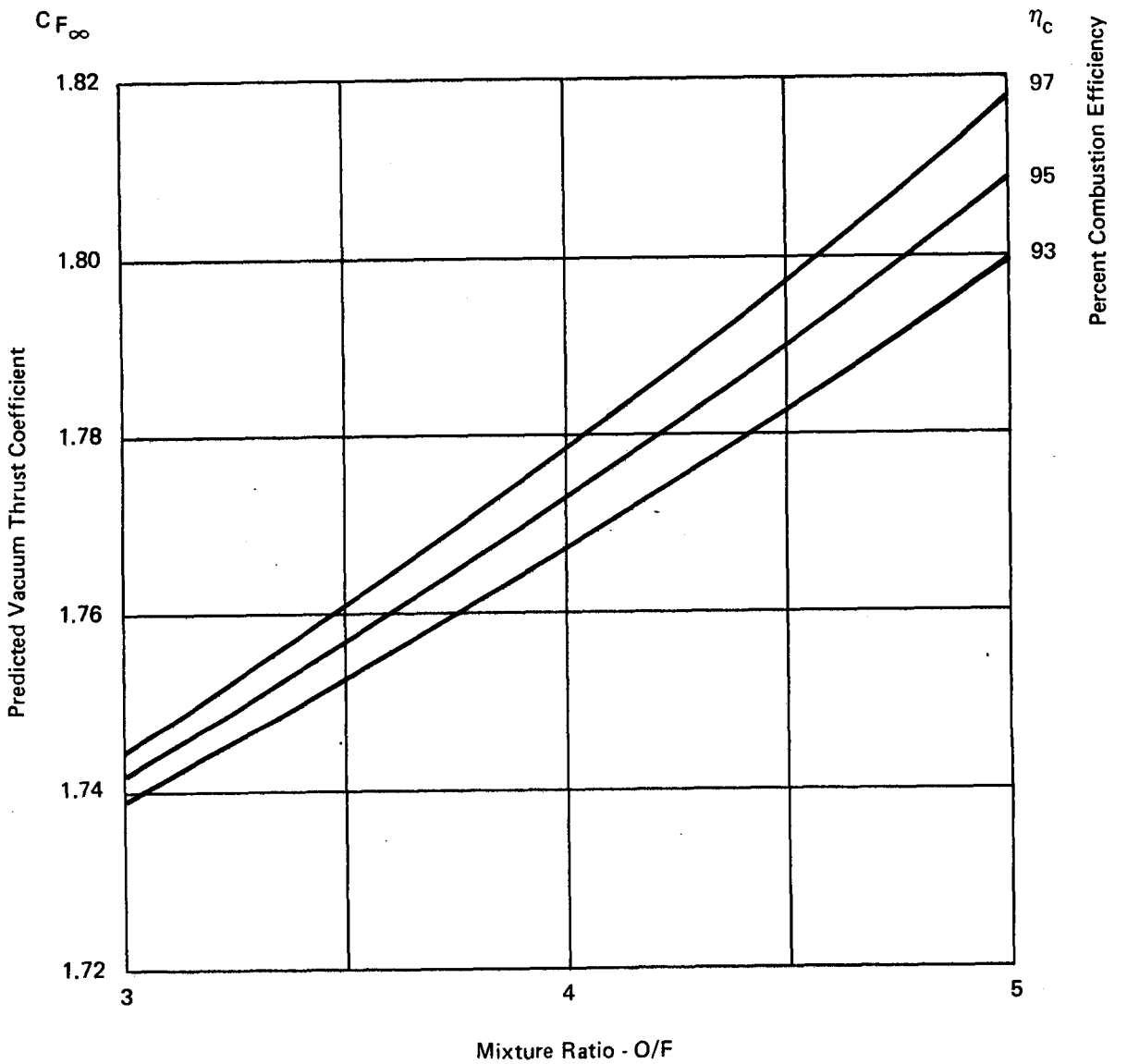

Figure 28. Thrust Coefficient versus Mixture Ratio and Combustion Efficiency

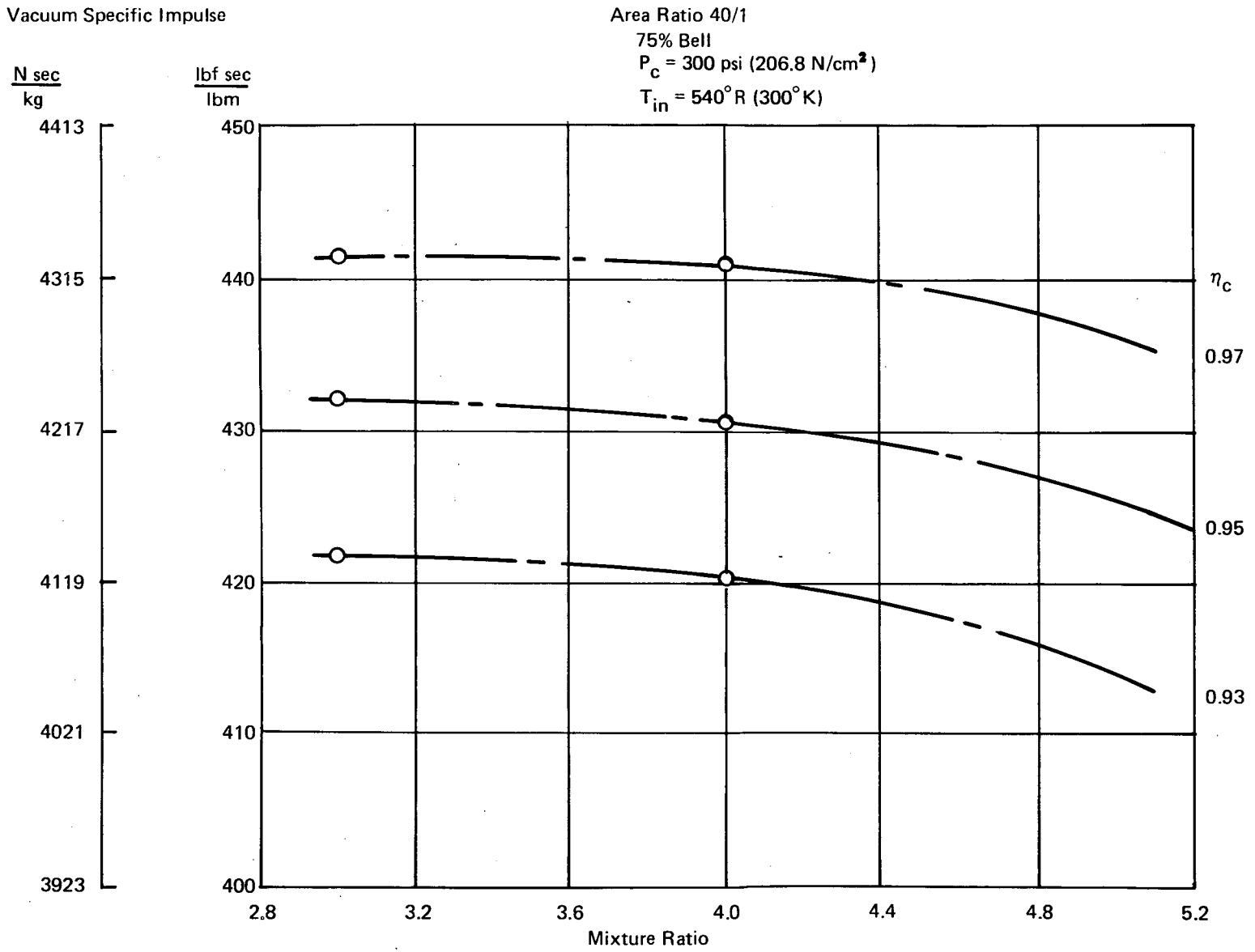

Figure 29. Predicted Vacuum Specific Impulse versus Mixture Ratio

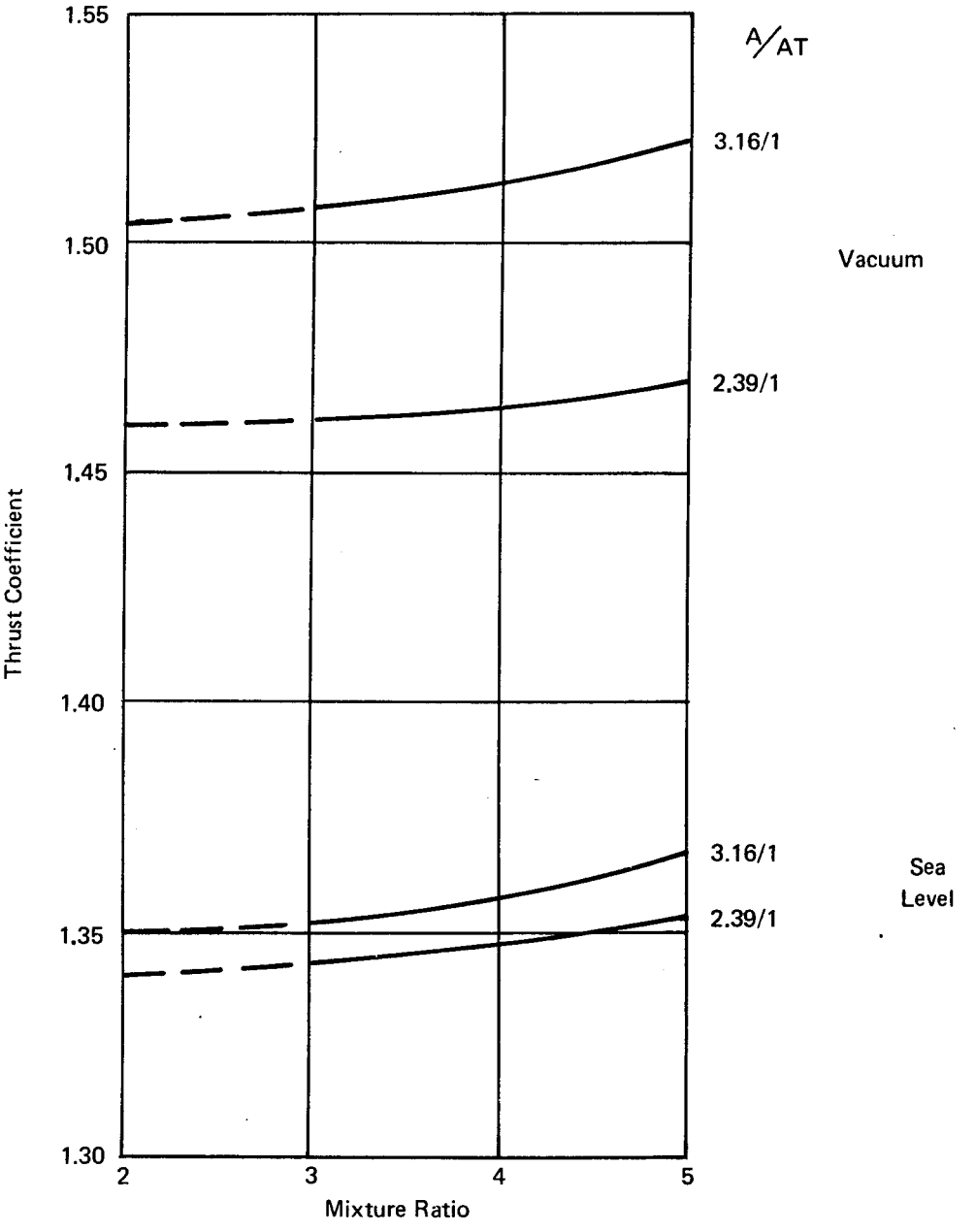

P_c = 300 psi (206.8 N/cm^2)

η_c^* = 97%

Figure 30. Predicted Conical Nozzle Thrust Coefficient versus Mixture Ratio

(8) Film and Dump Cooling Losses

The film- and dump-cooled TCA's were analyzed by assuming that combustion takes place at the increased mixture ratio resulting from hydrogen diversion, and that the hydrogen is then mixed with the main flow downstream – above the throat in the film cooling case, and at an area ratio of 10 for the dump-cooled case. At the point of mixing, mass, momentum and energy are conserved. The result can be shown to be thermodynamically equivalent to expansion of the premixed combustion gases from a reduced initial pressure.

A breakdown of the performance apportionment is presented in Figure 23. As expected, the fully regeneratively cooled case shows the highest performance, followed by film-cooled and the dump-cooled cases. Further details on thrust degradation with film and dump cooling may be found in Appendix C of this report.

b. Heat Transfer

(1) General

One-dimensional and two-dimensional heat-transfer analyses were made of the various cooled reverse-flow thrust chamber configurations, to examine their operational characteristics, i.e., wall temperatures, pressure drops, and performance losses. The ground rules and assumptions for these analyses are given in Table XIII.

TABLE XIII
HEAT TRANSFER GROUND RULES AND ASSUMPTIONS

Vacuum thrust, lbf	1500.0 (6 672 N)
Chamber pressure, psia	300.0 (206.8 N/cm^2)
Throat diameter, in.	1.90 (4.83 cm)
Nozzle exit area ratio	40/1
Overall mixture ratio, nominal	4/1
Total propellant flow at overall mixture ratio, lbm/sec	3.45 (1.566 kg)
Heating	
Combustion efficiency, percent	97.0
Cooling	
Inlet temperature, °F	80 (300°K)
Cooling enhancement from passage curvature, percent	0-100
Number of regenerative cooling passages	36
Exit Mach number	0.50
Wall material thermal conductivity	
Nickel 200 TD Nickel OFHC Copper Amzirc Copper Alloy	Temperature Dependent

Film- or internal-dump cooling in this design involves the injection of the fuel in the nozzle section to provide a protective film for the nozzle wall. If the gas is injected upstream of the throat, it is called film cooling; if the gas is injected downstream of the throat it is called dump cooling as noted earlier. Various materials, wall thicknesses and channel liner configurations were examined. This was done parametrically with the following cooling methods:

All regeneratively cooled
Film cooled
Supersonic dump cooled

The following paragraphs review the method of analysis and the results of application to the reverse flow engine. For each of the techniques used, a series of local heat balances are made to determine the heat flux and thrust chamber wall temperatures. These wall temperatures were controlled primarily by the three cooling techniques identified above.

(2) Regenerative Cooling

The analysis began with the desired maximum wall temperature specified. Families of cooling passage designs were constructed within this maximum temperature and for each cooling passage configuration, a coolant feed-pressure was determined. The steady-state heat transfer analysis was accomplished by specifying a nozzle wall shape, dividing the nozzle into a number of axial segments and performing heat balances on each segment. The heat flux at each segment was calculated assuming the thermal resistance to be the summation of resistances due to the gas-film boundary layer, the reciprocal conductance of the metal wall, and the coolant boundary layer. The heat-flux model was usually simplified to a one-dimensional flow, where the areas exposed to both boundary layers are equal. The temperature and pressure of the coolant at the outlet of the first segment becomes the input to the second segment, and so forth.

The "Reference Enthalpy" method of Eckert (Reference 11) was used to evaluate the transport coefficients of the high-speed combustion gases. This method considers compressibility effects, dissociation and recombination of species, and variable transport properties. The gas-film coefficient was calculated using a "turbulent-pipe-flow" equation with a modified correlation coefficient based on hydrogen-oxygen rocket test data, as given in Reference 12. The coolant side-film coefficient is calculated using the McCarthy-Wolf correlation as reported in Reference 13. An enhancement factor is added to account for additional cooling of outside walls of passages with curvature, as described in Reference 14. A more detailed description may be found in Appendix B.

The pressure drop in the coolant passages was calculated concurrently with the heat-transfer analysis. The calculation accounted for both friction and momentum change due to heating, plus velocity head losses at changes in flow area. For the configuration with a fuel-injection Mach No. of 0.5, the calculated injector pressure drop was 56 psi (38.6 N/cm^2) plus 5 psi (3.45 N/cm^2) expansion loss for a total injector ΔP of 61 psid (42.1 N/cm^2) at 300 psia (206.8 N/cm^2) chamber pressure. The pressure drop goal for the coolant passages was 14 psi (9.7 N/cm^2) to be compatible with the 375 psi (258.5 N/cm^2) valve outlet pressure

(3) Film Cooling

There is no exact analytical method which can be used to quantitatively determine the effect of film cooling. However, a number of different investigators have successfully

developed correlations of film-cooling effectiveness in terms of test data. The most widely used and accepted correlation for subsonic injection is the Hatch-Papell equation of Reference 15. This equation was used to determine the effectiveness of cooling reverse-flow H_2/O_2 engine at a nominal mixture ratio of 4:1 when injecting the coolant at a contraction ratio of 3.47 upstream of the throat. The results of a computer program to solve this equation are shown in Figures 31 through 33. Although not developed for the presence of a pressure gradient, this expression has demonstrated reasonably good results as shown in Reference 16.

Figure 31 shows the calculated effect of coolant injection angle (relative to the wall) on the adiabatic wall temperature, when 10% of the fuel flow is injected such that the velocities are matched at the point of injection. The advantage of injecting parallel to or as nearly parallel to the wall as possible is apparent.

Figure 32 is an extension of the above analysis to a greater portion of the nozzle. The solid lines show the effect of injection velocity on the wall-temperature distribution when 20% of the fuel flow is injected normally. As expected, the lower the velocity ratio, the less the penetration of the coolant into the main stream. Consequently, the coolant film remains intact longer, and the actual wall temperatures are lower. The dashed lines indicate a tangential injection which is parallel to the wall and which has an axial velocity ratio of 0.10. The effect on the wall temperature of increasing the flow rate from 10% to 20% is most pronounced within the throat region.

Calculated film temperature distributions with subsonic injection using the Hatch-Papell equation are shown in Figure 33. This temperature distribution was used for calculating the passage sizes of cooled engines with channeled passages. The film temperatures were calculated with injection parameters to simulate a swirl-type injection, where the injection angle, i, is zero and the coolant velocity, V_c, is one-tenth the gas velocity, V_g, i.e., i=0 and $V_c/V_g = 0.1$.

The use of film cooling would have the effect of requiring a lower coolant mass velocity with associated lower pressure drop for any regeneratively cooled section because of the reduced heat flux. However, there was a decrease in performance expected from the use of film cooling. As noted earlier, the I_{sp} goal could be achieved with the film coolant limited to 6% of the H_2 flow at a c* efficiency of 97%.

(4) Internal Dump Cooling

When coolant gases are injected downstream of the throat, the process involved is called internal dump cooling. In order to be effective, these injected gases must have supersonic velocities. Therefore, the relations used to predict the nozzle wall temperatures were related to supersonic injection of the coolant gases. The correlation equation chosen for supersonic injection was that of Zakkay, Sakell and Parthasarathy of Reference 17. As opposed to the subsonic correlation equation, there are no experimental data to suggest the applicability of that equation in a flow where a pressure gradient exists.

The initial calculations were made for injection at an area ratio of 6 downstream of the throat. The results are shown in Figure 34 for axial injection parallel to the wall through a convergent-divergent injection nozzle, such that the static pressures at the point of injection were matched.

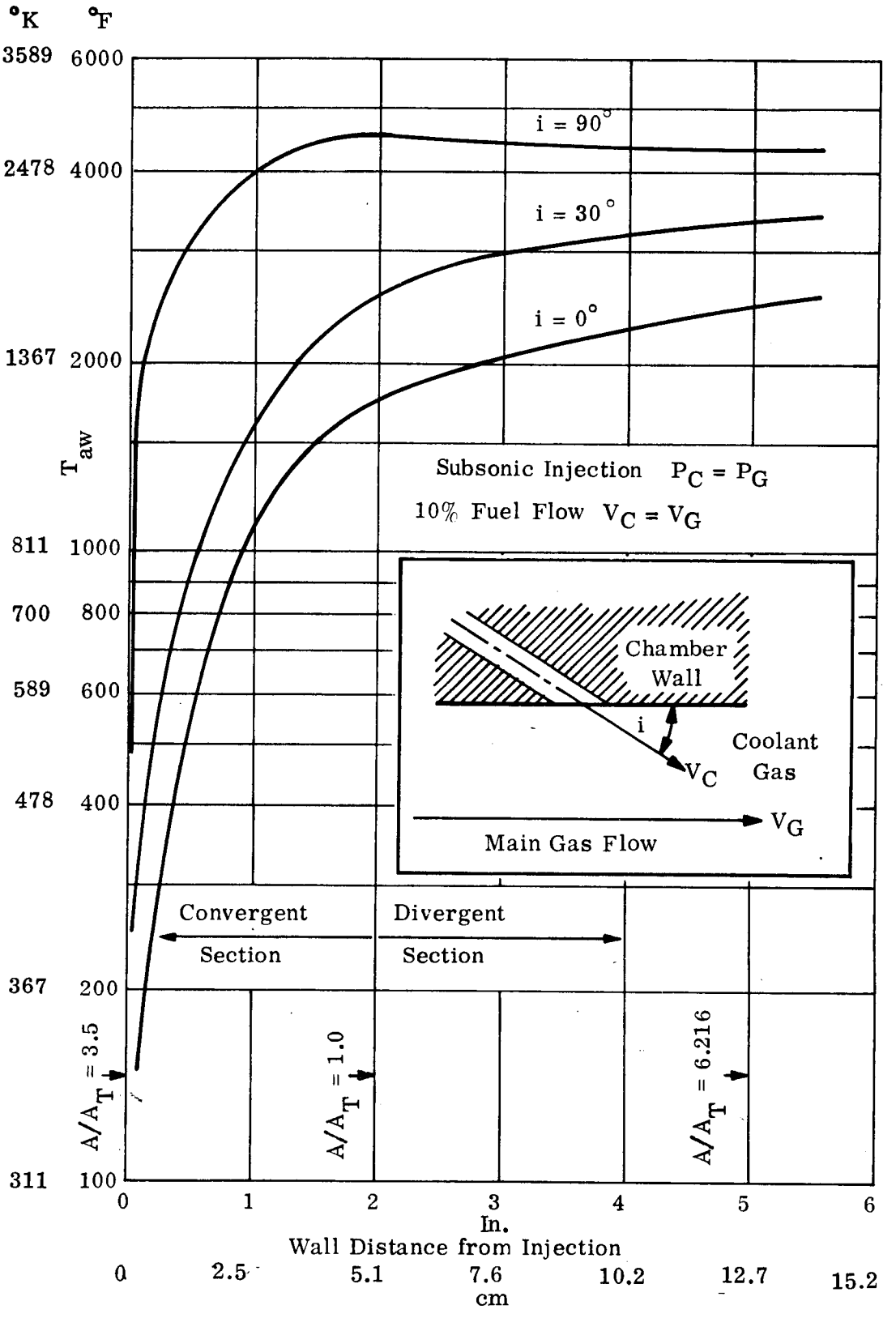

Figure 31 . Adiabatic Wall Temperature Distribution - Effect of Injection Angle

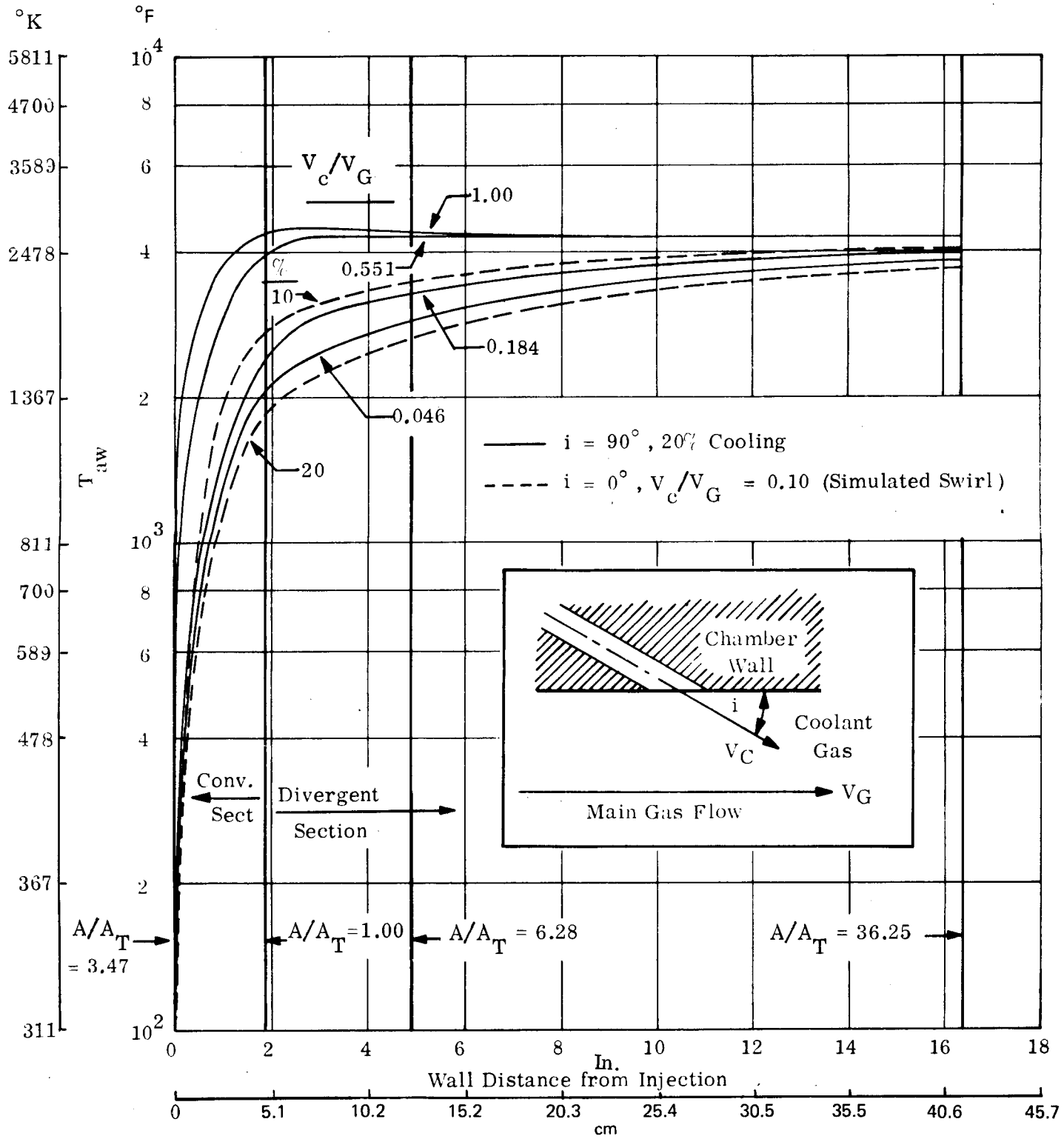

Figure 32. Wall Temperature Distribution, Subsonic Injection ($P_1 = P_2$)

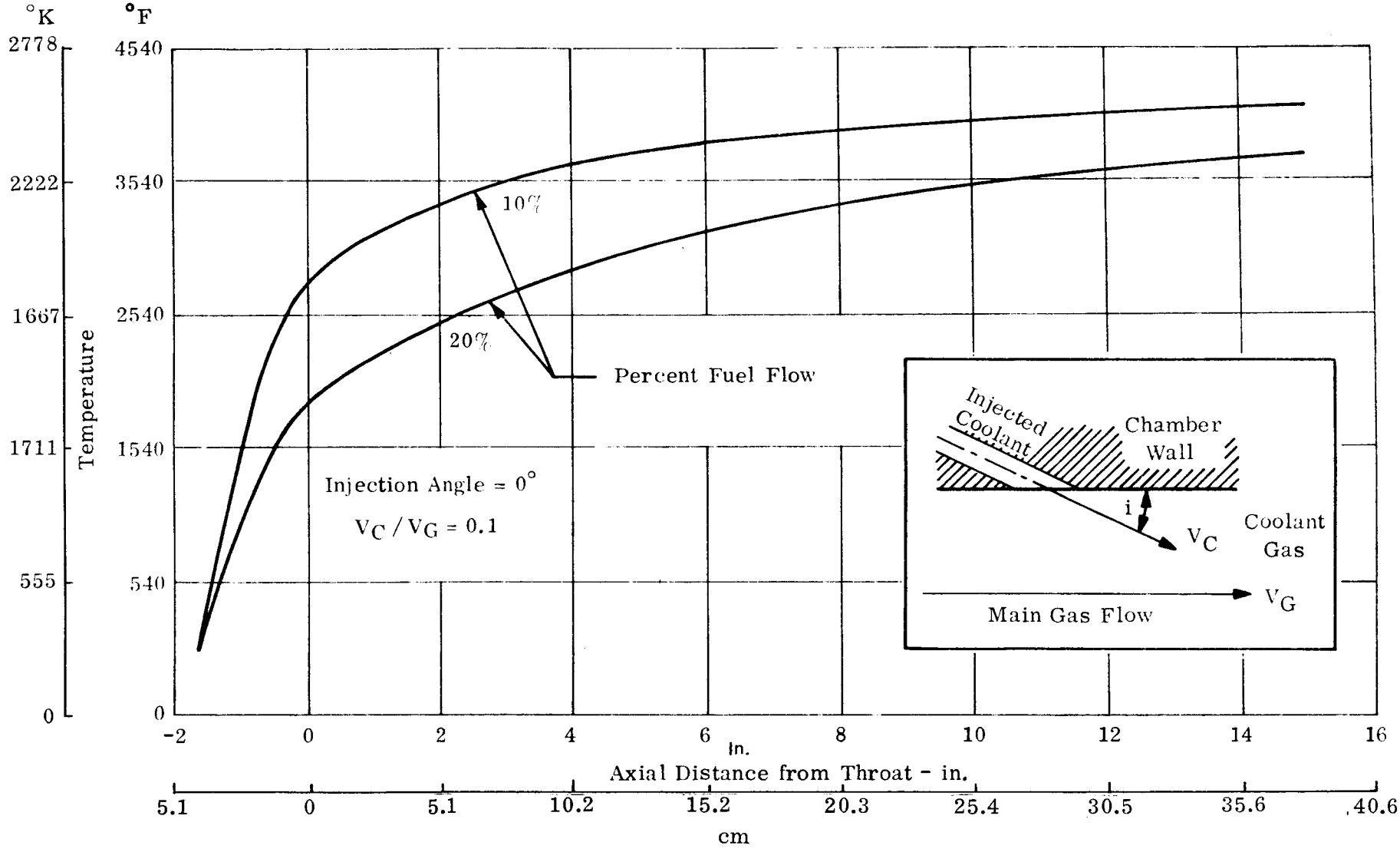

Figure 33. Film Temperature versus Axial Distance

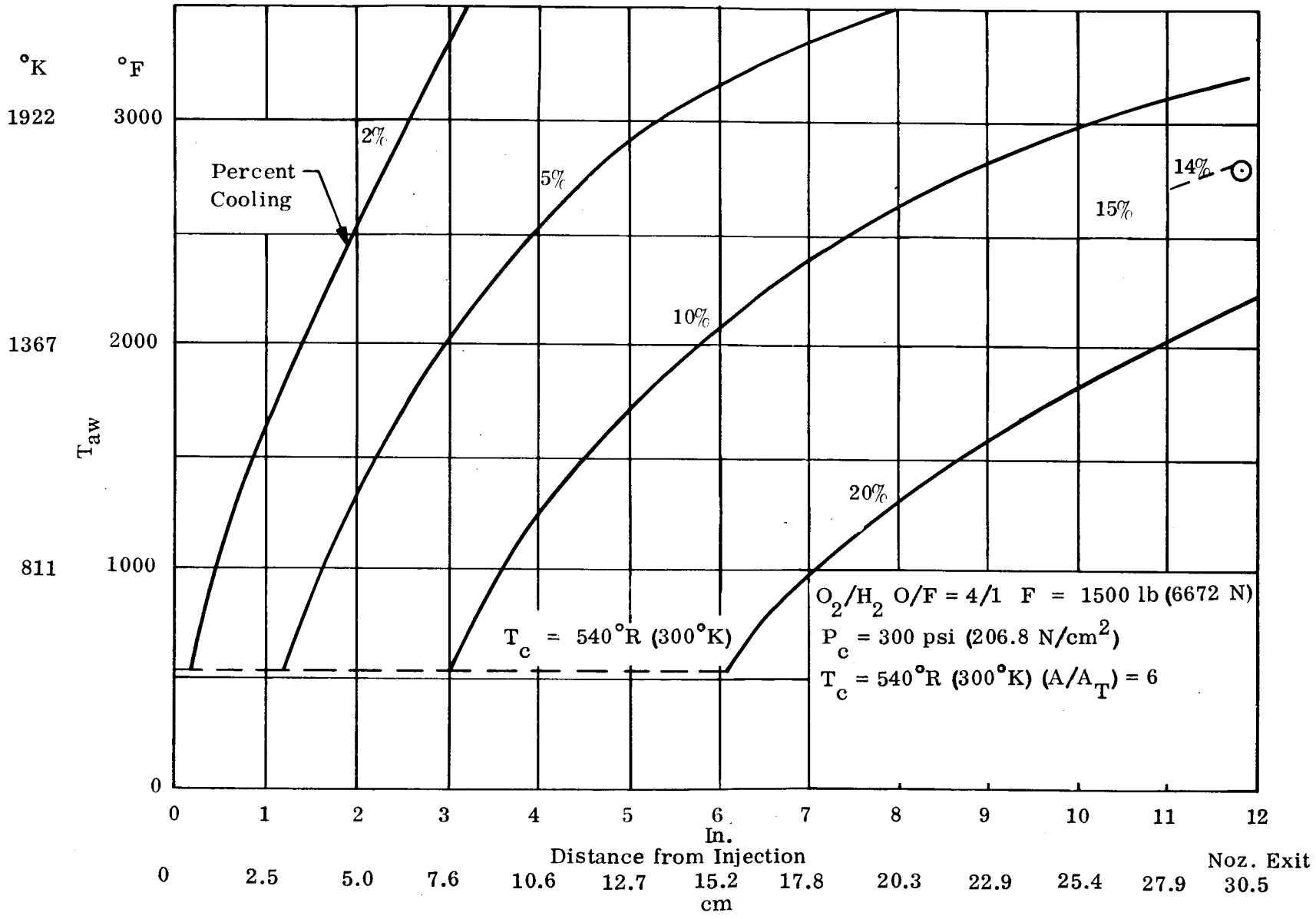

Figure 34. Adiabatic Wall Temperature Distribution with Film Cooling - Internal Dump

(5) Results of Wall Temperature and Pressure Drop Analyses, Normal Operation

Regeneratively Cooled Sections – Parametric solutions of coolant outlet temperatures, inlet pressures and coolant channel volumes were determined for various reverse flow engine configurations using the following variables:

Wall Temperatures	800-1500°F (700-1089°K)
Coolant inlet area ratio	4, 10, 40/1
Film cooling (percent of fuel flow rate)	0, 10, 20%
Dump cooling (percent of fuel flow rate)	10, 20%
Material	OFHC, Amzirc, Ni 200, TD Nickel

Typical results for regeneratively cooled sections are shown in Figure 35. Coolant-jacket pressure drops and coolant outlet temperatures are reduced by introducing the hydrogen at lesser area ratio and by cooling hotter walls.

The coolant total pressure was found to accumulate most rapidly in the subsonic nozzle and up to 2 inches (5.08 cm) aft of the throat as shown in Figure 36 (wall material-Nickel 200). Very little pressure drop results from cooling aft of the area ratio of 4:1. A small percentage (~ 10%) of the total passage volume exists forward of the area ratio of 4:1 for a nozzle designed to be cooled to an area ratio of 40:1.

Film or Dump Cooling – If some hydrogen were tapped off for internal or external dump cooling aft of an area ratio of 10:1, less fuel is available for cooling the throat and subsonic nozzle area. This will result in higher pressure drops because of physically smaller passages and higher coolant bulk temperatures as shown in Figure 37.

As a contrast to tapping off fuel for supersonic film cooling (dump cooling) the case for all regeneratively cooled nozzles, with various amounts of film cooling introduced subsonically, is shown in Figures 38, 39 and 40. The film cooling temperature distributions were taken from Figure 34 and illustrate the gross reduction in pressure drop with film cooling contingent on the applicability of the Hatch-Papell correlation for the instance of supersonic flow with a pressure gradient. Figure 38 shows that an all regeneratively cooled nozzle ($\epsilon = 40$) of Nickel 200 can have the pressure drop decreased from 83.5 to 78.5 psi (57.6 to 54.1 N/cm^2) by increasing the percent of film coolant from 5 to 10% while maintaining a 1000°F (811°K) wall temperature. Figure 29 shows that regeneratively cooling from the same area ratio (40:1) but with a copper-zirconium alloy, 10% film cooling will enable a 600°F (589°K) gas-side wall temperature to be maintained with a pressure drop of only 81 psi (55.9 N/cm^2). If the nozzle were cooled from an area ratio of ten, Figure 40, the 600°F (589°K) wall temperature can be maintained with 10% film cooling with about 79 psi (54.5 N/cm^2) drop. This shows that the use of 10% film cooling provides little pressure drop penalty, when changing the area at which regenerative cooling of the nozzle begins.

An external dump-cooled nozzle extension was analyzed to determine the feed-passage size and feed-pressure requirements for such a design. The extension was attached to a regeneratively cooled section as shown in configuration E in Table VIII. A design wall temperature

1 Dimensional Heat Flow
Mixture Ratio = 4:1
P_c = 500 psia

No Film Cooling
Wall Material - Ni 200
Coolant Inlet Temp. = 80°F (300°K)

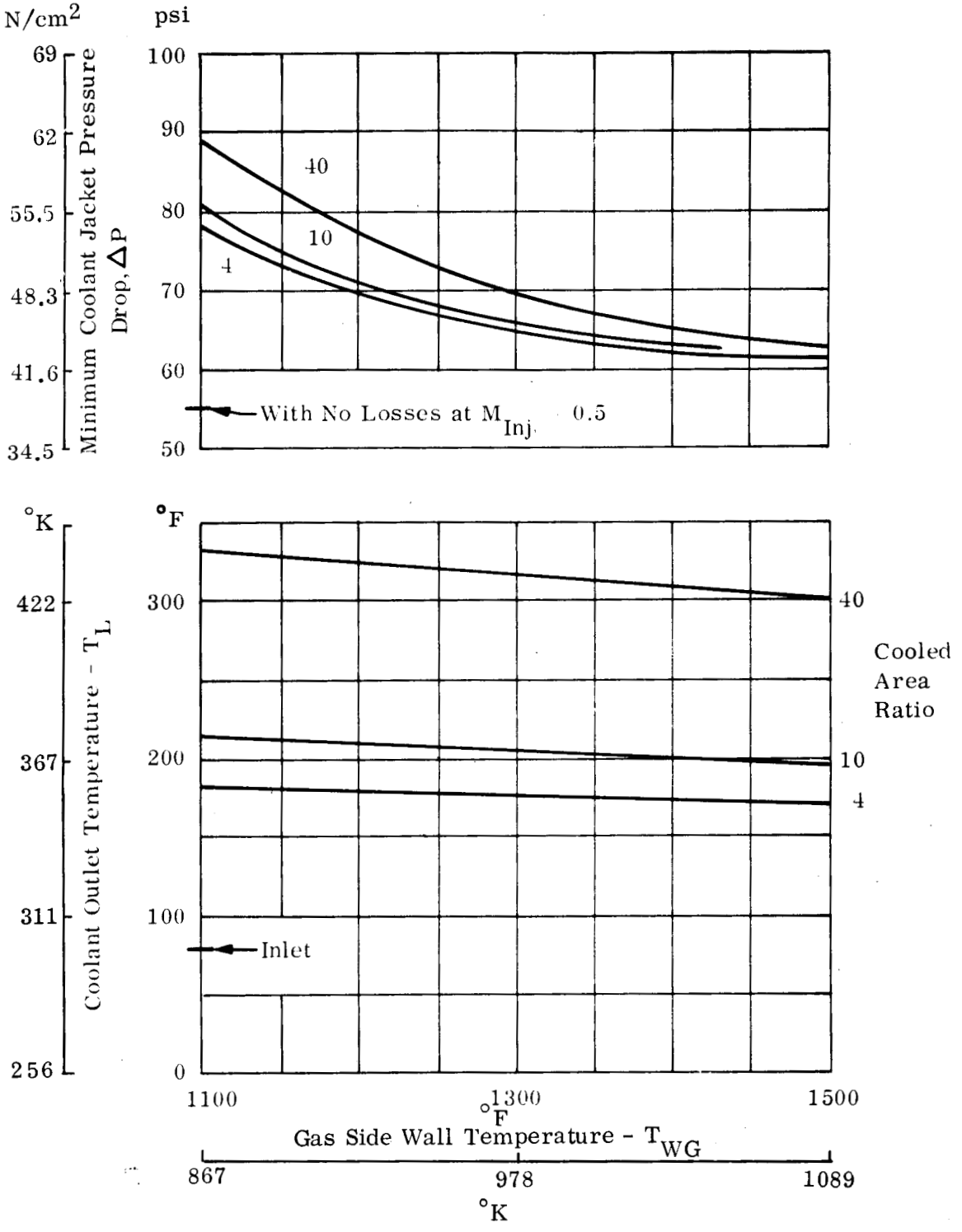

Figure 35. Pressure Drop and Coolant Outlet Temperature versus Wall Temperature

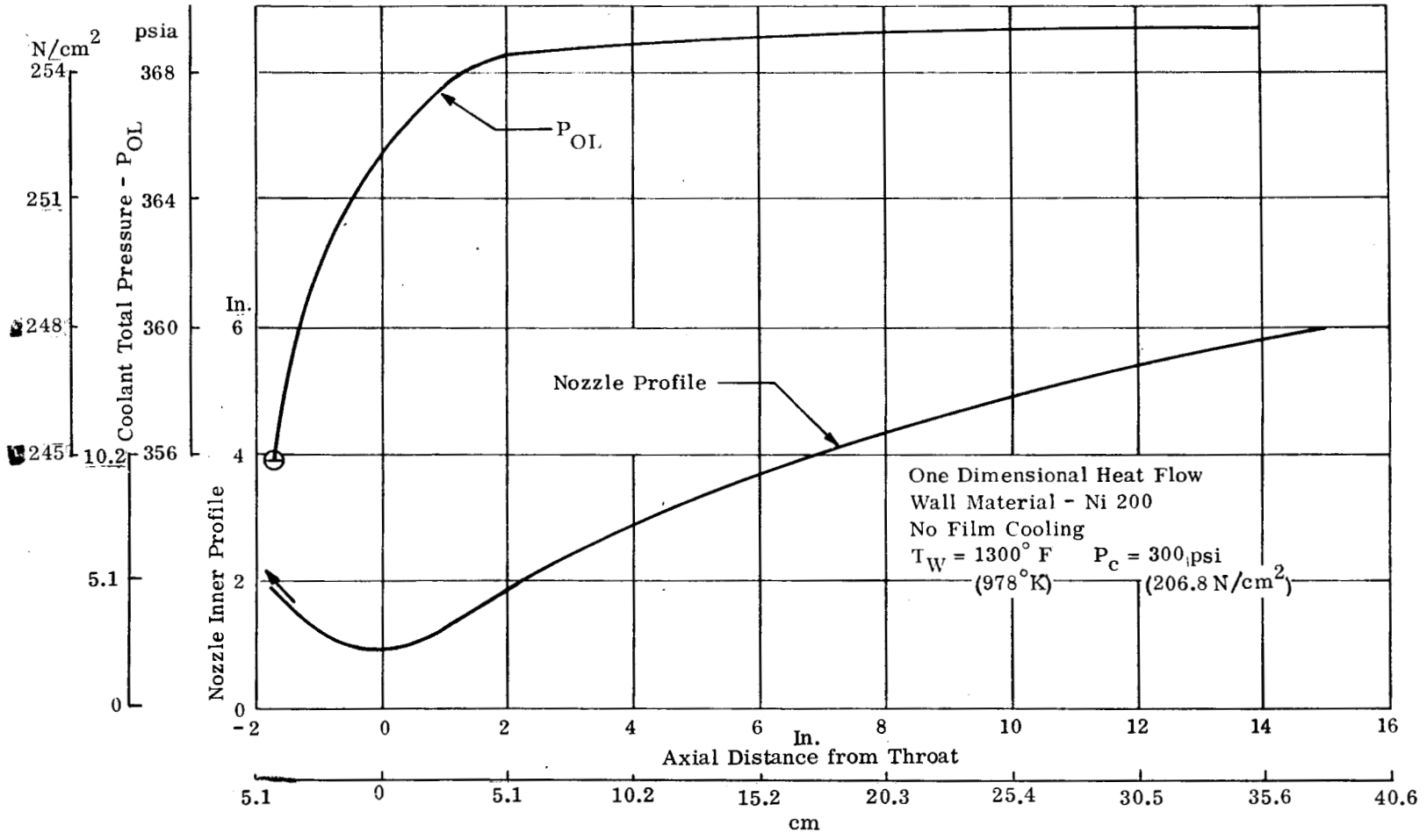

Figure 36. Regeneratively Cooled Design, Coolant Total Pressure Distribution

One Dimensional Heat Flow Chamber Pressure = 300 psia (206.8 N/cm^2)
Mixture Ratio = 4:1 No Inlet Losses
Coolant Inlet A/A_T = 10/1 Inlet Temperature = 80°F (300°K)
Wall Material = Ni 200

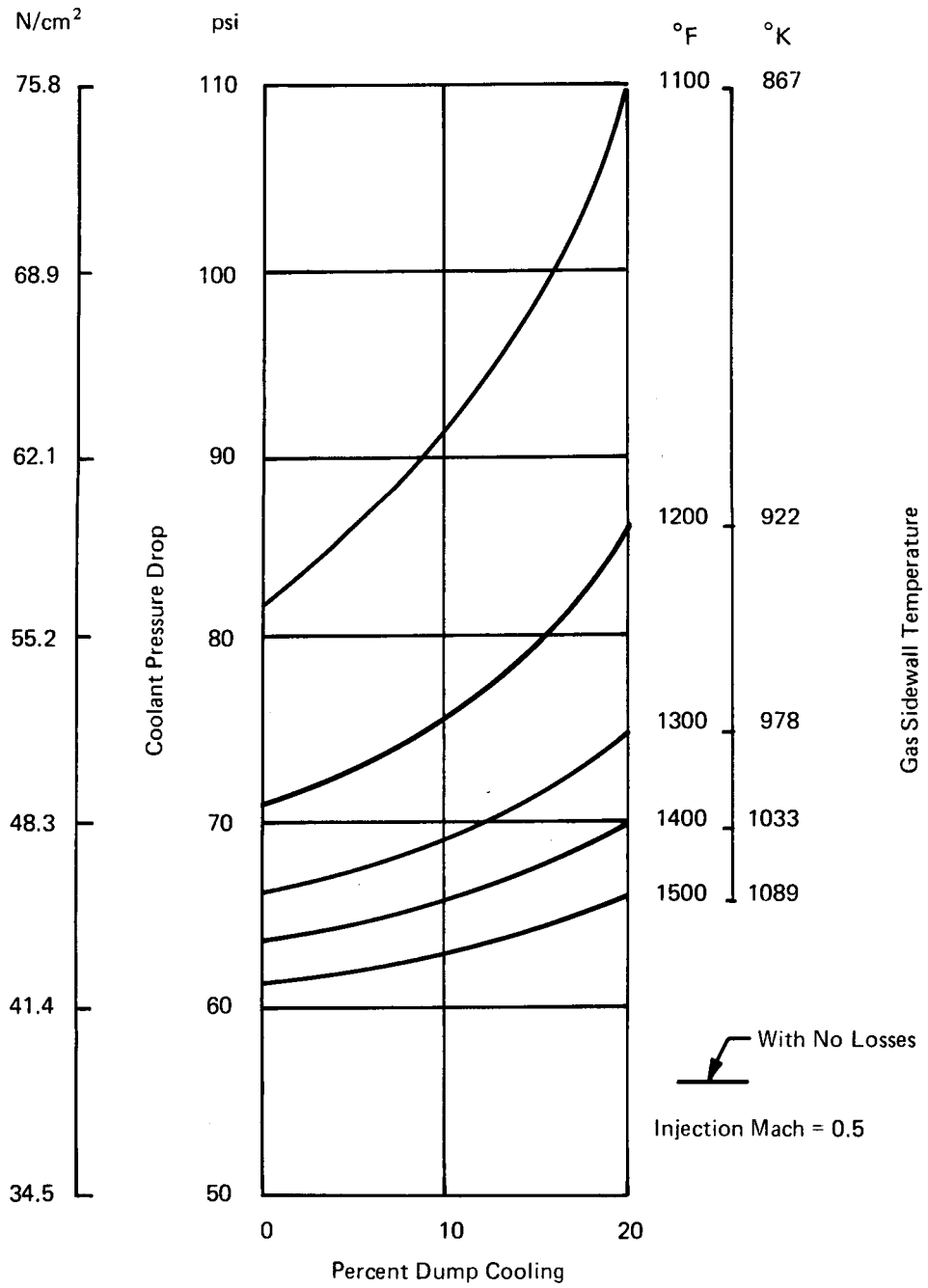

Figure 37. Regeneratively Cooled Design, Coolant Pressure Drop as a Function of Dump Cooling and Wall Temperature

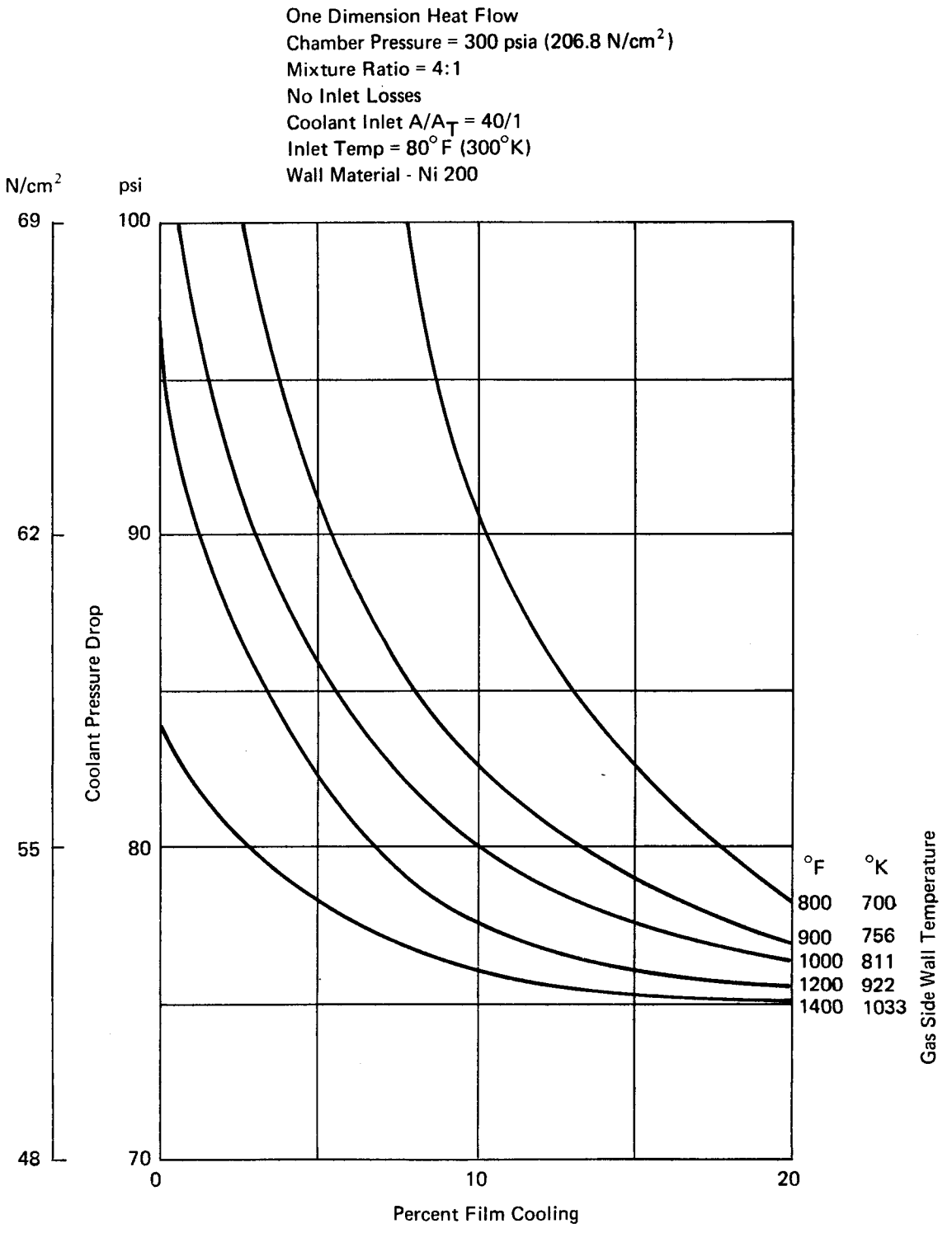

Figure 38. Regeneratively Cooled Design, Coolant Pressure Drop as a Function of Film Cooling and Wall Temperature

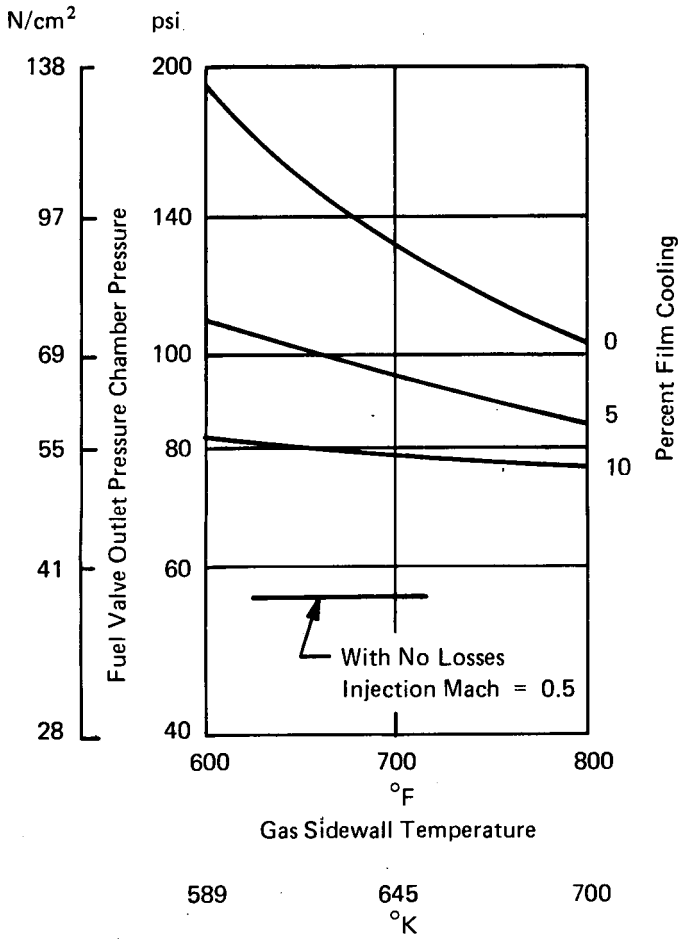

Modified Two-Dimensional Heat Flow
Chamber Pressure = 500 psia (345 N/cm^2)
Mixture Ratio = 4:1
Inlet Temperature = +80°F (300°K)
Coolant Inlet at 40:1
Includes 5 psi (3.4 N/cm^2) Entrance Loss Plus
15 psi (10.3 N/cm^2) for Channel Modifications

Figure 39. Regeneratively Cooled Design, Coolant Pressure Drop as a Function of Film Cooling and Wall Temperature

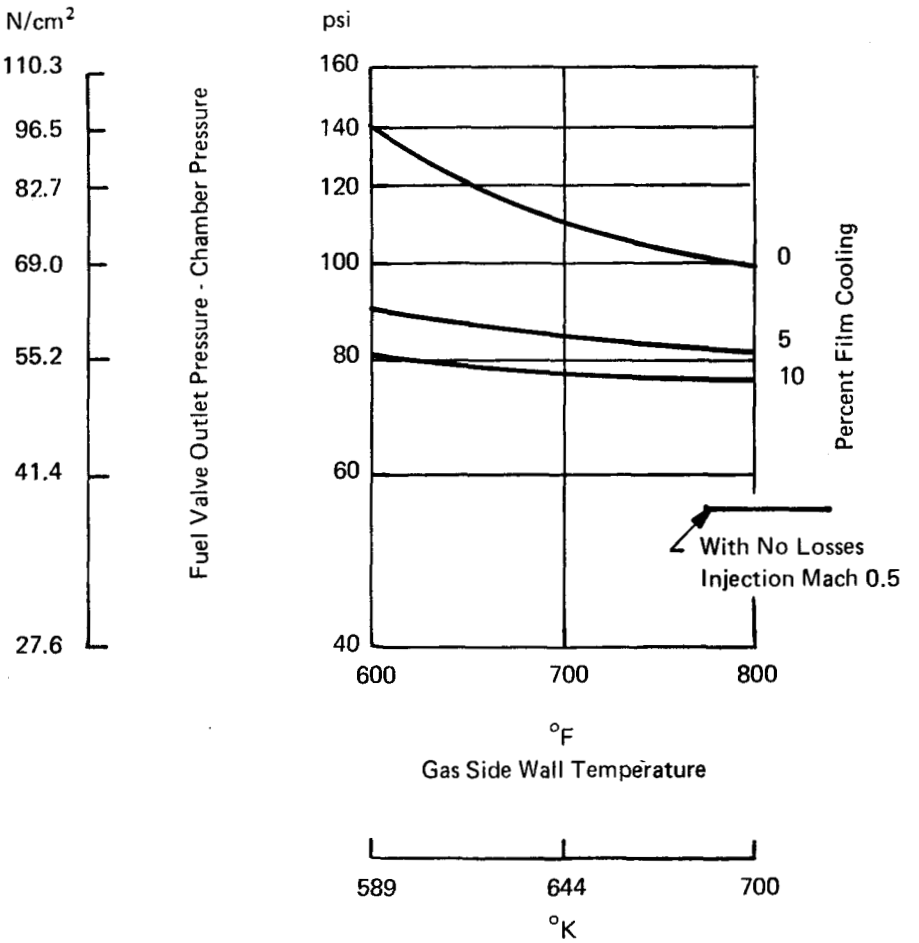

Modified Two-Dimensional Heat Flow
Chamber Pressure = 300 psia (206.8 N/cm^2)
Mixture Ratio = 4/1
Inlet Temperature = +80°F (300°K)
Coolant Inlet at 10/1
Includes 5 psi (3.4 N/cm^2) Entrance Loss Plus 15 psi (10.3 N/cm2) for Channel Modifications

Figure 40. Regereratively Cooled Design, Coolant Pressure Drop as a Function of Film Cooling and Wall Temperature

of 2000°F (1367°K) was assumed for the extension. Figure 41 shows resulting coolant-flow areas and parameters for the configuration without the benefit of film cooling. The flow area for the coolant assumes the use of 10% of the fuel flow.

The calculated effect of using various percentages of film and dump cooling, on the regenerative nozzle coolant pressure drop, for a 0.07 in. (0.178 cm) thick copper-zirconium channel wall is presented in Figure 42. The figure also shows the significant difference in ΔP caused by superimposing film cooling on the regeneratively cooled wall contingent upon the applicability of the equations employed in predictions.

Insulated/Radiation-Cooled Extension – Temperature distributions and insulation requirements were calculated for radiation cooled extensions attached to a regeneratively cooled nozzle section.

Figure 43, illustrates the calculated steady-state wall temperature of nozzle extensions insulated on the exterior and able to lose heat by radiation out the nozzle exit. The joint for attachment assumed for the analysis was at an area ratio of 6:1. An emissivity of 0.92 was used in the analysis. View factors, including radiation interchange between nozzle surfaces inside the nozzle varied from 0.145 at the forward end of attachment to 0.395 at the exit.

Two similar sets of wall temperature calculations were made for internal dump cooling where the hydrogen is injected in the supersonic nozzle at an area ratio of 6:1. The film temperature increase with axial distance towards the nozzle exit results in a low wall temperature increasing to a peak wall temperature within the nozzle and is in contrast to the wall temperature with no film cooling (local total temperature being constant). In the case of no film cooling, the wall temperature decreases constantly because of the diminishing heat-transfer coefficient and the increasing view-factor to space. The results plotted in Figure 43 illustrate that some degree of supersonic dump cooling is required to successfully demonstrate a radiation cooled extension which utilizes an oxidation resistant coating.

Nozzle Extension Insulation – The initial analysis of nozzle extension insulation was limited to an inner wall temperature of 2600°F (1700°K), compatible with assumed long term limits on oxidation resistant silicide coatings to be applied to a columbium extension shell. The exterior temperature of the nozzle was defined by the contract as 800°F (700°K). Table XIV gives the calculated thickness and weight for an insulation to meet the interior and exterior limits.

TABLE XIV
NOZZLE EXTENSION INSULATION

Outer Wrap	Altitude	Thickness		Insulation Weight	
		(in.)	(cm)	(lb)	(kg)
Stainless or Inconel	Sea Level	0.92	2.34	1.054	0.478
$\epsilon = 0.8$	Vacuum	0.85	2.16	0.973	0.442
Polished Stainless	Sea Level	1.47	3.73	1.683	0.763
or Inconel $\epsilon = 0.5$	Vacuum	1.36	3.46	1.558	0.706

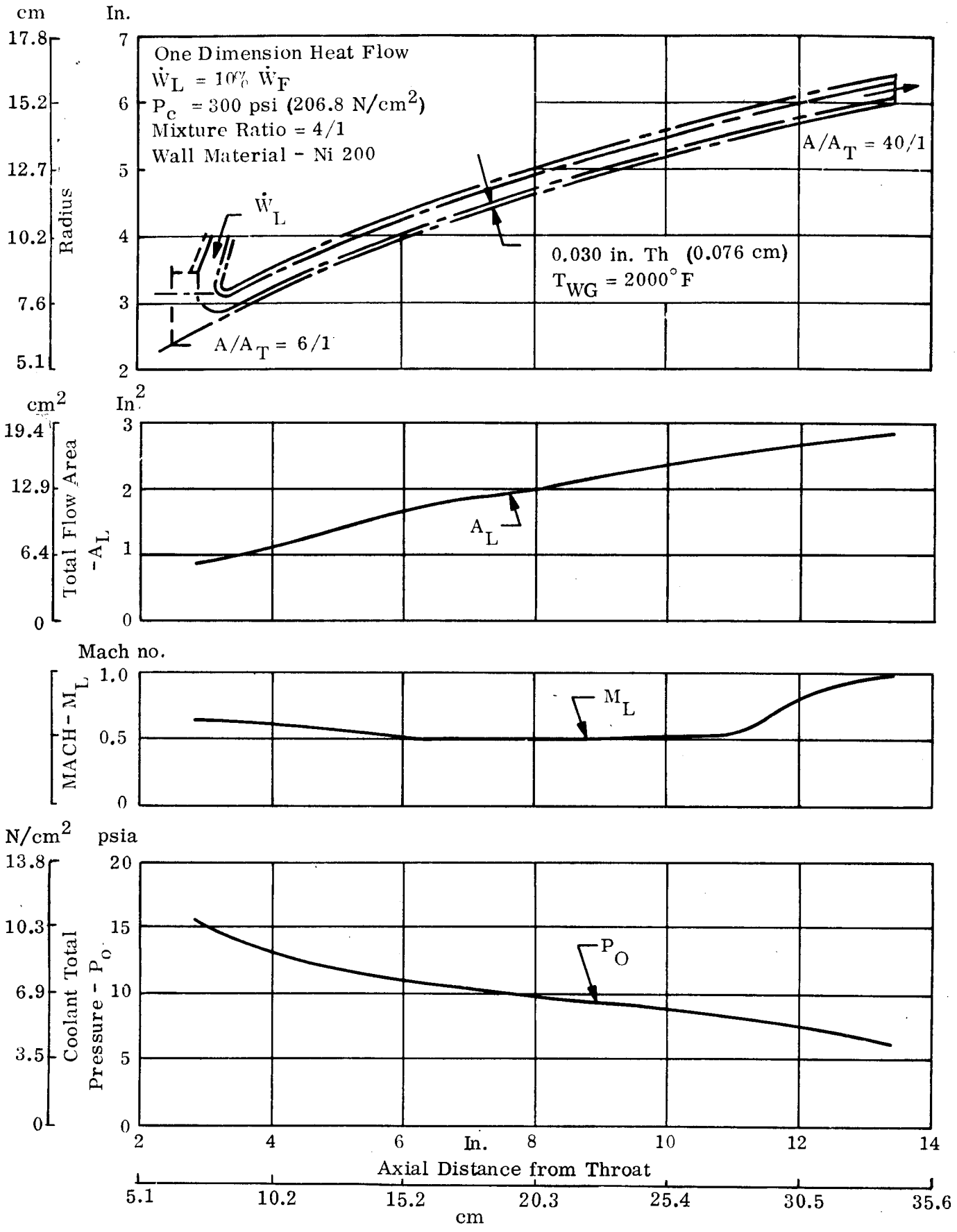

Figure 41. External Dump - Cooled Nozzle Extension

Modified Two-Dimensional Heat Flow
Chamber Pressure = 300 psia (206.8 N/cm^2)
Mixture Ratio = 4/1
Inlet Temperature = +80°F (300°K)
Coolant Inlet at 10/1
Includes 5 psi (3.4 N/cm^2) Entrance
Loss plus 15 psi (10.3 N/cm^2) for
Channel Modifications

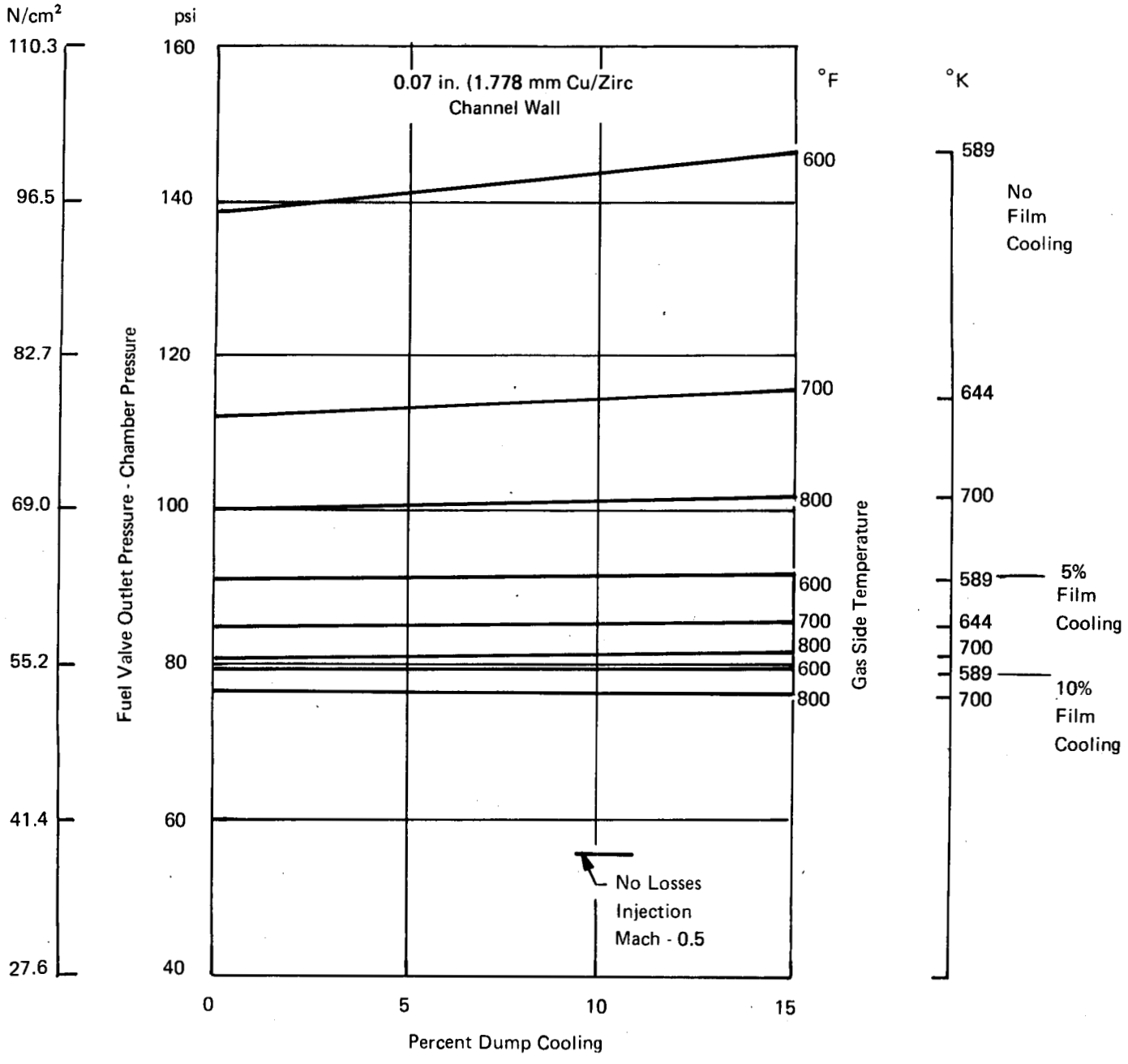

Figure 42. Regeneratively Cooled Design, Coolant Pressure Drop as a Function of Dump Cooling and Wall Temperature

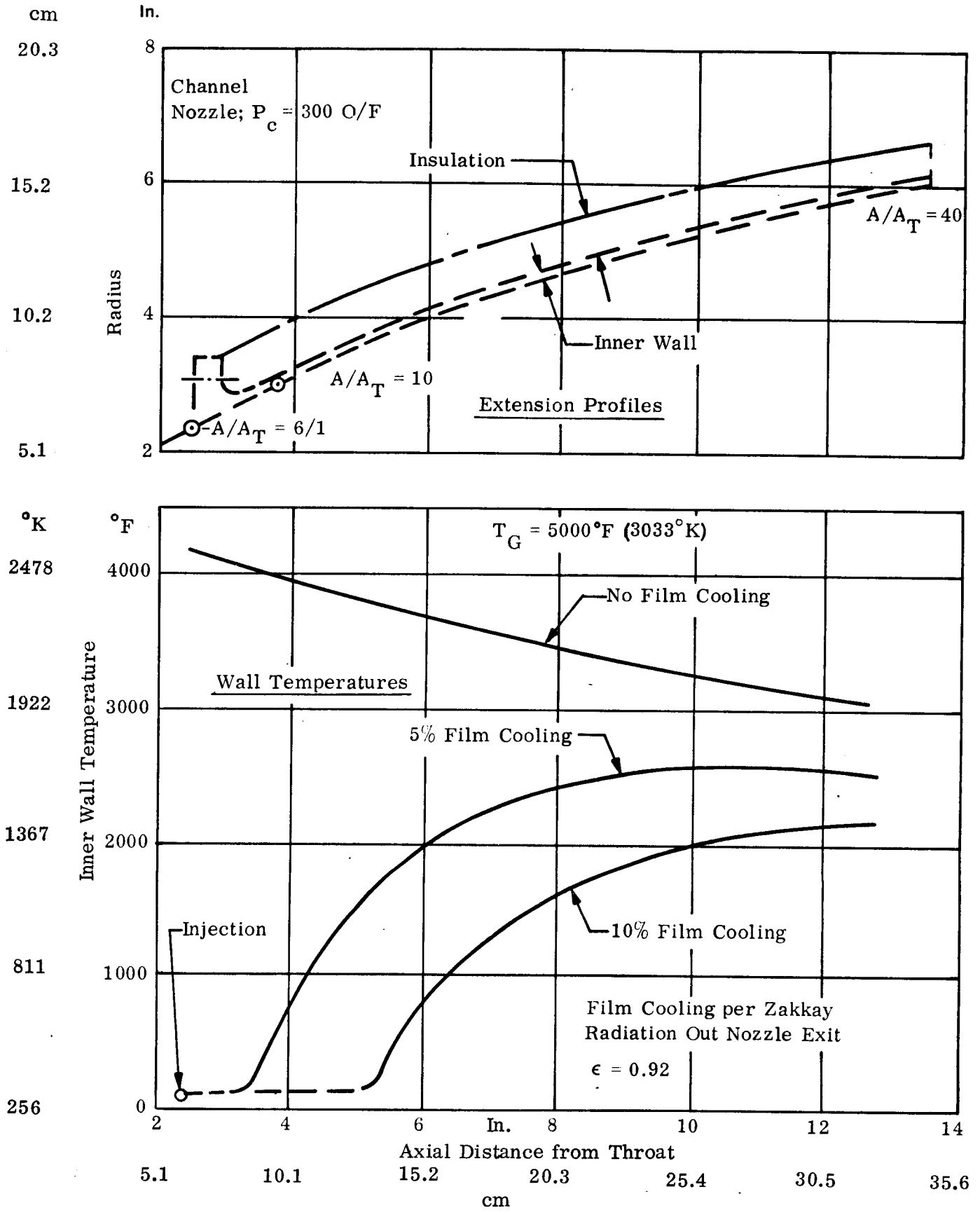

Figure 43. Radiation Cooled Nozzle Extension

The insulation taken for the analysis was Johns-Manville "Dynaflex", and was assumed to be in blanket form and secured on the exterior with Inconel or stainless foil. The density was taken as 6 lb/ft^3 (96.1 kg/m^3). Two thicknesses are shown for sea level and vacuum conditions in Table XIV.Thicknesses for sea level conditions are greater because air trapped in the insulation raises the thermal conductivity of the insulation. Changes in the emissivity of the outer wrap are shown also. If the emissivity of the outer wrap were reduced for a polished surface, the thickness will increase because of the reduced ability to radiate heat. The weights of insulation material to cover the nozzle extension from an area ratio of 6:1 at the joint to the exit (area ratio = 40:1) were based on a nozzle surface area of 329.1 square inches (2125 cm^2).

Use of an outer surface with the highest emissivity (0.8) results in the lightest weight, but highest heat rejection rate, 2.2 BTU/sec (2319 watts). Decreasing the emissivity would increase the thickness and weight and would decrease the heat rate proportionally.

The calculated insulation thicknesses were based on the temperature differential between the hot wall (T_{WG}) and the cool external wall (T_O) and the ability to cool by radiation. Reduction of the hot gas side wall temperature would reduce the required thickness of insulation in proportion to the reduced temperature differential.

(6) Off Design Operation

All previous discussions concerning the cooled reverse flow thruster have been at the nominal conditions of O/F = 4, P_c = 300 psia (206.8 N/cm^2) and 540°K (300°R) feed temperatures. However, it was necessary to consider the operation of the thrust chamber assembly at a range of conditions to meet the test firing requirements of the contract. Calculations were made to investigate the effect of varying coolant inlet temperature and combustion pressure on wall temperatures, pressure losses, coolant Mach number and H_2 injection velocity. These effects were calculated at an O/F of 4.0 and are shown in Figure 44. This task was accomplished by designing, in detail, a Nickel 200 channel liner with a wall 0.030 inch (0.076 cm) thick and 40 passages with linearly varying passage height and width as in Figure 45.

As expected, an increase in coolant inlet temperature resulted in an increase of coolant pressure drop and increase of injection velocity. The hot gas side wall temperature was shown to be near minimum at an inlet temperature of 80°F (300°K), and increases were predicted for either lower or higher inlet temperatures for the fixed passage liner. The maximum liner temperature occurred at 0.60 inch (1.52 cm) forward of the throat. Increasing the chamber pressure by increasing the propellant mass flow resulted in an increase in thrust with the fixed configuration. Increasing the chamber pressure was shown to cause the following:

Increase of the gas side wall temperature
Slight decrease of the coolant Mach number and outlet temperature
Slight change in ratio of chamber pressure drop to chamber pressure ($\Delta P/P_c$)

From Figure 44 it appears that the feed pressure would exceed the specification limit of 375 psia (258.5 N/cm^2) at high feed temperature conditions. The condition could be offset by an increase in the size of the coolant passages in the convergent nozzle to reduce the pressure losses. The associated wall temperature increase would not compromise the integrity of the liner.

The calculations indicated that relatively small changes in the throat section liner would be encountered at high and low P_c and feed temperatures. A large change of fuel injection Mach number could be expected for low feed temperature operation.

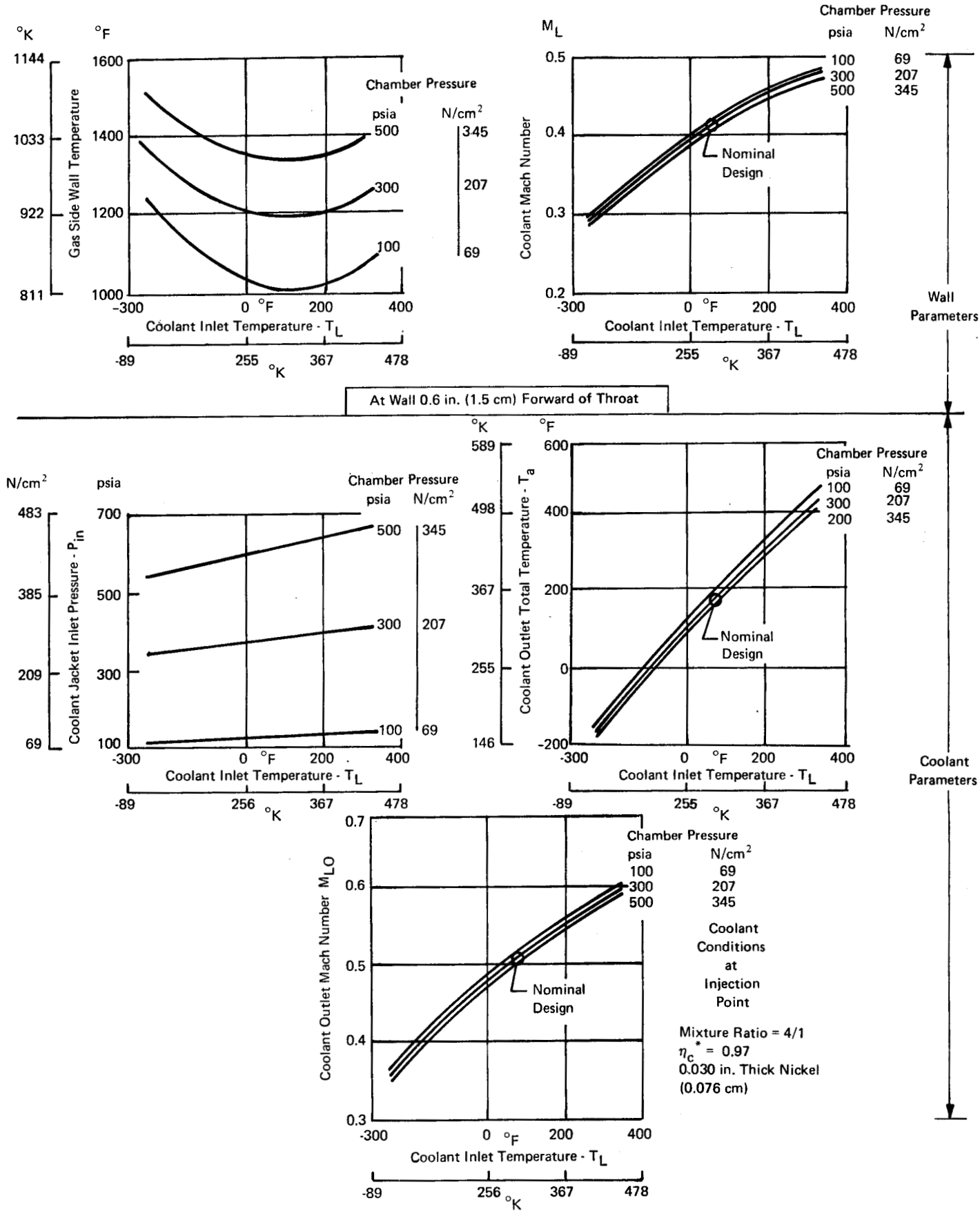

Figure 44. Heat Transfer Characteristics - Channel Type Nozzle, Off-Design Operation

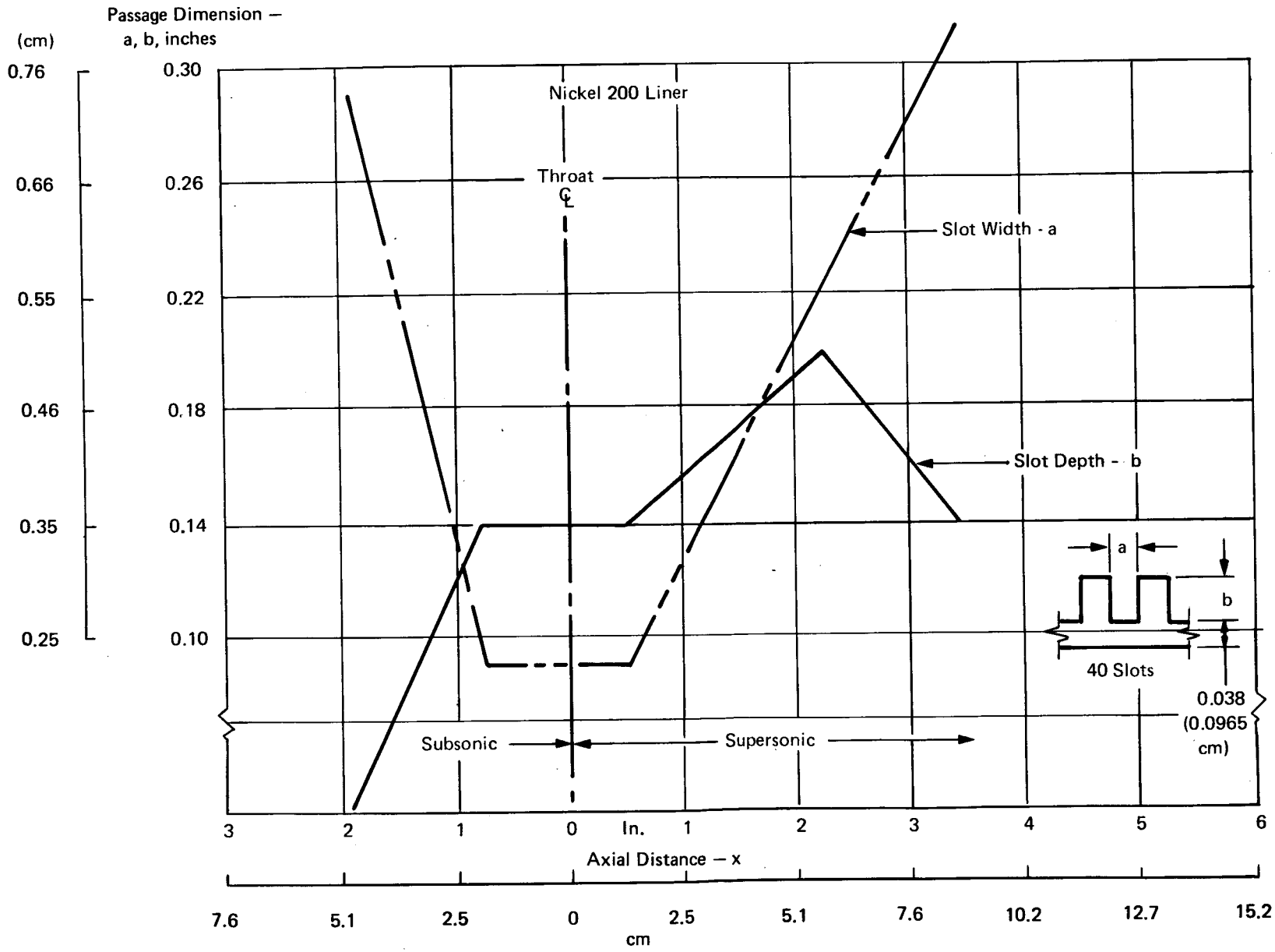

Figure 45. Cooling Passage Dimensions

c. Structural Cycle-Life Analyses

(1) Transient Heat Transfer Analysis

The primary structural problem encountered in attempting to meet the APS engine requirements was the stress induced by thermal cycling of the engine. These stresses are especially critical in the cooling passages of the regeneratively cooled section of the nozzle. To perform structural analysis on the engine, it was first necessary to perform a transient heat transfer analysis to predict thermal gradients and stresses setup in this region. The transient calculations were made for three basic types of construction with passage size as per Table XV. The three types were:

(1) Integral wall - liner and coolant passage closure of same material

(2) Free-standing liner - no attachment between liner and cooling passage closeout.

(3) Composite integral wall - liner and closure of dissimilar metals but fused together.

The following ground rules for wall sections and heat transfer parameters were assumed for the transient calculations:

Wall Section Parameters

Place of maximum heat flux 0.6 in. (1.5 cm) upstream of throat
Number of passages = 40
Total coolant flow = 0.690 lb/sec (0.313 kg/sec).
Passage width = 0.090 in. (0.229 cm).

Heat Transfer Parameters

Cooling enhancement for passage curvature = 100%
Coolant temperature at analysis point = 128°F (326.5°K)
Combustion Efficiency = 97%
Mixture Ratio = 4:1
Chamber Pressure = 300 psia (206.8 N/cm^2)
Mass of trapped H_2 in passage ignored

Temperature transients through walls on start-up were calculated using a simple step input of heat to the combustion side wall in terms of a gas temperature and a heat transfer coefficient. The analysis was made by construction of a nodal mathematical model and solving the model by a finite difference method using the IBM 360/65 computer. A typical start-up transient is shown on Figure 46 , leading to a steady-state temperature as shown for a sample wall [0.030 x 0.173-inch (0.0762 x 0.439-cm) slot] in Figure 47. The latter figure shows that temperatures in copper liners are affected more by geometry (outer closure) than the nickel liners, because of their ability to conduct heat up the web.

A minimum number of nodes was used to perform the analysis,one on each surface of the 0.030-inch (0.076-cm) wall; thus it was not possible to show the nonlinearity (if any) of the temperature gradient through the wall. To verify this analysis technique, a simplified one-

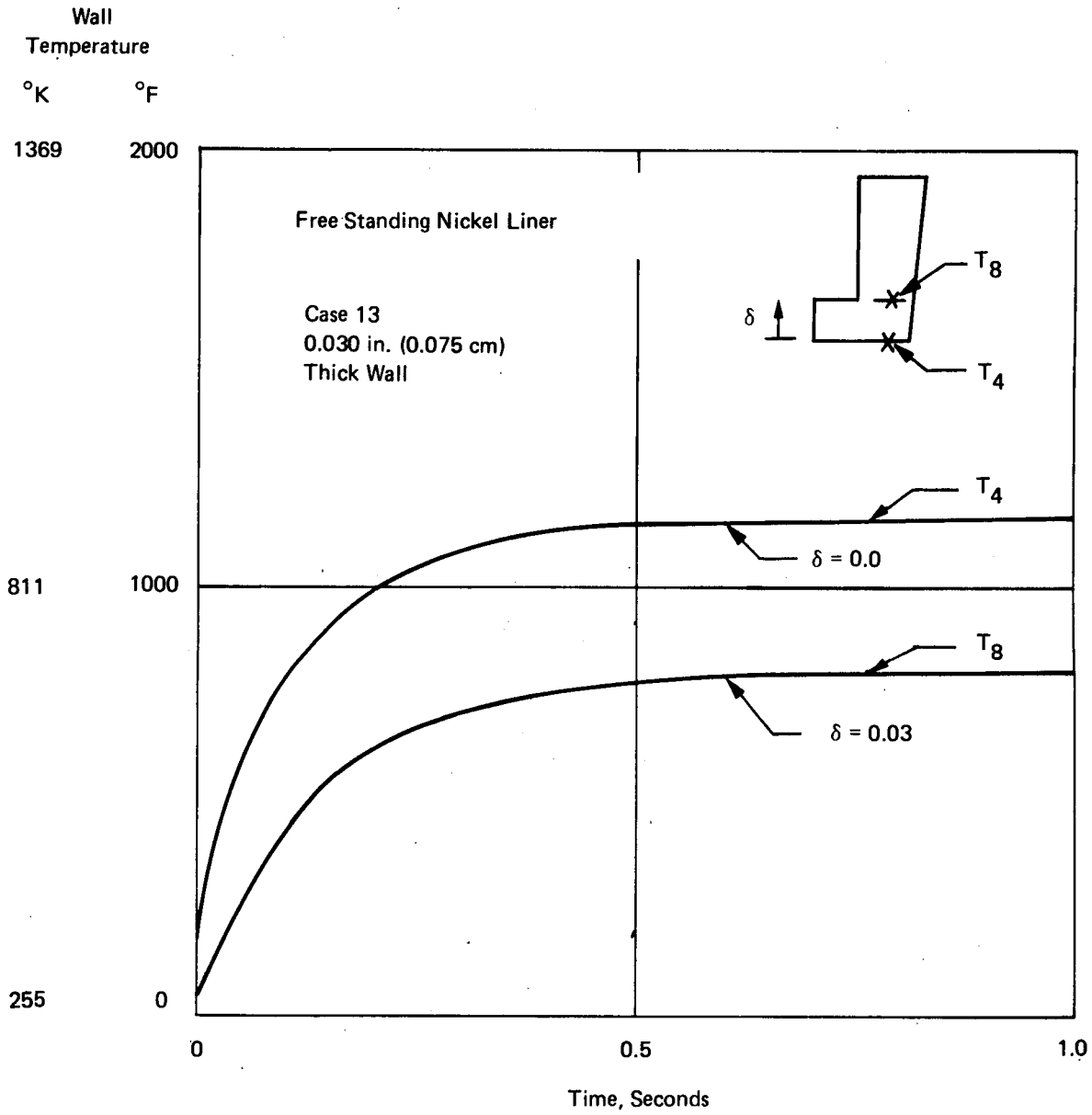

Figure 46. Typical Temperature Transient

dimensional analysis through a thick wall was conducted with results shown in Figure 48. The wall temperature stabilized in approximately 0.5 seconds and the gradient was linear through the wall, confirming the adequacy of the basic calculations.

The shutdown analyses were conducted for the cases listed in Table XVI. Initial temperature distributions were from the start-up analysis, and the time dependent temperature distribution was calaculated based on the flow of heat by conduction only within the wall. No heat was allowed to be removed from the section by the coolant or by radiation. The time to stabilize (reach a constant temperature at all spatial nodes) is indicated on the table. The time is much shorter for copper than nickel, because the copper walls have a more uniform initial temperature and higher thermal conductivity.

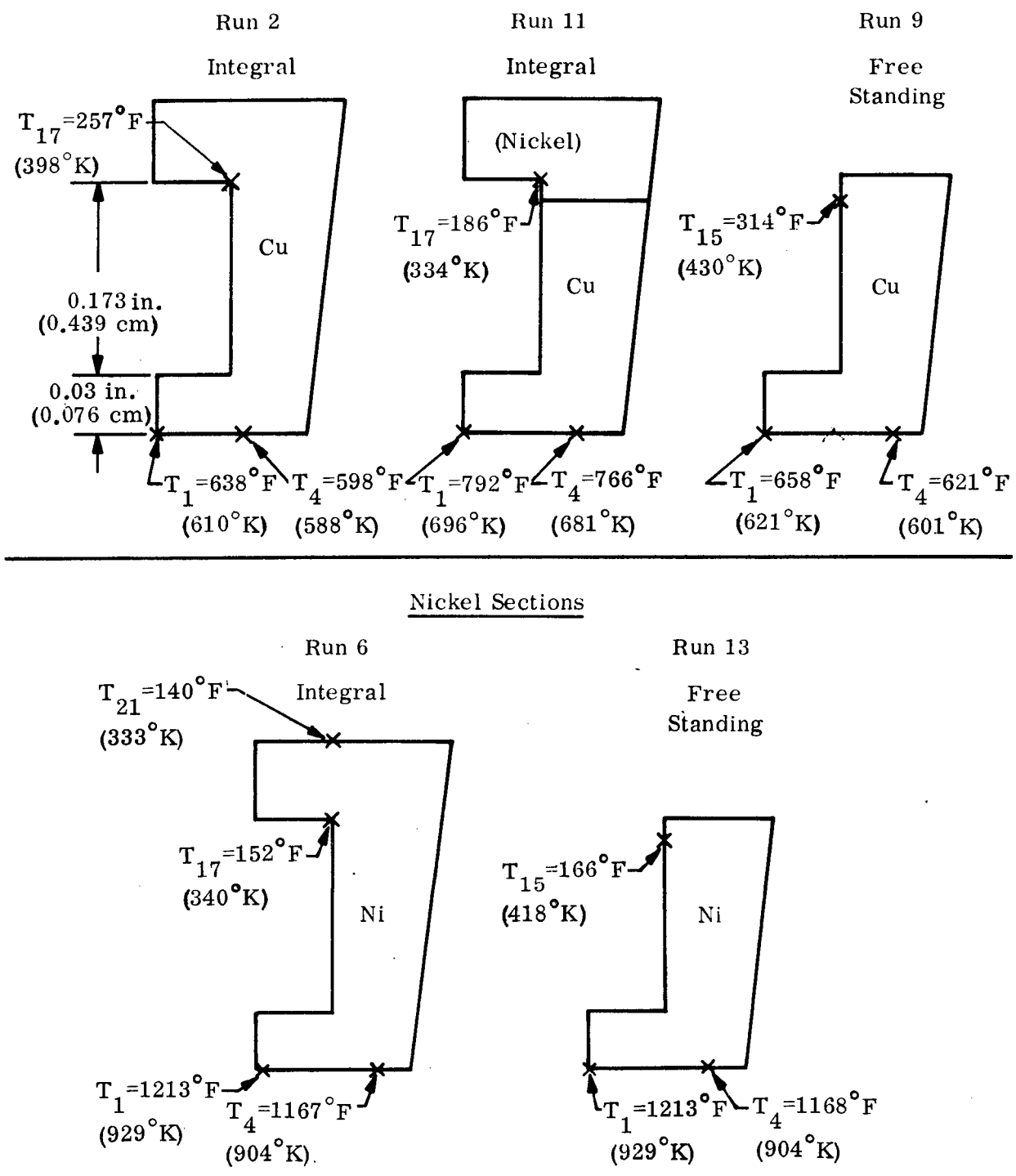

Figure 47. Construction and Material Effects, Steady-State Wall Temperatures

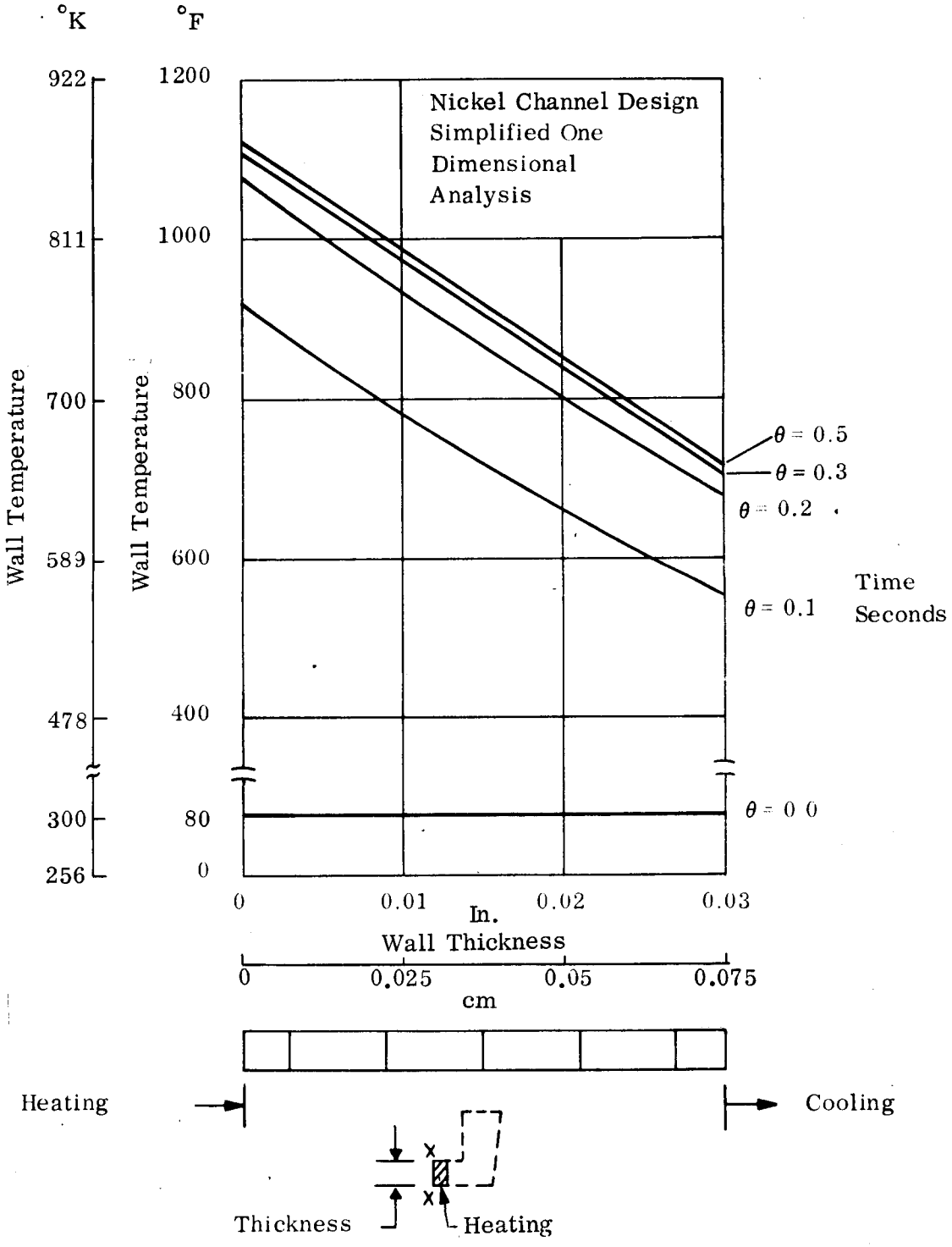

Figure 48. Wall Transient-Temperature Distribution

TABLE XV
LIST OF HEATING TRANSIENT ANALYSES

IBM Run No.	Type of Wall Construction	Combustion Efficiency	Wall Material	Passage Height (in.)	Passage Height (mm)	Wall Thickness (in.)	Wall Thickness (mm)	Time to Stabilize (secs)
1	Integral Wall	0.97	Copper	0.129	3.277	0.030	0.762	1.0
2		0.97		0.173	4.394	0.030	0.762	0.70
3		0.97		0.223	5.664	0.030	0.762	1.0
4		0.97		0.475	12.065	0.030	0.762	>1.0
5		0.97	Nickel	0.129	3.279	0.030	0.762	
6		0.97		0.173	4.394	0.030	0.762	2.0
7		0.97		0.223	5.664	0.030	0.762	2.0
8	Integral Wall	1.00		0.223	5.664	0.030	0.762	
9	Free Standing Liner	0.97	Copper	0.173	4.394	0.030	0.762	1.0
10		0.97		0.173	4.394	0.050	1.270	1.0
13		0.97	Nickel	0.173	4.394	0.030	0.762	1.0
14	Free Standing Liner	0.97		0.173	4.394	0.050	1.270	
11	Composite Integral	0.97	Copper Liner	0.173	4.394	0.030	0.762	1.0
	Wall Integral	0.97	+ Nickel Shell	0.173	4.394	0.030	0.762	
12	Composite Integral	0.97	Nickel Liner	0.173	4.394	0.030	0.762	1.0
			+ Copper Shell	0.173	4.394	0.030	0.762	1.0

No film cooling Passage width = 0.090 in. (2.286 mm)

Due to the parametric nature of the transient study, the transient flow of the hydrogen was ignored to simplify the analysis, and that omission was considered to be minor in its effect on the results. The section of wall was at the location of expected maximum heat flux and temperature gradients through the wall.

(2) Preliminary Thrust Liner Structural Analysis

The factors of safety used in the initial stress analysis of the thrust chamber were:

Material Yield - F.S. = 1.50
Material Ultimate - F.S. = 2.0

These factors were only applied to the stresses resulting from pressure loading. In conjunction with these factors minimum strength allowables, such as the "A" values of MIL-HDBK-5A, were used in the design along with the maximum expected operating temperatures. A factor of one was applied to all loads resulting from temperature gradients in the structure and were incorporated in addition to pressure stresses, in establishing fatigue capabilities which will be discussed below.

The preliminary nozzle liner calculations assumed that the section could be analyzed as an equivalent cylinder using the dimensions and temperatures of the throat station. Table XVII presents the nomenclature used for the analyses.

TABLE XVI
LIST OF SHUTDOWN ANALYSES

No.	Type of Wall Construction	Wall Material	Passage Height		Wall Thickness		Time To Stabilize
			in.	cm	in.	cm	sec
1.	Integral Wall	Nickel	0.129	3.277	0.030	0.076	2.0
2.	Integral Wall	Nickel	0.173	0.449	0.030	0.076	3.0
3.	Integral Wall	Nickel	0.223	0.566	0.030	0.076	4.8
4.	Integral Wall	Copper	0.192	0.488	0.030	0.076	0.5

TABLE XVII
NOMENCLATURE

R	mean radius of liner and/or closure (in.)
a, b	inner and outer radius of liner, respectively (in.)
T_i, T_o	inner and outer temperature of liner, respectively (^{0}F)
T_c	outer closure temperature (^{0}F)
α	coefficient of thermal expansion (10^{-6} in/in/^{0}F)
t	thickness of liner and/or closure (in.)
p_t	throat pressure (psia)
p_i	developed interface pressure (psi)
p_c	coolant pressure (psi)
p_{CR}	critical external buckling pressure (psi)
E	modulus of elasticity (10^6 psi)
μ	Poisson's ratio
ℓ	width of channel, cone length (in.)
P	developed longitudinal load resulting from differential thermal growth (lb)
A_H, A_L, A_C	longitudinal areas of components (in.^{2})
A	temperature parameter of land gradient = $\frac{4T_A - \Delta T_L}{\Delta T_L - 2T_A}$; $T_A = T_{MEAN} - T_{OUT}$; $\Delta T_L = T_{INNER} - T_{OUT}$
B	temperature parameter of land gradient = $\frac{T_A}{A+1}$
τ Avg	average cone radius (in.)
σ_e	effective uniaxial stress (psi)
σ_R,σ_L,σ_θ	radial, longitudinal, and circumferential stresses (psi)
σ_u	material ultimate stress (psi)
σ_f	actual fracture stress (psi)
R.A.	reduction in area
γ	developed cone angle (degrees)

Several regeneratively cooled designs were considered; these included an integral, rectangular-coolant channel structure in which the hot inner liner is metallurgically bonded to an electrodeposited outer closure or shell and also a free standing (nonintegral) liner and land configuration. The liner materials considered were: TD nickel, OFHC copper, zirconium copper (0.15% zirconium) and silver-copper (0.04% silver). The integral designs included electrodeposited nickel and copper. Since silver-copper and OFHC copper have essentially equal thermal conductivity and the former has superior strength properties, emphasis was placed on silver-copper.

Radial temperature gradients were determined for each configuration, initially assuming no film-cooling effects for the transient and steady-state operating conditions. The results showed that the inner liner developed a linear thermal gradient while that in the radial land was parabolic. The structural analysis, which incorporated the above gradients, was conducted for the circumferential and longitudinal directions at various times in the transient cycle to define the resultant stress and strain distributions.

For the integral wall designs, compatibility equations were derived for both directions and then were combined using the Von Mises yield criteria to arrive at an effective uniaxial stress and strain from which the thermal-fatigue life was determined. It was assumed that the radial land did not contribute any stresses in the circumferential direction. Therefore, the compatibility equation was the result of the differential thermal growths existing between the hot inner liner and outer closure shell. The compatibility equation used is:

$$\frac{2(1+\mu)\,\alpha_H\,(T_i - T_o)\,b}{t_H\,(b^2 - a^2)}\left[\frac{b^3}{6} - \frac{ba^2}{2} + \frac{a^3}{3}\right] + (1+\mu)\,\alpha_H\,(T_o - T_{Amb.}) + (p_t - p_i)\frac{R_H}{E_H\,T_H}^2 =$$

$$(1+\mu)\,\alpha_c\,(T_c - T_{amb}) + p_i\,\frac{R_c}{E_c\,t_c}^2$$

The equation was solved for the developed interface pressure (p_i) which was then used to determine the liner and closure stresses. The individual component stresses became:

Liner

$$\sigma_\theta = \pm\frac{\alpha_H \Delta TE_H}{2(1-\mu)} \pm \frac{p_c - p_t}{2}\frac{\ell^2}{t_H^2} - (p_i - p_t)\frac{R_H}{t_H}$$

Closure

$$\sigma_\theta = \pm\frac{p_i\,\ell^2}{2\,t_c^2} + p_i\,\frac{R_c}{t_c}$$

The compatibility equations for the longitudinal direction were derived across the interface joints of the liner-to-land, and land-to-closure. The criteria used was that the longitudinal strains were equal for the three components; thus the equations were:

Liner-to-Land Interface Joint

$$\frac{2\alpha_H (T_i - T_o)}{(1-2\mu^2)\, t_H (b^2 - a^2)} \left[\frac{b^3}{6} - \frac{ba^2}{2} + \frac{a^3}{3} \right] + (1+\mu)\, \alpha_H (T_o - T_{amb.}) - \frac{P_1}{A_H E_H} =$$

$$\alpha_L B \left(A + \frac{4}{3}\right) + \alpha_L (T_{o_L} - T_{amb.}) + (P_1 - P_2) \quad \frac{1}{A_L E_L}$$

Land-to-Closure Interface Joint

$$\alpha_L B \left(A + \frac{4}{3}\right) + \alpha_L (T_{o_L} - T_{amb.}) + (P_1 - P_2) \quad \frac{1}{A_L E_L} = (1+\mu)\alpha_C (T_C - T_{amb.}) + \frac{P_2}{A_C E_C}$$

These equations were solved for the interface loads (P_1, P_2) which are the result of the differential thermal expansion of the individual components.

The resulting component stresses were calculated with the following equations:

Liner

$$\sigma_L = \pm \frac{\alpha_H \Delta T E_H}{2(1-\mu)} - \frac{P_1}{A_H}$$

Land

(Because of the parabolic gradient, additional thermal stresses are developed.)

Hot Side

$$\sigma_L = -\alpha_L E_L B\left[A + \frac{8}{3}\right] + \frac{P_1 - P_2}{A_L}$$

Cold Side

$$\sigma_L = \alpha_L E_L B\left[A + \frac{4}{3}\right] + \frac{P_1 - P_2}{A_L}$$

Closure

$$\sigma_L = \frac{P_2}{A_C}$$

The criterion for establishing the closure thicknesses was based on maintaining a compression-mode stress throughout the inner liner at all times during the operating conditions, including transient and steady-state.

Once the maximum total stress location had been obtained in the structure, the effective uniaxial stress was determined from the Von Mises yield criteria, i.e.,:

$$\sigma_c = \frac{1}{\sqrt{2}}[\,\sigma_R - \sigma_L)^2 + (\sigma_L - \sigma_\theta)^2 + (\sigma_\theta - \sigma_R)^2\,]^{1/2}$$

The effective strain component was then obtained from the stress-strain temperature curve for the material. To be determine fatigue-life capability, it was assumed that the compression phase of a stress cycle does no damage from a fatigue criterion. Therefore, if the applied stress and/or strain was compression then the residual tension stress, if any, is determined during cool down and at room temperature. In general, the critical stresses occurred in the inner liner, which are compressively plastic at operating temperature. Figure 49 demonstrates the method used for determining the strain-range associated with the maximum developed residual tension-stress at room temperature. This strain was then incorporated in the Manson's formula relating total strain-range to fatigue-life, i.e.,

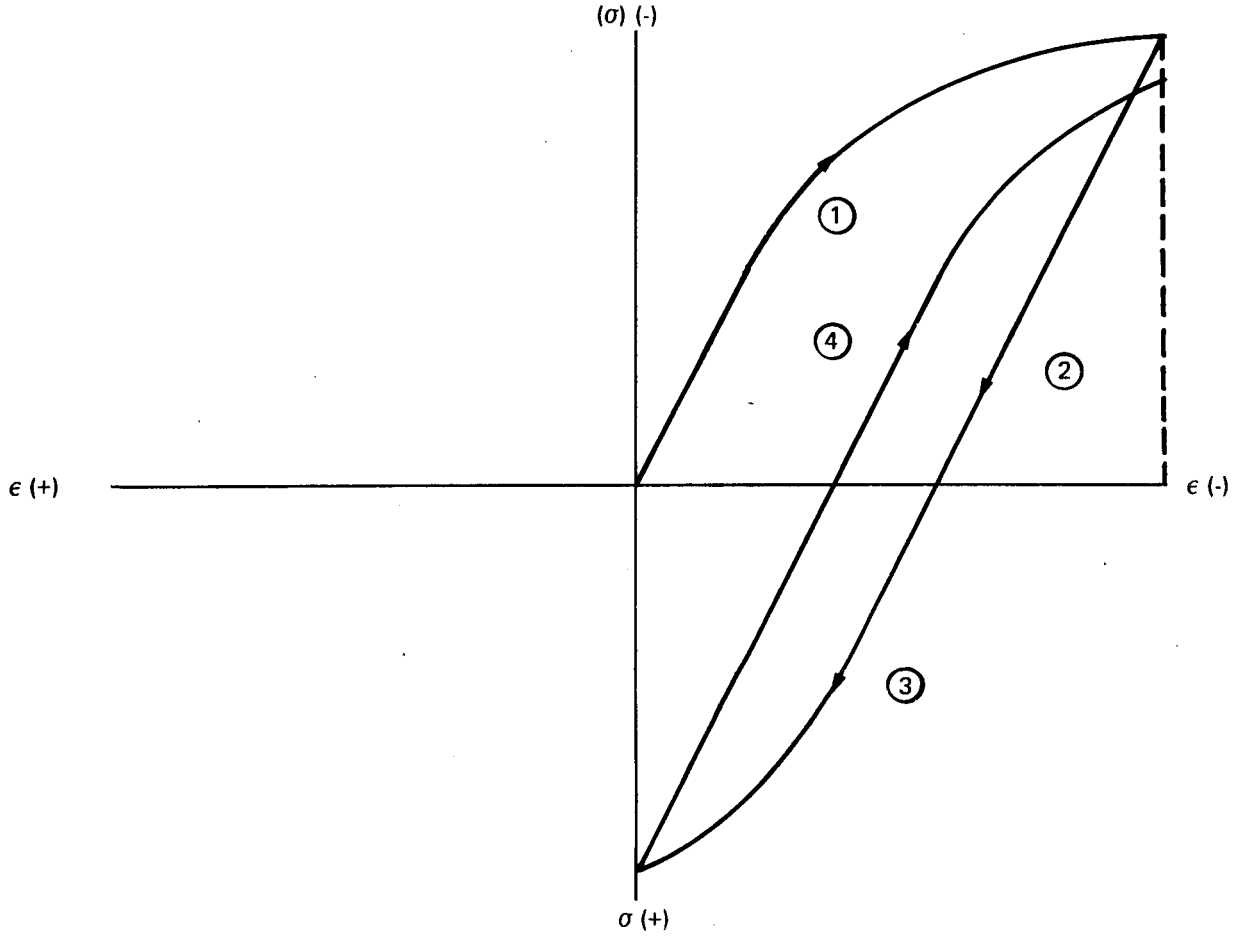

(1) Compressive stress buildup in the hot shell by the interface pressure as the result of differential thermal expansions.
(2) Elastic recoverable strain on cooldown as the interface pressure is relieved.
(3) Residual tensile stress in the hot shell as the result of cooldown.
(4) Stress reversal during recycle

Figure 49. Strain Range Based on Maximum Developed Residual Tension Stress

$$\epsilon_T = \frac{G}{E} N_f^{\gamma} + M N_f^{z}$$

where N_f = the number of cycles to failure

$$G = \frac{9}{4} \sigma_u \left(\frac{\sigma_f}{\sigma_u} \right)^{0.9}$$

$$\gamma = 0.083 - 0.166 \log \frac{\sigma_f}{\sigma_u}$$

$$M = 0.827\ D \left[1 - 82 \frac{\sigma_u}{E} \left(\frac{\sigma_f}{\sigma_u} \right)^{0.179} \right]^{-1/3}$$

$$z = 0.52 - 1/4 \log D + 1/3 \log \left[1 - 82 \frac{\sigma_u}{E} \left(\frac{\sigma_f}{\sigma_u} \right)^{0.179} \right]$$

and

$$D = - \text{Ln} (1 - \text{R.A.})$$

For the copper-liner-to-electrodeposited-copper closure design the critical stress occurred in the outer shell. The stress mode was tensile; therefore, the fatigue-life capability was determined during the operating conditions of the chamber.

The analysis of the free-standing liner designs used the same techniques as for the integral-wall configurations. Since there was no outer closure associated with this design, the compatibility equations are quite simplified, and also the total stress loading is reduced. An additional analysis is required for this design due to the potential of elastic buckling of the liner from external pressure in the "hot" condition. The following model was used for the required thickness:

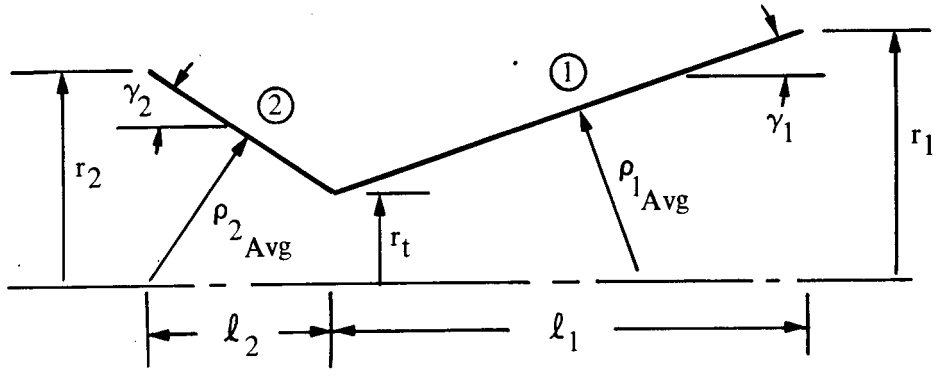

It was assumed that the liner was composed of two distinct conical shells with restraining boundaries at the throat and exit areas. The buckling equation used was:

$$P_{cr} = \frac{0.74E}{\left(\frac{\ell}{\rho_{Avg}}\right)\left(\frac{\rho_{Avg}}{t}\right)^{5/2}}$$

A factor of safety of two was also used in the analysis.

For each design the fatigue-life capability was determined for steady-state and pulse-mode operations. These were then incorporated into the cumulative-damage equation which is:

$$N = \frac{9 \times 10^5}{N_{f_p}} + \frac{1 \times 10^5}{N_{f_s}} + \frac{50}{t_r} \leqslant 1$$

N_{f_p} = Pulse-Mode-Fatigue Capability

N_{f_s} = Steady-State-Fatigue Capability

t_r = Time to Rupture in Hours

The time, t_r was determined from stress-rupture data based on the continuous load application resulting from the maximum thermal and mechanical stresses. If the sum of the three factors is greater than one, the design would not meet the life cycle criteria.

One method, which was apparently available for reducing the thermal load, was the application of film cooling. The predicted wall temperatures with film cooling were considerably less than without film cooling. Additional analyses were conducted assuming a 10% effective film cooling for the most promising designs.

Tables XVIII and XIX list the results of the analyses of these designs for the reverse-flow thrust chamber. It was apparent that the free-standing zirconium-copper liner exhibited the optimum fatigue characteristic for the stated design criteria. The free standing zirconium liner cummulative damage, N, was much less than 1. Several silver copper-alloy free-standing liner thicknesses were investigated without considering the previously stated buckling design mode to determine critical-fatigue parameters for each design. The result was that the pulse-mode factor increased while that for the steady-state decreased for increased liner thickness. The required liner thickness for the external pressure buckling design was 0.070 inch (1.778 mm) for both copper alloys. Table XIX shows a significant increase in fatigue capability for a 10% film-cooled design based on the predicted wall temperature reduction.

(3) Combustion Chamber and Nozzle Extension

The effectiveness of combustion chamber film cooling inherent in the reverse flow thrust chamber indicated essentially no problem in achieving combustion chamber wall temperatures which would be consistent with the life cycle requirements at nominal operating conditions. Preliminary calculations indicated that the stainless steel chamber and the anticipated maximum wall temperature of 1200 to 1300°F (922 to 978°K) [based on data from the 1K (4,448 N) engine] would far exceed the contract goals. Thermal review of off-design operation, high and low O/F at a P_c of 300 psia (206.8 N/cm^2), 100 and 500 psia (68.95 and 344.7 N/cm^2) chamber pressure at an O/F of 4 and low feed temperature operation appeared to present no problem. High feed temperature operation required empirical inputs

TABLE XVIII
CUMULATIVE DAMAGE – REGEN THROAT (0% FILM COOLED)
(9 x 10^5 PULSES, 1 x 10^5 STEADY STATE)

Chamber Design	Max. Wall Temp. (T_{wg})	Cumulative Damage Factors (0% Film-Cooled)						
		Pulse		Steady State		Creep		
		N_{fp}	$9 \times 10^5 / N_{fp}$	N_{fs}	$1 \times 10^5 / N_{fs}$	t_r	$50 / t_r$	N
Integral TD Ni/ED Ni	1190°F (917°K)	1.25 x 10^5	7.200	2.15 x 10^4	4.65	> 1000	0.050	11.900
Integral Ag Cu/ED Ni	780°F (689°K)	1.5 x 10^5	6.000	3.2 x 10^4	3.12	> 1000	0.050	9.170
Integral Ag Cu/ED Cu	619°F (599°K)	2.6 x 10^5	3.460	1.3 x 10^5	0.770	> 1000	0.050	4.280
Free-Standing Ag Cu [t = 0.030 in. (0.762 mm)]	640°F (611°K)	8.6 x 10^5	1.046	3.2 x 10^5	0.312	> 1000	0.050	1.408
[t = 0.050 in. (1.270 mm)]	676°F (631°K)	1.2 x 10^6	0.750	2.75 x 10^5	0.364	> 1000	0.050	1.164
[t = 0.070 in. (1.778 mm)]	715°F (653°K)	1.1 x 10^6	0.820	1.1 x 10^5	0.910	> 1000	0.050	1.780
Free-Standing Amzirc [t = 0.070 in. (1.778 mm)]	715°F (653°K)	4 x 10^9	–	7.6 x 10^5	0.130	> 1000	0.050	0.180
Free-Standing TD Ni (t = 0.030 in.) (0.76 mm)	1172°F (907°K)	9.2 x 10^6	0.098	4.6 x 10^4	2.170	> 1000	0.050	2.318
Free-Standing TD Ni (t = 0.050 in.) (1.27 mm)	1308°F (982°K)	2.0 x 10^8	0.005	2.6 x 10^4	3.85	> 1000	0.050	3.905

TABLE XIX
CUMULATIVE DAMAGE – REGEN THROAT
(10% FILM COOLED)(9 x 10^5 PULSES, 1 x 10^5 STEADY STATE)

Chamber Design	Max. Wall Temp. (T_{wg})	Cumulative Damage Factors (10% Film-Cooled)						
		Pulse		Steady State		Creep		
		N_{fp}	$9 \times 10^5 / N_{fp}$	N_{fs}	$1 \times 10^5 / N_{fs}$	t_r	$50 / t_r$	N
Integral TD Ni/ED Ni	692°F (640°K)	1.0 x 10^{12}	9.0 x 10^{-7}	2.1 x 10^6	0.048	> 1000	0.050	0.098
Integral Ag Cu/ED Ni	467°F (515°K)	8.0 x 10^5	1.125	1.9 x 10^5	0.526	> 1000	0.050	1.701
Integral Ag Cu/ED Cu	389°F (472°K)	1.0 x 10^6	0.90	5.4 x 10^5	0.185	> 1000	0.050	1.135
Free-Standing Ag Cu (t = 0.050 in.) (0.127 cm)	418°F (488°K)	3.3 x 10^7	0.027	7.2 x 10^6	0.014	> 1000	0.050	0.091

Preliminary structural calculations showed that a stainless steel nozzle extension would meet the life cycle requirements if the peak temperature were 2000°F (1367°K) or below, as previously discussed. The cycle life capability of the columbium oxidation-resistant coating was not amenable to analyses.

d. Selection of Configurations

The analyses of the candidate cooled thrust chamber configurations concluded that a fully regenerative cooled throat and nozzle extension, with some film cooling upstream of the throat, could meet the I_{sp} and fuel pressure drop goals and the specified 800°F (700°K) outside surface temperature at the expense of engine weight and the flexibility of vehicle installation. But the calculated effectiveness of the film cooling in the divergent nozzle was based on the projection of semi-empirical equations. The flexibility of vehicle installation was a consideration not explicitly included in the contract requirements. An external dump cooled nozzle extension (case E of Table VIII) had the undesirable features of both Isp loss relative to the fully regenerative cooled configuration while maintaining most of the weight associated with the regenerative cooled design. A free standing zirconium copper nozzle liner, the critical component for thrust chamber cycle life, indicated a capability in excess of the stated cycle life requirements without the use of additional film cooling. The attractive weight and vehicle installation flexibility of the dump cooled nozzle extensions presented the potential problem of Isp reduction below the contract goal if the required percentage of dump coolant exceeded approximately 7% of the total H_2 flow. The percentage of dump coolant necessary would be a function of the nozzle extension material selected, stainless steel, super alloy or columbium. A columbium extension would require the least dump cooling. The cycle life of the oxidation resistant coating of a columbium extension was not amenable to analysis. The analyses and characteristics of the reverse flow engine clearly identified a stainless steel combustion chamber. Thus the combustion chamber and nozzle section liner were fixed; the nozzle extension and the type of cooling to be employed had several alternatives.

The analyses of the candidate cooled thrust chamber configurations lead to the conclusion that both film cooling and dump cooling should be characterized with both regenerative and insulated nozzle extensions. The program scope did not permit separate thrust chamber assemblies for each of the configurations. Therefore, the recommendation was made to design altitude test hardware that would allow interchangeability of liners and nozzle extensions. Three regenerative cooled liners were proposed; one with regenerative cooling passages only, one with film cooling slots and one with provision for varying percentages of dump cooling. Two nozzle extensions were recommended; a drilled alumium extension which could be operated with either H_2 regenerative coolant or with water coolant and a columbium nozzle extension. The columbium extension was selected so that the widest range of dump cooling could be evaluated.

The proposed configurations of cooled thrust chamber hardware were approved by the NASA Lewis Project Manager together with a detailed plan of test firing evaluations. The detailed analyses for the test hardware design is described in the following subsections.

C. DETAILED ANALYSES OF COOLED NOZZLE LINERS, 540°R (300°K) FEED TEMPERATURE DESIGNS

1. Regeneratively Cooled, Nominal Test Conditions

a. Thermal Analyses and Passage Sizing

The detailed heat transfer analysis of the Amzirc nozzle liner included a sequence of analyses to size the coolant passages to provide cooling for a maximum combustion side wall temperature target of 750°F (672°K) at a chamber pressure of 300 psia (206.8 N/cm^2), O/F of 4.0 and a propellant inlet temperature of 540°R (300°K). The thermal conductivity of . was taken from Reference 18.

The starting point for the Amzirc liner analysis was the cooling passage geometry developed for the nickel 200 liner described in the off-design characteristics in the preceding subsection and whose passage dimensions are shown by Figure 45. Heights and widths of the rectangular passages had been determined by solving the coolant side heat transfer coefficient for a constant 1300°F (978°K) nickel wall temperature and the local heat flux. A layout drawing of the passage geometry was made with modifications to simplify the electrodischarge machining of the passages and to incorporate the detailed fuel injection geometry. A one dimensional heat balance was made to establish the coolant side (h_ℓ) and gas side (h_g) heat transfer coefficients at various stations where detailed two dimensional analyses were required using the passage geometry and a 0.070-inch (0.178 cm) thick Amzirc wall. The justification for use of the method for calculation of the heat transfer coefficients was made by correlations of the test data with analysis for the 1000 lbf (4448 N) reverse-flow engine presented in the Appendix B. Distribution of the nominal gas side heat transfer coefficient used in the analysis appears in Figure 50. The gas-side heat-transfer coefficient for the 1500 lbf (6672 N) engine was justified by heat rejection rates reduced from copper heat-sink test data developed during injector tests at sea level. The test results are presented in Section XI of this report.

Nodal cross-sectional mathematical models were made of the free-standing liner using the original passage dimensions of Figure 45. The results of the analysis indicated that the passages overcooled the copper alloy nozzle. This is attributed to the "fin effect" or the ability of the highly conductive material to conduct heat up the lands. Results of the calculations for the two-dimensional heat transfer models compared to the one-dimensional case are shown on Figure 51. A maximum deviation in excess of 20% aft of the throat is due in part to the change in passage depth to width ratio.

The two-dimensional heat transfer results of Figure 51 were used to update the coolant bulk temperature distribution solved in the initial one-dimensional analysis of the Cu-Zr liner. Iterations of these calculations were made with passage configuration modifications until a target wall temperature ≈ 750°F (672°K) was approached. The flow passage dimensions resulting from the calculations are presented in Figure 52. Significant temperatures through the Cu-Zr alloy wall at various stations are listed in Table XX. The nodal models are 1/80 of the local circumference because of symmetry about coolant passage and land of the 40-slot configuration.

The analysis included 18 nodal points for each segment. A short section of the liner at the point of fuel injection includes an integral cooling passage as shown in the table. The

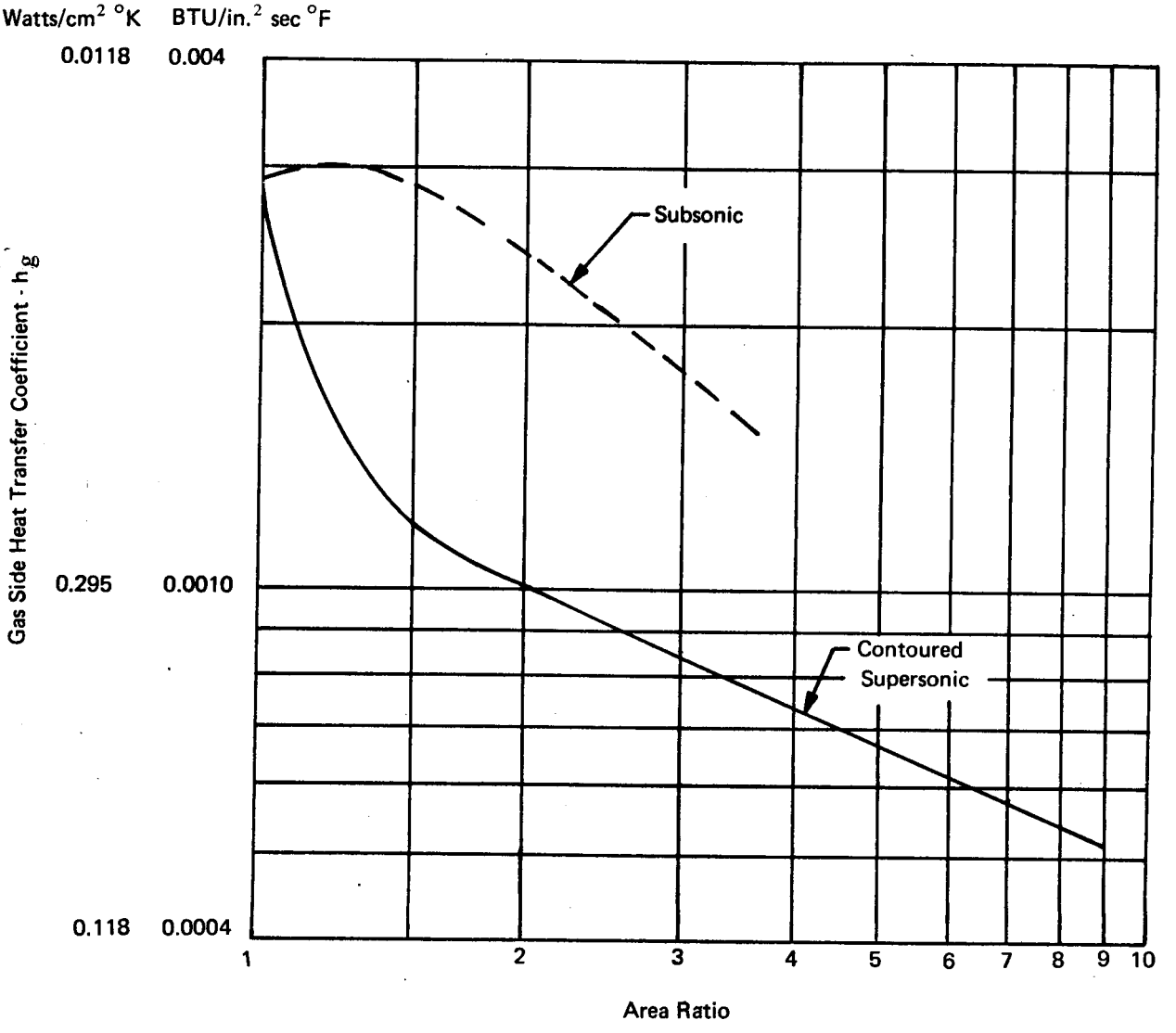

P_c = 300 psi (206.8 N/cm²)
O/F = 4/1
D_T = 1.90 in. (4.826 cm)
T_W = 750°F (672°K)

Figure 50. Gas-Side Heat Transfer Coefficient Distribution, Altitude Nozzle Liner

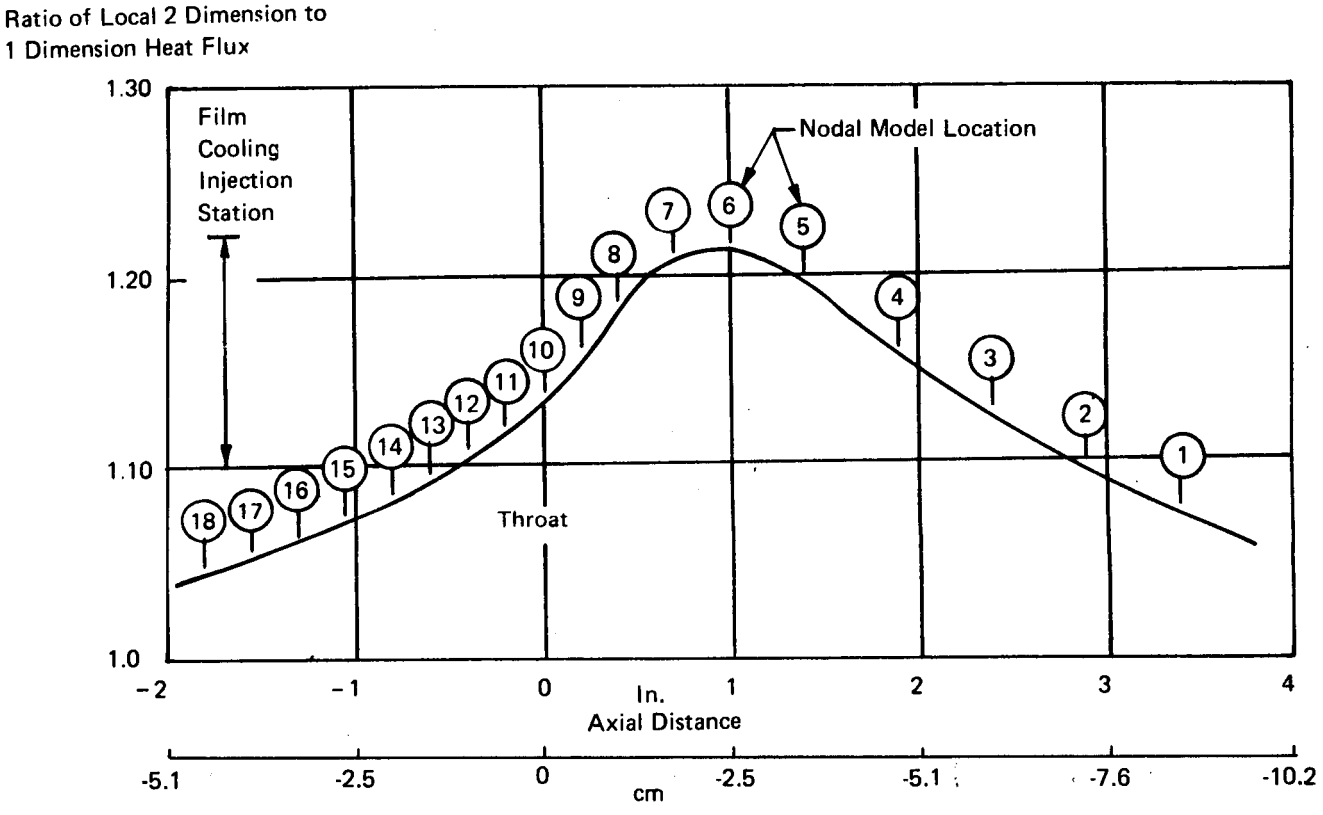

Figure 51. Two-Dimensional Heat Flux Deviation Distribution

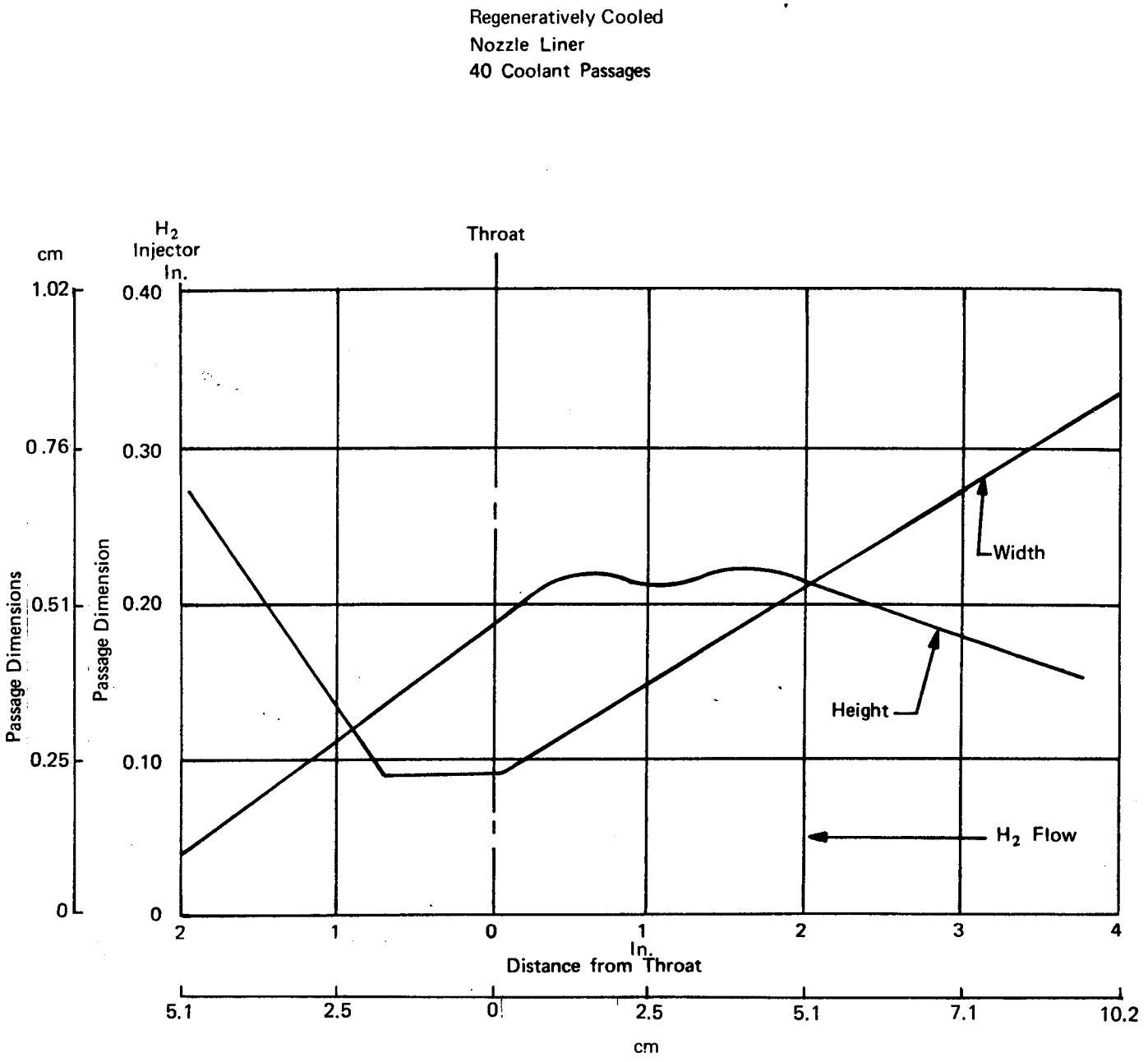

Figure 52. Rectangular Passage Dimensions - Altitude Nozzle

TABLE XX
WALL TEMPERATURE DISTRIBUTION REGENERATIVE LINER

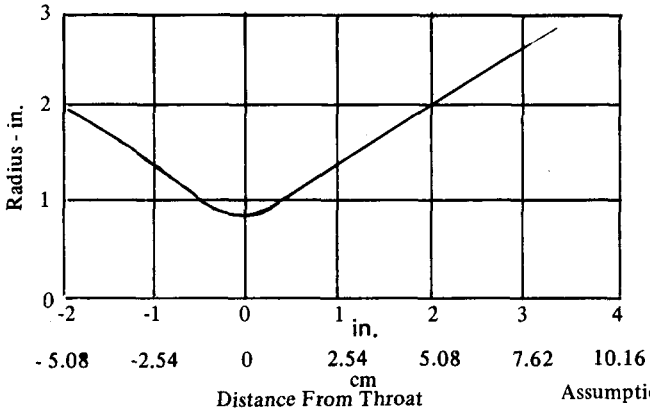

Assumptions

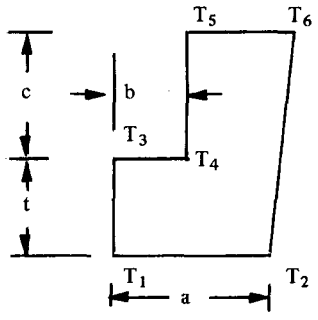

Free-Standing Sections

40 Passages
Mixture Ratio = 4/1

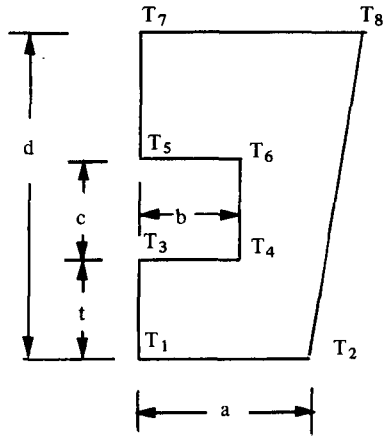

Integral Sections

	Dimensions											
	x		t		a		b		c		d	
	in.	cm	in.	cm	in.	cm	in.	cm	in.	cm	in.	cm
Subsonic Nozzle	0	0	0.070	0.178	0.0745	0.1892	0.045	0.1143	0.182	0.462		
	-0.4	-1.016	0.070	0.178	0.0778	0.1976	0.045	0.1143	0.161	0.409		
	-0.8	-2.032	0.070	0.178	0.0873	0.2217	0.0525	0.1334	0.121	0.307		
	-1.05	-2.667	0.070	0.178	0.0978	0.2484	0.0705	0.1791	0.102	0.259		
	-1.30	-3.302	0.070	0.178	0.1116	0.2835	0.088	0.2235	0.085	0.216		
	-1.55	-3.937	0.070	0.178	0.1271	0.3228	0.1068	0.2713	0.068	0.173		
	-1.80	-4.572	0.070	0.178	0.143	0.3632	0.124	0.315	0.053	0.135	0.375	0.9525
	-1.94	-4.928	0.070	0.178	0.157	0.3988	0.137	0.348	0.0438	0.1113	0.1838	0.4669
Altitude Supersonic Nozzle	0.7	1.778	0.070	0.178	0.0962	0.2443	0.0655	0.1664	0.220	0.559		
	1.4	3.556	0.070	0.178	0.1327	0.3371	0.0875	0.2223	0.220	0.559		
	2.4	6.096	0.070	0.178	0.1885	0.4788	0.1185	0.3010	0.20	0.508		
	3.4	8.636	0.105	0.2667	0.220	0.5588	0.150	0.3810	0.164	0.417		

	Wall Temperature															
	T_1		T_2		T_3		T_4		T_5		T_6		T_7		T_8	
	°F	°K	°F	°K	°F	°K	°F	°K	°F	°K	°F	°K	°F	°K	°F	°K
Subsonic Nozzle	675	631	666	626	534	552	496	531	258	400	268	404				
	686	637	654	619	548	560	505	536	290	417	306	425				
	706	648	715	652	577	576	538	554	358	454	381	467				
	748	671	725	659	611	595	568	571	405	481	424	491				
	715	652	692	641	596	587	552	562	422	490	437	499				
	680	633	659	622	577	576	539	555	449	505	463	513				
	552	562	522	545	468	515	414	486	255	397	288	415	271	406	272	407
	542	557	506	536	506	536	454	508	288	415	341	445	293	418	338	443
Altitude Supersonic Nozzle	593	585	581	579	543	557	514	541	352	451	357	454				
	650	617	634	608	612	596	581	578	457	510	466	514				
	745	669	725	659	709	649	683	635	610	595	623	601				
	729	661	719	655	691	639	672	629	617	598	627	603				

remaining sections are free-standing; there is no attachment between the liner and the aluminum shroud. In all cases some heat flows crosswise through the walls from the centerline of the passage over to and up the land.

The heat fluxes to the copper nozzle used in the injector test program were compared to a regeneratively cooled nozzle section with a coolant passage 0.090 inch (0.229 cm) wide by 0.173 inch (0.439 cm) deep or the regeneratively cooled liner passage dimensions just forward of the throat station. It was found, as shown in Figure 53 that the wall temperatures on the gas side of the 0.070 inch (0.178 cm) thick AMZIRC wall varied nearly linearly with the heat flux to the wall over the range of interest, heat flux to the copper wall from 7 to 15 BTU/in.^{2} sec (1144 to 2451 w/cm^2). The plot was prepared to relate the injector test data to operation with the regeneratively cooled nozzle section. The test data will be discussed further in Section XI. The lower limit of the test data, as indicated in Figure 53 is consistent with the heating rates assumed for the liner thermal analyses.

b. Pressure Drop

The calculations for the passage areas are constrained by the coolant jacket pressure drop. The overall pressure drop includes the fuel injection ΔP and the need to provide a smooth transition from the cooling passages to the point of fuel injection. The total ΔP target for the liner and fuel injector was set at 75 psi (51. N/cm^2) at 540°R (300°K) inlet. An increase in allowable pressure drop or a decrease of fuel injection velocity would allow design for a lower T_{wg} at the same condition of heat flux to the wall.

The calculated coolant flow parameters for the complete nozzle liner are depicted in Figure 54. The major portion of the pressure loss occurs in the liner upstream of the throat. The two inflection points on the coolant Mach number distribution are caused by:

1. Minimum flow areas at maximum heat flux locations near the nozzle throat, and

2. Reaccelerating the flow from areas of reduced cooling to a final high exit Mach number at the exit.

The variation of coolant total pressure in the passage as a function of surface roughness is presented in Figure 55. Increasing the surface finish roughness from an expected value of 63 microinches (1.6 μ) to 125 microinches (3.175 μ) would increase the feed pressure 2.0 psia (1.38 N/cm^2). Therefore, the effect of surface finish is small. The surface finish resulting from electrodischarge machining was considered acceptable.

c. Fuel Injector Flow Analysis

At the fuel injection station and for a short distance aft of that plane, the liner was defined as an integral configuration to provide dimensional stability of the fuel injection area and provide axial clamping of the liner. The hydrogen passage configuration was dictated not only by the requirement of cooling the wall but to provide, at the injector end, an injection velocity sufficient to assure high combustion efficiencies. This subject is also discussed in Section IV, Injector Design and Analyses.

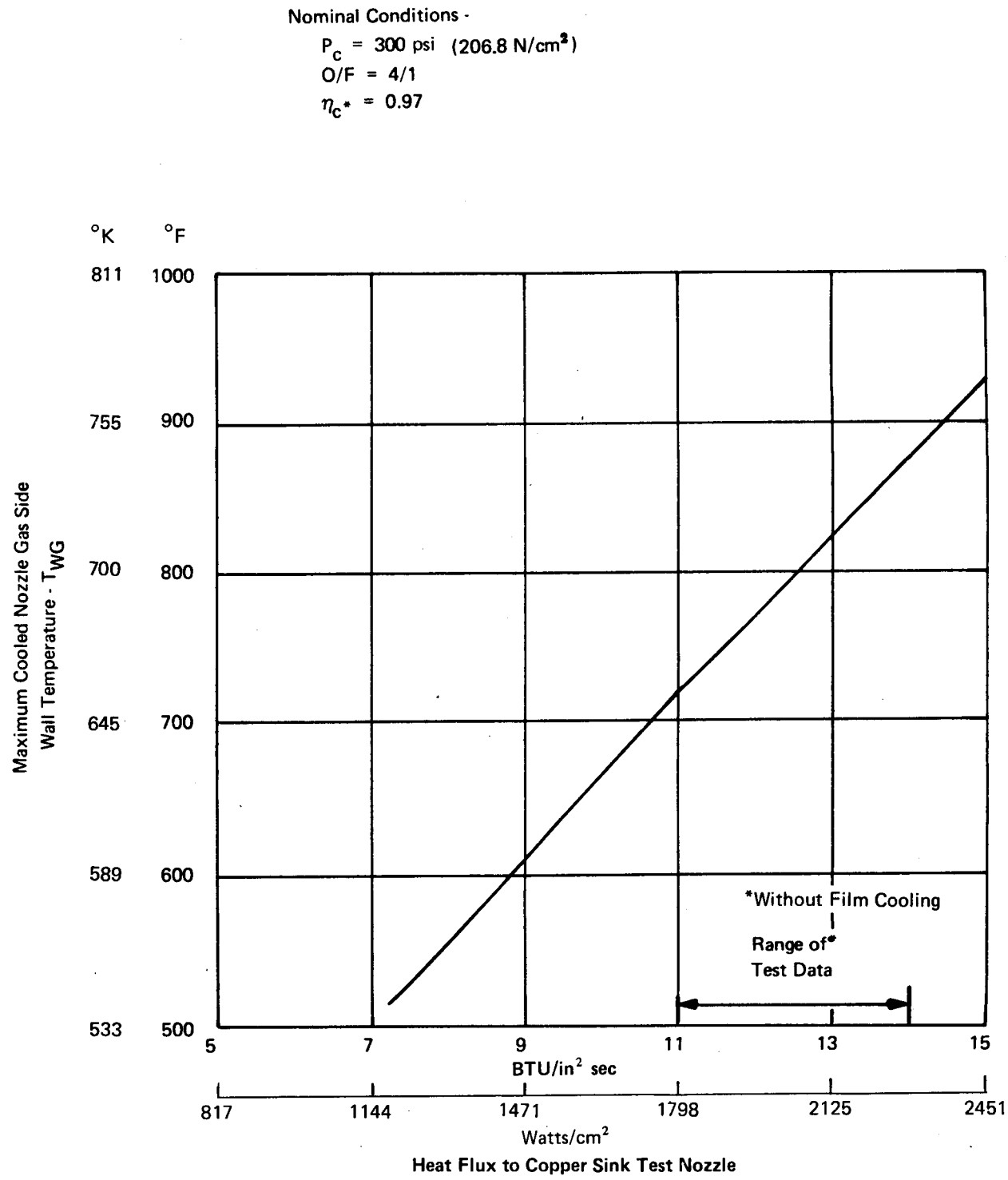

Figure 53. Wall Temperature versus Copper Test Nozzle Heat Flux

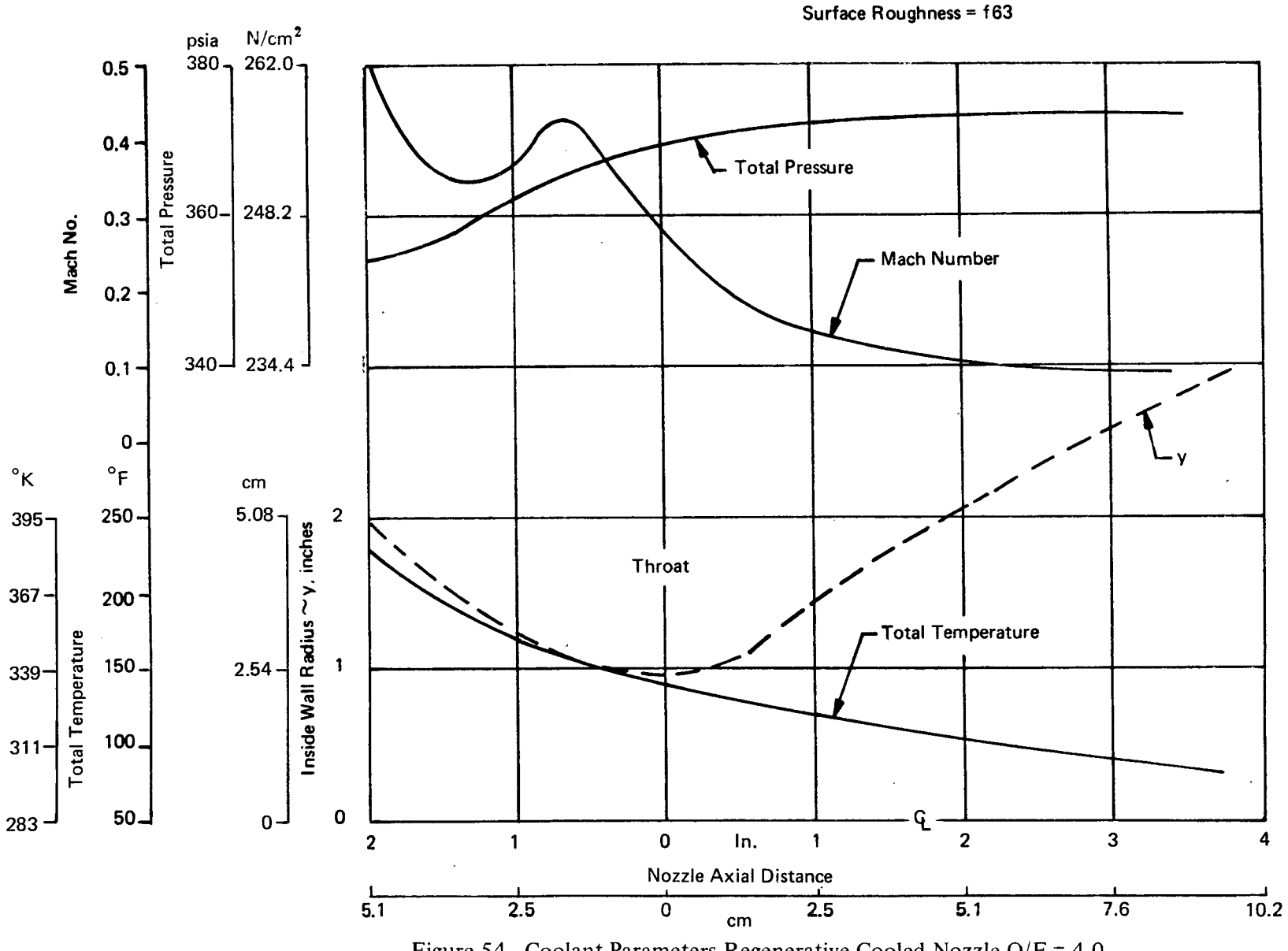

Figure 54. Coolant Parameters Regenerative Cooled Nozzle O/F = 4.0

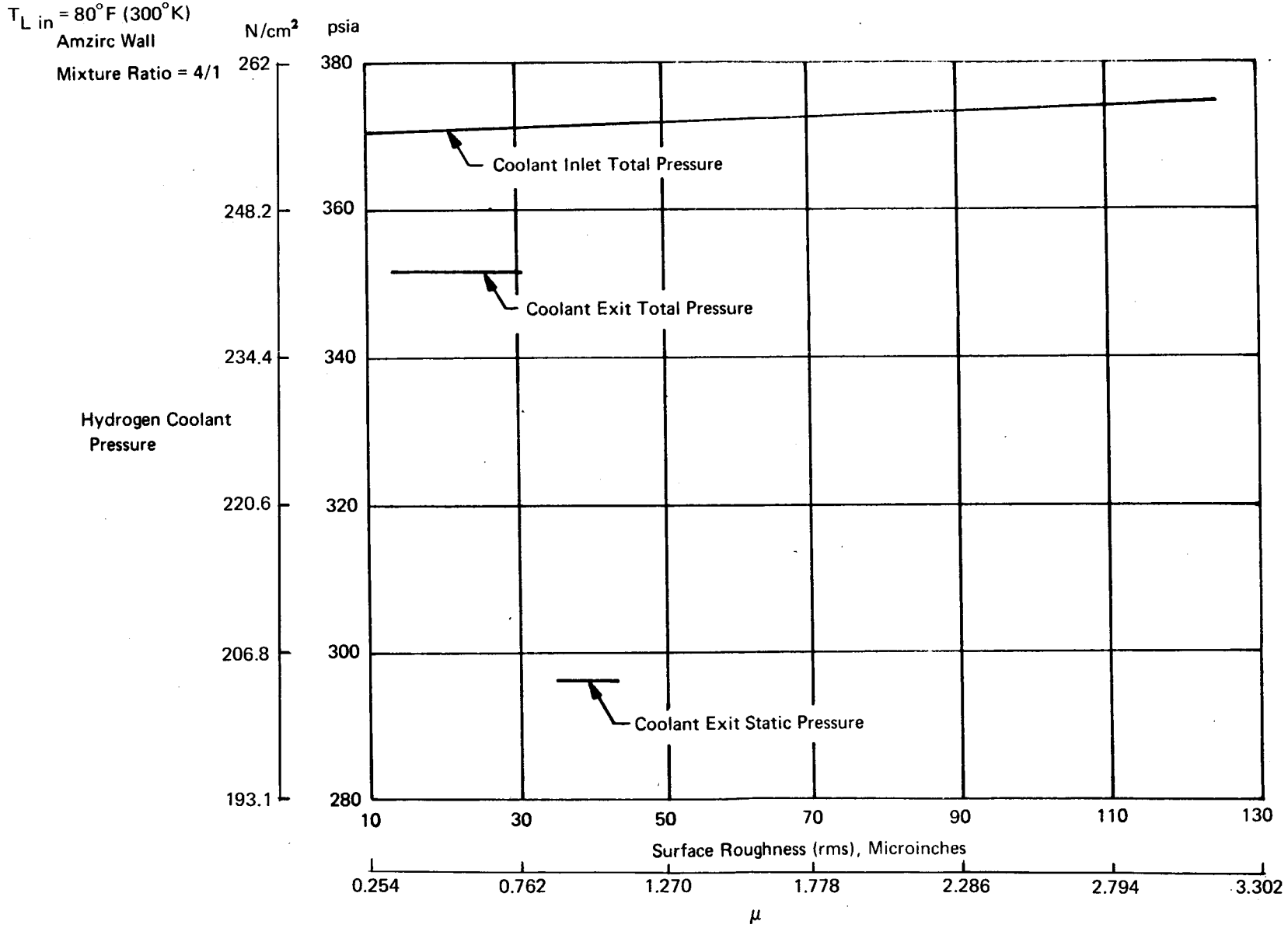

Figure 55. Coolant Passage Pressure versus Channel Surface Finish

Fuel injector exit flow areas were calculated using the law of continuity, a specified velocity and the exit total temperature of the H_2 regenerative coolant. The H_2 total temperature was a byproduct of the heat transfer analysis. The injection velocity was defined by the injector testing. The flow parameters, for the nominal case are:

Coolant Inlet Temperature, °R	540 (300°K)
Mixture Ratio	4/1
Coolant Outlet Total Temperature, °F	208 (371°K)
Coolant Flow Rate, lbm/sec	0.6896 (0.3131 kg/sec)
Exit Mach Number	0.513
Exit Sonic Velocity, fps	4680 (1427 m/sec)
Exit Velocity, fps	2403 (740 m/sec)
Exit Total Flow Area, in.^{2}	0.4713 (3.04 cm^2)

The individual fuel slots were calculated as 0.0438 inch (0.111 cm) high by 0.274 inch (0.695 cm) wide for the above conditions. The injector area to transition area was studied to establish the pressure drop of the length of passage 0.0438 inch (0.111 cm) x 0.274 inch (0.695 cm) included in the design. Frictional effects and heat addition to the hydrogen were included in the calculations. The calculated ΔP loss seen in Figure 56, increased rapidly with both surface finish and passage length, because of both high Mach number and small hydraulic diameter. The pressure drop characteristics dictated a minimum length of the fuel injection slot consistent with fabrication capability. A length, L, of 0.04 inch (0.102 cm) was specified for the slot depth after review with the EDM fabricator.

d. Structural Analysis

The preliminary structural investigation of the freestanding nozzle concept for the reverse flow thrust chamber, determined that a copper-zirconium (CU-Zr) alloy (AMZIRC) possesses the best characteristics for the engine design requirements of high thermal fatigue life and good creep deformation resistance. In addition, the resistance of the alloy to hydrogen embrittlement was rated as comparable to OFHC copper. The detailed structural analyses were conducted using the following room temperature properties of the zirconium copper material:

Ultimate Strength	-	45,000 psi (31,026 N/cm^2)
Yield Strength	-	33,000 psi (22,753 N/cm^2)
Elongation in 2 in (5.08 cm)	-	25%
Reduction in Area	-	80%

These properties can be considered the minimum which can be maintained through normal manufacturing techniques and after exposure to the engine temperature cycling. Although the effects of temperature on these properties is not directly available through the literature, strength/temperature plots were generated by using the direct ratio of the properties to a known strength variation curve for a similarly cold worked copper-zirconium alloy. Figure 57 shows the effects of temperatures on strength as determined by this method. Metallurgical tests are required to confirm the cyclic capability and creep life to confirm Manson's equation for Amzirc with the above minimum properties.

The elevated temperature Cu-Zr material properties were incorporated into the structural (thermal and pressure) analysis to update the operating fatigue life capabilities (pulse and

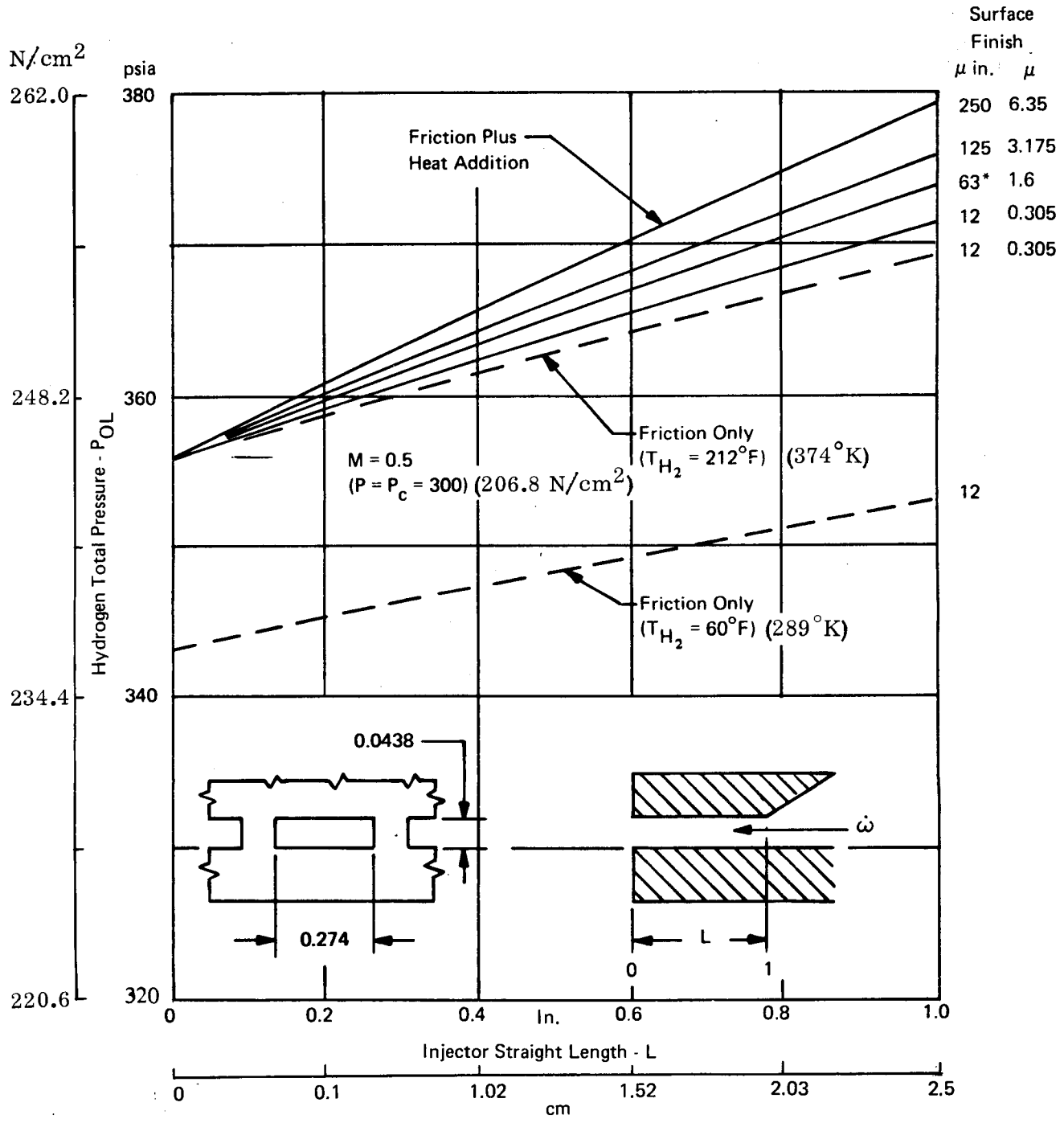

Figure 56. Total Pressure Loss in a Constant Area Injector Exit

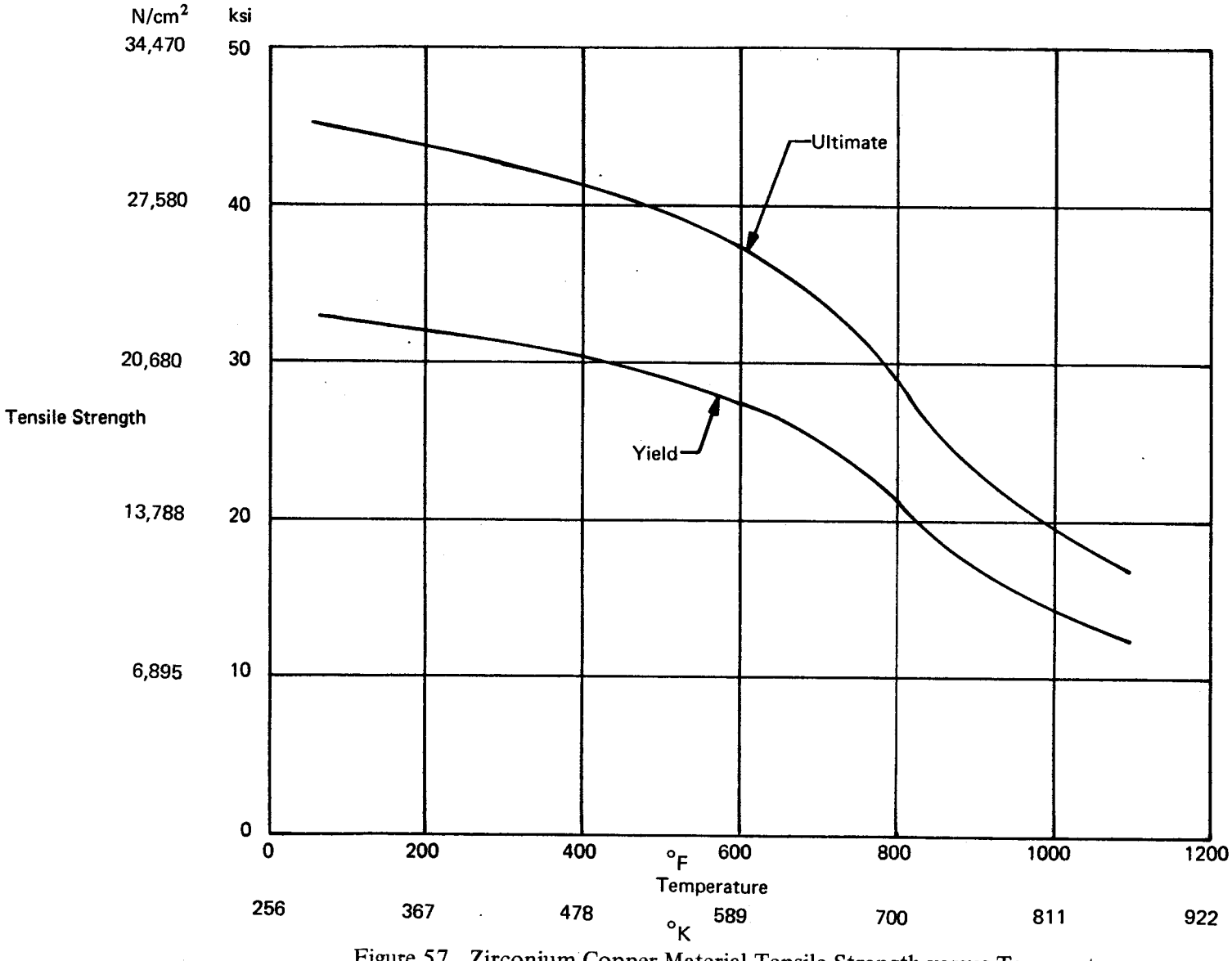

Figure 57. Zirconium Copper Material Tensile Strength versus Temperature

steady-state) of the liner. The effects of 5 and 10% film cooling on the fatigue life capabilities were also determined for the Cu-Zr material, as shown in Table XXI. The film cooling analysis was limited to a station 0.6 inch (1.52 cm) forward to the throat. Also shown in the data for the silver-copper alloy corrected to a 0.070 inch (0.178 cm) wall thickness where the 0.070 in. (0.178 cm) thickness was established by buckling calculations. The table shows that the Cu-Zr material exhibits excellent fatigue life characteristics for the chamber nominal operating conditions and for the condition of a maximum liner wall temperature of 715°F (652°K). Based on these results, it was apparent that the Cu-Zr alloy would provide the design life capabilities with margin and a small amount of film cooling could provide an increase in the design margin of the predicted film cooling temperature reductions. The analysis for the complete axial temperature profile for the film cooling cases would not show as large an improvement as that calculated for 0.60 inch (0.152 cm) forward of the throat.

TABLE XXI
CUMULATIVE DAMAGE FACTORS
LINER THICKNESS = 0.070 in.

Film Cooling %	Material	Max. Wall Temp. Twg. °F	Max. Wall Temp. Twg. °K	Cumulative Damage Factors: Pulse N_{f_p}	Pulse $9. \times 10^5$ N_{f_p}	Steady State N_{fs}	Steady State $1. \times 10^5$ N_{fs}	Creep t_R	Creep 50 t_R	N
0	Ag. Copper	715.2	652.9	1.1×10^6	0.82	1.1×10^5	0.91	>1000	0.050	1.78
0	Amzirc	715.2	652.9	$4. \times 10^9$	-	7.6×10^5	0.13	>1000	0.050	0.18
5	Ag. Copper	525.3*	547.4*	7.6×10^6	0.12	4.7×10^5	0.21	>1000	0.050	0.38
5	Amzirc	525.3*	547.4*	$> 10^{12}$	-	1.3×10^8	-	>1000	0.050	0.05
10	Ag. Copper	439.9*	499.9*	2.8×10^7	0.03	1.25×10^6	0.08	>1000	0.050	0.16
10	Amzirc	439.9*	499.9*	$> 10^{12}$	-	$> 10^{12}$	-	>1000	0.050	0.05

* 0.6 in. (15.24mm) Forward of Throat Only

A parametric investigation was conducted on the nozzle section liner to determine the effects of gas side wall temperatures on the structural cumulative damage factor. The results of these analyses for a Cu-Zr alloy are shown in Figure 58 . It becomes apparent from this curve that the cumulative damage factor increases significantly above about 700°F (645°K) and that an optimum chamber design would be one in which the T_{wg} is maintained at or below that temperature. The "optimum" chamber is associated with the distinction between pulse and steady-state operation as described in the following paragraph.

A study was conducted on the liner to determine the critical thermal and pressure stress distribution versus chamber operating time to define pulse and steady-state stress levels. It was found that the stresses reached steady-state values fairly early in the duty cycle, at approximately 0.2 second. Therefore, a criterion was established in which a stress of about one-half that at steady-state was selected for a pulse mode stress level. This particular stress occurred at 50 milliseconds into the duty cycle; thus, the pulse mode loading environment was defined as that which existed at 0.050 second of engine operation. The restrictiveness of this definition would be

$$N = \frac{9 \times 10^5}{N_{f_P}} + \frac{1 \times 10^5}{N_{f_S}} + \frac{50}{t_R}$$

N	N_{f_P}	N_{f_S}	t_R
1.0	1×10^8	1.07×10^5	> 1000
0.5	3.6×10^9	2.1×10^5	> 1000
0.1	$>10^{10}$	2.3×10^7	> 1000

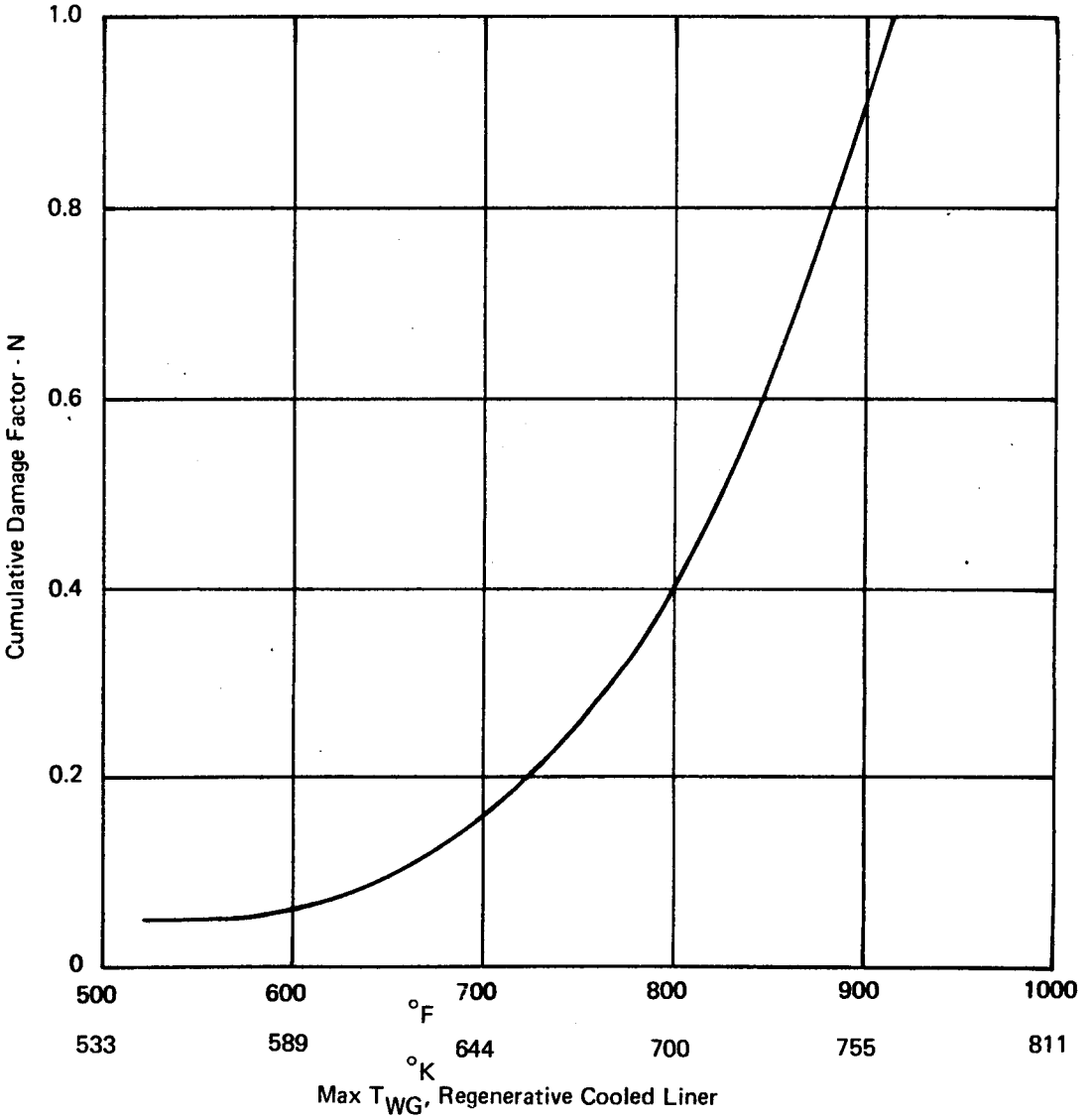

Figure 58. Free Standing Amzirc Liner - Cumulative Damage Factor versus T_{wall} Gas

eliminated for liner temperatures associated with a cumulative damage of about 0.2 or below because the steady-state firing capability would approach or exceed 1 x 10^6 cycles.

In order to ensure a free-standing nozzle under all operating conditions, a two-dimensional thermal expansion analysis was also conducted for the selected liner configuration. Temperatures from the two-dimensional heat transfer analysis were incorporated into a structural finite element program which was used to define the growth profile of the nozzle. The resultant thermally deflected shape was then used to define the inner contour of the two-piece aluminum shroud to ensure that there would be no interference of the structures at the operating temperatures. An additional detailed analysis was conducted to determine the radial growth of the liner flange at the H_2 injector end where the liner is fixed axially. Due to the radial growth of the flange at this location a radial clearance of 0.007 inch (0.018 cm) was incorporated to guarantee an elastic stress distribution in the flange and to minimize thermal distortion of the liner.

2. Regeneratively Cooled Nozzle Liner, Off Design

The coolant passage dimensional distribution was considered correctly sized for the nominal condition of

Mixture Ratio = 4/1
Fuel Inlet Temperature = 540°R (300°K)

Additional calculations were then undertaken to examine wall temperatures, total rejected heat and coolant inlet pressure drop as a function of contract defined extremes of mixture ratio and coolant inlet temperature for the fixed configuration liner.

The thermal models were solved for the conditions of high and low inlet temperatures 800 and 200°R (444 and 111°K) with the passage geometry determined for the 540°R (300°K) case. The liner temperature profile comparison for the three feed temperatures is presented in Table XXII. The maximum temperature predicted was 947°F(782°K) at 1.05 inches (2.67 cm) forward of the throat at the high feed temperature limit. That temperature was not far removed from the predicted maximum temperature to assure compliance with the life cycle requirement for 540°R (300°K) feed propellants, Figure 59.

It was found from the company's 1000 lbf (4448 N) tests that there was a reverse-flow engine variation of heat rejection with mixture ratio that differed slightly from theoretical over-excursions in mixture ratio from 3/1 through 5/1. Theoretical, in this case, is meant the assumption of gas species corresponding to the overall mixture ratio forming the gas side boundary layer and the applicability of the equations used to calculate the gas side heat flux. Predicted heat rejection rate as a function of mixture ratio appearing in Figure 59 was calculated with modification of the theoretical expressions based on the 1K (4448 N) data.

The expected coolant outlet temperature is a variable in the continuity equation used to calculate the fuel injection parameters for the 40 rectangular slots that exit into the chamber. Injection parameters were calculated using the predicted outlet temperature as a function of mixture ratio and inlet temperature is presented in Table XXIII. Coolant jacket pressure drops were predicted in a similar manner, using the data from the 1000 lbf (4448 N) to calculate the drops. This is shown in Figure 60.

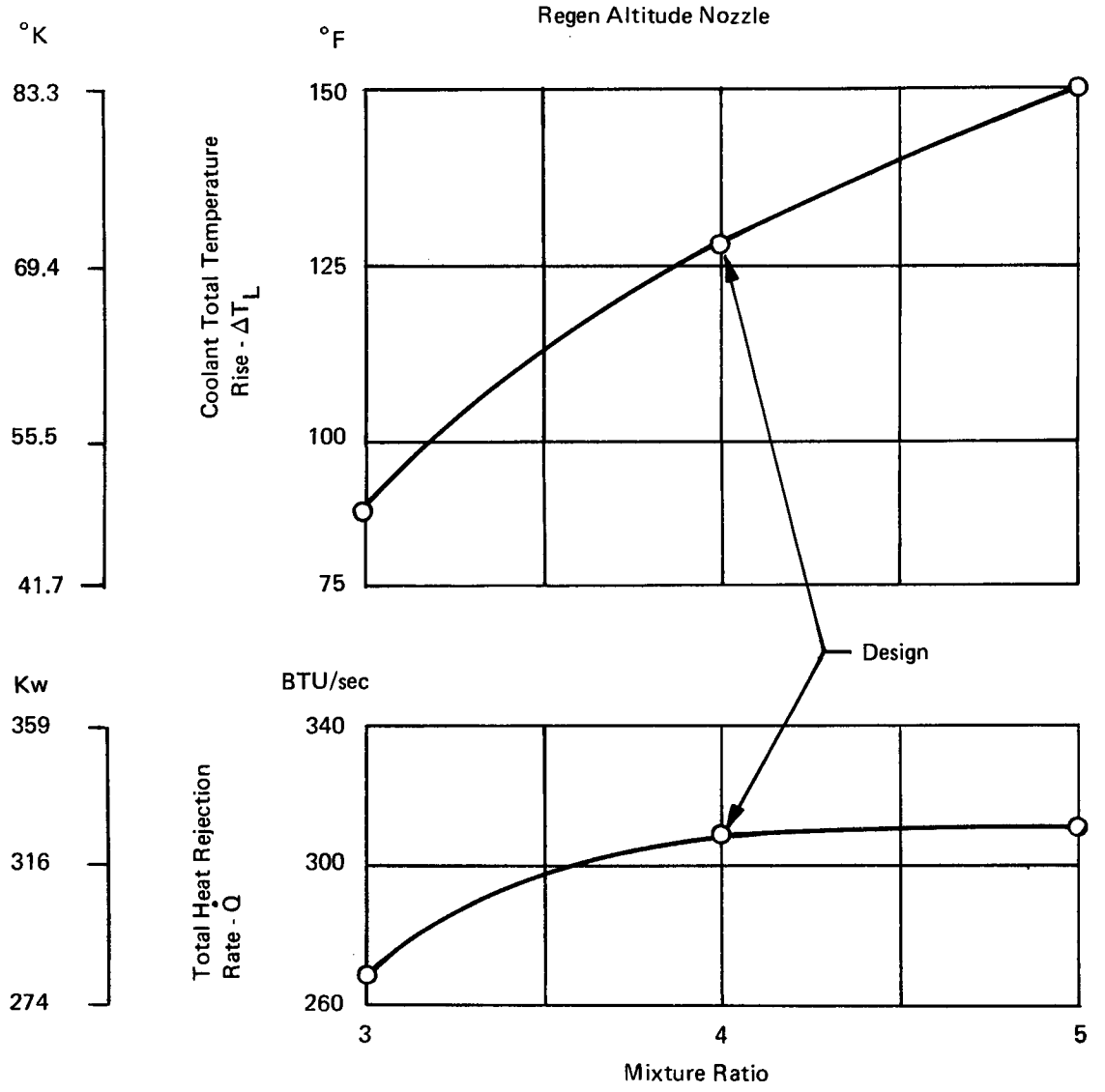

Figure 59. Heat Rejection versus Mixture Ratio

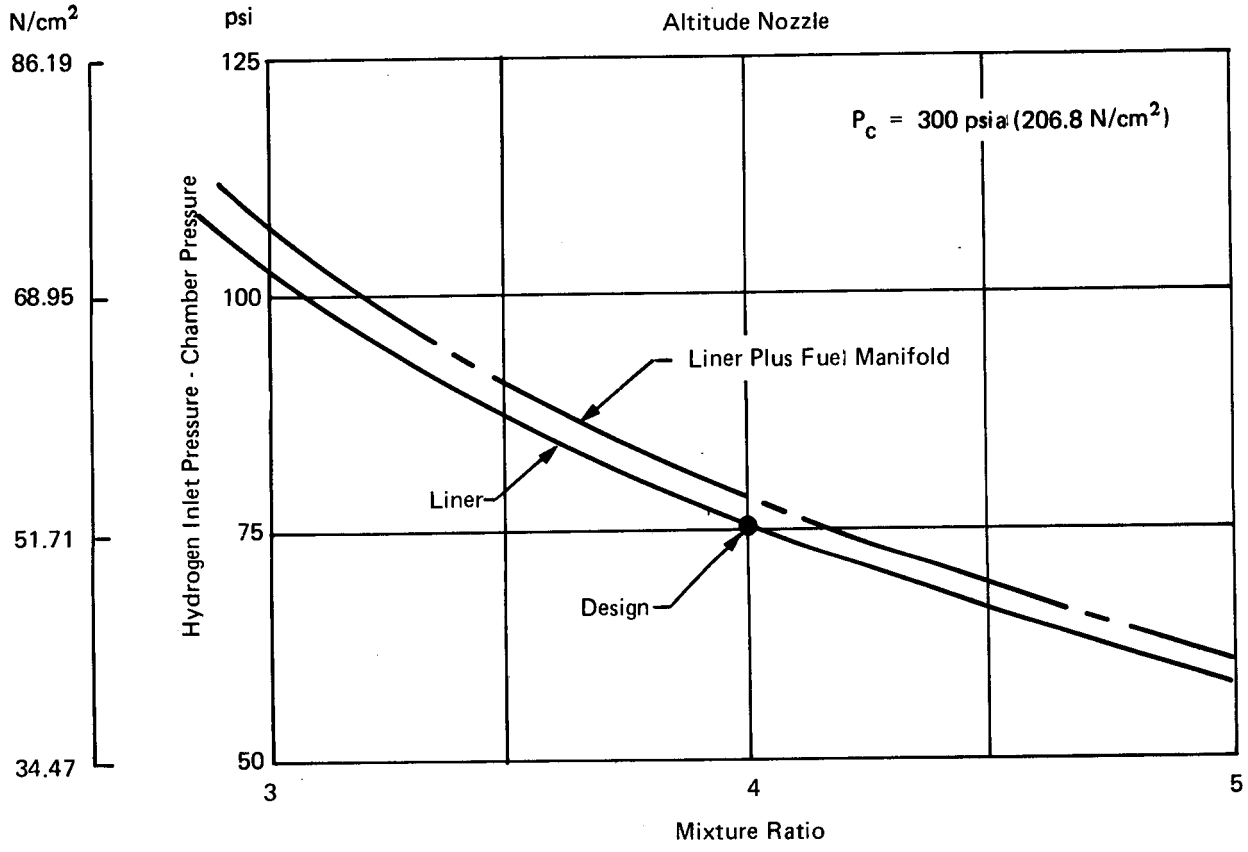

Figure 60. Hydrogen Coolant Pressure Drop versus Mixture Ratio

TABLE XXII

SUMMARY OF NODAL TEMPERATURES WITH VARIOUS COOLANT INLET TEMPERATURES

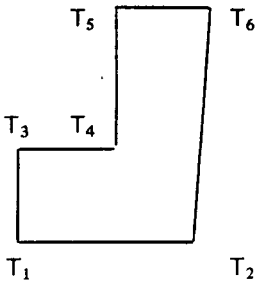

	Temp.	2.4 in. (0.61 cm) Aft of Throat						0.4 in. (0.102 cm) Forward of Throat						1.05 in. (3.17 cm) Forward of Throat					
		°F	°K	°F	°K	°F	°K	°F	°K	°F	°K	°F	°K	°F	°K	°F	°K	°F	°K
	T_{in}	80	300	-260	111	340	444	80	300	-260	111	340	444	80	300	-260	111	340	444
	T_1	745	663	793	696	906	759	681	634	494	530	889	750	748	671	598	588	947	782
Altitude	T_2	725	658	773	685	888	749	648	616	459	505	858	732	725	658	572	573	926	770
Nozzle	T_3	709	649	759	677	872	740	537	554	346	448	751	673	610	594	458	504	815	708
8636-470044	T_4	688	638	736	664	852	729	499	532	302	423	717	654	568	571	407	482	777	687
	T_5	610	594	658	621	780	689	284	413	53	285	520	544	404	480	223	369	627	604
	T_6	623	602	670	628	791	695	300	422	72	296	535	553	424	491	245	392	645	614

3. Regenerative/Film Cooled Liner

The major regenerative/film cooled liner design was identical to the regeneratively cooled liner up to the point of the film injection. The heat rejection and coolant pressure distribution within the passages of a regeneratively cooled liner with film cooling were calculated to furnish the coolant stagnation conditions required for sizing film cooling slots. The slots were added 1.69 inches (4.293 cm) forward of the throat to inject six percent of the hydrogen rearward along the liner wall. The selection of 6% of the flow for film cooling is based on the parametric studies described earlier.

The first step in the analysis was to determine the film temperature along the wall which would reject heat to the coolant. The method of Hatch and Papell, described previously, was used for the calculations. Pertinent parameters included the effective film coolant injection slot width and the angle of injection with respect to the wall. The injection slot width was converted to an equivalent annulus 0.016 inch (0.041 cm) wide at the injection station. The basic dimension of the slot width was based on the coolant temperature and pressure at the film cooling slot inlet and the orifice flow coefficient as described in Appendix C. The film coolant inlet pressure and temperature were iteratively determined starting with the heat transfer and pressure drop calculations for the regeneratively cooled liner without film cooling. The calculations were made using 17 axial elements in a similar fashion as the regenerative design but instead of a constant exhaust total temperature heating the walls, the gas film temperature as calculated with the Hatch-Papell correlations was employed as the driving temperature. Figure 61 is the film temperature distribution used for the heat transfer and pressure drop calculations.

TABLE XXIII

FUEL INJECTOR PARAMETERS, ALTITUDE NOZZLE 8636-470044

Coolant Inlet Temperature (°R)	540°R (300°K)						250°R (139°K)					
Mixture Ratio	3	3	4	4	5	5	3	3	4**	4**	5	5
Coolant Outlet Total Temperature	193°F	363°K	208°F	371°K	218°F	377°K	-106°K	197°K	-92°F	204°K	-83°F	210°K
Coolant Flow Rate	0.8487 lb/sec	0.3843 kg/sec	0.6896 lb/sec	0.3131 kg/sec	0.5926 lb/sec	0.2690 kg/sec	0.8487 lb/sec	0.3843 kg/sec	0.6896 lb/sec	0.3131 kg/sec	0.5926 lb/sec	0.2690 kg/sec
Exit Mach No.	0.618	0.618	0.513	0.513	0.447	0.447	0.463	0.463	0.385	0.385	0.336	0.336
Sonic Velocity	4576 fps	1390 m/sec	4680 fps	1423 m/sec	4744 fps	1445 m/sec	3423 fps	1042 m/sec	3512 fps	1068 m/sec	3567 fps	1085 m/sec
Exit Velocity	2828 fps	862 m/sec	2403 fps	732 m/sec	2121 fps	645 m/sec	1582 fps	472 m/sec	1353 fps	412 m/sec	1199 fps	365 m/sec
Estimated Coolant Inlet Pressure	398 psia	274.4 N/cm^2	375 psia	268.6 N/cm^2	355 psia	244.5 N/cm^2	359 psia	247.5 N/cm^2	345 psia	237.9 N/cm^2	333 psia	229.6 N/cm^2

Coolant Inlet Temperature (°R)	200°R (111°K)						800°R (444°K)					
Mixture Ratio	3	3	4**	4**	5	5	3	3	4**	4**	5	5
Coolant Outlet Total Temperature	-166°F	163°K	-153°F	171°K	-145°F	775°K	446°F	504°K	461°F	512°K	470°F	517°K
Coolant Flow Rate	0.8487 lb/sec	0.3843 kg/sec	0.6896 lb/sec	0.3131 kg/sec	0.5926 lb/sec	0.2690 kg/sec	0.8487 lb/sec	0.3843 kg/sec	0.6896 lb/sec	0.3131 kg/sec	0.5926 lb/sec	0.2690 kg/sec
Exit Mach No.	0.423	0.423	0.353	0.353	0.308	3.308	0.719	0.719	0.598	0.598	0.520	0.520
Sonic Velocity	3130 fps	953 m/sec	3215 fps	979 m/sec	3267 fps	994 m/sec	5324 fps	1622 m/sec	5447 fps	1658 m/sec	5518 fps	1680 m/sec
Exit Velocity	1323 fps	403 m/sec	1134 fps	345 m/sec	1006 fps	306 m/sec	3827 fps	1163 m/sec	3254 fps	990 m/sec	2870 fps	875 m/sec
Estimated Coolant Inlet Pressure	347 psia	239.2 N/cm^2	337 psia	232.4 N/cm^2	328 psia	226.1 N/cm^2	444 psia	306.1 N/cm^2	410 psia	282.7 N/cm^2	481 psia	331.6 N/cm^2

Exit Static Pressure = 296.1 psia (204.1 N/cm^2)

Coolant Exit (Fuel Injection) Flow Area = 0.47128 $in.^2$ (3.03825 cm^2)

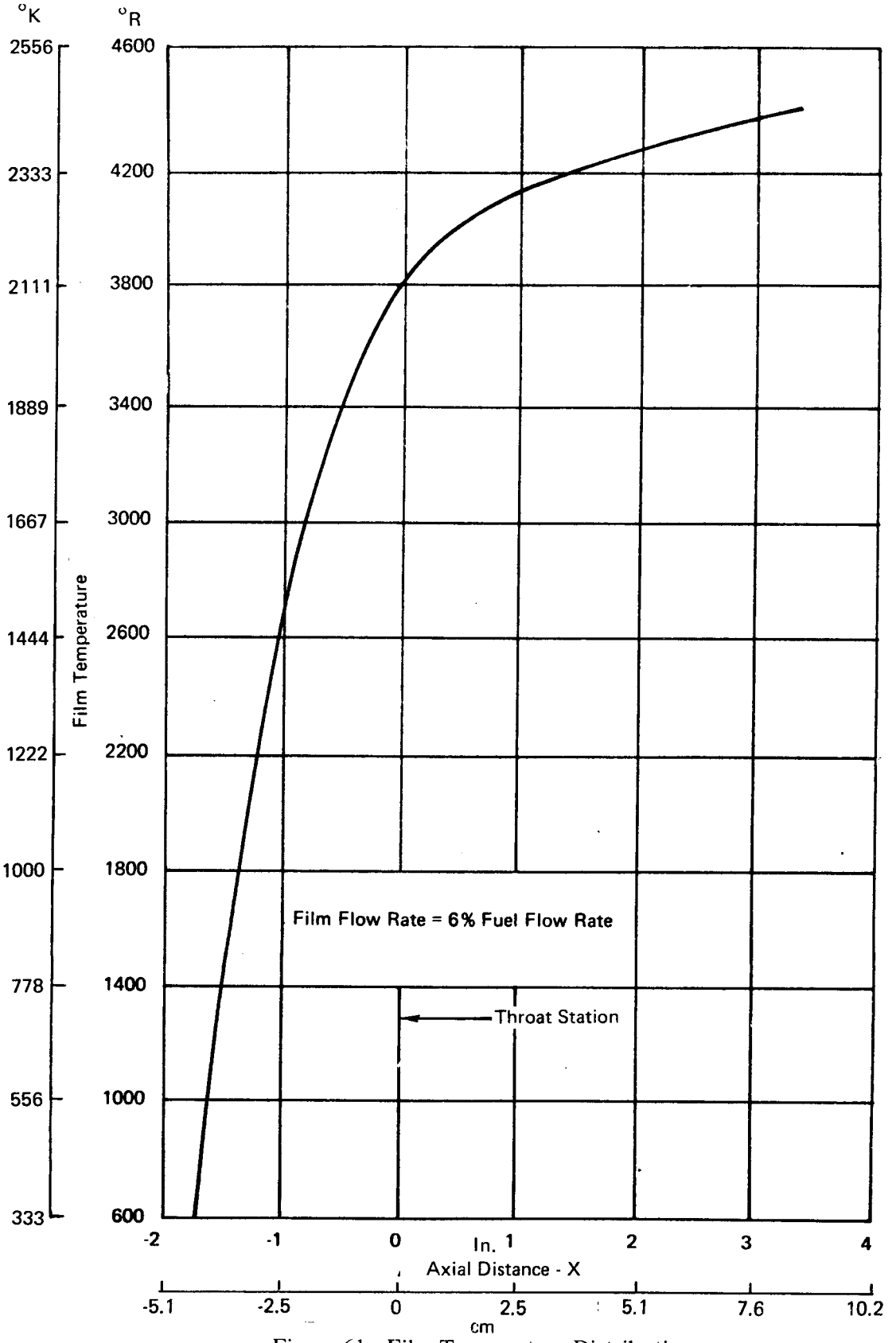

Figure 61. Film Temperature Distribution

A schematic sketch of the flow conditions in the passages of the film cooled liner is shown in Figure 62. The addition of the film coolant slots and the reduction of the hydrogen injector flow results in slightly reduced fuel injection areas and regenerative passage areas near the point of injection.

An assumed surface roughness (rms) of 63 microinches (1.6 μ) was used to determine the pressure loss due to friction in the regeneratively cooled passages. The comparison summary of Table XXIV gives the exit and inlet coolant flow parameters of the regenerative and regenerative plus film cooled nozzles. The increased feed pressure for the film cooled design results from:

1. Maintaining 2,400 fps (731.5 m/sec) injection velocity with cooler injected fuel by increasing the required total pressure at exit. The injected fuel is cooler due to the heat flux reduction predicted for the film-cooled liner.

2. Reducing the flow area and increasing the Mach number between the film injection station and the point of H_2 injection increases frictional losses.

TABLE XXIV
FUEL FLOW PARAMETERS FOR ALTITUDE CHANNEL NOZZLES

	Outlet Total Temp		Outlet Flow Area		Exit Mach No.	Exit Velocity		Outlet Total Pressure		Inlet Total Pressure		Loss In Total Pressure	
Nozzle	(°F)	(°K)	(In.^{2})	cm^2	(-)	(Fps)	(m/sec)	(psia)	(N/cm^2)	(psia)	(N/cm^2)	(psi)	(N/cm^2)
Regeneratively Cooled	209	372	0.48224	3.11141	0.503	2357	718	351.87	242.60	373.11	257.46	21.24	14.86
6% Film Cooled	178	354	0.42744	2.75784	0.520	2377	724	356.02	245.47	380.06	262.26	24.04	16.79

Exit (Fuel Injection) Static Pressure = 296.1 psia (2.0415 N/cm^2)

A comparison of the predicted temperature distributions in the regeneratively and film cooled liners is shown on Table XXV . The difference in maximum wall temperatures with and without film cooling is more pronounced near the injector where the difference between film and overall recovery gas temperature is a maximum.

4. Regenerative/Dump Cooled Liner

The parametric heat transfer design studies of the insulated radiation cooled nozzle extensions showed that supersonic dump cooling aft of an area ratio of 10:1 would be necessary to demonstrate a nozzle extension with a maximum temperature that would not exceed upper limits of oxidation resistant coatings.

The liner was designed for 6% dump cooling by maintaining the principal coolant passage dimensions of the regeneratively cooled liner, reducing the fuel injector height from 0.0438 inch (0.111 cm) high to 0.0400 inch (0.102 cm) high and adding dump cooling slots to a dump coolant distribution manifold.

	①*	⑴A	②	②A	③	③A
Total Temperature, °F (°K)	178.48	(354.53)	166.18	(347.69)	80.0	(300.0)
Total Pressure, psia (N/cm²)	356.02	(245.5)	361.32-365.0	(249-251.7)	380.06	(262.0)
Mach Number	0.5199	(0.5199)	0.3403	(0.3403)	0.091	(0.091)
Passage Area, sq. in. (sq.cm)	0.42744	(2.75784)	0.5825	(3.75829)	1.932	(12.4653)
Flow Rate, lbm/sec (kg/sec)	0.64822	(0.29402)	0.6896	(0.31279)	0.6896	(0.31279)
Axial Station, in. (cm)	-1.937	(-4.92)	-1.69	(-4.293)	3.75	(9.525)
Pressure, psia (N/cm²)	296.1	(204.2)	333.49	(229.8)	377.74	(260.4)

* Points ①, ② and ③ refer to the diagram below, ⑴A, ②A and ③A are the metric conversions

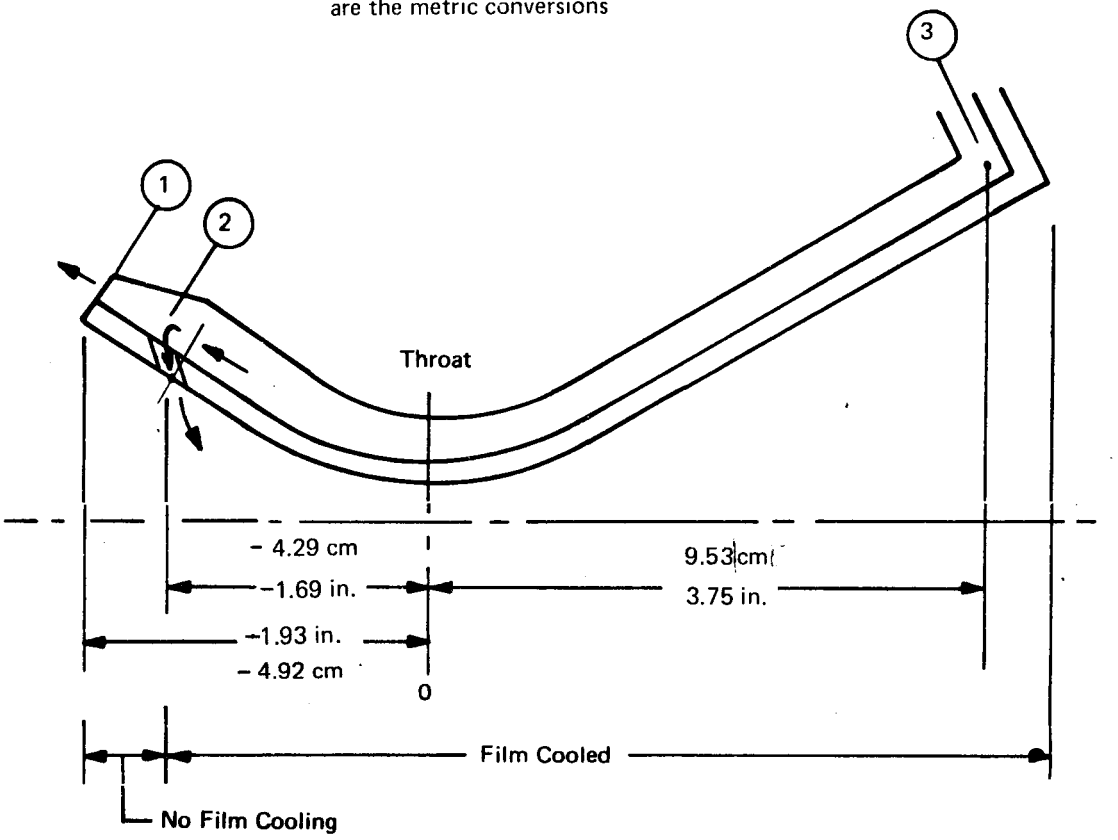

Figure 62. Coolant Stagnation Conditions - 6% Film Cooling

Twenty circular sonic metering orifices were sized to feed 0.06896 lbm/sec (0.03128 kg/sec) to the dump cooling manifold which, in turn, fed 80 supersonic flat nozzles, providing expansion to match the local main stream wall pressure of 4.116 psia (2.838 N/cm²). The expanded nozzles distributed the metered flow over 80% of the local perimeter.

Dump cooled tests with variable dump cooling rates were accomplished by changing the number of round metering orifices. The calculation and matching operation of the distribution holes is presented in Appendix C.

TABLE XXV
COMPARISON OF FILM AND REGENERATIVELY COOLED AMZIRC CHANNEL LINER TEMPERATURE DISTRIBUTION

	Divergent Nozzle																				Throat			
Station	1				3				5				7				10							
X	3.4		8.636		2.4		6.096		1.4		3.556		0.70		1.778		0		0					
Passage Size	inch		cm		inch		cm		inch		cm		inch		cm		inch		cm					
	W	H	W	H	W	H	W	H	W	H	W	H	W	H	W	H	W	H	W	H				
	0.30 by 0.164		0.762 by 0.417		0.237 by 0.20		0.602 by 0.508		0.175 by 0.220		0.444 by 0.559		0.131 by 0.220		0.333 by 0.559		0.090 by 0.182		0.229 by 0.462					
Heating Mode	°F		°K		°F		°K		°F		°K		°F		°K		°F		°K					
	R	F	R	F	R	F	R	F	R	F	R	F	R	F	R	F	R	F	R	F				
Wall Temp T_1	729	679	660	633	745	672	669	629	650	576	617	576	593	506	585	556	675	521	631	544				
Wall Temp T_2	719	670	655	628	725	654	659	619	634	562	608	568	581	496	578	531	666	514	626	541				
Wall Temp T_3	691	643	640	613	709	640	650	611	612	543	596	557	543	465	557	514	534	408	552	482				
Wall Temp T_4	672	625	629	603	688	620	638	600	581	517	578	542	514	440	541	501	496	387	531	471				
Wall Temp T_5	617	574	598	574	610	550	595	561	457	409	510	483	352	305	541	425	258	215	398	375				
Wall Temp T_6	627	584	604	580	623	561	602	567	466	417	515	487	357	309	454	427	268	222	403	379				

	Convergent Nozzle																			
Station	12				14				15				16				17			
X	-0.4		-1.016		-0.8		-2.032		-1.05		-2.667		-1.30		-3.302		-1.55		-3.937	
Passage Size	inch		cm		inch		cm		inch		cm		inch		cm		inch		cm	
	W	H	W	H	W	H	W	H	W	H	W	H	W	H	W	H	W	H	W	H
	0.09 by 0.161		0.229 by 0.409		0.105 by 0.121		0.267 by 0.307		0.141 by 0.102		0.358 by 0.259		0.176 by 0.085		0.447 by 0.216		0.213 by 0.068		0.541 by 0.173	
Heating Mode	°F		°K		°F		°K		°F		°K		°F		°K		°F		°K	
	R	F	R	F	R	F	R	F	R	F	R	F	R	F	R	F	R	F	R	F
Wall Temp T_1	686	481	581	522	706	422	648	490	749	385	671	498	715	280	653	416	680	184	634	358
Wall Temp T_2	654	460	619	512	715	428	653	494	725	375	658	464	692	282	641	412	659	185	622	358
Wall Temp T_3	543	385	557	470	577	351	576	451	611	323	595	435	595	253	586	396	577	175	576	353
Wall Temp T_4	505	361	536	456	538	330	554	439	568	305	571	425	552	242	562	390	539	173	555	352
Wall Temp T_5	290	222	417	379	358	236	454	386	405	237	481	387	422	207	490	371	449	167	505	348
Wall Temp T_6	306	233	425	385	381	248	467	393	424	245	491	391	437	211	499	373	463	168	513	349

* R = Regenerative 8636-470044 Liner
F = 6% film cooled 8636-470076 Liner

Injection station 1.69 inches (4.29 cm) upstream of throat

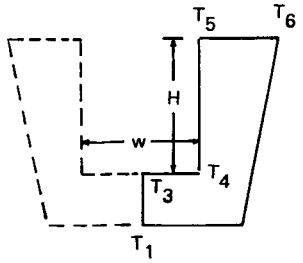

D. DETAILED ANALYSES OF NOZZLE EXTENSIONS

1. Nozzle Contour

The basic nozzle contour for the configuration studies was selected to provide high performance with a relatively short overall length. A 75% bell nozzle with a circular arc one-half of the throat diameter was maintained for the detailed nozzle design. The detailed method of contour analysis, applying aerodynamic relationships to optimizing the supersonic flow (Rao nozzle) as a function of length is presented in detail in Appendix C of this report. Thermodynamic properties of shifting equilibrium combustion gas, computed by the ICRPG ODE computer program, was used for the nozzle design.

Aerodynamic performance, a result of the nozzle design, is dependent to some extent on the shape of the wall in the vicinity of the nozzle throat. An investigation of the effect of the downstream wall radius at the throat on performance of the area ratio 40:1 nozzles was accomplished by designing families of nozzles of various lengths with downstream wall to throat radius ratios varying between 0.4:1 to 2:1. For any nozzle length, the aerodynamic performance increases with diminishing radius ratio reaching a limit at a radius ratio of 0.0. Results of this study appear in Figure 63. The nozzle profile with a symmetric curved wall radius, as a maximum limit is identified on the figure and is associated with a bell length when expanded for optimum length. Shifting to a slightly longer nozzle, 75% bell, but decreasing the radius ratio to 0.4:1, 1.4 seconds of impulse is gained. The aerodynamic efficiency is 98.8% relative to theoretical maximum. This variation of aerodynamic performance with radius ratio is illustrated in Figure 64 with the maximum value of 464.4 seconds (4534 N sec/kg) (extrapolated) at a ratio of 0.0 which is a sharp throat.

The design profile of the 75% bell length nozzle for the altitude test hardware is presented in Figure 65. A 2.04 inch (5.68 cm) upstream wall radius which is larger than the 1.90 inch (4.83 cm) radius used in the parametric analysis was found to have a negligible effect on the performance as both are large enough to provide nearly a 100% subsonic aerodynamic efficiency (discharge coefficient). Other results of the nozzle design are listed in Table XXVI. Of particular interest is the Mach number at the wall which was subsequently used for boundary layer analyses such as gas side heat transfer coefficient and viscous drag.

A portion of the digital computer output of the nozzle design is the static pressure at the wall. This pressure is plotted on Figure 66 and was used as input to structural analyses. Pressures upstream of the throat up to the fuel injector are one dimensional pressures found from the isentropic relationships between area ratio and pressure ratios relative to Mach number = 1.0. The pressure at the exit lip of the area ratio = 40:1 nozzle is 0.96 psia (0.66 N/cm^2). With a chamber pressure of 300 psia (206.8 N/cm^2), the nozzle can be expected to flow full at a pressure of 3.6 psia (2.48 N/cm^2) at 34K ft (10,350 m) as per "Handbook of Supersonic Aerodynamics," Volume 6, Figure 6-18.

The axisymmetric case presented previously was taken as a point of departure for scarfed nozzles of a wide variety of thrust inclination angles which might be installed in a space vehicle for reaction control. The scarfed portion would be a conical extension to the contoured axisymmetric nozzle. Design data and Bell Aerospace background experience with scarfed nozzles are presented in Appendix C.

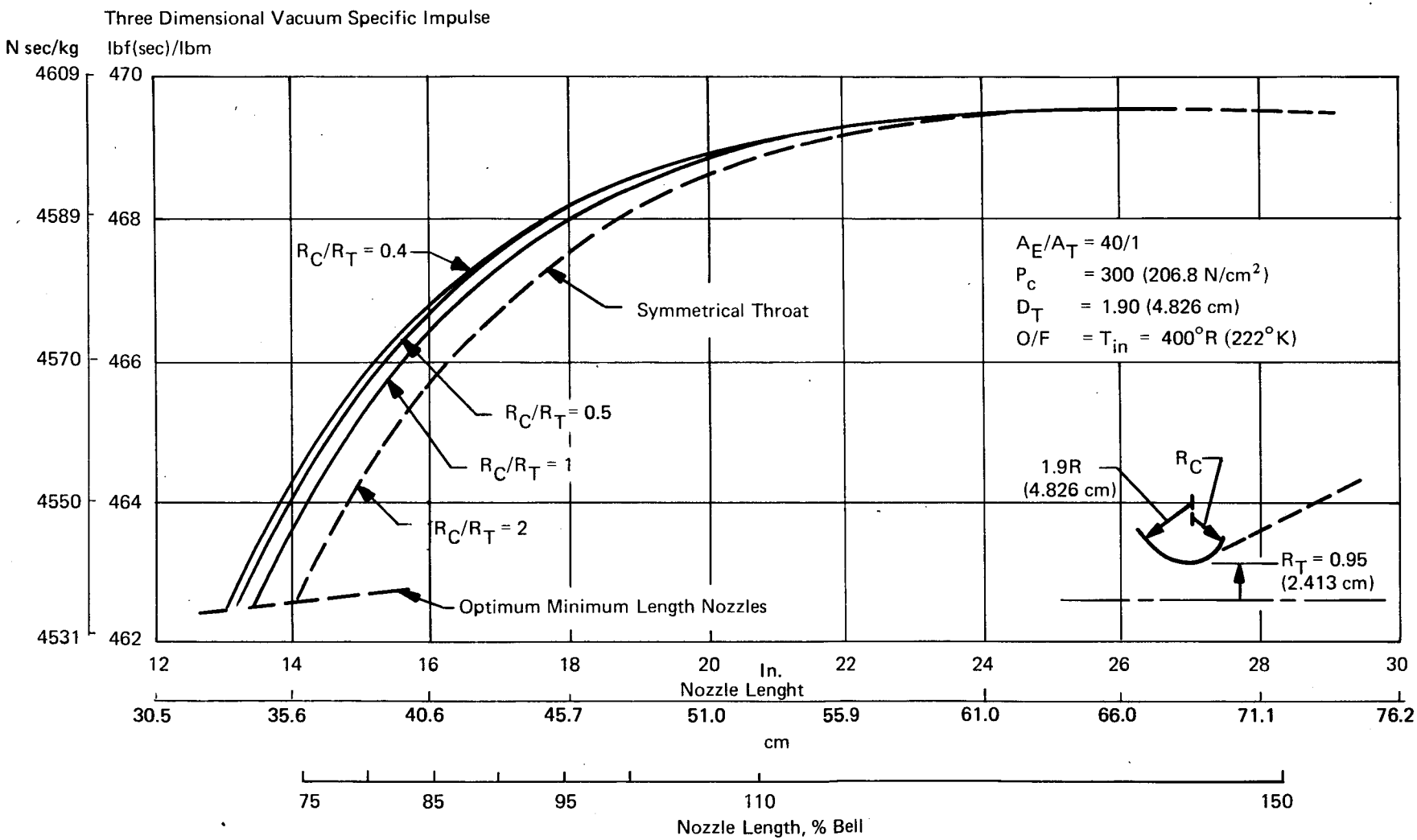

Figure 63. Three-Dimensional Specific Impulse versus Nozzle Length

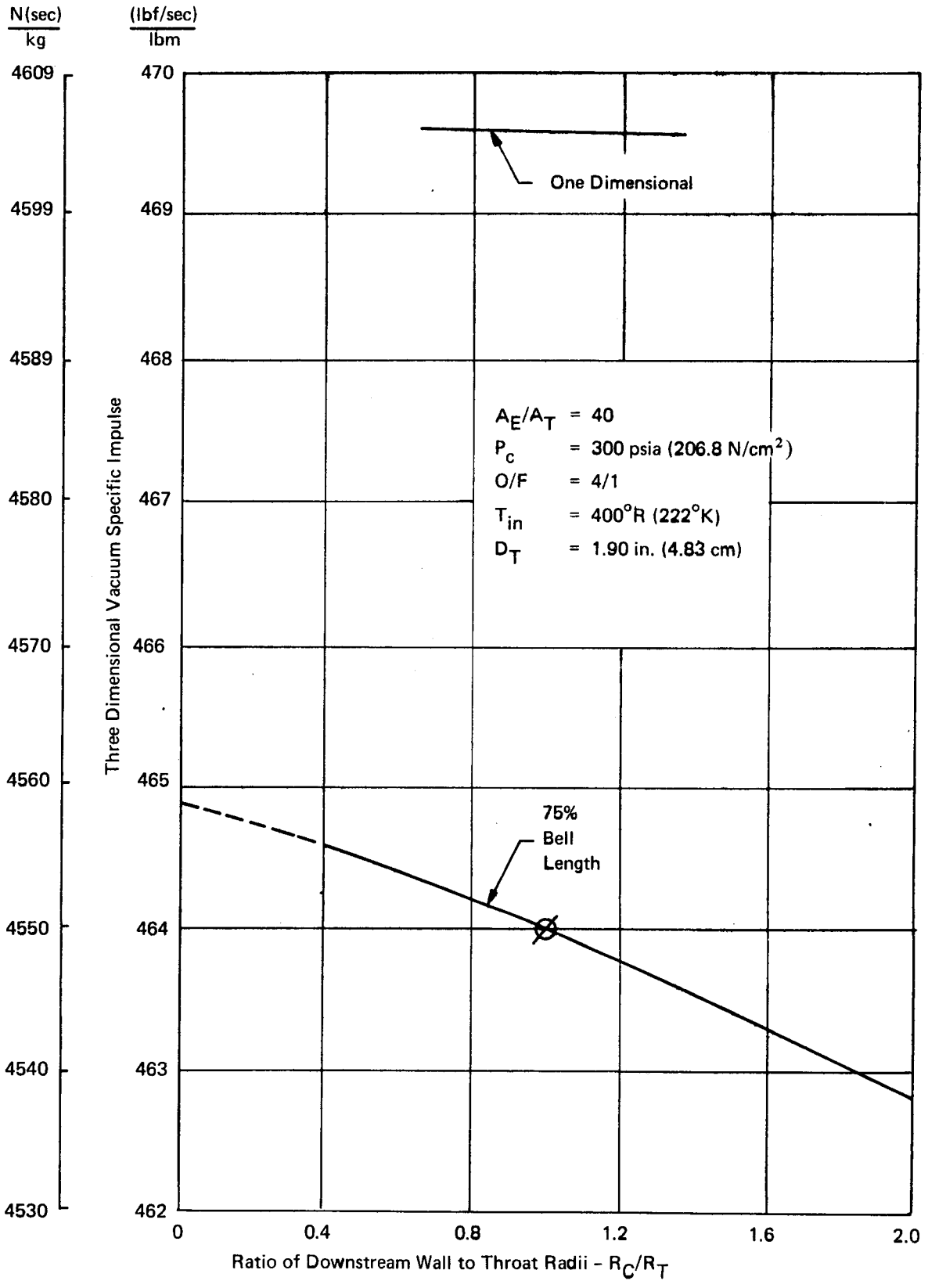

Figure 64. Three-Dimensional Specific Impulse versus Downstream Radius Ratio

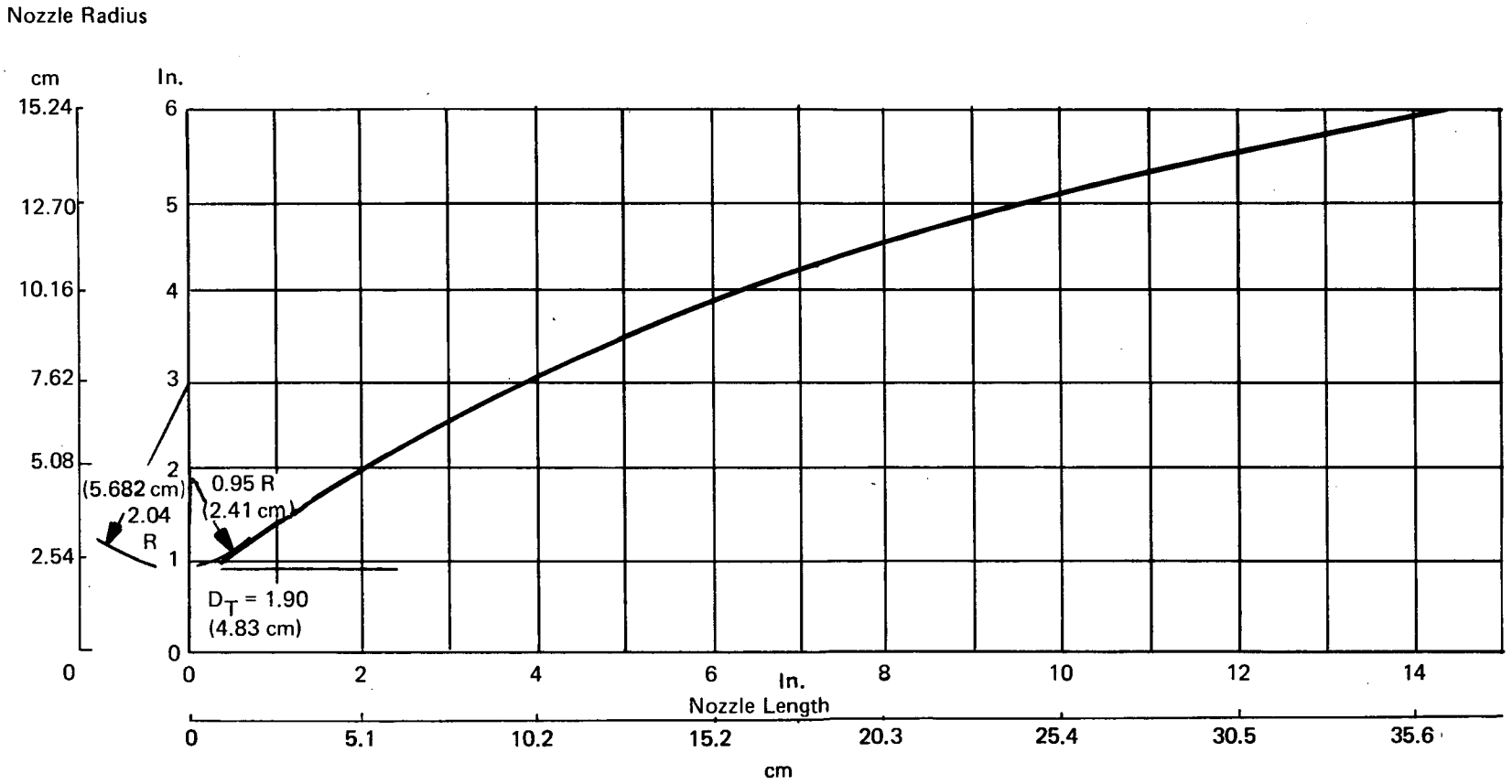

Figure 65. 75% Bell Length Nozzle Profile

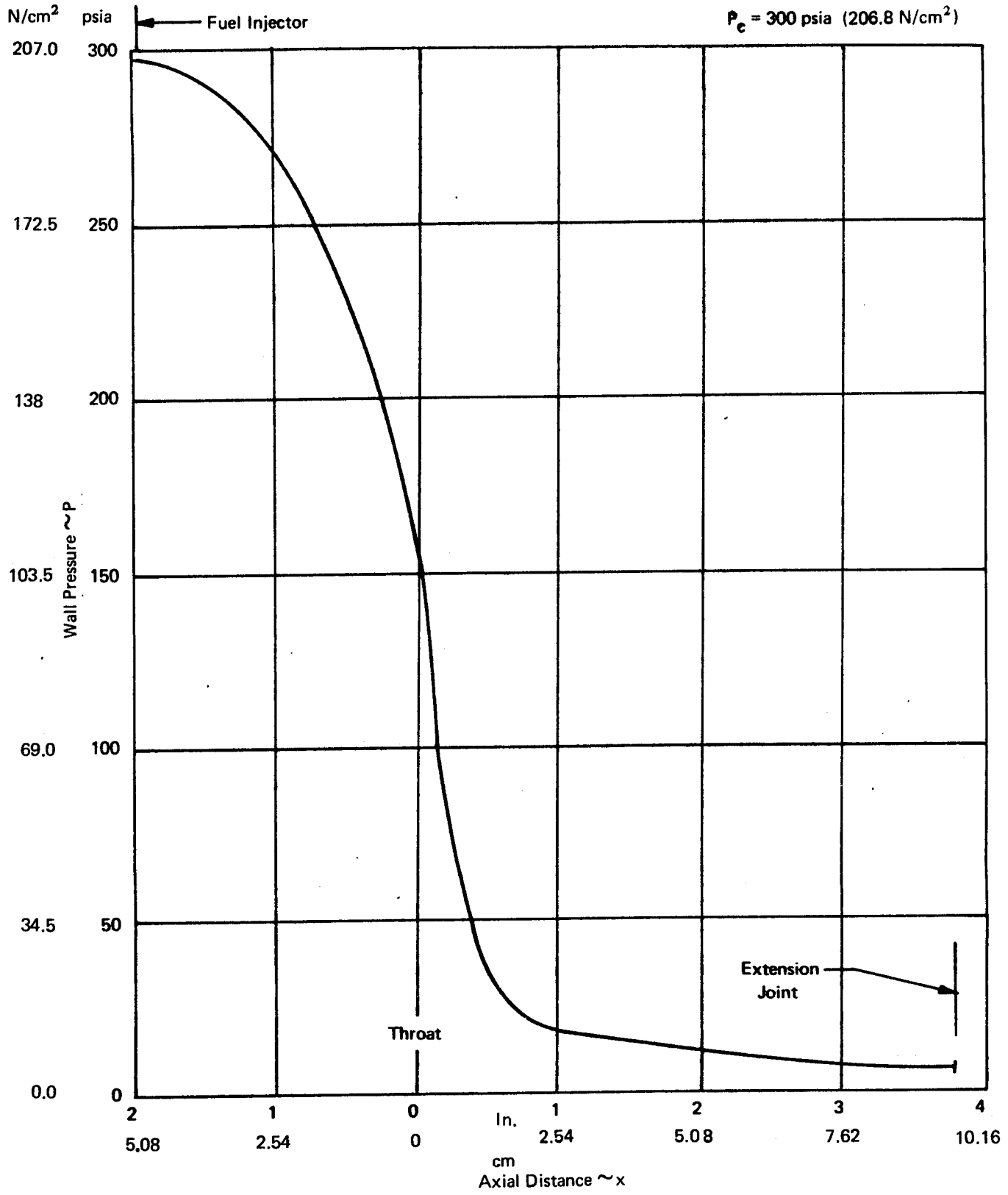

Figure 66. Wall Pressure Distribution Altitude Nozzle Liner

TABLE XXVI
NOZZLE WALL PARAMETERS 75% BELL NOZZLE

Axial Station from X Throat		Radial Distance from Y Centerline		Pressure		Wall Angle (Degrees)	Mach Number	Ratio of Specific Heats	Velocity at Wall	
(in.)	cm	(in.)	cm	(psia)	N/cm^2				(FPS)	m/sec
0.2718	0.6904	0.9897	2.5138	70.91	48.89	16.62	1.642	1.199	8446	2574
0.4949	1.2698	1.0891	2.7663	31.34	21.61	31.40	2.118	1.224	10242	3122
1.558	3.9573	1.7887	4.5433	12.78	8.81	31.67	2.607	1.245	11681	3560
2.004	5.0902	2.053	5.2146	10.12	6.98	30.31	2.734	1.250	11991	3655
3.030	7.6962	2.622	6.6599	6.57	4.53	27.15	2.969	1.259	12510	3813
4.039	10.2591	3.109	7.8969	4.73	2.78	24.43	3.150	1.266	12862	3920
4.979	12.6467	3.517	8.9306	3.67	2.53	22.20	3.292	1.271	13112	3997
6.025	15.3035	3.920	9.9568	2.90	2.00	20.08	3.426	1.276	13329	4063
7.017	17.8222	4.267	10.8382	2.39	1.65	18.31	3.536	1.280	13496	4114
7.993	20.3022	4.574	11.5914	2.02	1.39	16.77	3.634	1.284	13633	4155
9.029	22.9337	4.872	12.3749	1.73	1.19	15.32	3.727	1.287	13757	4193
9.964	25.3086	5.118	12.9997	1.52	1.05	14.14	3.803	1.289	13853	4222
10.963	27.8460	5.359	13.6122	1.34	0.92	12.98	3.874	1.295	13944	4250
12.029	30.5537	5.594	14.2088	1.19	0.82	11.86	3.945	1.299	14029	4276
13.174	33.4620	5.823	14.7907	1.06	0.73	10.77	4.021	1.300	14110	4301
14.155	35.9537	6.008	15.2603	0.96	0.66	9.91	4.082	1.300	14171	4319

2. Thermal Analyses

a. General

The fuel-cooled channel liner extended into the supersonic nozzle to an area ratio of 10:1. A bolt on nozzle extension was attached to further expand the nozzle to the exit at an area ratio of 40:1. Two types of extensions were designed and tested during the program. These were water (or fuel) cooled and radiation cooled. The thermal analysis effort was directed to cooling passage definition, wall temperatures, insulation requirements and joint seal temperature predictions.

Firing data at a simulated vacuum altitude with the drilled and radiation cooled nozzles provided heat transfer data that permitted a refinement in the calculations of the heat rejection rates by the exhaust gas in the nozzle extension which was culminated in the verification of the predictions of shell temperatures of an insulated radiation cooled extension, fired for an extended duration of 500 seconds. The review of the thermal analysis includes discussion of the original assumptions and the iterative use of test data to make the final prediction.

b. Drilled Configuration

The analysis of the integral wall regeneratively cooled nozzle extension was directed towards three metals: nickel, aluminum and stainless steel. Calculations of an H_2 regeneratively cooled nozzle, which were carried out during the parametric studies led to the definition of sixty-four 0.25 inch (0.635 cm) diameter passages to provide adequate cooling (mass velocity) for the nominal conditions of

P_c = 300 psi (206.8 N/cm^2)
Mixture Ratio = 4/1
Combustion Efficiency = 97%
Coolant Inlet Temperature = 60°F (271°K)
No film or dump cooling

The coolant was to enter at the maximum area ratio and flow single pass forward toward the joint at an area ratio of 10:1.

Two dimensional steady-state nodal mathematical models were constructed at two nozzle stations as part of the detailed design. Solution of the models with appropriate boundary conditions and thermal conductivities resulted in temperatures shown in Table XXVII. Low weight and thorough background in the deep hole drilling technique with aluminum led to the selection of that metal. Structural calculations established that the aluminum would function adequately at the predicted temperatures. Pressure drop calculations made for the drilled hydrogen cooled aluminum extensions resulted in the following:

Outlet Pressure	375 psia (258.6 N/cm^2)
Average Mach Number	0.0461
Total Pressure Loss in Drilled Passages	1.0 psi (0.69 N/cm^2)

Annular manifolds connecting the drilled passages were sized for a coolant Mach number of 0.07 and a possible maximum loss (dynamic pressure) of 1.28 psi (0.89 N/cm^2) for entrance and turning losses.

The parameters for water cooling of the drilled aluminum nozzle were established to add simplicity to the test program. The nozzle extension heat data could be more easily obtained with water cooling. Local heat fluxes were examined and it was determined that a water velocity of 4.4 fps (1.34 m/sec) would provide adequate cooling. This velocity, flowing through the 64 drilled passages, would absorb the total heat flow to the nozzle extension. The theoretical gas side heat transfer coefficient with a mean correlation constant distribution was used for the analysis. Subsequent testing, to be discussed later in this section, led to the conclusion that the coefficient should be reduced. In summary, the water-cooled parameters for the drilled aluminum nozzle were:

Water Coolant Velocity, fps	4.4 (1.34 m/sec)
Water Flow Rate, lbm/sec	6.0 (2.724 kg/sec)
Heat Rejection Rate, BTU/sec	401 (4.23 x 10^5 watts)
Temperature Rise of Water, °F	67 (37.2°K)
Maximum Heat Flux, BTU/in.^{2} sec	1.93 (315.5 watts/cm^2)
Upper Limit of Nucleate Boiling, BTU/in.^{2} sec	2.76 (451.0 watts/cm^2)

The heat rejection by the exhaust gas to the divergent nozzle, 75% bell length, was calculated with a heat transfer coefficient in the form of a pipe flow equation for fully developed turbulent flow. The equation employed was:

TABLE XXVII
REGENERATIVE COOLED NOZZLE EXTENSION WALL TEMPERATURES

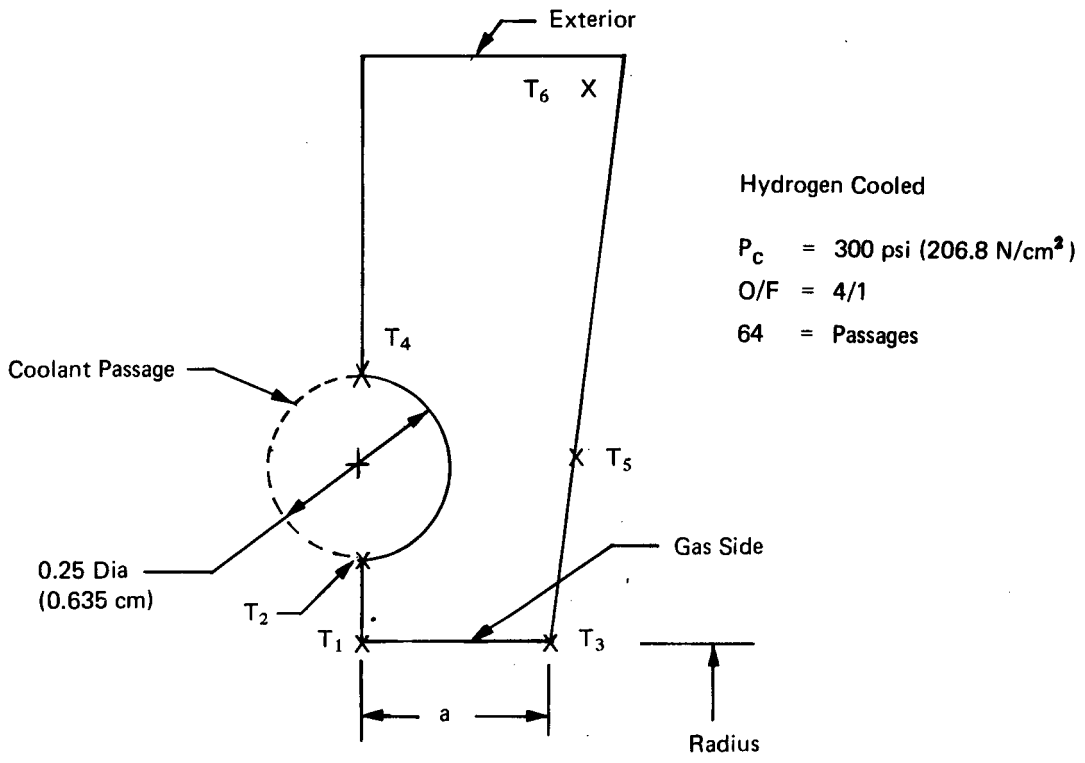

	Area Ratio = 11.7/1					
	Radius = 3.25 in. (8.255 cm) a = 0.1592 in. (0.4035 cm)					
	Temperatures					
	°F	°K	°F	°K	°F	°K
	Nickel		Aluminum		Stainless	
T_1	959	788	737	665	1249	949
T_2	869	739	707	649	1213	929
T_3	910	762	709	650	1030	828
T_4	302	423	412	485	220	378
T_5	512	540	537	554	462	513
T_6	317	431	421	490	234	385

	Area Ratio = 38.2/1					
	Radius = 5.71 in. (14.50 cm) a = 0.288 in. (0.731 cm)					
	Temperatures					
	°F	°K	°F	°K	°F	°K
	Nickel		Aluminum		Stainless	
T_1	504	535	418	488	699	645
T_2	458	510	400	478	551	562
T_3	514	541	413	407	809	705
T_4	268	494	320	433	174	352
T_5	364	458	359	455	409	483
T_6	314	430	339	444	282	412

$$S_T^* \ [P_R^*]^{0.7} = C \ [R_E^*]^{-0.2}$$

where

S_T = Stanton number
P_R = Prandtl number
R_E = Reynolds number
C = correlation constant
* = superscript for reference conditions.

Details on the use of the equation are found in Appendix B. The correlation coefficient (C) used with the equation was assumed to have a distribution through the nozzle as shown in Figure 67 With this figure and the Mach number distribution in the nozzle found during the design (contouring) of the nozzle, local heat balances to the water cooled section were made assuming a constant nozzle total temperature for mixture ratio 4/1 and integrated over the entire surface at various mixture ratio. This is shown in Figure 68 which is based on the heat transfer coefficient distribution with the 100% correlating coefficient.

As the firing test data was examined, it was noted that the predicted heat rejection rate was lower than observed and a gas temperature probe was inserted between the water coolant passages 2.15 inches (5.4 cm) forward of the exit lip extending into the gas stream to measure the gas temperature adjacent to the wall. This was a bare wire probe which was considered to read 12.7% lower than a true value due to the high velocity across the probe. Table XXVIII shows the comparison of the measured and predicted heat rejection rates and gas temperatures for regenerative and dump cooled configurations. A comparison of Table XXVIII and Figure 67 would indicate that a lower estimate of the gas heat transfer coefficient would produce better correlation with test data.

c. Radiation Cooled

The temperature distributions for the radiation-cooled extensions were calculated, based on Zakkay, Ref. 17, and compared with measured (Pyroscanner) test data. The heat rejection ratio to the water-cooled extension were found to be overpredicted as described in the preceding subsection and deviations from theory of the magnitude and distribution of the radiation-cooled extension temperatures were also noted. The gas film coefficients originally calculated for the hot wall extensions were reassessed by referral to the water-cooled nozzle tests and a final best predicted insulated radiation-cooled extension with 7-1/2% dump cooling was made. Details of the steps in the thermal analysis leading to the wall temperature predictions for the final, long duration firings with the radiation-cooled extension are presented in the following paragraphs.

As was mentioned earlier in the method of calculation of radiation-cooled extensions that the heat loss by radiation takes place both from:

(1) The exterior of the shell to the environment.
(2) The internal surface out the open nozzle exit to the environment.

An insulated nozzle would have an equilibrium wall temperature higher than the "bare" nozzle because of the reduction in radiative cooling from the exterior shell. The gray body view factor for radiation loss out the exit plane of the nozzle is calculated to include radiation interchange within the divergent nozzle and was found to vary from 0.13 at the throat to 0.43 at the exit.

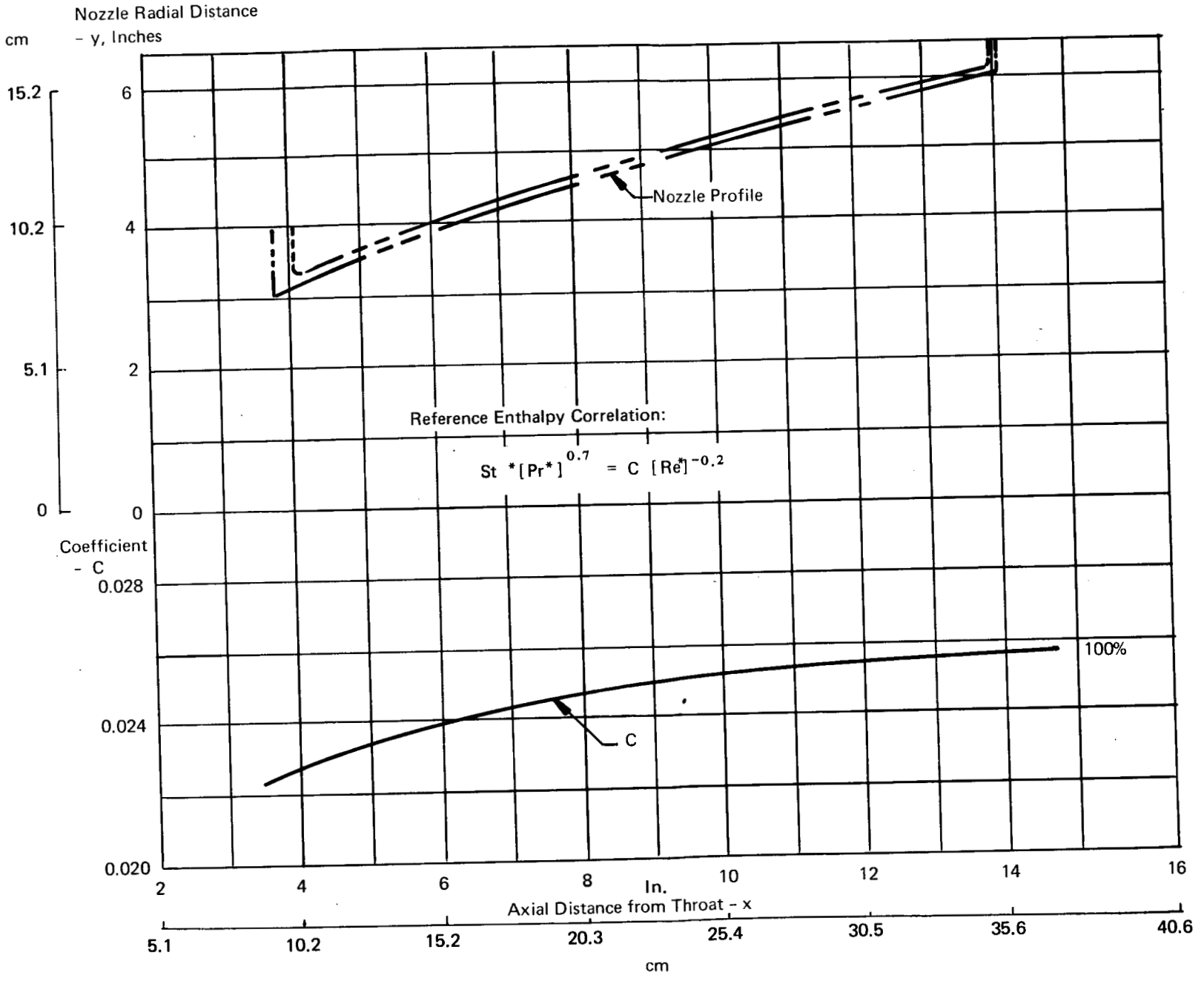

Figure 67. Gas-Side Heat Transfer Coefficient Distribution - Nozzle Extension

TABLE XXVIII
WATER-COOLED NOZZLE EXTENSION HEAT REJECTION AND MEASURED GAS TEMPERATURE

Test No.	Mixture Ratio	Percent Dump Cooling	Predicted Nozzle Heat Rejec.		Act. Noz. Heat Rejec.		Act. Meas. Gas Temp.		Corrected Measured Gas Temp.		Gas Temperature Inferred From Heat Rejection	
			(B/sec)	KW	(B/sec)	KW	(°F)	°K	*(°F)	°K	**(°F)	°K
1BN-640	4.13	0.0	396	418	215	265	—	—	—	—	—	—
1BN-655	4.17	6%	—	—	240	253	2531	1666	2910	1872	2200	1478
1BN-656	2.99	6%	—	—	207	218	2041	1390	2358	1566	1970	1350
1BN-657	4.77	6%	—	—	192	202	1784	1247	2069	1405	1820	1267

* Corrected for velocity loss per Moffat, Reference 42
** From Figure 67 at actual heat rejection, 100% h_g

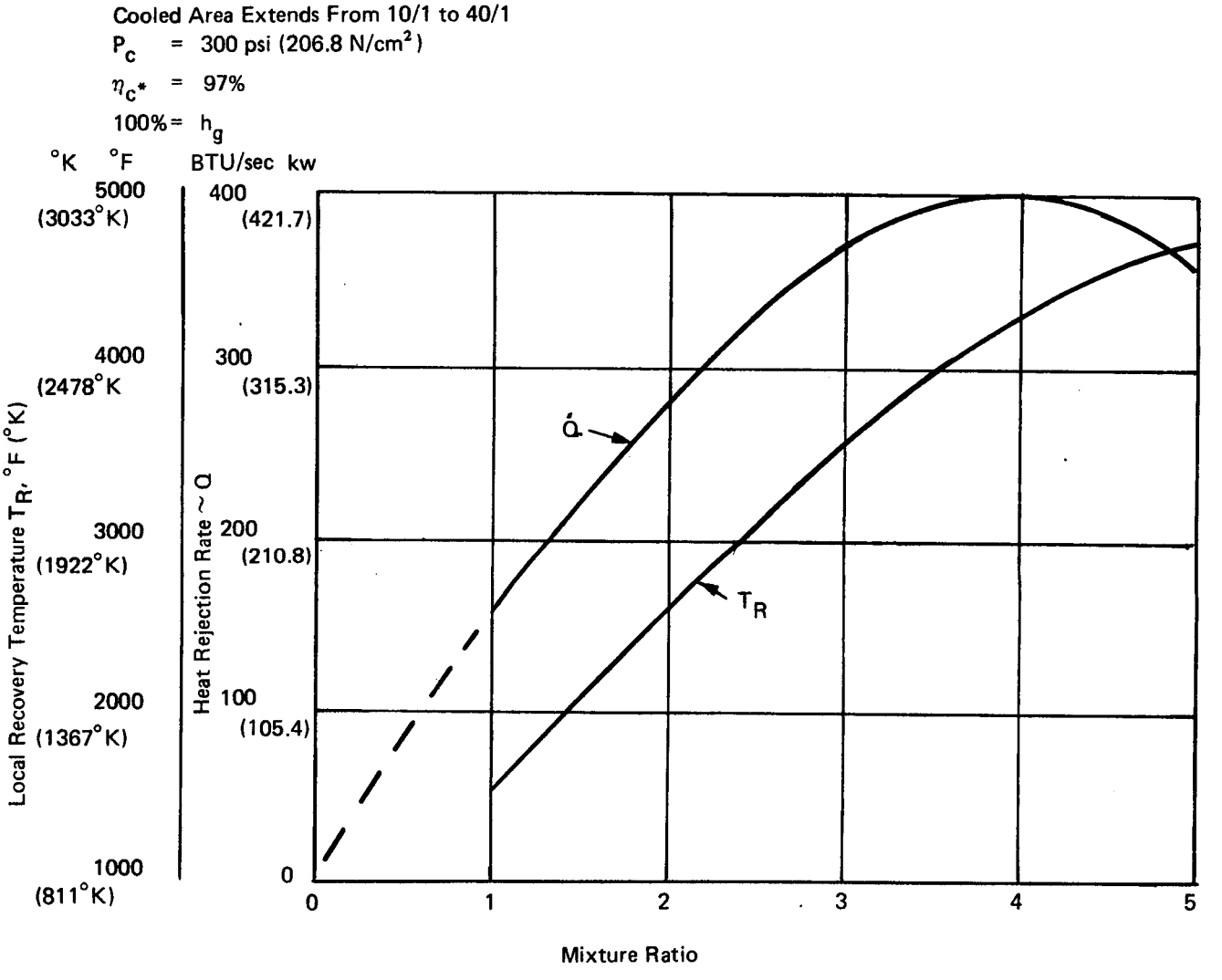

Figure 68. Heat Rejection Rate versus Mixture Ratio Water-Cooled Nozzle Extension

Predicted equilibrium temperature distributions along the radiation-cooled extension (no external insulation) were made for the nominal mixture ratio 4:1 with various amounts of supersonic dump cooling. The wall temperature with no dump cooling was made with the assumption of the recovery temperature at overall mixture ratio, and a combustion efficiency = 97%. A comparison of test and predicted radiation wall temperatures as in Figures 69 and 70 shows that the predicted wall temperature for the regenerative tests (0% dump cooling) compared reasonably well with the test data but the dump cooled calculations were under predicting temperatures toward the attachment station. A more accurate method of calculating the gas temperature distribution and local heat-transfer coefficients was required to predict operation with an insulated nozzle extension. The approach to improving the predictions consisted of:

(1) Superseding the dump-cooled adiabatic wall gas temperature distribution (calculated using Zakkay's method) by use of the actual wall temperature measurements.

(2) Making corrections on the gas-side heat-transfer coefficients, using water-cooled nozzle heat rejection rates with dump-cooled firings.

The measured wall temperatures for the dump-cooled extension were used to calculate the local gas temperature (T_R) by adding the ratio of radiative heat flux ($\dot{q}_{rad}$) to gas side heat transfer coefficient (h_g) to the wall temperature.

$$T_R = T_w + \frac{1}{h_g} (\dot{q}_{rad})$$

The total heat rejection rate to the water-cooled extension was calculated with the gas temperatures derived from radiation-cooled tests and correspondingly reduced cold-wall, gas-side heat transfer coefficients. These calculations are presented in Figure 71 with a point representative of the tests with 3% dump cooling.

Figure 71 indicates the use of 79% of the theoretical heat transfer coefficient to provide agreement between predicted values and test data. For simplicity's sake, 80% of the heat transfer coefficient value distribution in Figure 67 was used for the final insulated nozzle extension temperature predictions.

The selection of the percent of supersonic dump cooling for the 500 sec firing with an insulated nozzle extension was made for the demonstration of the lowest extension temperature consistent with the program target specific impulse of 435 sec (4266 N sec/kg). A plot of I_{sp} versus percent of dump cooling indicated that 435 sec (4266 N sec/kg) could be achieved with 7-1/2% dump cooling. That coolant flow corresponded to a radiation cooled extension temperature of 1900°F (1293°K) (Figure 72), an insulated and extension temperature approaching 2300°F (1515°K) (Figure 73).

The high temperature insulation specified on Figure 73 was selected on the basis of its mechanical properties for extended periods of use. The properties of Johns-Manville "Dynaflex" were originally examined in Reference (19) which proved inadequate for accurate thermal conductivity in vacuum. The work of Rolinski, Reference (20), was obtained for more complete data. "Dynaflex" is basically an alumina-silica fiber with chromia additive. Other properties are shown in Table XXIX.

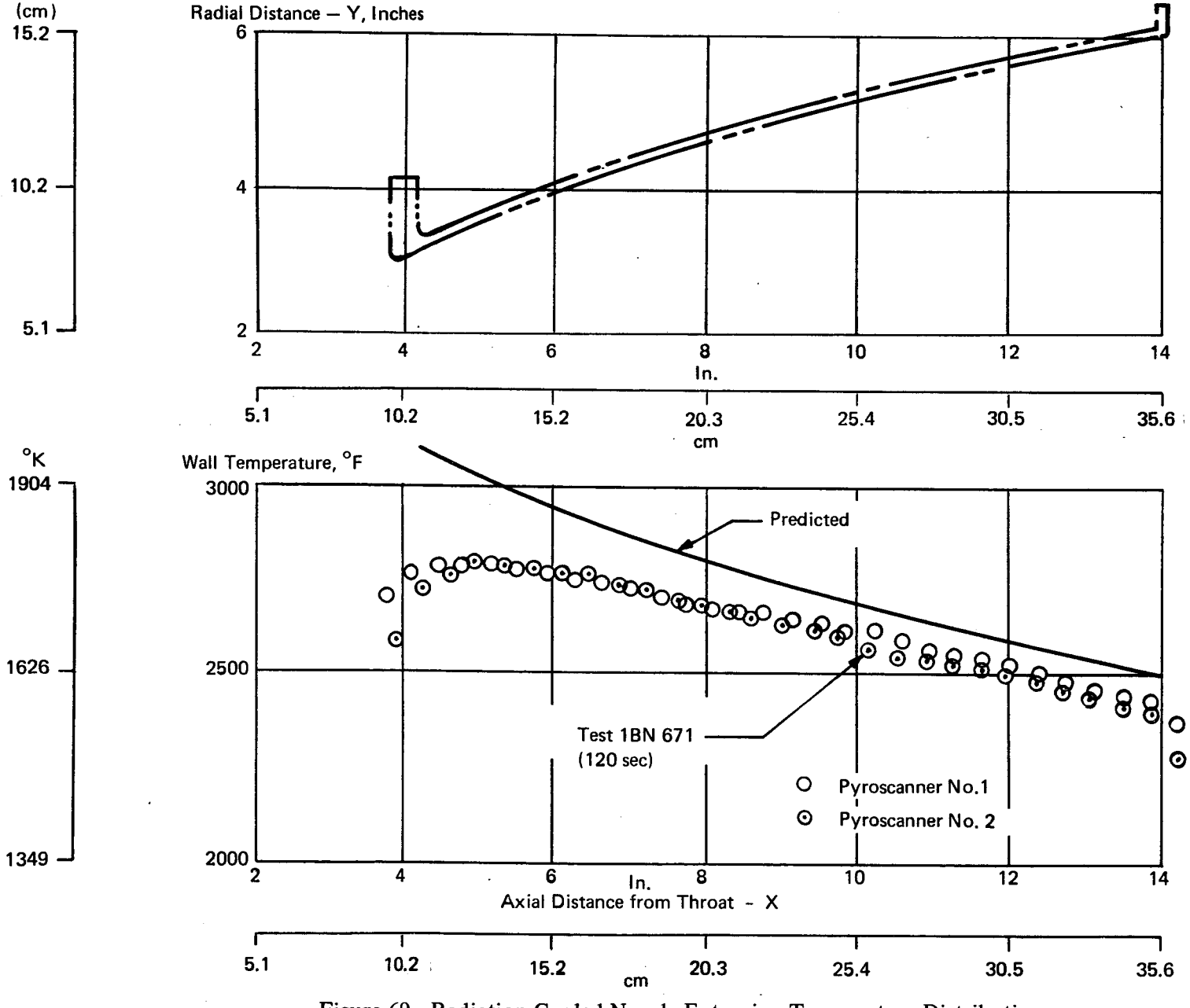

Figure 69. Radiation Cooled Nozzle Extension Temperature Distribution

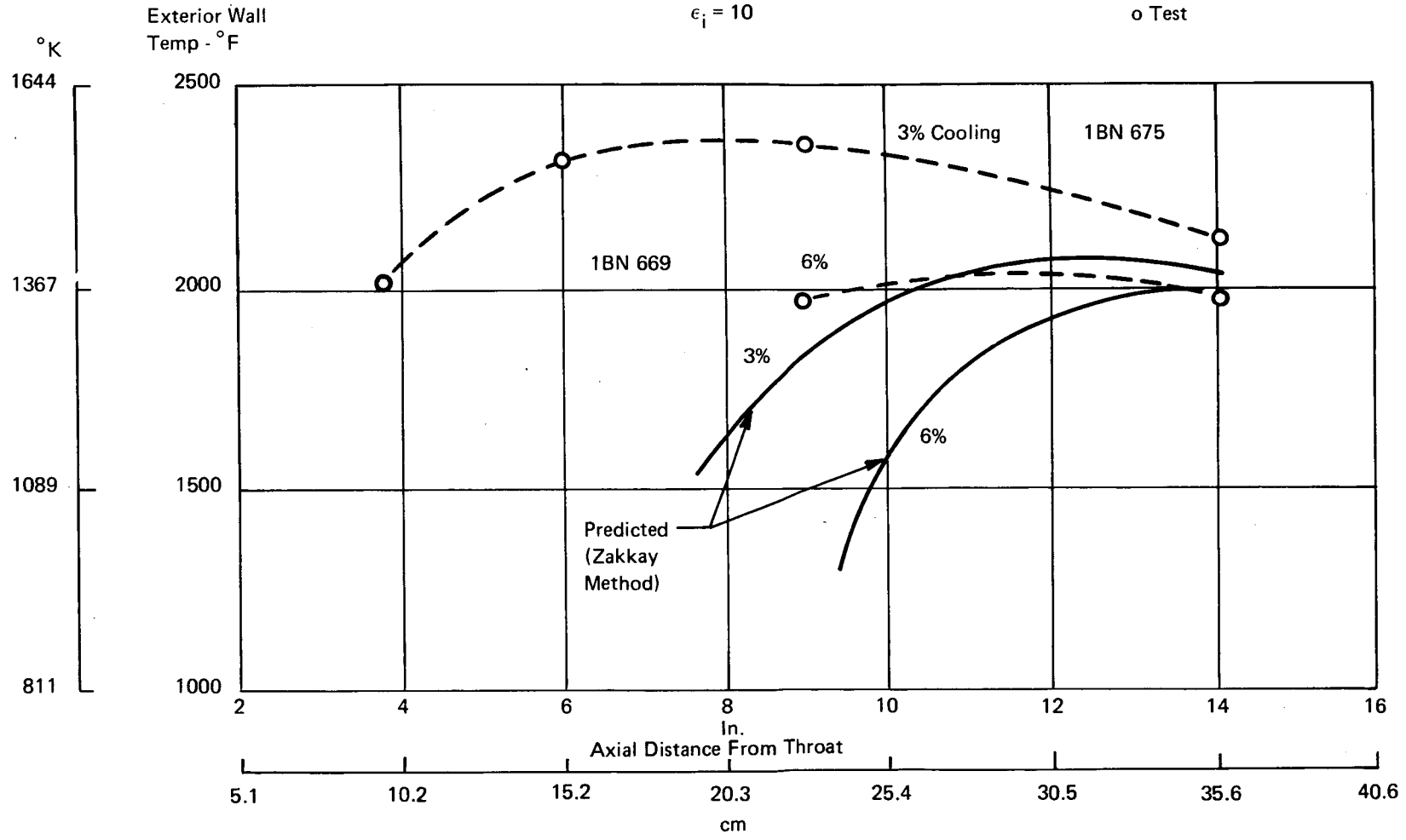

Figure 70. Model 8636 Dump Cooling - Radiation Cooled Nozzle Extension

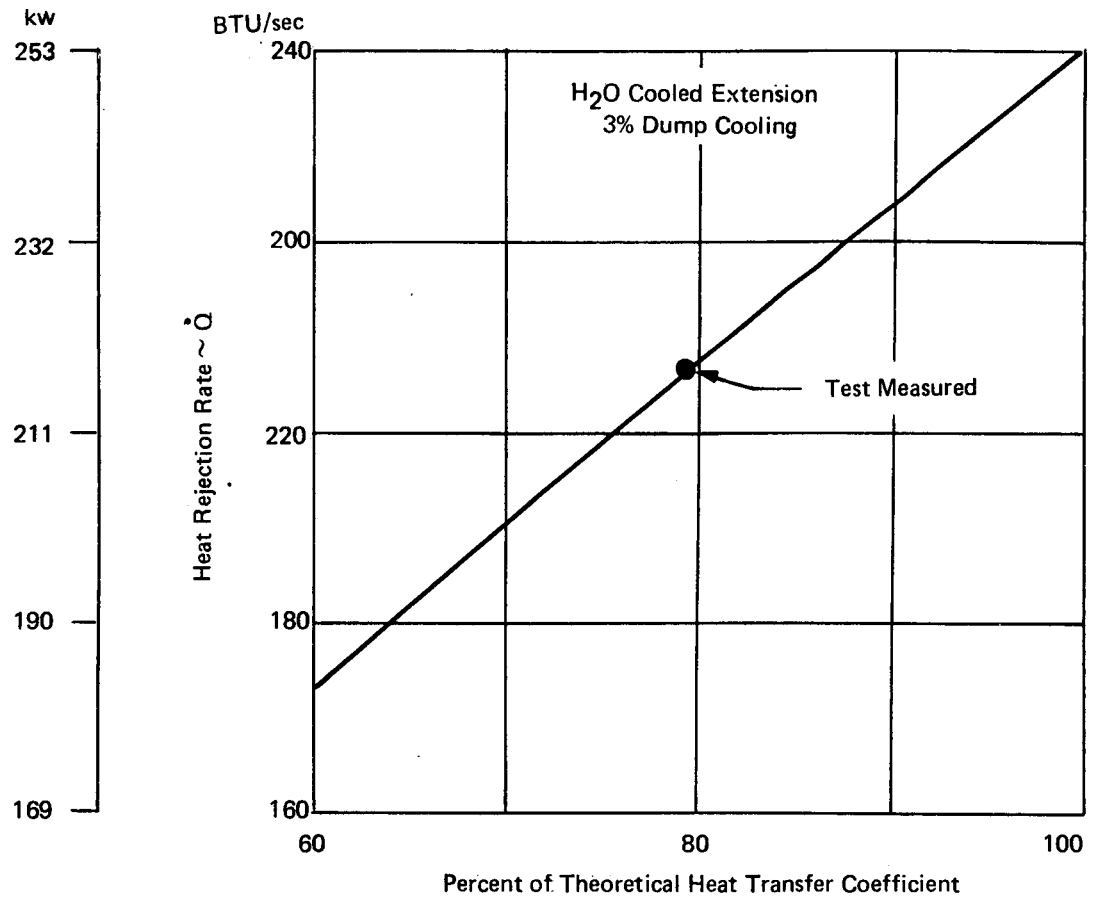

Figure 71. Heat Rejection Rate versus Percent Heat Transfer Coefficient

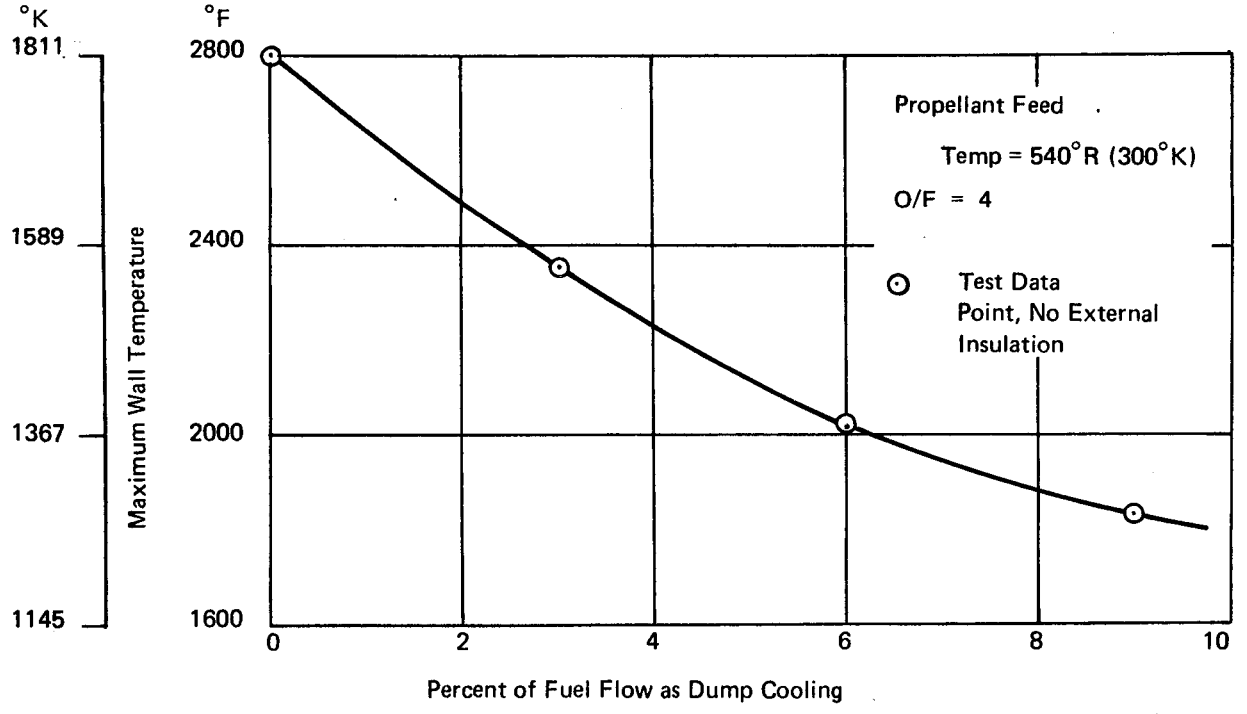

Figure 72. Maximum Radiation Cooled Nozzle Extension Temperature versus Percent Dump Cooling

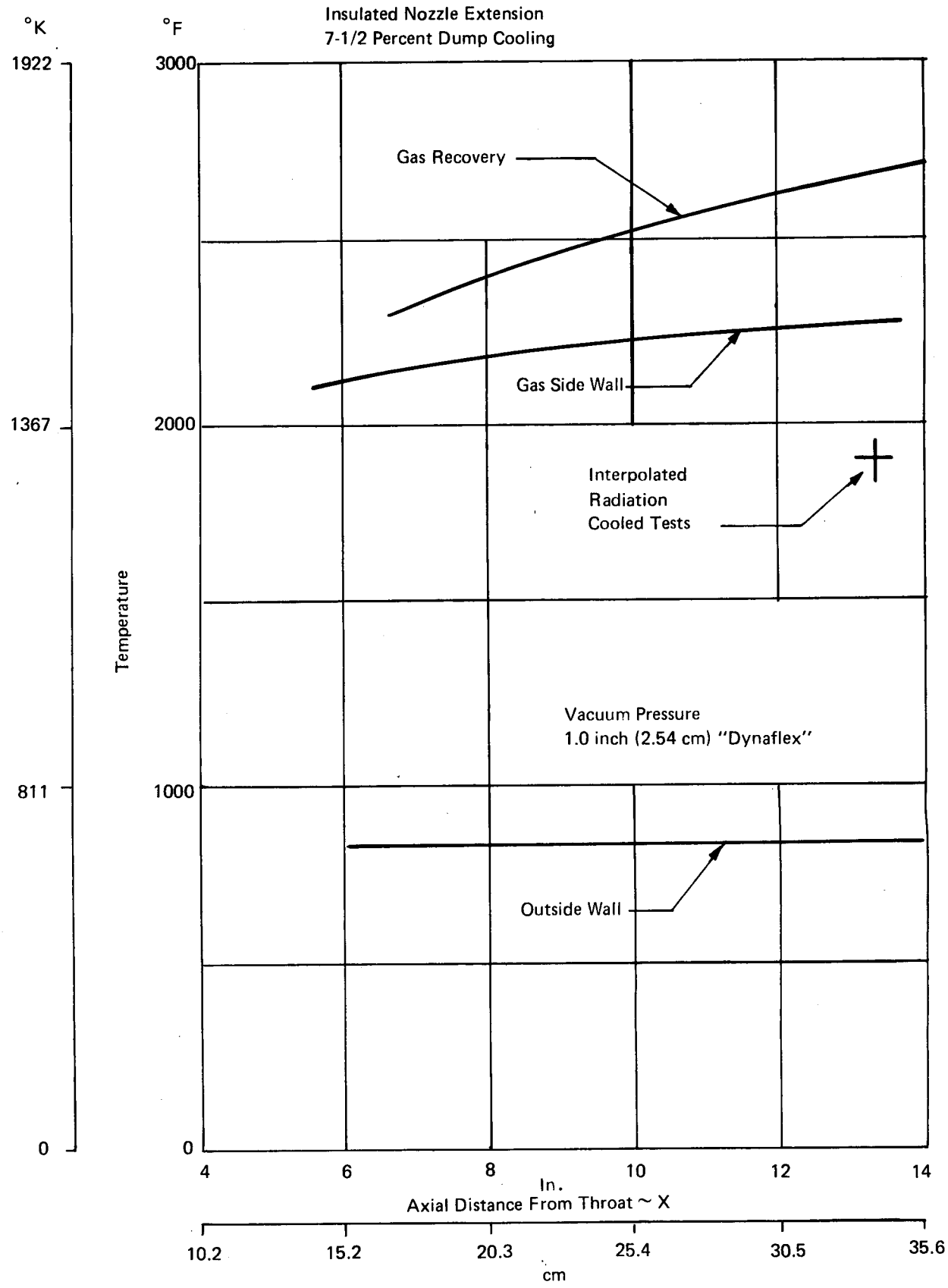

Figure 73. Predicted Temperature Distribution – Insulated Nozzle Extension

TABLE XXIX

CHARACTERISTICS OF "DYNAFLEX" INSULATION

Maximum Rated Temperature, °F	2800 (1811°K)
Density, lb/ft^3	8-10 (128.1-160.2 kg/m^3)
Fiber Diameter, microns	3.5
Unidimensional Shrinkage After 2 Hours	2.9% (2600°F) (1700°K)
Chemical Composition	SiO_2 (56.9%)
	Al_2O_3 (37.6%)
	Cr_2O_3 (4.5%)
Manufacturer	Johns-Manville Inc.

The temperature distribution of Figure 73 was predicted for the extension which was to be insulated with two 0.50-inch (1.27 cm) thick layers of "Dynaflex". For purposes of calculation, it was assumed the radiation-cooled wall temperature distribution for 7-1/2% dump cooling would be shaped similarly to the 9% data but with 1900°F (1311°K) maximum. The recovery temperature was calculated with 80% of the ideal heat transfer coefficient, as described previously. Final heat balances were made for an exterior emissivity of 0.9 and a mean thermal conductivity of 0.43 BTU in/ft^2 hr °F (223.1 joule/meter hr °K).

d. Attachment Flanges

The water-cooled nozzle extension flange attachment was analyzed to determine the steady-state temperature of three Viton O-rings (two O-rings sealing the Amzirc liner and an O-ring seal in the attachment flange) and bolt heads holding the extension to the manifold assembly. A nodal mathematical model was solved for the nominal operating conditions with 6 lb/sec water (2.724 Kg/sec) flow at 120°F (320°K) in the nozzle extension. The temperature of the Viton O-ring seals was taken as the average of the two metal surface temperatures at their tangent points. These were found to be

Forward Liner O-Ring	=	431°F (495°K)
Aft Liner O-Ring	=	489°F (527°K)
Extension Flange O-Ring	=	203°F (368°K)

The bolt head temperature was calculated as 158°F (343°K). The predictions indicated no temperature problems in the water-cooled extension test setup.

The radiation-cooled extension used supersonic dump cooling of the nozzle extension with insulation attached to the exterior of the nozzle extension, blocking heat loss by radiation to the surroundings except a small area in the outer diameter of the attachment flange. The nodal model, with predicted results, is shown in Figure 74. The local film temperature within the columbium extension was determined from the measured fully radiation cooled extension test data. Steady-state temperatures of the gas filled stainless steel O-ring, piston ring and Viton O-ring were of principal interest. The same nominal boundary conditions were used for the dump-cooled analysis as on the previously described water-cooled nozzle extension joint. Results of the analysis indicated no structural problems for seals, bolts or miscellaneous hardware for cyclic life.

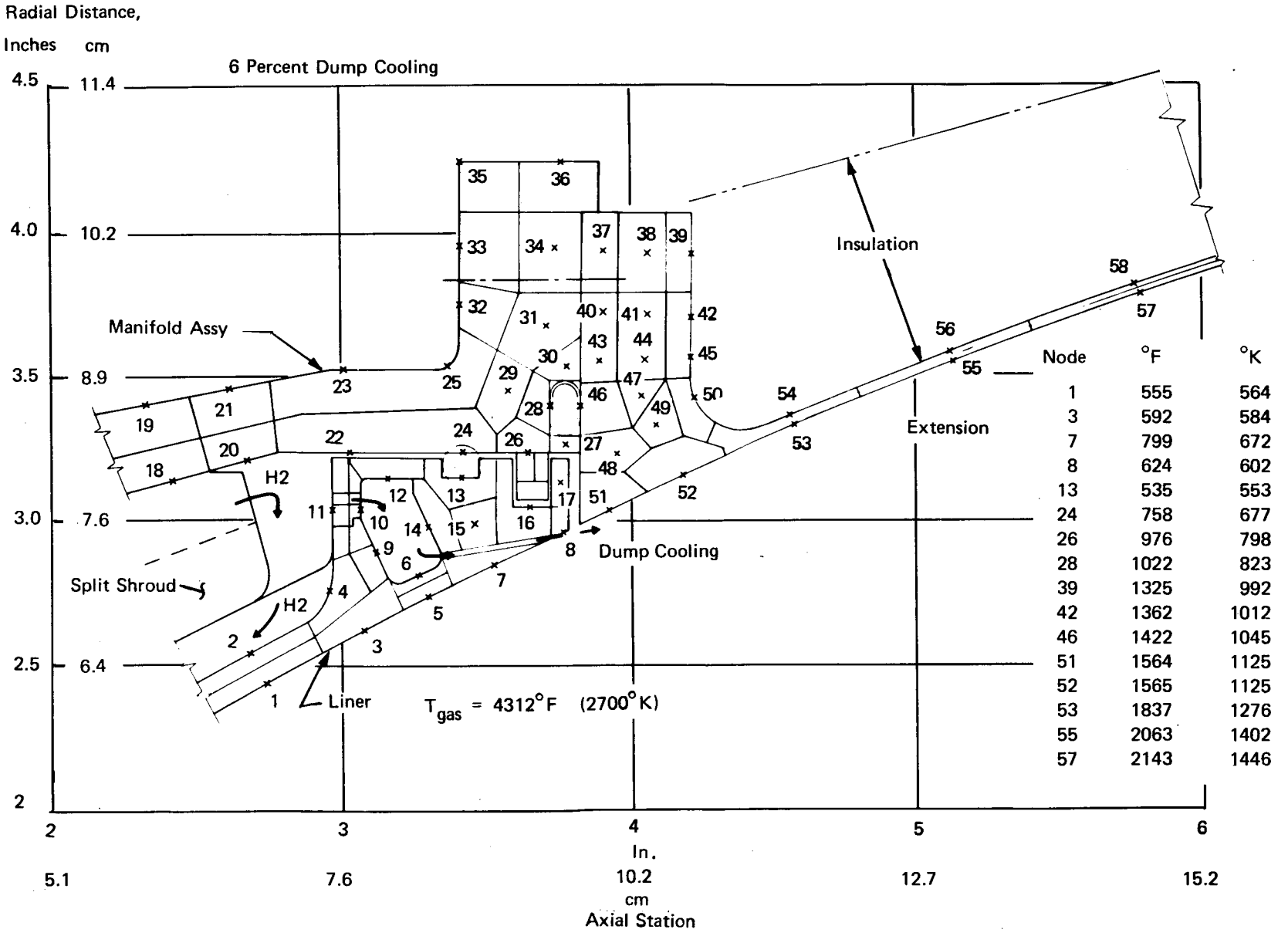

Figure 74. Joint of Columbium Extension and Dump Cooled Nozzle

E. DETAILED ANALYSIS OF COOLED SEA-LEVEL NOZZLE

A sea-level conical nozzle was designed for company-sponsored reverse-flow engine testing. As in the case of the contract altitude nozzle, the liner was regeneratively cooled with coolant slots EDM'd in Amzirc alloy to provide the capability of long-duration firings. The data base established by NAS3-14353 dictated that the subsonic nozzle and fuel injector be identical to the contract altitude nozzle; that is , the liner was designed with an integral channel cross section at the fuel injector end and free-standing sections aft of the fuel injector. The sea-level nozzle differed from the altitude nozzle in that the supersonic nozzle was defined as a 15° semidivergent angle conical nozzle expanded to an area ratio of 3.16:1. This area ratio is such that the exhaust is expanded to nearly sea-level atmospheric pressure at the nominal operating point and the exhaust streamlines leave the conical nozzle with little change in flow direction. Exhaust gas heating of the aft surface of the sea-level thrust chamber assembly was therefore prevented.

Coolant passage dimensions of the sea-level nozzle were determined for the channel type liner by stipulating the same cross-sectional coolant flow area at each divergent nozzle area ratio as in the altitude nozzle design previously described. Temperature distributions through the liner wall at 12 stations were calculated by construction of nodal mathematical models and solving with the appropriate boundary conditions. The computed gas side heat transfer coefficient is presented in Figure 75. The distribution of the coefficient reflects the difference in Mach number distributions between the conical and contoured nozzles. Passage dimension and wall temperatures solved as a result of the analysis are given in Table XXX. The temperature distribution in the subsonic nozzle is approximately 20° less than the altitude nozzle at all stations upstream of the throat because the integrated heat rejection aft of the throat is less than the altitude nozzle liner.

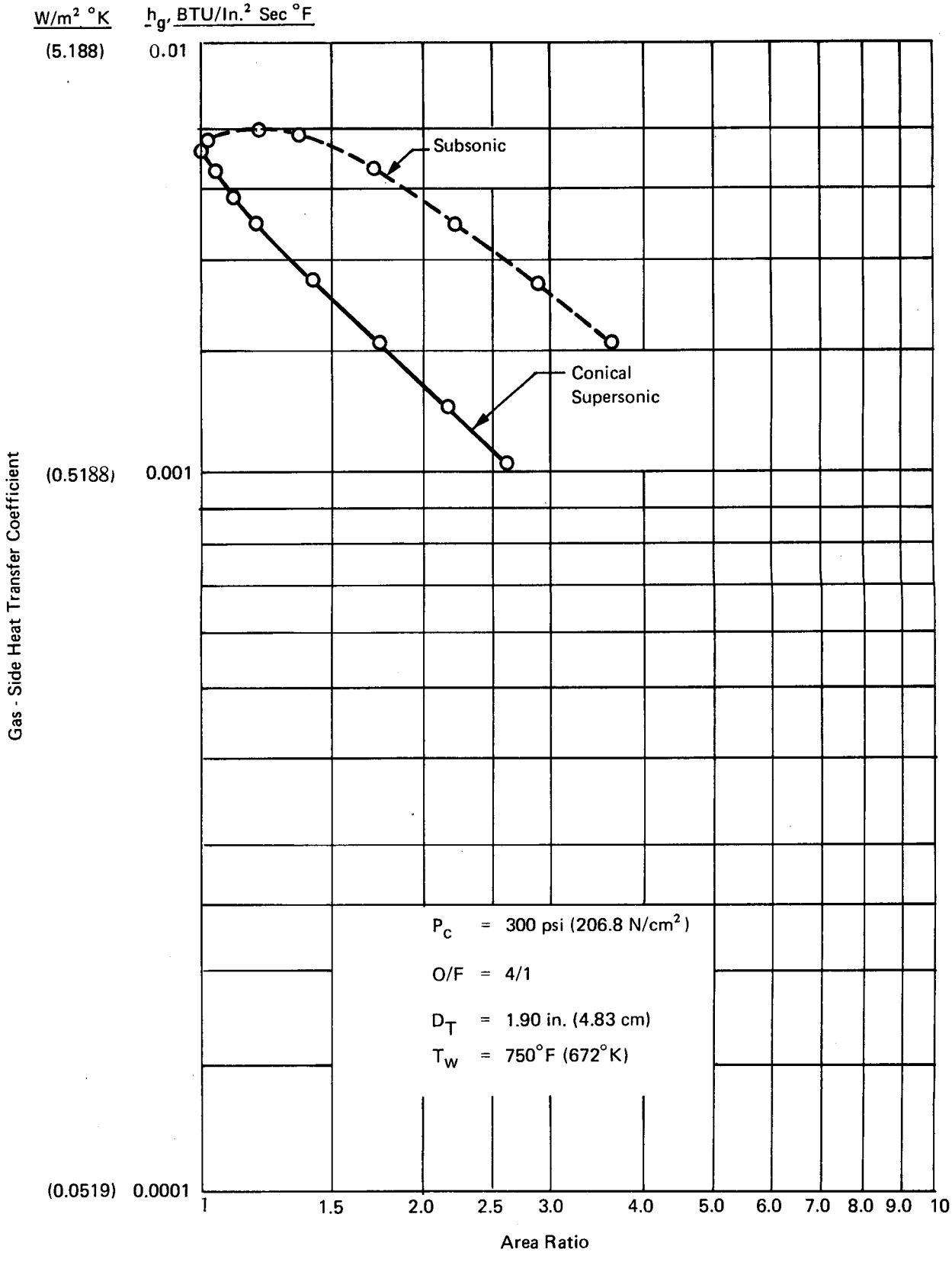

Figure 75. Gas-Side Heat Transfer Coefficient Distribution Sea-Level Nozzle 8636-470047

TABLE XXX
WALL TEMPERATURE DISTRIBUTION
SEA LEVEL LINER

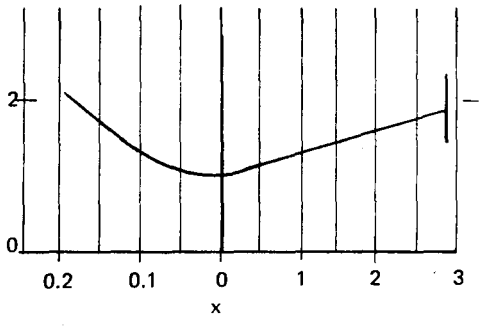

Sea-Level Conical Nozzle

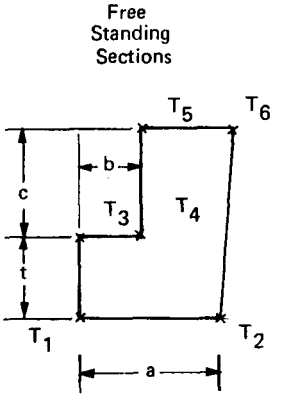

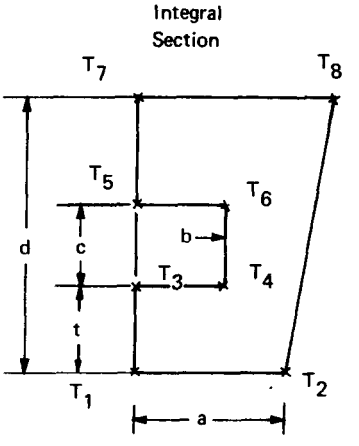

Assumptions: 40 Passages
Mixture Ratio = 4/1

	Dimensions											
	x		t		a		b		c		d	
	in.	cm	in.	cm	in.	cm	in.	cm	in.	cm	in.	cm
Subsonic Nozzle	0	0	0.070	0.178	0.0745	0.1892	0.045	0.1143	0.182	0.4623		
	-0.4	-1.016	0.070	0.178	0.0778	0.1961	0.045	0.1143	0.161	0.4089		
	-0.8	-2.032	0.070	0.178	0.0873	0.2217	0.0525	0.1334	0.121	0.3073		
	-1.05	-2.667	0.070	0.178	0.0978	0.2484	0.0705	0.1791	0.102	0.2591		
	-1.30	-3.302	0.070	0.178	0.1116	0.2835	0.088	0.2235	0.085	0.2159		
	-1.55	-3.937	0.070	0.178	0.1271	0.3228	0.1065	0.2705	0.068	0.1727		
	-1.80	-4.572	0.070	0.178	0.143	0.3632	0.124	0.3150	0.053	0.1346	0.375	0.9525
	-1.94	-4.928	0.070	0.178	0.157	0.3988	0.137	0.3480	0.0438	0.1113	0.1838	0.4669
Sea-Level Conical Supersonic Nozzle	0.4	1.016	0.070	0.178	0.0815	0.2070	0.0465	0.1181	0.177	0.4496		
	0.8	2.032	0.070	0.178	0.0888	0.2256	0.052	0.1321	0.187	0.4750		
	1.30	3.302	0.070	0.178	0.089	0.2261	0.0585	0.1486	0.206	0.5232		
	2.34	5.944	0.070	0.178	0.121	0.3073	0.0725	0.1842	0.247	0.6274		

	Wall Temperature															
	T_1		T_2		T_3		T_4		T_5		T_6		T_7		T_8	
	°F	°K	°F	°K	°F	°K	°F	°K	°F	°K	°F	°K	°F	°K	°F	°K
Subsonic Nozzle	661	623	652	618	519	543	481	522	242	390	253	396				
	674	630	641	612	530	550	492	529	277	409	243	418				
	695	642	704	647	566	626	527	548	346	448	370	461				
	741	667	718	655	603	591	561	530	397	476	417	487				
	708	649	685	637	589	583	595	558	415	480	430	495				
	667	624	646	615	564	569	525	547	435	498	449	505				
	545	558	515	541	461	512	407	482	248	393	281	411	264	402	265	402
	535	553	499	532	499	532	447	504	281	411	334	451	286	414	331	439
Sea-Level Conical Supersonic Nozzle	790	694	779	688	686	637	652	618	466	515	482	523				
	760	678	748	671	674	630	640	611	450	506	463	513				
	737	665	724	658	670	628	635	609	464	514	474	519				
	672	629	657	621	626	604	596	587	445	503	455	509				

F. ANALYSES OF LOW PROPELLANT FEED TEMPERATURE ALTITUDE TEST HARDWARE

1. Baseline Dump-Cooled Liner

A low-inlet-temperature AMZIRC liner was designed in a similar fashion as the ambient-temperature liner, differing only in the dimensions of the fuel injector orifices. Thermal analyses had shown, as in Table XXII, that operating the regeneratively cooled liner designed for 540°R (300°K) inlet coolant with 250°R (139°K) coolant would not be detrimental structurewise, and that the calculated total heat rejection does not vary significantly with inlet temperature. On that basis, a dump-cooled nozzle liner was designed for 250°R (139°K) H_2 feed temperature and 6% fuel dump cooling with the fuel injector sized for an injection velocity similar to that for the ambient-temperature liner. Table XXXI lists the critical flow parameters of the injector orifices, 40 in number, 0.023 inches (0.058 cm) high and 0.274 inches (0.696 cm) wide. The table shows that the coolant Mach number at 250°R (139°K) feed is higher than for the ambient coolant design and hence would require higher feed pressure to maintain the desired injection velocity at the rated propellant flow rate. The table also gives the calculated flow parameters for the 250°R (139°K) feed liner when operated with 540°R (300°K) feed H_2.

Although the baseline 250°R (139°K) feed temperature liner was designed for 6% dump cooling, dump-cooling holes were provided for only 3% dump coolant in the final assembly and that revised configuration was fired in the simulated altitude tests.

TABLE XXXI
FUEL INJECTOR PARAMETERS
(Low Temperature Altitude Nozzle Liner, Baseline 6% Dump Cooling)

Coolant Inlet Temperature, °R	250* (139°K)	540 (300°K)
Mixture Ratio	4/1	4/1
Coolant Flow Rate, lbm/sec*	0.6482 (0.2943 kg/sec)	0.6482 (0.2943 kg/sec)
Exit Mach Number	0.674	0.869
Exit Velocity, fps	2356 (718 m/sec)	3915 (1167 m/sec)
Injector Total Pressure, psia	401 (276.5 N/cm²)	484 (333.7 N/cm²)

*Design Point: Exit Static Pressure = 296.1 psia (204.2 N/cm²)
Coolant Exit (fuel injector) flow area = 0.2521 in.² (1.627 cm²)
Fuel Flow Rate = 0.6896 lbm/sec (0.3130 kg/sec)

2. Dump-Cooled Liner, Changed Fuel Injection Station

The second nozzle section for Amendment 2 of the contract incorporated a changed station of H_2 injection as shown in Figure 76. Figure 76 includes the 540°R (300°K) liners' H_2 injection station for reference. The pressure drop of the second low-temperature liner section is designed for 75 psi (51.7 N/cm²) or 20 psi (13.8 N/cm²) less than the baseline liner described previously. The reduction of design ΔP resulted in an injection velocity of 2190 fps (668 km/sec) with an engine H_2 feed temperature of 250°R (139°K). The regenerative passages of the second liner were essentially the same as the earlier designs because of the insensitivity of the maximum liner temperature with H_2 feed temperature.

A discussion of the selection of the changed point of fuel injection for the second low feed temperature test hardware assembly is given in Section IV, Injector Design and Analyses.

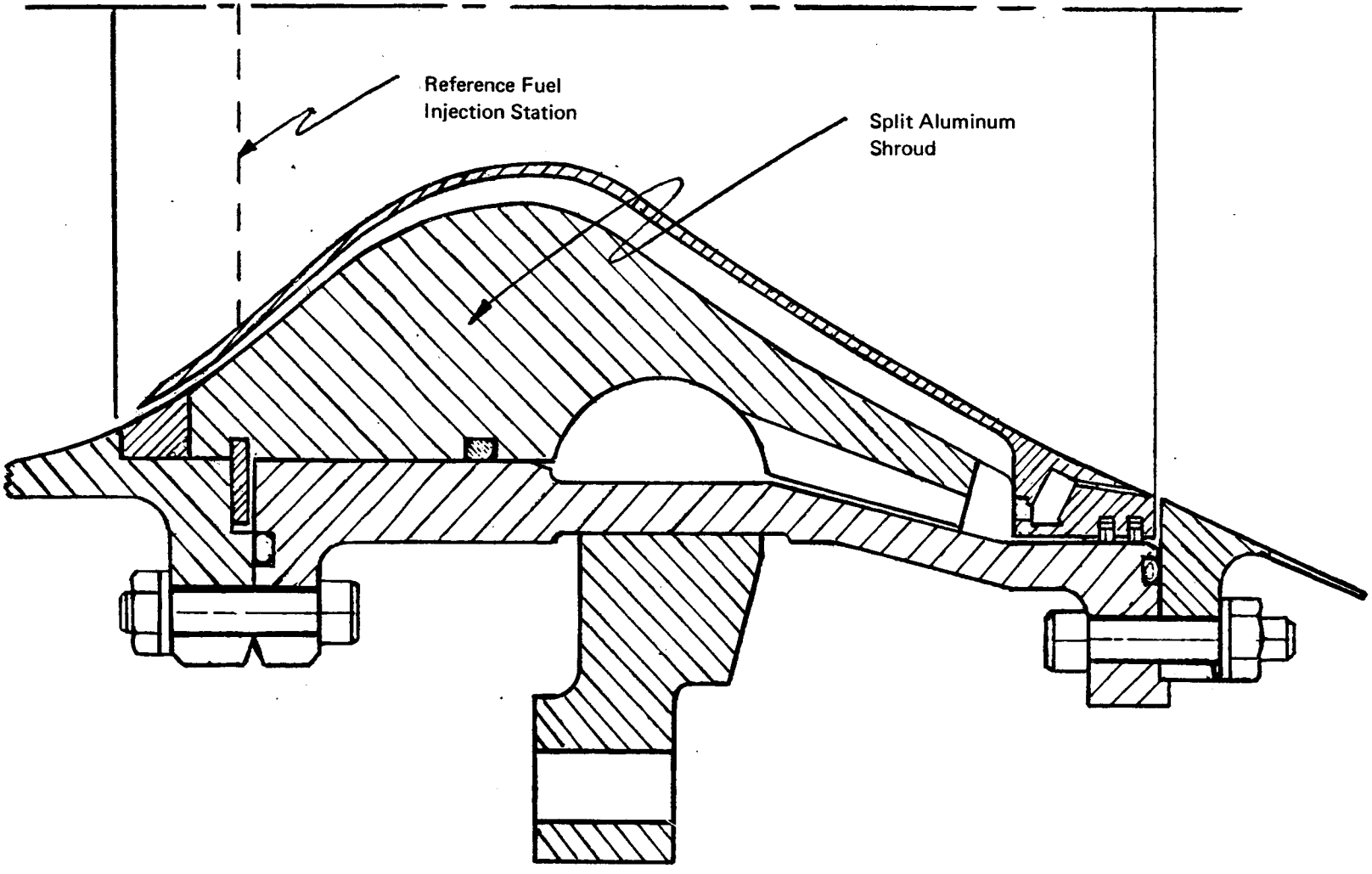

Figure 76. Nozzle Section - Changed Fuel Injection Station

VII. THRUST CHAMBER FABRICATION

A. GENERAL

The thrust chamber fabrication effort included the spherical thrust chambers, igniter plug adapters, the nozzles or nozzle extensions and associated metal seals, snap rings, "O" rings and various metal fasteners (i.e., nuts, bots, washers, etc.). The method of assembling the various components is described in this section.

The major elements of this task consisted of the following:

(1) Heat sink/sea level thrust chamber (combustion chambers, igniter plug adapters, nozzles and thrust chamber assembly).

(2) Cooled/altitude thrust chamber (combustion chamber, igniter plug adapters, nozzle extensions, and thrust chamber assembly).

B. HEAT SINK/SEA LEVEL THRUST CHAMBER

The spherical combustion chambers and the uncooled (heat sink) nozzles were used with the various oxidizer and fuel injector assemblies for short duration (approximately 2 to 3 seconds) evaluation. This test effort resulted in early characterization of the 1500-lb (6672N) thrust design. Although the tests were of short duration, the spherical combustion chambers were capable of steady state, long duration firings.

1. Combustion Chambers

Three spherical combustion chambers [a 22 L* (0.559m), 32 L* (0.813m), and 42 L* (1.067m)] were fabricated for use with the heat sink/sea level hardware. Each chamber was machined from 304L SST bar.

A summary of these chambers fabricated is listed in Table XXXII. A photograph is included in Figure 77.

TABLE XXXII
HEAT SINK/SEA LEVEL HARDWARE
IGNITER ADAPTERS
COMBUSTION CHAMBERS AND NOZZLES

Part Number	Part Name	Material	Qty.
8636-470020-1	Chamber L* = 32 (0.831 m)	SST, 304L	1
8636-470021-1	Chamber L* = 42 (1.067 m)	SST, 304L	1
8636-470022-1	Chamber L* = 22 (0.559 m)	SST, 304L	1
8636-470	Igniter Plug Adapter	SST, 304L	2
8636-470017-1	Nozzle (with Thermocouples)	OFHC Copper	1
8636-470017-3	Nozzle (without Thermocouples)	OFHC Copper	1

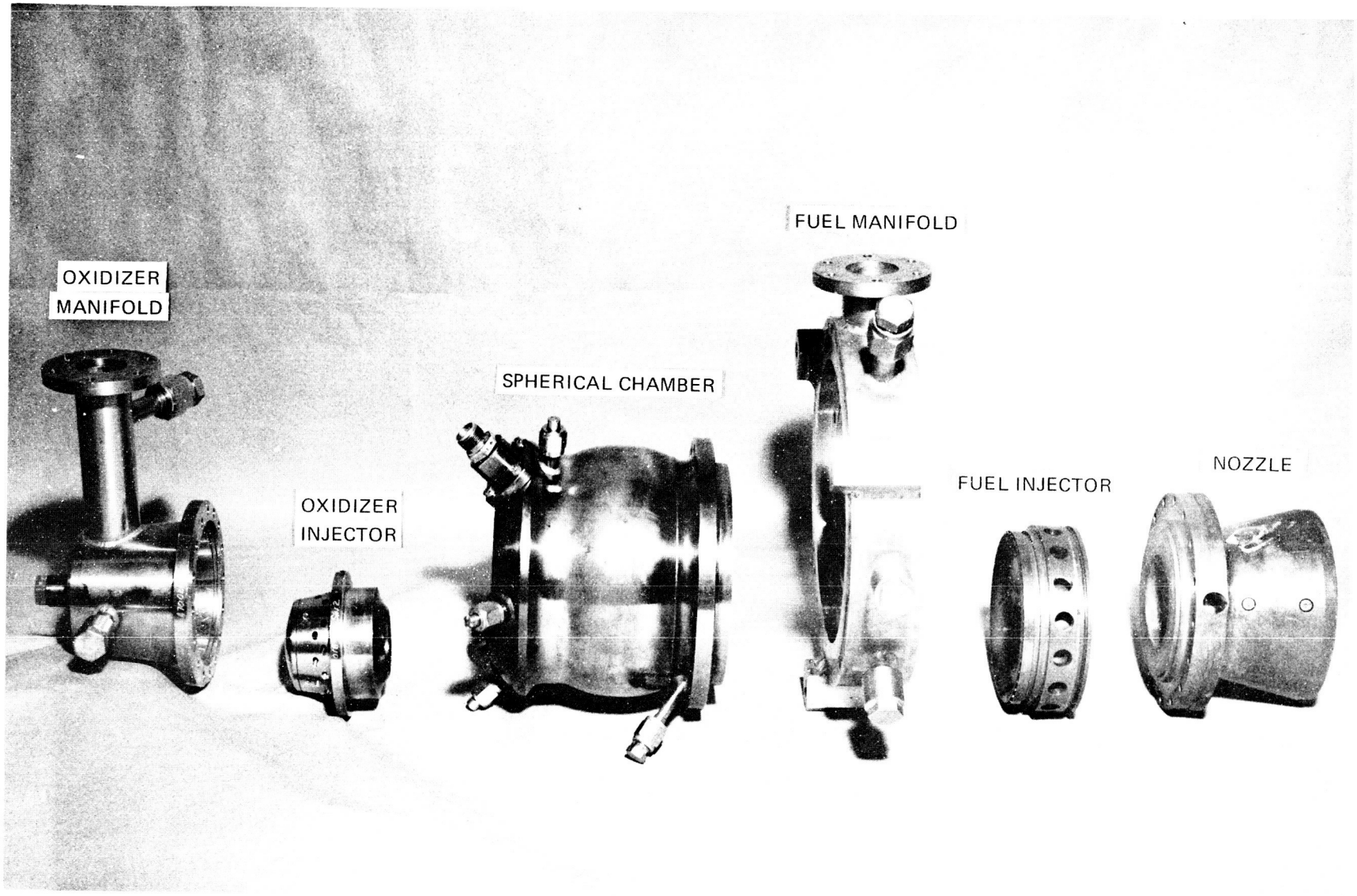

Figure 77. Heat Sink/Sea Level Chamber Assembly

2. Igniter Plug Adapters

Two igniter plug adapters were fabricated for use with the heat sink hardware. One adapter was used to attach the igniter plug to the combustion chamber, the other served as a spare. The adapters were machined from 304 SST bar. A reference to the fabrication of these adapters is listed in Table XXXII.

3. Nozzles

Two heat-sink nozzles were fabricated, one with provisions for six thermocouple attachments (three axial stations at two different circumferential locations). Each thermocouple was attached to an "island" by insertion in a drilled hole and "peened" in place. The second nozzle did not have the thermocouple installation. Each nozzle interfaced with the fuel injector assembly and incorporated the throat section and divergent nozzle section to an area ratio of 3.16. Each nozzle was machined from an oxygen free copper bar. The thermocouple "islands" were EDM'd.

A summary of these nozzles is also listed in Table XXXII and a photograph is also shown in Figure 77.

4. Thrust Chamber Assembly

The assembly methods of the thrust chamber assembly is listed below:

(a) Although the spherical combustion chamber had provisions for two igniter ports only one was used with the heat sink hardware. The other port was plugged. The igniter adapters were bolted to the combustion chamber and a Viton "O" ring was used as a seal.

(b) The oxidizer injector was installed in the combustion chamber and retained in place by the oxidizer manifold assembly which was bolted to the combustion chamber. Viton "O" rings were used as seals.

(c) The fuel manifold was bolted to the combustion chamber, without the bolts being torqued. The fuel injector was then installed in the chamber and manifold assembly. Then the nozzle was bolted to the fuel manifold, retaining the fuel injector in place, and all bolts torqued. Viton "O" rings were used at all seal locations.

A cross section of the heat sink/sea level thrust chamber assembly is shown in Figure 78, and a photograph of the assembly is given in Figure 77.

C. COOLED/ALTITUDE THRUST CHAMBER

The same basic spherical combustion chamber design used for the uncooled/heat sink hardware was used for the cooled/altitude hardware. Since the throat section and divergent nozzle section to an area ratio of 10:1 was integral with the fuel injector only nozzle extensions were fabricated from an area ratio of 10:1 to 40:1. This hardware allowed for steady state, long duration testing at simulated altitudes of approximately 100,000 feet (30,480m) during Task IX. The hardware fabricated in this task follows:

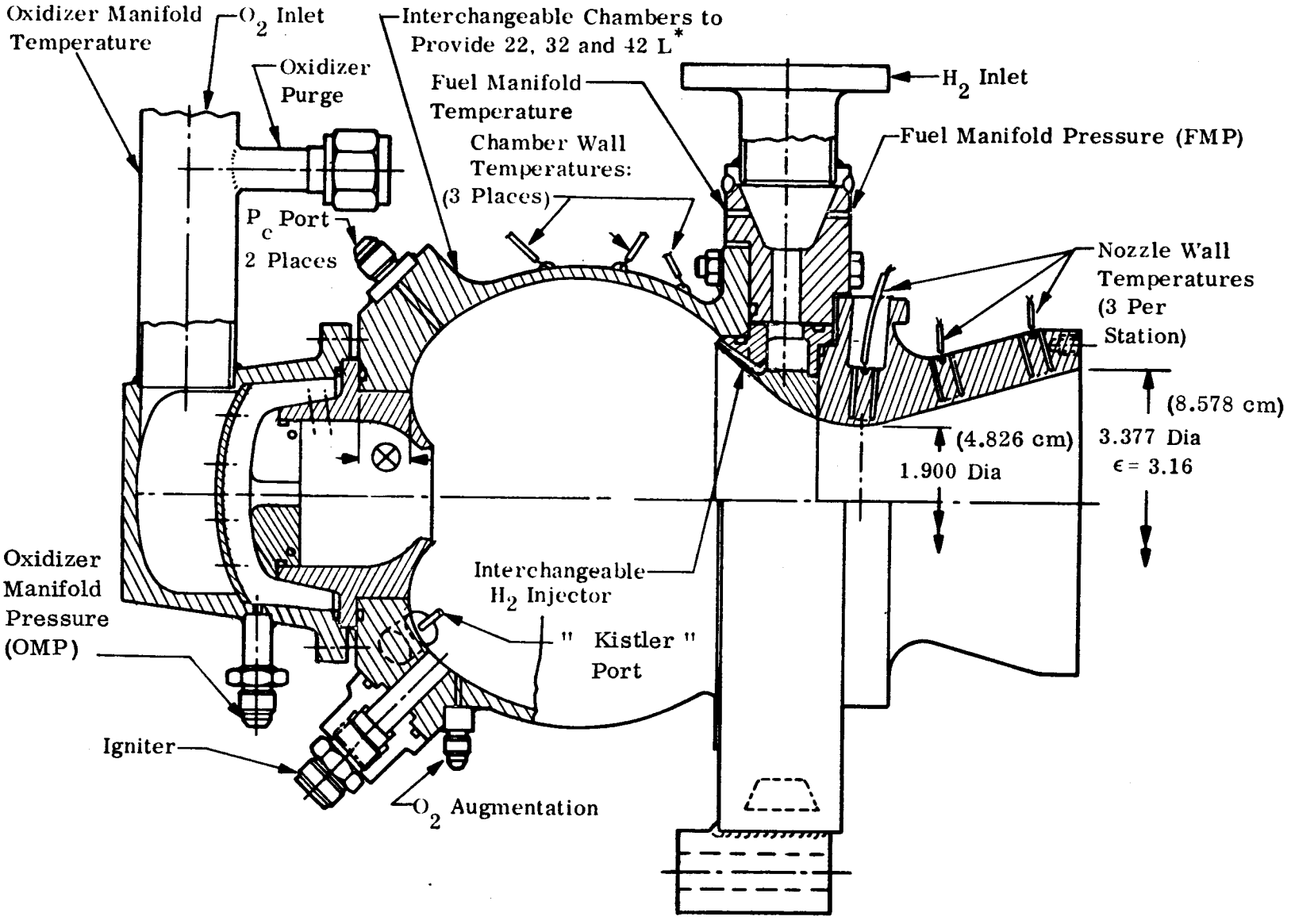

Figure 78. Heat Sink Thrust Chamber Assembly

1. Combustion Chambers

Two types of spherical combustion chambers were used for this task, the type for the standard fuel injection station and the other for the modified fuel injection station for low propellant temperature evaluation. Three combustion chambers were used for the standard fuel injection station, the 32L* (0.813m) SST, 304L chamber fabricated for the uncooled/heat sink evaluation but modified for interface with the regeneratively cooled fuel injector, a 32L* (0.813m) Multimet chamber, and a 32L* (0.813m) SST 304L chamber with an integral nozzle retainer ring. One 32L* (0.813m) SST 304L combustion chamber was fabricated for use with the high fuel injection station hardware. A nozzle retainer ring was fabricated for use with the standard type chamber.

A summary of the parts fabricated is listed in Table XXXIII. A photograph of the modified fuel injection station chamber is shown in Figure 79. The combustion chambers were machined from SST 304L or Multimet bar. The nozzle retainer ring was machined from SST 304L plate.

TABLE XXXIII
COOLED/ALTITUDE HARDWARE
COMBUSTION CHAMBERS IGNITER PLUG ADAPTERS
AND NOZZLE EXTENSIONS

Part Number	Part Name	Material	Qty	Function
8636-470	Chamber, Assembly of, 32L* (0.183 m)	Multimet	1	
8636-470020-5A	Chamber, Assembly of, 32L* (0.813 m) (Reworked)	SST, 304L	1	
8636-970125-1	Chamber, Assembly of 32L* (0.813 m)	SST, 304L	1	Equivalent of 8636-470020-5 with Integral Nozzle Retainer Ring
8636-470093-1	Chamber, Assembly of, 32L* (0.813m)	SST, 304L	1	Used with High Injection Point Liner
8636-470	Igniter Plug Adapter, Cooled	SST, 304L	2	
8636-470040-1	Drilled Nozzle Extension, Assembly of	Heat Treated to T-6 Condition	1	
8636-470037-1	AFT Manifold	Al, 6061-T651 Heat Treated to T-4 Condition	1	
8636-470038-1	Forward Manifold	Al, 6061-T651 Heat Treated to T-4 Condition	1	
8636-470039-1	Nozzle Extension	Al, 6061-T651 Heat Treated to T-4 Condition	1	
8636-470041-1	Manifold Cover	Al, 6061-T651 Heat Treated to T-4 Condition	1	
8636-470041-3	Manifold Cover	Al, 6061-T651 Heat Treated to T-4 Condition	1	
8636-470042-1	Fitting	Al, 6061-T651 Heat Treated to T-4 Condition	2	
8636-470056-1	Radiation Cooled Nozzle Extension		1	
8636-470056-3	Flange	Columbium Alloy C103 (Cb-10% H_f - 1% Ti)	1	
8636-470056-5	Nozzle Cone	Columbium Alloy C103 (Cb-10% H_f - 1% Ti)	1	
–	Insulation Blanket	Dynaflex	1	

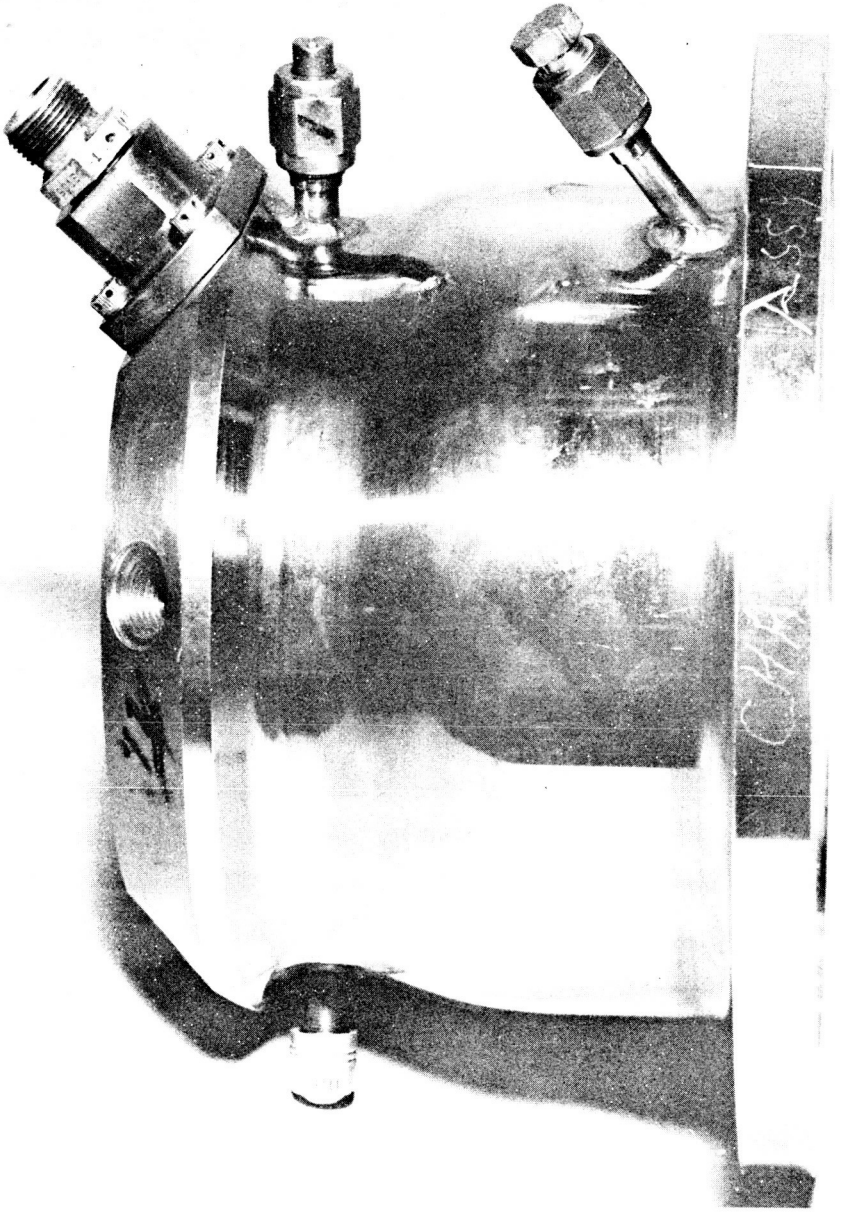

Figure 79. Modified Fuel Injection Station Chamber

2. Igniter Plug Adapters

Two types of adapters were used for the cooled/altitude chamber evaluation. The same adapters as fabricated for use with the uncooled/heat sink hardware and an oxidizer-cooled adapter. The oxidizer-cooled igniter plug adapter was cooled with the igniter oxidizer augmentation flow and was used for the long duration 500-sec test. This cooled adapter was machined from SS 304L stock with SS tubing welded for inlet and outlet connections. A cross section and a photograph of this cooled adapter are shown in Figures 80 and 81, respectively, and the adapter is listed in Table XXXIII.

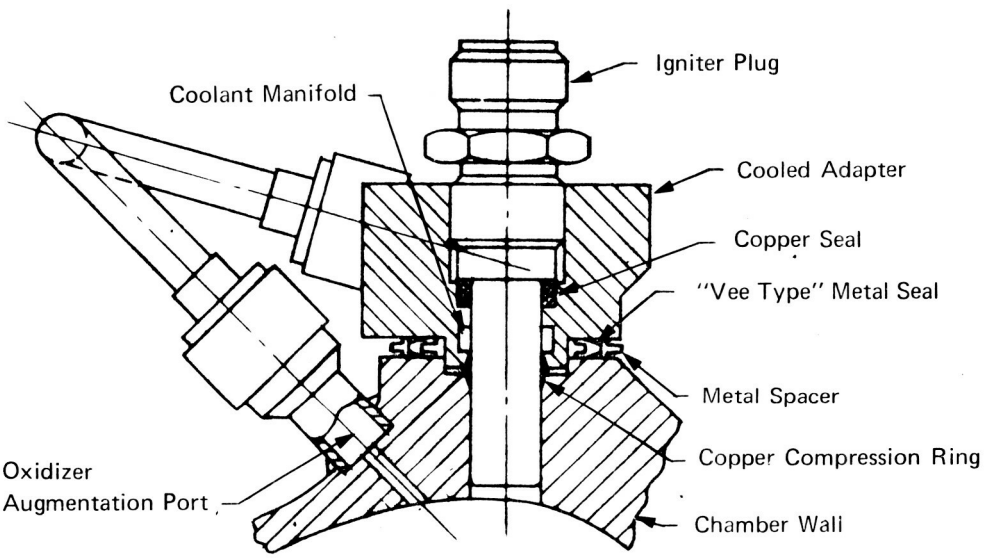

Figure 80. Cooled Igniter Plug Adapter

3. Nozzle Extensions

Two types of nozzle extensions were fabricated for evaluation of the cooled/altitude hardware; a water-cooled, drilled aluminum extension and an uncooled (or radiation-cooled) columbium extension. Each extension had the same interface configuration at the area ratio of 10:1 and the same internal contour to an area ratio of 40:1.

a. Water-Cooled, Aluminum Nozzle Extension

This nozzle extension could also be cooled with gaseous H_2 and consisted of six basic parts; the aft manifold, the forward manifold, the nozzle extension, two manifold covers and the fittings. A summary of these parts is listed also in Table XXXIII. A cross section is shown in Figure 82 and two photographs are shown in Figures 83 and 84.

The method of fabrication and assembly follows:

(1) Nozzle Extension - Machined from 6061-T4 forged billet. Cooling passages were drilled holes. The 0.25-in. (6.35mm) diameter cooling passages were formed by drilling from each end. The quality of the drilling was very high with mismatch between the two mating passages within 0.002 in. (0.051mm). The deep hole drilling operation was performed by 20th Century Machine Co.

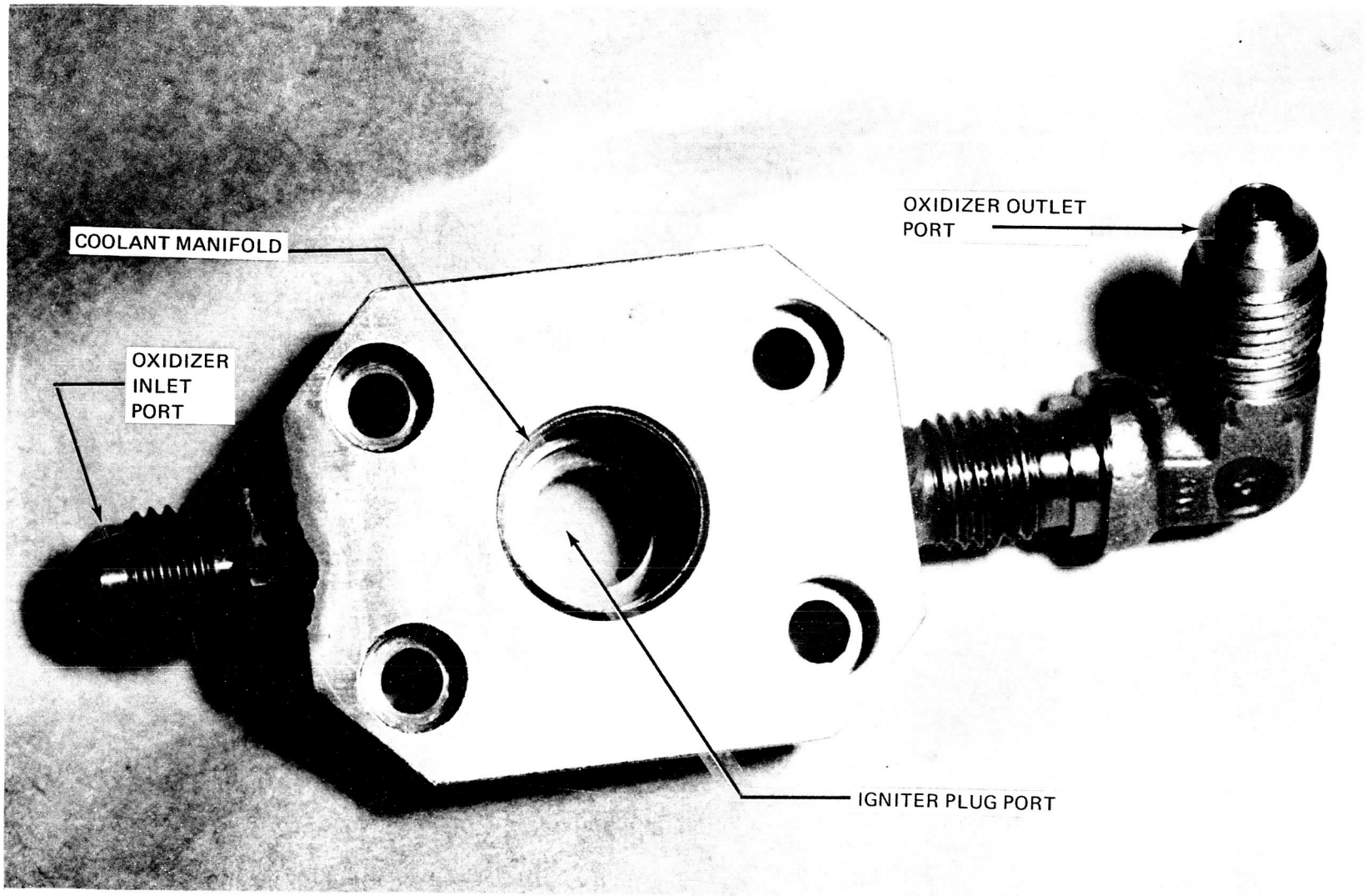

Figure 81. Cooled Igniter Plug Adapter

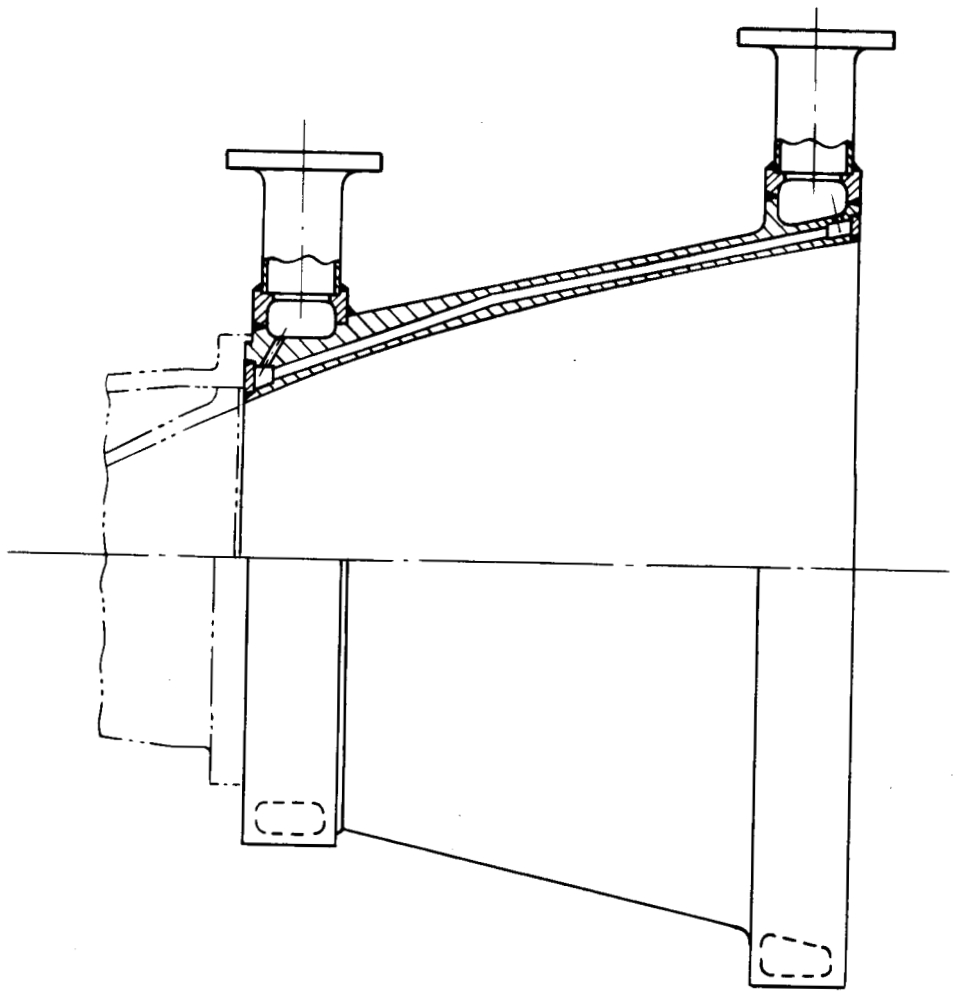

Figure 82. Water Cooled Aluminum Nozzle Extension

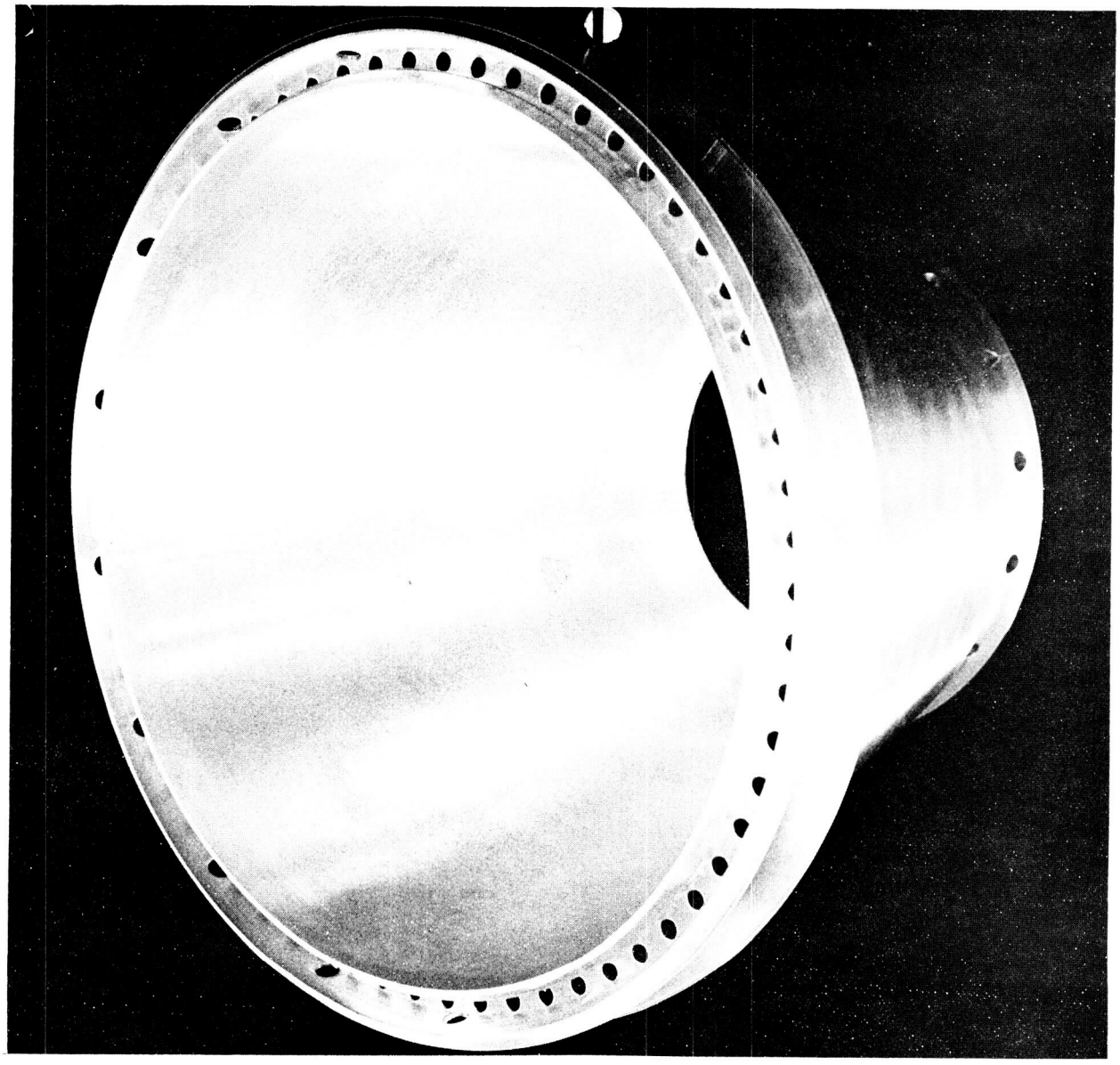

Figure 83. Water Cooled Aluminum Nozzle Extension-Drilled Subassembly

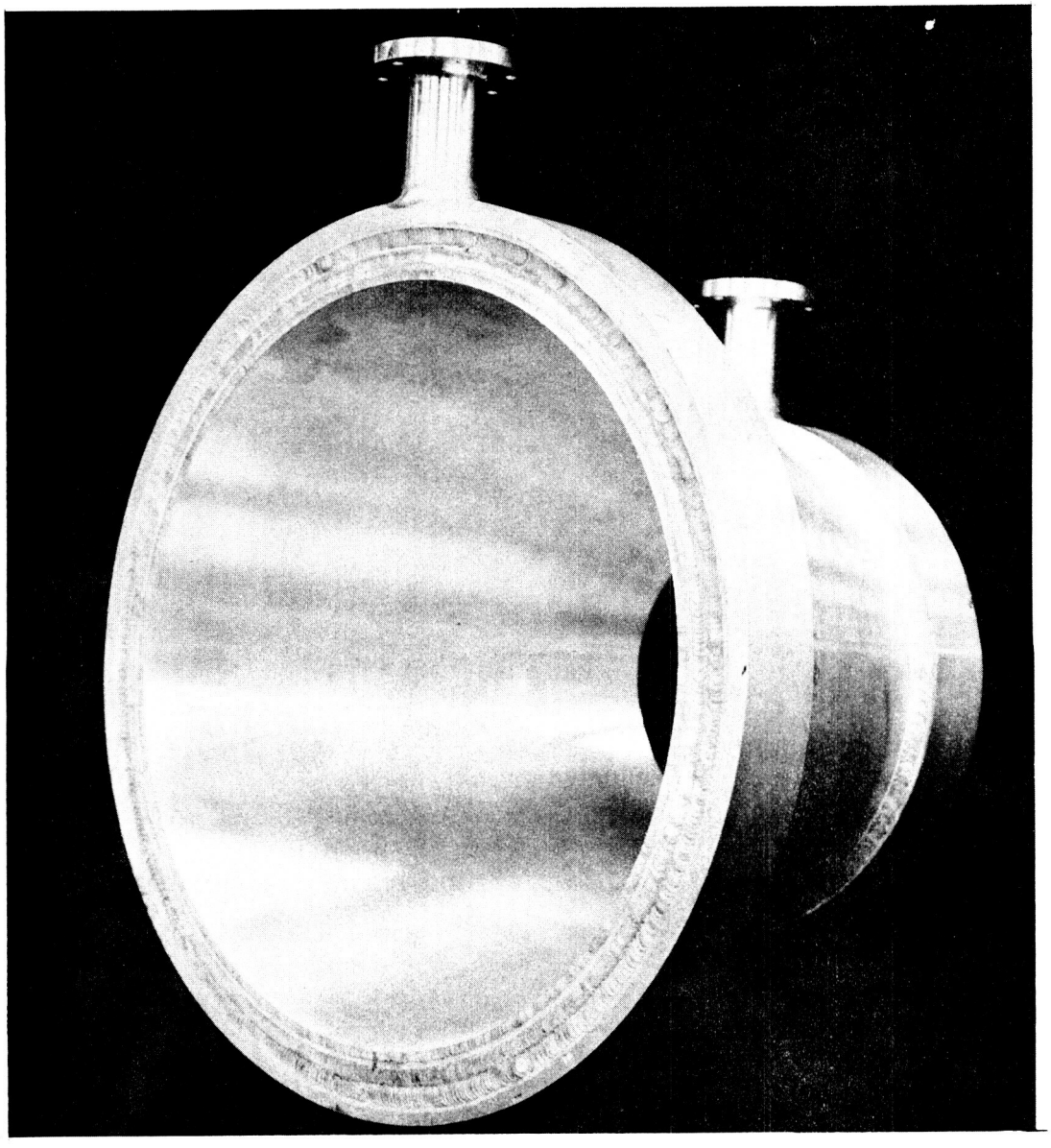

Figure 84. Water Cooled Aluminum Nozzle Extension Assembly

(2) Manifold Covers - Machined from 6061-T651 Aly plate and solution heat-treated to T4 condition.

(3) Manifold Inlet and Outlet Fittings - Machined from 6061-T651 Aly bar and solution heat-treated to T4 condition.

(4) Nozzle Extension Assembly - Manifold covers and fittings were TIG welded to extension. Assembly was heat treated to T6 condition after welding and final machined. Heli-Coil inserts were installed in bolt holes.

b. Uncooled (Or Radiation-Cooled) Columbium Nozzle Extension

This nozzle extension in the radiation-cooled configuration consisted of two basic parts, the flange and the nozzle cone. An insulation blanket of one inch thick "Dynaflex" with fiberglass tape overwrap was used for the insulated long duration, 500-sec test. A summary of these parts is listed also in Table XXXIII. A cross section and photograph of the radiation cooled extension are shown in Figure 85 and included in Figure 86, respectively.

A method of fabrication of the radiation cooled extension follows:

(1) Nozzle Cone - Formed from C103 (Cb-10% H_f - 1% Ti) Columbium alloy sheet 0.040 thick in halves and EB seam welded to form a conical nozzle which was then spun and planished over a mandrel to the desired contour.

(2) Flange - Machined from C103 (Cb-10% H_f - 1% Ti) Columbium alloy disc.

(3) Nozzle Extension Assembly - Mounting flange was EB welded to nozzle cone and final machined. After final machining all surfaces except the flange face were coated with an R512A silicide coating (Sylcor).

4. Thrust Chamber Assembly

The thrust chamber assembly cross section is shown in Figure 87 and a photograph of the assembly is given in Figure 86.

The assembly methods of the cooled thrust chamber assembly is listed below:

a. Two igniter ports were used for the cooled/altitude hardware. The standard adapters were bolted to the chamber and sealed with Viton "O" rings. The Oxidizer-cooled adapters were also bolted to the chamber and sealed with metal "V" seals.

b. The oxidizer injector was installed in the combustion chamber and retained in place by the oxidizer manifold assembly which was bolted to the combustion chamber. Viton "O" rings were used as seals.

c. The nozzle retainer ring was installed on the nozzle end of the combustion chamber with flush head screws.

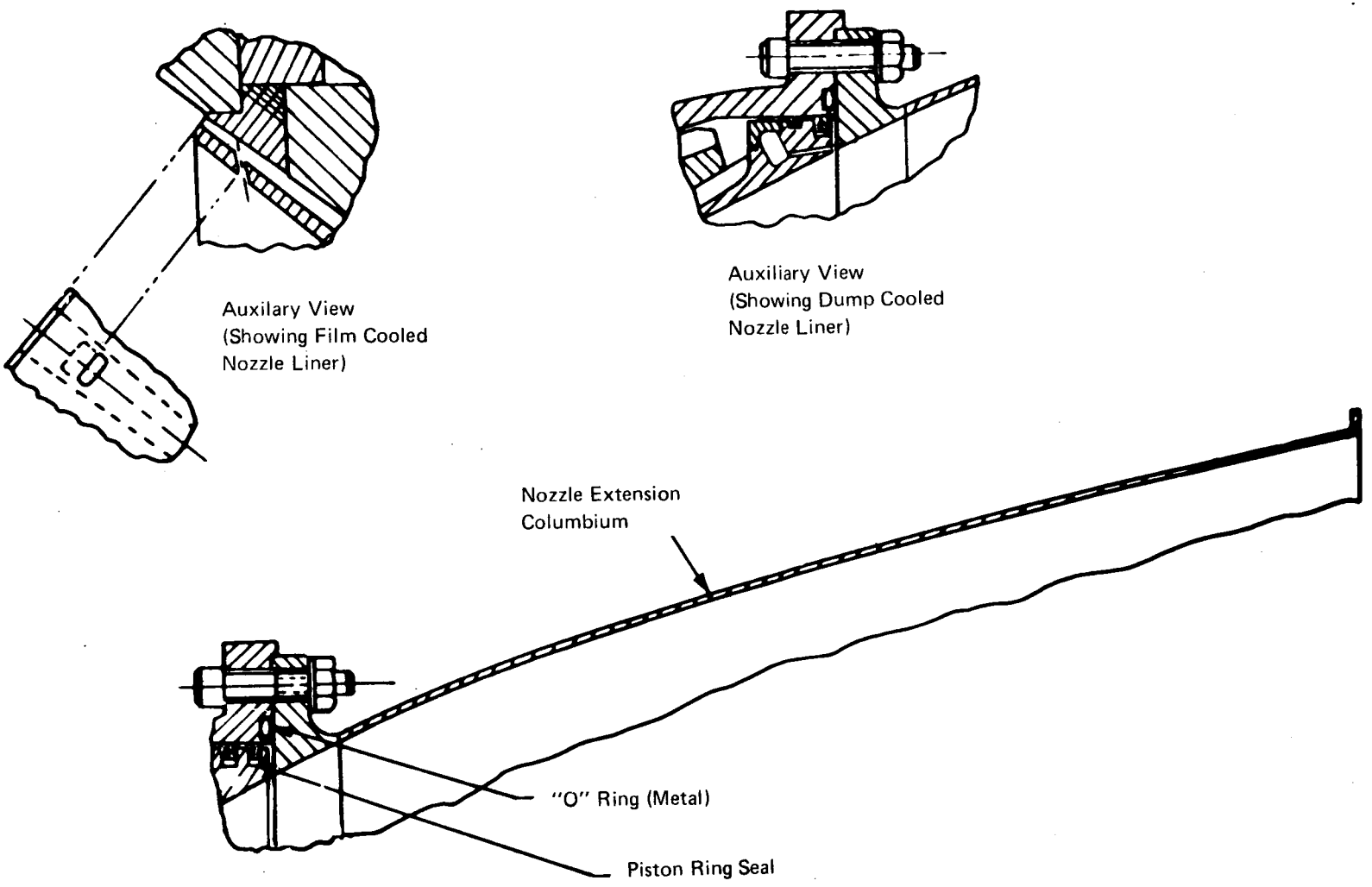

Figure 85. Cooled Chamber Design Details and Cb Nozzle Extension

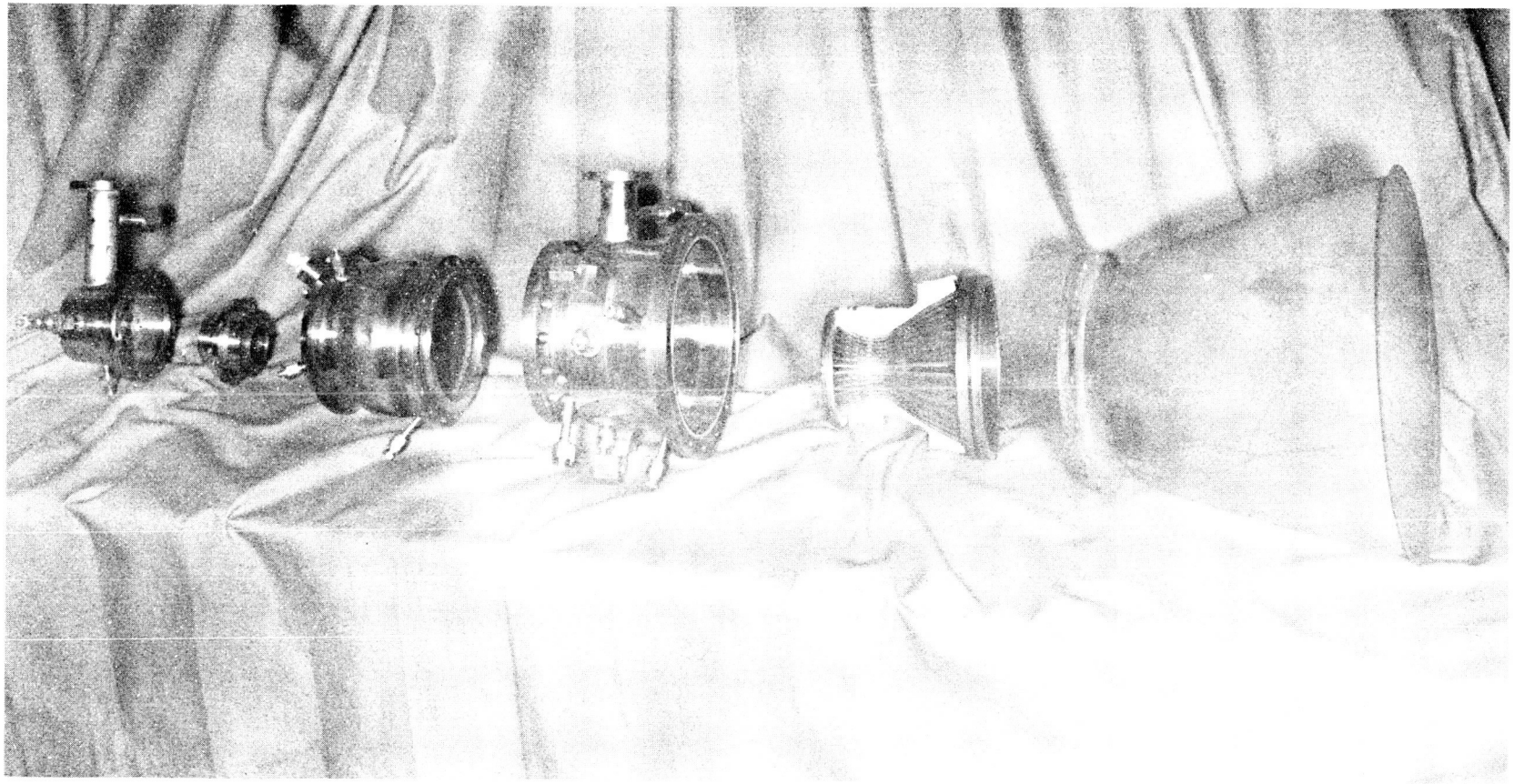

Figure 86. Cooled/Altitude Thrust Chamber Assembly

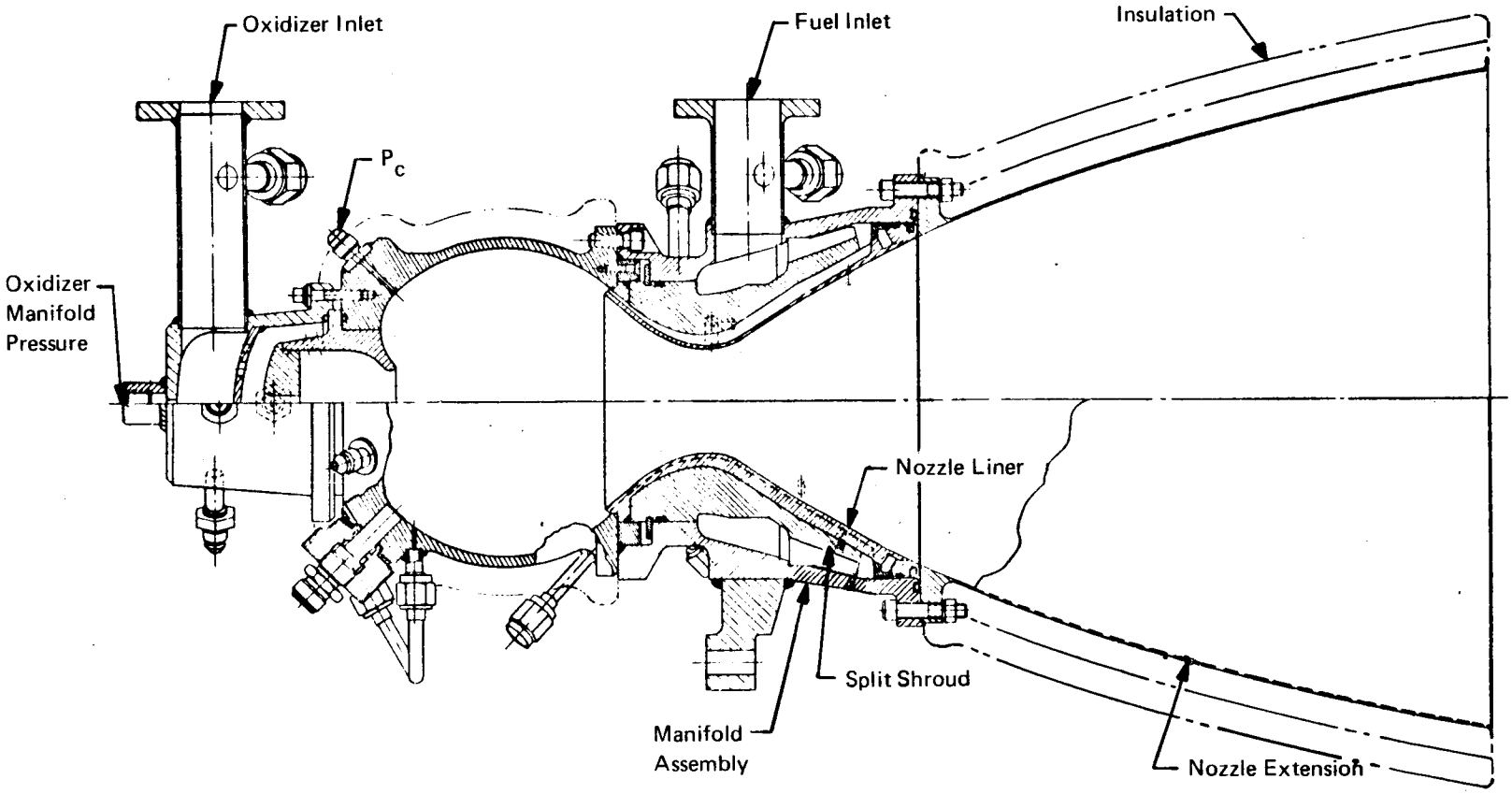

Figure 87. 1500 lb (6672N) Thrust Altitude Test Assembly – Cb Extension

d. The nozzle shroud halves were positioned on the nozzle liner and this assembly was slid into the fuel manifold assembly. A snap ring was installed in a groove machined in the shroud to maintain proper positioning of the liner and shroud assembly on the manifold assembly. A Viton "O" ring was used as a seal between the shroud and manifold at the injector end of the nozzle assembly. At the exit end of the nozzle assembly several configurations were used for sealing between the nozzle liner and manifold; two expanding type piston rings of Haynes No. 25 Stellite (AMS 5759) (supplied by Precision Piston Ring, Inc.), two Viton "O" rings, and a combination of a piston ring and one "O"ring. This nozzle assembly was bolted to the combustion chamber, with Viton "O" rings being used as seals between the nozzle liner and the nozzle retainer ring, and at the interface of the chamber mounting flange and the fuel manifold flange.

e. Either the drilled, water-cooled nozzle extension or the radiation-cooled nozzle extension were bolted to the fuel manifold. The drilled nozzle extension was used in combination with all three nozzle liners, a Viton "O" ring being used as a seal at the mounting interface. The radiation-cooled nozzle extension was used in combination with the regeneratively cooled and the dump-cooled nozzle liner with a metal "O" ring being used as a seal at the mounting interface.

VIII. IGNITION SYSTEM ANALYSIS AND DESIGN

A. GENERAL

The design and incorporation of an igniter system for the reverse flow thruster was given considerable attention although the program work statements did not include the development of ignition components. The demonstration of altitude ignition (100,000 ft) (30,480 m) and the operation in pulse mode required that some sufficiency in the ignition capability be incorporated into the program. As a consequence, care was taken in the selection of components to give reasonable certainty that proper ignition could be obtained.

Reasonable certainty of ignition was claimed from previous sea-level test programs, indicating that a simple system incorporating an igniter plug directly mounted in the combustor produced acceptable ignition. The desirability of such a simple system not requiring additional components such as valves, sequence timing or other items was amplified by the restricted funding of the program. Thus, the initial ignition system design considered the sea level experience and incorporated a spark-plug ignitor directly into the combustion chamber wall.

The next selection criterion was related to component type. Here consideration was primarily given to such items as frequency and power output. Augmentation, spark gap and spark-plug position were additional secondary considerations requiring definition. The frequency and power output of spark propagation were considered of primary importance as the ignition, using only an igniter plug, takes place as the propellant composition and pressure are in a transitional period in the chamber. This condition may differ from a torch igniter where a steady propellant flow may be established in the torch before the spark is propagated.

The problem of ignition of main propellants was thus considered to be one of igniting in transitional flow under a wide latitude of conditions. To insure ignition at the optimum conditions, a high frequency of spark generation was initially requested and this request, in turn, set the stage for demands of power output, exciter type and other specific design features. The principal component defined by frequency was the exciter where the higher frequencies may be obtained with an inductive discharge (ID) unit while the capacitive discharge unit produces a more powerful, lower frequency spark. A minimum frequency (desired) of 500 sparks per second dictated the use of an inductive unit as no capacitive units are commercially available in the higher frequency range. A Bendix unit having approximately 900 sparks per second was selected and used until it was subsequently found that the plug/connector/cable system was apparently sensitive to moisture. Then a company-sponsored capacitive discharge unit was used to augment the Bendix unit. In general, both units produced satisfactory ignition as long as care was taken to ensure drying of the plug and cable. Finally, when most of the performance duration and environmental tests had been conducted, several altitude starts were conducted with a single ignition system (either CD or ID) to confirm that either system could ignite the chamber.

B. SELECTION CRITERIA

A simple electrical ignition system was selected for initial evaluation with the reverse-flow engine. This ignition system consisted of electrical spark components, including an igniter plug with an electrical exciter and harness and a secondary oxidizer injection port. The igniter plug was mounted directly in the spherical chamber wall so that the igniter plug electrode was mounted flush with the inside of the chamber wall. The oxidizer injection port was available so that oxidizer could be supplied locally upstream of the igniter plug to provide a high mixture ratio for ignition.

1 to 2% of the total oxidizer can be introduced about 1/2 inch (1.27 cm) upstream of the igniter plug resulting in a local oxidizer-rich mixture. This ignition system had previously been tested at the 50 and 1000 lb (222.41 and 4448N) thrust levels. A total of 100 successful tests were conducted at chamber pressures between 45 and 250 psia (31 and 172 N/cm^2) at ambient temperatures and sea-level conditions. The test series on the 50 lb (222.41 N) thrust unit established the preferred igniter plug location at the oxidizer end of the chamber. Ignition delays were experienced with the igniter plug located near the fuel injector. With the igniter plug at the oxidizer end of the chamber, rapid ignition was obtained with and without oxidizer augmentation. All testing at the 1000 pound (4448 N) thrust level was successfully made with the igniter plug located at the oxidizer end of the injector. The spark gap was provided by an annulus between the center electrode and the chamber wall. Duration tests up to 120 seconds and pulses of 300 milliseconds were made with no apparent effect on the exposed plug. The spark gap was 0.040 to 0.050 in. (0.102 to 0.127 cm) with a spark energy of approximately 4 millijoules and a spark frequency of 2500 Hz. A Mallory exciter was used as the power supply.

To meet both program cost and schedule limitations, only available (off-the-shelf) electrical exciter and igniter plugs were considered. The principal concern for the selection of these components was to provide a spark of sufficient energy and frequency to ensure reliable ignition under all conditions. A schematic of the dual ignition system used for the cooled chamber is shown in Figure 88.

The overall operating parameters defined for the electrical ignition system were as follows:

Mixture Ratio	-	5.0 or higher
Pressure	-	2 psia (1.38 N/cm^2) or higher
Ignition Energy	-	5 millijoules minimum
Spark Frequency	-	500 sparks/sec minimum
Life	-	1,000,000 pulses
Input Voltage		Minimum Variation

1. Igniter Selection Criteria

Exciter – Various vendors were contacted to determine the availability of electrical exciters for use on this program. As a result of these contacts, Mallory, General Laboratory Associates and Bendix Electronics Division indicated having available exciters. Initially, preference was given to a high energy level capacitive discharge exciter rather than the lower energy level inductive discharge exciter.

This preference was made based on the assumption that a capacitve discharge system could be readily modified to give a frequency in the 500 to 1000 Hz range. Subsequent information has indicated that the frequency can be readily achieved. However, with existing systems, the output energy is lowered to a point where there appears to be little difference in the systems. A spark energy (at the igniter plug) of 5 millijoules or more has been selected as a suitable energy level for ignition of gaseous O_2/H_2 under these conditions.

This selected energy level was based upon ignition data obtained by Pratt & Whitney and the Bureau of Mines. Ignition limits investigated by Pratt & Whitney during RL-10 engine tests were conducted with a torch igniter and demonstrated successful ignition at the 1 to 2 psia

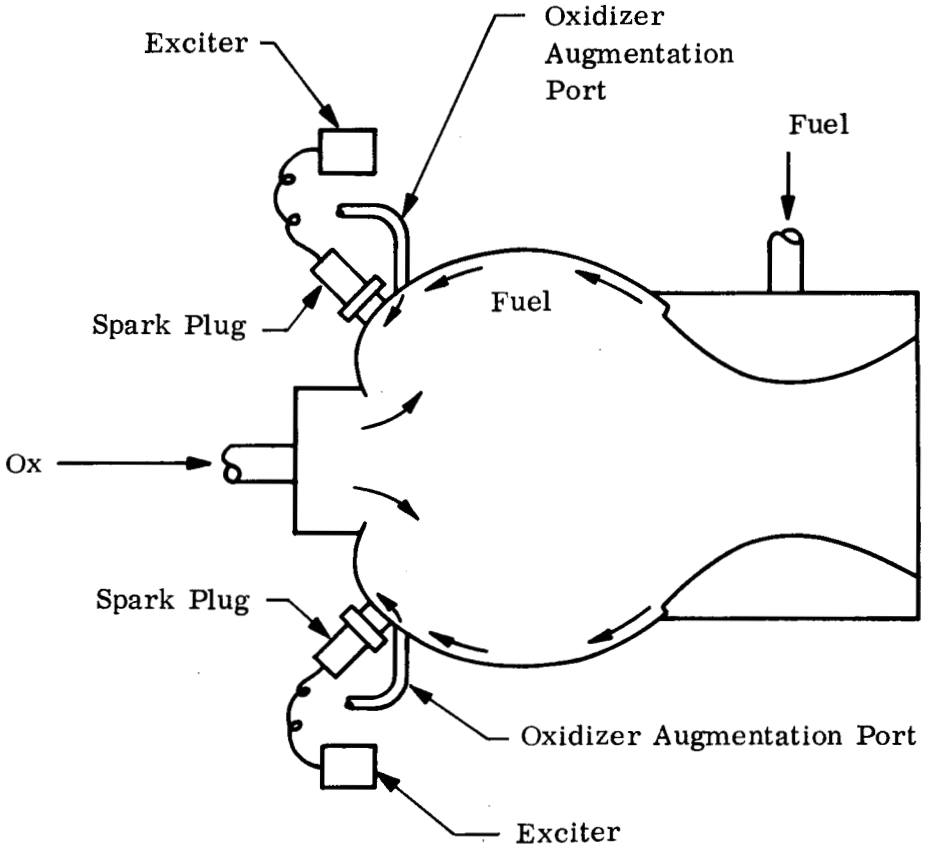

Figure 88. Ignition System Configuration - Cooled Chamber

(0.69 to 1.38 N/cm^2) level. These data were used as the basis for our study and 2 psia (1.38 N/cm^2) was selected as a practical ignition pressure for our analytical studies and ignition design point.

Analyses with oxidizer augmentation have been conducted to determine the rate of combustion chamber pressurization and the rate of mixture ratio variation during the start sequence. As revealed in Figure 89 chamber pressure of 2 psia (1.38 N/cm^2) would be obtained 9.5 milliseconds after valve signal using ambient temperature propellant. Only one millisecond is required to double this pressure indicating rapidity of pressurization (lowering the risk of no ignition) and the desirability of rapid sparking. Figure 90 shows the change in mixture ratio with time where both the local O/F ratio at the igniter plug and the mean (overall) O/F ratio start oxidizer-rich and add fuel with time. The local O/F ratio is 40:1 at an ignition pressure of 2 psia (1.38 N/cm^2)and the mean O/F ratio is 5:1.

To establish a practical spark ignition energy level, data from Pratt & Whitney (Ref. 21) at the Bureau of Mines (Ref. 22) were adjusted by using the equation $E \propto 1/p^2$ (where E is ignition energy and p is ambient gas pressure) recommended by the Bureau of Mines (Figure 91). The Pratt and Whitney data are the most conservative and would predict a 0.5 millijoule requirement for 2 psia (1.389 N/cm^2) ignition pressure. Similar examination of the Bureau of Mi nes data predicts a 0.08 millijoule energy requirement at 2 psia (1.389 N/cm^2). To account for the many unknowns of gaseous O_2/H_2, ignition under all conditions, a factor of 10 was applied to the most conservative data (P&W) resulting in a 5 millijoules energy level as the requirement at the igniter plug. A minimum spark rate of 500 sparks/second was also selected with a more desirable rate being 1000 sparks/second. This was to provide at least one spark every two milliseconds during engine pulse operation.

Bench tests conducted on the highest-energy-available Bendix exciters revealed that the best unit for our application was an inductive discharge exciter. This exciter produced an energy at the plug of from 5 to 12 millijoules at 30 vdc with a rate of 1000 sparks/second. This Bendix exciter was apparently the only unit available that met the spark rate, cost, and schedule limits, and was therefore used during the initial evaluation testing.

a. Igniter Plug

Contact was made with Auburn Spark Plug Co., Bendix Electronics Division, A.C. Division, and Champion to determine the availability of spark plugs. Consideration was given to the desirability of air gap or surface gap plugs and to special-purpose designs if available. Secondary consideration was given to the tip of the surface-gap plug, which appeared to be available only with a semiconductor coating in the size desired.

The decision to use a surface-gap plug was based on several factors including previous experience in aircraft (altitude operation) and a very mundane consideration of availability. Additionally, consideration was given to the capability of recessing the plug in the chamber wall, thus forming an "air gap" chamber. The final feature of the plug was removal of the semiconductor from the end of the insulation, reducing any electrical leakage at that surface as much as possible for use with the I.D. system.

One additional design which was attempted, was the use of glaze on the plug tip to eliminate the effects of moisture and increase the reliability. Unfortunately only one plug was received during the program and no conclusion could be drawn from the tests conducted.

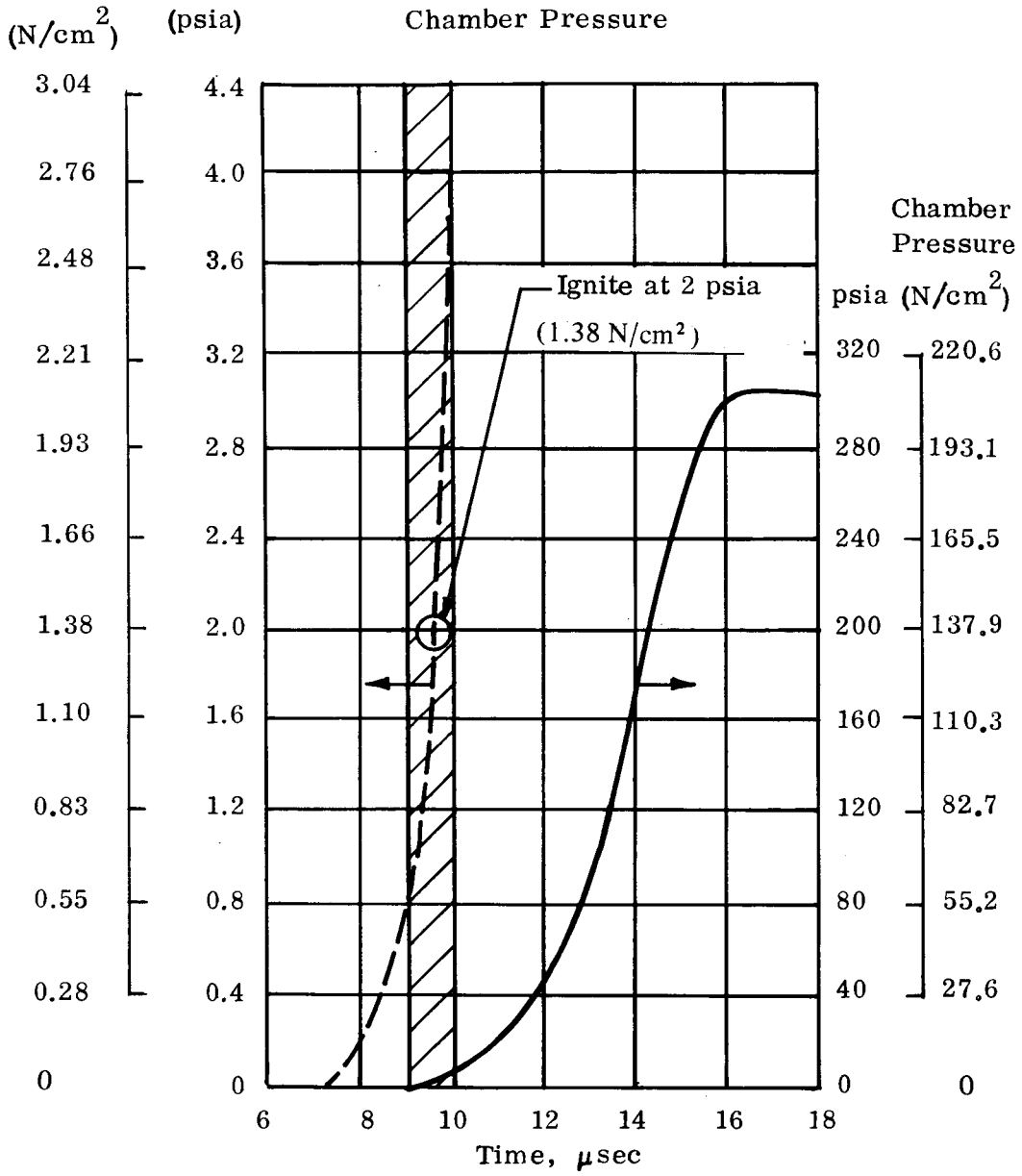

Figure 89. Chamber Pressure versus Time

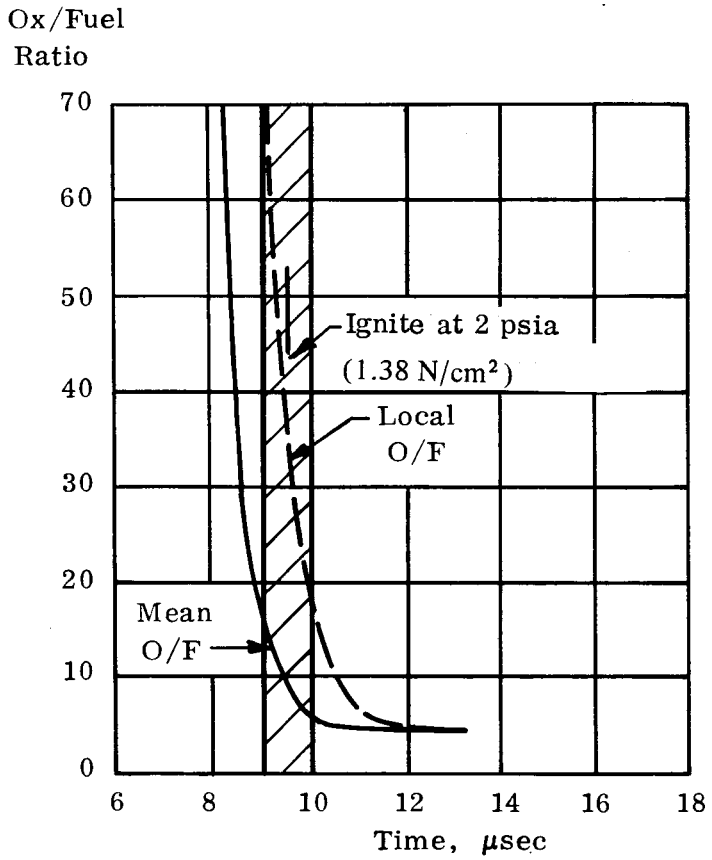

Figure 90. Mixture Ratio versus Time

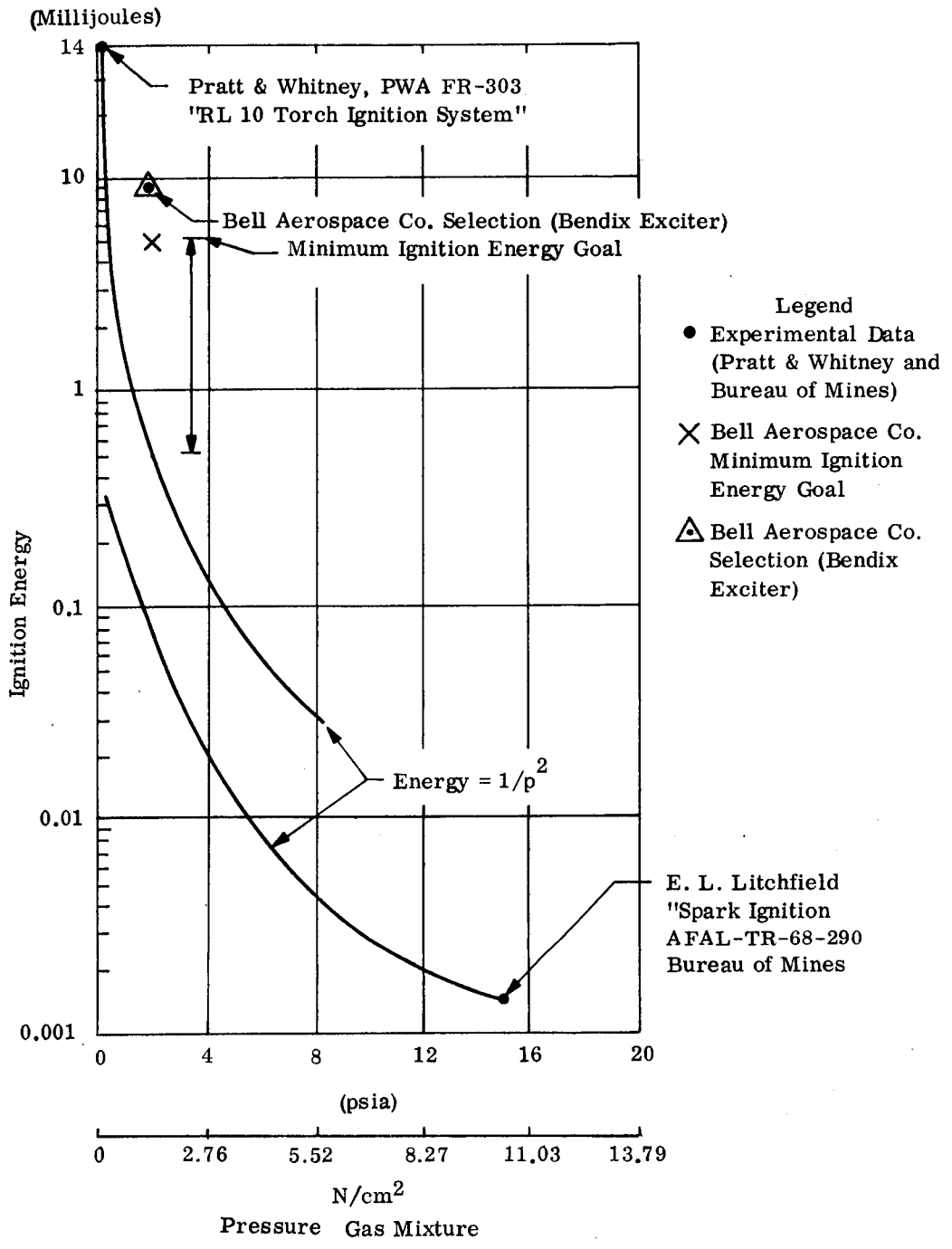

Figure 91. Ignition Energy for O_2 - H_2 Gaseous Propellants (MR = 37:1)

One final comment on plugs should be made relative to cooling. Although the chamber wall of the reverse-flow chamber runs very cool by rocket engine comparison, the 1200 to 1600°F (922° to 1144°K) maximum temperature is a little warm for the plug. The plug itself is much less susceptible to temperature than the silicon rubber grommet used in the lead wire to seal the connection at altitude. This rubber connector would normally be good to 500°F (533°K). On heat soak (particularly with an insulated engine) the plug became too hot, the connector was destroyed and terminals damaged. This condition was encountered on the first long-duration test. The cooling scheme used for insulated chamber tests was very successfully employed, with the coolant flow of the oxidizer augmentation used to cool the plug. A seal stand-off arrangement was also used on the plug base to reduce the heat flow outward. This scheme (Figure 91) was successfully employed on the insulated chamber test (500 seconds) and the plug lead combination was used on additional testing after the duration test.

2. Selected Ignition Components

The Bendix inductive discharge exciter coupled with an ignition harness and igniter plug comprised the ignition system used on the majority of the tests conducted. The primary consideration in the selection was frequency of the spark where the Bendix unit was considered capable of producing 1000 sps and a nominal rate of 900 sps at the 28-volt input normally used in the test cell. The harness or oxidizer-to-plug cable was fabricated with a monitoring capability so the frequency could be measured in operation. The use of this monitor was discontinued during subsequent operation as it affected other monitored test parameters due to its high noise level.

The selected Bendix exciter unit had the following characteristics:

a. Model No. 10-81110-3
b. Input Voltage - 18 to 30 vdc
c. Spark Energy - 10 millijoules @ 28 vdc
d. Spark Rate - 1000 sparks/sec (at 30 vdc)
e. Operating Altitude - Sea Level to 100,000 ft. (30,480 m)
f. Frequency Control - Vibrator
g. Operating Temperature - 65°F to +165°F (219 to 347°K)

This type of exciter unit was initially designed for operation on jet aircraft turbine engines and the Talos Missile.

a. Igniter Plug

The Bendix surface-gap igniter plug (or equivalent Champion) was used. This plug was modified slightly by increasing the radial surface gap from 0.030 to 0.050 inch (0.076 to 0.127 cm) to provide an increased breakdown voltage. The plug diameter and overall size were compatible with thrust chamber hardware design. This type of plug has also been used with the jet turbine engines; therefore, no development time was required.

The selected igniter plug had the following major characteristics:

Model - 10-390150-1 Bendix (or FHE146-7A Champion)
Operating Temperature (at sparking end) - 1200°F (922°K)

Leakage Rate - Less than 10 cc/min (at 300 psi) (206.8 N/cm^2)
Operating Pressure - 700 psia (482.6 N/cm^2)

b. Ignition Lead (Cable)

The Bendix ignition lead was used. It was designed for use with the referenced exciter unit to provide high operational reliability. This lead was modified to include an inductive pick-up coil located around the high tension cable to monitor the sparking rate of the system.

The selected lead had the following major characteristics:

a. Model - 10395019-1
b. Igniter Terminal - 90° terminal capable of 400°F (478°K) operation
c. Conduit Assembly - Convoluted and brazed core covered with copper inner braid and nickel outer braid. Brazed at both terminal ends and tested to 50 psig. (34.47 N/cm^2)
d. Wire - MIL-C-3702 5 mm
e. Exciter Terminal - 200°F (367°K) operation
f. Monitor - Inductive coil monitor around cable.

c. Capacitive Discharge Exciter

During the conduct of the test program, both at sea level and at altitude, the susceptability of the spark plug to moisture produced a number of ignition malfunctions. This malfunction (no start) condition was drastically reduced by drying the plugs prior to installation and by using care to have a dry and clean fit on the plug-cable connection. Although this drying procedure was adequate for the test cell, altitude drying for shuttle application would be far too uncertain for reproducible operation. For this reason a capacitive discharge exciter was ordered and used to reduce the uncertainty of starts.

Due to the nature of this program (which did not include separate ignition tests within the budgeted schedule) the starting capability was mostly related to ensuring some kind of ignition to obtain performance data rather than the evaluation or optimization of the starting sequence. Beginning at run 1BN 687 two ignition systems were used for all tests. Some starting tests were subsequently made with only one ignition system (either the ID or CD) and will be remarked on separately. However, in general, the two systems were used together, with the first system consisting of the Bendix Exciter, cable and igniter plug and the second system consisting of a GLA CD exciter and cable with a Bendix plug.

The capacitive discharge exciter selected for use with this program was made by General Laboratory Associates (GLA) and carried the model number 48488. This unit had the following characteristics:

Model No. 48488
Input Voltage - 14 to 30 Vdc
Spark energy - 10 millijoules
Spark rate - 270 @ 28 Vdc
Operating altitude - sea level to 100,000 ft (30,480 m)
Frequency control - Solid State Converter
Operating temperature - 65°F to +165°F (219 to 347°K)

C. FIRE TEST RESULTS

The primary purpose of the ignition system used on this program was to generate a spark which in turn would ignite the primary propellants and produce combustion from which performance parameters could be measured and the general acceptability of the engine could be defined. Thus, both by definition of the program objectives and by the monetary allowance, ignition was relegated to a secondary priority. However, it had been projected that a simple ignition system would be sufficient to ignite the reverse-flow engine. This system should have been sufficient to accomplish the purpose of evaluation of the general concept of the type of engine to be tested.

Originally the concern of the ignition system was that of producing sufficient power to the plug and sequencing the power properly to produce the spark which would propagate the combustion process. The original task was to select a type of component which would insure some confidence that ignition would be obtained. Further, it was considered that a variation in the propellant lead or lag could be incorporated by sequencing the individual propellant valves thus producing the optimum condition of propellant entry during initiation of the combustion wave.

During the test program, it was also of interest to examine the possibility of a propellant trap when the fuel flowed past the cavity created by recessing the ignitor plug. An oxidizer-rich mixture would be encountered if, for example, an oxidizer lead were used followed by the fuel entry. In practice, very little was changed as the initial tests using the Bendix inductive discharge spark system produced sufficiently reproducible starts. It was felt that additional funding to evaluate different starting conditions was unwarranted.

These initial starts were conducted at sea level using the heat-sink hardware. Further, the testing was conducted in a region without weather control and a substantial amount of humidity was encountered throughout the initial heat-sink hardware evaluation program. During this program a number of misstarts were attributed to moisture collecting somewhere within the body of the igniter plug, allowing a reduction in the spark energy at the tip of the plug. This in turn reduced the energy available for propagation of the combustion wave. In general, it can be stated that this condition was rectified by setting up a drying procedure to use with the test equipment. Prior to a test, the spark plug was removed from the hardware, placed in a heated vacuum oven for approximately two hours and then reinstalled in the engine. In general, starts were then reproducibly propagated. Most tests were conducted with a dual ignition system with each system consisting of the Bendix inductive discharge exciter with the associated cable and igniter plug.

A dual ignition system was used on almost all of the altitude testing. In fact, the dual system was used on all tests to obtain general engine data, with the exception of those tests to evaluate a single type of ignition system. The procedure generated for drying the plugs developed during the sea-level testing was incorporated directly into the operating conditions of the altitude cell. Although it was speculated that the rise to altitude would remove all moisture, this was not proven and drying was used to enhance the probability of starts. The benefit of this procedure appeared in instances where altitude starts were not obtained on the engine. The plugs were removed from the chamber, dried in a heated evacuated oven, replaced in the chamber and subsequent starts produced. Some speculation may be involved that other factors than moisture may have caused the nonignition occurrences. However, the only known variant, between the initial no-start attempts and the second attempts where combustion was obtained, was the removal, drying and replacing of the spark plugs involved.

Although there were several instances where starts did not occur, in general, the starting system was very successful in producing results within the test cell. Not only were there quite a number of starts produced (3489); but the starts were produced under a wide variety of conditions, not the least of which was a chamber pressure variation of 100 to 500 psia (68.9 and 344.7 N/cm^2), propellant temperatures ranging from approximately 200°R (111°K) to 800°R (444°K). Adding to the variable of altitude where ignition was obtained from sea level to 100,000 ft (30,480 m), the combined test variables where ignition occurred were wide enough to assume that more data should be accumulated to optimize the simple ignition system which was used.

Oxidizer Augmentation

Provision was made in the design of the ignition system to inject a small amount of oxidizer in the combustion chamber wall ahead of the igniter plug, as the fuel sweeps through the chamber. This augmentation port was used to provide a film of oxidizer over the immediate vicinity of the spark plug during the ignition process. Analysis of the propellant entering sequence indicated that the oxidizer from the augmentation port would enter the chamber approximately 1 msec after the entry of the oxidizer through the primary swirl cup injector. This oxidizer was acquired from a tap in the upstream portion of the oxidizer injector inlet housing and a simple 1/8-inch (0.32 cm) diameter line led to the augmentation port. Initially, some concern was given to the possible higher temperature produced by this augmentation oxidizer; therefore, one of the plugs was recessed 0.170 inch (0.432 cm) and the augmentation was deleted to offset this possibility.

Subsequent testing indicated that the recessed plug did not react differently than the nonrecessed plug. This comparison produced the conclusion that the elimination of the augmentation had little effect on durability of the spark plug. The use of the recessed-oxidizer spark plug showed that this configuration without augmentation was not infallible in producing ignition. The conclusion was reached that moisture was the predominant factor in preventing ignition, while other variables were somewhat secondary. This instance also initiated the consideration that ID spark would probably remain susceptable to moisture; therefore, a CD system having a higher peak spark energy would produce a more reliable ignition system.

D. COOLED IGNITER PLUG DESIGN

1. General

A cooled igniter plug adapter was designed to reduce the temperature at the igniter plug/electrical harness interface to a value less than 500°F (533°K) to preclude damage to the igniter plug and electrical harness connector. This design incorporated four basic modifications from the standard igniter plug adapter:

a. Provision for cooling with the igniter oxidizer augmentation flow around the igniter plug (just below the igniter plug/adapter seal region). The nominal amount of oxidizer augmentation flow for this configuration is approximately 0.7% of the total oxidizer flow.

b. Thermally isolating the adapter from the spherical chamber by use of a minimum "contact area" spacer. This spacer increased the interface resistance and controlled the amount of compression of the seal.

c. Use of a Lo-load "vee type" metal seal (Inconel "X", silver coated, supplied by Advanced Products Co.) between the igniter adapter and the spherical chamber. This seal replaced the "Viton" O-ring used with the standard adapter and increased the seal temperature capability from approximately 700°F (644°K) to >1600°F (1144°K).

d. Use of a copper compression ring located between the coolant manifold and the tip of the igniter plug. This compression ring prevented leakage along the "shank" of the igniter plug.

A cross section of the cooled igniter plug adapter is shown in Figure 92 and a photograph is presented in Figure 93.

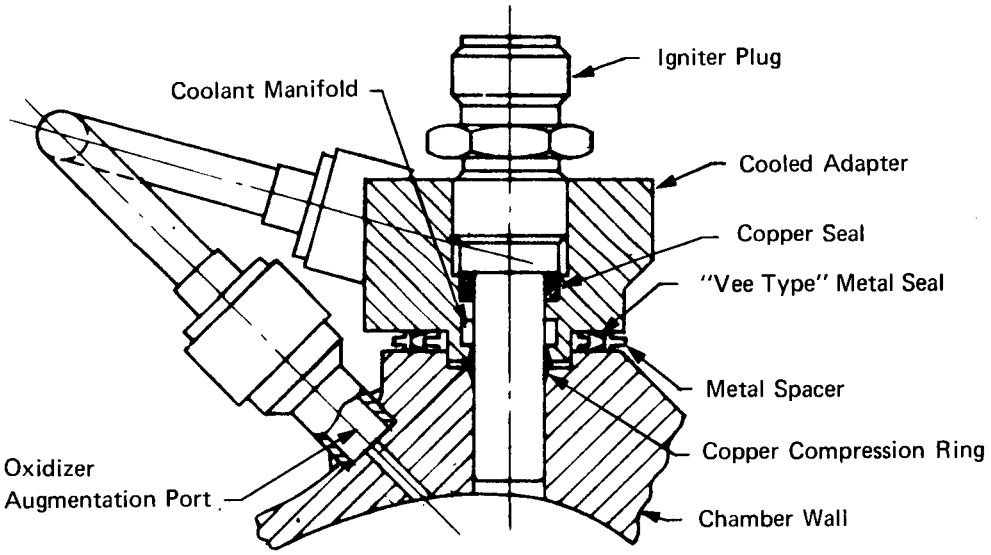

Figure 92. Cooled Igniter Plug Adapter

2. Analysis

Design and thermal analyses were conducted on this oxidizer-augmentation-cooled igniter-plug adapter configuration. The following design inputs were applied to the analysis:

a. P_c = 300 psia (206.8 N/cm^2)
b. O/F = 4
c. $W_{ox\ Total}$ = 2.76 lb/sec (1.253 kg/sec)
d. Oxidizer coolant flows varied from 0.5% to 5.0% of a total oxidizer flow
e. Chamber wall temperature at adapter interface = 1200°F (922°K).

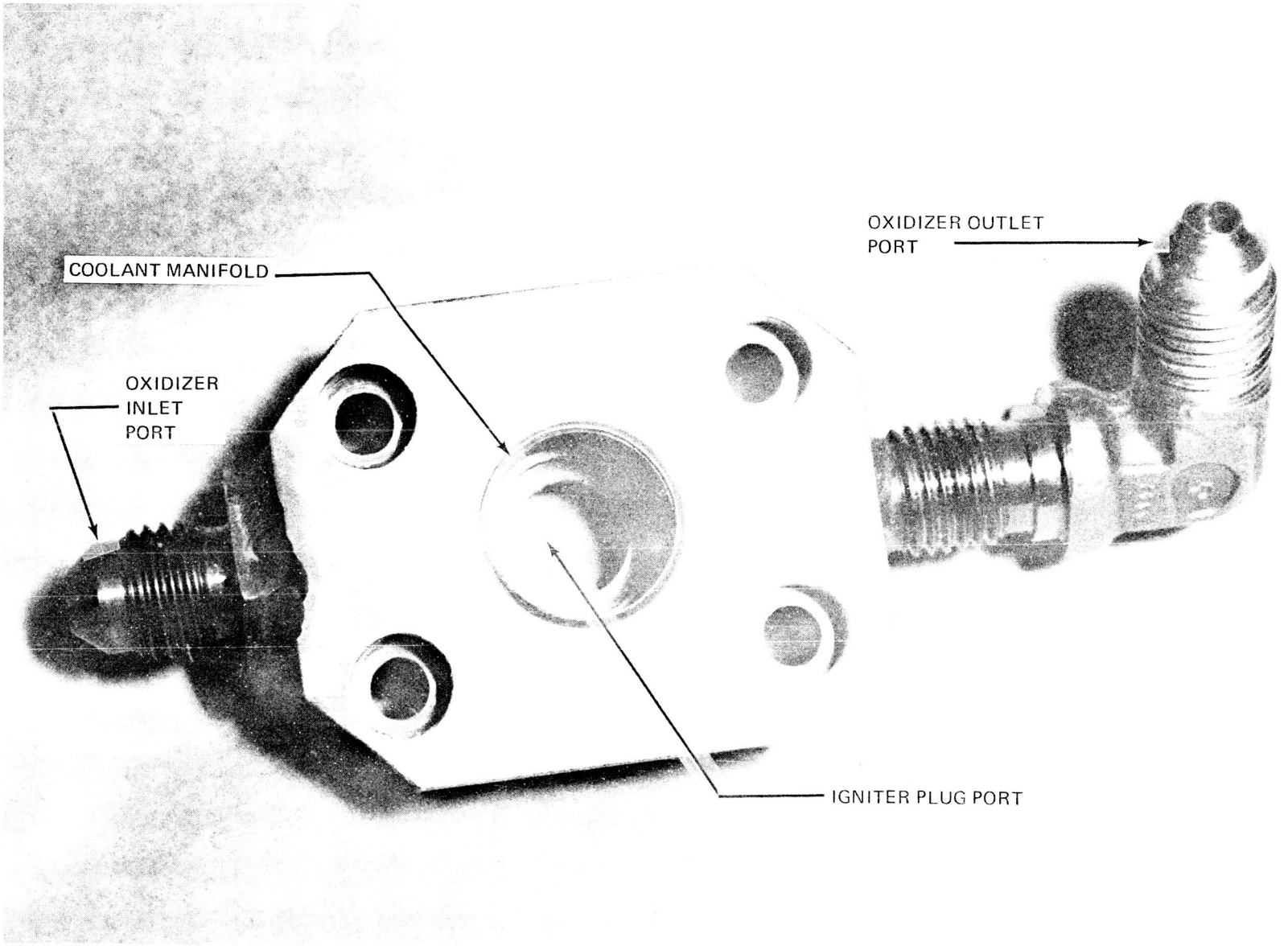

Figure 93. Cooled Igniter Plug Adapter

An analysis was first conducted for three different spacer and seal configurations:

a. The standard adapter/chamber interface (no spacer) but with oxidizer augmentation cooling.

b. The same as (a) except with a spacer, thereby increasing joint resistance, and a metal "V" seal.

c. The same as (a) except with a minimum contact area spacer and a metal "V" seal.

The basic configuration is shown in Figure 94 and a simple series/parallel resistance flow circuit was made as given in Figure 95. In these analyses it was assumed no oxidizer coolant flowed along the shank of the igniter plug into the chamber even though a definite seal was not provided. The temperature of the igniter adapter wall for these different configurations is shown in Figure 96. The major proportion of the heat flows through the chamber wall and across the spacer joint into the coolant wall machined in the adapter. Coolant flow requirements are found by determining the heat flow rates (Q) for various spacers and temperature differentials ($1200\text{-}T_{wL}$). The coolant flow rate is found from the coolant heat transfer coefficient (h_L) determined from the heat flow rate and the temperature (T_L).

$$\dot{Q} = \left[\frac{1}{R_1 + \frac{1}{\frac{1}{R_2} + \frac{1}{R_3}}} + \frac{1}{R_4}\right]\left[1200 - T_{wL}\right] = h_L A_s \left[T_{wL} - T_L\right]$$

The coolant surface area (A_s) is the total surface area of the annular groove.

The oxygen coolant flow rate required to maintain the wall temperature was found from the following form of Nusselt number equation.

$$N_L = 0.023 \left[\frac{\dot{W}}{A}\right]^{0.8} \frac{1}{D^{0.2}} \left[\frac{C_p{}^{0.4}\, K^{0.6}}{N^{0.4}}\right]_L \left[\frac{T_L}{T_{wL}}\right]^{0.34}$$

A narrow-faced spacer (8636-470118) is more effective in blocking heat than are full-width seals or no spacer, similar to the 8636-470024 adapter which is bolted directly on the chamber.

The selected adapter/seal configuration, incorporating a copper seal, was analyzed. This analysis differs from the preceding analysis in that a copper ring is compressed between the adapter, chamber wall and igniter plug shank to prevent coolant flow from the annular coolant passage down the igniter plug shank into the chamber, bypassing the oxidizer augmentation function. The copper ring forms a thermal short-circuit across the chamber/igniter/adapter interface resulting in a complex heat flow path. A high (3000 BTU/ft² hr°F) (4.324×10^2 watt/meter² °K) joint conduction was used for the compression ring because of the wedging nature of the seal surfaces. The thermal model is given in Figure 97 and the temperature of the igniter adapter wall and the igniter plug wall (igniter sleeve) for various coolant flowrates is shown in Figure 98.

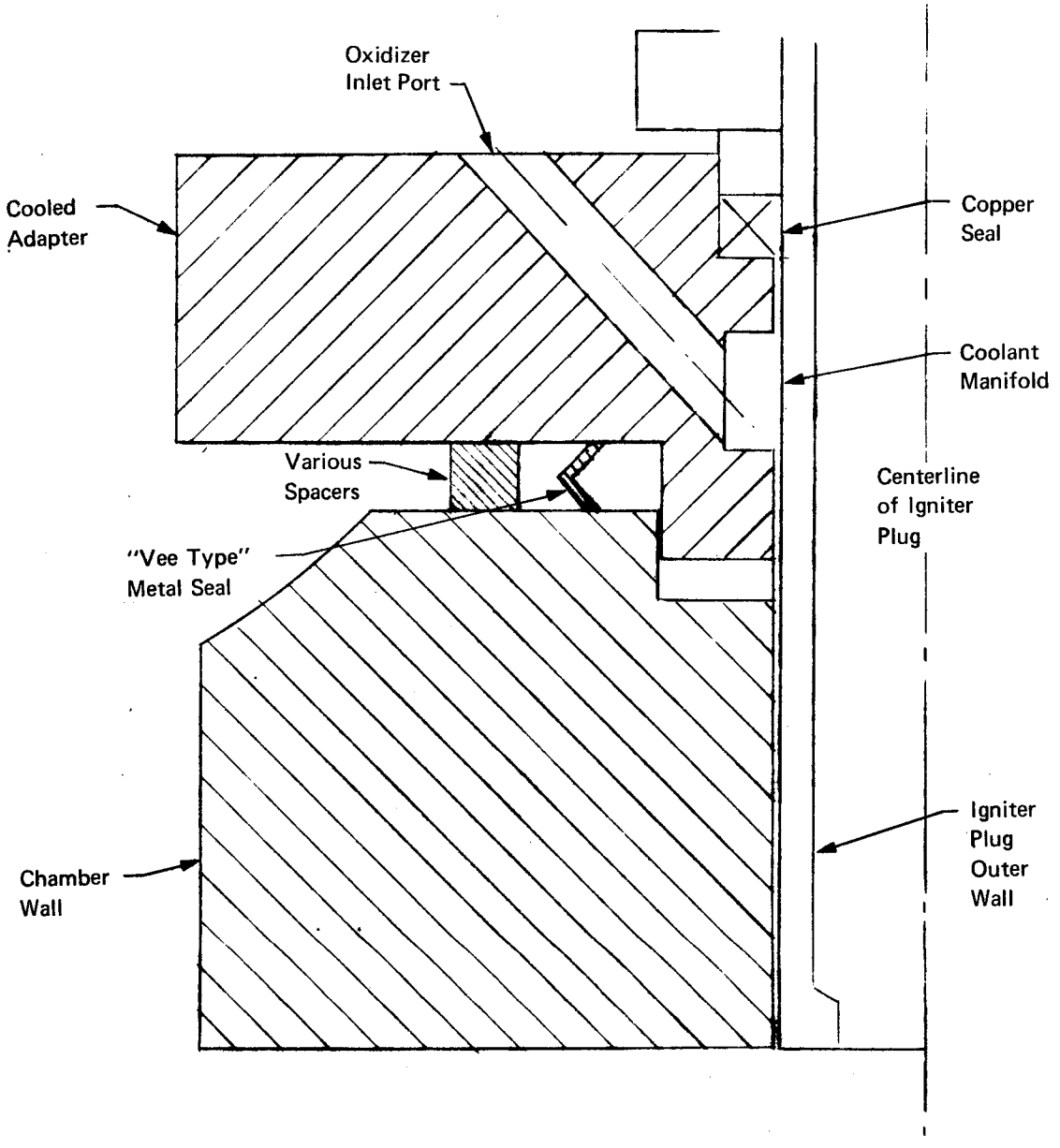

Figure 94. Basic Model Cooled Igniter Plug Adapter

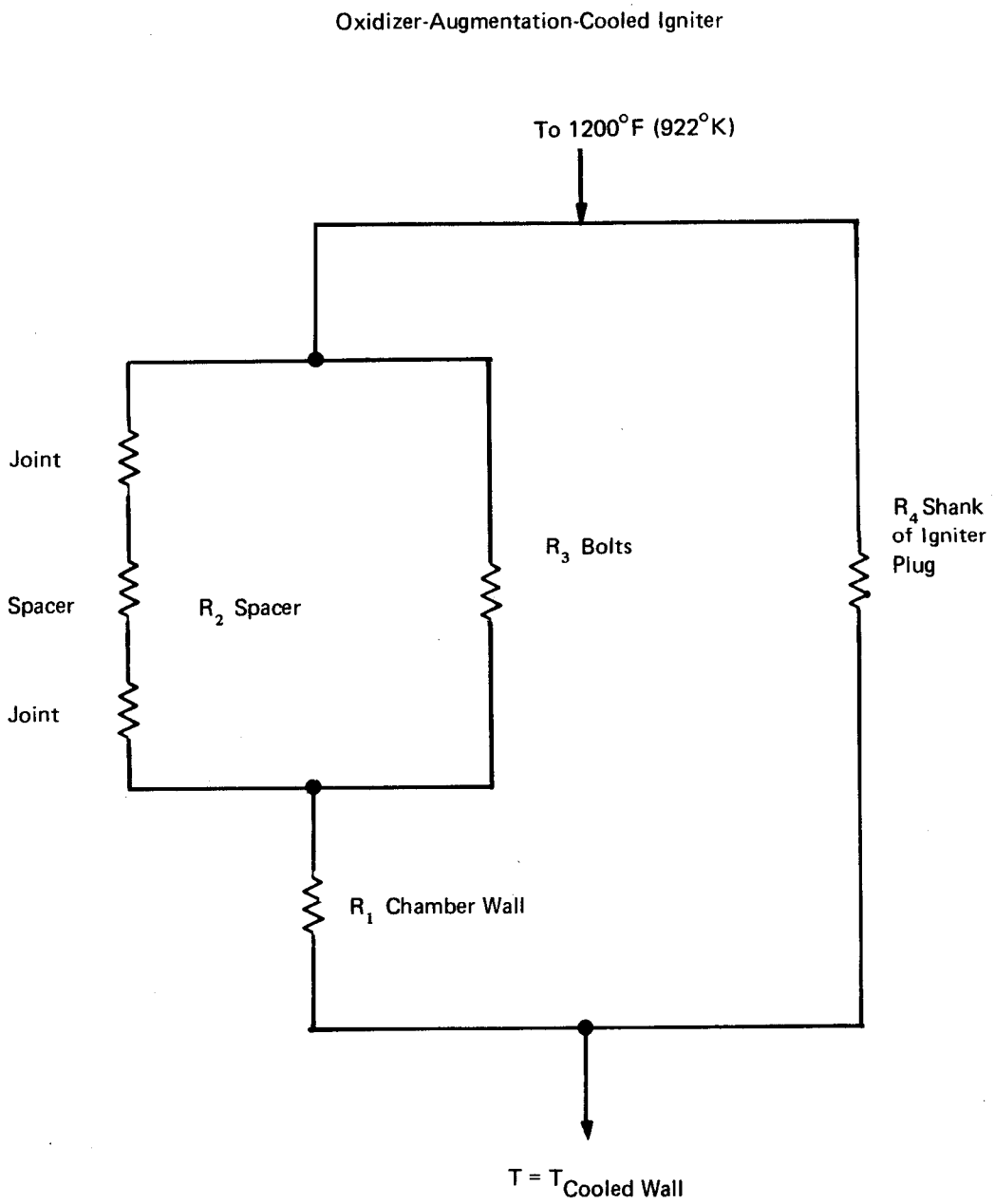

Figure 95. Simplified Igniter Heat Flow Network

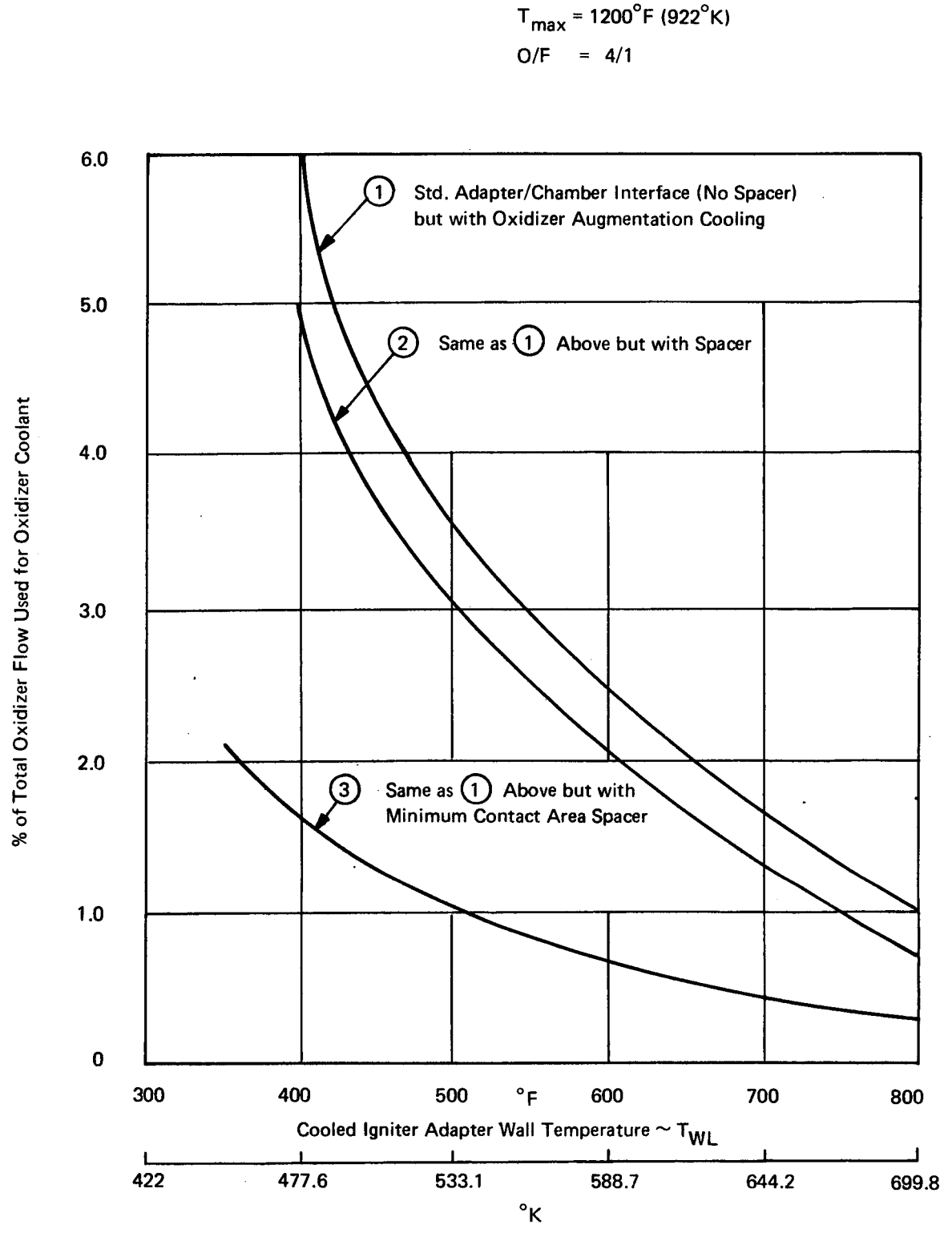

Figure 96. Oxidizer Augmentation Cooling With Bendix Champion Igniter

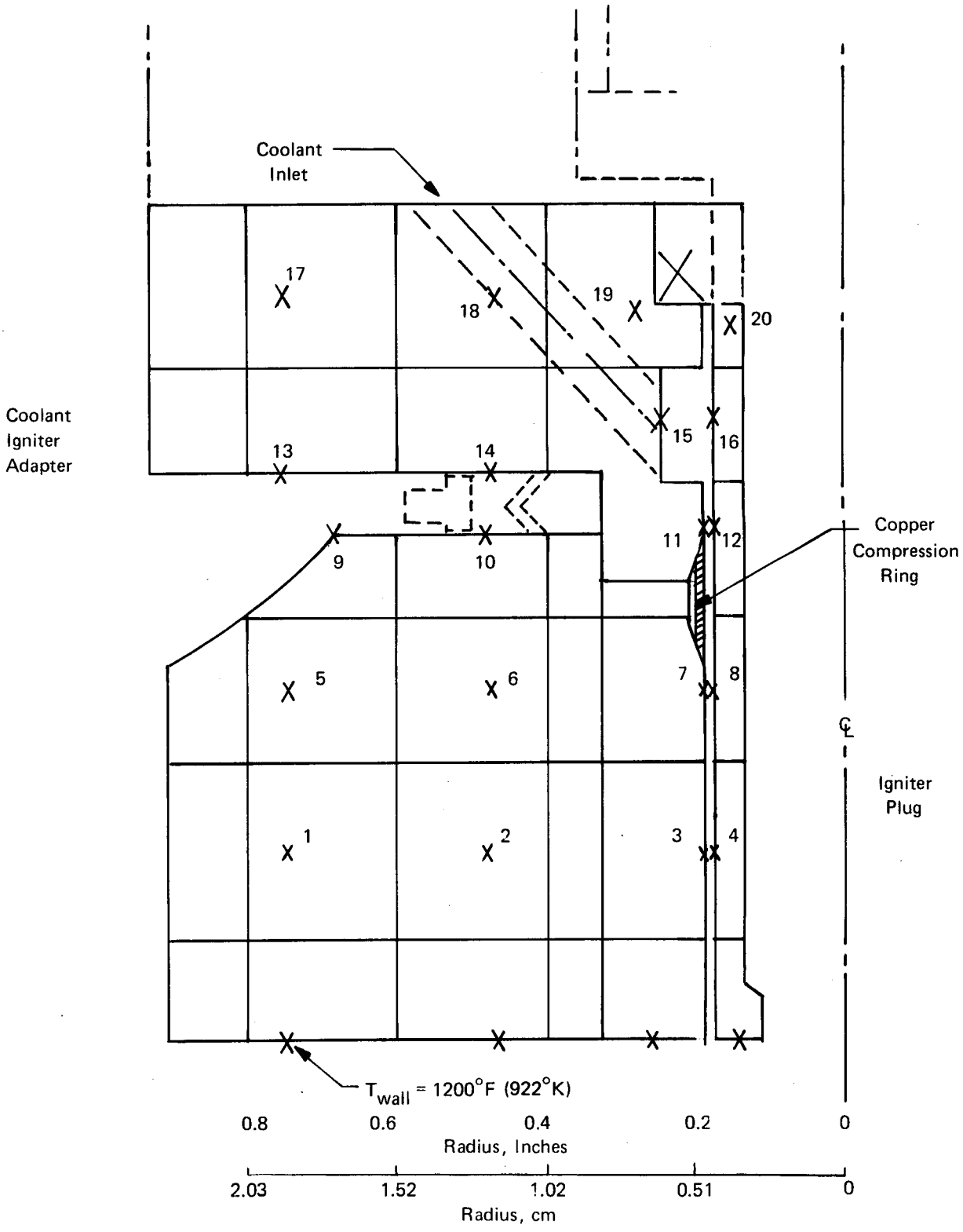

Figure 97. Oxidizer Augmentation Cooled Igniter Adapter Thermal Model (With Compression Ring)

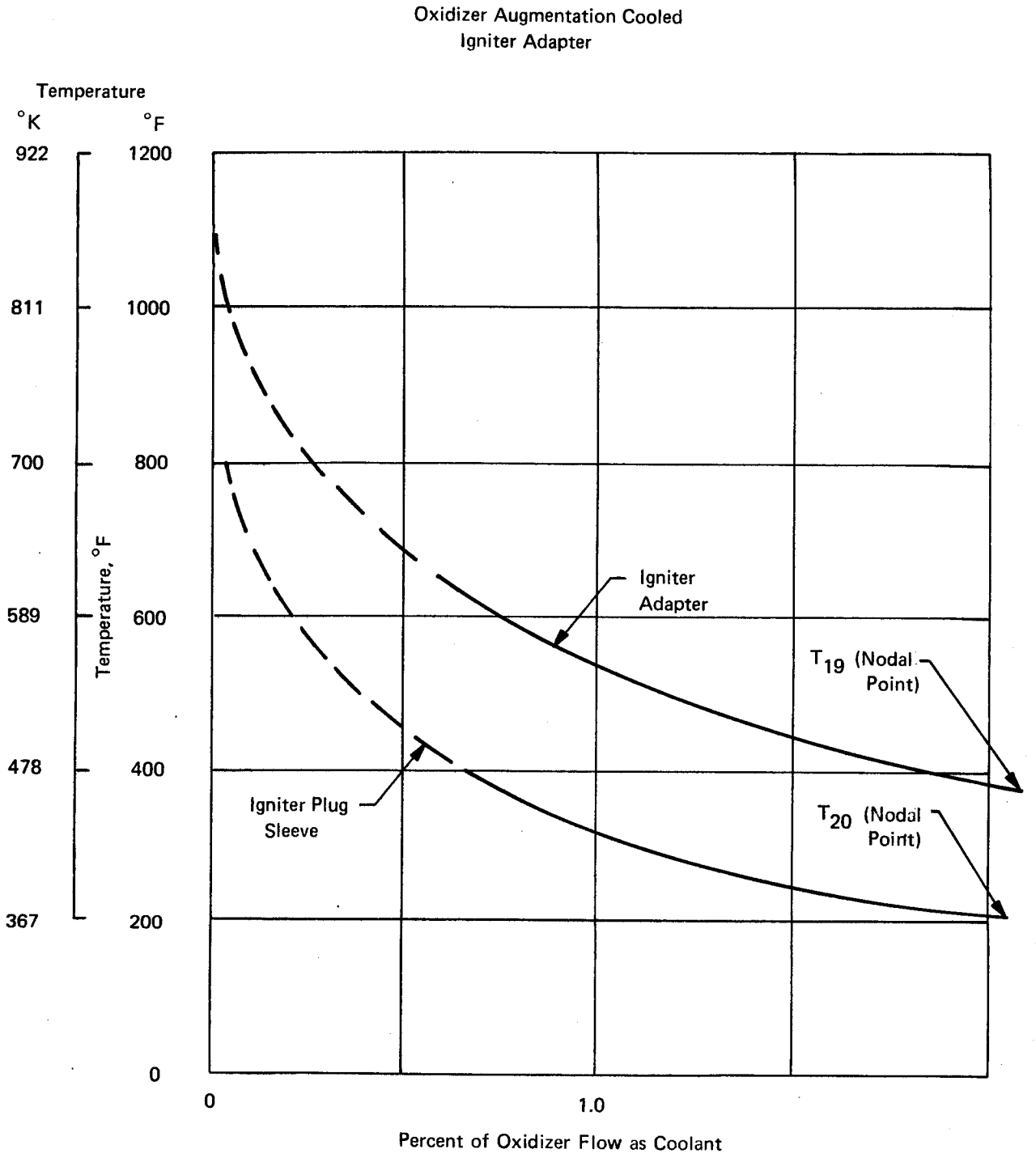

Figure 98. Temperature versus Percent Oxidizer Coolant

This analysis reveals the igniter sleeve temperature (nodal point 20) is less than 400°F (477.6°K) with 0.7% oxidizer augmentation flow. Therefore, the igniter plug/connector interface temperature is less than 400°F (477.6°K) resulting in a margin of more than 200°F (366.5°K).

Additional thermal analyses were conducted on other methods of igniter plug cooling. These analyses are included in the Appendix.

3. Test Results

Two cooled igniter adapters were used for the 500-second test firing. Nominal oxidizer augmentation was used for each igniter adapter. A thermocouple was attached to the body of one igniter plug, (at the connector). Post-run examination of the two igniter plugs and the two electrical harnesses revealed the following:

a. Both electrical harness connectors and both igniter plug connectors revealed no overheating.

b. The temperature on the igniter plug connector (measured by a thermocouple) was less than 170°F (350°K).

c. One igniter plug showed no unusual heating conditions.

d. The other igniter plug was damaged in the area from the tip to the adapter interface (near the copper seal). Approximately 0.5 inch (12.7 mm) of the igniter tip was "burned away." Slight melting of the chamber wall in the vicinity of the igniter plug also occurred.

This damage to the one igniter plug is attributed to leakage of the oxidizer augmentation cooling past the copper compression ring. During the installation of this igniter plug (prior to test), difficulty was encountered which necessitated partial removal of the igniter plug and then retightening. This procedure allowed initial compression and seating of the copper compression ring, followed by relaxation and then attempted resealing. It is probable that the copper compression ring did not re-seal entirely, thereby allowing a sufficient amount of the oxidizer augmentation flow to leak past the compression ring, along the shank of the igniter plug and form a combustable mixture hot enough to melt the igniter plug tip and a portion of the chamber wall. It should be realized that a greater amount of oxidizer flow (greater than the undefined leak) could be considered quite acceptable due to sufficient cooling of the igniter plug shank and much higher mixture ratios, resulting in much lower temperatures.

With a proper installation of the copper compression ring and a leakage test of the installation, it is apparent that this type of cooled igniter plug adapter is a satisfactory configuration.

IX. IGNITION SYSTEM FABRICATION AND CHECKOUT

As previously discussed in the Ignition System Analyses and Design section, two basic types of ignition systems were purchased from vendors and used during this program. Initially, two inductive discharge (I.D.) systems were obtained from Bendix Corporation. These ignition systems provided the desirable "fixed" energy level of approximately 10 millijoules and a spark rate of approximately 900 sparks/sec. During the last quarter of this program two General Laboratory Associates (GLA) ignition systems were also made available. The first of the two C.D. systems used was a capacitive discharge type at a "fixed" energy level – approximately 10 millijoules and approximately 270 sparks per second at a 28-volt input. An available variable energy (GLA) C.D. ignition system was also used for a limited number of tests near the end of the program. Although the ignition system could provide a variable spark energy, it was set up to deliver 10 millijoules of energy at a spark rate of approximately 250 per second.

A photograph of the Bendix Corporation exciter, lead cable and igniter plug is shown in Figure 99. A photograph of the GLA exciter and lead cable with a Champion igniter plug is given in Figure 100.

The major ignition system components consisted of the following:

1. Exciters and Lead Cables
2. Igniter Plugs

A. EXCITERS

The exciters and lead cables obtained for this program are listed in Table XXXIV. Two Bendix Corporation fixed-energy inductive-discharge exciters were purchased for use on the program. In addition, two General Laboratory Associaties fixed-energy, capacitive-discharge exciters were made available for use. Two lead cables for the Bendix Corporation exciters were also purchased items. The variable energy GLA exciter used in the latter test series is also listed in Table XXXIV.

B. IGNITER PLUGS

The surface gap igniter plugs obtained for this program are listed in Table XXXV. The initial igniter plugs purchased from Bendix Corporation did not include a Saurisen cement filler between the electrical connector outer shell and the internal insulator. The subsequent igniter plugs incorporated this rework to improve the structural support in the connector region. The Champion igniter plugs incorporated a one piece insulator and a close fitting insulator/connector shell interface.

C. CHECKOUT TESTS

1. Vendor Tests

The Bendix Corporation exciter system was component bench tested by the vendor. The performance of the entire system was estimated based upon three bench tests and is shown in Figure 101.

The GLA exciter system component bench test results conducted at the vendor are also shown in Figure 102.

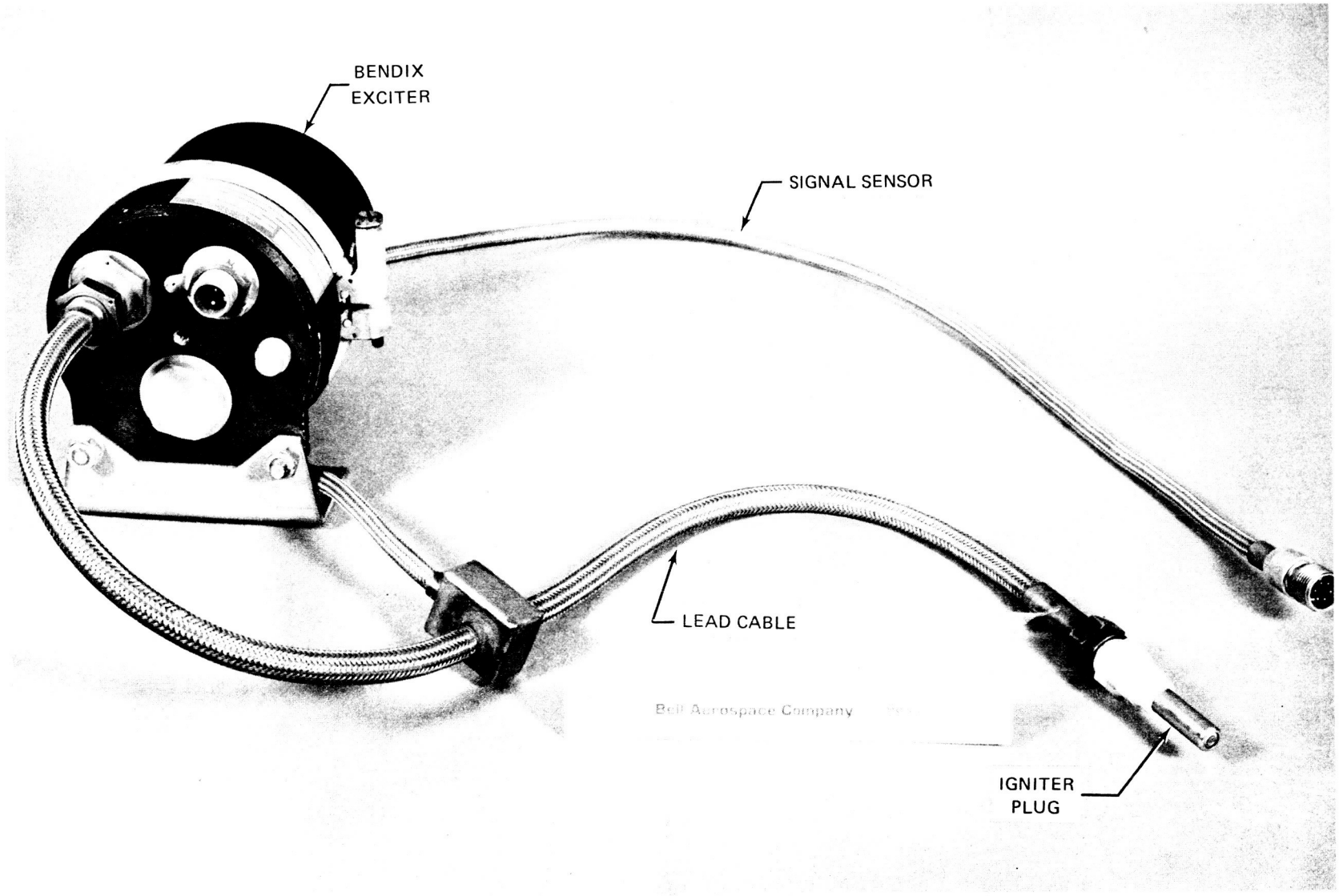

Figure 99. Bendix Ignition System

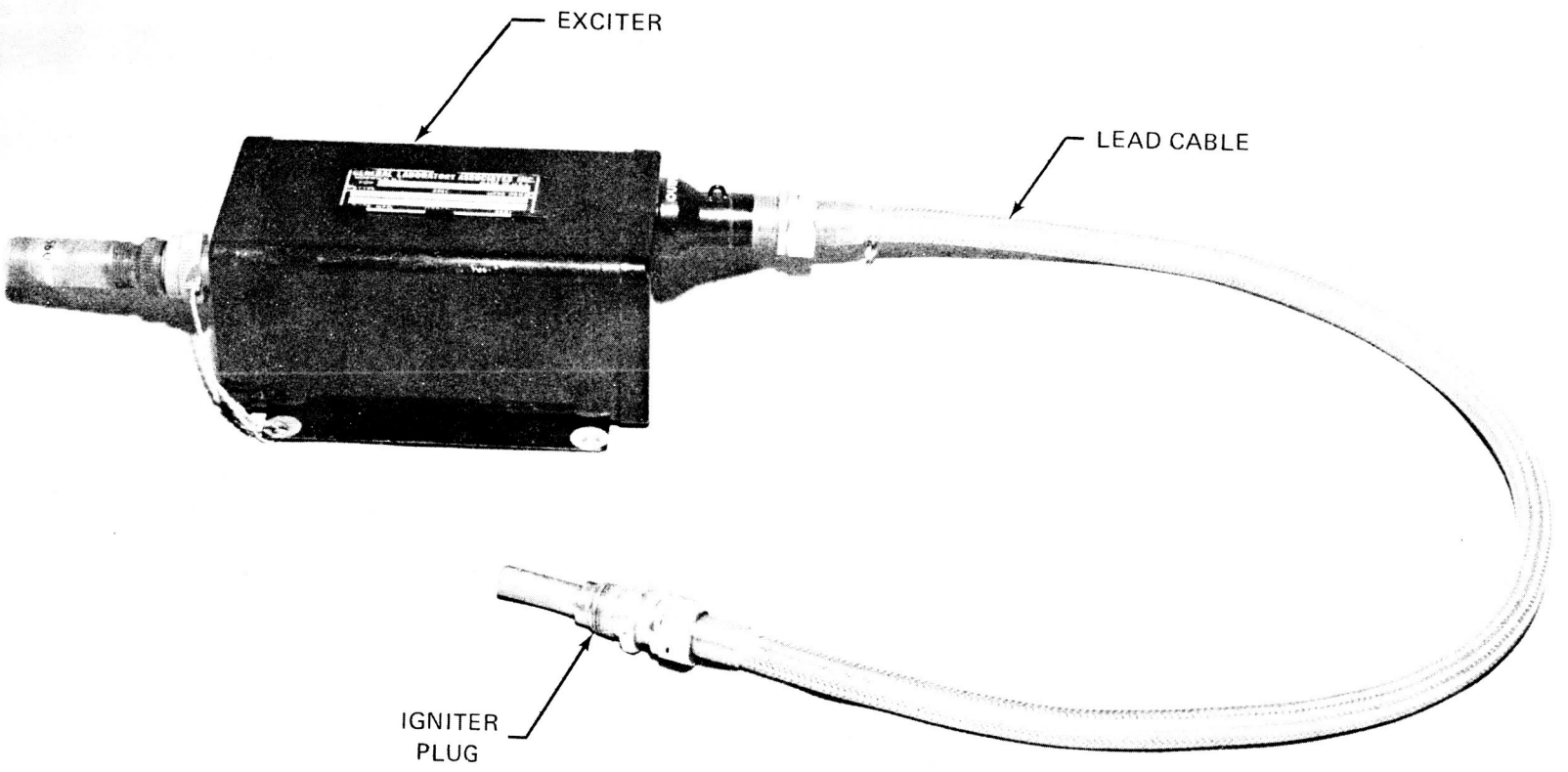

Figure 100. GLA Exciter and Lead Cable and Champion Igniter Plug

2. BAC Tests

Each exciter, lead cable and at least one of each type igniter plug was bench tested at BAC to assure proper operation prior to installation in the test cell. Checkout tests were also conducted to assure nominal operating conditions after initial test cell installation.

TABLE XXXIV
EXCITERS AND LEAD CABLES

Supplier	Component	Model No.	Quantity
Bendix Corp.	Inductive Discharge Exciter	10-81110-3	2
Bendix Corp.	Lead Cables with Monitor	10-395019-1	2
General Laboratory Associates	Capacitive Discharge Exciter	48488	2
General Laboratory Associates	Lead Cables	48487	3
General Laboratory Associates	Control Unit (Variable Energy)	484517	1
General Laboratory Associates	Compositor (Variable Energy)	48489	1

TABLE XXXV
IGNITER PLUGS (SURFACE GAP)

Supplier	Model No.	Quantity
Bendix Corporation	10-390150-1	5
Bendix Corporation	10-390150-1 Modified with Saurisen Cement	11
Champion	AA-1395-1	3

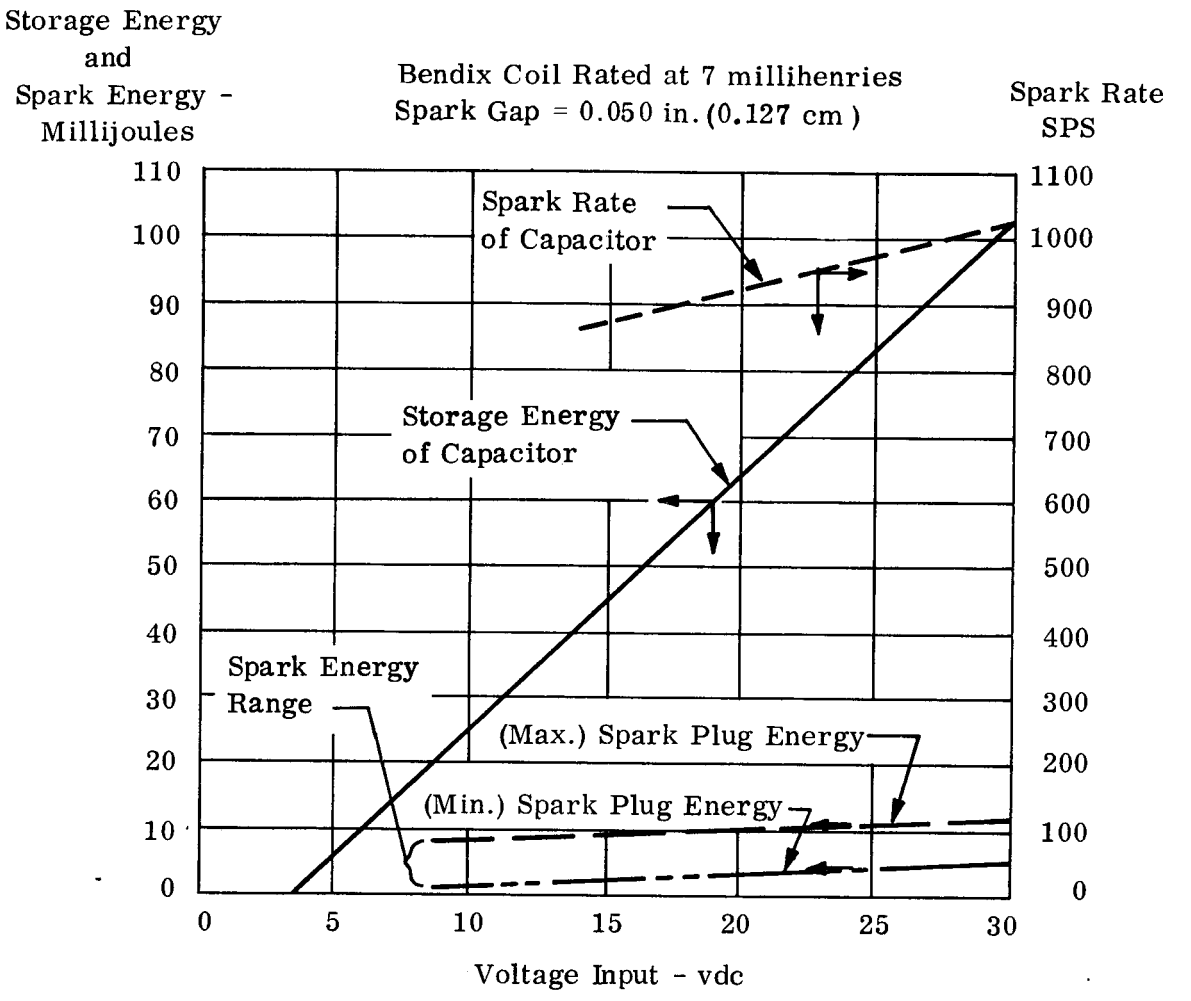

Figure 101. Ignition System Operating Characteristics

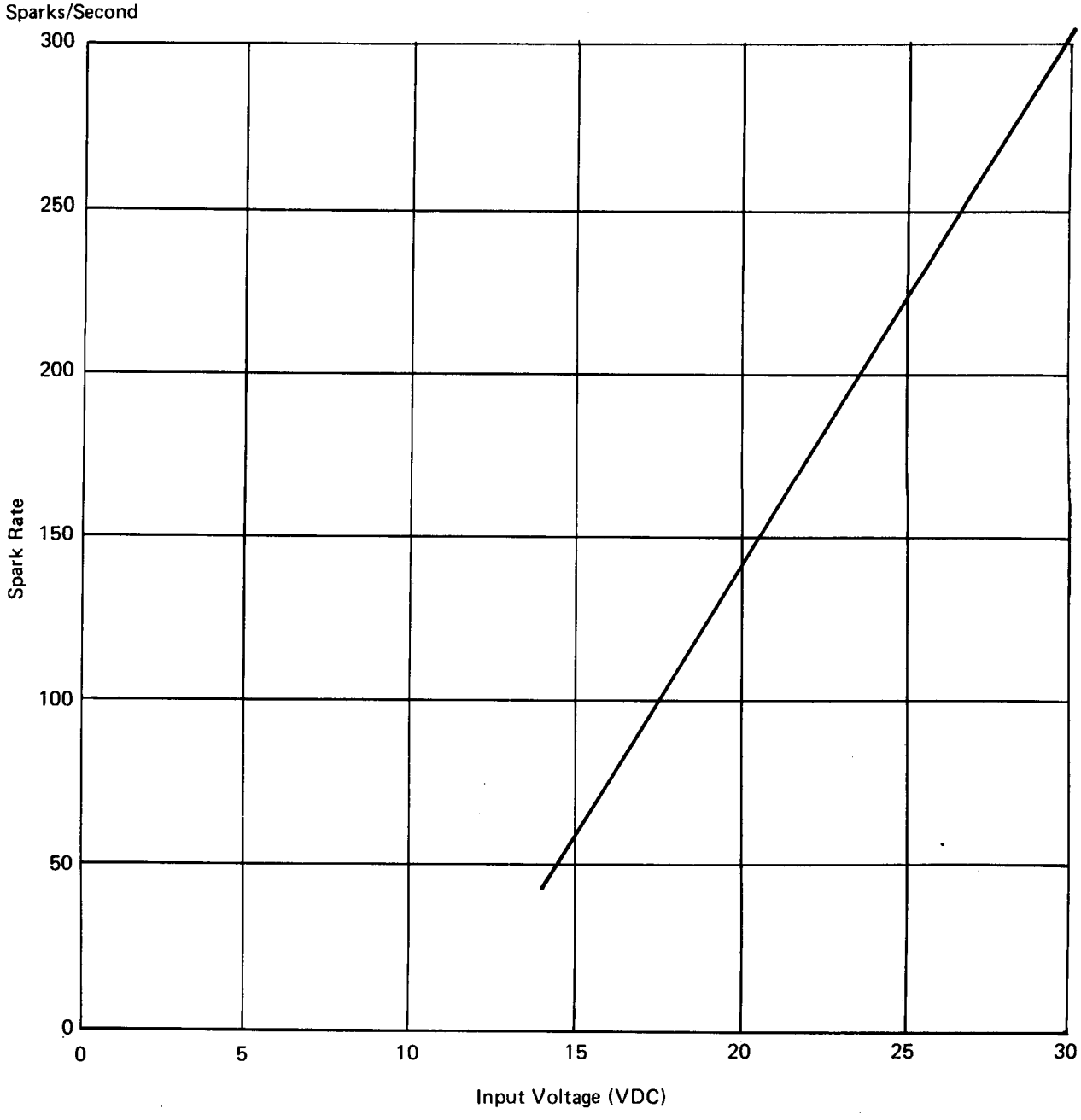

Figure 102. GLA "Fixed Energy" Exciter Calibration
(Spark Energy 10 MJ)

X. PROPELLANT VALVES

A. VALVE SELECTION

The propellant valve preparation task of the contract required the analysis of gaseous hydrogen and gaseous oxygen valves, the fabrication or procurement and checkout of valves for injector, and thrust chamber firing tests. Maximum use of existing off-the-shelf designs and/or hardware was to be made. The operating characteristics of the valves were to be consistent with the range of test conditions defined for thrust chamber testing. The valve opening and closing times were specified as 10-15 milliseconds and a nominal flow pressure drop of 25 psi (17.2 N/cm^2) was required. The internal leakage rate was set at 10^{-7} lb/sec (4.536×10^{-8} kg/sec). A flight-weight configuration was not required and the valve cycle life did not need to conform with the 1×10^6 cycle thrust chamber life. The thrust chamber firing test plan required valving which could provide for the lead of one propellant or simultaneous flow of both propellants to the combustion chamber.

The process of valve selection to meet all of the above requirements included consideration of valve types, and actuator configurations. The selection of the type of actuator lead to the definition of a pilot solenoid valve. The selection considerations and analyses are summarized in the following paragraphs.

The following valve configurations were eliminated as possible candidates for the reasons indicated:

Butterfly Valves - This design is not recommended for sizes of two inches (5.08 cm) or smaller or for high pressure systems.

Gate Valve or Blade Valves - These designs are usually not recommended for high-pressure systems because of the high seat loadings which occur with high inlet feed pressures.

Sleeve Valve or Spool Valve - These designs are usually not recommended for service requiring low leakage rates. Low leakage rates require extremely close tolerances and high surface finishes.

Thus, the most logical candidates for consideration were the ball valve and the poppet valve. The next step was to determine the flow areas required for both ball and poppet valves. The following gas flow formula was used for the calculation.

$$\dot{w} = \frac{8.02\, C_d\, A_2\, P_1}{\sqrt{RT}} \sqrt{\frac{K}{K-1}\left[\left(\frac{P_2}{P_1}\right)^{\frac{2}{K}} - \left(\frac{P_2}{P_1}\right)^{\frac{K+1}{K}}\right]} \times \frac{1}{\sqrt{1 - \left(\frac{A_2}{A_1}\,\frac{\rho_2}{\rho_1}\right)^2}}$$

where

$\dot{w}$ = 0.69 lb/sec (0.313 Kg/sec) H_2 gas

C_d = 0.95 for ball valve and 0.65 for poppet valve

A_2 = Ball hole area or poppet seat area, $in.^2$ (cm^2)

P_1 = 400 psia (275.8 N/cm^2)

R = 766.8 ft/°R (110.7 m/°K)

T = 530°R (294°K)

K = 1.4 for H_2 gas or O_2 gas

P_2 = 375 psi (258.6 N/cm^2)

ΔP = 25 psi (17.2 N/cm^2) - Used for calculations and for comparative sizes.

A_1 = 1.042 in.^{2} (6.726 cm^2) (based on valve upstream size of 1-1/4 in. (3.175 x 10^{-2} m) OD with 0.049-in. (0.1245 cm) wall thickness or an ID of 1.152 in. (2.93 cm) and A_1 = 1.042 in.^{2} (6.726 cm^2).

Comparative results for each type valve were as follows.

Parameter	Ball Valve	Poppet Valve
ΔP	25 Psi (17.2 N/cm^2)	25 Psi (17.2 N/cm^2)
Seat Area	0.524 in.^{2} (3.581 cm^2)	0.681 in.^{2} (4.394 cm^2)
Seat Diameter (min.)	0.817 in. (2.075 cm)	1.108 in. (2.814 cm)
Stroke		0.277 in. (0.704 cm)

The results indicated the poppet type valve would be larger than the ball type valve.

Another factor in the selection of the valve design was the schedule consideration. A ball valve, to accomplish the engine design objectives, was available for use without modification while the selection of a poppet design would have required some valve development effort. As a result of the above considerations, the ball valve was considered the most logical candidate.

The selection of an actuator type is dependent on such factors as energy source, response times, leakage rates, weight, envelope size and cycle life. The energy to actuate the valve may be derived from hydraulic, electric or pneumatic sources. The hydraulic and electrical types were eliminated as possible candidates for the following reasons:

Electric Type - Electric energy may be employed to magnetically actuate the propellant valve. A direct acting type valve was investigated where the valving element was moved from its seat by means of an electrically actuated coil. To meet the maximum pressure drop of 25 psi (17.2 N/cm^2), a stroke of over 0.225 in. (0.57 cm) was required. To open in a maximum of 0.030 second with this stroke would have required an exceedingly high electrical power requirement which in turn would have required a large and heavy coil.

Hydraulic Type - The use of a hydraulic fluid to actuate the valve would have presumed the availability of a hydraulic pump or a pressurized reservoir. Since the high pressure reverse flow APS engine employed gases as the propellant media, the hydraulic type actuator was not considered practical. Other factors eliminating the hydraulic type were the temperature requirement of 200°R (111°K) to 850°R (472°K) and the larger size solenoid valve which would be required to meet open and close response times.

After concluding that a pneumatic actuator was the logical candidate, several type pneumatic actuators were considered:

Rotary - Although a number of rotary actuators have been developed in recent years to provide direct reciprocating rotation of valves, the majority have been designed for hydraulic fluids. The use of gases would have entailed some development effort to prove an adequate design for minimizing the leakage problems and the inherent high breakout torques.

Double Acting Piston - The conventional double acting piston utilizes pressure on one side of the piston to open and on the opposite side to close. This is usually accomplished by means of a four-way solenoid valve. The main disadvantage of this design is that it does not have the capability of "fail safe" closed provisions in the alloted closing time of 0.015 second when power is lost.

Thus, the spring return piston actuator type was selected as the most logical actuator. Pressure is admitted to, and vented from, the gas side of the actuator by means of a solenoid actuated three-way pilot valve. The extensive experience at Bell Aerospace Co. with that type actuator (LM, Agena, Rascal), indicated that the actuator would meet opening and closing response times, repeatability, test cycle life and leakage requirements with the least amount of development time and cost.

The solenoid valve selected was a Skinner pilot actuated solenoid valve which had been used with great success on the Rascal and Agena programs. The valve was also selected because it was available and it was known that it could meet the required response times. The electrical delay of the solenoid was approximately 0.006 second with a shuttle poppet time of less than 0.008 second. Because the flow is introduced to the main valve actuator piston before the shuttle poppet is fully opened, the overall electrical delay of the solenoid valve was well under the allowable response time of 0.015 second.

B. VALVE VENDOR SELECTION

In order to meet the allowable pressure drops, the opening and closing response times, leakage and cycle life requirements for the 1500-lb (6,672N) thrust engine, the type of valve selected as the most logical candidate was a ball valve employing a pneumatic actuator with a spring return piston. For the development testing of the high-pressure reverse-flow engine, the following additional ground rules were established in conformance with the contract work statement:

(1) The test valves would be individual valves rather than bipropellant valves. This would enable the evaluation of engine starts with propellant sequencing. By electrically interconnecting the test valves, a simulation of a bipropellant valve could be achieved.

(2) The test valves would not be flight weight. Externally, the bodies would be rough machined but internally the dimensions and parts would be similar to flight type valves.

(3) The cycle life of the test valve would not be demonstrated.

A survey was conducted of various ball valve manufacturers to determine the availability of off-the-shelf designs to meet the requirements. Flodyne Control, Inc. was found to have the required valve. Calculations disclosed a ball having a 0.818-in. (2.08 cm) flow hole would permit a maximum pressure drop of 25 psi (17.2 N/cm^2) for the rated oxidizer or fuel flows. Flodyne's standard size ball valves have 3/4-(1.9 cm) or 1-in. (2.54 cm) hole sizes. The 1-in. (2.54 cm) size was selected. The pressure drop through the 1-inch flow holes for rated flows was calculated as 9 psi (6.205 N/cm^2) maximum.

Flodyne's ball valve design employed a rack and pinion to rotate the balls (Figure 103). This design had proven itself to be very successful for long cycle life and for rapid opening and closing response. The rack and pinion arrangement transmits the linear motion of the piston to the rotary motion required for the ball and shaft. The rack is an integral part of the piston while the pinion is part of the shaft.

Three valves were purchased from Flodyne and were received during the month of November 1970.

C. VALVE CHECKOUT TESTS

Prior to receipt of the ball valves from Flodyne, three normally open pilot-operated solenoid valves were reworked to normally closed type valves. The pilot poppet strokes were adjusted to give similar opening and closing response times for each solenoid. The average opening and closing response times at 28 Vdc for the three solenoid valves were 0.011 second and 0.007 second, respectively.

The apportionment for the opening response times was as follows:

From	To	Time (sec)
Electrical Switch Actuation	Start of Poppet Movement	0.005
Electrical Switch Actuation	End of Pilot Poppet Movement	0.008
Electrical Switch Actuation	Start of Main Poppet Movement	0.008
Electrical Switch Actuation	End of Main Poppet Movement	0.011

The apportionment for the closing response times was as follows:

From	To	Time (sec)
Electrical Switch Actuation	Pilot Poppet Valve Full Closed	0.004
Electrical Switch Actuation	Main Poppet Valve Full Closed	0.007

The solenoid valves were leak tested satisfactorily at 3.00 (2.068), 600 (413.7) and 900 (621 N/cm^2) psig.

The average electrical characteristics of the three valves were recorded:

Coil Resistance	12.75 ohms
Coil Inductance	39.5 millihenries

Upon receipt of the propellant valves from Flodyne, the three solenoid valves were assigned and installed onto the three propellant valves. Leakage tests were conducted on the propellant valve assemblies with the following results:

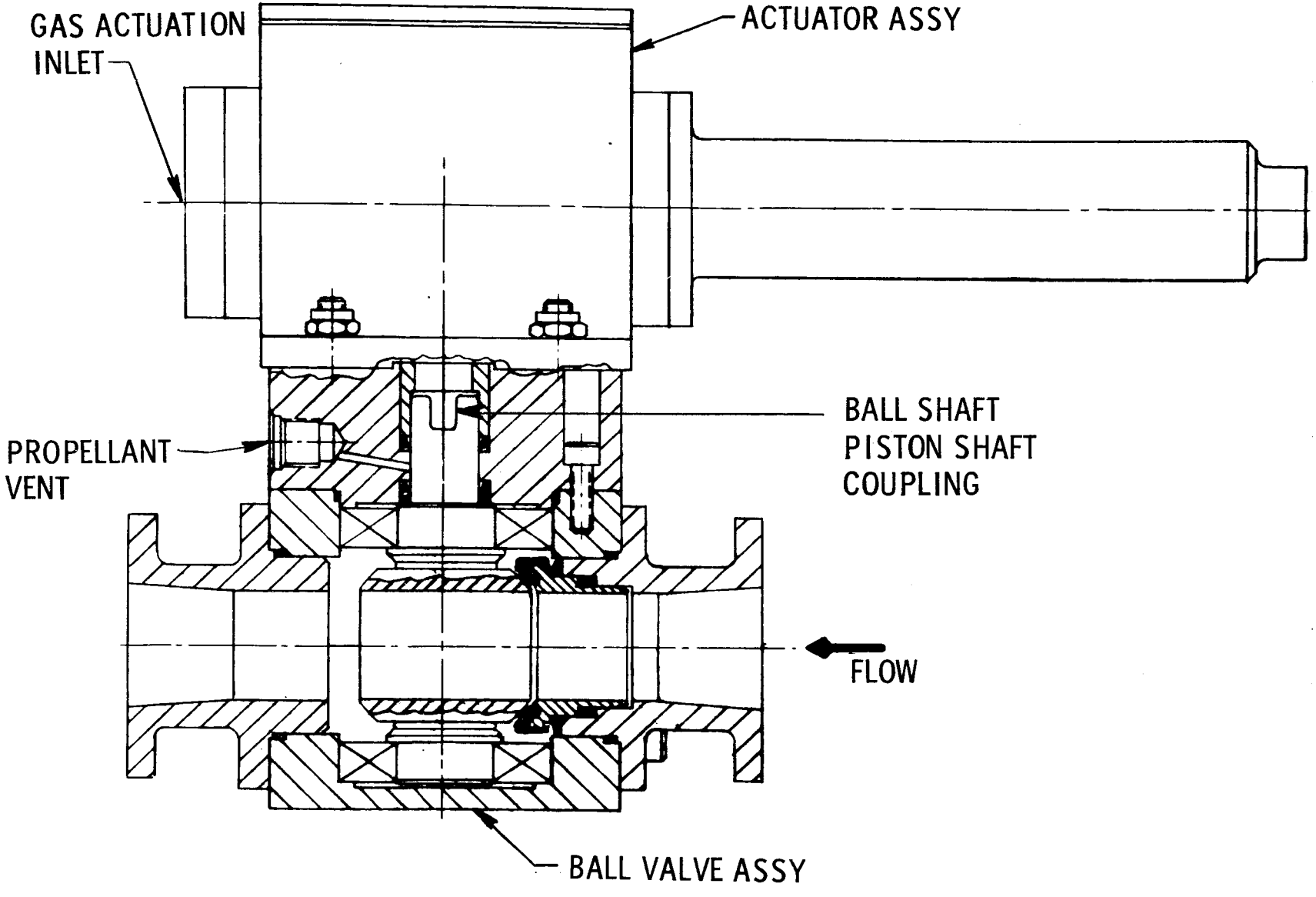

Figure 103. APS Engine Propellant Valve

Test Location	Inlet Pressure psig (N/m^2)	N2 Gas Leakage (CC/min.)		
		S/N-1	S/N-2	S/N-3
Seat	3 (2.068)	0	0	0
Seat	400 (275.8)	0	0	0
Seat	600 (413.7)	0	0	0
Shaft	3 (2.068)	0	0	0
Shaft	400 (275.8)	0.73	0	0
Shaft	600 (413.7)	1.40	0	0

No further testing was conducted on valves S/N-1 and S/N-2. They were assembled on the reverse-flow engine for engine testing.

A pressure actuation test was conducted on valve S/N-3 with the following results.

Condition	Cycle No. 1				Cycle No. 2			
	Pressure Required psig	Pressure Required N/cm^2	Force Required lb	Force Required N	Pressure Required psig	Pressure Required N/cm^2	Force Required lb	Force Required N
Start Opening	350	243	428	1 904.0	340	241	417	1854.9
Fully Open	650	448	796	3 541.0	645	445	790	3514.1
Start Closing	540	352	662	2944.7	550	379	675	3,002.5
Fully Closed	270	176	331	1427.4	280	183	343	1525.7

Test results indicated the following:

Spring Compressed Load	=	730 lb (3247.2N)
Spring Installed Load	=	380 lb (1700.3N)
Spring Rate	=	636 lb per inch (1,114 N/cm)

D. VALVE HISTORY DURING ENGINE TESTS

Engine firing tests were started in December 1970. The valve opening and closing response times were satisfactory. The contract requirement of maximum opening and closing times were 0.030 second (0.015 second for electrical and 0.015 second for mechanical delay) while the actual opening and closing response times were 0.014 second. The apportionment was as follows:

From elect. switch to prop valve Start Open	0.010 sec
From prop valve start to prop valve Full Open	0.004 sec
Total Opening Time	0.014 sec
From elect. switch to prop Valve Start Close	0.009 sec
From prop valve start to prop Valve Full Close	0.005 sec
Total Closing Time	0.014 sec

A total of over 162 hot firing runs were conducted on the valves in the sea level test cell with no problems. During the initial phase of testing in the altitude cells failure of the valve coupling by the shearing of either the male tang on the ball shaft or the related female tangs on the pinion shafts occurred on three Flodyne valves. A review of test results was conducted. The piston travel times recorded for opening were very repeatable and averaged between 0.004 to 0.005 second. The piston travel times recorded for closing were very repeatable and averaged between 0.005 to 0.006 second. At the start of the program, the opening and closing time requirement for the mechanical travel of the valve was defined as 0.015 second maximum. Thus, the valves had been designed and stressed for opening and closing travel times of 0.012 to 0.015 second. Since acceleration is a function of time squared (t^2), the full travel of the piston, ball and shaft in 0.004 second gave torsional shear stress load 14.5 times greater than that for a 0.015 sec piston travel. The fast opening and closing response time was attributed to the large size of the pilot-operated solenoid valves which were used in conjunction with the Flodyne valves. The calculated solenoid valve seat size to open and close the ball valve in 0.012 to 0.015 second was determined to be equal to an effective seat diameter of 0.14 in. (0.356 cm). The solenoid valves used had an effective seat diameter of 0.24 in. (0.61 cm) since that size solenoid was available.

In order to continue with the engine program after the ball shaft failures, the decision was made to slow the opening and closing mechanical response times by orificing the inlet and vent ports of the solenoid valve. The results were as follows:

Period	Orifice Size In Inlet (inch)	Opening Time (sec)			Orifice Size In Vent Port (inch)	Closing Time		
		Elect	Mech	Total		Elect	Mech	Total
Before	-	0.010	0.004	0.014	-	0.009	0.005	0.014
After	0.078 (0.198 cm)	0.010	0.022	0.032	0.093 (0.236 cm)	0.009	0.024	0.033

Engine tests were conducted satisfactorily with the orifices until the month of October when pulse tests were required. The orifice sizes were changed to decrease the opening and closing times to the contract requirement. The valve operation was as follows:

Period	Orifice Size In Inlet (inch)	Open Time (sec)			Orifice Size In Vent Port (inch)	Close Time		
		Elect	Mech	Total		Elect	Mech	Total
Before Change	0.078 (0.198 cm)	0.010	0.022	0.032	0.093 (0.236 cm)	0.009	0.024	0.033
After	0.081 (0.206 cm)	0.010	0.016	0.026	0.109 (0.277 cm)	0.009	0.016	0.025

A total of over 4000 pulse cycles were made with the total opening and closing times of less than 0.030 second with no further problem of shearing of the ball shafts.

XI. INJECTOR TESTS

A. OXIDIZER CUP COLD FLOW TESTS

Cold flow testing of oxidizer cup configurations was conducted early in the contract effort to assist in the O_2 injector design. The tests included:

(1) Characterization of the cup employed for hot firing of the 1K (4,448N) engine.

(2) Flow tests of candidate 1.5K (6,672N) cup models for comparison with the 1K (4,448N) cup.

(3) Test of the 1.5K (6,672N) models with back pressure to provide accurate cup pressure drop values.

Tests (1) and (2) above were carried out with ambient back pressure with N_2 flow rates which matched the volumetric flow rate of O_2 at the 1K (4,448N) and 1.5K (6,672N) design points.

Figure 104 presents pitot tube measurements of the flow boundary and maximum axial velocity for the 1K injector and a 1.5K (6,672N) O_2 cup with no center flow. The swirl hole size and the diameters of the 1.5K (6,672N) injector provided the same ratio of $\frac{D_1 D_2}{A_S}$ as the 1K (4,448N) cup, where A_S is the total area of the swirl holes. The tests confirmed that equal ratios $D_1 D_2 / A_S$ exhibited similar flow patterns. The gas efflux angle, which is based on the two sets of data points closest to the cup outlet, was essentially equal.

Test data for 1K (4,448N) and 1.5K (6,672N) oxidizer cups is with center flow as given in Figure 105 which presents plots of the radial distribution of the axial velocity component at three downstream locations. The 1.5K (6,672N) configuration employed for the data of Figure 105 was taken as the baseline configuration. The various configurations tested and the observed gas efflux angles are presented in Table XXXVI.

The characterization of the swirl cup flow and the subsequent hot test firings as described in the following subsections showed that the combustion efficiency of the 1K (4,448N) unit was duplicated by the 1.5K (6,672N) cup which had the same ratio of $D_1 D_2 / A_S$ and the same fuel injection velocity. The cold flow testing of candidate cup configurations was employed successfully to scale from 1.0K (4,448N) and a design P_C of 250 psia (172.4 x 10^5 N/cm^2) to the contract nominal operating conditions. Performance improvements were achieved at increased ratios of $D_1 D_2 / A_S$ and higher velocity fuel injectors.

B. HEAT SINK TCA FIRINGS

1. Test Objectives

The primary purpose of the injector firings at sea level was the definition of fuel and oxidizer injectors to be employed with or incorporated into the cooled thrust chamber hardware which was to be tested in a simulated altitude environment. The successful demonstration of the contract specific impulse goal required injectors capable of achieving a high percentage of c*. The specific c* goal was 97% of the theoretical shifting value at a chamber pressure of 300 psia (206.8 N/cm^2) and a mixture ratio of 4. The cycle life requirement dictated effective and uniform

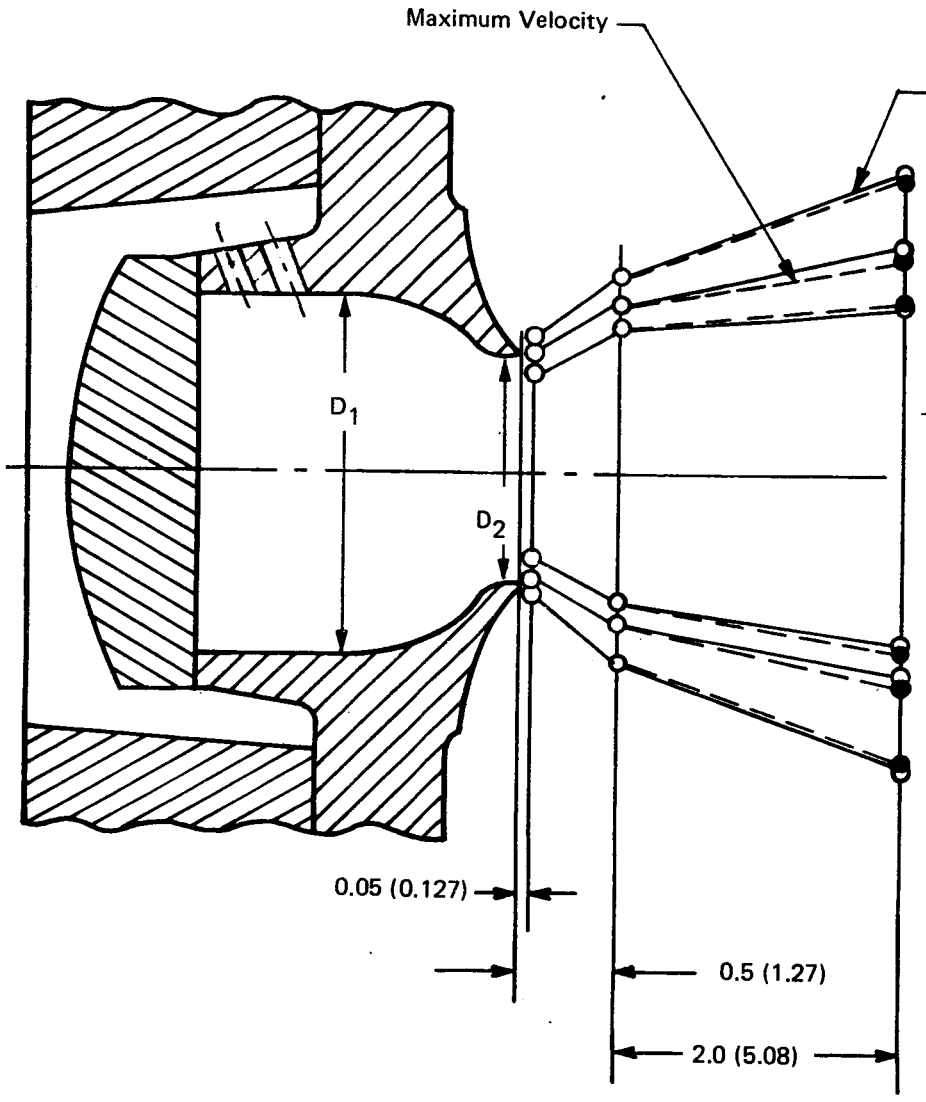

in.	mm
+0.50	(12.7)
0.25	(6.4)
0	
-0.25	(6.4)
-0.50	(12.7)

Model Parameters

1 k (4448N) Injector			1.5 k (6672 N) Injector		
	in.	cm		in.	cm
D_s	= 0.1406	(0.35)	D_s	= 0.166	(0.42)
D_1	= 1.594	(4.05)	D_1	= 1.902	(4.83)
D_2	= 1.00	(2.54)	D_2	= 1.189	(3.03)

Figure 104. Heat Sink Thrust Chamber Assembly

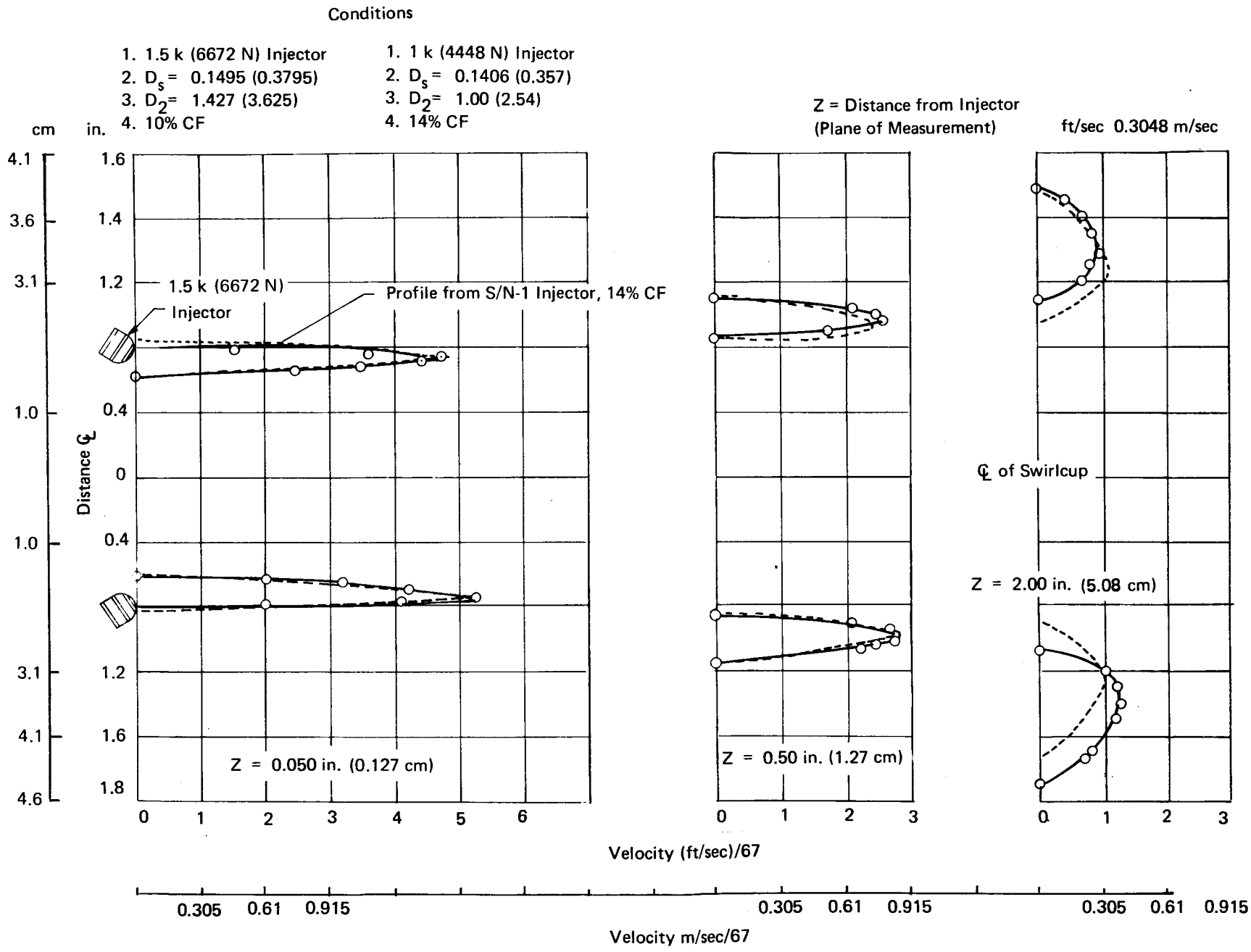

Figure 105. Oxidizer Flow Model Comparison of Radial Distribution of Axial Components of Gas Flow

TABLE XXXVI
SUMMARY – O_2 CUP COLD FLOW TESTS

1 K (4448N) D_1		D_2		As		% Center Flow	Va ⚠		Efflux Angle
in.	mm	in.	mm	$in.^2$	mm^2		fps	m/sec.	
1.594	40.5	1.00	(25.4)	0.373	176.2	0	485	147.5	21
						14	334	101.7	26
						21	239	72.8	26
				0.471		0	441	134.2	17
						14	297	90.5	23
						21	237	72.2	25
1.5 K (6672N)									
1.90	48.3	0.951	24.2	0.418	270	10	615	187.2	22
				0.519	335		602	183.5	22
		1.189	30.2	0.418	270		415	126.3	26
				0.519	335	0	544	165.8	20
						10	390	118.7	22
		1.427	36.25	0.418	270	0	444	135.2	22
						5	366	111.3	25
						10	330	100.5	28
				0.519	335	0	416	126.5	21
						5	357	108.5	23
						10	333	101.3	25

⚠ Max. Axial Velocity 0.050 in. (1.27 mm) From Cup Outlet Plane

cooling of the combustion chamber and throat. The achievement of high combustion efficiency and adequate cooling was constrained by the injection pressure drop.

Secondary test objectives included the assessment of the valves and ignition system selected to support the thrust chamber characterization.

The initial contract requirements encompassed fuel and oxidizer injectors designed for a propellant feed temperature of 540° R (300° K). The contract was amended after the injector firings to include testing of an injection system designed for 250° R (139° K) H_2 and 375° R (208.3° K) O_2 feed temperatures. The injector test firings were carried out at a nominal feed temperature of 540° R (300° K); the definition of the low temperature design hardware was made from the cooled thrust chamber firings at altitude.

A description of the injectors' design characteristics and the variables selected for injector test evaluation is presented in Section IV.

2. Test Chronology

The tests conducted at sea level with the heat sink injector test hardware are summarized in Table XXXVII. All tests were carried out with ambient propellant feed temperatures. The hardware configuration tested, the performance data as measured for the firing, and the data corrected

TABLE XXXVII

MODEL 8636 TEST DATA - SPACE SHUTTLE (1 of 3)

		Hardware Configuration				Test Performance Data										Corrected Data to 540°R(300°K)						Efficiency	
IAW Cell Run No.	Date	Cup (deg)	* Fuel Inj.	% Ctr Flow	Thrust Chamber	P_c psia	P_c N/cm^2	WT lb/sec	WT Kg/sec	MR	Thrust lbf	Thrust N	c* ft/sec	c* m/sec	I_{sp} SL	c* ft/sec	c* m/sec	I_{sp} SL	C_f SL	I_{sp} vac	C_f vac	% c*	% I_{sp} vac
992	12/4/70	28	-5	10	-020	288.8	199.1	3.319	1.506	3.07	1081.8	4802	7883	2403	325.9	7932	2418	329.6	1.3370	368.9	1.4961	94.6	91.2
993	12/4/70	28	-5	10	-020	307.5	212.0	3.573	1.621	3.50	1160.9	5164	7799	2377	324.9	7846	2391	328.6	1.3476	365.0	1.4970	94.3	90.6
994	12/9/70	28	-1	10	-020	304.4	209.9	3.563	1.616	3.90	1157.6	5149	7741	2358	324.9	7776	2370	328.1	1.3576	364.5	1.5080	94.3	91.1
995	12/14/70	28	-1	10	-020	305.6	210.7	3.628	1.645	4.23	1169.4	5201	7654	2333	322.3	7689	2344	325.6	1.3622	361.4	1.5121	94.1	91.0
996	12/18/70	28	-5	10	-020	302.6	208.6	3.576	1.624	3.99	1153.7	5131.5	7667	2337	322.6	7703	2348	325.9	1.3611	362.4	1.5139	93.6	90.8
997	12/21/70	28	-5	10	-020	303.7	209.4	3.602	1.635	4.22	1151.9	5123.5	7614	2321	319.8	7655	2333	323.3	1.3588	359.6	1.5116	93.7	90.5
998	12/21/70	28	-5	10	-020	305.7	210.8	3.581	1.621	3.54	1154.5	5135	7711	2350	322.4	7761	2366	326.2	1.3525	362.9	1.5043	93.3	90.2
999	12/21/70	28	-5	10	-020	306.9	211.6	3.542	1.607	3.30	1152.9	5128	7827	2386	325.5	7880	2402	329.5	1.3452	366.5	1.4965	94.3	90.8
1000	12/21/70	28	-5	10	-020	301.9	208.2	3.624	1.644	4.56	1134.7	5046.7	7523	2293	313.1	7563	2305	316.5	1.3465	352.7	1.5003	93.6	89.5
1003	12/30/70	28	-9	10	-020	299.2	205.3	3.629	1.646	4.43	1128.1	5018	7424	2263	310.8	7460	2274	314.0	1.3543	349.8	1.5085	91.9	88.5
1004	1/4/71	28	-9	10	-020	294.8	203.3	3.582	1.625	4.32	1110.8	4941.1	7383	2250	310.1	7415	2260	313.1	1.3586	348.7	1.5133	91.1	88.0
1005	1/5/71	28	-1	10	-020	301.0	207.5	3.629	1.646	3.76	1131.8	5034.1	7430	2265	311.9	7468	2276	315.2	1.3578	350.6	1.5104	90.3	87.4
1006	1/5/71	28	-1	10	-020	297.1	204.8	3.618	1.641	4.15	1114.0	4955.3	7356	2242	307.9	7391	2253	311.0	1.3541	346.5	1.5086	90.3	87.1
1009	1/8/71	28	-1	10	-020	308.6	212.8	3.556	1.613	3.18	1144.2	5089.5	7737	2358	321.7	7788	2274	325.5	1.3448	362.0	1.4957	93.0	89.6
1010	1/8/71	28	-1	10	-020	309.1	213.1	3.599	1.633	3.52	1151.7	5123	7658	2334	320.0	7705	2362	323.7	1.3517	359.8	1.5024	92.6	89.4
1011	1/8/71	28	-1	10	-020	303.8	209.5	3.388	1.537	2.77	1118.1	4973.5	7984	2434	330.0	8042	2451	334.1	1.3367	372.4	1.4900	95.7	92.0
1012	1/8/71	28	-1	10	-020	304.1	209.7	3.590	1.629	4.87	1138.0	5062	7541	2298	317.0	7575	2309	320.2	1.3599	356.2	1.5131	94.7	91.2
1013	1/12/71	28	-1	10	-020	302.0	208.2	3.508	1.591	3.99	1121.9	4990.3	7648	2331	319.8	7692	2345	323.4	1.3528	360.3	1.5070	93.5	90.2
1014	1/12/71	28	-1	10	-020	306.2	211.1	3.426	1.554	2.85	1127.4	5014.7	7919	2414	329.0	7974	2430	333.0	1.3435	370.7	1.4957	94.9	91.6
1015	1/12/71	28	-1	10	-020	300.8	207.4	3.613	1.639	5.16	1128.3	5018.8	7377	2248	312.3	7412	2259	315.5	1.3695	351.2	1.5244	93.7	90.7
1016	1/13/71	28	-1	1.5	-020	306.7	211.5	3.512	1.593	4.03	1138.9	5066	7738	2358	324.3	7783	2372	328.0	1.3559	364.7	1.5074	94.7	91.4
1017	1/13/71	28	-1	1.5	-020	316.9	218.5	3.513	1.593	2.61	1162.1	5169	7994	2436	330.8	8063	2458	335.4	1.3382	372.1	1.4849	95.9	92.0
1018	1/13/71	28	-1	1.5	-020	309.3	213.2	3.631	1.647	5.30	1138.9	5066	7548	2301	313.7	7585	2312	317.0	1.3445	352.4	1.4947	96.4	91.4
1019	1/13/71	28	-1	1.5	-020	308.0	212.4	3.511	1.593	4.10	1135.1	5049	7774	2370	323.3	7821	2384	327.0	1.3455	363.7	1.4964	95.4	91.3
1020	1/13/71	28	-1	1.5	-020	311.7	214.9	3.475	1.576	2.59	1144.0	5089	7948	2422	329.2	8020	2444	333.9	1.3395	371.0	1.4886	95.3	91.7
1021	1/14/71	28	-1	5	-020	307.0	211.7	3.488	1.582	4.20	1137.2	5059	7743	2350	326.1	7777	2370	329.3	1.3623	365.5	1.5119	95.1	91.9
1022	1/15/71	28	-1	5	-020	301.5	208.0	3.433	1.557	4.02	1101.4	4899	7725	2354	320.8	7760	2365	324.0	1.3433	360.9	1.4965	94.4	90.4
1023	1/15/71	28	-1	5	-020	304.4	209.9	3.421	1.552	4.02	1119.0	4978	7826	2385	327.0	7863	2397	330.3	1.3516	367.4	1.5033	95.7	92.1
1024	1/18/71	28	-1	5	-020	308.0	212.4	3.350	1.520	2.52	1117.5	4971	8080	2463	333.6	8148	2483	338.1	1.3351	375.8	1.4841	96.9	92.9
1025	1/18/71	28	-1	5	-020	304.1	209.7	3.531	1.602	5.41	1120.3	4983	7568	2307	317.3	7604	2318	320.5	1.3563	356.2	1.5072	97.0	92.7
1026	1/20/71	25	-1	5	-020	304.4	209.9	3.454	1.567	4.08	1115.4	4962	7711	2350	322.9	7746	2361	326.1	1.3546	362.7	1.5064	94.4	91.0
1027	1/20/71	25	-1	5	-020	313.5	216.2	3.426	1.554	2.64	1133.9	5043	8005	2440	331.0	8070	2460	335.4	1.3371	372.4	1.4846	95.9	92.0
1028	1/20/71	25	-1	5	-020	301.8	208.1	3.417	1.549	3.97	1110.3	4939	7727	2345	324.9	7765	2366	328.3	1.3602	365.3	1.5134	94.4	91.4
1029	1/20/71	25	-1	5	-020	308.0	212.4	3.360	1.524	2.54	1112.6	4949	8020	2444	331.1	8088	2465	335.6	1.3350	373.3	1.4851	96.2	92.3
1030	1/21/71	23	-1	5	-020	304.0	208.9	3.381	1.534	3.19	1110.3	4939	7860	2396	328.4	7905	2409	332.0	1.3513	369.0	1.5020	94.4	91.3
1031	1/22/71	23	-1	5	-020	305.2	210.4	3.324	1.508	2.51	1105.6	4918	8034	2449	332.6	8082	2463	336.3	1.3386	374.0	1.4890	96.1	92.5
1032	1/22/71	23	-1	5	-020	298.7	205.9	3.382	1.534	3.91	1096.4	4877	7708	2349	324.2	7744	2360	327.5	1.3605	364.4	1.5141	94.0	91.1
1033	1/22/71	23	-1	5	-020	298.0	205.5	3.342	1.516	3.81	1087.2	4834	7760	2365	325.3	7794	2375	328.5	1.3559	365.8	1.5099	94.3	91.3
1034	1/27/71	28	029-1	5	-021	302.7	208.7	3.461	1.570	3.05	1131.9	5035	7971	2429	327.1	8027	2447	330.9	1.3266	359.7	1.4418	95.7	92.1
1035	1/27/71	28	029-1	5	-021	305.1	210.4	3.504	1.589	3.12	1142.1	5080	7934	2418	325.9	7991	2436	329.8	1.3279	358.2	1.4423	95.4	91.7
1036	1/27/71	28	029-1	5	-021	307.3	211.9	3.623	1.643	4.03	1155.3	5139	7729	2346	318.9	7778	2371	322.6	1.3343	350.0	1.4478	94.7	91.1
1037	1/27/71	28	029-1	5	-021	294.9	203.3	3.586	1.627	4.43	1093.7	4865	7494	2284	305.0	7533	2296	308.1	1.3161	335.8	1.4344	92.8	88.3
1038	1/27/71	28	029-1	5	-021	301.4	207.8	3.500	1.588	3.91	1130.6	5029	7802	2378	323.0	7842	2390	326.3	1.3387	354.5	1.4545	95.1	92.0
1039	1/28/71	28	029-1	5	-021	292.4	201.6	3.526	1.599	4.28	1090.5	4855	7492	2284	309.2	7527	2294	312.2	1.3345	340.1	1.4539	92.3	89.1
1041	2/1/71	28	029-1	5	-020	301.8	208.1	3.444	1.562	3.12	1112.9	4950	7983	2433	325.0	8038	2450	328.8	1.3161	357.7	1.4317	95.9	91.6
1042	2/1/71	28	029-1	5	-020	304.9	202.2	3.521	1.597	4.00	1132.4	5037	7846	2392	321.6	7889	2405	325.0	1.3255	353.1	1.4399	95.9	91.8
1043	2/1/71	28	029-1	5	-020	312.5	215.5	3.522	1.598	2.76	1148.0	5106	8036	2449	325.9	8103	2470	330.2	1.3109	358.3	1.4225	96.4	91.6
1044	2/1/71	28	029-1	5	-020	303.9	209.5	3.572	1.620	4.65	1134.0	5044	7706	2349	317.5	7748	2362	320.8	1.3322	348.5	1.4470	96.2	92.2
1045	2/3/71	28	029-1	5	-020	301.3	207.7	3.414	1.549	3.08	1106.6	4922	7915	2412	324.3	7963	2427	327.8	1.3245	356.5	1.4403	95.0	91.3

*Design Mach No. (540°R = 300°K Injection Temp.)

-1; 0.50 -9; 0.56

-5; 0.40 029-1; 0.50

TABLE XXXVII (2 of 3)

IAW Cell Run No.	Date	Hardware Configuration				Test Performance Data										Corrected Data to 540°R (300°K)						Efficiency	
		Cup (deg)	* Fuel Inj.	% Ctr Flow	Thrust Chamber	P_c psia	P_c N/cm^2	WT lb/sec	WT Kg/sec	MR	Thrust lbf	Thrust N	c* ft/sec	c* m/sec	I_{sp} SL	c* ft/sec	c* m/sec	I_{sp} SL	C_f SL	I_{sp} vac	C_f vac	% c*	% I_{sp} vac
1046	2/3/71	28	029-1	5	-020	304.8	210.2	3.500	1.588	4.01	1129.3	5023	7810	2380	322.6	7847	2392	325.8	1.3357	353.7	1.4501	95.5	92.0
1047	2/3/71	28	029-1	5	-020	306.1	211.1	3.421	1.552	2.55	1117.9	4973	8026	2446	326.9	8084	2464	330.8	1.3164	359.4	1.4304	96.1	91.9
1048	2/3/71	28	029-1	5	-020	300.8	207.4	3.510	1.592	4.63	1120.0	4982	7685	2342	319.1	7720	2353	322.1	1.3425	350.0	1.4585	95.8	92.6
1049	2/4/71	28	029-1	5	-020	304.9	210.2	3.444	1.562	3.08	1119.0	4877	7914	2412	324.9	7962	2427	328.4	1.3271	356.8	1.4416	95.0	91.3
1053	2/4/71	28	029-1	5	-020	305.5	210.6	3.380	1.533	2.56	1111.7	4945	8080	2463	328.7	8134	2479	332.4	1.3149	361.3	1.4291	96.7	92.3
1054	2/4/71	28	029-1	5	-020	301.7	208.0	3.488	1.582	4.53	1116.2	4965	7732	2357	320.0	7769	2368	323.1	1.3382	351.1	1.4538	96.0	92.6
1055	2/8/71	28	029-1	5	-022	299.4	206.4	3.435	1.558	3.01	1086.5	4833	7779	2371	316.4	7826	2385	319.8	1.3148	348.1	1.4313	93.3	89.1
1056	2/8/71	28	029-1	5	-022	301.6	207.9	3.500	1.588	4.08	1100.9	4897	7627	2325	312.4	7665	2336	315.6	1.3245	343.1	1.4402	93.4	89.4
1057	2/8/71	28	029-1	5	-022	297.4	205.1	3.427	1.554	2.60	1074.1	4778	7720	2353	313.4	7777	2370	317.2	1.3121	345.5	1.4295	92.5	88.3
1058	2/8/71	28	029-1	5	-022	299.4	206.4	3.533	1.603	4.57	1095.2	4872	7528	2295	310.0	7564	2306	313.0	1.3315	340.4	1.4480	93.6	89.9
1059	2/9/71	34	029-1	5	-020	302.0	207.2	3.378	1.532	2.97	1102.9	4906	7953	2424	326.5	8000	2438	330.0	1.3271	358.7	1.4426	95.3	91.7
1060	2/10/71	34	029-1	5	-020	304.5	209.9	3.419	1.551	3.78	1121.3	4988	7916	2413	327.9	7955	2424	331.2	1.3394	359.5	1.4540	96.2	93.0
1061	2/10/71	34	029-1	5	-020	305.1	210.3	3.400	1.542	2.57	1110.2	4938	7978	2432	326.5	8045	2452	330.8	1.3228	359.4	1.4371	95.6	91.8
1062	2/10/71	34	029-1	5	-020	303.5	209.3	3.504	1.589	4.38	1121.4	4988	7701	2347	320.0	7742	2360	323.3	1.3437	351.0	1.4586	95.2	92.1
1063	2/10/71	34	029-1	5	-020	307.8	212.2	3.459	1.569	3.08	1125.0	5004	7910	2411	325.2	7968	2429	329.2	1.3291	357.2	1.4424	95.1	91.5
1064	2/11/71	28	-9	5	-020	284.1	195.9	3.594	1.630	3.04	1174.5	5223	7981	2433	327.0	8027	2447	330.6	1.3251	370.9	1.4868	95.7	91.7
1065	2/11/71	28	-9	5	-020	297.5	205.1	3.856	1.759	4.02	1242.9	5531	7788	2374	322.4	7826	2386	325.7	1.3392	363.3	1.4936	95.2	91.0
1066	2/11/71	28	-9	5	-020	301.1	207.6	3.753	1.702	2.70	1244.0	5536	8100	2469	331.5	8155	2480	335.4	1.3234	374.0	1.4760	96.9	92.4
1067	2/11/71	28	-9	5	-020	298.5	205.8	3.863	1.752	4.40	1249.9	5553	7801	2378	323.6	7835	2388	326.8	1.3419	364.3	1.4958	96.4	92.1
1068	2/12/71	28	030-5	5	-020	237.4	163.7	3.621	1.728	2.75	1185.6	5277	7987	2434	327.6	8034	2449	331.2	1.3264	371.1	1.4861	95.6	91.7
1069	2/12/71	28	030-5	5	-020	304.3	209.8	3.820	1.733	2.52	1261.2	5613	8006	2440	330.1	8059	2456	334.0	1.3332	371.7	1.4840	95.8	91.9
1070	2/12/71	28	030-5	5	-020	305.0	210.3	3.924	1.780	3.72	1279.9	5696	7804	2379	326.2	7844	2391	329.6	1.3520	366.3	1.5025	94.7	91.3
1071	2/12/71	28	030-5	5	-020	303.9	209.5	3.959	1.796	4.07	1277.0	5683	7700	2347	322.6	7737	2358	325.9	1.3553	362.2	1.5063	94.3	90.9
1072	2/15/71	39	030-5	5	-020	297.8	205.3	3.719	1.687	3.03	1240.4	5521	8053	2454	333.5	8100	2463	337.2	1.3393	376.0	1.4936	96.6	93.0
1073	2/15/71	39	030-5	5	-020	287.9	198.6	3.686	1.669	3.68	1199.3	5338	7854	2394	325.3	7898	2407	328.9	1.3399	368.0	1.4992	95.3	91.6
1074	2/15/71	39	030-5	5	-020	285.3	196.7	3.939	1.787	3.95	1122.8	4996	7283	2220	285.1	7321	2231	288.2	1.2665	324.8	1.4273	88.9	81.3
1075	2/15/71	39	030-5	5	-020	293.4	202.3	3.614	1.639	2.36	1203.9	5358	8163	2488	333.1	8229	2508	337.5	1.3195	377.5	1.4759	97.9	93.5
1076	2/16/71	28	029-1	5	-020	297.0	204.8	3.357	1.523	3.85	1098.7	4887	7851	2393	324.7	7886	2404	327.8	1.3373	356.6	1.4548	95.5	92.4
1077	2/16/71	28	029-1	5	-020	298.5	205.8	3.523	1.598	5.24	1097.9	4884	7518	2291	311.7	7550	2301	314.5	1.3402	341.9	1.4571	95.7	92.2
1078	2/16/71	28	029-1	5	-020	303.1	209.0	3.463	1.571	4.57	1112.4	4948	7720	2353	319.2	7756	2364	322.3	1.3369	350.0	1.4520	96.0	92.4
1079	2/17/71	39	029-1	5	-020	307.5	212.0	3.376	1.527	3.26	1126.8	5012	8081	2463	333.8	8117	2474	336.9	1.3354	365.5	1.4488	97.1	93.8
1080	2/17/71	39	029-1	5	-020	316.3	218.1	3.461	1.570	2.73	1149.0	5101	8108	2471	332.0	8160	2487	335.7	1.3235	363.7	1.4338	97.0	92.9
1081	2/17/71	39	029-1	5	-020	300.7	207.3	3.621	1.643	4.70	1050.1	4671	7360	2243	290.0	7391	2253	292.7	1.2740	319.3	1.3900	91.9	84.6
1082	2/17/71	39	029-1	5	-020	306.6	211.4	3.463	1.571	4.11	1122.9	4995	7846	2391	324.3	7883	2403	327.5	1.3365	355.3	1.4503	96.2	92.6
1083	2/18/71	39	029-1	5	-020	287.5	198.2	3.534	1.603	5.36	989.3	4401	7210	2198	274.9	7236	2206	277.2	1.2325	304.5	1.3539	92.1	82.5
1084	2/19/71	39	-9	5	-020	298.5	205.8	3.808	1.732	4.32	1251.1	5571	7882	2402	328.5	7914	2412	331.6	1.3431	369.6	1.5026	97.2	93.2
1085	2/19/71	39	-9	5	-020	300.7	207.3	3.913	1.775	4.89	1254.0	5581	7727	2355	320.5	7761	2366	323.7	1.3418	360.7	1.4954	97.1	92.4
1086	2/19/71	39	-9	5	-020	295.6	203.8	3.397	1.541	5.23	1229.8	5473	7617	2322	315.7	7649	2331	318.8	1.3407	355.9	1.4968	96.9	92.1
1087	2/22/71	39	-9	5	-020	307.6	212.1	3.771	1.711	3.19	1271.3	5657	8160	2487	337.0	8207	2500	340.7	1.3357	378.9	1.4854	98.0	93.8
1088	2/22/71	39	-9	10	-020	309.5	213.4	4.875	2.211	3.31	1272.3	5662	7984	2433	328.3	8023	2445	331.6	1.3298	368.3	1.4769	96.0	91.2
1089	2/22/71	39	-9	10	-020	314.3	216.7	4.018	1.823	4.18	1297.9	5776	7811	2381	323.1	7850	2393	326.5	1.3381	361.8	1.4830	96.0	91.0
1090	2/23/71	39	-9	10	-020	289.0	199.3	3.703	1.680	4.51	1187.2	5281	7791	2375	320.5	7819	2383	323.3	1.3306	361.1	1.4859	96.6	91.5
1092	3/5/71	23	029-1	5	-020	298.8	206.0	3.406	1.545	3.83	1096.0	4870	7772	2369	321.9	7808	2380	325.0	1.3392	353.4	1.4560	94.5	91.5
1095	3/5/71	23	029-1	5	-020	296.9	204.7	3.488	1.581	5.18	1093.0	4805	7539	2298	313.5	7570	2307	316.2	1.3441	343.9	1.4617	95.7	92.6
1096	3/8/71	25	029-1	5	-020	306.1	211.1	3.572	1.619	3.88	1118.0	5973	7675	2339	317.5	7716	2352	320.8	1.3377	348.1	1.4517	93.5	90.3
1098	3/9/71	25	029-1	5	-020	301.7	208.0	3.578	1.623	5.54	1114.0	4955	7452	2271	311.3	7480	2280	313.9	1.3503	340.8	1.4659	95.9	92.9
1100	3/10/71	25	029-1	10	-020	304.8	210.1	3.525	1.599	4.29	1112.0	4846	7629	2356	315.5	7664	2366	318.5	1.3372	345.8	1.4517	94.0	90.5
1102	3/11/71	25	029-1	10	-020	293.3	202.2	3.356	1.522	3.99	1066.0	4786	7711	2350	317.6	7744	2360	320.6	1.3319	349.2	1.4509	94.2	90.8
1103	3/11/71	25	029-1	10	-020	303.3	210.1	3.683	1.671	5.80	1113.0	4951	7266	2215	302.2	7293	2223	304.8	1.3444	330.8	1.4595	94.4	91.0

TABLE XXXVII (3 of 3)

IAW Cell Run No.	Date	Hardware Configuration				Test Performance Data										Corrected Data to 540°R (300°K)						Efficiency	
		Cup (deg)	Fuel Inj.	% Ctr Flow	Thrust Chamber	P_c psia	P_c N/cm^2	WT lb/sec	WT Kg/sec	MR	Thrust lbf	Thrust N	c* ft/sec	c* m/sec	I_{sp} SL	c* ft/sec	c* m/sec	I_{sp} SL	C_f SL	I_{sp} vac	C_f vac	% c*	% I_{sp} vac
1106	3/12/71	28	029-1	10	-020	301.3	207.7	3.445	1.565	3.99	1095	4871	7732	2355	317.9	7768	2368	321.0	1.3294	348.9	1.4450	94.4	90.7
1107	3/12/71	28	029-1	10	-020	301.1	207.6	3.512	1.593	5.01	1096	4875	7565	2306	312.1	7595	2315	314.8	1.3337	342.2	1.4496	95.5	91.6
1109	3/12/71	28	029-1	10	-020	299.5	206.5	3.446	1.563	3.88	1084	4822	7669	2337	314.5	7705	2348	317.5	1.3260	345.4	1.4425	93.4	89.6
1110	3/12/71	28	029-1	10	-020	301.3	207.7	3.561	1.615	5.11	1094	4866	7467	2276	307.3	7497	2285	310.0	1.3304	337.0	1.4462	94.6	90.5
1111	3/15/71	28	-9	15	-020	303.7	209.4	3.910	1.774	3.57	1266	5737	7858	2395	323.8	7889	2405	326.8	1.3327	364.0	1.4846	94.9	90.5
1113	3/15/71	28	-9	15	-020	293.6	202.4	3.928	1.782	5.26	1222	5439	7562	2305	311.1	7588	2313	313.8	1.3307	350.9	1.4878	96.3	90.9
1114	3/16/71	28	-9	15	-020	298.1	205.5	3.806	1.726	3.93	1228	5466	7891	2405	322.6	7922	2415	325.6	1.3224	363.7	1.4772	96.2	91.0
1115	3/16/71	28	-9	15	-020	297.5	205.1	3.960	1.796	5.32	1231	5479	7568	2307	310.9	7597	2316	313.7	1.3287	350.4	1.4838	96.6	90.9
1121	3/22/71	28.4	-9	5	-020	269.7	186.0	3.378	1.532	3.60	1094	4866	8037	2450	325.0	8076	2461	328.4	1.3082	371.3	1.4793	97.2	92.3
1122	3/22/71	28.4	-9	5	-020	297.2	204.9	3.719	1.687	3.54	1221	5434	8040	2451	329.1	8079	2462	332.5	1.3240	372.1	1.4816	97.0	92.0
1123	3/22/71	28.4	-9	5	-020	305.3	210.5	3.833	1.739	4.38	1261	5612	7888	2404	324.6	7922	2415	327.8	1.3313	365.0	1.4824	97.4	92.2
1126	3/23/71	28.4	-9	5	-020	307.2	211.8	4.014	1.821	5.27	1279	5692	7714	2351	318.7	7743	2360	321.6	1.3363	357.7	1.4865	98.3	92.7
1127	3/23/71	28	-9	5	-020	307.8	212.2	3.459	1.569	4.20	1121	4986	7856	2394	324.1	7888	2404	327.2	1.3345	363.9	1.4843	96.5	91.5
1128	3/23/71	28	-9	5	-020	303.3	209.1	3.462	1.570	4.66	1104	4911	7735	2358	318.9	7767	2367	321.9	1.3336	358.6	1.4857	96.4	91.3
1129	3/24/71	35	-9	5	-020	283.6	195.5	3.624	1.644	3.49	1167	5191	7920	2414	321.9	7955	2425	325.0	1.3146	365.2	1.4773	95.5	90.7
1130	3/24/71	35	-9	5	-020	292.3	201.5	3.880	1.760	4.77	1204	5323	7624	2324	303.0	7655	2333	313.2	1.3166	350.8	1.4744	95.4	89.5
1132	3/25/71	28.4	-9	5	-020	68.2	47.0	0.886	0.382	4.76	187	831	7902	2409	211.1	7933	2418	214.0				98.8	
1133	3/25/71	28.4	-9	5	-020	122.1	84.2	1.538	0.698	3.68	421	1893	8152	2485	273.8	8196	2498	277.2				98.9	
1134	3/25/71	28.4	-9	5	-020	100.3	69.2	1.257	0.546	3.46	321	1428	8197	2498	255.5	8243	2511	258.9				99.0	
1135	3/25/71	28.4	-9	5	-020	106.9	73.7	1.414	0.641	5.24	356	1583	7765	2367	252.1	7797	2376	255.0				98.8	
1136	3/26/71	28.4	-9	5	-020	295.0	203.4	3.722	1.688	3.63	1215	5408	8000	2438	326.3	8038	2450	329.6	1.3193	368.7	1.476	96.8	91.7
1137	3/30/71	28	-9	10	-020	290.0	200.6	3.555	1.612	4.16	1105	4915	7725	2355	320.8	7755	2364	323.8	1.3433	362.0	1.502	94.8	91.0
1138	3/30/71	28	-9	10	-020	292.3	201.5	3.542	1.607	5.13	1111	4942	7551	2302	313.8	7580	2310	316.7	1.3442	353.9	1.502	95.7	91.3
1139	3/30/71	28	-9	10	-020	443.5	305.8	4.022	1.824	3.29	1735	7718	8080	2463	345.5	8128	2477	349.3	1.3826	375.5	1.487	97.3	93.0
1140	3/31/71	28	-9	10	-020	517.2	356.7	6.663	3.023	6.03	2155	9585	7470	2277	323.4	7497	2285	326.2	1.4234	351.2	1.533	97.9	93.5

to a nominal 540° R (300° K) propellant inlet temperature are presented in the table. The corrected data includes adjustment for the heat loss to the combustion chamber and nozzle during the short duration firings. The final columns of Table XXXVII, % c* and % I_{sp}, are further corrected to vacuum operation and include the corrections for 540° R (300° K) nominal inlet temperature and the heat lost to the test hardware. The sea level test facilities, data acquisition and data reduction; and the heat sink thrust chamber assembly are described elsewhere.

The data reported in Table XXXVII were not corrected for a change of flow calibration which occurred after the completion of the injector tests. A standard nozzle had been calibrated on a subcontract basis prior to the sea level tests. Descrepancies in that calibration became apparent but could not be resolved. A recalibration of the standard nozzle was carried out and the impact on the sea level tests was to increase the % c* and % I_{sp} by approximately 1%. The cost of correcting the data was not considered justified in that the relative performance of the injector combinations tested was sufficient to select the injectors for the subsequent thrust chamber testing at altitude.

The injector testing was initiated with firings of a 28° efflux angle (see Section V.C) oxidizer cup with 10% centerflow and a fuel injection velocity of 1720 ft/sec (524 m/sec.) equivalent to a Mach number of 0.40 at 540° R (300° K) H_2 injection temperature. The chamber L* was 32 inches (81.3 cm). The 28° cup was identified by cold flow testing as described in the preceding subsection. The injector combination was operated over a mixture ratio range of 3.0 to 5.0 with P_c held at a nominal of 300 psia (206.8 N/cm^2). The basic evaluation of all injector combinations consisted of several firings at various points from 3.0 to 5.0 mixture ratio at the nominal chamber pressure. Subsequent firings evaluated the following variables and test conditions:

		Run No.
(a)	Fuel Injection Mach Number; 0.50, 0.56	992-1015
(b)	% Centerflow, 1.5 and 5%	1016-1025
(c)	O_2 Gas Efflux Angle 25, 23°	1026-1033
(d)	Chamber L* 22, 42 inches (55.9, 106.7 cm)	1034-1058
(e)	O_2 Gas Efflux Angle 34°	1059-1063
(f)	Additional Data Points with M = 0.56	1064-1067
(g)	Film Cooling Tests	1068-1075
(h)	Check Firings	1076-1079
(i)	Chamber Efflux Angle 39°	1079-1090
(j)	Additional Data Points, 25, 23° cups	1092-1103
(k)	Check Firings	1106-1110
(l)	15% Centerflow	1111-1115
(m)	Gas Efflux Angle 28.4°, 35°	1121-1130
(n)	High and Low P_c	1132-1140

Several times during the tests, h, k and part of runs m above, check firings were carried out to assess the data repeatability. Those firings showed consistent operation within instrumentation tolerances. The initial test series, (a) through (h), followed the plan of evaluation of injector variables as described in Section IV. A general trend of increasing combustion efficiency with increased efflux angle and/or increased total O_2 injection velocity was explored with tests at efflux

angles of 35, 39 and 28.4°. The final series of firings was conducted to access the operation at the contract required chamber pressure limits.

The film cooling tests, g above, were part of the original program plan. The assurance of 1 x 10^6 total firing-cycle capability of the regenerative cooled throat section required low maximum material temperatures. Supplementary throat film cooling was included for additional insurance that the required operating temperatures could be achieved. The design approach to supply more throat film cooling than provided by the basic reverse flow combustion process is presented in Figure 106. A small percentage of the H_2 flow was bled from each of the regenerative cooling passages upstream of the H_2 injector station.

3. Percentage of Shifting c* Achieved

The highest percentages of theoretical shifting characteristic velocity obtained with the various configurations of fuel and oxidizer injectors tested are presented in Figure 106. The data is for operation at a chamber pressure of 300 psia (206.8 N/cm^2) with a chamber of 32 inches (81.3 cm) L*. Two configurations of injectors met or exceeded the c* goal of 97%-configurations with 39.4° and 28.4° oxidizer injection angles with 5% oxidizer centerflow and with a fuel injector Mach number of 0.56. Data for the 39.4° oxidizer cup with 10% centerflow and fuel Mach number of 0.56 is included on the figure to show the effect of increasing centerflow on the %c* with that configuration. The increased centerflow reduced the performance slightly over 1%. Data for the 39.4° oxidizer cup, 5% centerflow and a fuel injection Mach number of 0.50 shows a rapid fall off the % c* above a mixture ratio of 4.0. That performance loss was undoubtedly associated with the interaction of the oxidizer cone directed combustion zone and the H_2 flow near the point of H_2 injection. That interaction could result in a partial blockage of the design flow of H_2 along the walls to the plane of O_2 injection. The wide angle of oxidizer injection for the 39.4° unit relative to the other cups evaluated apparently caused the greater sensitivity to fuel injection Mach number.

The performance achieved with the 39.4° and 28.4° oxidizer cups was obtained at the expense of relatively high oxidizer ΔP, 217 and 247 psi (149.5 N/cm^2 and 170 N/cm^2) respectively, at a mixture ratio of 4.0. The configurations also exhibited the relatively high throat heat flux as will be discussed in the following subsection.

The performance of the low heat rejection fuel and oxidizer configurations are compared in Figure 107. The 28° oxidizer cup with 5% centerflow and fuel injection M_N of 0.5 provides the same performance as the 28°, 10%, 0.56 assembly which exceeds 95% c* over the mixture ratio range of 2.5 to 5.5. The % c* for the 28° cup with 10% centerflow with M_N = 0.50 is about 1 percent lower. The oxidizer pressure drop of the 28° cup is 133 (90.8 N/cm^2) and 106 psi (73.0 N/cm^2) with 5 and 10% centerflow, respectively which favors the 28°, 10% 0.56 injector combination.

The general trend of increasing performance with increasing fuel injection Mach number is depicted in Figure 108 for the 28° cup with 10% centerflow. It may be noted that throughout this discussion the reference to fuel injection M_N is based on the fuel flow for a mixture ratio of 4 at a P_c of 300 psia (206.8 N/cm^2). The trend of increasing c* with fuel velocity was also noted with other oxidizer cups and in particular, the 0.56 Mach number fuel injector was required with the 39.4° cup to prevent a performance fall off above a mixture ratio of 4.0. The chamber design studies indicated that the fuel injection at a Mach number of 0.56 was consistent with a total fuel pressure drop (regeneratively cooled passage plus injection ΔP's) of 75 psia (51.6 N/cm^2) for the nozzle cooled to an area ratio of ϵ = 10.

Symbol	Oxidizer Angle	% Center Flow	Fuel Mach No.
□	39.4°	5	0.56
△	39.4°	10	0.56
▽	28.4°	5	0.56
○	39.4°	5	0.50

P_c = 300 psia (206.8 N/cm^2)
L^* = 32 (81.3 cm)
Heat Sink Chamber

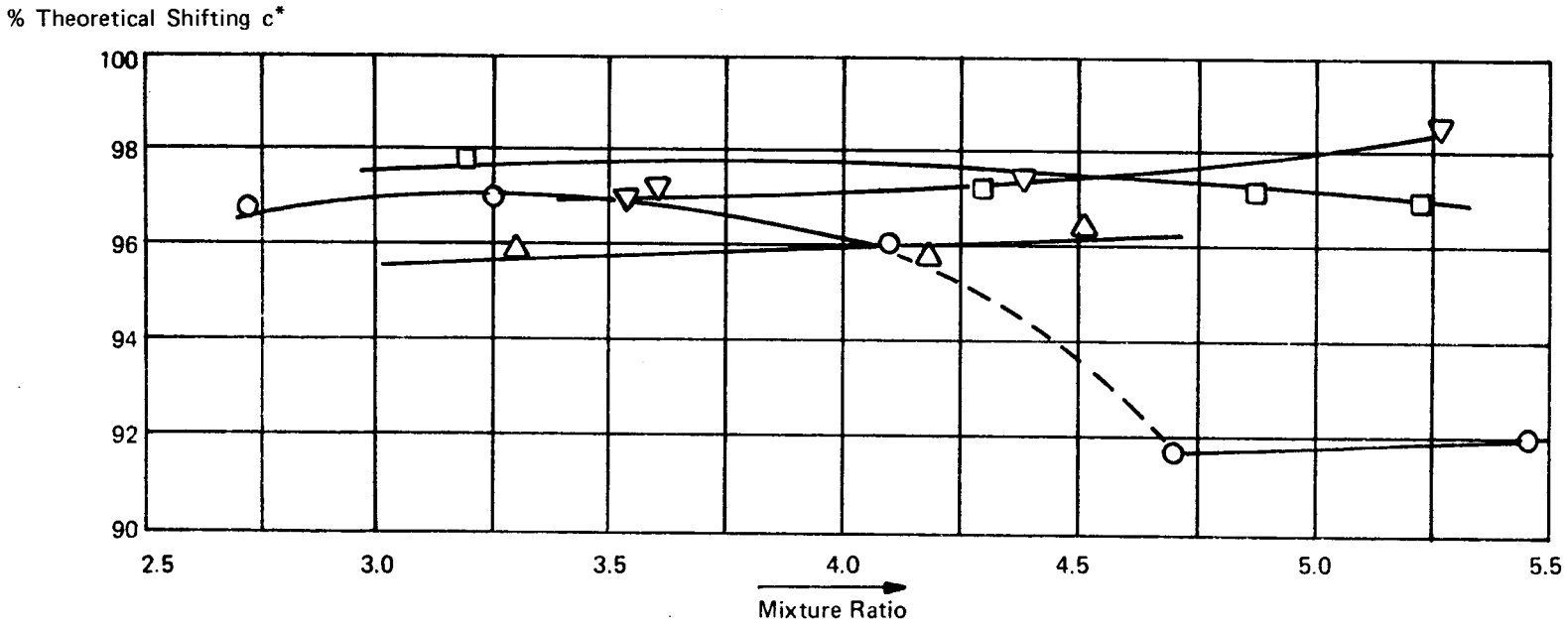

Figure 106. Percent Theoretical Shifting c* versus Mixture Ratio

Symbol	Oxidizer Angle	% Center Flow	Fuel Mach No.
□	28°	10	0.56
◇	28°	5	0.50
⬡	28°	10	0.50

P_c = 300
L^* = 32
Heat Sink Chamber

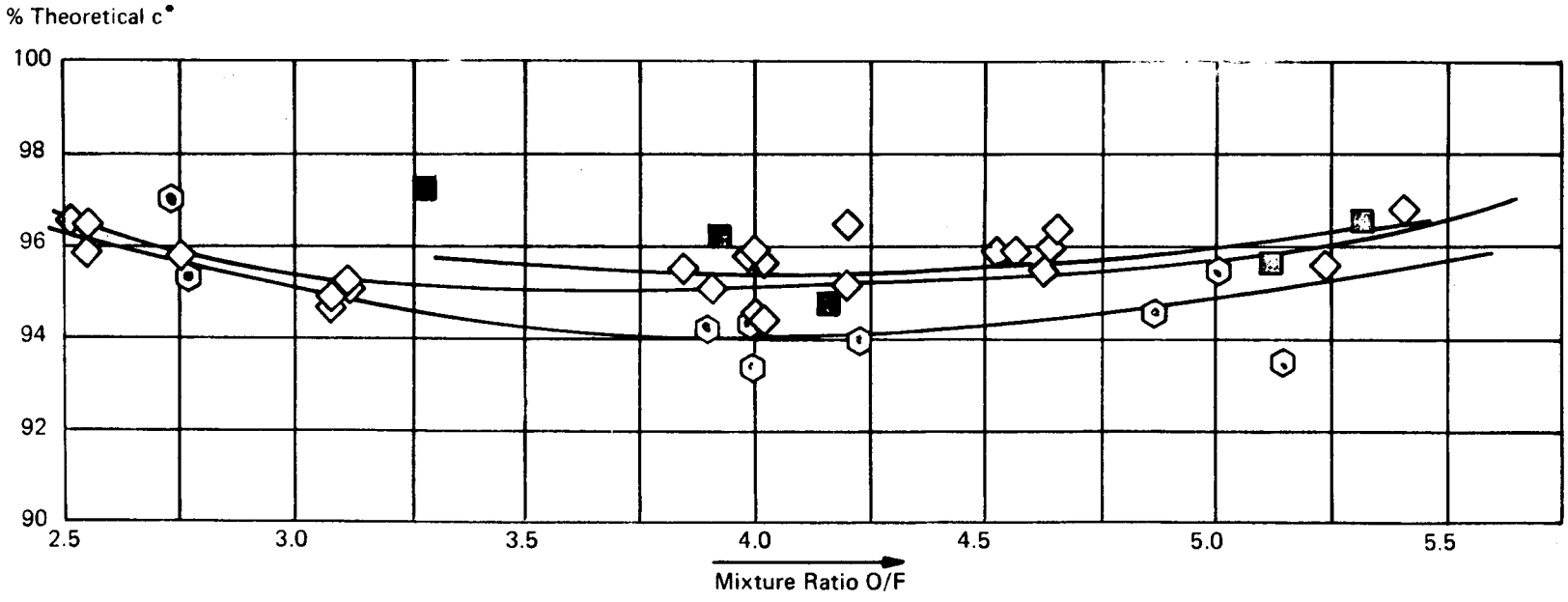

Figure 107. Percent Theoretical c* versus Mixture Ratio

A trend of increasing performance with increasing oxidizer injection angle was noted during the injector testing (Figure 109). Optimized % c* with 5% centerflow is shown in Figure 110 which compares operation with 1.5, 5, 10 and 15% oxidizer cup centerflows.

Characteristic velocity variation with a chamber L* of 32 in. (81.3 cm) is shown by the data of Figure 111 for operation of 28°, 5%, M_N = 0.50 injectors with L*'s of 22, 32, and 42 (55.9, 81.3, and 106.7 cm). The performance fall off with the 42-in. (106.7 cm) combustion chamber again appears to be the result of the combustion zone interaction with the fuel because the larger L* chamber resulted in a greater longitudinal distance between the stations of fuel and oxidizer injection.

Film cooling of the throat section was evaluated by adding slots just aft of the plane of fuel injection. The slots diverted part of the fuel along the nozzle wall as shown in Figure 112. The performance obtained with the film cooling is included in the figure and is compared with configurations of the 28° cup with fuel injection Mach numbers of 0.50 and 0.40. The actual film cooling was approximately 15% at an O/F of 4.0. This film coolant flow was associated with a nominal fuel injection Mach number of approximately 0.45. The lower fuel injection velocity of the film cooled nozzle is considered to be at least partially responsible for the lower performance. Unfortunately the inability to separate performance losses due to film cooling and fuel velocity reduction clouded these test results. Subsequent to this test series, a coolant slot definition test was performed, which included a program of cold flowing two-dimensional models similar to the coolant cross section shown on Figure 112. The information gained by the cold flow tests was employed to define the film cooling slots of the regeneratively cooled nozzle section for altitude testing.

Operation at high and low P_c was carried out with two different injector combinations as noted on Figure 113. The high pressure drop of the 28.4° oxidizer cup precluded its use for high P_c operation. The data of Figure 113 indicates increased performance at both high and low P_c relative to operation at 300 psia (206.8 N/cm^2) for each injector combination. The operation of the 28.4° cup at low P_c resulted in a pressure drop of 247 psi (170.2 N/cm^2) which is still a higher percentage of chamber pressure than observed at 300 psia (206.8 N/cm^2). The increased relative ΔP plus the reduced energy release per unit volume at 100 psia chamber pressure resulted in a higher % c*. The performance increase at high P_c is apparently indicative of the general trend of increasing % c* with the absolute values of oxidizer and fuel injector ΔP.

The selection of the oxidizer and fuel injectors for the thrust chamber cooling tests favored the 28°, 10%, M_N = 0.56 configuration on the basis of oxidizer injector pressure drop. The higher % c* of the 28.4°, 5%, M_N = 0.56 combination was obtained with the penalty of increased ΔP. The 39.4° oxidizer cups provided high % c* with the additional characteristic of greater sensitivity to fuel injector M_N. The large reduction of H_2 fuel injection Mach number at low-temperature operation indicated that the 39.4° O_2 cup is not acceptable for the thrust chamber assembly tests.

The absolute value of c* achieved was known to be approximately 1% higher than reported in Table XXXVII due to a flow calibration change as described in the preceeding subsection. The absolute value of c* of the 28° cup was therefore acceptable for the I_{sp} goal of 435 seconds ($4266 \frac{N\ sec}{kg}$).

Symbol	Oxidizer Angle	% Center Flow	Fuel Mach No.
○	23°	5.0	0.50
□	25°	5.0	0.50
◇	28°	5.0	0.50
⬡	39.4	5.0	0.50

P_c = 300 psia (206.8 N/cm^2)
L^* = 32 in. (81.3 cm)
Heat Sink
Chamber

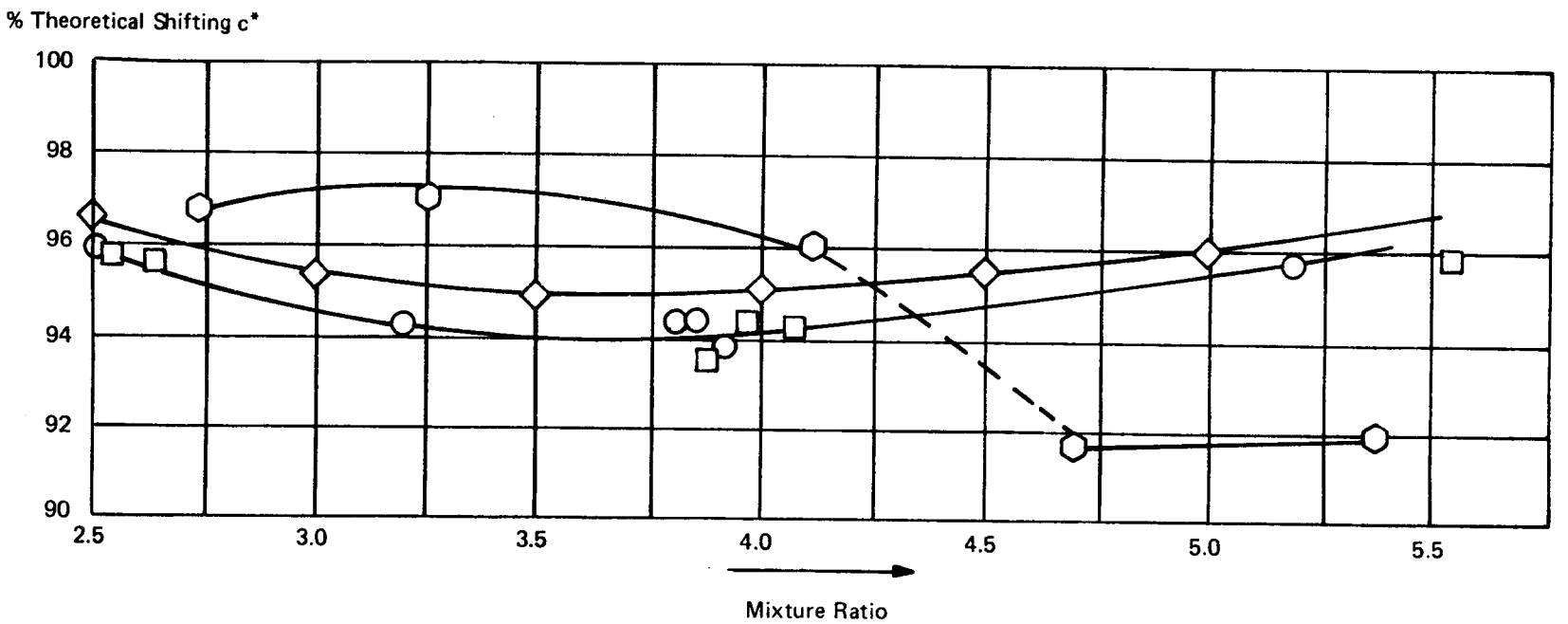

Figure 109. Percent Theoretical Shifting c* versus Mixture Ratio

Symbol	Oxidizer Angle	% Center Flow	Fuel Mach No.
○	28°	1.5	0.50
◇	28°	5	0.50
□	28°	10	0.50
△	28°	15	0.50

P_c = 300 psia (206.8 N/cm^2)
L^* = 32 in. (81.3 cm)
Heat Sink
Chamber

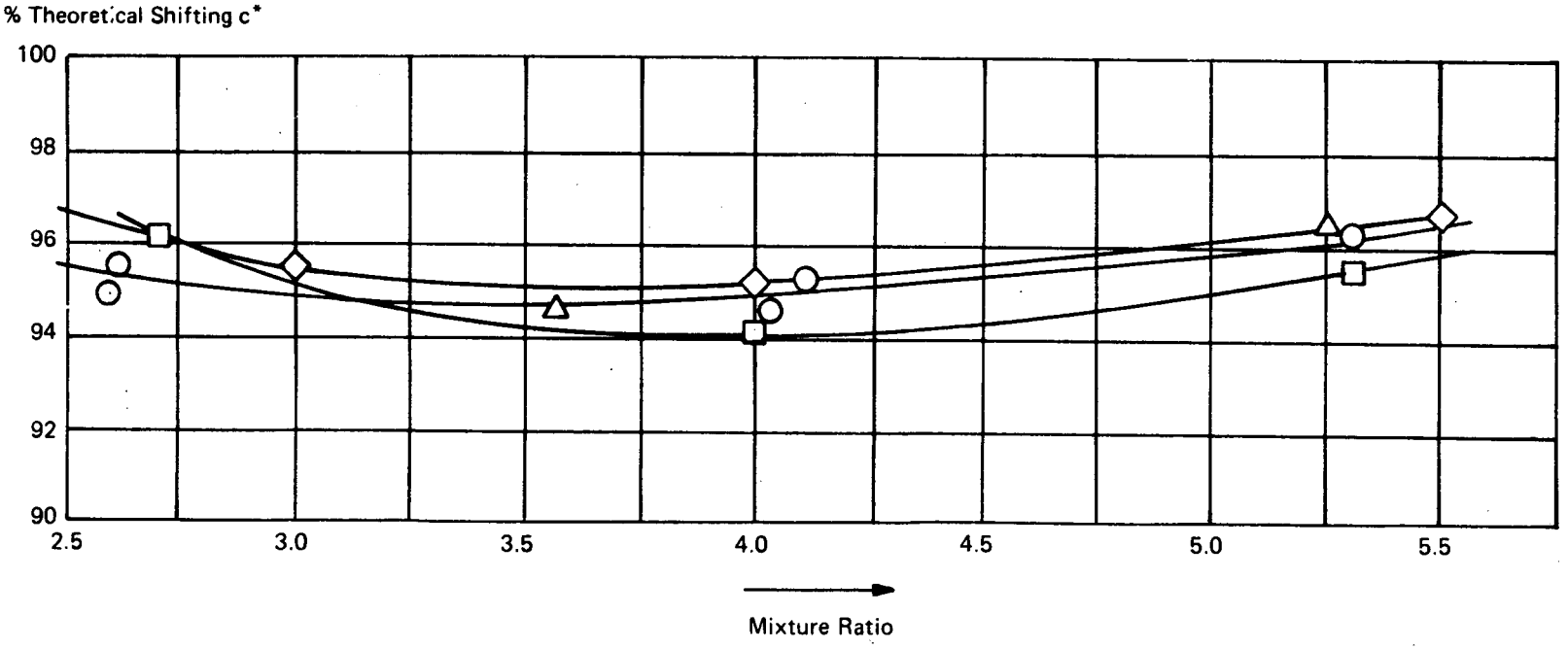

Figure 110. Percent Theoretical Shifting c* versus Mixture Ratio

Symbol	Oxidizer Angle	% Center Flow	Fuel Mach No	Chamber L*
○	28°	5	0.5	32
□	28°	5	0.5	42
△	28°	5	0.5	22

P_c = 300 psia (206.8 N/cm²)
Heat Sink
Chamber

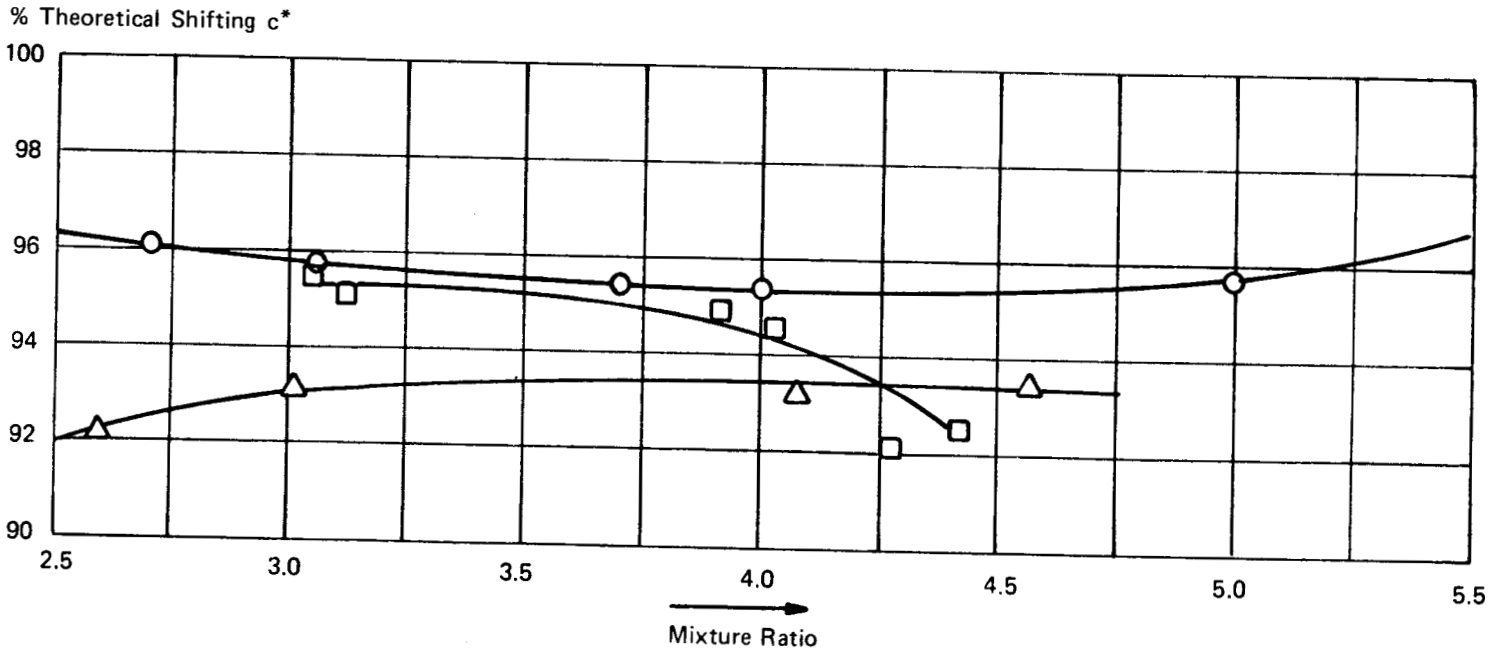

Figure 111. Percent Theoretical Shifting c* versus Mixture Ratio

Symbol	Oxidizer Angle	% Center Flow	Fuel Mach No.
○	28°	5	0.50
□	28°	5	0.45
△	28°	5	0.40

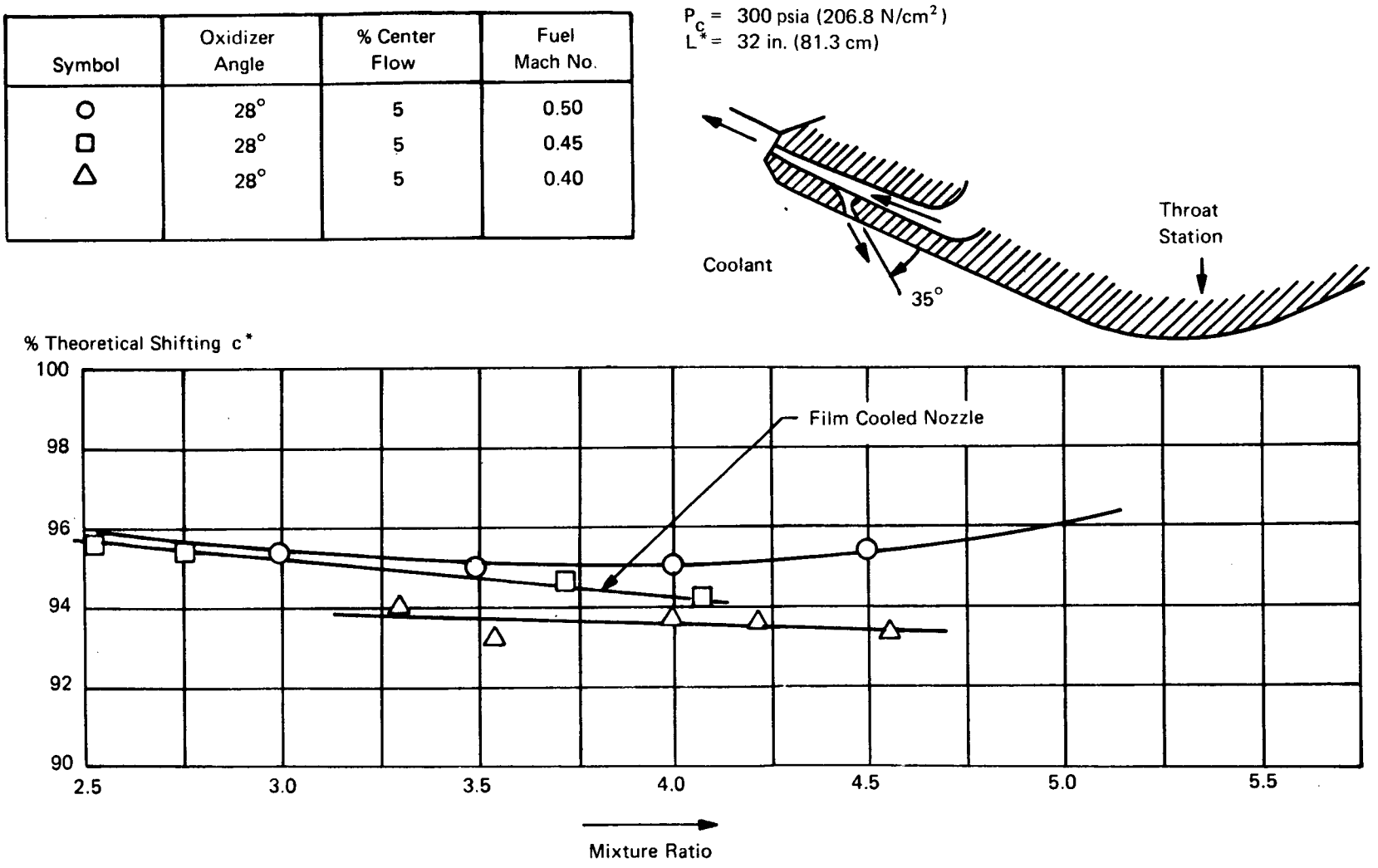

Figure 112. Percent Theoretical Shifting c* versus Mixture Ratio

Symbol	Oxidizer Angle	Nominal % Center Flow	Nominal Fuel Mach No.
○	28°	10	0.56
□	28.4°	5	0.56

High P_c
Low P_c
L^* = 32 in. (81.3 cm)
Heat Sink
Chamber

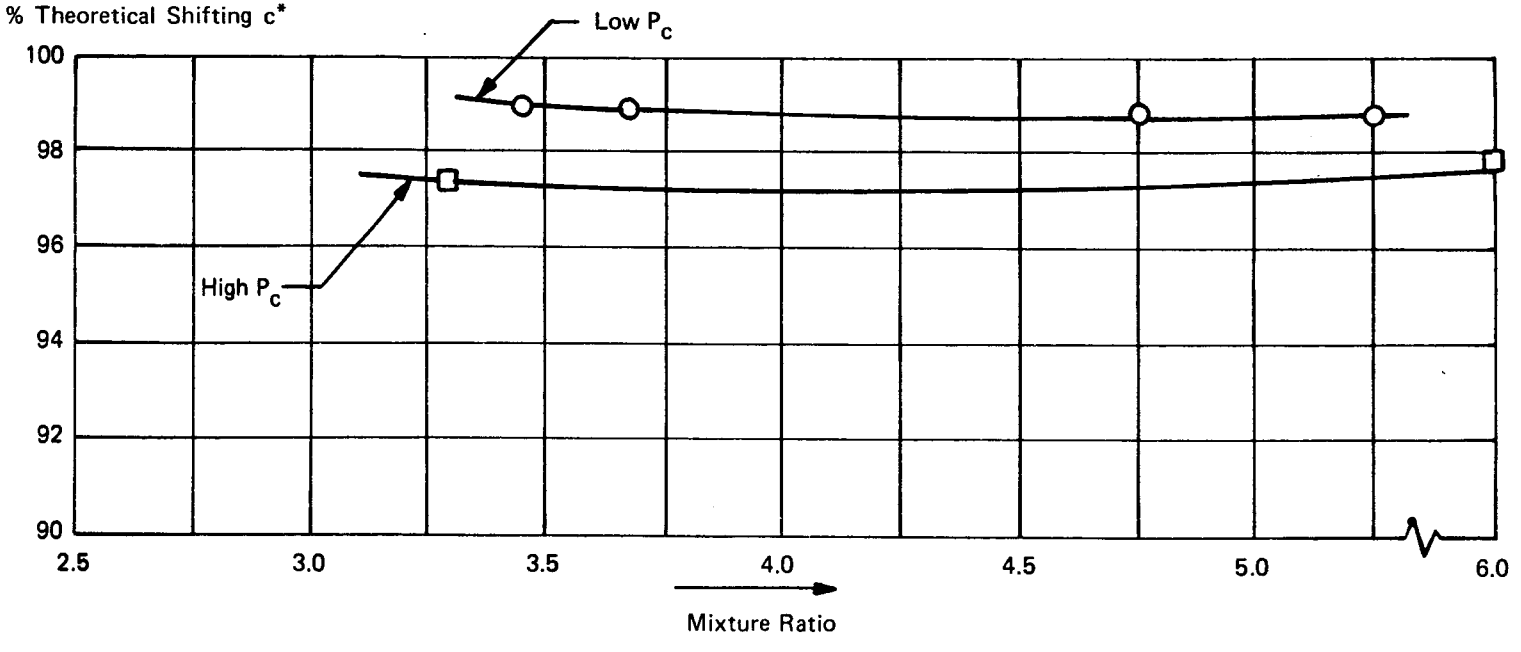

Figure 113. Percent Theoretical Shifting c* versus Mixture Ratio

4. Heat Flux Data and Analyses

The transient temperature histories recorded at the throat station and at two points downstream of the throat were employed to determine an average heat flux for each of the injector combinations tested. The configuration of the nozzle and thermocouple installation is shown in Figure 114. The technique of deriving the average heat flux includes solution of the one-dimensional, nonsteady heat flow equation is shown in Appendix C.

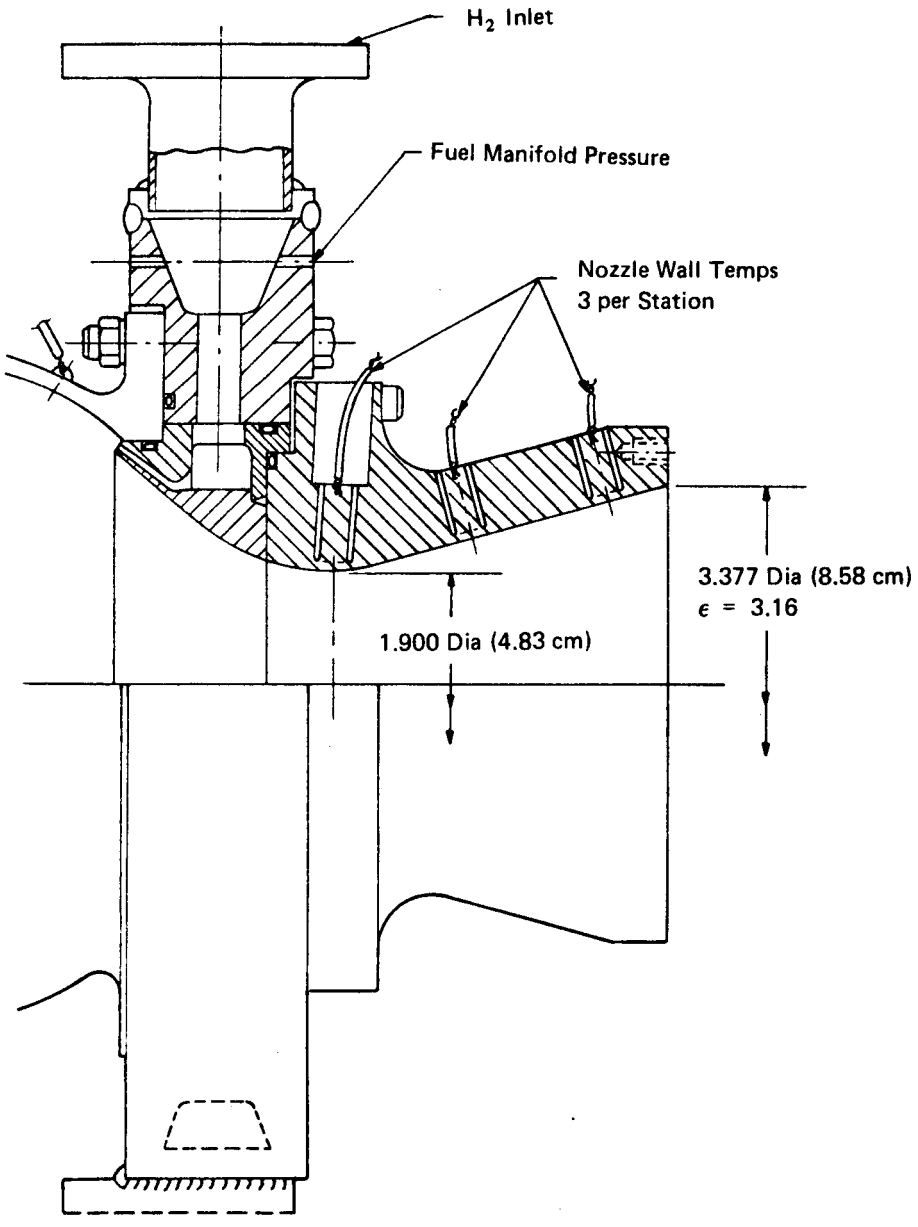

Figure 114. Heat Sink Thrust Chamber Assembly

The heat flux data for several of the oxidizer and fuel injectors tested are presented in Figure 115 and 116. The injector combinations can be grouped by relative heat flux as follows: lows:

$\dot{Q}$:	High	Intermediate	Low
	39.4°/5%/0.56	39.4°/10%/0.56	28.0°/10%/0.56
	28.4°/5%/0.56	25.0°/5%/0.50	28.0°/10%/0.50
	28.0°/1.5%/0.50	23.0°/5%/0.50	28.0°/5%/0.50

where the oxidizer angle is given first, the oxidizer cup % centerflow is second and the third value is the fuel injection Mach number. The measured combustion efficiency of the above configurations showed that, in general, the high heat flux is obtained with the highest performance configurations as would be anticipated while the low heat flux data is obtained with configurations exhibiting intermediate percentages of theoretical c*. The lowest heat flux is also obtained with 28° oxidizer cup with 5% or 10% centerflow and with a fuel injection Mach number of 0.50 and 0.56. The heat flux data for the fuel injector configuration with throat film cooling slots was in the range of 7 to 8 BTU/in.^{2}-sec (1.14 to 1.31 Kw/cm^2). That indication of heat flux reduction by film cooling could not be accepted as absolute due to the low c* performance exhibited by the configuration.

The analysis of the heat sink hardware heat flux data required analytical predictions of the operation of regenerative cooled hardware given those heat fluxes and the comparative effect on the life cycle capability of the regenerative cooled throat. Extrapolation of the heat sink hardware heat flux data to the gas side wall temperature of a regenerative cooled throat section is discussed in Section VI.A. The calculation of life cycle capability of the regenerative cooled throat is also described in that section by the definition of the cumulative damage, N. N equal to 1 indicates that the contract life cycle requirements of 900,000 pulses, 100,000 cycles of steady state operation and an accumulated running time of 50 hours can be met. Values of N less than 1 would indicate that the life cycle requirements are exceeded. The value of N is primarily a function of the maximum gas-side wall temperature. A plot of N versus the maximum gas-side wall temperature is presented in Figure 117 for the regenerative throat configuration selected for the altitude test hardware based on heat sink hardware data. Superposition of the extrapolated values of maximum gas wall temperatures from the injector tests relates the heat flux data to the contract life cycle requirements. Figure 117 shows that all injector combinations tested were capable of meeting the life cycle requirements at the nominal operating conditions.

The projected life cycle capability of the regeneratively cooled throat section included the definition of pulse operation as a firing of 50 milliseconds duration. The selection of 50 milliseconds was based on a transient thermal/structural analysis which is described in Section VI.B of this report. The transient analysis showed that the maximum stresses in the throat section occurred at 0.10 to 0.20-second firing time. The contract pulse mode requirement was interpreted as the definition of operation which was less severe than steady state operation. The assumption of a stress level of 50% of the maximum for a steady-state firing lead to the 50 ms pulse definition.

The thermal/structural analyses prediction of essentially the same cumulative damage (less creep damage) for firings from 0.10 second to the maximum firing duration of 500 seconds indicated that the 50 ms pulse definition could be an optimisitic description of the pulse mode oper-

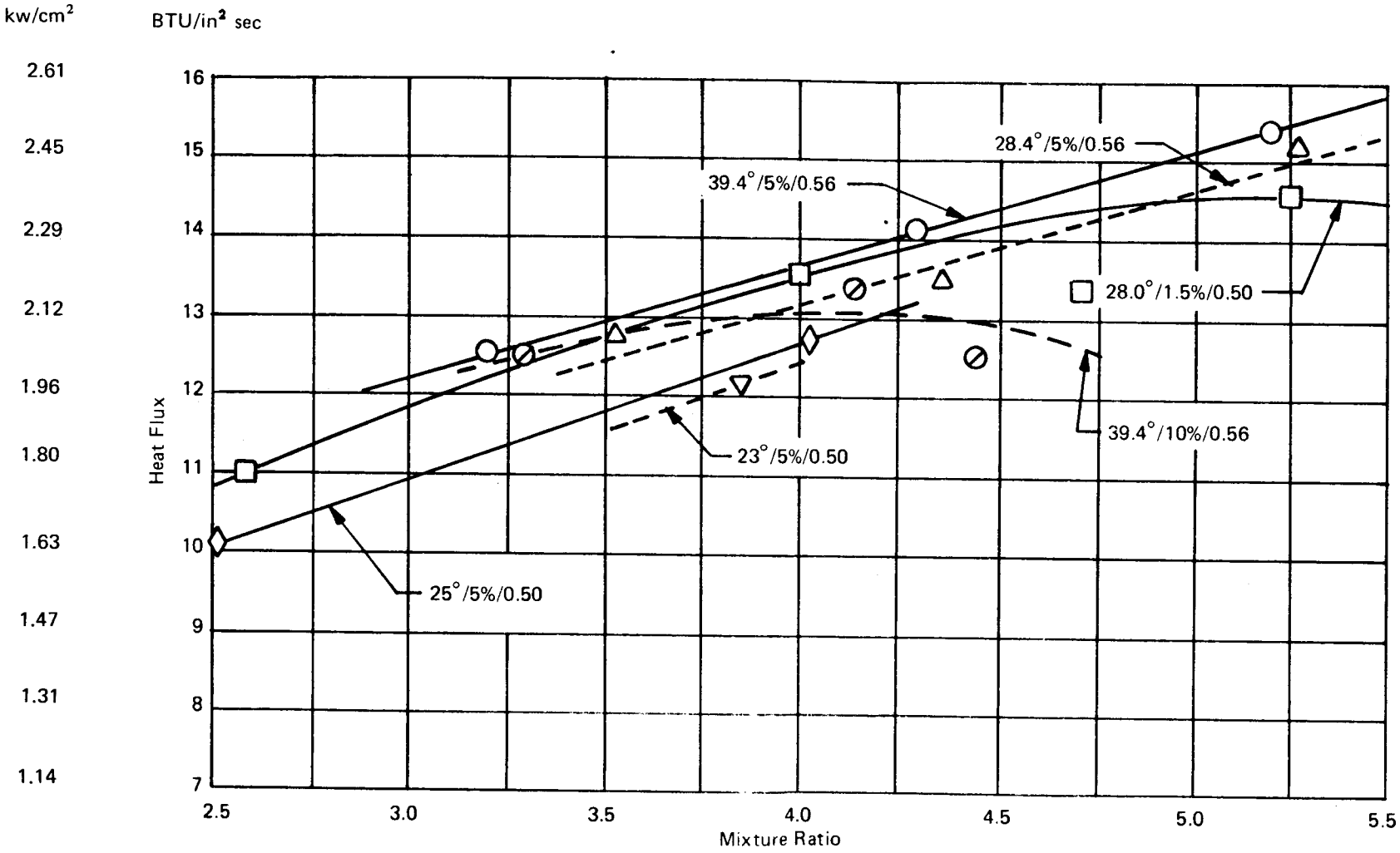

Figure 115. Heat Sink Hardware - Throat Heat Flux versus Mixture Ratio

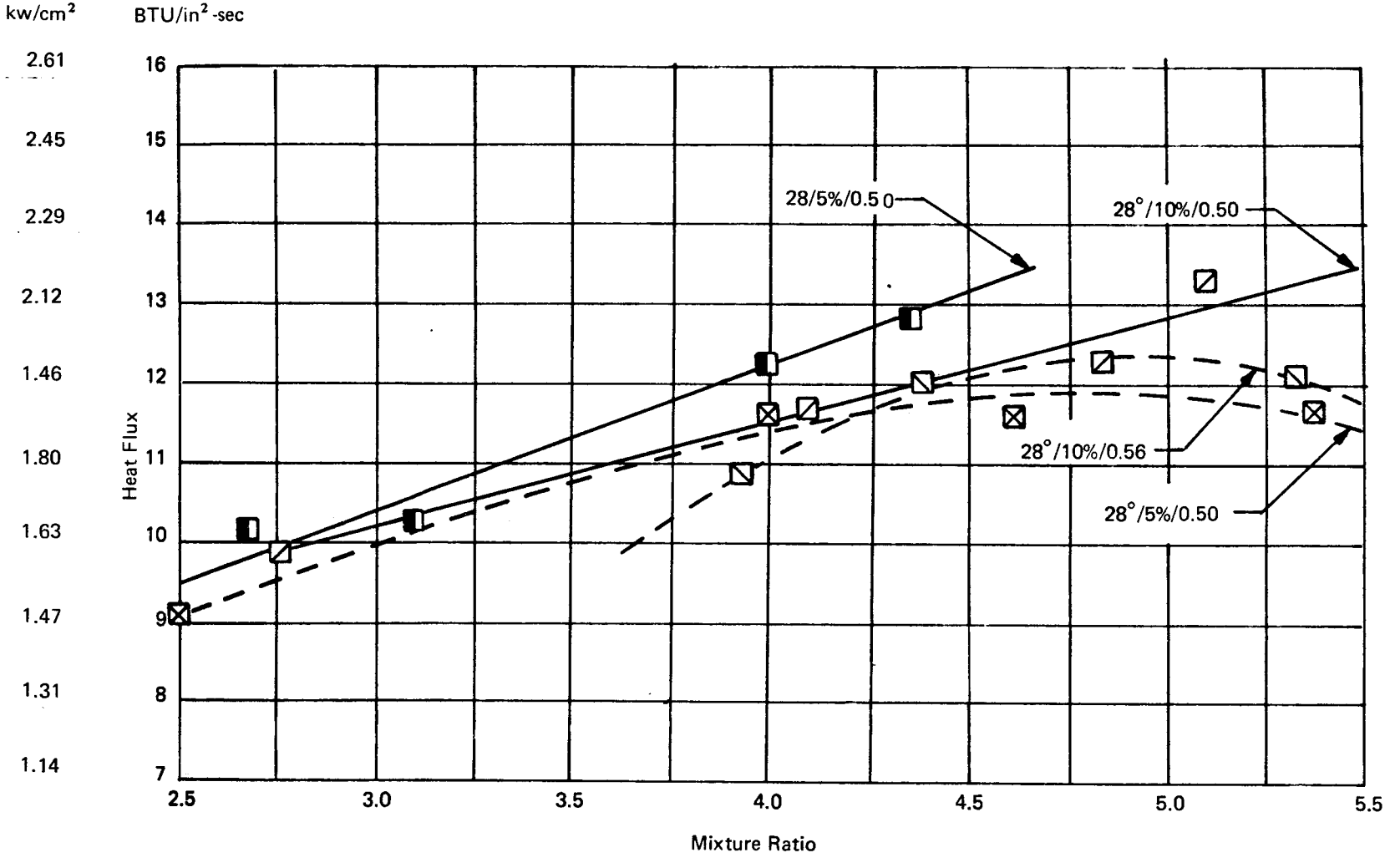

Figure 116. Heat Sink Hardware - Throat Flux versus Mixture Ratio

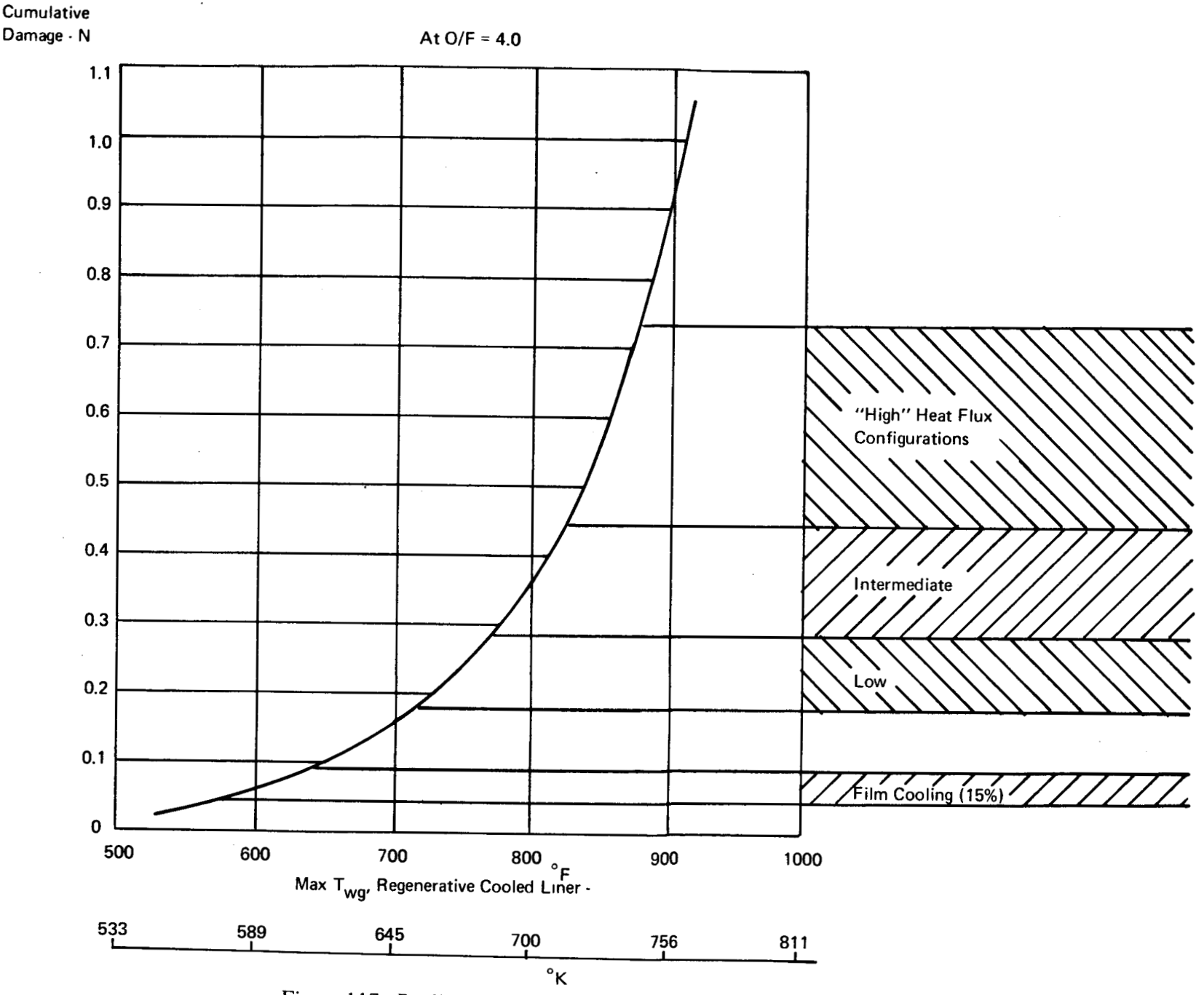

Figure 117. Predicated Cumulative Damage versus Temperature

ation. That optimism dictated a conservative selection of injector combination based on heat flux data. The low heat flux injectors were the principle candidates. The performance and pressure drop characteristics of the low heat flux configurations showed that the 28° oxidizer cup with 10% center flow and with a fuel injector Mach number of 0.56 were the primary configurations for altitude testing.

The projected throat liner life cycle of the selected injectors included over 700,000 steady state firings for operation with 540°R (300°K) propellants at nominal P_C and O/F. That steady state life plus the possibility of some further improvements by film cooling indicated that the reverse flow engine would approach 1×10^6 cycles of operation without restriction on firing duration. There would be no need to distinguish between pulse mode and steady-state operation within the accumulated firing time of 50 hours. Therefore, the total analysis of the injector heat flux data indicated that projected life cycle requirements of the reverse flow thrust chamber throat section would exceed the contract requirements.

C. REGENERATIVE COOLED, SEA-LEVEL TEST THRUST CHAMBER

A 1500-lb (6672N) thrust regeneratively cooled, sea-level reverse flow chamber was evaluated on company sponsorship to determine operating characteristics at special conditions. The configuration of this chamber was very similar to the regeneratively cooled, altitude hardware evaluated on the contract program. The only difference was the provision for sea-level testing and the use of a heavy-walled, three-piece spherical chamber. The internal contour of the spherical chamber and the oxidizer injector design was identical to the program hardware. The regeneratively cooled AMZIRC nozzle liner and fuel injector was the same configuration also, except for the conical shaped, 15° half-angle, sea-level nozzle. This sea-level nozzle internal profile was identical to the sea-level design used early in the contract program.

The major design features of this chamber were as follows:

Thrust	=	1500 lb (6672 N) (at ϵ = 40)
Chamber Pressure	=	300 psia (206.8 N/cm^2) nominal
Nozzle Area Ratio	=	3.16
Chamber L*	=	32 in. (81.3 cm)

A cross section of this design is given in Figure 118 and a photograph of the hardware is shown in Figure 119.

This hardware was used for a limited number of bomb stability tests and to determine the effect of variations in the fuel injector orifices. Discussion of these test results follows.

1. Bomb Stability Tests

The spherical chamber incorporated a bomb port that allowed installation of a radially directed bomb located near the oxidizer end of the chamber and directed toward the convergent nozzle.

Three bomb-stability tests were conducted on this hardware using the regeneratively cooled AMZIRC nozzle liner and the oxidizer vortex injector with 10% center flow and the cup with α = 6.44. Each test was approximately 0.5 sec duration with the bombs ignited at approximately 0.3 sec after chamber pressure rise. Two bomb sizes were used: a 2-grain and a 7-grain size. Chamber pressure overpressure in excess of 50% was obtained with the 7-grain bomb with recovery in less than 3 milliseconds. Some shrapnel damage was noted in the convergent nozzle section of the AMZIRC liner after the 7-grain bomb tests.

Summarizing these bomb tests:

Test	Bomb Size and Type	Overpressure	Recovery
1	2 grain (Lead Azide/PETN)	25%	2-3 ms.
2	7 grain (Lead Azide/PETN)	54%	2-3 ms.
3	7 grain (Lead Azide/PETN)	48%	2-3 ms.

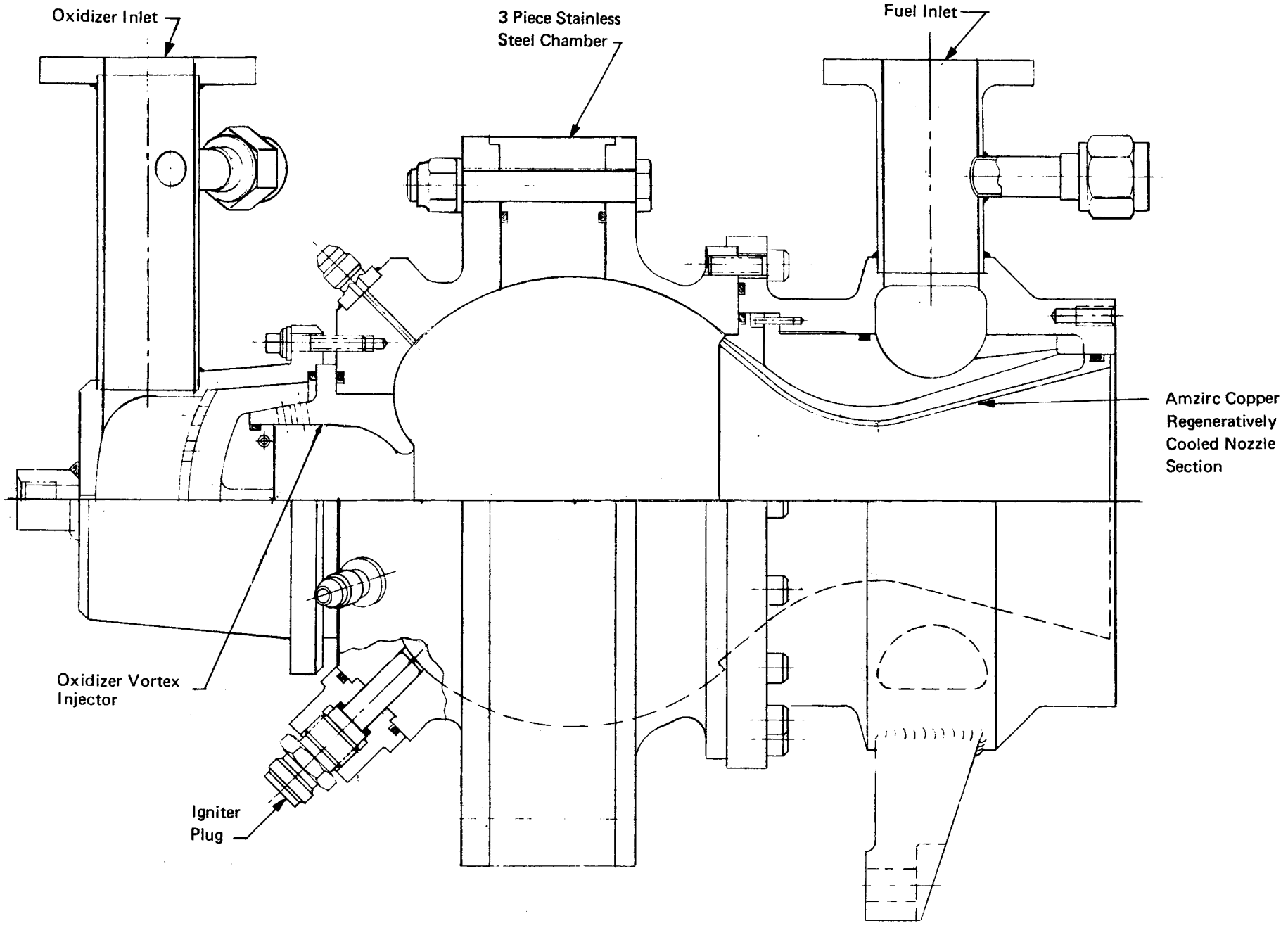

Figure 118. Regeneratively Cooled, Sea-Level Test Thrust Chamber

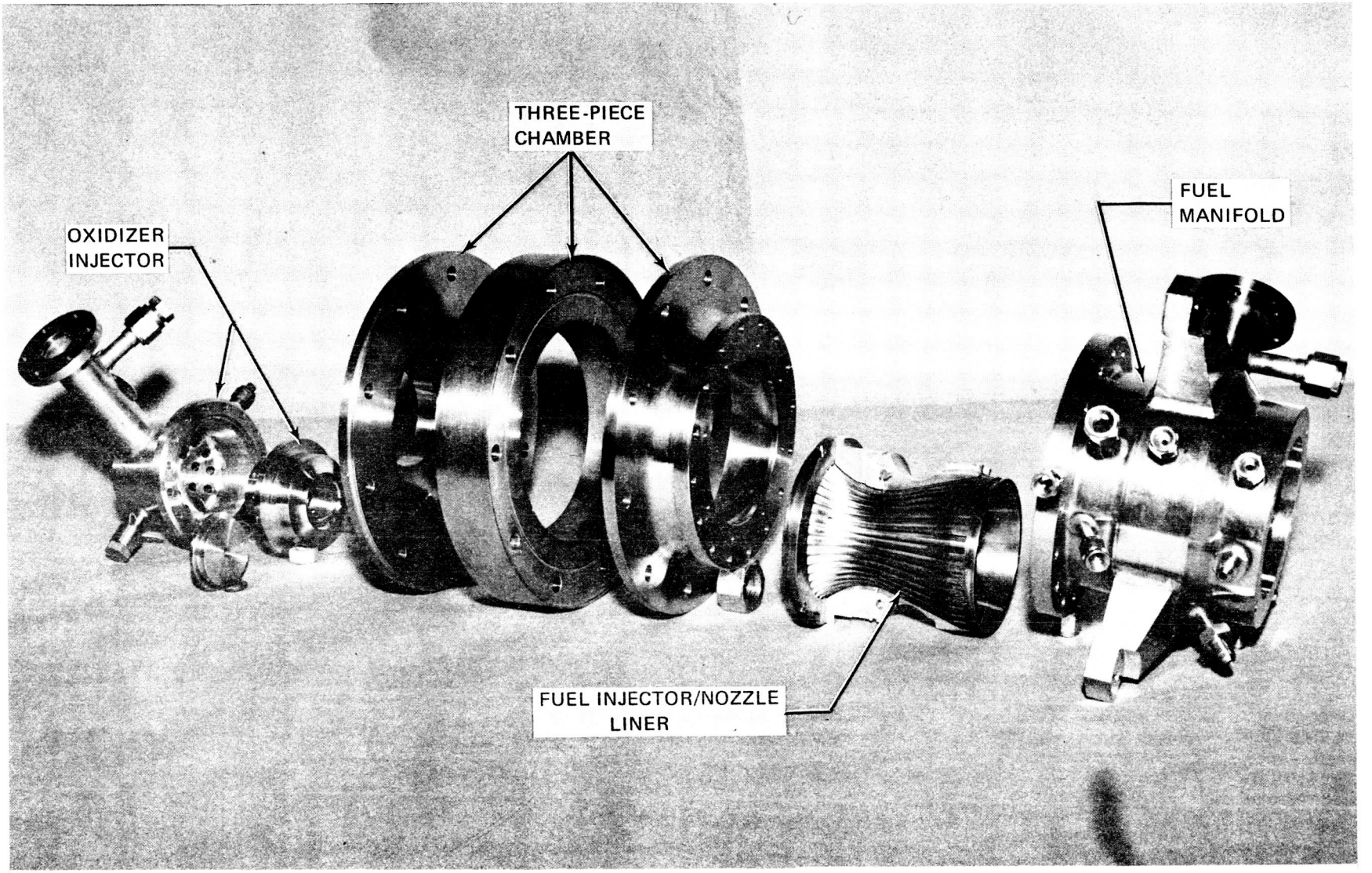

Figure 119. Regenerative Cooled, Sea-Level Test Thrust Chamber

2. Fuel Injection Slot Geometry

Due to indications of slight overheating in the spherical chamber wall at the exit of the fuel injector orifices (in line with the lands) a limited test series was conducted to determine the effect of modification to the fuel injector orifices. Six variations were incorporated in the AMZIRC liner in the land area at the fuel injector slot exit.

Five slots were reworked for each of four types of modification and three slots were reworked for two other types of modification. The purpose of each modification was to provide a means of directing more H_2 into the land area between the fuel injector slots. This would reduce or eliminate possible recirculation of combustion gases and therefore reduce overheating of the chamber wall during extended duration testing.

These six modifications consisted of:

Modification No.	Land Modification	Quantity Modified
1	Chamfered Lands (0.025 in. deep) (0.064 cm)	5
2	Recessed Lands (0.025 in. deep) (0.064 cm)	5
3	Partial (Inside) Recessed Lands (0.015 in high) (0.038 cm) and (0.025 in. deep) (0.064 cm)	3
4	Drilled Lands (2 Holes)	5
5	Arched Recessed Lands (0.025 in. deep) (0.064 cm)	5
6	Partial (Outside) Recessed Lands (0.015 in. high) (0.038 cm) and (0.025 in. deep) (0.064 cm)	3

These six types of modifications are shown in Figure 120.

A total of five tests were conducted on this modified hardware with test durations from 2 sec to 60 sec with a total of 107 seconds accumulated. Due to the limited duration accumulated in this test series only slight thermal discoloration patterns were noted on the chamber wall. The results were only qualitative, but did indicate improvement with the recessed land modification (modification No. 1) and the arched recessed land modification (modification no. 4). Since the arched modification was easier to incorporate in an available piece of hardware and provided more structural support to the exit lip of the land, this configuration was selected for modification of the fuel injector on the contract program.

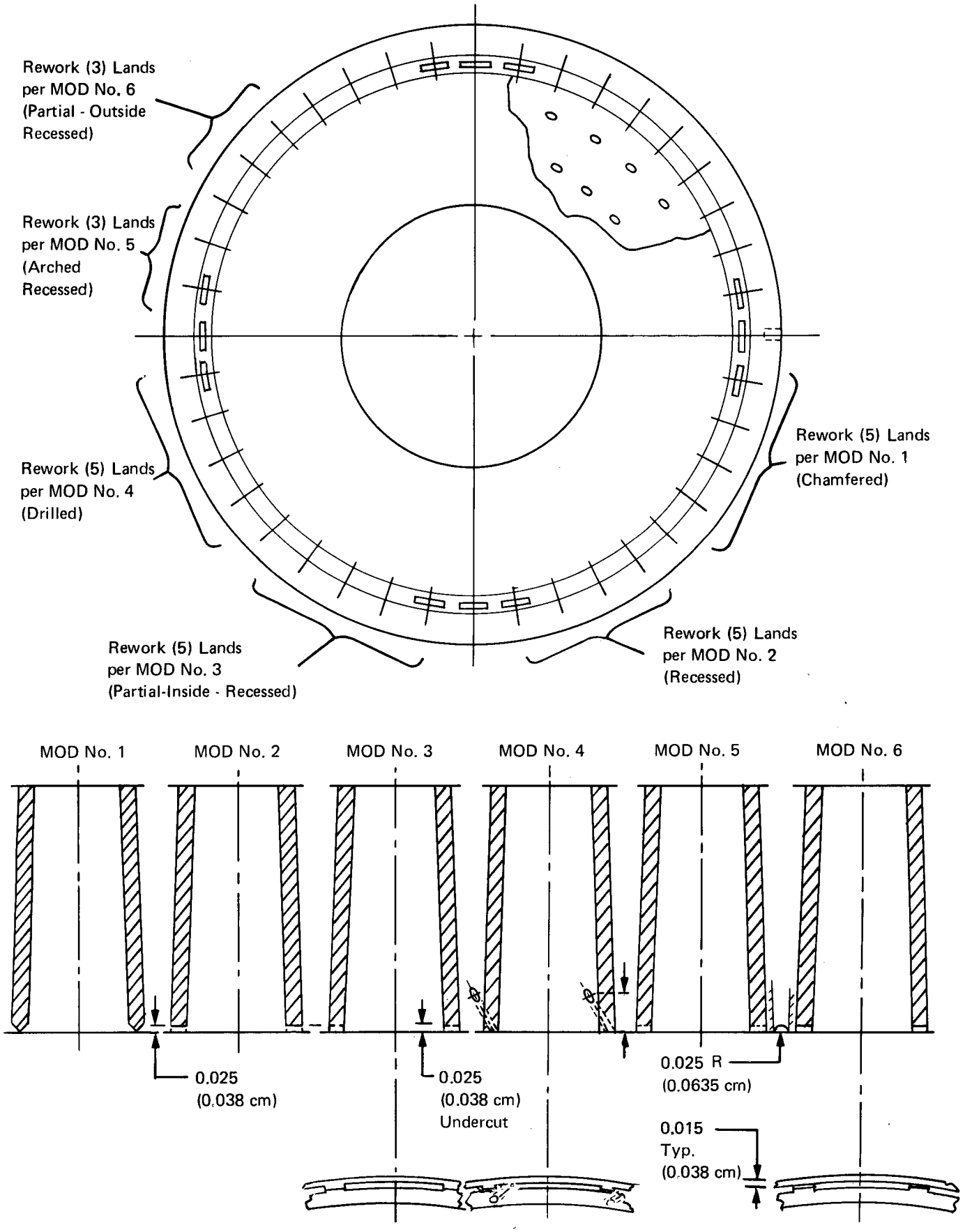

Figure 120. Fuel Injector Slot Modification

XII. THRUST CHAMBER COOLING TESTS

A. GENERAL DESCRIPTION

A primary purpose of the thrust chamber cooling tests was to provide data at altitude operating conditions which would be sufficient to design an engine applicable to the APS requirements. To accomplish this, a variety of hardware was fabricated and selected for tests dependent upon the purpose or parameter to be evaluated. Testing fell into several general categories. Initial tests were made to establish a performance level for continued operation. Next, tests were conducted to evaluate the effect of two different cooling schemes on the base performance, then duration tests and further limit tests for evaluating P_c variations, and the effect of using propellant temperatures from 200°R (111°K) to 800°R (444°K). The final test grouping is related to the evaluation of response characteristics to establish pulse mode performance with a variety of conditions of on-time and down-time between pulses.

In general, the entire test program could be classed as very successful. All of the initially stated program goals appear to be met or exceeded. This program was surprisingly flawless, considering the number of new or innovated pieces of hardware tested and the somewhat complex altitude operating facility required to produce the test environment.

The data obtained during this altitude test program is included as Table XXXVIII. An analysis of this data is included in the following sections of this report. Prior to presenting this analysis, it may be valuable to explain several of the columns in the data table.

C^* (P_c) is calculated from the standard value of

$$C^*(P_c) = \frac{P_c \, A_t \, g}{\dot{W}_t}$$

P_c = chamber pressure (test corrected)

A_t = Throat area measured

g = Gravity (32.174) ft/sec² (9.8066 m/sec²)

and $\dot{W}_t$ = Measured Propellant Flow

$$C^*(F) = \frac{F}{\dot{W}_t} g \, \frac{1}{C_{Fx}}$$

F_∞ = thrust vacuum

C_{Fx} = Predicted thrust coefficient for configuration tested

It also should be mentioned that Q nozzle extension is obtained from the water temperature rise used for cooling. This parameter is the total Q obtained by subtracting the temperature in from the temperature out of the water flowing through the aluminum nozzle extension and multiplying this value times the water flow rate.

TABLE XXXVIII
STEADY-STATE DATA SUMMARY (1 of 4)

Test No.	Run Duty Time	$r_{o/f}$	P_c psia N/cm^2	F_∞ lb N	c^*_{test} (P_c) (1) * ft/sec M/sec	c^*_{test} (2) (F) * ft/sec M/sec	$I_{sp_\infty test}$ lb-sec/lb N-sec/kg	C_{f_∞}	$\eta_{c^*}(P_c)$ *%	ηI_{sp} *%	W_f lb/sec kg/sec	W_o lb/sec kg/sec	ΔP_o (3) (omp-P_c) psi N/cm^2	ΔP_f (3) (fmp-P_c) psi N/cm^2	Max Temp Ch Skin °F °K	Max Temp Noz Throat °F °K	Max Temp Noz Ext °F °K	$Q_{Noz\ Ex}$ BTU/sec J/sec	Ox Line Temp	Fuel Line Temp	Remarks	IGN Sys No. 1	IGN Sys No. 2	Chamber	Ox Cup	Ox Cap	Fuel Inj.	Noz Ext
634	1.0	5.03	302	1555	7726	7697	434.3	1.811	97.2	92.2	0.594	2.986	124	76	75	400	-	65	536	534	Checkout Run	B	G	020-5	018-1	019-1 (10%)	046-1 (Regen)	040-1 (H_2O)
			208	6917	2355	2346	3946.4				0.2694	1.3544	85	52	297	478		68578	298	297	Short Duration							
635	0.9	3.51	304	1477	8106	7887	430.5	1.710	97.4	90.8	0.762	2.670	109	98	87	353	-	61	542	541	Checkout Run							
			210	6570	2471	2404	3911.8				0.3456	1.2111	75	68	304	452		64357	301	301	Short Duration							
636	5.0	3.56	309	1560	8040	8077	442.3	1.772	96.7	93.3	0.774	2.754	107	105	504	405	-	224	533	534	Checkout							
			213	6939	2451	2462	4019.0				0.3511	1.2492	74	72	535	480		236329	296	297								
637	19.8	3.21	291	1454	8056	8079	438.9	1.755	96.3	92.8	0.787	2.525	93	114	652	374	-	214	532	535	Checkout							
			201	6467	2455	2462	3988.2				0.3570	1.1453	64	79	618	463		225779	296	297								
638	19.9	3.86	310	1569	7981	7992	440.3	1.777	96.7	92.8	0.734	2.830	111	97	1154	419	-	251	532	533	Hardware Eval. Mixture							
			214	6979	2433	2436	4000.9				0.3329	1.2837	77	67	897	488		264815	296	296	Ratio Series							
640	20.0	4.13	299	1518	7904	7902	437.6	1.783	96.5	92.3	0.677	2.793	112	86	1223	447	-	252	536	540	↕							
			206	6752	2409	2409	3976.3				0.3071	1.2669	77	59	935	504		265870	298	300								
641	20.0	4.66	294	1518	7813	7828	438.7	1.808	97.0	92.8	0.612	2.849	121	73	1272	468	-	256	530	532								
			203	6752	2381	2386	3986.3				0.2776	1.2923	83	50	962	515		270090	294	296								
642	20.0	4.36	106	539	7839	7786	432.4	1.777	97.2	91.3	0.232	1.014	43	30	1118	529	-	73	531	532	Hardware Eval. Mixture							
			73	2397	2389	2373	3929.1				0.1052	0.4600	30	21	877	549		77018	295	296	Ratio Series							
643	5.8	3.41	99	496	8146	8110	442.8	1.751	98.0	93.5	0.254	0.866	35	38	408	366	-	-	533	532	Short Test on Fuel Supply							
			68	2206	2483	2472	4023.6				0.1152	0.3928	24	26	482	459			296	296	↕							
644	19.8	3.87	482	2458	7856	7935	436.8	1.791	95.2	-	1.156	4.470	177	155	1377	372	-	360	535	537								
			332	10933	2395	2419	3969.1				0.5244	2.0276	122	107	1020	462		379814	297	298								
645	20.2	4.09	500	2561	7860	7923	438.7	1.797	94.5	92.5	1.146	4.690	189	151	1440	359	-	378	541	543	↕							
			345	11391	2396	2415	3986.3				0.5198	2.1274	130	104	1055	455		398805	301	302	Short Test on Fuel Supply							
648	19.9	4.05	301	1527	8029	8018	444.3	1.781	97.8	93.6	0.681	2.756	192	88	1364	339	-	251	543	542	Hardware Eval. Mixture				018-3A	019-3 (5%)		
			208	6792	2447	2444	4037.2				0.3089	1.2501	132	61	1013	444		264815	302	301	Ratio Series							
649	20.1	3.29	305	1523	8239	8230	449.1	1.755	98.6	94.8	0.791	2.600	187	114	1113	280	-	238	539	541	↕							
			210	6774	2511	2509	4080.8				0.3588	1.1794	129	79	874	411		251100	299	301								
650	19.9	4.92	306	1576	7864	7806	440.7	1.805	98.6	93.4	0.604	2.972	186	72	1494	351	-	273	537	542	Hardware Eval. Mixture							
			211	7010	2397	2379	4004.5				0.2740	1.3481	128	50	1085	450		288026	298	301	Ratio Series							
651	19.7	4.30	287	1459	7970	7916	440.9	1.781	97.8	93.0	0.624	2.685	205	80	1319	328	-	249	542	551	Hardware Evaluation				18-7			
			198	6490	2429	2413	4006.3				0.2830	1.2179	141	55	988	438		262705	301	306								
655	19.8	4.17	298	1528	7939	7957	441.9	1.792	97.1	93.2	0.669	2.790	194	96	1337	434	-	240	547	548	Film Cooled Nozzle Eval.				018-3A		046-5 (6% F)	
			205	6797	2420	2425	4015.4				0.3035	1.2655	134	66	998	497		253210	304	304	↕							
656	40.2	2.96	301	1496	8186	8179	442.1	1.741	97.6	93.8	0.855	2.529	179	140	1009	302	-	209	541	525								
			208	6654	2495	2493	4017.2				0.3878	1.1472	123	97	816	423		220503	301	292								
657	20.0	4.77	286	1429	7288	7168	395.8	1.749	90.9	83.3	0.625	2.984	208	84	556	356	-	192	541	535								
			197	6356	2221	2185	3596.5				0.2835	1.3535	143	58	564	453		202568	301	297	Film Cooled Nozzel Eval.							
658	19.9	3.90	298	1539	7883	8015	442.5	1.807	95.6	93.2	0.709	2.769	195	95	1247	388	-	162	532	544	Dump Cooled Nozzle						046-7 (6% D)	
			205	6845	2403	2443	4020.9				0.3216	1.2560	134	66	948	471		170916	296	302	Eval.							
659	12.2	4.72	284	1435	7045	7038	387.0	1.769	87.6	81.9	0.649	3.060	209	82	428	369	-	134	531	543	↕							
			196	6383	2147	2145	3516.6				0.2944	1.3880	144	57	493	460		141375	295	302								
661	20.1	2.82	299	1510	8092	8225	443.8	1.766	96.3	94.3	0.890	2.513	177	137	970	328	-	139	530	539								
			206	6716	2466	2507	4032.7				0.4037	1.1399	122	94	794	438		146651	294	299					018-1			
662	20.1	4.79	271	1376	7083	7076	390.1	1.773	88.4	82.6	0.609	2.919	164	77	504	392	-	130	534	545								
			187	6120	2159	2157	3544.7				0.2762	1.3241	113	53	535	473		137155	297	303						019-1 (10%)		
663	19.7	4.41	286	1455	7163	7196	395.0	1.776	88.2	83.4	0.680	3.00	139	88	379	380	-	133	536	544								
			197	6472	2183	2193	3589.2				0.3084	1.3608	96	61	466	467		140320	298	302						019-9 (15%)		
664	20.0	4.52	282	1433	7092	7124	391.0	1.775	87.6	82.6	0.664	3.00	125	85	286	373	-	134	535	543	Dump Cooled Nozzle							
			194	6374	2162	2171	3553.8				0.3012	1.3608	86	59	414	463		141375	297	302	Eval.							

LEGEND

*Corrected to (300°K) propellant temperature for ambient tests only

B	Bendix Excitor	GR	GLA, Recessed 0.170 in.
BR	Bendix Recessed 0.170 in.	GFA	GLA, Flush mounted, oxidizer augmentation
BFA	Bendix, Flush Mounted, Oxidizer Augmentation	GFAV	GLA, Flush mounted, oxidizer augmentation, variable output
G	GLA Excitor		

(1) c* based on measured P_c and standard calculation

(2) c* based on measured F and relation $c^* = \frac{I_{sp}g}{C_f}$

(3) ΔP through thrust chamber only

TABLE XXXVIII
STEADY-STATE DATA SUMMARY (2 of 4)

Test No.	Run Duty Time c	$r_{o/f}$	P_c psia N/cm²	F_∞ lb N	$c^*_{test(P_c)}$ (1) * ft/sec M/sec	$c^*_{test(F)}$ (2) * ft/sec M/sec	$I_{sp_\infty test}$ lb-sec/lb N-sec/kg	C_{f_∞}	$\eta_{c^*(P_c)}$ *%	ηI_{sp} *%	W_f lb/sec kg/sec	W_o lb/sec kg/sec	ΔP_o (3) (omp-P_c) psi N/cm²	ΔP_f (3) (fmp-P_c) psi N/cm²	Max Temp Ch Skin °F °K	Max Temp Noz Throat °F °K	Max Temp Noz Ext °F °K	$Q_{Noz\ Ext}$ BTU/sec J/sec	Ox Line Temp	Fuel Line Temp	Remarks	IGN Sys No. 1	IGN Sys No. 2	Chamber	Ox Cup	Ox Cap	Fuel Inj.	Noz Ext
665	20.0	4.15	276	1404	7246	7313	400.5	1.779	88.5	84.4	0.681	2.824	128	92	316	369	-	547	539	547	Dump Cooled Nozzle	B	B	020-5	018-3	019-1	046-7	040-1
			190	2645	2209	2229	3639.2				0.3089	1.2810	88	63	431	460		133990	299	304	Duration Series					(10%)	(6% D)	(H_2O)
666	22.9	3.55	296	1533	7836	8019	439.2	1.804	94.3	92.6	0.767	2.723	115	109	1149	310	2039	-	539	546	↕				018-1			056-1
			204	6819	2388	2444	3990.9				0.3479	1.2352	79	75	894	428	1388		299	303								(RAD)
667	50.1	3.81	306	1592	7770	7985	439.6	1.822	94.0	92.6	0.753	2.869	122	104	1253	450	2122	-	537	544	Dump Cooled Nozzle							
			211	7081	2368	2434	3994.5				0.3416	1.3014	84	72	952	504	1434		298	302	Duration Series							
669	116.8	3.90	306	1596	7775	7973	439.9	1.822	94.3	92.7	0.741	2.887	124	101	1266	459	2142	-	535	545	Altitude Cell Shutdown							
			211	7099	2370	2430	3997.2				0.3361	1.3095	85	70	959	510	1445		297	303								
670	31.1	3.73	300	1493	7986	7904	432.4	1.747	96.5	91.4	0.730	2.724	114	92	1021	328	2801	-	489	540	Regen Nozzle Duration						046-1	
			207	6641	2434	2409	3929.1				0.3311	1.2356	79	63	823	438	1812		272	300	Series						(Regen)	
671	124.7	4.17	300	1508	7884	7786	430.3	1.759	96.4	91.3	0.677	2.829	119	80	1233	403	2944	-	533	524	Altitude Cell Shutdown							
			207	6708	2403	2373	3910.0				0.3071	1.2832	82	55	940	479	1891		296	291								
672	4.8	5.04	299	1560	7640	7671	432.9	1.824	96.2	91.9	0.596	3.007	136	67	691	439	2880	-	540	540	Post Duration Evaluation							
			206	6939	2329	2338	3933.6				0.2703	1.3640	94	46	639	499	1856		300	300								
673	5.1	5.47	278	1404	7101	6992	390.0	1.768	90.8	83.3	0.556	3.043	144	61	260	400	2218	-	540	540								
			192	6245	2164	2131	3543.8				0.2522	1.3803	99	42	400	478	1488		300	300	Post Duration Evaluation							
675	29.8	3.83	302	1570	7827	8007	441.0	1.814	94.8	93.0	0.738	2.823	121	108	1182	383	2420	-	540	539	Reduced % Dump Cooled						046-7A	
			208	6983	2386	2441	4007.2				0.3348	1.2805	83	74	912	468	1600		300	299	Eval.						(3% D)	
676	4.9	4.79	292	1537	7620	7756	435.6	1.840	95.0	92.2	0.610	2.919	139	80	730	435	2289	-	541	542	Reduced % Dump Cooled							
			201	6837	2323	2364	3958.2				0.2767	1.3241	96	55	661	497	1527		301	301	Eval.							
677	313.6	3.89	306	1569	7948	7994	441.0	1.787	96.4	92.9	0.727	2.830	-	103	2126	753	2476	-	531	538	Duration (Hardware							
			211	6979	2423	2437	4007.2				0.3298	1.2837	-	71	1437	674	1631		295	299	Rework Completed)							
678	30.0	4.60	296	1553	7699	7815	437.0	1.829	95.4	92.4	0.635	2.919	130	89	1567	451	-	-	533	527	Reduced % Dump Cooled							
			204	6908	2347	2382	3970.9				0.2880	1.3241	90	61	1126	506			296	293	Eval.							
679	5.0	5.36	285	1520	7482	7614	432.4	1.827	95.3	92.2	0.553	2.962	133	69	1023	618	-	-	532	527	↕							
			197	6761	2281	2321	3929.1				0.2508	1.3436	92	48	824	599			296	293								
680	20.1	5.16	286	1503	7578	7639	431.6	1.835	95.8	91.8	0.566	2.917	133	75	1633	470	-	-	533	527								
			197	6685	2310	2328	3921.8				0.2567	1.3232	92	52	1163	517			296	293								
681	9.8	5.15	259	1365	7489	-	429.3	1.846	95.5	92.3	0.517	2.664	97	46	1097	334	-	-	382	340								
			179	6072	2283		3900.9				0.2345	1.2084	67	32	865	441			212	189								
682	20.0	3.77	274	1413	7917	8047	442.7	1.802	95.7	93.4	0.669	2.524	108	107	1328	413	-	-	539	536								
			189	6285	2413	2453	4022.7				0.3035	1.1449	74	74	993	485			299	298								
683	20.0	5.62	282	1497	7537	7563	432.4	1.847	96.9	92.6	0.523	2.939	138	69	1686	522	-	-	541	539	Reduced % Dump Cooled							
			194	6659	2297	2305	3929.1				0.2372	1.3331	95	48	1192	545			301	299	Eval.							
684	14.8	6.03	270	1393	6380	-	358.0	1.807	83.7	77.7	0.554	3.337	83	42	154	318	-	-	277	245	④ Low Temp Eval. at	BR	BFA					
			186	6196	1945		3253.0				0.2513	1.5137	57	29	341	432			154	136	Min. Temp.							
685	10.1	7.45	271	1416	5693	-	323.2	1.828			0.518	3.864	98	36	120	336	-	-	264	229	④ Low Temp Eval. at							
			187	6298	1735		2936.8				0.2345	1.7527	68	25	322	442			147	127	Min. Temp.							
686	9.0	4.87	280	1457	6409	-	363.9	1.829	81.6	78.7	0.682	3.320	70	55	969	338	-	-	261	228	④ Chamber Erosion to							
			193	6481	1953		3306.7				0.3094	1.5060	48	38	794	443			145	127	Cold Ox (Hardware							
																					Rework Completed)							
687	10.0	3.81	289	1511	7096	-	404.3	1.835	87.6	87.1	0.777	2.960	99	67	521	289	-	-	298	253	④ Low Temp Eval ⑤		GFA	020-5A				
			199	6721	2163		3673.8				0.3524	1.3427	53	46	545	416			166	141								
688	10.0	4.24	288	1515	7052	-	403.7	1.843	87.5	86.9	0.716	3.037	81	59	-158	-204	-	-	302	256	④ Revised Min. Temp.							
			199	6739	2149		3668.3				0.3248	1.3776	56	41	168	142			168	142								
689	10.0	4.47	285	1501	6952	-	398.6	1.846	87.0	85.8	0.688	3.078	82	56	-152	-204	-	-	308	256	④							
			197	6676	2119		3622.0				0.3121	1.3962	57	39	171	142			171	142								
690	10.1	4.55	288	1509	7397	-	422.9	1.841	93.1	91.3	0.643	2.924	74	75	435	322	-	-	292	207	↕							
			199	6712	2255		3842.8				0.2917	1.3263	51	52	497	434			162	115	④ Revised Min. Temp.							

*Corrected to (300°K) propellant temperature for ambient tests only

④ Flowmeters calibrated at room temperature only

⑤ Reworked Chamber

(1) c* based on measured P_c and standard calculation

(2) c* based on measured F and relation $c^* = \frac{I_{sp}{}^g}{C_f}$

(3) ΔP through thrust chamber only

TABLE XXXVIII
STEADY-STATE DATA SUMMARY (3 of 4)

Test No.	Run Duty Time	$r_{o/f}$	P_c psia N/cm^2	F_∞ lb N	c^*_{test} (P_c) (1) * ft/sec M/sec	c^*_{test} (F) (2) * ft/sec M/sec	I_{sp_∞} test lb-sec/lb N-sec/kg	C_{f_∞}	η_{c^*} (P_c) *%	ηI_{sp} *%	W_f lb/sec kg/sec	W_o lb/sec kg/sec	ΔP_o (3) (omp-P_c) psi N/cm^2	ΔP_f (3) (fmp-P_c) psi N/cm^2	Max Temp Ch Skin °F °K	Max Temp Noz Throat °F °K	Max Temp Noz Ext °F °K	$Q_{Noz\ Ext}$ BTU/sec J/sec	Ox Line Temp	Fuel Line Temp	Remarks	IGN Sys No. 1	IGN Sys No. 2	Chamber	Ox Cup	Ox Cap	Fuel Inj.	Noz Ext
691	10.1	5.01	287	1513	7064	-	405.8	1.850	90.0	87.8	0.620	3.108	80	56	538	316	-	-	300	216	④ Revised Min. Temp.	BR	GFA	020-5A*	018-1	019-1	096-7A	056-1
			198	6730	2153		3687.4				0.2812	1.4098	55	39	554	431			167	120						(10%)	(3% D)	(RAD)
692	10.0	4.95	291	1537	6891	-	396.5	1.853	86.4	84.1	0.651	3.225	86	45	609	320	-	-	308	220	④							
			201	6837	2100		3602.9				0.2545	1.4629	59	31	594	433			171	122								
693	9.9	4.95	281	1437	6330	-	352.6	1.794	80.6	76.2	0.685	3.392	87	46	573	321	-	-	300	209	④							
			194	6392	1929		3204.0				0.3107	1.5386	60	32	574	434			167	116								
694	9.9	3.04	287	1461	7094	-	393.4	1.786	87.1	86.0	0.920	2.794	68	78	220	329	-	-	288	209	④ Revised Min. Temp.							
			198	6499	2162		3574.7				0.4173	1.2674	47	54	378	438			160	116								
695	9.3	3.48	295	1534	7109	-	402.0	1.821	87.2	87.0	0.852	2.964	84	74	508	303	-	-	337	239	④ LowTemp Eval							
			203	6823	2167		3652.9				0.3865	1.3445	58	51	538	424			187	133								
696	10.0	4.19	299	1562	7051	-	401.3	1.833	87.5	86.4	0.750	3.142	92	59	755	309	-	-	341	242	④ Interim Temp							
			206	6948	2149		3646.5				0.3402	1.4252	63	41	675	427	-	-	189	134								
697	10.0	4.17	300	1560	7109	-	403.1	1.826	88.4	86.7	0.748	3.122	91	59	730	313	-	-	346	250								
			207	6939	2167		3662.8				0.3393	1.4161	63	41	661	429			192	139								
698	10.0	4.78	300	1570	7024	-	400.7	1.837	89.0	86.3	0.677	3.240	98	50	1044	312	-	-	351	256								
			207	6983	2141		3641.0				0.3071	1.4697	68	34	835	429			195	142	④ Interim Temp							
707	19.8	3.94	311	1599	7812	7861	432.5	1.805	94.9	91.3	0.747	2.949	125	87	1310	351	1966	-	521	526	Increased % Dump			020-5			046-7B	
			214	7112	2381	2396	3930.0				0.3388	1.3377	88	60	983	450	1348		289	292	Cooled Eval						(9% D)	
708	19.9	3.24	310	1556	7958	8022	435.3	1.764	95.2	91.1	0.842	2.731	107	108	1174	297	2016	-	519	522								
			214	6921	2426	2445	3955.4				0.3819	1.2388	74	74	908	420	1375		288	290								
709	20.0	4.63	310	1596	7598	7673	427.6	1.814	94.2	90.6	0.663	3.070	134	69	1526	397	2045	-	519	520	Increased % Dump							
			214	7099	2316	2339	3885.5				0.3007	1.3926	92	48	1103	476	1392		288	289	Cooled Eval							
710	0.7	3.77	313	1567	7976	7930	435.0	1.758	96.4	91.8	0.756	2.846	116	88	444	346	-	-	519	525	Test Cell Stop							
			216	6970	2431	2417	3952.7				0.3429	1.2909	80	61	502	448			288	292								
711	19.8	3.97	312	1586	7816	7878	433.9	1.790	95.0	91.6	0.735	2.921	117	83	1337	362	2018	-	521	520								
			215	7055	2382	2401	3942.7				0.3334	1.3250	81	57	998	457	1377		289	289	Test Cell Stop							
714	2.1	2.97	310	1558	8127	8230	445.3	1.766	96.8	94.4	0.882	2.617	99	124	314	272	-	-	531	528	Prel Eval for Pulse Tests	GFA	BFA					
			214	6930	2477	2509	4046.3				0.4001	1.1871	68	85	430	407			295	293								
715	2.1	3.03	314	1580	8124	8119	445.2	1.767	96.9	94.4	0.880	2.668	102	122	358	282	-	-	530	528								
			217	7028	2476	2475	4045.4				0.3992	1.2102	70	84	454	412			294	293								
716	2.1	3.01	314	1577	8132	8220	445.0	1.764	97.0	94.4	0.885	2.660	100	123	384	288	-	-	529	527								
			217	7014	2479	2505	4043.6				0.4014	1.2066	69	85	469	415			294	293	Prel Eval for Pulse Tests							
743 ⑤	500.0	4.06	331.0	1706	7725	7762	431.2	1.797	94.3	90.5	0.782	3.174	121	97	1372	-	2178	-	494	502	Insulated Chamber Eval			125-1	018-1W	019-1W	046-7B	
			228	7588	2355	2366	3918.2				0.3547	1.4397	83	67	1018		1465		274	279						(10%)	(7½% D)	
750	9.8	3.49	308	1602	8581	-	487.1	1.828	101.5	100.8	0.732	2.557	155	129	1425	-	-	-	762	773	④ High Temp Eval			020-5				
			212	7126	2615		4426.1				0.3320	1.1599	107	89	1047				423	429								
751	10.1	2.79	316	1609	8831	-	490.9	1.790	103.0	102.0	0.863	2.412	135	168	1304	-	-	-	762	764	④							
			218	7157	2692		4460.7				0.3915	1.0941	93	116	980				423	424								
752	10.1	2.74	317	1602	8971	-	496.1	1.781	104.6	103.1	0.863	2.367	134	170	1330	-	-	-	769	773	④							
			219	7126	2734		4507.9				0.3915	1.0737	92	117	994				427	429								
753	10.1	3.54	307	16631	8801	-	502	1.836	104.2	103.8	0.704	2.490	155	120	1537	-	-	-	777	774	④							
			212	7130	2683		4561.5				0.3193	1.1295	107	83	1109				432	430								
754	10.2	4.15	300	1575	8207	-	470.6	1.846	99.2	97.8	0.650	2.697	157	102	1544	-	-	-	736	754	④ High Temp Eval							
			207	7006	2501		4276.2				0.2948	1.2235	108	70	1113				409	419								
755	10.2	3.63	260	1364	8600	-	468.3	1.753	100.6	97.5	0.601	2.183	215	249	1507	544	-	-	702	701	④ Low Temp Design			095-1	018-15	019-13	077-7	
			179	5800	2621		4255.3				0.2726	0.9902	148	172	1093	558			390	389	Eval						(3% D)	
756	10.4	42.2	301	1532	8303	-	453.0	1.776	101.0	95.7	0.641	2.705	211	207	1611	553	-	-	673	679	④ High Temp							
			208	6814	2531		4161.7				0.2908	1.2270	145	143	1150	563			374	377								

* Corrected to (300°K) propellant temperature for ambient tests only

⑤ Data reduction method differed due to recording problems

④ Flowmeters calibrated at room temperature only

(1) c* based on measured P_c and standard calculation

(2) c* based on measured F and relation $c^* = \frac{I_{sp^g}}{C_f}$

(3) ΔP through thrust chamber only

TABLE XXXVIII
STEADY-STATE DATA SUMMARY (4 of 4)

Test No.	Run Duty Time	$r_{o/f}$	P_c psia N/cm²	F_∞ lb N	c* test (P_c) (1) * ft/sec M/sec	c* test(F) (2) * ft/sec M/sec	I_{sp_∞} test lb-sec/lb N-sec/Kg	C_{f_∞}	η_{c^*} (P_c) *%	ηI_{sp} *%	W_f lb/sec Kg/sec	W_o lb/sec kg/sec	ΔP_o(3) (omp-P_c) psi N/cm²	ΔP_f(3) (fmp-P_c) psi N/cm²	Max Temp Ch Skin °F °K	Max Temp Noz Throat °F °K	Max Temp Noz Ext °F °K	$Q_{Noz\ Ext}$ BTU/sec J/sec	Ox Line Temp	Fuel Line Temp	Remarks	IGN Sys No. 1	IGN Sys No. 2	Chamber	Ox Cup	Ox Cap	Fuel Inj.	Noz Ext
757	9.9	2.57	271	1311	8854	-	464.6	1.690	103.7	97.6	0.792	2.031	177	237	1256	439	-	-	678	682	④ High Temp	GFA	BFA	093-1	018-15	019-13	077-7 (3% D)	056-1 (RAD)
			187	5831	2699		4221.7				0.3593	0.9213	122	163	953	499			377	379								
758	10.2	4.15	308	1555	8332	-	456.0	1.762	101.1	95.3	0.663	2.747	204	200	1489	570	-	-	668	654	④							
			212	6917	2540		4143.5				0.3007	1.2460	141	138	1083	572			371	363								
759	10.2	4.61	315	1617	8094	-	450.5	1.792	100.0	94.8	0.640	2.950	197	193	1542	588	-	-	628	624	④ High Temp							
			217	7192	2467		4093.6				0.2903	1.3381	136	133	1112	582			349	347								
760	10.1	3.95	287	1474	7591	-	427.5	1.814	93.6	92.8	0.697	2.750	154	149	734	94	-	-	346	283	④ Low Temp Design Eval							
			198	6556	2314		3884.6				0.3162	1.2474	106	103	663	308			192	157								
763	10.2	2.96	304	1537	7745	-	428.9	1.783	94.6	93.4	0.904	2.678	150	200	591	3	-	-	370	259	④							
			210	6837	2361		3897.3				0.4101	1.2147	103	138	584	257			206	144								
764	10.4	4.61	298	1552	7616	-	434.7	1.838	95.6	94.4	0.637	2.934	186	118	944	148	-	-	382	274	④							
			205	6903	2321		3950.0				0.2889	1.3309	128	81	780	338			212	152								
765	10.2	3.69	284	1448	7757	-	434.2	1.802	95.3	93.4	0.712	2.623	161	146	783	76	-	-	390	276	④ Low Temp Design Eval							
			196	6441	2364		3945.4				0.3230	1.1898	111	101	690	298			217	153								
766	9.8	4.48	294	1514	7343	-	415.6	1.822	91.8	89.1	0.665	2.979	106	138	917	147	-	-	323	305	④ Low ΔP ox Eval				018-11	019-11		
			203	6734	2238		3776.4				0.3016	1.3513	73	95	765	337			179	169								
767	10.0	4.25	285	1463	7302	-	411.3	1.814	90.6	88.1	0.677	2.879	101	146	910	174	-	-	331	313	④ Low ΔP ox Eval							
			197	6507	2226		3737.4				0.3071	1.3059	70	101	761	352			184	174								
768	10.1	3.95	270	1380	7670	-	427.9	1.797	94.6	91.9	0.651	2.573	88	155	624	267	-	-	408	277	④ Fuel Position Change Eval				018-13	019-1	092-1 (3% D)	
			186	6138	2338		3888.2				0.2953	1.1671	61	107	602	404			226	154								
771	10.2	3.94	314	1611	7640	-	427.7	1.802	93.3	92.0	0.763	3.005	104	173	572	266	-	-	411	251	④							
			217	7166	2329		3886.4				0.3461	1.3631	72	119	573	403			573	403								
772	10.1	3.00	316	1594	7805	-	430.9	1.778	95.3	93.8	0.924	2.775	96	192	356	170	-	-	430	244	④							
			218	7090	2379		3915.5				0.4191	1.2587	66	132	453	350			239	136								
773	10.0	4.79	314	1636	7569	-	430.1	1.830	95.4	92.5	0.657	3.146	118	137	708	320	-	-	432	244	④ Fuel Position Change Eval							
			217	7277	2307		3908.2				0.2980	1.4270	81	94	649	433			240	136			G FAV					
779	10.0	4.06	298	1524	7404	-	413.7	1.799	91.9	89.0	0.728	2.956	108	210	826	199	-	-	334	254	④ Ox ΔP Increase Eval				018-11	019-11		
			205	6779	2257		3759.2				0.3302	1.3408	74	145	714	366			186	14								
780	10.0	3.06	301	1511	7624	-	418.2	1.766	93.1	91.1	0.891	2.723	95	207	544	77	-	-	328	242	④							
			208	6721	2324		3800.1				0.4042	1.2352	66	143	558	298			182	134								
781	9.8	5.12	298	1549	7294	-	414.3	1.829	93.2	89.4	0.611	3.128	116	163	892	284	-	-	327	254	④							
			205	6890	2223		3764.6				0.2771	1.4189	80	112	751	413			182	141								
782	9.9	4.40	298	1534	7426	-	417.3	1.810	92.7	89.7	0.680	2.996	108	198	850	223	-	-	325	266	④ Ox ΔP Increase Eval							
			205	6823	2263		3791.9				0.3084	1.3590	74	137	728	379			181	148								

(1) c* based on measured P_c and standard calculation

(2) c* based on measured F and relation $c^* = \frac{I_{sp}^{g}}{C_f}$

(3) ΔP through thrust chamber only

Corrected to (300°K) propellant temperature for ambient tests only

④ Flowmeters calibrated at room temperature only

TABLE XXXIX
IGNITION TEST SERIES

	Ignition System Location		Plug Position		Ox. Aug.		Tests		
	Top	Bottom	Bendix	GLA	Top	Bottom	Amb.	High Temp.	Low Temp.
1	Bendix	Bendix	-	-	None	None	634 - 680 682, 683	-	681
2a	Bendix	GLA	Recessed	Flush	None	Yes	707 - 711	-	687 - 698
2b	GLA	Bendix	Flush	Flush	Yes	Yes	714-747, 775	750 - 759	760 - 773
3a	-	GLA	-	Flush	None	Yes	702		
b	-	GLA	-	Flush	None	None	703		
c	-	GLA	-	Recessed	None	None	704		
d	-	GLA	-	Recessed	None	Yes	705		
4	-	Bendix	Flush		None	Yes	712		
5	-	GLA Variable	-	Flush	None	Yes	776, 785		779 - 782

B. PERFORMANCE

The initial performance evaluation test series was performed on the thrust chamber shown in Figure 121 and consisted of the oxidizer injector and thrust chamber (32 L*) (81.3 cm) established as a baseline with the sea level heat sink thrust chamber tests. The cooled, area-ratio-10, nozzle and the water-cooled, 40/1-area-ratio, nozzle extension were new pieces of hardware constructed for the altitude evaluation program. Initial testing was conducted with the regeneratively cooled nozzle which had no further auxiliary cooling and was the first of three nozzle sections to be evaluated. Both the valves and the igniter system used on the sea level test program were used to complete the engine assembly. Actuation of the valves both for opening and closing was by a separate pneumatic helium system which was subsequently changed to nitrogen. The initial test program objectives were to establish the merits of using a regeneratively cooled nozzle which either incorporated or varied the location of auxiliary cooling in the Amzirc nozzle liner wall. The two positions for auxiliary cooling were established as a point near the injection orifices in the convergent section of the nozzle and termed as film cooling or a second position in the divergent nozzle at the nozzle extension joint and termed as dump cooling. The location of these auxiliary cooling locations may be noted in the cross-sectional chamber view shown in Figure 122 and the details in Figure 123.

The initial performance series was conducted using the water-cooled nozzle since an established heat rejection rate for the combustor (reverse flow) had not been previously demonstrated. As a consequence, the various nozzle types with auxiliary cooling were initially used to establish the performance numbers and the heat rejection in the nozzle extension portion of the chamber. Originally, we considered using this water cooled nozzle extension as a regeneratively cooled unit. However, as the program progressed, information from the prime contractor indicated the lack of interest in a fully regeneratively cooled configuration; therefore, this type of testing was not conducted during the program. Initial test results indicated that a performance value of nearly 440 seconds (4315 N sec./kg) could be expected with no auxiliary cooling in the nozzle region. Further evaluation, using the water cooled aluminum nozzle extension, indicated that with 6% of the fuel allowed to pass through the convergent nozzle film coolant ports or through the dump coolant ports in the divergent

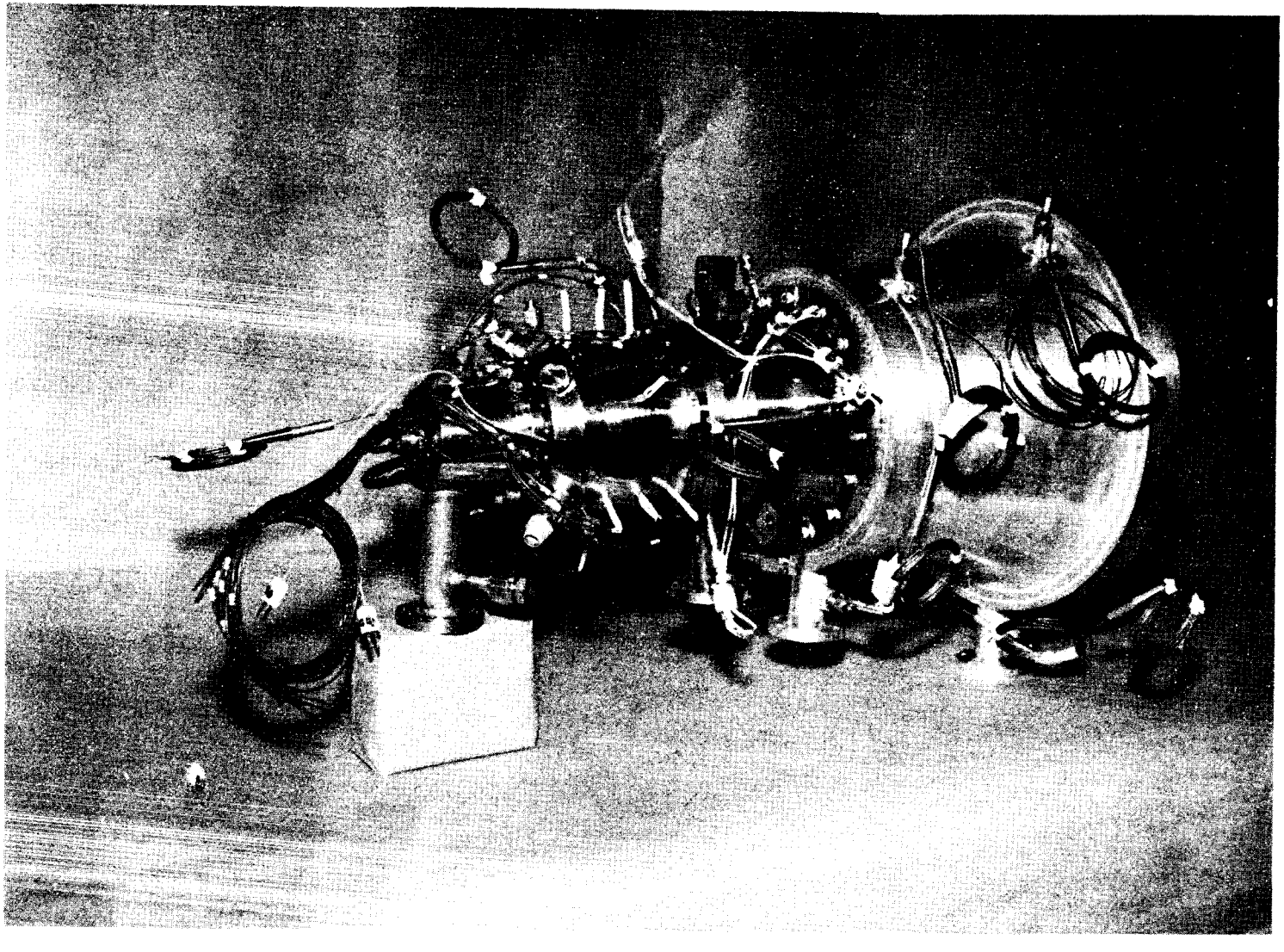

Figure 121. Altitude Thruster with Water Cooled Nozzle Extension

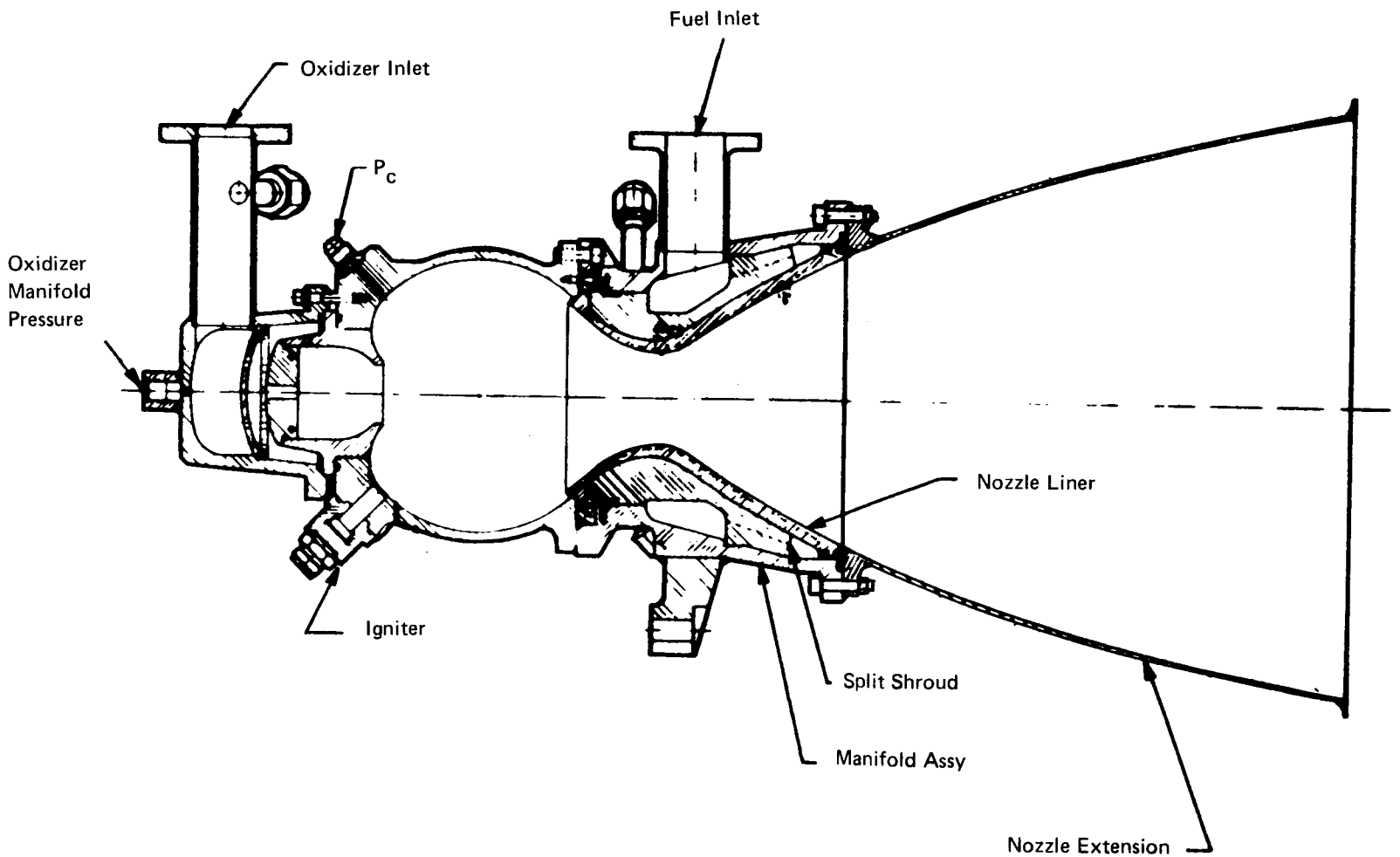

Figure 122. 1500-lb 6672 N Thrust Altitude Test Assembly – Cb Extension

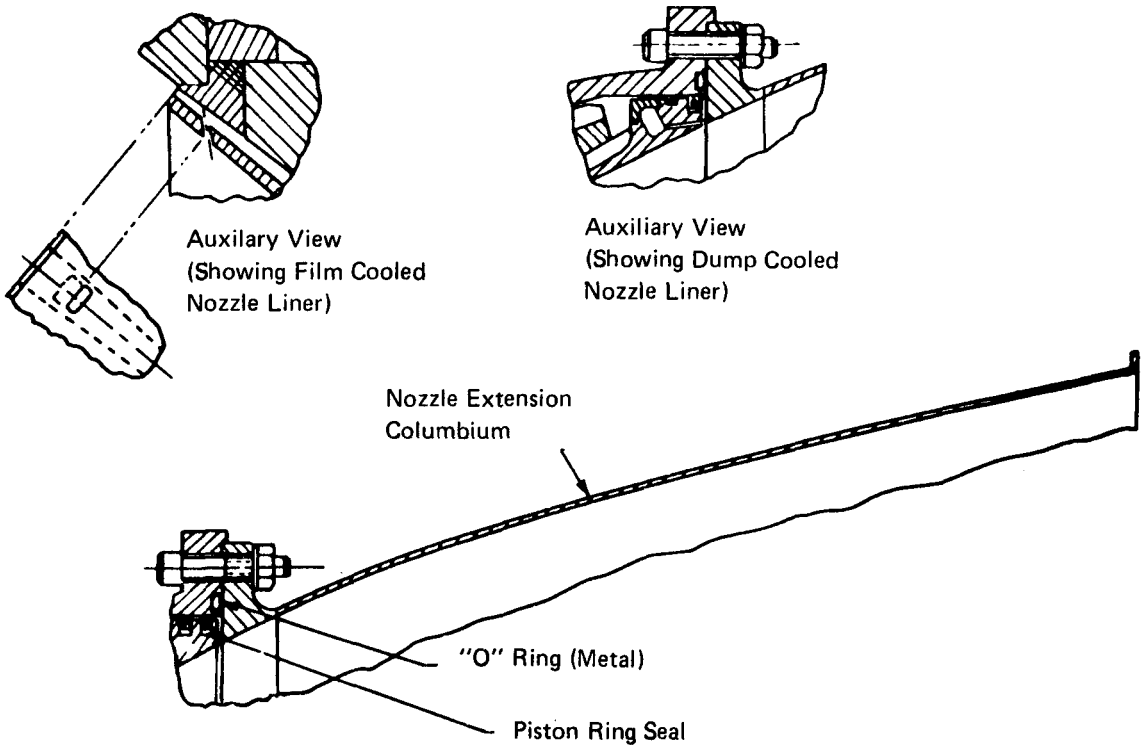

Figure 123. Cooled Chamber Design Details

nozzle showed that very little, if any, change in performance was experienced. This small loss in performance still allowed the performance valve to exceed the goal of 435 seconds (4266 N sec./kg) (Table XL).

TABLE XL
HEAT REJECTION DATA - ALUMINUM NOZZLE EXTENSION

	BTU/Sec	KW/Sec
Regeneratively Cooled Nozzle	251	265
Regenerative/Film-Cooled Nozzle	240	253
Regenerative/Dump-Cooled Nozzle	130	137

The difference in the results was in the divergent nozzle heat rejection where a rather significant reduction, of nearly 50%, was encountered with the dump-cooled configuration, while the film-cooled nozzle values were reduced insignificantly. Therefore, all effort related to the film-cooled configuration was halted and further effort was concentrated on variation of the dump-cooled configuration.

C. OXIDIZER INJECTOR EFFECTS

The test data summary of the sea-level evaluation series indicated a definite relationship between the oxidizer injector and the performance obtained on the thrust chamber. A series of tests was also conducted on the altitude thrust chamber to confirm this information and to indicate any differences involved between the altitude or regenerative thrust chamber testing and the heat-sink hardware. It was also conducted to see what variance could be expected from the hardware selected for general testing (28° cup with 10% centerflow) and that of the higher performance oxidizer configurations used in the heat-sink chamber tests. Results of the tests shown in Figure 124 indicate that as much as 5 seconds (49 N sec./kg) might be gained by using a test configuration of a lesser centerflow and a slightly higher oxidizer emittance angle. However, lower performance was encountered in the use of the 39° cup configuration where the performance obtained was slightly below that of the 28.4° configuration. Since both higher angle oxidizer configurations produced higher heat rejection rates and the 28° cup originally selected produced performance approximately as predicted (exceeding the program goal), no further attempts were made to optimize the oxidizer configuration. The original selection of the 28° cup with 10% cap configuration was used.

D. THRUST COEFFICIENT

Another parameter closely examined in the course of the initial test program was the thrust coefficient (C_{f_∞}). Initially, there had been some concern that the reverse-flow chamber performance calculations could not be handled in a conventional manner, so the predictions for operation might be invalid. This was not the case. In fact, it appears that conventional means can be used in a very reasonable fashion. Some corrections were incorporated into the data before interpretation. In the case of chamber pressure, the measured value was corrected for the cross flow expected at the measuring orifice and for a standard nozzle correction with the relatively high contraction ratio used on this chamber. These two corrections are standard and should present no difficulties in the normal usage of the reverse flow thrust chamber data. A second method of handling the data may be related to the value of expected or predicted c*. It has become standard procedure at Bell Aerospace Company to vary the C_F expected based on the c* or operating efficiency of the engine. As the performance decreases, the theoretical expansion which can be obtained also decreases the gas expansion initiated from the lower enthalpy regime. The predicted C_{f_∞} displayed in Figure 125 has been decreased from the lower energy level and assumes that expansion is initiated based on 97% obtained c*. This figure shows the comparison of data from the tests conducted on the regeneratively cooled nozzle only. It is admitted that when either fuel film or dump cooling is used the theoretical values change and so the C_f predicted value would also vary. In the case displayed, a very encouraging comparison was obtained. When the test data with the two chamber pressure corrections were compared to the theoretical C_f for the lower energy expansion condition, a very close correlation resulted. This indicated that the reverse flow engine could be designed by using conventional theoretical methods for predicting performance, as long as the design parameters stayed within reasonable limits of previously demonstrated hardware.

E. DUMP-COOLED NOZZLE EFFECTS

The use of dump cooling in the nozzle extension would obviously allow more latitude in the design of a thrust chamber to lower temperatures in the nozzle extension or to use less exotic materials. This consideration incorporated the hypothesis that the space shuttle engine would probably incorporate a variety of nozzle installations including various scarf angles as well as area ratios. On this basis, it was presumed that the initial design of the engine would include a standard combustion

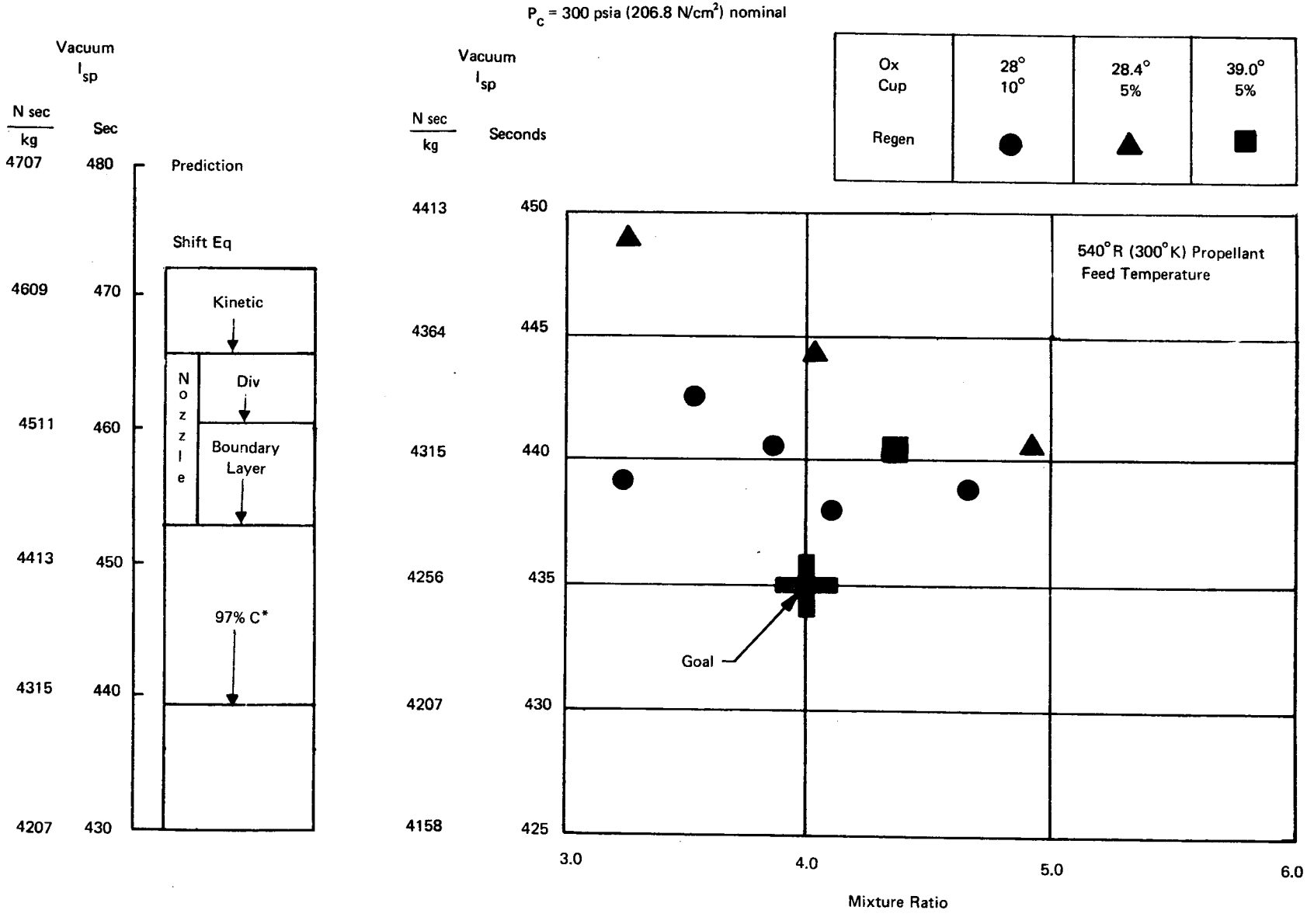

Figure 124. 1500-lb (6672 N) Thrust Altitude Test Results – I_{sp} versus O/F

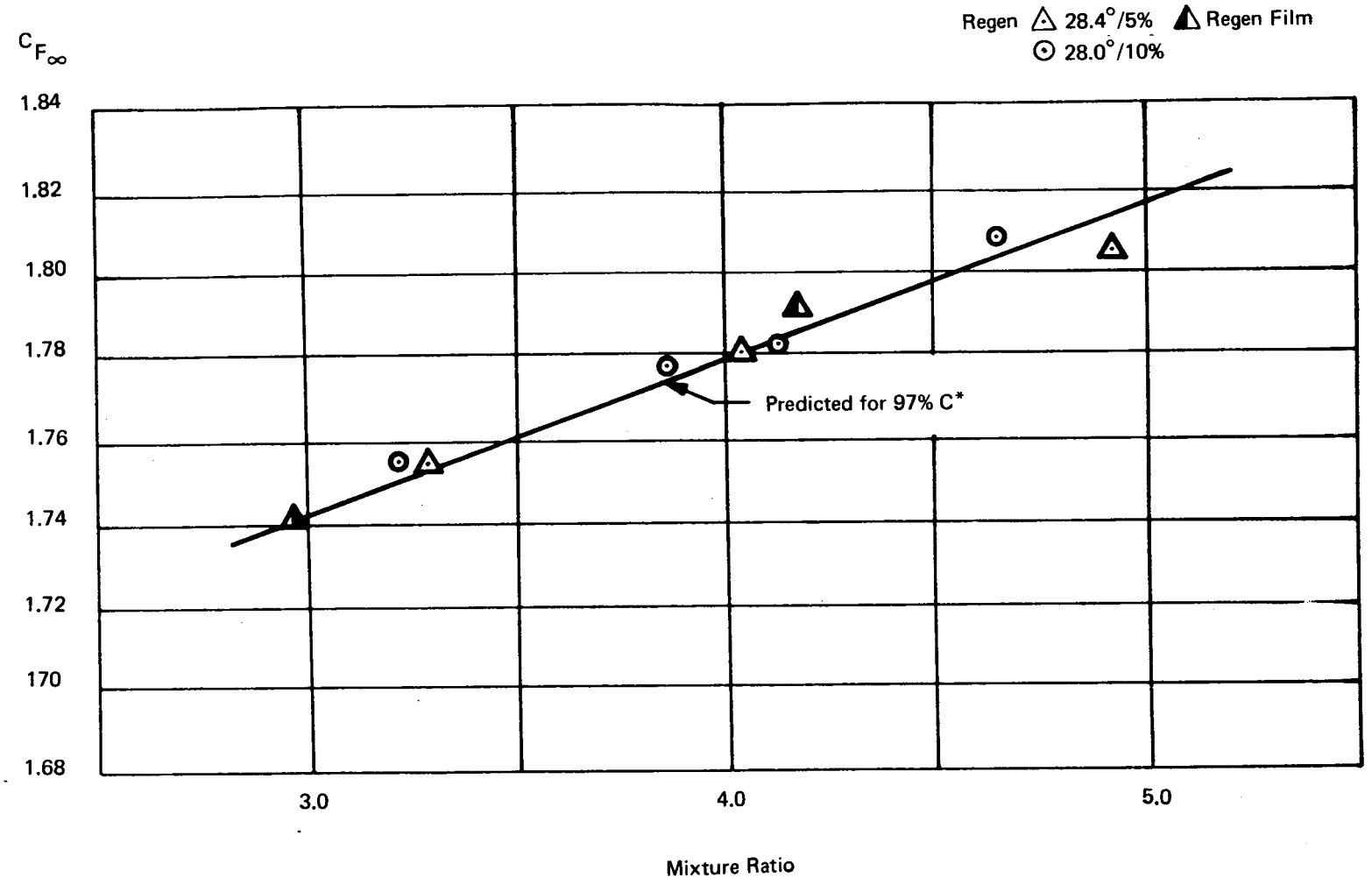

Figure 125. C_{F_∞} versus Mixture Ratio

engine, indicating that the entire nozzle extension should be enclosed in some manner. The engine should be capable of operating as a wrapped, insulated or buried configuration. Considering a sheet metal nozzle extension, the divergent nozzle was initially predicted to operate at approximately 3700°F (2311°K) in a buried or fully insulated environment. Since this temperature is somewhat above the current state of the art for long-duration operation, it was considered probable that the nozzle would either be cooled by regenerative techniques or by auxiliary fuel cooling on the internal surface of the nozzle extension. This auxiliary cooling was thus the task of the dump-cooled nozzle configuration.

The initial dump-cooled nozzle design was for 6%. The predicted performance loss was approximately 2.5 seconds. It was further predicted that an 800-900°F (700 - 756°K) maximum nozzle temperature reduction would also be achieved with this configuration. The previous discussion as well as Table XL indicated that a significant reduction in heat rejection was displayed when the dump-cooled nozzle was used on the thrust chamber. Also, a minimal loss in performance was indicated as shown in Figure 126. These encouraging results indicated that not only could the reverse flow thrust chamber achieve the high performance goals of the program, but also auxiliary cooling could be used in a "metal nozzle extension" resulting in simplifying the design. Subsequent testing on the program used what was called 3, 6 and 9% dump cooling configurations. These data are compared in Figure 126.

One caution should be used in the interpretation of the percentage of dump cooling quoted. The 6% dump coolant was a design value properly calculated and computerized; however, no calibration of this percentage of flow was attempted within the scope of the program. Further, the 3% dump cooling used was obtained by plugging one half of the metering orifices going into the dump-cooled nozzle manifold at the downstream location of the nozzle liner. Since it was expected that the copper wiring used to plug the film-cooled orifices would probably have enlarged them, the 9% dump cooling was obtained by drilling two additional metering orifices per each orifice which then remained for 3% dump coolant. The exactness of the percentage values quoted is questionable. However, the use of comparative values seems reasonable.

F. HEAT REJECTION

As on all rocket engine developments, performance is so integrally involved with heat rejection that a discussion of performance cannot be complete without comparable displays of temperature or heat rejection values. One value of heat rejection, that of the water-cooled nozzle extension, has already been displayed in Table XL indicating that the temperature could be adjusted as desired in the nozzle extension by the use of auxiliary cooling. A more precise determination of heat rejection values of the chamber were involved since the temperatures obtained were used to define structural margins which would allow the prediction of multi-cycle long-duration operating capability. To obtain data, 20-second operation was used in most cases. A typical thermocouple trace for this time period is demonstrated in Figure 127. On this chart, the values are displayed for varying mixture ratio and chamber pressure for the selected oxidizer injector configuration. In addition, the typical values for dump coolant (6%) are included for comparison purposes. Note that the uncooled chamber, represented by values of T1, T2 and T3, was designed for approximately 1650°F (1172°K) maximum temperature. At this maximum design temperature, the cycle life goal (1×10^6) would be significantly exceeded. Therefore, 1650°F (1172°K) becomes a goal for the chamber temperature on this program. The other design temperatures significant to this data are temperatures 4 and 5, which are

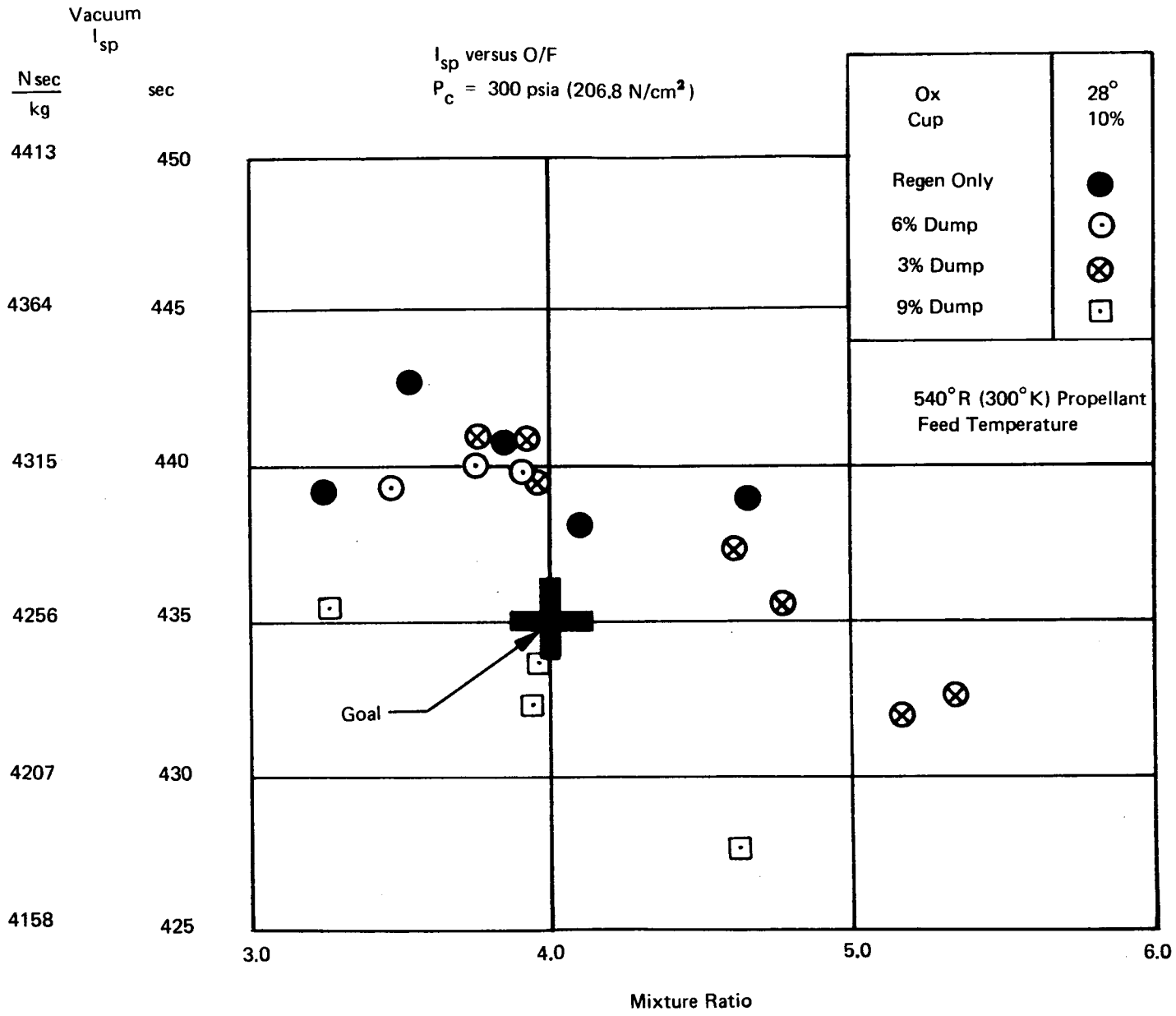

Figure 126. 1500-lb (6672 N) Thrust Altitude Test Results I_{sp} versus O/F

Regeneratively Cooled - 20-sec Firings

P_c	300 psia (206.8 N/cm^2)						100 psia (68.95 N/cm^2)		500 psi (344.7 N/cm^2)	
O/F	°F	3.21 °K	°F	4.13 °K	°F	4.66 °K	°F	4.36 °K	°F	4.09 °K
T1	1041	(834)	1223	(935)	1271	(962)	1118	(877)	1440	(1055)
T2	975	(797)	1083	(858)	1220	(933)	1113	(874)	1276	(965)
T3	517	(542)	648	(616)	715	(653)	683	(636)	777	(687)
T4	584	(580)	697	(643)	728	(660)	779	(521)	609	(594)
T5	470	(517)	579	(577)	612	(596)	659	(622)	488	(526)

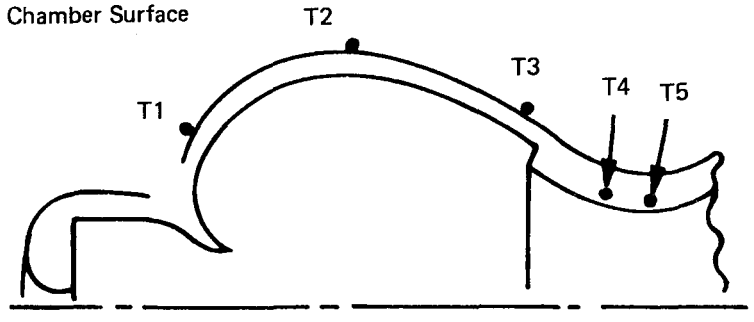

Dump Cool at 116 sec

P_c	3.00 psia Nom (2.07 N/cm^2)	
O/F	3.90	
T1	1297°F	(977°K)
T2	1106°F	(870°K)
T3	657°F	(621°K)
T4	704°F	(647°K)
T5	536°F	(554°K)

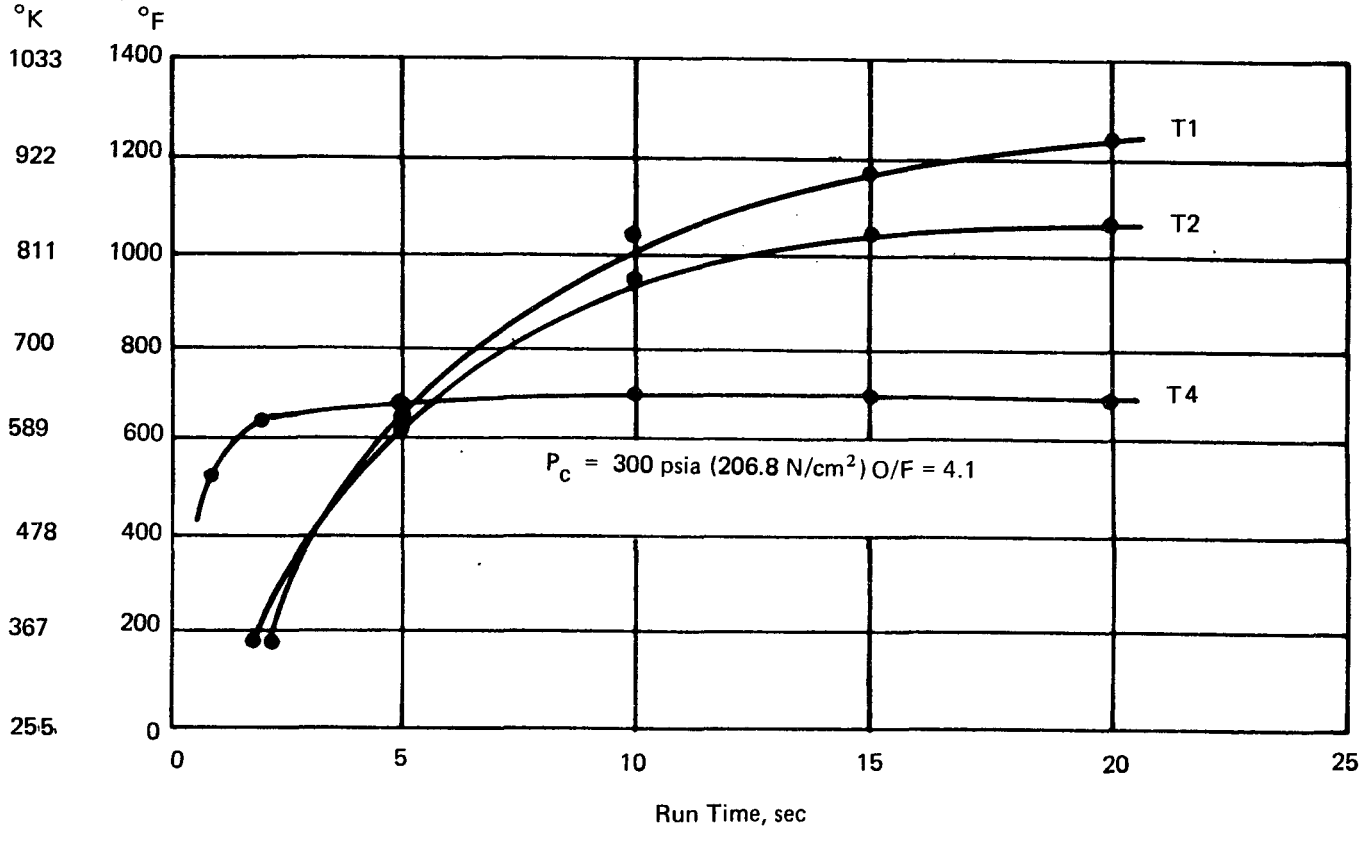

Figure 127. Maximum Temperatures - 28.0°/10% Cup

the inner AMZIRC liner temperatures for the nozzle. The design maximum to obtain the million cycle capability is approximately 915°F (764°K). The temperature value observed on this program is significantly reduced from this maximum, indicating that a substantial margin exists with the designs tested.

Another view of this data may be seen in Figure 128 where the maximum temperature for the chamber has been plotted versus chamber pressure with an additional point at mixture ratio of 5. The values displayed are for a radiation-cooled chamber. However, only a small increase in temperature would be displayed with a fully insulated unit. The calculated increase, even at the 1600°F (1144°K) point, would only about 50°F (28°K). Therefore, from this chart the date would imply that the engine would operate even at the mixture ratio of 5 and 500 psia (344.7 N/cm^2) chamber pressure over the desired cycle life.

A check was also made on the predicted land temperature for the regeneratively cooled nozzle. This predicted versus test data are shown in Figure 129. From the information generated, a very reasonable correlation is displayed, and predicted values for design use are reasonable for future analytical exercises. Figure 130 shows the correlation of the increase of the fuel temperature passing through the regeneratively cooled nozzle with test values displayed. Again a reasonable correlation exists between the predicted value and the data obtained. A value of 100% enhancement was used in calculating the predicted temperature rise for hydrogen.

The radiation-cooled temperature for the non-fuel-cooled nozzle extension was also calculated (see Figure 131). The prediction of a variety of dump cooling configurations was also made. Here a prediction was difficult as no previous data existed in the definition of h_g or the amount of film which may be adjacent to the wall for cooling purposes. So, an empirical approach was taken where the data obtained from the tests using the different dump cooling rates were used to substantiate the type of prediction which could be expected from a theoretical analysis. The test data obtained are shown in Figure 132. The previously displayed baseline for nonauxiliary cooling is shown in the top curve of the test data. The additional curves represent the various dump cooling configurations tested. It may be noted that points plotted are cumulative points at those particular locations, and the data were taken in a complete map of the nozzle extension from pyroscanner data. It has been found in the past that pyroscanner information is extremely accurate. In fact, the calibration of thermocouples at these temperatures was greatly enhanced with the use of pyroscanner information.

It may be noted that these data were all for radiation-cooled nozzle configurations. Initial tests were made in a radiation configuration both to determine the operating temperatures for a buried installation and to allow more temperature coverage by using the optical pyrometer. The addition of insulation was postponed until measured nozzle extension data became available so that a more accurate prediction for the buried installation could be made. Figure 132 data were used in the definition of the type of thrust chamber configuration that was to be used for long duration tests. Estimates had been made, indicating that a radiation-cooled nozzle temperature of approximately 2000°F (1367°K) would probably increase by 200°F (111°K) with the addition of a blanket of insulation. Figure 132 indicates that if a 2100°F (1423°K) temperature were desired, for example, using a Hastelloy nozzle extension, 1900°F (1311°K) or approximately 7.5% dump cooling configuration would be a reasonable value to test for long duration. This was one of the factors involved in the selection of 7.5% dump cooling for the 500-sec. insulated chamber test which was later conducted.

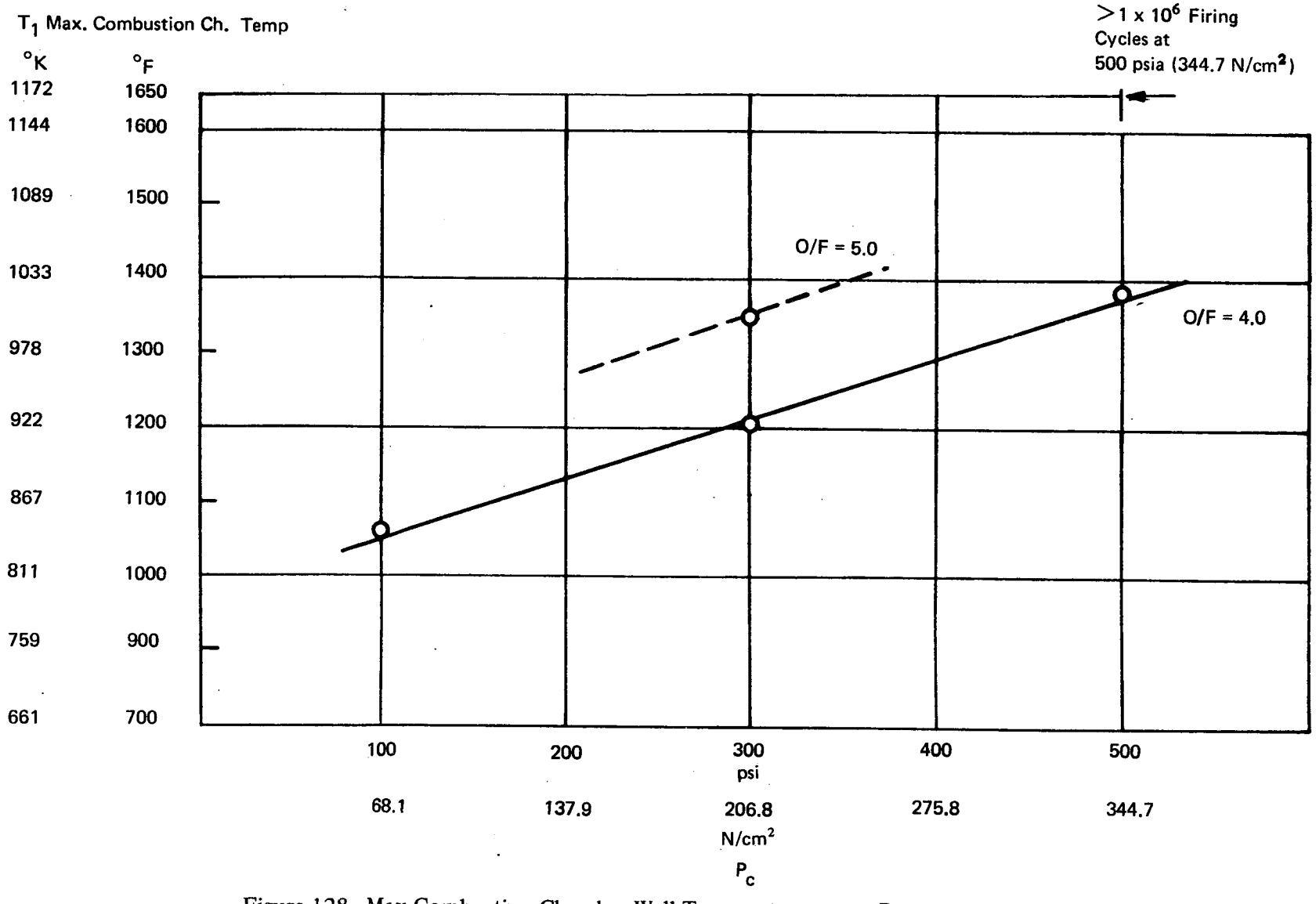

Figure 128. Max Combustion Chamber Wall Temperature versus P_c (Regenerative Nozzle)

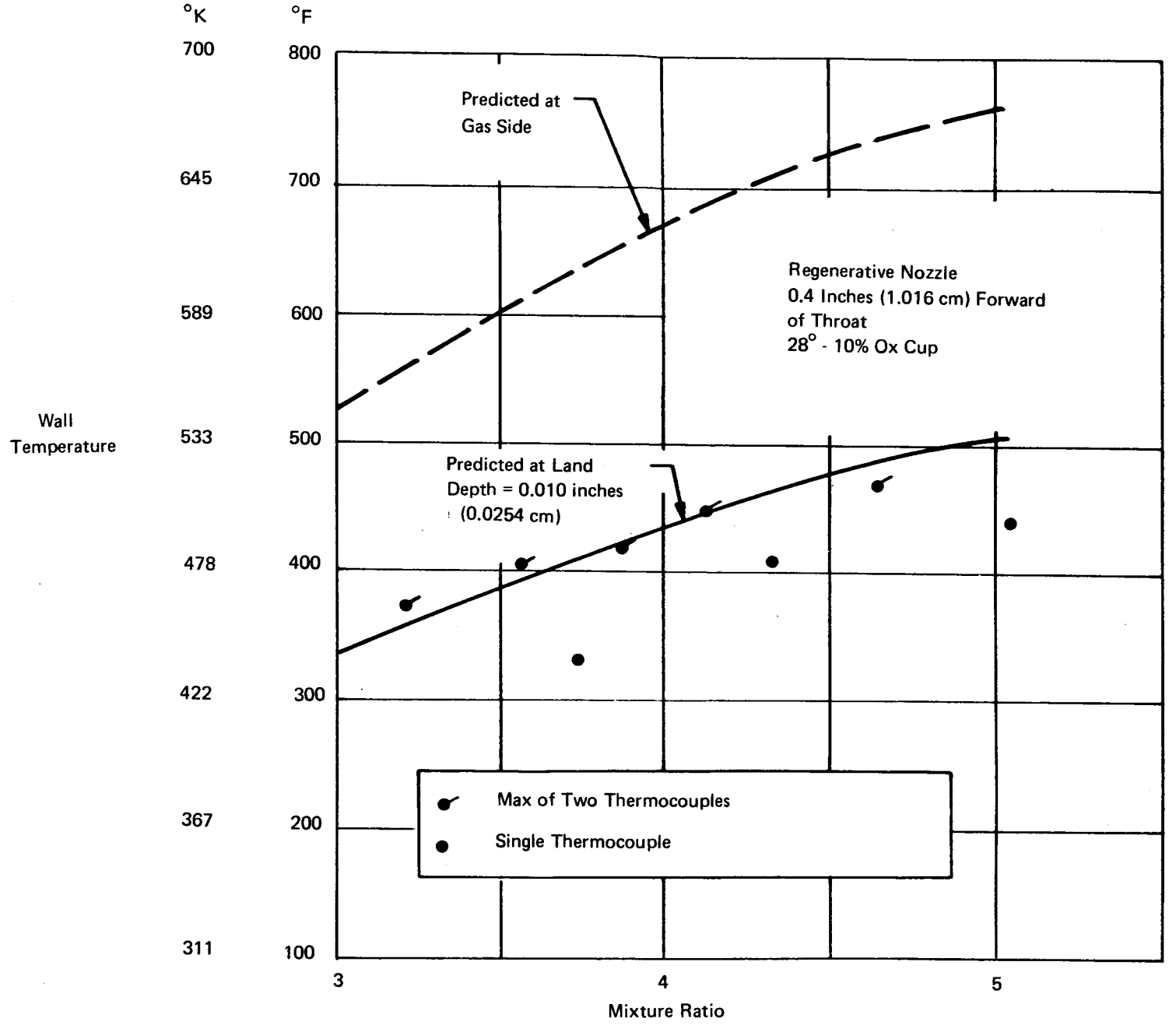

Figure 129. Wall Temperature versus Mixture Ratio

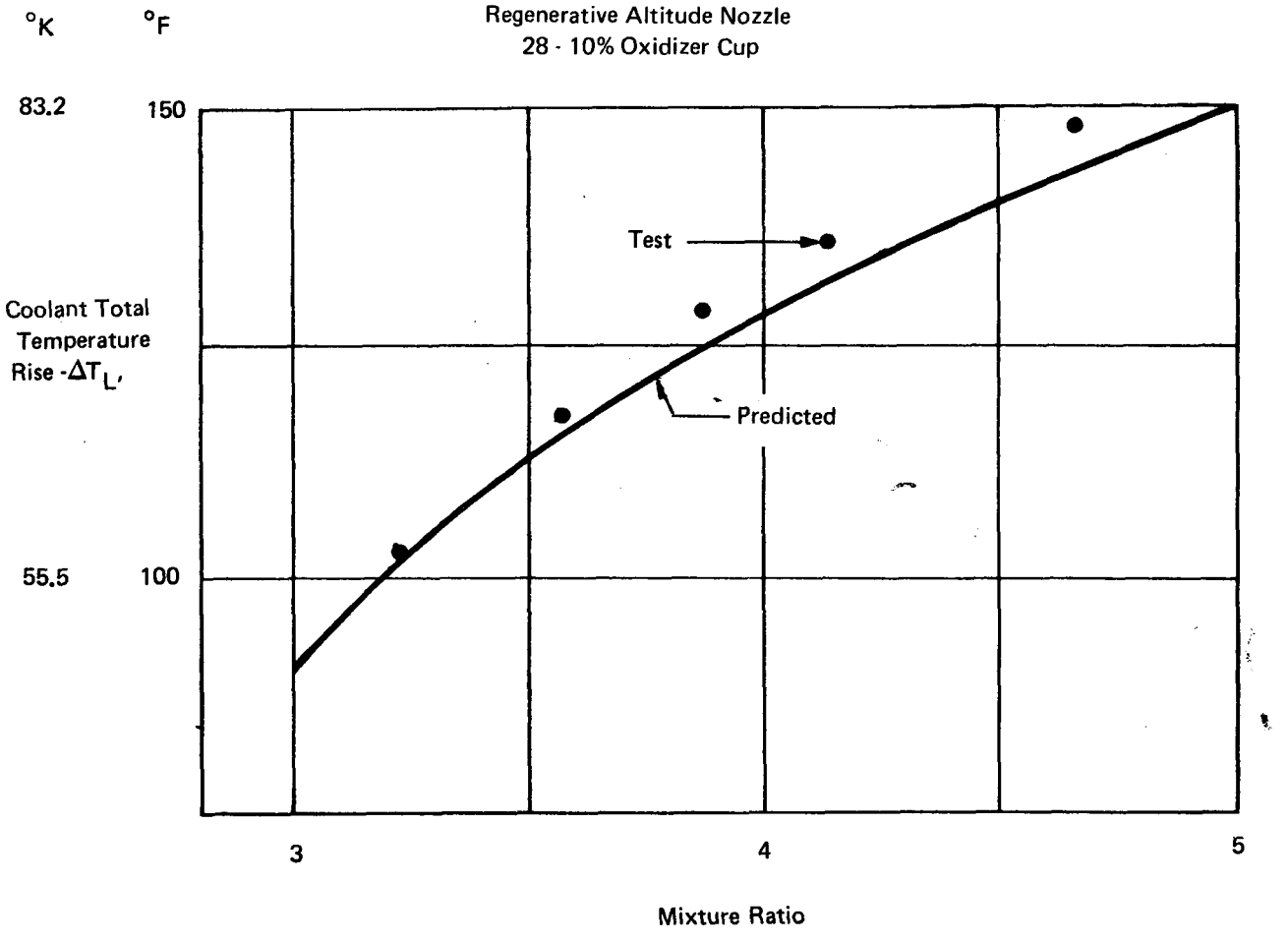

Figure 130. Heat Rejection versus Mixture Ratio

G. CHAMBER PRESSURE TESTS

A series of four tests were conducted to evaluate the effects of high and low chamber pressure. Two tests were conducted at each of the extreme pressures. Data obtained are presented in Figure 133 and indicate that no large excursion in performance would be expected over the operating range indicated. It is suggested that caution be exercised in using the actual performance values, as the data base was quite small and minor changes would probably result if a larger sampling were taken.

H. DURATION EVALUATION

Four long-duration tests were attempted during the course of the program. One of these tests was a buried installation demonstration test where the chamber was fully insulated to obtain the required maximum 800°F (700°K) external temperature. The first three tests conducted were with radiation components at both the combustion chamber location and the nozzle extension. Each of the initial three tests was to demonstrate a different nozzle extension temperature. All tests were conducted with the same columbium nozzle extension.

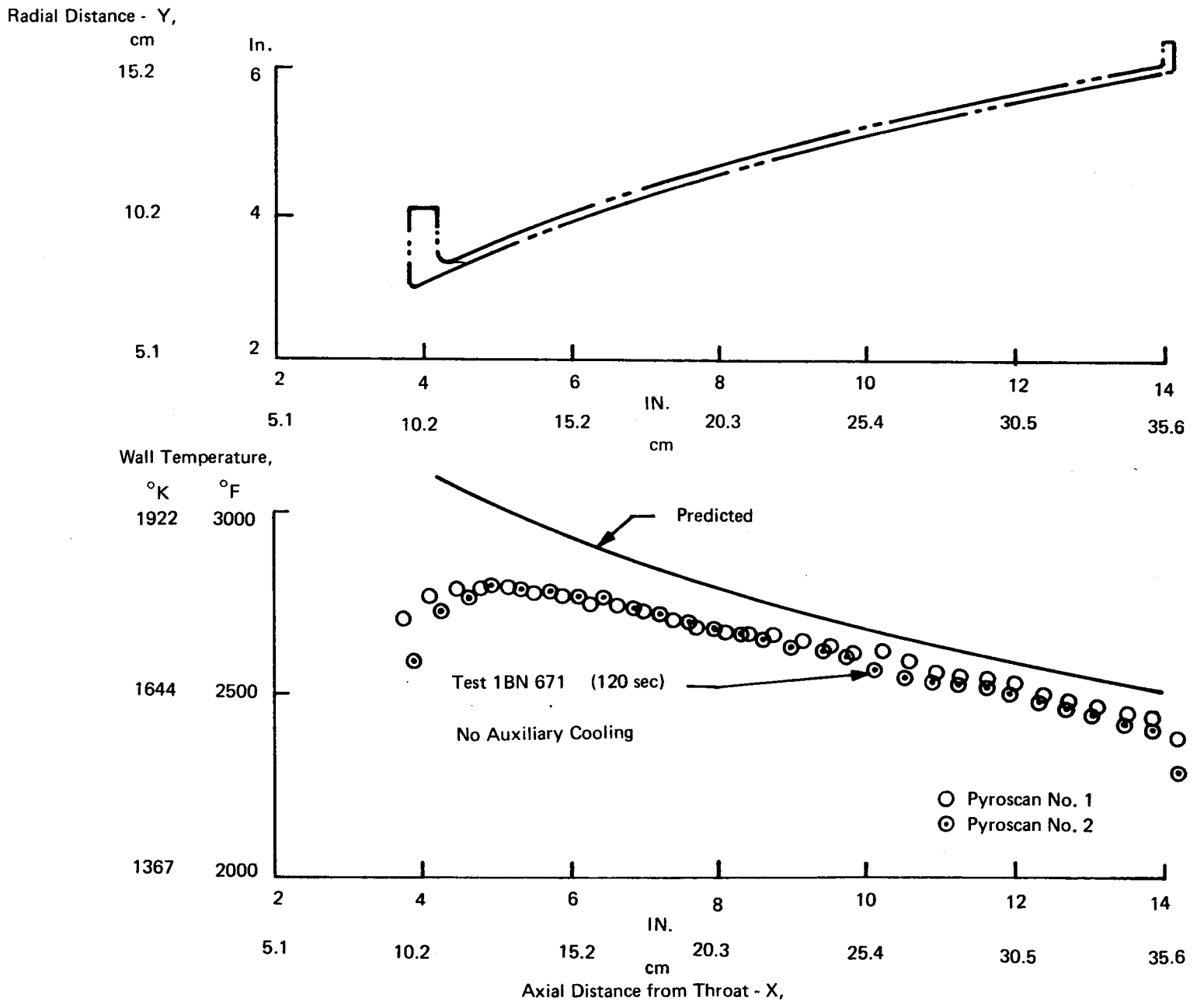

Figure 131. Radiation Cooled Nozzle Extension Temperature Distribution

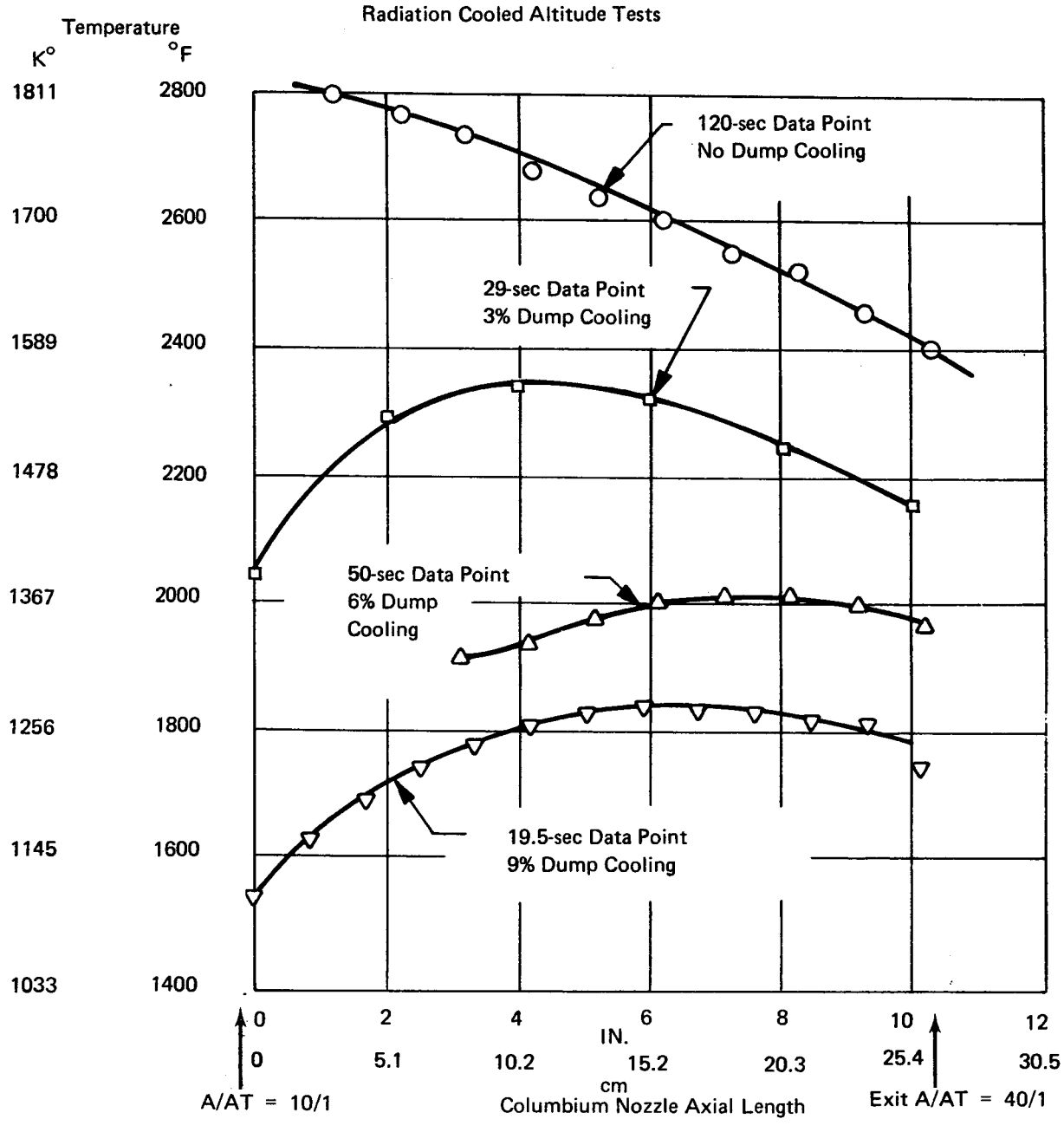

Figure 132. Columbium Nozzle Extension Temperature

High and Low P_c

I_{sp_∞} versus P_c

O/F = 4.0 Nominal

P_c psia	P_c N/cm^2	O/F	Data Pt. sec	$I_{sp\infty}$	$I_{sp\infty}$ N sec/Kg
106.1	73.154	4.36	19.4	432.7	4243.3
99.3	68.465	3.41	1.0	443.1	4345.25
482.0	332.327	3.87	15.0	437.0	4285.43
500.3	344.945	3.09	19.6	438.6	4301.12

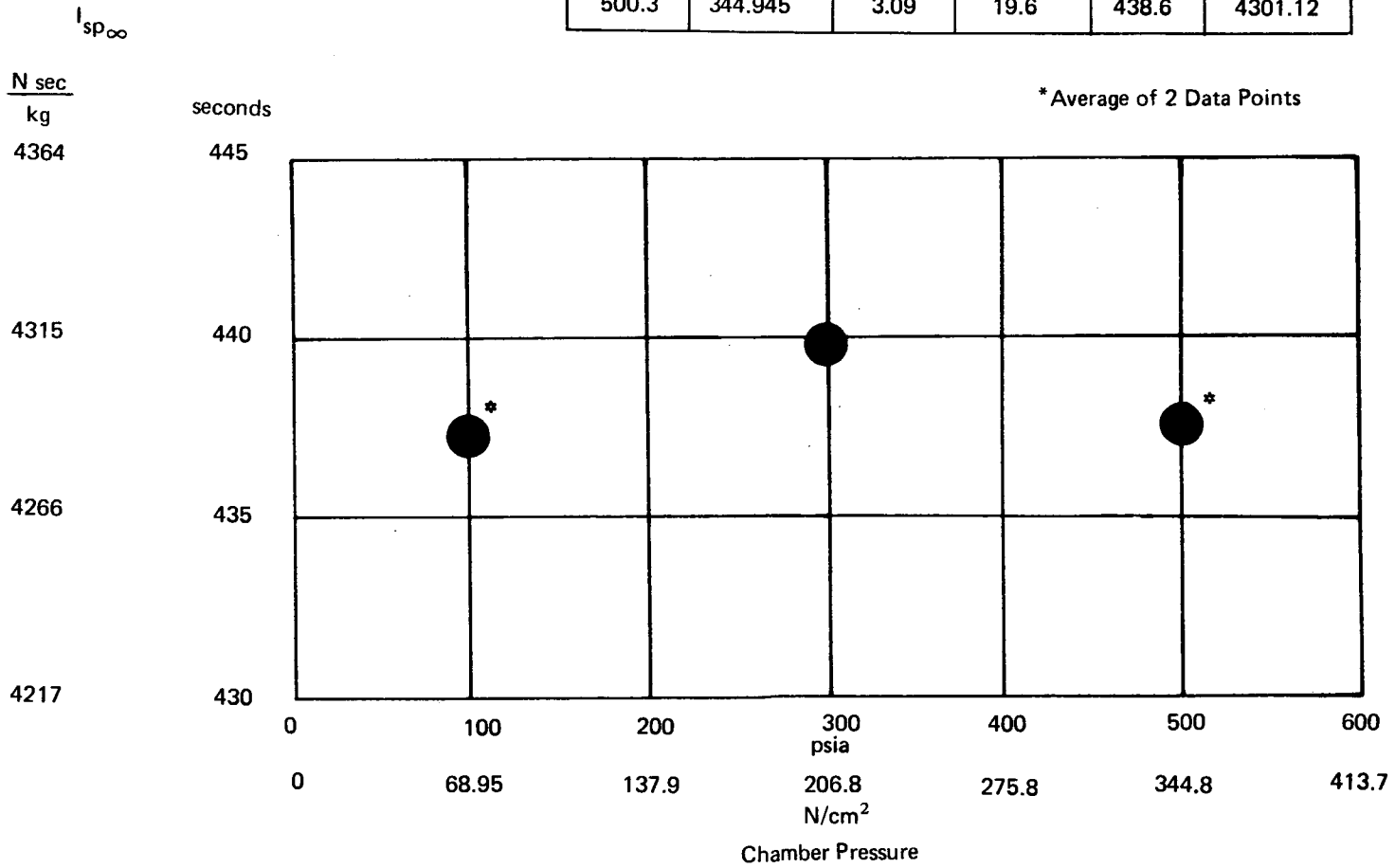

Figure 133. 1500-lb (6672 N) Thrust Altitude Test Results

The initial long-duration test was run 1BN 669, which included a 6% dump-cooled nozzle. The run was scheduled for 200 seconds and was stopped somewhat short of this value when the altitude chamber automatic shutdown system was actuated due to propellant exhaustion. Temperatures of the chamber and operating parameters indicated that the run could have continued for the desired duration.

The second attempt at long duration was conducted without auxiliary cooling in the nozzle. This test run, 1BN 671,was again halted prior to the desired 200 seconds as a test cell pressure switch, installed as a safety device, overheated and halted the operation of the test. At the time of the test there were no indications that the run could not have continued, and it was suggested that the chamber could have been restarted (achieved on the following test). However, on these tests it was demonstrated that some leakage was involved in the nozzle-to-nozzle extension housing O-ring seal and that leakage at that joint was encountered. Disassembly of the engine indicated that the O-rings at the oxidizer injector end of the chamber were also somewhat degraded but not sufficiently to warrant changing the configuration.

The next duration test was run 1BN 677 and was conducted with 3% dump cooling in the divergent nozzle. In this case the test continued some 300 seconds. At approximately 200 seconds it appeared that some leakage existed at the oxidizer cup O-rings, and an overheating condition became obvious on the TV monitor as the run time progressed. This condition eventually affected the chamber pressure lead-in wire and as a consequence the pressure signal was lost and the run was terminated. In observing the data from this test, it was obvious that the basic run hardware was acceptable for the long-duration operation. However, some of the individual features of the hardware, i.e. O-ring locations in the oxidizer injector-to-chamber joint were unsatisfactory and should be changed prior to a buried installation test. In addition, the O-rings at the igniter ports were also eliminated and the plug connectors to the exciter lead in wire were protected from a heat-soak condition.

Preliminary testing conducted for performance, heat rejection, and durability had also indicated a number of modifications to the hardware to be incorporated prior to the demonstration of the 800°F (700°K) ambient temperature operating capability. These modifications included the cooling of the igniter plugs with the oxidizer used in the augmentation. This was accomplished by routing the oxidizer from the injector through a coolant jacket surrounding the igniter plug and thence into the previously used augmentation port. Both spark plugs were equipped in this manner. The next modification was to weld the oxidizer injector cup and cap together. This separate assembly had previously used an O-ring seal which was felt to be unsatisfactory for the long-duration test. Additional seals which were changed included the oxidizer cup-to-cap where metal seals were installed instead of the normal composition O-rings and at the igniter plug where metal seals were installed to allow for the higher temperature operation. In addition, the thermocouple lead-in ports to the nozzle, previously sealed with Teflon inserts, were capped, eliminating these measurements which were not considered essential for the duration test.

Since no pyroscanner data could be obtained on the long duration test with the nozzle insulated, thermocouple installations were made to obtain comparative buried extension installation data. The thermocouples were inserted through the insulation with an internal tab applying some pressure to ensure a good contact with the surface of the nozzle. Subsequent thermocouple data obtained during the test indicated that the installation was successful in obtaining the required data. However, the data from the thermocouple compared to the pyroscanner data, where no joint calibration was performed, may show difference in recorded values. Insulation of the chamber was made in a crude but effective manner by wrapping two layers of half inch Dynaflex material around the uncooled portions of the chamber. The insulation was held in place with a covering of tape fiberglass

and sewn through the material with a strand of the fiberglass material. The thermocouples that were installed through the insulation were potted with a high temperature epoxy and thermocouples were installed on the external surface of the wrapped nozzle to measure external temperatures. The test of the thrust chamber installation, shown in Figure 134, was nondramatic in terms of other previously witnessed operation as there was no visible heating in the chamber or nozzle extension regions. A rather dull viewing period of 500 sec. resulted. Post-test examination of the hardware indicated the only damage to occur was one slight erosion point around an area where leakage occurred from the oxidizer augmentation port (the second port showed no visible damage whatsoever), with the balance of the hardware being in excellent condition.

The performance recorded for the long-duration test was slightly less than had been predicted. The original data (Table XXXVIII, Figure 126) indicated that 7 1/2% dump cooling should produce a specific impulse of 435 seconds (4266 N sec./kg). The data shown in Figure 126, was the primary reason for incorporation of the 7 1/2% configuration. Since 435 seconds I_{sp} (4266 N sec./kg) was the stated performance goal of the program, the recording of 431 seconds (4227 N sec./kg) on this long-duration test was disappointing. However, there was an additional hardware change made which was considered to be responsible for this change. This change was in the recessing of the land area in the fuel orifices.

The change to the land area of the fuel orifices was made because long-duration tests had resulted in some erosion marks immediately downstream of the fuel injection ports at the location of the land area. This erosion was attributed to the aspiration of the combustion gases into the region of the land, resulting in local heating. This erosion had occurred on short-duration tests and the concern was that long-duration testing would result in damaging erosion of the chamber wall. So, the dump-cooled nozzle fuel injector land area was modified prior to the long-duration test. This modification consisted of recessing the land area by approximately 0.040 inch (0.102 cm) in an eliptical pattern. It was hoped that recessing the land area would draw a small amount of fuel into the land region immediately adjacent to the injection port and either dilute the aspirated combustion gases or produce sufficient pressure to reduce the flow into the region. Observation of the hardware after test indicated that the modification was moderately effective, as portions of the chamber were not eroded while other portions of the chamber were only lightly eroded. In general, the erosion was significantly reduced over what would have been projected had the modification not been incorporated. This seemingly successful erosion reduction modification had an apparent side effect in reducing performance of the engine. The modification to the land area was apparently sufficient to have changed the velocity in the injection orifices. The lower velocity of the orifices was responsible for the somewhat reduced performance exhibited on the 7.5% dump-cooled nozzle configuration. Further tests to gain back the originally achieved performance while eliminating erosion were recommended but fell beyond the scope of available program funding.

The insulated chamber duration test produced the first heat rejection data for the insulated chamber configuration. In a previous discussion, it had been indicated that a temperature rise of some 200°F (111°K) was expected by insulating the nozzle extension. From the test data obtained, it appeared this 200°F (111°K) increase was only slightly optimistic; the level of predicted temperature increase as shown in Figure 135 is in reasonable agreement with predicted values. The radiation-cooled curve presented is a summation of the data shown in Figure 132 and represents the maximum nozzle temperature without regard to nozzle station. Table XLI is presented as a summation of data obtained and may be used for projection to flight weight designs. The maximum temperatures indicated at the top of the figure refer to those values demonstrated in Figure 132. Suggested material usage limits are included at the bottom of the figure. The columbium nozzle extension could be used

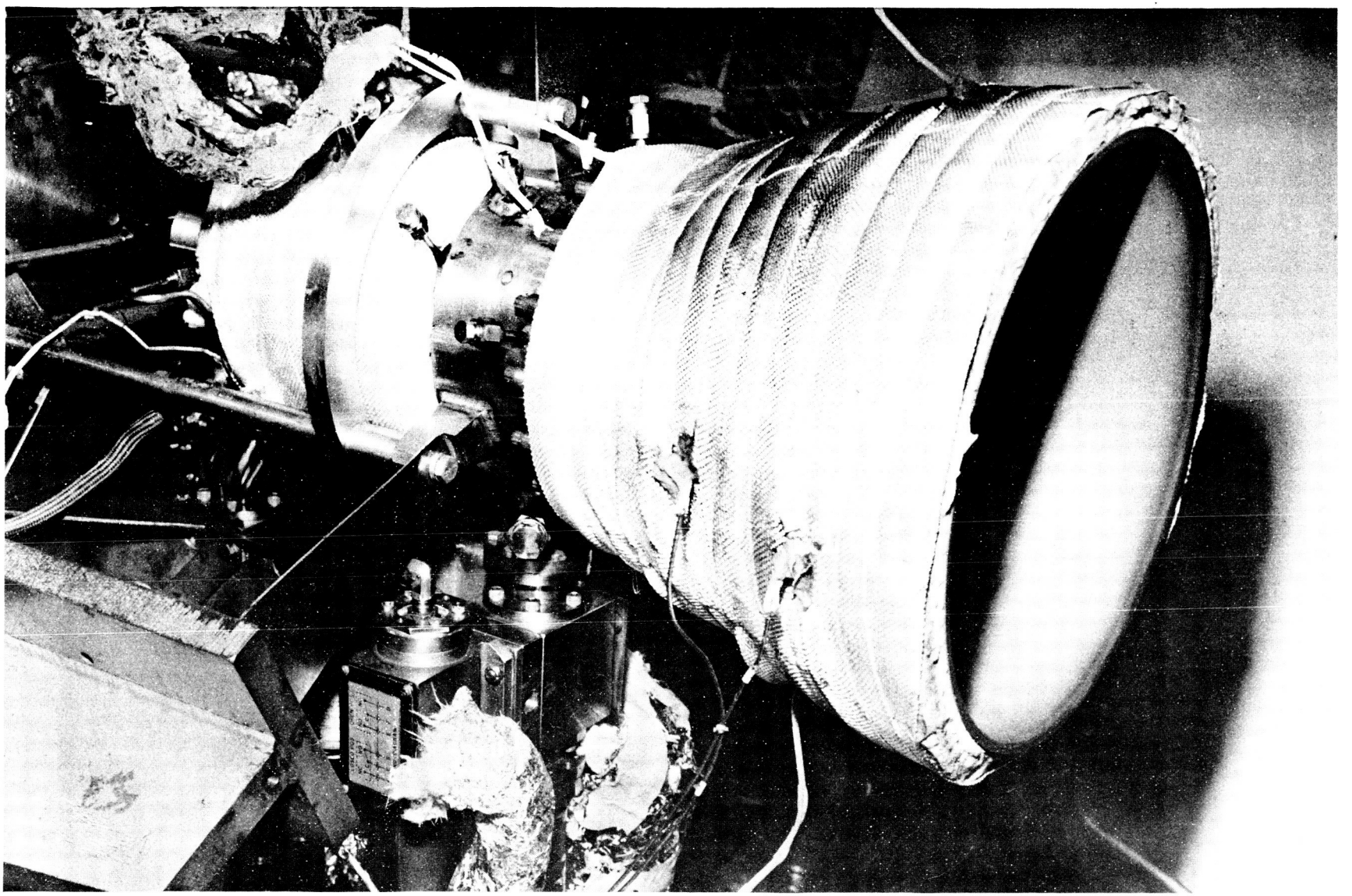

Figure 134. Reverse-Flow Thrust Chamber Assembly (with Wrapped Insulation)

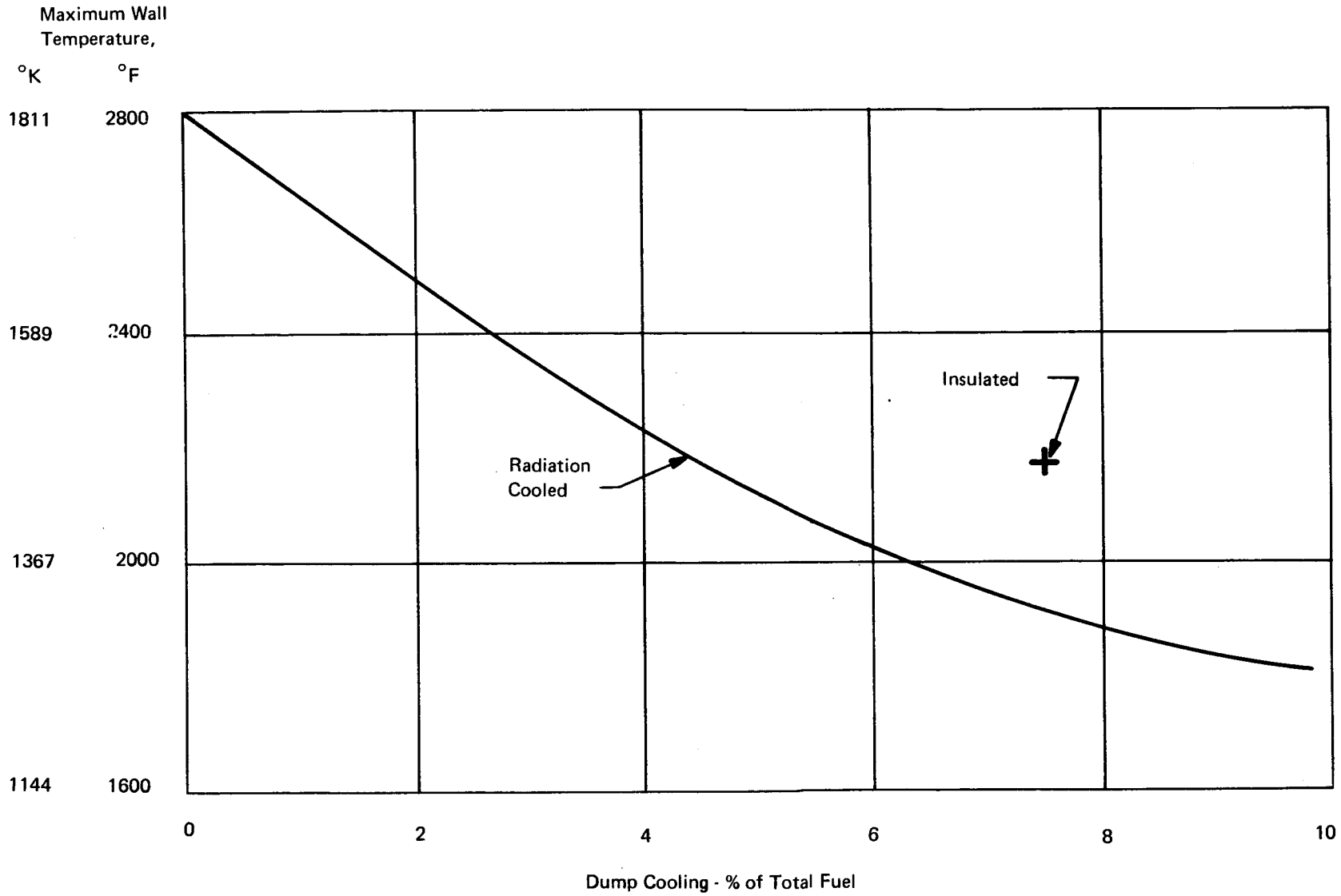

Figure 135. Maximum Radiation-Cooled Nozzle Extension Temperature

TABLE XLI
COLUMBIUM NOZZLE EXTENSION TEMPERATURE

% Dump Cooling	Maximum Temp.	
	°F	°K
0	2800	1811
3	2370	1572
6	2020	1378
9	1840	1278
Run Conditions	O/F = 4	
	P_c = 300 psia (206.8 N/cm²)	
	Pft = 540°R (300°K)	
Alernate Buried Engine Configurations		
-Cb Extension	2600°F (1700°K) and below	
-SS Type Extension	2100°F (1423°K) and below	

above 2600°F (1700°K) for shorter durations or single missions. In fact, with replaceable components, this temperature limit could be extended to as high as 3100 or 3200°F (1977 or 2033°K), allowing more latitude in the design of the dump-cooling requirements desired. The alternate configuration using stainless steel type materials, which may include the super alloys of the Haynes 25 family, could be useful to 2100°F (1423°K). The structural analysis was made using Haynes 25 at 2100°F (1423°K) and indicated that the cycle life desired could be achieved. Test data indicate that only a slight increase in dump cooling to a value near 8% would be adequate to perform the required life demonstration.

I. PROPELLANT TEMPERATURE EXCURSIONS

One of the objectives of the program was to examine the difficulties encountered while operating the reverse flow engines over a propellant temperature excursion from 200°R (111°K) to 800°R (444°K). A significant secondary objective was to examine the possibility of one hardware design which would operate over the entire temperature range. If performance variations occurred, it was then the objective to explore the range of temperatures which may be usable. The program results indicated the reverse flow engine could operate over a wide range but a performance variation should be expected. It was initially assumed and confirmed that the performance was tied to fuel velocity and that low temperature, low velocity, fuel at the cold temperature was responsible for a substantial performance decrease. New hardware, increasing the fuel velocity at cold temperature, was defined and an extension of the program conducted which included two additional hardware designs to operate at the cold temperature conditions.

The velocity decrease is quite substantial as the density of the hydrogen changes approximately proportional to the temperature changes. Thus, the change from 540°R (300°K), the initial design point, to 250°R (139°K), which was the suggested vehicle optimum, would cause a reduction of velocity of nearly 50%. Thus, injection at 2400 ft/sec (730 m/sec) on the ambient design would be reduced to 1200 ft/sec (365 m/sec). The performance dropoff predicted from theoretical calculations was approximately 30% compared to a value of nearly 10% encountered in going from 2400 ft/sec (730 m/sec) at ambient temperature to a 200°R (111°K) fuel temperature.

TABLE XLII
LOW-TEMPERATURE TEST DATA

Fuel Position	Oxidizer Cup	Fuel Velocity Ratio (To Ambient Design)	Fuel Temperature °R	Fuel Temperature °K	Oxidizer Temperature °R	Oxidizer Temperature °K	Average I_{sp} lbf-sec/lbm	Average I_{sp} N sec/kg	Remarks
Baseline	Ambient Design Full Velocity	Full	Ambient		Ambient		440	4395	(3% Dump Cooled)
Baseline	Ambient Design 1/2 Velocity	1/2	260	144	300	167	403	3952	(3% Dump Cooled)
Baseline	Cold Design Full Velocity	Full	250	139	380	211	431	4227	(3% Dump Cooled)
Baseline	Cold Design 2/3 Velocity	Full	310	172	325	181	413	4050	(3% Dump Cooled)
Modified	Cold Design 1/2 Velocity	0.8	250	139	425	236	429	4207	(3% Dump Cooled)
Modified	Cold Design 2/3 Velocity	0.8	260	144	330	183	417	4089	(3% Dump Cooled)

Note: Theoretical Performance at 250°R (139°K) Ambient - 10 Seconds

The cold temperature nozzle design was made to increase the velocity to value of the ambient temperature hardware as originally designed, so the design point was again 2400 ft/sec (730 m/sec) at the 250°R (139°K) design point. In examining the test data, it may be noted that the theoritical performance decrease expected from the ambient temperature to cold conditions was about 10 seconds. The initial velocity dropoff is shown by the first two lines in Table XLII. They indicate that some 20 seconds (186 N sec/kg) of performance was lost due to the fuel velocity. The third line of the figure represents the redesigned hardware indicating that the performance was returned to the original efficiency. In the design, all other parameters of the chamber were held constant including the location of the oxidizer and fuel injection points. The fourth line of the figure represents data obtained when a lower velocity oxidizer cup, and consequent pressure drop was installed on the assembly. Although the temperatures are varied on the test data, it was felt that the higher than desired oxidizer temperature should have produced a higher performance value. Since this was not the case, a substantial performance loss was exhibited indicating a performance trend for the hardware.

The last two lines of Table XLII represent data which were obtained on a redesigned combustor unit where the fuel injection location was changed. On previous designs, the fuel injection location was about at the mid point between the maximum diameter of the spherical chamber and the throat. The redesign or modified location was about halfway between the maximum diameter and the original fuel injection location. This position is shown schematically in Figure 136. The purpose of moving the fuel location was twofold. First, data were to be collected on the effect of the location change. Second, and more clinically, the change was made to examine the hypothesis that a lower pressure

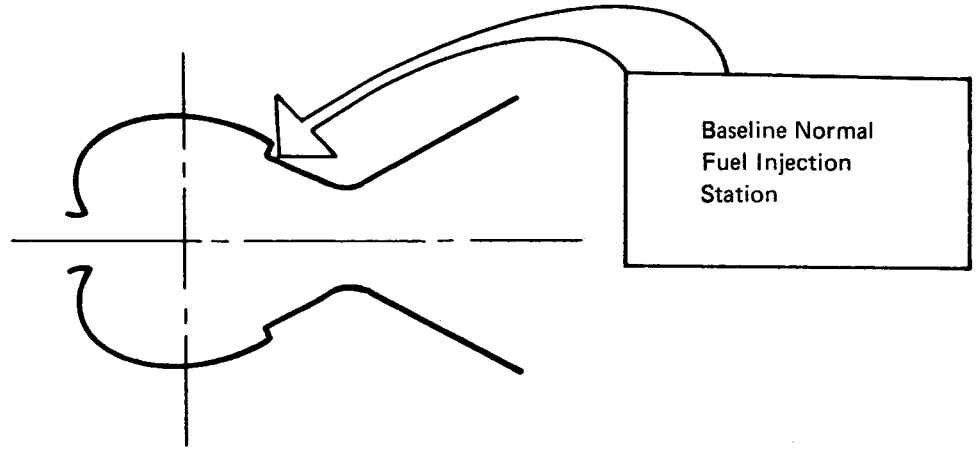

- Fuel Injection Area Decreased - Same Velocity
- Oxidizer Injection Area Decreased - Same Velocity
- New Nozzle Liner Required

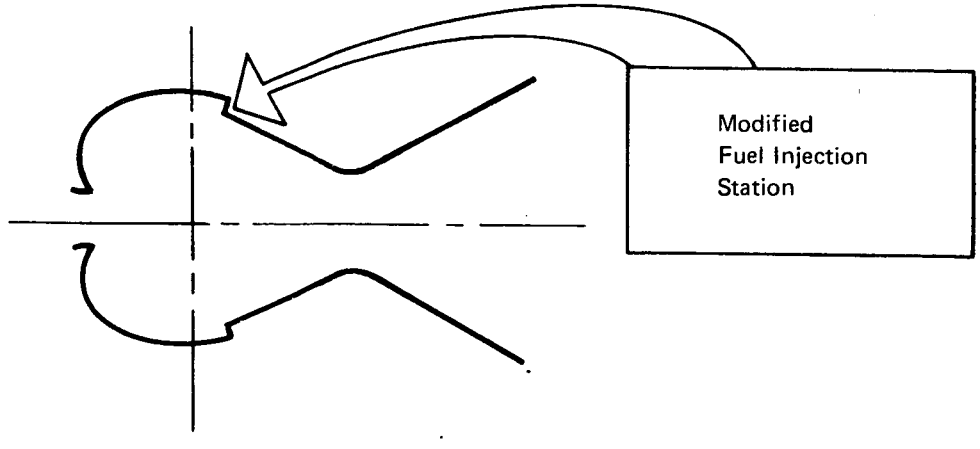

- Fuel Injection Area Decreased To Reduce ΔP 20%
- Oxidizer Injection Area Area Decreased - Same Velocity
- New Nozzle Liner, Chamber and Nozzle Housing Required

Figure 136. Low Temperature Design Modification

drop might be usable if fuel propellant path length was reduced. The latter hypothesis appears to have been confirmed in the data figure presented. Some doubt may be exhibited due to the slightly higher temperature of the test oxidizer; however, we consider that since the true temperature is more representative of the design critical parameter, the hypothesis will be confirmed and optimum position of the fuel location will also be a variable in future studies. The achievement of nearly the same performance for the changed location with a 20% reduction and pressure drop or about half the velocity for the oxidizer and 80% for the fuel indicates that the same performance level could be obtained with this changed fuel configuration.

The final series of low temperature tests were conducted on the modified fuel configuration with increased oxidizer velocity. Since previous testing had indicated that a higher oxidizer velocity produced increased performance, it was expected that the value of 429 sec (4207 N sec/Kg) would be exceeded. The last line on the figure does not indicate this to be the case. Difficulties encountered in maintaining a constant cold temperature are indicated and may have had some countereffect; however, the data were interpreted to mean that a probable optimum oxidizer velocity was involved and this value had been exceeded on the last test series. Admittedly, lower oxidizer temperature coupled with a higher oxidizer velocity produces two variables which defies distinction without further testing.

Before leaving the subject of cold temperature operation it would appear to be appropriate to comment on the instrumentation used to obtain these data. Again, a program constraint was encountered as the scope of the program did not include the rather costly process of operating instruments at cold temperatures. As a consequence, all of the data used was obtained on instrumentation calibrated at ambient temperatures and then extrapolated to the cold conditions by use of density and other standard parameter extrapolations. Running checks were made of different instrumentation to see if variance would be obvious, but none was found for such instruments as chamber pressure and thrust. However, in the case of hydrogen flow measurement a discrepancy was encountered at the very low temperatures. Both the fuel flow and the oxidizer flow were monitored with a combination of two methods. One was the calibrated flow meter and the other was the relationship between the weight flow and ΔP of the system which compensated for the temperature decrease and consequent density increase. Although this check of propellant flow accuracy is somewhat crude the data did indicate that all oxidizer flows to the coldest temperature used followed the curve which would be expected for a temperature and density change. The fuel flow indicated some difficulty in measurement below 250°R (139°K). Although some flow meter data at this temperature correlated with ΔP data, other data bits indicated a falloff of as much as 30% in weight flow. The intermittancy or at least the uncertainty of the data acquisition would indicate that dependency on this meter at the low temperature was inappropriate. Fortunately, the very cold temperature testing was only exploratory in nature and after the initial tests were conducted the balance of the program was performed at or above 250°R (139°K) where consistent data was obtained with the ITT Barton turbine meter. The swirl meters used at ambient temperatures appeared to be ineffective at cold temperatures and were not used during the low temperature program.

J. HIGH PROPELLANT TEMPERATURE TESTS

A series of tests between runs 1BN 750 and 759 evaluated the high temperature operating characteristics of the basic and low temperature designed hardware. The initial program required the evaluation of the hardware designed at 540°R (300°K) to be tested at approximately 800°R (444°K), the cold hardware 250°R (139°K) fuel and 375°R (208°K) oxidizer design was to be evaluated at approximately 600°R (333°K). The data from the two series of tests are shown in Table XLIII and indicate a high level of performance can be achieved. In fact, the data indicates that the results

TABLE XLIII
HIGH-TEMPERATURE TEST DATA

Fuel Position	Oxidizer Cup	Fuel Velocity Ratio (to Ambient Design)	Fuel Temp. °F	Fuel Temp. °K	Oxidizer Temp. °F	Oxidizer Temp. °K	Average I_{sp} lbf-sec/lbm	Average I_{sp} N-sec/kg	Remarks
Baseline	Ambient Design 1-1/2 Velocity	1-1/2	768	676	762	679	470	4609	7-1/2% Dump Cooling
Baseline	Cold Design 2 Velocity	2	660	623	670	628	456	4472	3% Dump Cooling

produce an inordinately high performance, which is partially attributed to the increased velocity of the fuel. However, the data indicate a near-theoretical achievement of performance which seems unlikely. Again, some conjecture must be made as to the accuracy of instrumentation at this higher level. An exercise was performed to correlate the difference in pressure drop between the high temperature and ambient temperature test series. No significant changes in the data seemed to be indicated from this exercise. Other exercises to examine data inputs, calibrate numbers and computer input values were as equally unproductive and it remained that the level of performance was a bit above that which was hoped for in the initial design.

K. IGNITION TESTS

Although the evaluation of ignition was not a stated program objective, the engine ignition characteristics are so intimately involved with operation that some evaluation was necessary just to establish test procedures. Further, the unique design of the reverse flow combustor warrants a re-evaluation of previous information to establish applicability. Previous testing with smaller thrusters of the reverse flow configuration had all been conducted with an ignition system incorporating an igniter plug, flush mounted in the wall of the combustion chamber. At a time coinciding with the beginning of this program, one of these company-developed units was tested at altitude at the Marshall Space Flight Center with substantial success, using the simple nonsequenced ignition system. Because of the success of the Marshall testing and the previously demonstrated company efforts at ambient pressures, a simple ignition system was used during this program.

This simple ignition system is described in Section VIII. Briefly, it consists of a 28-volt power source, a Bendix inductive exciter and a lead from the exciter to a flush mounted surface gap spark plug. A 1/8-inch (0.318 cm) line feeds oxidizer from the inlet housing. A small orifice provides oxidizer augmentation, completing the system. All of the altitude tests conducted on the program used an ignition system of this type or one with various innovations incorporated.

Although this system worked with great success, improvement was considered desirable. The first problem was the sensitivity of the ignitor plug to moisture. The exact method of moisture degradation was not identified but misfires did occur and the same plugs produced starts after drying in a vacuum oven. The result of this condition was to incorporate a drying procedure for use in the test cell, in addition to incorporating a capacitive discharge unit which would produce a higher peak spark power with the same energy level. Subsequently, a capacitive discharge system was installed and both the inductive and capacitive systems were used for most of the remaining tests. The exception to this

ignition arrangement occurred when we wanted to know whether either system would function individually. So, a series of tests were conducted with the capacitive discharge unit (GLA, Run 702-705) and also with the Bendix (Run 712) inductive discharge unit individually.

The results of these series of tests are interesting. No ignition malfunction was encountered. In fact, in the case of the ID system, the ignitions were immediate and reproducible and demonstrated the most desirable start characteristics of any series examined. A typical pulse obtained on this series is shown in Figure 137 where the small oscillation at the left side of the slope of the parameter is the ignition point. The test series was conducted with a slight delay incorporated into the fuel valve when it was determined that the normal sequence of propellants into the thrust chamber resulted in a slight fuel lead. Since it was desirable to initiate combustion with a zone rich in oxidizer, the delay was placed in the starting sequence to obtain a 0 to 1 msec oxidizer lead.

This sequence of events with the rapid spark cycling of the inductive discharge ignition system and the slight oxidizer lead produced excellent ignition and leads us to recommend that these two features be incorporated into a final design. Also, a spark system more tolerant to moisture accumulation leads to a further recommendation that a capacitive discharge system or some redesign of the igniter plug should be incorporated.

The tests just described yielded encouraging results for the recommendation of a simplified ignition system for this type of thruster; however, further testing was not accomplished to confirm these results. Leakage of the actuator seals of the valve required replacement of these units and the timing sequence necessary to achieve the results described earlier was not obtained again on the program. So, further efforts should be expended to define either the sequence of events leading to the satisfactory operation of the simple igniter system or, more broadly, to evaluate a torch ignition system similar to those developed under NASA-sponsored programs.

L. PROJECTED LIFE CYCLE CAPABILITY

The projected life cycle capability for each of the thrust chamber components was examined as to component temperatures obtained in test. The objective of the exercise, that a million cycles could be achieved, was in conformance with the work statement. For the sake of this analysis, the million cycles were interpreted to mean 900,000 pulses of approximately 50-msec duration and 100,000 pulses reaching steady-state temperatures. The 50-msec test value was defined on the basis that the steady state was not reached during that period of time resulting in a cold pulse. In combination with a duration requirement of 50 hours, the equation of evaluation used is:

$$N = \frac{900{,}000}{N_{fp}} + \frac{100{,}000}{N_{fs}} + \frac{50}{T_N}$$

where

N = number of cycles
N_{fp} = number of design pulses
N_{fs} = number of design steady-state tests
T_N = creep time (hr)

This equation was applicable to the regenerative portion of the nozzle which was considered to be the critical section from all design aspects. Temperatures obtained during the regeneratively cooled

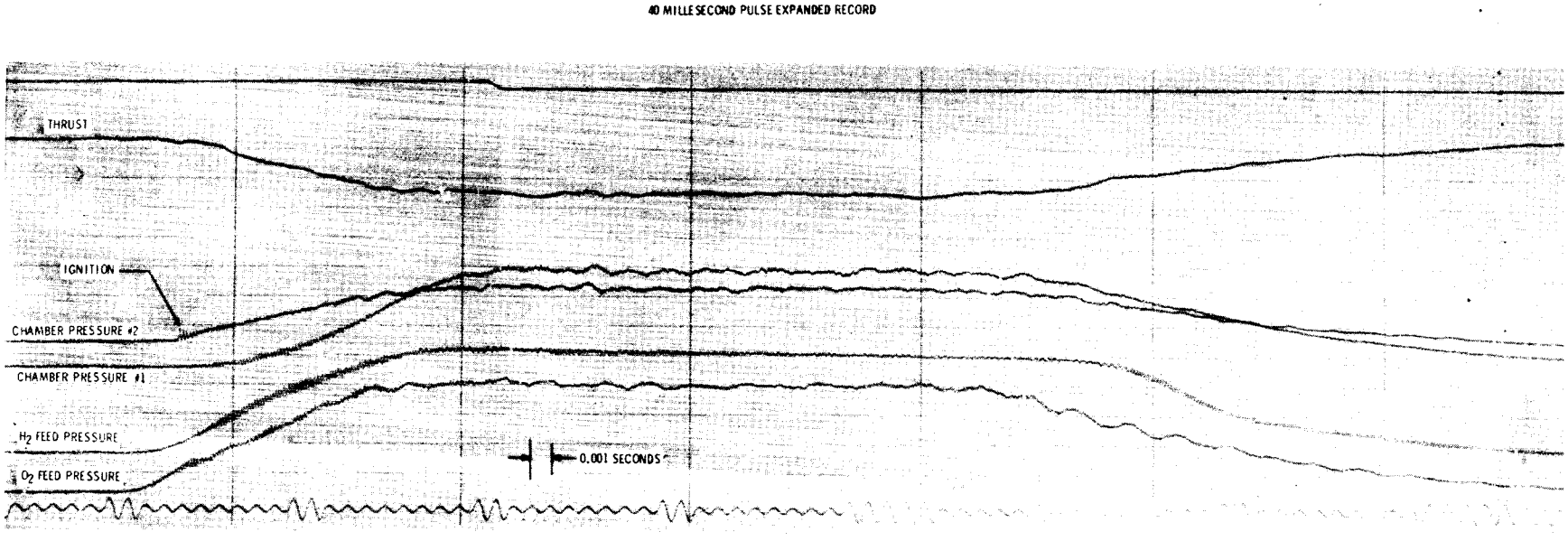

Figure 137. Typical Pulse

tests were used as the basis of extrapolation to duration. This value has been plotted in Figure 138 which shows that the previously mentioned 915°F (764°K) nozzle temperature goal would reach a value of N = 1 and just meet the required million-cycle capability. So, the value for the oxidizer 28° cup/cap combination plotted would show that the duration capability would be exceeded. In fact, the cumulative life would be exceeded greatly as shown in the third item of Table XLIV. Table XLIV also shows the resultant duration capability for each component of the thruster subsequent to testing. The figure shows that none of the designs suggested were critical to meeting the million-cycle capability.

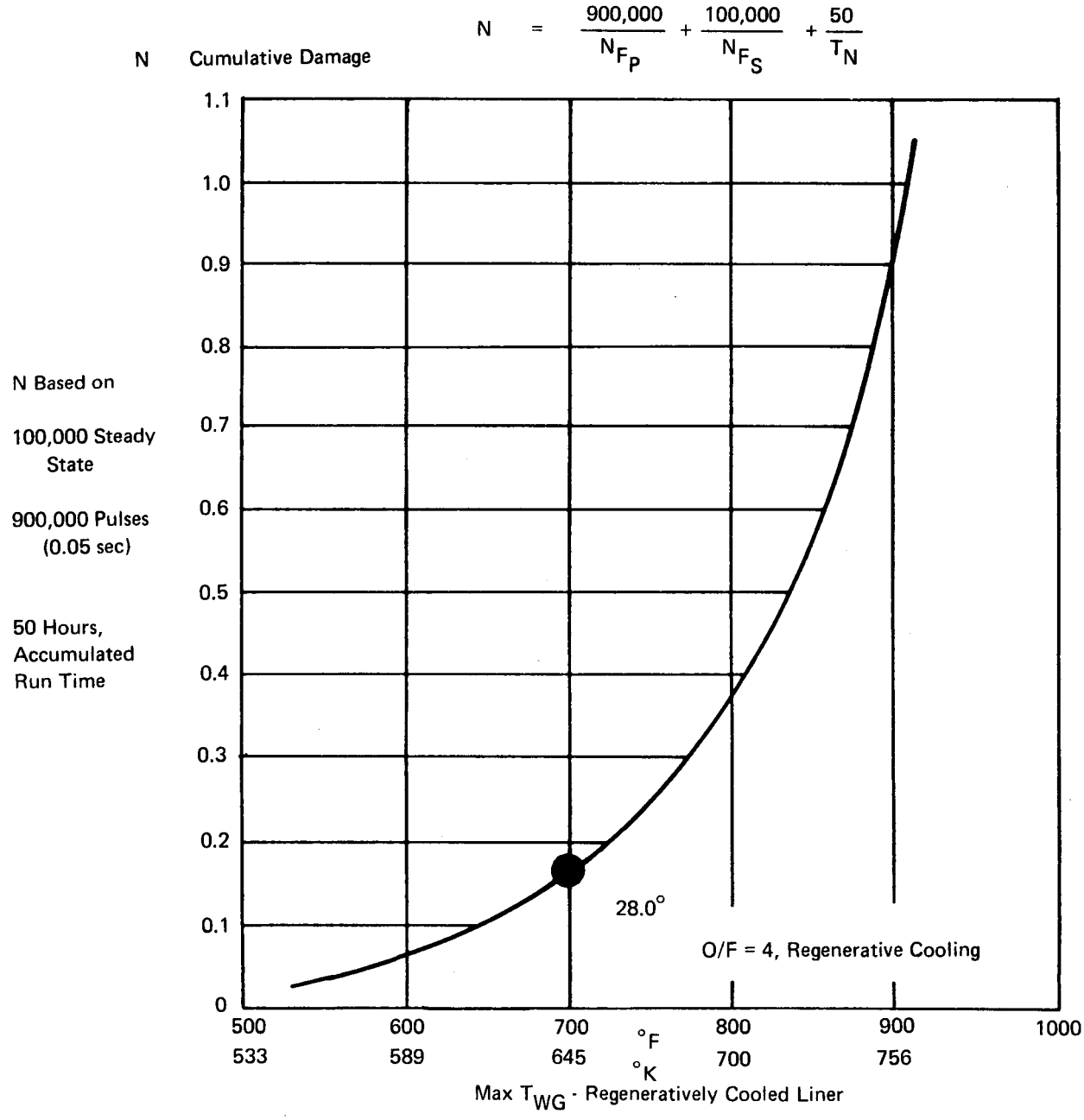

Figure 138. Predicted Cumulative Damage versus Temperature

TABLE XLIV
CYCLE CAPABILITY STUDY RESULTS

		Steady State Cycles (100,000)	Pulses (900,000)	Duration (50 Hr)
1	Ox Inlet	$>10^7$	——→	>50 Hr
2	Combustion Chamber	$>10^7$	——→	>50 Hr
3	Nozzle Liner	760,000	$\gg$900,000	>50 Hr
4	Nozzle Housing	$>10^7$	——→	>50 Hr
5	SS Type Nozzle Extension at 2100°F (1423°K)	$>10^6$	——→	>50 Hr

The durability was exceeded in enough cases that redesigns would appear to be applicable to reduce cost and weight. This led to additional configurations as shown in Table XLV. Although the Amzirc material clearly shows a margin over any nickel design proposed, the latter material was included due to the possible subjection of the hardware to reentry conditions producing temperatures too high for the Amzirc material. Table XLV was also used as a basis for preliminary design of a flight weight chamber.

TABLE XLV
NOZZLE SECTION CUMULATIVE DAMAGE CALCULATIONS

Configuration	Liner	Closeout	Jacket	Calculated Steady State (Pulse)* Firing Capability
Free Standing	Amzirc	Al Shroud or Ed Cu	SS	760,000 ($\geqslant 1 \times 10^7$)
Integral	Amzirc	Ed Cu	SS	490,000 (9×10^6)
Integral	Td Ni	Ed Ni ——→ Ed Cu	 SS	23,000 16,000
Free Standing	Td Ni	Al Shroud	SS	100,000

*0.050 sec Pulse Width Ed = Electro Deposited

M. POST TEST HARDWARE EXAMINATION

The post test condition of the altitude hardware was in excellent condition. There was some minor erosion during the tests, but it was related to either the investigative nature of the hardware or to a condition limit encountered during test.

The two most observable hardware descrepancies were related to a cold test condition and long duration operation, respectively. Both resulted in combustion chamber erosion. The first, cold temperature, incidence was noted on test 1BN686. It was suspected that some slushing or liquification of the oxidizer occurred inadvertently. On this test contamination of the fuel passages was known to have occurred. The result was a chamber erosion streak attributed to both conditions coming about at the same time. The second incidence was quite minor with erosion about one spark plug occuring on the long insulated test. This occurrence was attributed to a faulty installation, as there were no signs of similar erosion on the second plug.

Further remarks related to the combustion chamber were that the post test surface condition remained smooth with some heat marks but no regions presented concern. One area at the fuel orifice was examined for redesign as small indentations occurred in the chamber wall in line with the land between the slot orifice. No real concern was given to this condition even though a redesign was incorporated as a part of the long, buried chamber test. This redesign consisted of recessing the nozzle lands so that some cross flow across the orifice exit would occur. Examination of test results indicates that the modification was moderately successful from the standpoint of erosion but also resulted in a minor loss of performance. A further redesign of this exit seems warranted.

a. The Amzirc nozzle liners and components were in excellent condition at the conclusion of testing. The O-ring seals, designed to permit thermal growth of the liner, may require redesign for extended and repeated operation. (The seals were in excellent condition following the 500-second duration test.)

b. The oxidizer injector, both cup and cap, were in excellent condition at the conclusion of testing. No problems are anticipated using the welded assembly.

c. The spark plug installation was redesigned from an uncooled configuration to one cooled with oxygen. The redesign was necessitated when spark plug overheating occurred on some of the extended tests. The oxygen cooled configuration was successfully evaluated on the 500-second test. This cooling arrangement is applicable for the spark plug installation as well as for a torch igniter configuration. A redesign assembly change is advisable to preclude oxygen leakage around this installation.

d. Two types of nozzle extensions (water cooled and radiation cooled) were used on this program with excellent results. The first was a drilled, water-cooled, aluminum design which allowed the measurement of the overall nozzle extension heat rejection. This hardware held up well and was in excellent condition at the conclusion of testing.

   The second design was a columbium nozzle with an oxidation-resistant coating. This lightweight nozzle was considered attractive for a flightweight configuration. It was exposed to 2115 seconds of firing time including a continuous 500-second, buried-firing duration. The extension was also exposed to a 2500-cycle, pulse-mode operation of 50 milliseconds on time and 100 milliseconds off time per pulse. A total of 3400 starts were made on the extension.

No problems were encountered with the columbium nozzle extension or its coating. At the conclusion of testing this hardware was also in excellent condition.

e. Off-the-shelf Flodyne ball type valves were used throughout the test program. Results were good. Some problems were encountered when the valve opening and closing times were 4 milliseconds or less. The ball actuating shaft failed in shear after varying amounts of cycle time. This problem was resolved by shaft redesign and by slower operating times. Some seat leakage was encountered at high and low temperatures but this was attributed to improper seals since these valves were not modified specifically for the program.

XIII. PULSING TESTS

A. GENERAL

The pulsing test program was performed to evaluate the response and capability of operation in pulse mode of the reverse flow, 1500 pound (6672N) thrust APS engine.

The engine configuration used for this evaluation was that selected for the thrust chamber cooling testing. The only change incorporated was the use of blow-down operation of the test stand which in turn did not affect the engine hardware in any way. The pulse testing consisted of three groups of short duration firings. The first group established pulse performance as a function of the on-off duty cycle with a baseline engine configuration. The second group was used to evaluate engine modifications to improve pulse mode operation. The last group provided a limited demonstration of pulse operation endurance, and off-design. Firings of 1 second to 30 milliseconds duration were made with 0.1, 1, 5, and 30 seconds between pulses.

Test data for the pulse series were obtained by a blow-down method. The propellant feed system was stabilized, measured and then a blow-down pulse series made. Remeasuring of the system after the test determined propellant expended for the series.

Engine operating conditions, pressures and temperatures, and timing data such as time from valve opening to engine ignition, time to 90% P_C etc., further characterized the pulse mode operation. The pulse mode tests conducted are shown in Table XLVI. Table XLVII lists the test conditions, while Table XLVIII is a summary of pulse data, and Table XLIX lists the individual pulse impulse data.

The Group I tests consisted of durations as short as 30 milliseconds to demonstrate operation approaching 50 lb-second (222.4 N-sec) impulse. This group also identifies pulse series which provide an indication of the I_{sp} average for engine operation heated from previous pulses and pulse operation with the engine hardware at ambient temperature at the start of the pulse series.

Group II presents pulse testing to assess changes to engine operating characteristics which may become desirable as a result of initial testing. Initial test results indicated the desirability of investigating propellant sequence which was performed in this group.

The Group III tests provided O/F and average I_{sp} data for operation at P_C = 300 (206.8 N/cm ^{2}), at mixture ratios of 3, 4, and 5. It also provided endurance demonstration with a continuous 2500 pulse series (0.05 second on an 0.10 second off).

B. TEST SETUP

1. Hardware Configuration

The thrust chamber configuration tested incorporated components selected from the results of the thrust chamber cooling program. A diagram of the assembly is shown in Figure 139 and photograph of the engine installed in the altitude test cell in Figure 140. Thrust chamber components varied during testing included the oxidizer cup/cap combination and the regeneratively cooled nozzle. The nozzle changes were made to vary the nozzle divergence dump cooling, and also to incorporate the nozzle designed for cold testing. The oxidizer parts used are as follows:

TABLE XLVI
PULSE MODE TESTS CONDUCTED

Group I	On Time (sec)	Off Times (sec) 1	5	30
I-1	1.00	6	3	3
	0.40	4	4	4
I-2	0.40			(B) 5
I-3	0.10			(B) 15
I-4	0.05			(B) 15
I-5.1	0.10	(B) 20		
I-5.2	0.10		(B) 20	
I-6.1	0.05	(B) 20		
I-6.2	0.04	(B) 20		
I-6.3	0.03	(B) 20		
I-6.4	0.40	(B) 5		
Group II				
II-1	0.1		(B) 20	2ms Fuel Delay*
II-2	0.04	(B) 20		2ms Fuel Delay*
II-3	0.1		(B) 20	4ms Fuel Delay*
II-4	0.04	(B) 20		
Group III				
III-1	0.1	(B) 20	(r = 3.0)	
III-2	0.1	(B) 20	(r = 5.0)	
III-3.1	2500 at 0.05 On and 0.1 Off (r = 4.0; P_c = 300 psi (206.8 N/cm^2)			
III-3.2	0.1	(B) 20		

*Delay references current setup (10/1/71) which at best has 2 ms fuel lead in test chamber.

(B) Blow-Down Operation

LEGEND

B	Bendix Excitor
BR	Bendix Recessed 0.170 in.
BFA	Bendix, Flush Mounted, Oxidizer Augmentation
G	GLA Excitor
GR	GLA, Recessed 0.170 in.
GFA	GLA, Flush mounted, oxidizer augmentation
GFAV	GLA, Flush mounted, oxidizer augmentation, variable output

* 1 second blow-down test data taken at beginning and end of test.

TABLE XLVII
PULSE MODE TEST CONDITIONS (1 of 2)

Test No.	On/Off Time sec	Total No. of Pulses	$R_{o/f}$	P_c psia	Total Impulse lb-sec / N-sec	Avg Imp. per Pulse lb-sec / N-sec	Avg. I_{sp} lb-sec/lb / N-sec/kg	Inst. I_{sp} lb-sec/lb / N-sec/kg	OLT °R / °K	FLT °R / °K	Ign. Sys. No. 1	Ign. Sys. No. 2	Chamber	Oxid. Cup	Oxid. Cap	Fuel Inj.	Nozzle Ext.
702	1/2	15	4.1	305	-	-	-	434 3944	509/483 283/268	503/438 279/243	-	GFA	020-5	018-1	019-1 (10%)	046-7B (3% D)	056-1 (RAD)
703	1/2	15	4.1	303	-	-	-	437 3971	529/508 204/282	517/466 287/259	-	GF					
704	1/2	15	4.1	304	-	-	-	435 3953	517/497 232/276	504/461 280/256	-	GR					
705	1/2	15	4.2	310	-	-	-	436 3962	509/486 283/270	484/450 269/250	-	GRA					
712	1/2	15	3.8	307	-	-	-	439 3989	532/527 296/293	528/525 293/292	-	BFA				046-7B (9% D)	
717	1/1	6	4		9979 44387	1665 7397	-	-	530 294	531 295	GFA						
718	1/5	3	4		5026 22356	1675 7450	-	-	531 295	540 300							
719	1/30	2			3354 14919	1677 7459	-	-	529 294	539 299							
720	0.4/1	4			2633 11712	658 2927	-	-	530 294	533 296							
721	0.4/5	4			2676 11903	669 2976	-	-	530 294	538 299							
722	0.4/30	3			1999 8892	666 2962	-	-	530 294	538 299							
725	0.4/30	5			3071 13660	614 2731	418.5 3802.8	-	530 294	534 297							
726	0.1/30	15			2456 10924	164 729	412.0 3743.7	-	535 297	536 298							
727	0.05/30	13			1259 5600	94 418	413.4 3756.4	-	531 295	530 294							
728	0.1/5	19			3156 14038	166 738	413.3 3755.5	-	531 295	531 295							
729	0.1/1	20			3301 14683	165 734	430.1 3908.2		531 295	531 295							
730	0.05/1	18			1673 7442	94 418	440.0 3998.1	-	531 295	531 295							
731	0.04/1	20			1542 6859	77 342	-	-	529 294	529 294							
732	0.03/1	11			635 2824	58 258	406.5 3693.7	-	528 293	528 293							
733	0.4/1	4			2494 11093	623 2771	-	-	526 292	526 292							
734	0.1/5	20			3344 14874	167 743	422.0 3834.6	-	528 293	530 294							
735	0.04/1	20			1570 6983	79 351	410.8 3732.8	-	523 291	526 292							

Not Available as Test Data - Nominal Test Condition Mixture Ratio (4)

Not Available as Test data - Nominal Test Condition 300 psia

TABLE XLVII
PULSE MODE TEST CONDITIONS (2 of 2)

Test No.	On/Off Time sec	Total No. of Pulses	Ro/f	P_c psia	Total Impulses lb-sec / N-sec	Avg. Imp. per Pulse lb-sec / N-sec	Avg. I_{sp} lb-sec/lb / N-sec/kg	Inst. I_{sp} lb-sec/lb / N-sec/kg	OLT °R / °K	FLT °R / °K	Ign. Sys. No. 1	Ign. Sys. No. 2	Chamber	Oxid. Cup	Oxid. Cap	Fuel Inj.	Nozzle Ext.
736	0.1/5	20	Not Available	↑ Not Available as Test Data - Nominal Test Condition 300 Psia	3348 14892	167 743	446.0 4052.7	-	523 291	525 292	GFA	BFA	020-5	018-1	019-1 (10%)	046-7B (9% D)	056-1 (RAD)
737	0.04/1	20			1568 6974	79 351	438.1 3980.9	-	524 291	525 292							
738	0.03/1	17	4		1034 4599	61 267	409.7 3722.8	-	528 293	526 292							
739	0.4/1	5	4		3205 14256	641 2851	-	-	526 292	525 292							
740	0.1/1	19	3		3187 14176	168 747	429.2 3900.0	-	525 292	525 292							
741	0.1/1	19	5		3237 14398	180 801	439.1 3990.0	-	532 296	532 296							
742	0.05/0.1	122	4		-	-	-	-	530 294	530 294							
744	0.05/0.1	420	4		-	-	-	-	530 294	530 294				018-1W	019-1W	046-7C (7 1/2% D)	
745	0.05/0.1	2500	4		-	95	-	-	527 293	526 292							
747	0.1/1	20	4		3527 15688	176 783	-	-	539 299	530 294	GFA	BFA	020-5	018-1W	019-1W	046-7C	056-1
775	2/1	15	4		-	-	-	-	375 208	250 139	GFA	BFA	093-1	018-13	019-1	092-1 (3% D)	
776	2/1	15	4		-	-	-	-	375 208	250 139	-	G FAV	093-1	018-11	019-11		
785	0.2/1	15	4	↓	4518 20096	301 1339	-	-	375 208	250 139	-	G FAB	093-1	018-11	019-11	092-1 (3% D)	056-1

TABLE XLVIII
SUMMARY PULSE DATA – INFINITE ALTITUDE

Run IBN	Group	No. of Pulses	On Time	Off Time	Impulse lb-Sec	Impulse N-Sec	Average Specific Impulse I_T Integral W_T (lbf/sec)/(lbm)	N-Sec/kg	Impulse/Pulse (AVG) lb-Sec	Impulse/Pulse (AVG) N-Sec
732	I-6.3	11	0.03	1	635	2,829.62	406.5	3,986.33	58	258.00
738	I-6.3	17	0.03	1	1034	4,599.46	409.7	4,017.72	61	271.33
731	I-6.2	20	0.04	1	1542	6,859.16	-		77	342.50
735	II-2	20	0.04	1	1570	6,893.71	410.8	4,028.50	79	351.39
737	II-4	20	0.04	1	1568	6,974.81	438.1	4,295.24	79	351.39
727	I-4	13	0.05	30	1259	5,600.30	413.4	4,054.00	94	418.11
730	I-6.1	18	0.05	1	1673	7,441.87	440.0	4,314.85	94	418.11
742	III-3.1	144	0.05	0.1	-	-	-	-	-	418.11
744	III-3.1	420	0.05	0.1	-	-	-	-	-	418.11
745	III-3.1	2500	0.05	0.1	-	-	-	-	95	422.56
726	I-3	15	0.10	30	2456	11,916.80	412.0	4,040.27	164	729.51
728	I-5.2	19	0.10	5	3156	14,038.60	412.3	4,043.21	166	738.40
729	I-5.1	20	0.10	1	3301	14,673.60	430.1	4,217.77	165	733.96
734	II-1	20	0.10	5	3344	14,874.80	422.0	4,138.34	167	742.82
736	II-3	20	0.10	5	3348	14,892.60	446	4,373.79	167	742.82
740	III-1	19	0.10	1	-	-	-	-	-	742.82
741	III-2	19	0.10	1	3237	14,398.90	439.1	4,306.03	180	800.64
747	III-3.2	20	0.10	1	3527	15,688.90	329.1 *	3,727.28	176	782.85
720	-	4	0.40	1	2633	11,712.20	-	-	658	2,926.93
721	-	4	0.40	5	2676	11,916.80	-	-	669	2,975.85
722	-	3	0.40	30	1999	8,891.99	-	-	666	2,962.52
725	I-2	5	0.40	30	3071	13,660.50	418.5	4,104.01	614	2,731.21
733	I-6.4	4	0.40	1	2494	11,093.90	-		623	2,771.23
739	I-6.4	5	0.40	1	3205	14,256.50	-		641	2,855.76
717	-	6	1.00	1	9979	44,388.80	-		1663	7,397.39
718	-	3	1.00	5	5026	22,356.80	-		1675	7,450.77
719	-	2	1.00	30	3354	14,919.30	-		1677	7,459.66

* Flow Data Questionable

TABLE XLIX
INDIVIDUAL PULSE IMPULSE DATA - INFINITE ALTITUDE (Sheet 1 of 4)

Run 1BN	717		718		719		720		721		722		725	
	Impulse/Pulse													
On/Off (sec)	1/1		1/5		1/30		0.4/1		0.4/5		0.4/30		0.4/30	
Pulse No.	lb sec	N sec	lb sec	N sec	lb sec	N sec	lb sec	N sec	lb sec	N sec	lb sec	N sec	lb sec	N sec
1	1679	7468.56	1686	7499.70	1677	7459.66	658	2926.93	664	2953.62	666	2962.52	638	2837.96
2	1643	7308.43	1663	7397.39	1677	7459.66	655	2913.58	667	2966.96	667	2966.96	618	2749.00
3	1660	7384.05	1677	7459.66			656	2918.03	671	2984.76	-	-	615	2735.66
4	1667	7415.18					664	2953.62	674	2998.10	666	2962.52	602	2677.83
5	1672	7437.42											598	2660.04
6	1658	7375.15												
7														
8														
9														
10														
11														
12														
13														
14														
15														
16														
17														
18														
19														
20														
Total Impulse	9979	44,388.8	5026	22,356.8	3354	14,919.3	2633	11,712.2	2676	11,916.8	1999	8891.99	3071	13,660.5
Avg. Impulse per Pulse	1663	7397.39	1675	7450.77	1677	7459.66	658	2926.93	669	2975.85	666	2962.52	614	2731.21
Average Specific Impulse $\frac{\text{N sec}}{\text{kg}}$ (sec)	-	-	-	-	-	-	-	-	-	-	-	-	418.5	4104.0

TABLE XLIX

INDIVIDUAL PULSE IMPULSE DATA - INFINITE ALTITUDE (Sheet 2 of 4)

Run 1BN	726		727		728		729		730		731	
Pulse No.	Impulse/Pulse											
On/Off (sec)	0.1/30		0.05/30		0.1/5		0.1/1		0.05/1		0.04/1	
Pulse No.	lb sec	N sec	lb sec	N sec	lb sec	N sec	lb sec	N sec	lb sec	N sec	lb sec	N sec
1	167	742.82	93	413.66	-	-	171	760.61	-	-	78	346.94
2	168	747.26	94	418.11	170	756.16	168	747.26	-	-	78	346.94
3	164	729.47	94	418.11	168	747.26	166	738.37	94	418.11	79	351.39
4	167	742.82	93	413.66	169	751.71	167	742.82	94	418.11	78	351.39
5	159	707.23	93	413.66	170	756.16	169	751.71	93	413.66	78	351.39
6	166	738.37	94	418.11	169	751.71	168	747.26	94	418.11	78	351.39
7	163	725.02	95	422.56	170	756.16	168	747.26	94	418.11	78	351.39
8	164	729.47	-	-	169	751.71	166	738.37	93	413.66	79	342.50
9	164	729.47	94	418.11	167	742.82	166	738.37	92	409.22	78	351.39
10	165	733.92	94	418.11	165	733.92	164	729.47	94	418.11	76	338.05
11	162	720.58	93	413.66	165	733.92	163	725.02	94	418.11	78	351.39
12	162	720.58	94	418.11	168	747.26	165	733.92	93	413.66	76	338.05
13	160	711.68	93	413.66	165	733.92	165	733.92	93	413.66	76	338.05
14	163	725.02	92	409.22	164	729.47	164	729.47	93	413.66	76	351.39
15	162	720.58	-	-	163	725.02	163	725.02	92	409.22	76	338.05
16					163	725.02	162	720.58	93	413.66	76	338.05
17					163	725.02	160	711.68	93	413.66	76	338.05
18					164	729.47	161	716.13	92	409.22	76	338.05
19					163	725.02	162	720.58	92	409.22	76	338.05
20					162	720.58	160	711.68	92	409.22	76	338.05
Total Impulse	2456	11,916.8	1259	5600.30	3156	14,038.6	3301	14,673.6	1673	7441.87	1542	6859.16
Avg. Impulse per Pulse	164	729.47	94	418.11	166	738.37	165	733.92	94	418.11	77	342.50
Average Specific Impulse (sec) $\frac{\text{N sec}}{\text{kg}}$	412.0	4040.3	413.4	4054.0	412.3	4043.2	430.1	4217.8	440.0	4314.8	-	-

TABLE XLIX
INDIVIDUAL PULSE IMPULSE DATA - INFINITE ALTITUDE (Sheet 3 of 4)

Run	732		733		734		735		736		737	
	Impulse/Pulse											
On/Off (sec)	0.03/1		0.4/1		0.1/5		0.04/1		0.1/5		0.04/1	
Pulse No.	lb sec	N sec	lb sec	N sec	lb sec	N sec	lb sec	N sec	lb sec	N sec	lb sec	N sec
1	-	-	-	-	172	765.06	80	355.84	170	756.16	80	355.84
2	-	-	637	2833.52	171	760.61	80	355.84	172	765.06	80	355.84
3	-	-	622	2766.79	171	760.61	78	346.94	170	756.16	79	351.39
4	-	-	623	2771.23	169	751.71	79	351.39	171	760.61	77	342.50
5	-	-	612	2722.31	171	760.61	78	346.94	171	760.61	80	355.84
6	-	-			170	756.16	79	351.39	171	760.61	80	355.84
7	-	-			170	756.16	80	355.84	168	747.26	80	355.84
8	59	262.44			168	747.26	80	355.84	168	747.26	79	355.84
9		-			168	747.26	79	351.39	168	747.26	79	351.39
10	59	262.44			167	742.82	79	351.39	168	747.26	79	351.39
11	-	-			166	738.37	78	346.94	166	738.37	79	346.94
12	57	253.55			166	738.37	78	346.94	167	742.82	78	346.94
13	58	258.00			166	738.37	78	346.94	166	738.37	78	346.94
14	56	249.10			165	733.92	79	351.39	167	742.82	78	346.94
15	57	253.55			164	729.47	78	346.94	166	738.37	76	388.05
16	58	258.00			165	733.92	78	346.94	163	725.02	78	346.94
17	58	258.00			166	738.37	77	342.50	167	742.82	78	346.94
18	58	258.00			164	729.47	77	342.50	163	725.02	77	342.50
19	57	253.55			163	725.02	77	342.50	165	733.92	76	338.05
20	58	258.00			162	720.58	77	342.50	162	720.58	76	720.58
Total Impulse	635	2824.2	2494	11093.9	3344	14874.8	1570	6983.71	3348	14892.6	1568	14892.6
Average Impulse Per Pulse	58	258.00	623	2771.23	167	742.82	79	351.39	167	742.82	79	742.82
Average Specific Impulse (sec) $\frac{\text{N sec}}{\text{Kg}}$	406.5	3986.33	-	-	422.0	4138.34	410.8	4028.50	446.0	4373.79	438.1	4373.79

*Flow Data Questionable

TABLE XLIX

INDIVIDUAL PULSE IMPULSE DATA - INFINITE ALTITUDE (Sheet 4 of 4)

Run	738		739		740		741		747		785	
	Impulse/Pulse											
On/Off (sec)	0.03/1		0.4/1		0.1/1		0.1/1		0.1/1		0.2/1	
Pulse No.	lb sec	N sec	lb sec	N sec	lb sec	N sec	lb sec	N sec	lb sec	N sec	lb sec	N sec
1	-	-	670	2980.31	-	-	-	-	180	800.64	299	1330.02
2	-	-	647	2878.00	173	769.50	175	778.40	181	805.09	307	1365.60
3	61	271.33	637	2833.52	171	760.61	175	778.40	181	805.09	300	1334.47
4	61	271.33	629	2797.93	171	760.61	175	778.40	182	809.54	307	1365.60
5	60	266.89	622	2766.79	169	751.71	174	773.95	179	796.19	300	1334.47
6	61	271.33			170	756.16	171	760.61	179	796.19	297	1321.12
7	61	271.33			169	751.71	170	756.16	181	805.09	299	1330.02
8	61	271.33			168	747.26	169	751.71	178	791.74	298	1325.57
9	61	271.33			168	747.26	171	760.61	177	787.30	299	1330.02
10	62	275.78			169	751.71	169	751.71	176	782.85	299	1330.02
11	62	275.78			169	751.71	170	756.16	176	782.85	302	1343.36
12	61	271.33			167	742.82	170	756.16	175	778.40	299	1330.02
13	60	266.89			166	738.37	170	756.16	174	773.95	305	1356.71
14	-	-			166	738.37	170	756.16	176	782.85	302	1343.36
15	60	266.89			166	738.37	170	756.16	175	778.40	309	1374.50
16	61	271.33			165	733.92	169	751.71	174	773.95		
17	62	275.78			165	733.92	168	747.26	174	773.95		
18	61	271.33			165	733.92	167	742.82	172	765.06		
19	61	271.33			166	738.37	168	747.26	169	751.71		
20	61	271.33			164	729.47	166	708.37	169	751.71		
Total Impulse	1034	4599.46	3205	14256.5	3187	14176.5	3237	14398.9	3527	15688.9	4518	20097.1
Average Impulse Per Pulse	61	271.33	641	2855.76	168	747.26	180	800.64	176	782.85	301	1338.91
Average Specific Impulse (sec) $\frac{\text{N sec}}{\text{Kg}}$	409.7	4017.72	-	-	429.2	4208.94	439.1	4306.3	329.1*	3727.28*	-	-

*Flow Data Questionable

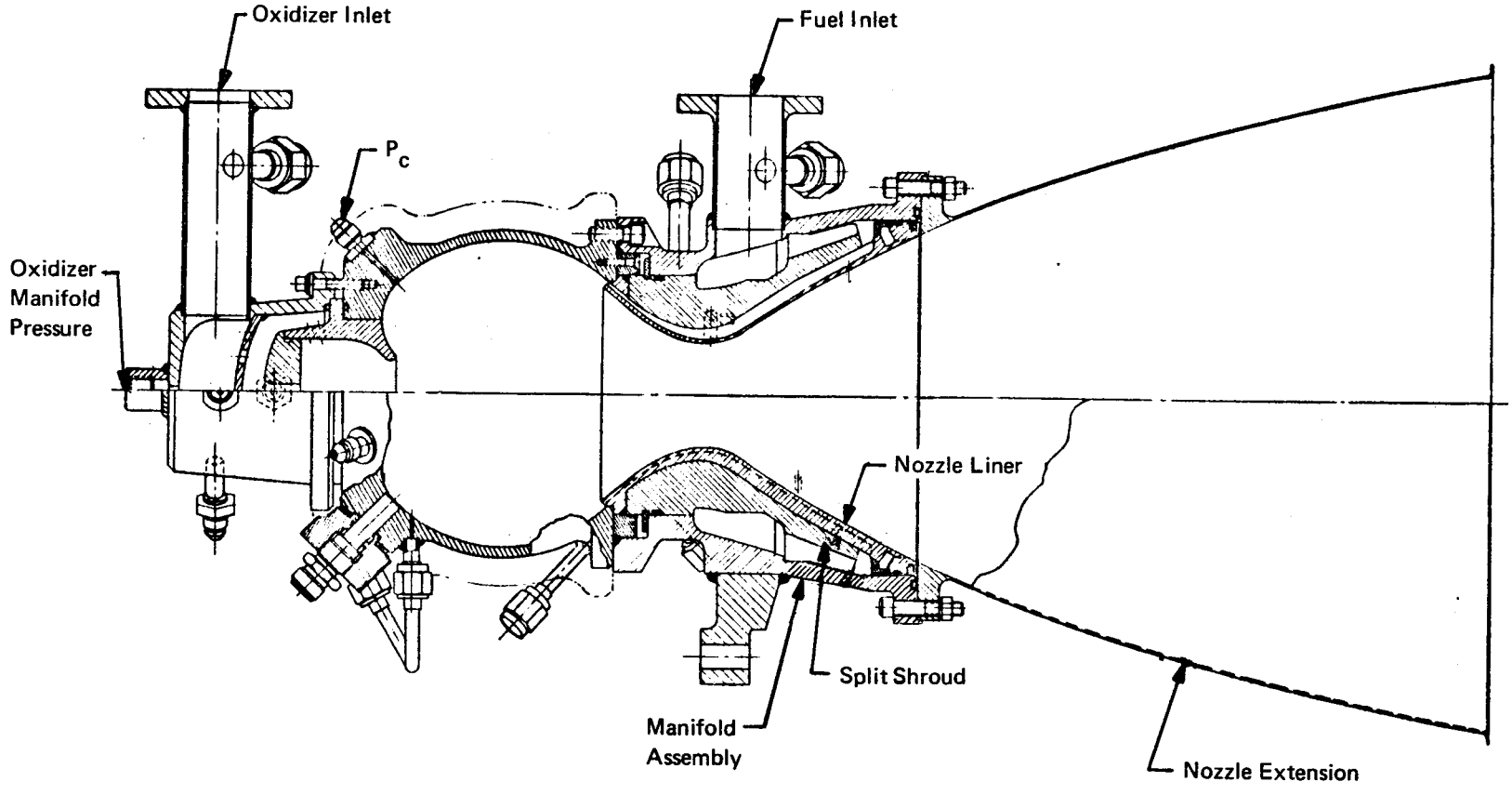

Figure 139. 1500-lb (6672 N) Thrust Altitude Test Assembly – Cb Extension

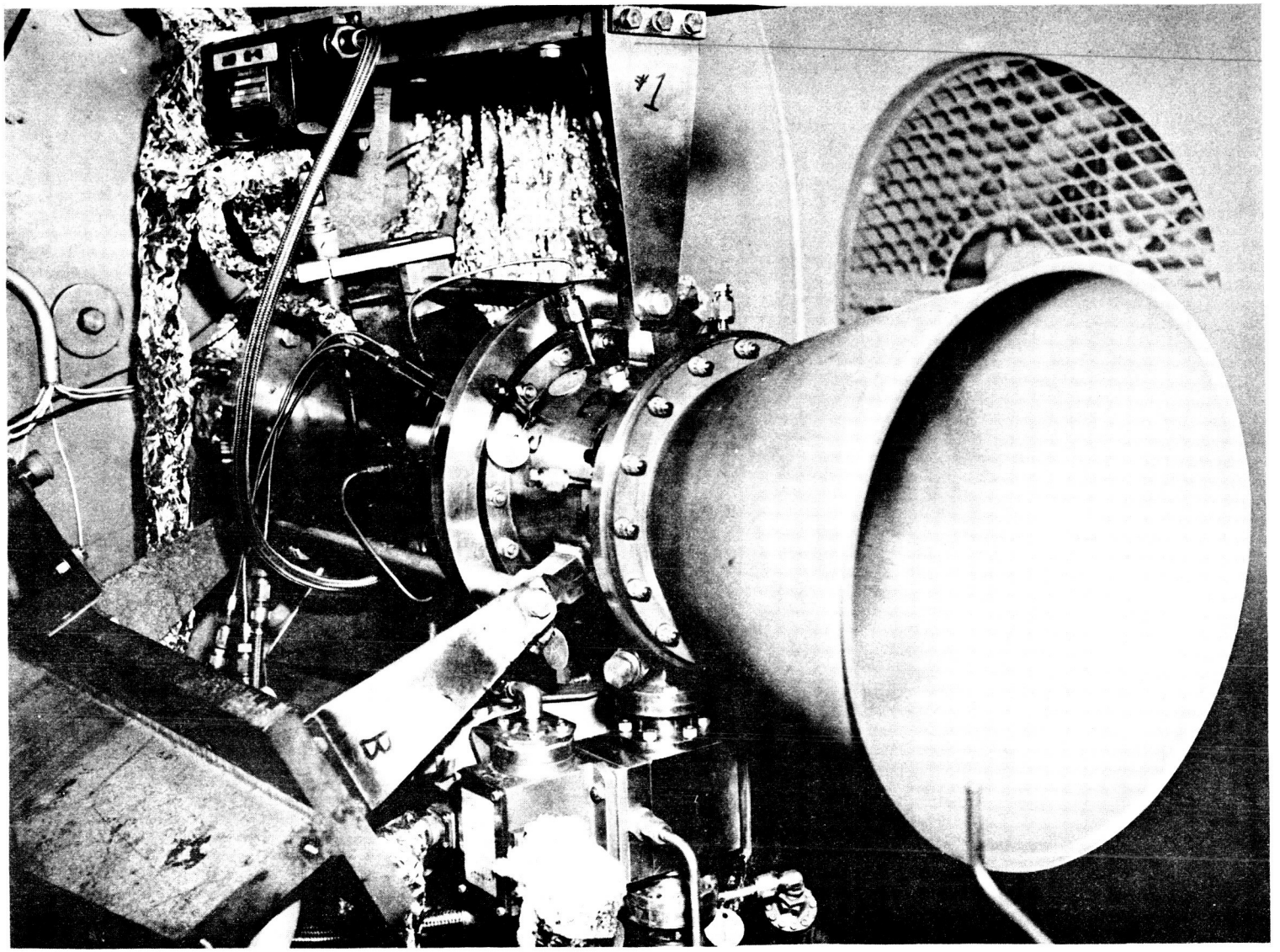

Figure 140. 1500-lb (6672 N) Thrust Engine Installed in Altitude Test Cell

Part No./Name

8636-473018-1/Cup
8636-473019-1/Cap (10% C.F.)

8636-473018-13/Cup
8636-473019-1/Cap (10% C.F.)

The regeneratively cooled nozzle sections used, included the following:

Part Number	% Dump Coolant
8636-470046-7A	3
8636-470046-7B	9
8636-470047-7C	7 1/2
8636-4700092-1	3

The chamber used, 8636-470020-5, had a characteristic length of 32 inches (81.3 cm).

a. Ignition System

The same Bendix and General Laboratory Associates ignition systems were used on the pulse test program as on the thrust chamber cooling tests. The best characteristics of ignition from the cooled chamber altitude test program were incorporated into the start system for the pulse testing. This included flush mounted spark plugs with oxidizer augmentation.

The ignition system assembly consisted of redundant, exciters, harnesses, and spark plugs. One exciter was a Bendix unit and the other a GLA unit. The Bendix and GLA harnesses were interchangeable and selection was based on availability. Both Bendix and Champion spark plugs were used and again selection was based on availability.

A typical flush mounted spark plug with oxidizer augmentation is shown in Figure 139. The augmentation is upstream of the spark plug and is swept across the spark plug by the reverse flow of the fuel. The nominal characteristics of the system are given in Table L.

TABLE L
IGNITION SYSTEM

	Bendix	GLA
Input Voltage	24 vdc	24 vdc
Storage Energy	79 millijoules	50 millijoules
Spark Rate	850 sps	210 sps
Input Current	5.0 amps peak	5 amps peak
Pulse Duration	0.5 milliseconds	2 milliseconds
Spark Plug		
Annular Gap	0.05 inch(0.127cm)	
Energy	11 millijoules	
Breakdown Voltage (Sea Level)	2400 vdc	

C. DISCUSSION OF TEST RESULTS

A total of 33 pulse tests were performed with the number of pulses made in each test varying from 3 to 2500. The total number of pulses obtained was approximately 3400. Pulse "on" times were varied from 30 milliseconds to 1.0 second. "Off " times were varied from 0.1 second to 30 seconds. All tests were performed at altitude.

In summary, pulse repeatability was excellent and impulse per pulse for a given "on" time did not vary more than 7.9%. Pulse repeatability within a pulse series with good ignition characteristics was also good and was within 6%. This repeatability was considered excellent considering the manner in which the data were taken. No previous experience had been logged with the test facility. In addition a blow-down system does not normally produce the accuracy attributed to a steady-state measuring system.

1. Pulse Specific Impulse Versus On/Off Time

One objective of the pulse test was to determine the effects of pulse "on/off" times on performance. Table XLVIII shows the pulse data grouped by "on" times which were varied from 0.030 second to 1.00 second and Figure 141 is a plot of specific impulse versus pulse "on" time for various "off" times between pulses. The data are shown in comparison to predicted values for pulses with fixed transient lossess.

An examination of these data would not produce much confidence in the repeatability of the test data. However, a comparison to the predicted curves indicates the data fall in a bandwidth approximately ±5% wide.

This scatter of data for this type of testing is not unusual. Without a more rigorous analysis, a discussion of accuracy is premature; but the ±5% value for scatter could be used as a reasonable approximation.

2. Impulse Versus Pulse Width

The impulse data, which were computed by integrating thrust (See Appendix A on data reduction methods), showed that impulse per pulse versus pulse "on" time to be linear. This indicates the start and shutdown transient impulse is repetitive even for 30-millisecond pulses. The data are shown in Figure 142 and Table XLVIII and XLIX.

Two 20-pulse test series were made at a 30-millisecond "on", 1-second "off", duty cycle. The average impulse/pulse for each of the two series was 58 and 61 lb-sec (258.0 and 271.3 N-sec). The maximum variation within a pulse series was 3 lb-sec (13.3 N-sec) or less than 6%. The data indicate that a 50 lb-sec (222.4 N-sec) pulse can be achieved with a pulse "on" time of slightly less than 30 milliseconds.

Three 20-pulse test series were made at a 40 millisecond "on", 1 second "off", duty cycle. The average impulse/pulse for each of the three series was 77, 79, and 79 lb-sec (342.5, 351.4 and 351.4 N-sec) and maximum variation within a pulse series was 3 lb-sec (13.3 N-sec) or 4%.

Five pulse series were made with 50 millisecond "on" times and "off" times of 0.1 to 30 seconds. The number of pulses varied from 13 to 2500. The average impulse/pulse ranged from 94 to 95 lb-sec (418.1 and 422.6 N-sec) with a maximum variation within a pulse series of 6 lb-sec (26.7 N-sec) or 6.5%.

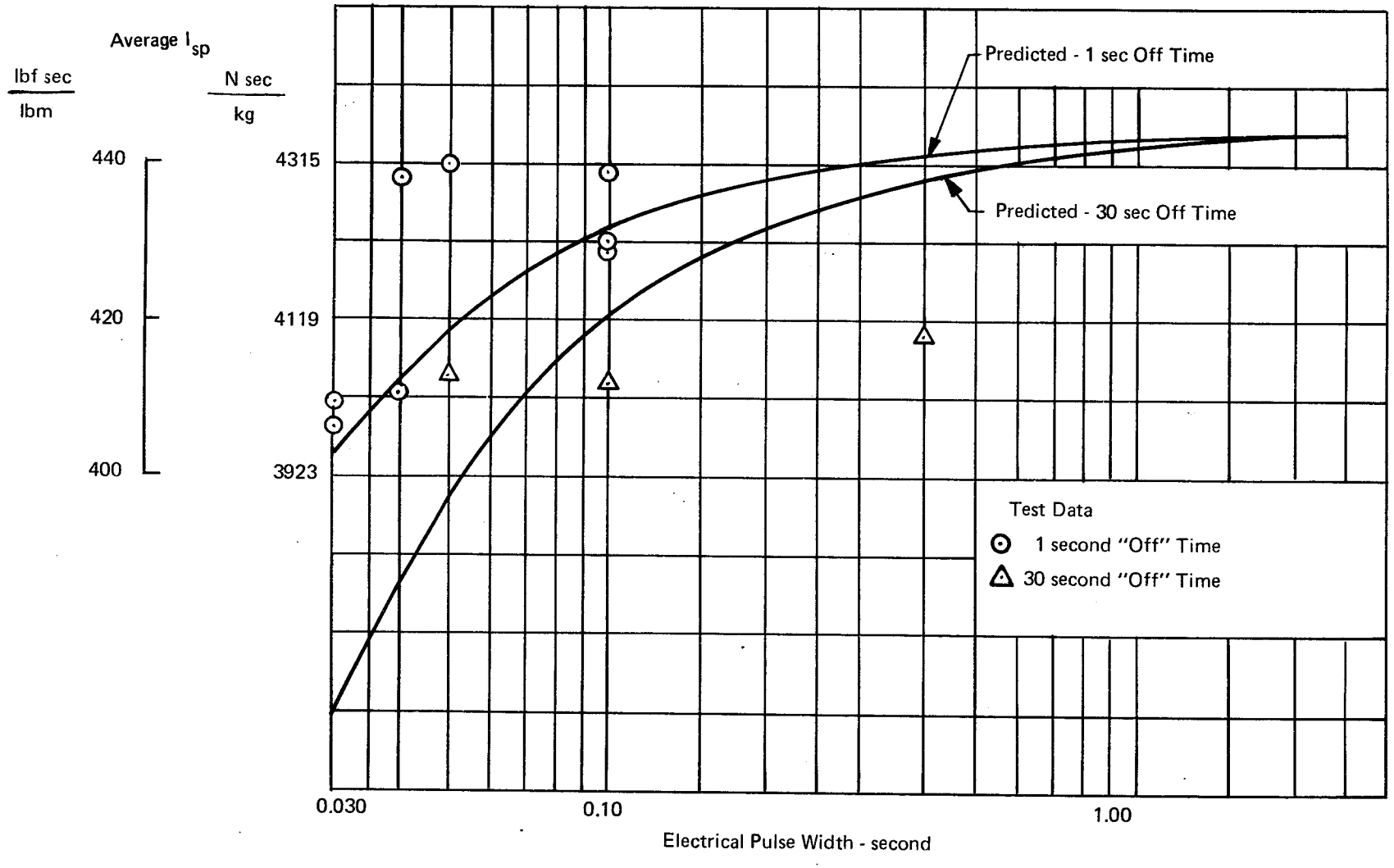

Figure 141. Average I_{sp} versus Electrical Pulse Width (Data For Infinite Altitude)

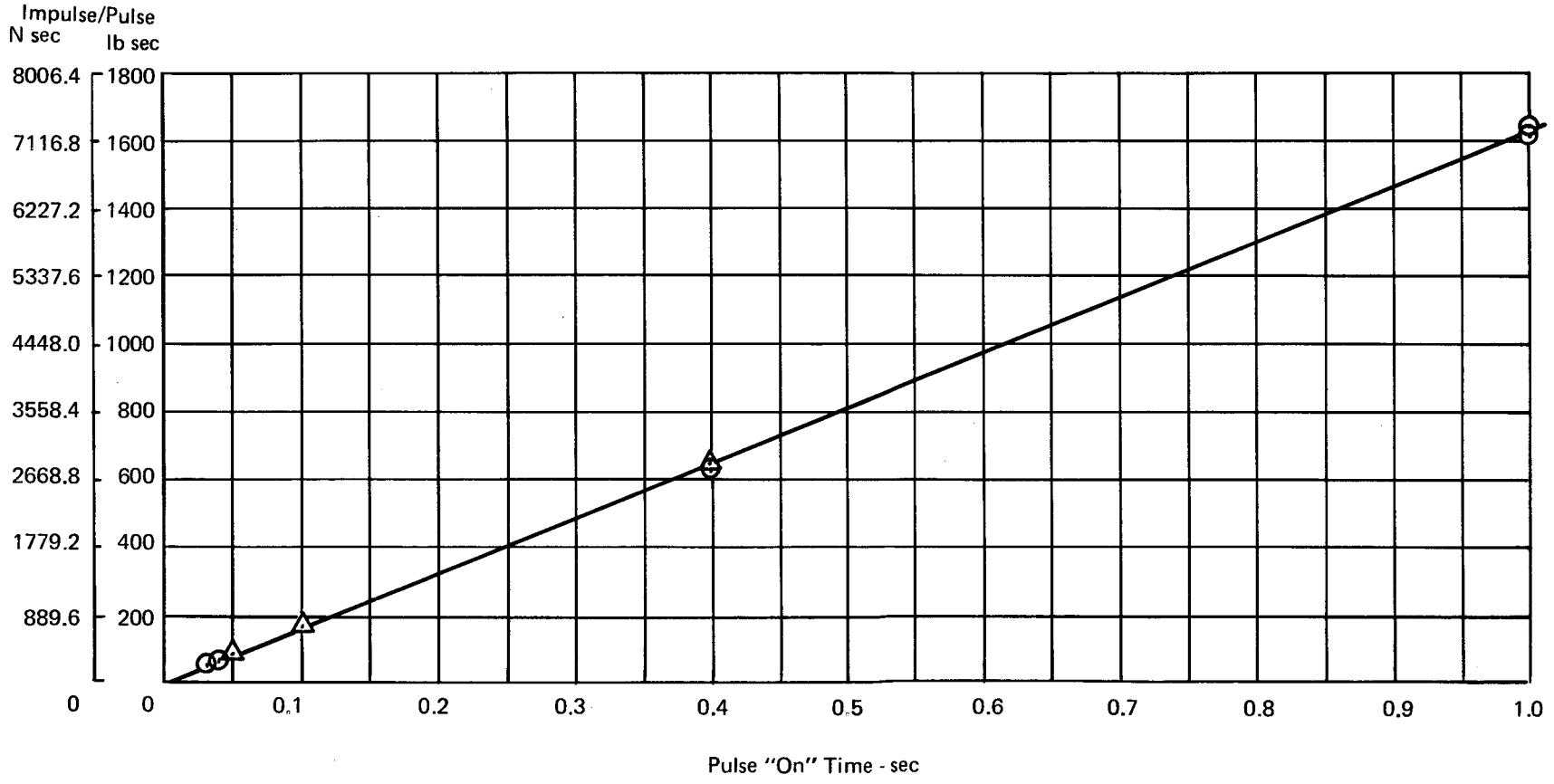

Figure 142. Impulse/Pulse versus Pulse "On" Time

Eight pulse series were made with 100-millisecond "on" time and "off" times ranging from 1 second to 30 seconds. The number of pulses varied from 15 to 20 pulses per series. The average impulse per pulse series ranged from 164 to 180 lb sec (729.5 to 800.6 N sec). The maximum variation within a pulse series was 13 lb-sec (57.8 N-sec) or less than 7.8%.

Six pulse series were made with 400 millisecond "on" times and "off" times ranging from 1 to 30 seconds with the number of pulses ranging from 4 to 5. The average impulse per pulse series varied from 614 to 669 lb sec (2731.1 to 2975.7 N sec) with a maximum variation within a pulse series of 48 lb sec (213.5 N sec) or approximately 7.9%.

Three pulse series were made with 1 second on times and off times of 1, 5, and 30 seconds. The pulses varied from 3 to 6. The average impulse per pulse series ranged from 1663 to 1677 lb sec, (7400.4 to 7462.7 N sec) while the maximum variation within a pulse series was 41 lb sec (182.4 N sec) or approximately 2.6%.

3. Pulse Repeatability

Table LI summarizes the pulse tests by on/off times and lists the maximum variation of individual pulses for each pulse series. The maximum variation occurred during the 400 milliseconds on, 1 second off duty cycle.

The 2500-pulse test data are listed in Table LII , showing the first 21 pulses, 21 pulses in the middle of the run and the last 21 pulses. The average of each of these groups shows there is a maximum variation of 0.5 lb sec (2.224 N sec) or less than 0.6%. Figures 143, 144, 145, are oscillograms of these same pulses showing thrust, chamber pressure and feed pressures. Excellent repeatability is observed in the start and shutdown transients, and the steady-state portion of the pulses.

TABLE LI
PULSE TESTS SUMMARY

Hardware	Pulse "On" Time sec	Pulse "Off" Time sec	No. of Pulses	Max Variation Impulse/Pulse %
Same	0.03	1	28	5.5
Same	0.04	1	60	4.0
Same	0.05	0.1	2940	6.5
Same	0.05	1	20	2.2
Same	0.05	30	20	3.3
Same	0.10	1	80	7.8
Same	0.10	5	59	6.2
Same	0.10	30	15	5.7
Same	0.40	1	13	7.9
Same	0.40	5	4	1.4
Same	0.40	30	3	6.8
Same	1.00	1	6	2.6
Same	1.00	2	75	2.7
Same	1.00	5	3	1.6
Same	1.00	30	2	0.2

TABLE LII
2500-PULSE IMPULSE DATA – INFINITE ALTITUDE
RUN 1BN 745

Beginning Pulses			Mid-Run Pulses		Ending Pulse		
	Impulse/Pulse		Impulse/Pulse			Impulse/Pulse	
Pulse No.	(lb-sec)	(N-sec)	(lb-sec)	(N-sec)	Pulse No.	(lb-sec)	(N-sec)
1	95	422.56	95	422.56	2480	94	418.11
2	99	440.36	94	418.11	2481	95	422.56
3	98	435.91	96	427.01	2482	94	418.11
4	95	422.56	95	422.56	2483	95	422.56
5	95	422.56	94	418.11	2484	94	418.11
6	95	422.56	93	413.66	2485	96	427.01
7	96	427.01	94	418.11	2486	96	427.01
8	95	422.56	96	427.01	2487	96	427.01
9	95	422.56	96	427.01	2488	95	422.56
10	95	422.56	96	427.01	2489	95	422.56
11	96	427.01	96	427.01	2490	93	413.66
12	95	422.56	95	422.56	2491	94	418.11
13	95	422.56	94	418.11	2492	95	422.56
14	93	413.66	93	413.66	2493	95	422.56
15	93	413.66	94	418.11	2494	94	418.11
16	95	422.56	95	422.56	2495	94	418.11
17	95	422.56	95	422.56	2496	94	418.11
18	95	422.56	94	418.11	2497	95	422.56
19	95	422.56	94	418.11	2498	94	418.11
20	95	422.56	95	422.56	2499	95	422.56
21	94	418.11	95	422.56	2500	93	413.66
Total Impulse	1998	8887.55	1989	8847.51		1986	8834.17
Avg. Impulse Per Pulse	95.1	423.01	94.7	421.23		94.6	420.78
Max Δ Within Pulse Series	6	26.69	3	13.34		3	13.34

Difficulty was encountered with the chamber pressure transducer near the end of the run, resulting in erroneous P_c deflections. The thrust deflection was consistent throughout the 2500 pulses. The pulses shown are characteristic of all pulse duty cycles, where no difficulties were encountered with the ignition system or instrumentation.

4. Effects of Ignition Delay

An analytical model was established to predict pulse mode impulse for 30 and 50-millisecond pulse widths and varying ignition delay times. The model assumed propellants were simultaneously injected into the chamber.

Four pulse series were examined for the effect of ignition delay as shown in Table LIII The ignition delay is defined as the elapsed time between rise of feed pressure and the rise of chamber pressure. The data presented are for representative pulses.

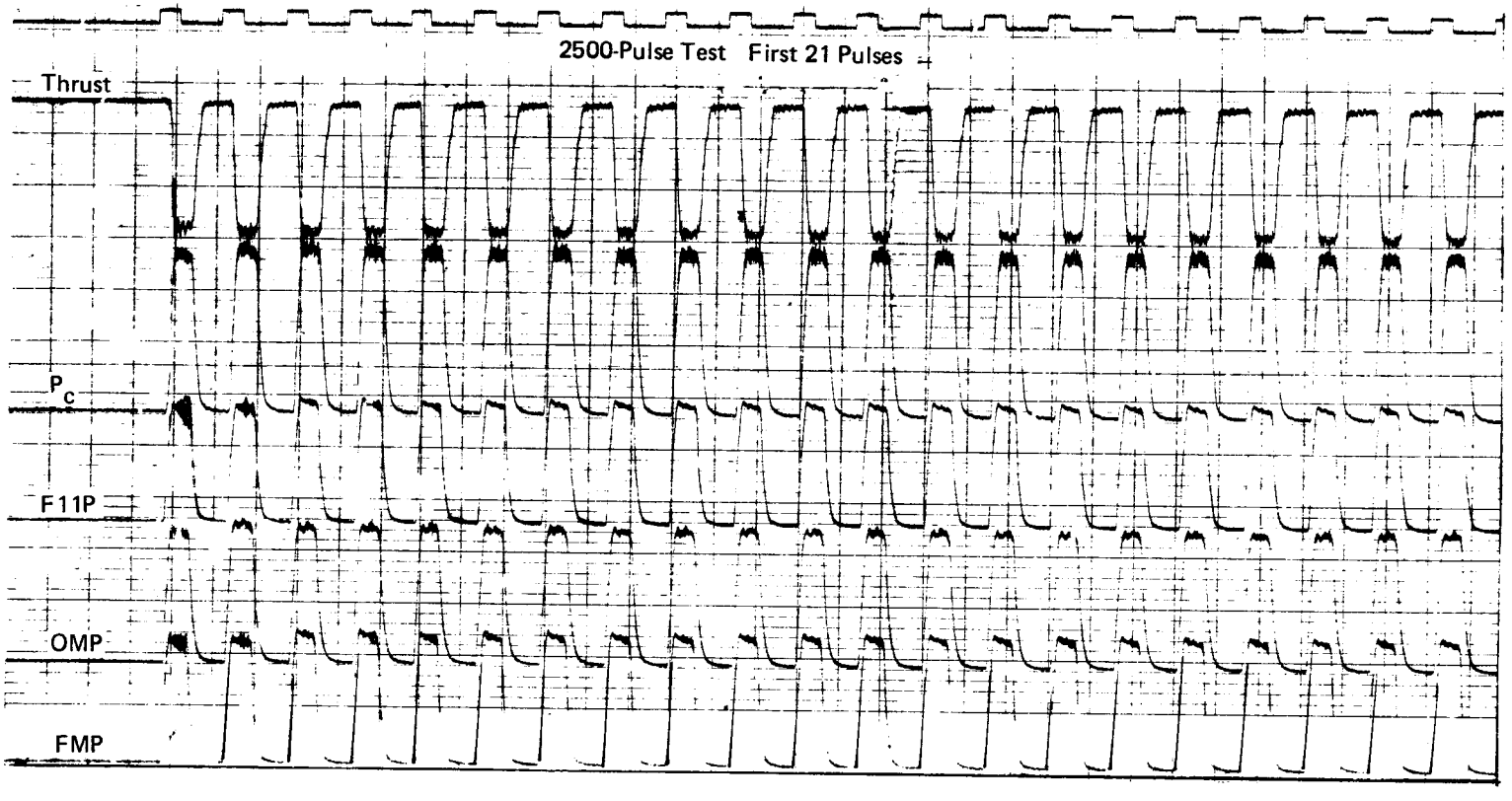

Figure 143. 2500-Pulse Test – First 21 Pulses

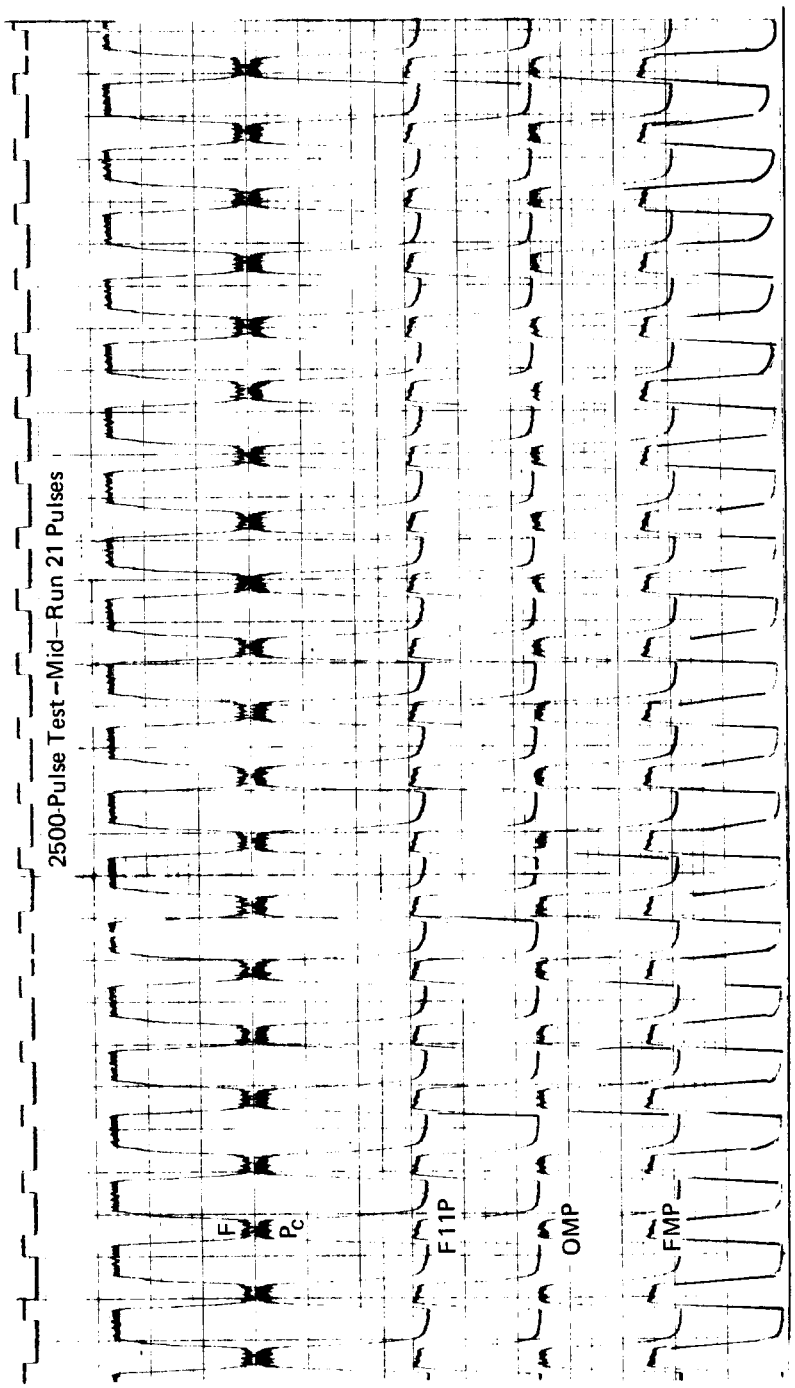

Figure 144. 2500-Pulse Test – Mid-Run 21 Pulses

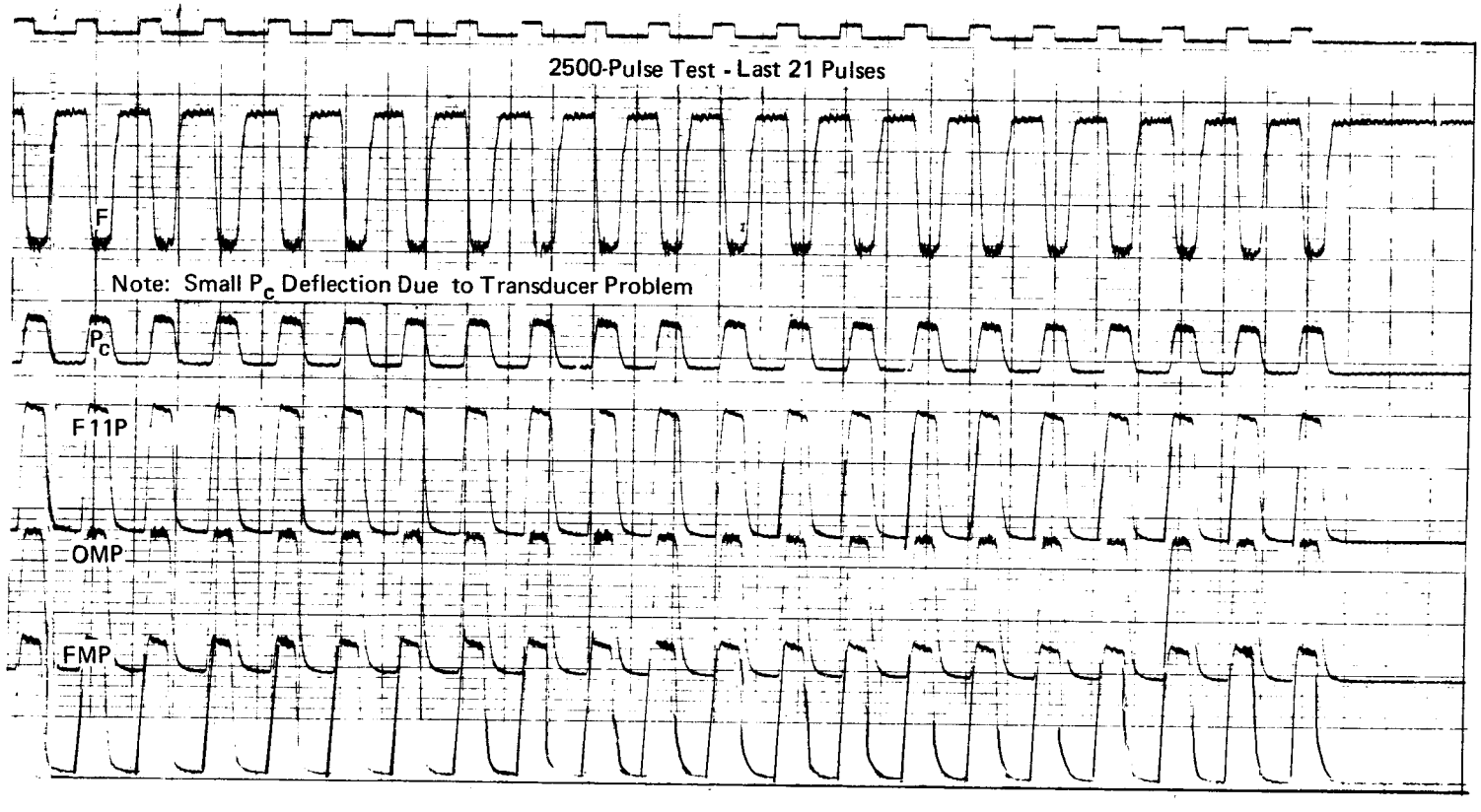

Figure 145. 2500-Pulse Test – Last 21 Pulses

TABLE LIII
IGNITION DELAY EFFECT RESULTS

	Test No. 732			Test No. 738			Test No. 730			Test No. 727		
	On/Off Time 0.03/1 sec			On/Off Time 0.03/1 sec			On/Off Time 0.05/1 sec			On/Off Time 0.05/30 sec		
Pulse No.	Impulse lbf sec	Impulse N sec	Delay Time ms	Impulse lbf sec	Impulse N sec	Delay Time ms	Impulse lbf sec	Impulse N sec	Delay Time ms	Impulse lbf sec	Impulse N sec	Delay Time ms
1	59	262.44	4.0	61	271.33	3.5	94	418.11	5.5	93	413.66	6.5
2	59	262.44	3.5	61	271.33	3.0	94	418.11	5.0	94	418.11	5.5
3	57	253.55	6.0	60	266.89	5.5	93	413.66	3.0	94	418.11	4.0
4	58	257.45	5.0	61	271.33	4.5	94	418.11	7.5	93	413.66	5.0
5	56	249.10	7.5	61	271.33	6.0	94	418.11	2.5	93	413.66	6.5
6	57	253.55	5.0	61	271.33	4.5	93	413.66	5.0	94	418.11	5.5
7	58	257.45	4.0	61	271.33	5.5	92	409.22	3.5	95	422.56	5.0
8	58	257.45	5.0	62	275.78	4.0	94	418.11	4.0	94	418.11	3.5
9	58	257.45	4.0	62	275.78	4.0	94	418.11	4.0	94	418.11	3.5
10	57	253.55	6.5	61	271.33	4.5	93	413.66	3.0	93	413.66	4.0
11	56	249.10	4.0	60	266.89	6.0	93	413.66	4.5	94	418.11	4.0
12				60	266.89	6.0	93	413.66	4.5	93	413.66	3.0
13				61	271.33	5.0	92	409.22	4.5	92	409.22	5.0
14				62	275.78	4.0	93	413.66	2.5			
15				61	271.33	4.0	93	413.66	2.5			
16				61	271.33	4.0	92	409.22	5.0			
17				61	271.33	5.0	92	409.22	5.0			
18				61	271.33	5.0	92	409.22	4.5			

Figure 146 shows both the predicted and test results. The test results are lower than predicted and is partly attributed to propellant sequencing. The tests were performed with an approximate 2 millisecond fuel lead whereas the predicted was based on simultaneous injection of propellants.

The 30 millisecond pulse data indicated a slightly decreasing impulse for greater ignition delays over the time delay range of 3 to 7.5 ms, while the 50 ms data indicated a relatively constant impulse over the time delay range of 2.5 to 7.5 ms. For an ignition delay of 5 ms, the 30 ms data were 8.3% lower than predicted and the 50-ms data were 7.6% lower than predicted.

The study resulted in the conclusion that ignition delay had little effect on the pulse performance as long as the delay time was less than the time to establish full propellant flow.

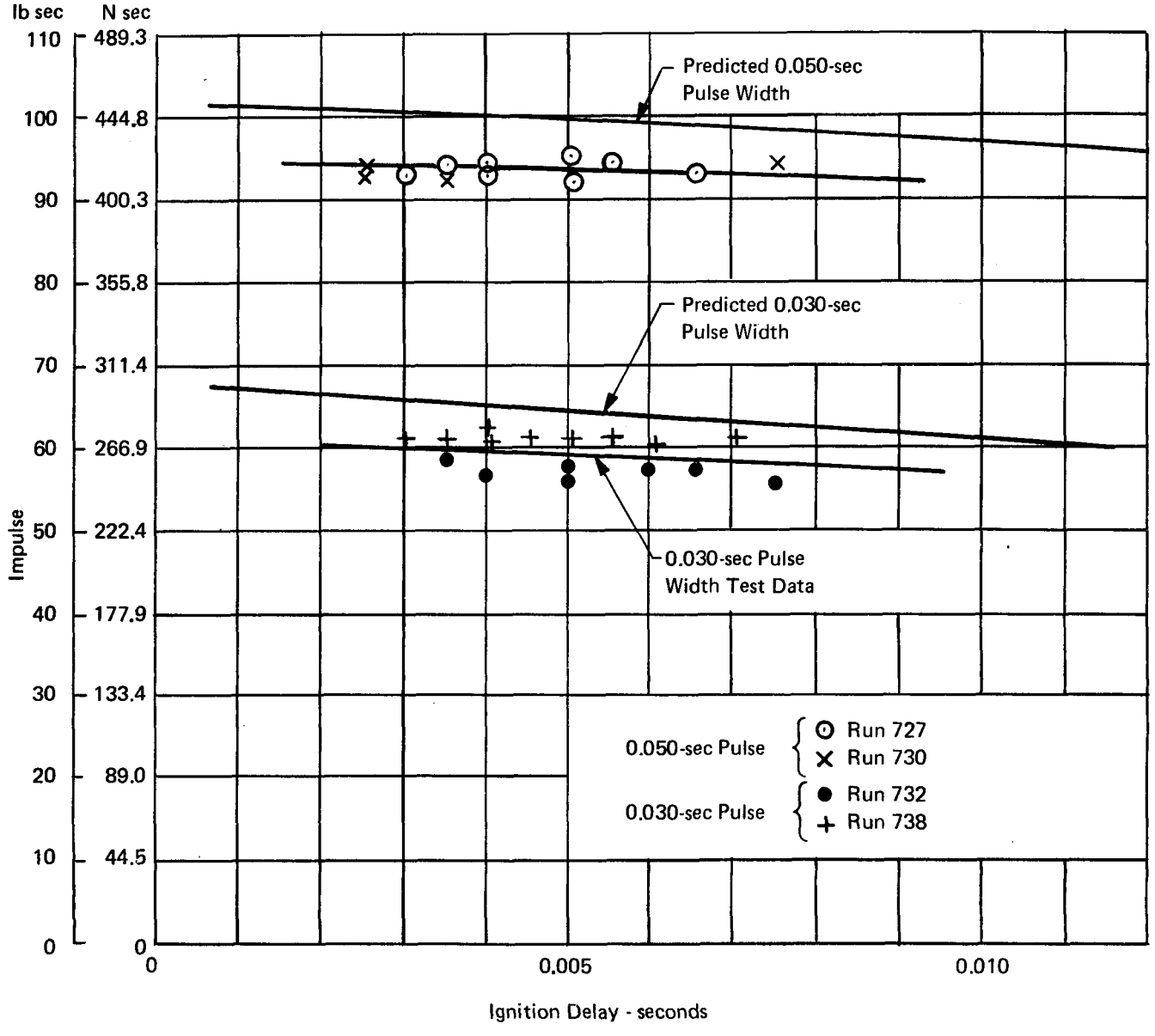

Figure 146. Pulse Mode Impulse versus Ignition Delay for 0.030 and 0.050 Sec Pulse Width

a. Pulse Mode Propellant Sequence

Propellant sequence was investigated to determine what effects it may have on pulse impulse. The sequence of propellant entry for the majority of tests was to use simultaneous valve signals which resulted in a 2 ms fuel lead.

Tests were made with 2 ms and 4 ms fuel delay from this reference. Thus, three sequence points were evaluated: 2 ms fuel lead, zero fuel lead, and 2 ms fuel lag. Table LIV is a summary of the results for two pulse duty cycles: (1) 0.1 second on/5 seconds off, and (2) 0.04 seconds on/1 or 5 seconds off. Based on the observed results, the simultaneous injection of propellants gives the highest pulse impulse, although a ±2 ms variation causes little variation.

TABLE LIV
PROPELLANT SEQUENCE VARIATION

Run No.	Fuel Lead-ms	On/Off Time-sec	Imp./Pulse Avg.		Δ Within Series
			lb sec	N sec	
728	2	0.1/5	164	729.47	8
734	0		165	733.92	10
736	-2		165	733.92	10
731	2	0.04/1	76	338.05	3
735	0	0.04/5	78	346.94	3
737	-2	0.04/5	77	342.50	4

b. Pulse Mode Mixture Ratio

Pulse mode tests were performed over a mixture ratio range of 3 to 5 to observe the effects of mixture ratio variation on pulse impulse. The only conclusion from the effort was that the mixture ratio variation was smaller than the variation in individual pulses. The pulse duty cycle was 0.1 second "on" and 1 second "off". Because of data scatter and insufficient data points no conclusions were drawn from this data (Refer to Table LV).

TABLE LV
MIXTURE RATIO VARIATION

Run No.	$R_{o/f}$	On/Off Time	Impulse/Pulse (avg.)		Δ Within Series	
			lb sec	N sec	lb sec	N sec
729	4	0.1/1	165	733.92	11	48.93
740	3	0.1/1	173	769.50	9	40.03
741	5	0.1/1	180	800.64	9	40.03
747	4	0.1/1	176	782.85	13	57.82

XIV. SUMMARY OF TEST RESULTS

During the program, tests were conducted at both sea level and at simulated altitude to evaluate a variety of reverse flow engine components. Testing encompassed variations in operating parameters such as chamber pressure and mixture ratio. Environmental conditions were varied from 200°R (111°K) to 800°R (444°K). Durations of engine "on time" were varied from 0.030 seconds in pulse-mode testing to 500 seconds in steady state.

In general, the reverse flow engine produced results equal to or exceeding requirements. In steady-state performance the design objective was 435 seconds (4266 N sec/Kg) and was exceeded by three different configurations. The duration test of 500 seconds in an insulated configuration (to simulate a buried installation) was conducted without incidence and could have been continued indefinitely if facilities or budget had not been limiting factors.

Tests at a given propellant condition indicated that a wide latitude of chamber pressure and mixture ratio variations can be tolerated without a large performance variation. Propellant temperature was found to have a greater effect, but, if hardware changes were incorporated, equally efficient operation could be maintained.

The major accomplishments of the program can be summated in the following statements:

- Program has demonstrated that the reverse flow thruster can achieve APS performance.
- Altitude ignition of primary flows was demonstrated
- Cooling techniques for the reverse flow thruster were demonstrated
- Insulated chamber operation was demonstrated
- Pulse mode operation was demonstrated – to 65 lb sec (29.5 kg/sec)
- Cold propellant performance was demonstrated.

The above statements summarize those items which were accomplished during the course of testing. In addition, more specific items are tabulated for comparison to the program objectives. This comparison is made in Table LVI.

TABLE LVI
CONTRACT REQUIREMENT AND DEMONSTRATION COMPARISON

Design Point	Contract Requirements NAS3-14353	Demonstrated
Thrust	1500 lbf (6672 N)	1500 lbf (6672 N)
Chamber Pressure	300 psia (206.8 N/cm^2)	300 psia (206.8 N/cm^2)
Mixture Ratio	4.0	4.0
Feed Pressure	100 psi (68.95 N/cm^2)	110 (75.84 N/cm^2) Oxidizer 90 (62.06 N/cm^2) Fuel
Area Ratio	40	40
H_2 Feed Temp	540 and 250°R (300 and 139°K)	540 and 250°R (300 and 139°K
O_2 Feed Temp	540 and 375°R (300 and 208°K)	540 and 375°R (300 and 208°K)
Min Impulse Bit	50 lb/sec (222.5 N/sec)	65 lb/sec (289.1 N/sec)
Max Firing Duration	1000 Sec	500
Life Cycle Pulses	9×10^5	($>>10^6$)
Steady State	1×10^5	(7.6×10^5)
Cumulative	50 hr	(>50 hr)
Max External Temp	800°F (700°K)	496°F (531°K)
Operating Range		
P_c	100 - 500 psia (68.95 - 344.7 N/cm^2)	100-500 psia (68.95 - 344.7 N/cm^2)
O/F	3 - 5	3 - 5
Feed Pressures	As Required	—
O_2 Feed Temp	Saturated Gas - 800°R (444°K)	261 - 777°R (145 - 432°K)
H_2 Feed Temp	200 - 800°R (111 - 444°K)	207 - 774°R (115 - 430°K)
Duration	500 sec	500
Goal		
Specific Impulse (I_{SP})	435 sec ($\frac{4266\ N/sec}{kg}$)	440+ sec ($\frac{4315 + N\ sec}{kg}$)

XV. FLIGHT WEIGHT REVERSE FLOW ENGINE PRELIMINARY DESIGN

A. APPROACH

The NAS 3-14353 program scope and the desire to characterize several variations of thrust chamber throat and nozzle extension cooling dictated the test firing of interchangeable, nonflight weight thrust chamber components. To incorporate interchangeability, flanged assemblies were employed as described in the preceding sections of this report and with the exception of the throat liner, the individual part thicknesses were established primarily for ease of fabrication. For example, the spherical combustion chamber was 0.20 inches (0.508 cm) thick whereas the required wall thickness, based on the maximum operating temperature and an extreme chamber pressure of 500 psia (344.7 N/cm^2), would be less than 0.10 inches (0.254 cm). Therefore, a baseline of the flight weight thrust chamber consisted of a direct extrapolation of the test hardware to a flight configuration by the definition of welded joints and with section and wall thicknesses based on the test defined operating temperatures and structural margins consistent with a flight configuration. The test hardware configuration selected for the exercise was the regenerative cooled throat and the dump cooled nozzle extension. Low propellant feed temperatures were assumed for the design of the flight weight engine.

The baseline flight weight TCA was then studied for weight reduction and improved reliability through alternate configurations of the nozzle liner and stainless steel jacket to eliminate mechanical seals. Primary emphasis was placed on expansion joints to supersede the piston ring seal of the test hardware liner. A parallel effort was carried out to establish a direct joining technique for the zirconium copper liner and stainless steel nozzle section shell. The work led to a chamber layout with a calculated weight approaching 10 lb (4.54 kg) at the design thrust, P_c and area ratio defined by the contract.

A nickel liner throat was also analyzed because of the potential engine requirement of withstanding reentry heating. A columbium nozzle extension would be included for that environment.

Preliminary engine valve and ignition subassemblies specifications were prepared and inputs received from several suppliers. Those inputs plus in-house valve preliminary designs were reviewed and components selected to complete the flight weight engine definition. Several alternate arrangements of valve-to-chamber mounting were considered prior to the selection of the final configuration.

Subsequent paragraphs of this section will present a summary of the work outlined above. Figure 147 shows the configuration of the flight weight engine resulting from the studies.

B. THRUST CHAMBER ASSEMBLY

1. Thermal Analyses, Nozzle Section

Several arrays of steady-state two-dimensional analyses were made of the regeneratively cooled thrust chamber liner wall as an input to the stress analysis calculations. Variables in the arrays were:

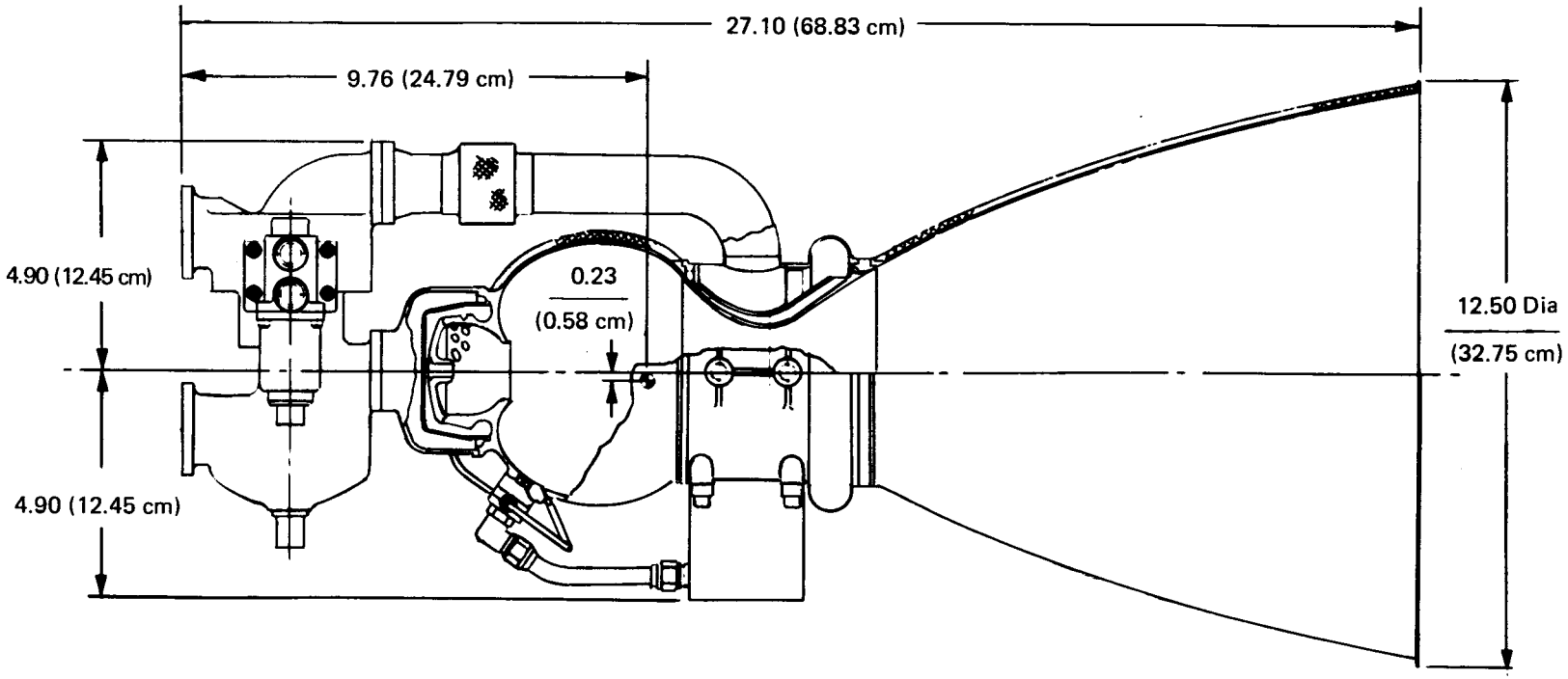

Figure 147. Flight Weight 1500 LBF (6672 N) APS Engine

Types of construction (integral, free standing)

Materials of construction (zirconium, copper, nickel)

Wall Thickness

Axial Location

Cooling side boundary conditions were made to simulate 250°R (139°K) hydrogen engine feed temperature. The basic ground rule was to make nodal models of wall and channel configurations with the same passage dimensions as presented earlier for the contract demonstration hardware (Section VII). Conductance between nodes was made in conformance with change in material, change in wall thickness or top closure. The models were solved with the nominal combustion side boundary conditions corresponding with

Chamber Pressure	300 psia (206.8 N/cm^2)
Mixture Ratio	4/1
Combustion Efficiency	97%

Equilibrium temperature distributions at several locations on the liner are presented in Table LVII and LVIII. The data of Table LVII show the cross section temperatures as a function of the thickness of the hot gas wall at the throat station, X =0.0. Table LVIII presents the calculated temperatures at various axial positions forward and aft of the throat station.

The calculations included minor adjustments of the heat transfer equations resulting from the earlier comparison of predicted temperatures and test firing temperature measurements.

2. Structural Analyses, Nozzle Section

a. Nozzle Section – Unrestricted Axial Growth

The desire to define an all-welded nozzle section for the improved reliability of that configuration presented the structural problem of providing for the longitudinal thermal growth of the liner assembly. For a liner extending to a divergent nozzle area ratio of 10 (the same as the test hardware) the calculated maximum thermal expansion for various liner configurations were as follows:

Free-standing Amzirc	0.018 inches (0.046 cm)
Integral Amzirc/ED Copper	0.009 inches (0.003 cm)
Free-standing TD Nickel Liner	0.020 inches (0.051 cm)

The maximum thermal expansions were based on the longitudinal and axial temperature gradients at steady-state operation.

The first nozzle section design concept investigated used a short bellows to absorb most of the differential expansion. The bellows arrangement shown in Figure 148, was modified to provide better attachment and a lower spring rate as shown in Figure 149.

TABLE LVII
VARIABLE WALL THICKNESS ANALYSES
FLIGHT WEIGHT THRUST CHAMBER

Study A: Integral Wall, Nickel

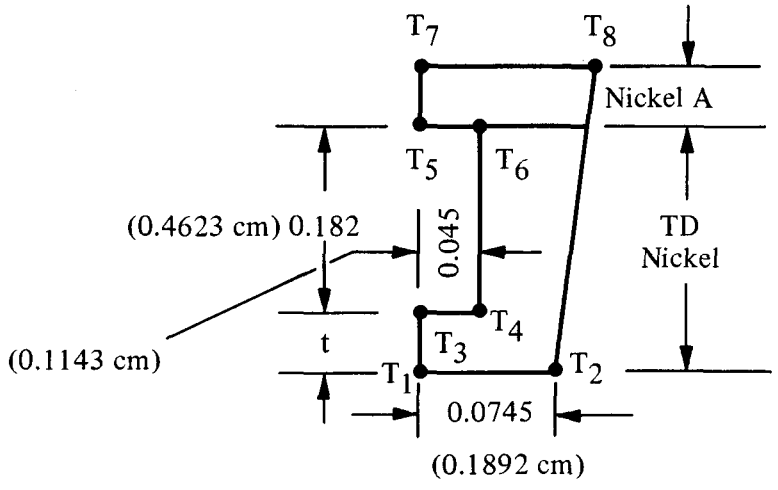

	X	t		T_1	T_2	T_3	T_4	T_5	T_6	T_7	T_8
in.	0.0	0.015	°F	986	752	758	508	-151	-134	-145	-121
cm.	0.0	0.038	°K	803	673	676	537	172	181	175	188
in.	0.0	0.020	°F	1005	821	708	502	-151	-140	-147	-121
cm.	0.0	0.051	°K	814	712	649	534	172	178	174	188
in.	0.0	0.030	°F	1070	953	634	481	-152	-140	-148	-122
cm.	0.0	0.076	°K	850	785	608	522	171	178	173	188

Study B:Free Standing Nickel

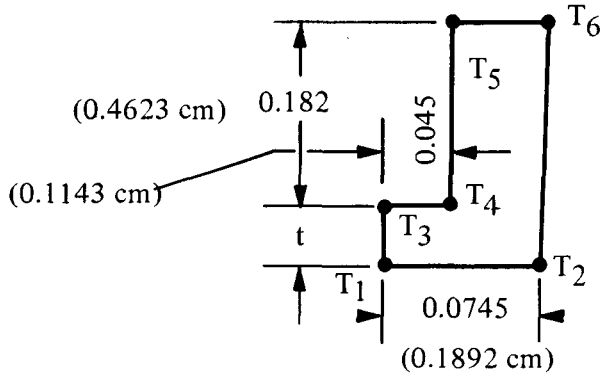

	X	t		T_1	T_2	T_3	T_4	T_5	T_6
in.	0.0	0.030	°F	1065	948	640	468	-118	-102
cm	0.0	0.076	°K	847	782	611	516	190	199
in.	0.0	0.050	°F	1221	1169	551	425	-122	-106
cm	0.0	0.127	°K	934	905	562	492	188	197
in.	0.0	0.060	°F	1301	1264	516	404	-124	-108
cm	0.0	0.152	°K	979	958	542	480	187	196

TABLE LVII (CONT)
VARIABLE WALL THICKNESS ANALYSES
FLIGHT WEIGHT THRUST CHAMBER

Study C: Integral Composite

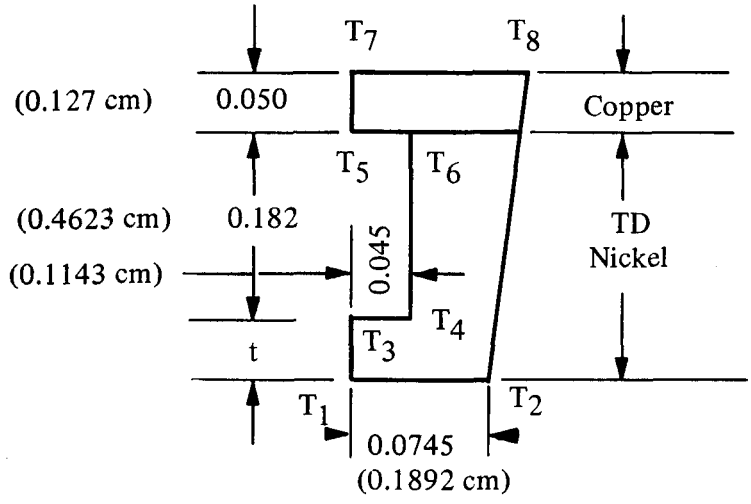

	X	t		T_1	T_2	T_3	T_4	T_5	T_6	T_7	T_8
in.	0.0	0.015	°F	985	750	757	507	-140	-139	-139	-137
cm.	0.0	0.038	°K	803	672	676	537	178	178	178	179
in.	0.0	0.020	°F	1004	820	708	501	-141	-139	-140	-137
cm.	0.0	0.051	°K	813	711	649	534	177	178	178	179
in.	0.0	0.030	°F	1069	952	633	480	-142	-140	-141	-138
cm.	0.0	0.076	°K	850	784	608	522	177	178	177	179

TABLE LVIII
VARIABLE AXIAL LOCATION ANALYSES
FLIGHT WEIGHT THRUST CHAMBER

Study D: Integral Wall, Copper

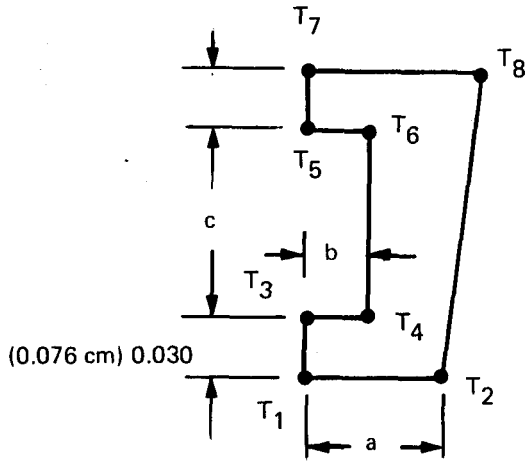

	X	a	b	c		T_1	T_2	T_3	T_4	T_5	T_6	T_7	T_8
In.	-1.05	0.0978	0.0705	0.102	°F	475	390	416	322	21	64	31	73
cm.	-2.667	0.2485	0.1891	0.2591	°K	520	472	487	434	267	291	273	296
in.	0.0	0.0745	0.045	0.182	°F	400	356	342	278	-44	-32	-39	-25
cm.	0.0	0.1892	0.1143	0.4623	°K	478	453	446	416	231	244	234	242
in.	1.4	0.1327	0.875	0.220	°F	438	379	422	359	160	183	164	188
cm.	3.556	0.3371	0.2223	0.5588	°K	499	466	490	455	345	358	347	360
in.	3.4	0.220	0.150	0.164	°F	466	380	456	375	213	269	217	284
cm.	8.636	0.5588	0.381	0.4166	°K	515	467	509	464	374	405	376	413

Study E: Free Standing Nickel

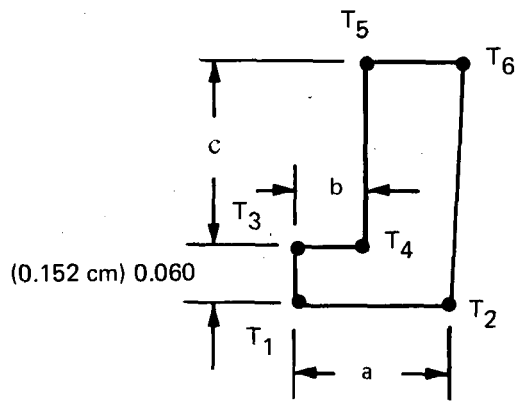

	X	a	b	c		T_1	T_2	T_3	T_4	T_5	T_6
in.	-1.05	0.0978	0.0705	0.102	°F	1314	1216	525	417	-13	30
cm.	-2.667	0.2485	0.1891	0.2591	°K	986	931	547	487	248	272
in.	0.0	0.0745	0.045	0.182	°F	1302	1263	516	400	-124	-108
cm.	0.0	0.1892	0.1143	0.4623	°K	979	957	542	478	187	196
in.	1.4	0.1327	0.0875	0.220	°F	986	876	747	592	102	130
cm.	3.556	0.3371	0.2223	0.5588	°K	803	732	670	585	199	328
in.	3.4	0.220	0.150	0.164	°F	959	845	795	664	389	436
cm.	8.636	0.5588	0.381	0.4166	°K	788	725	697	625	472	498

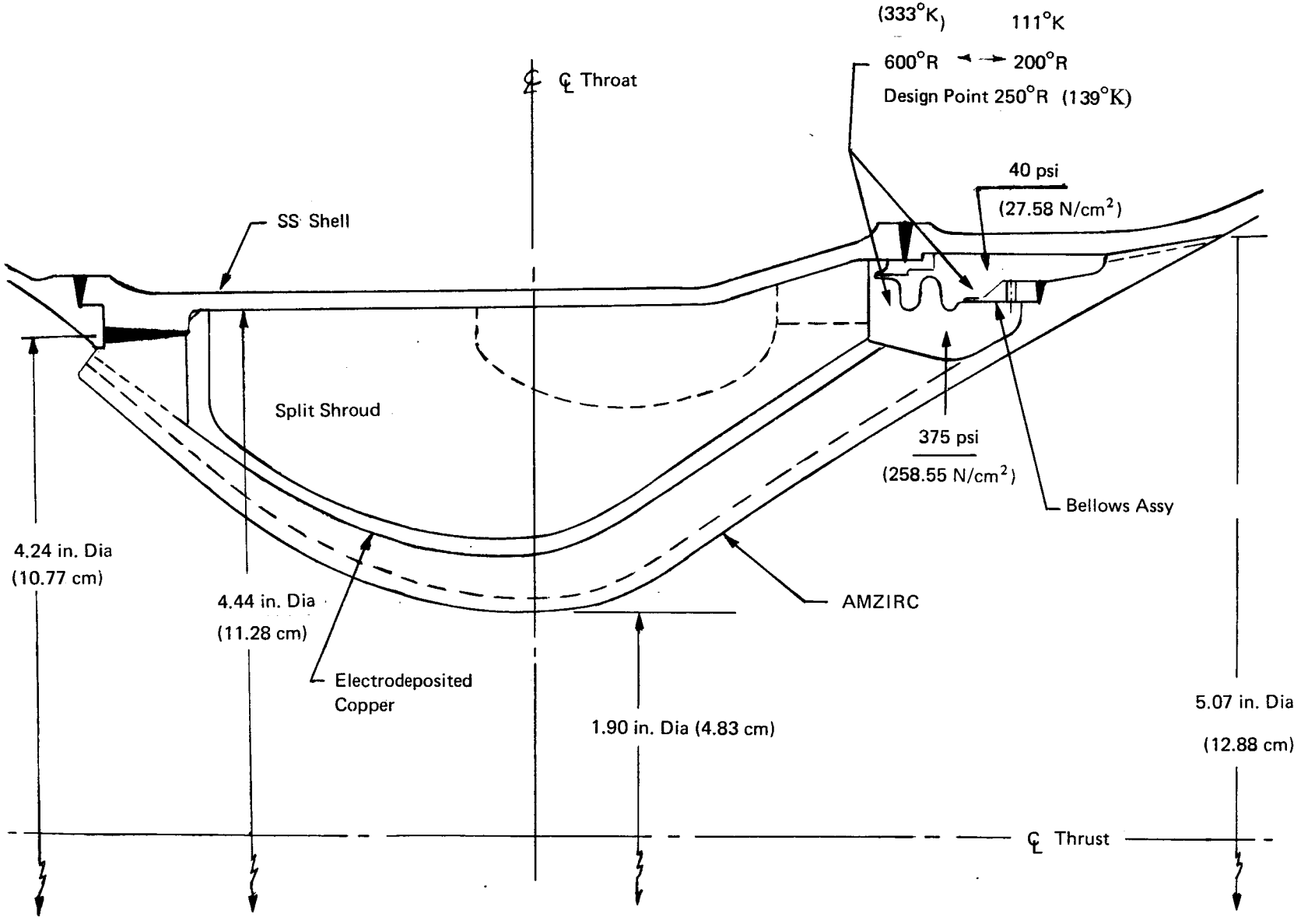

Figure 148. Short Bellows Arrangement

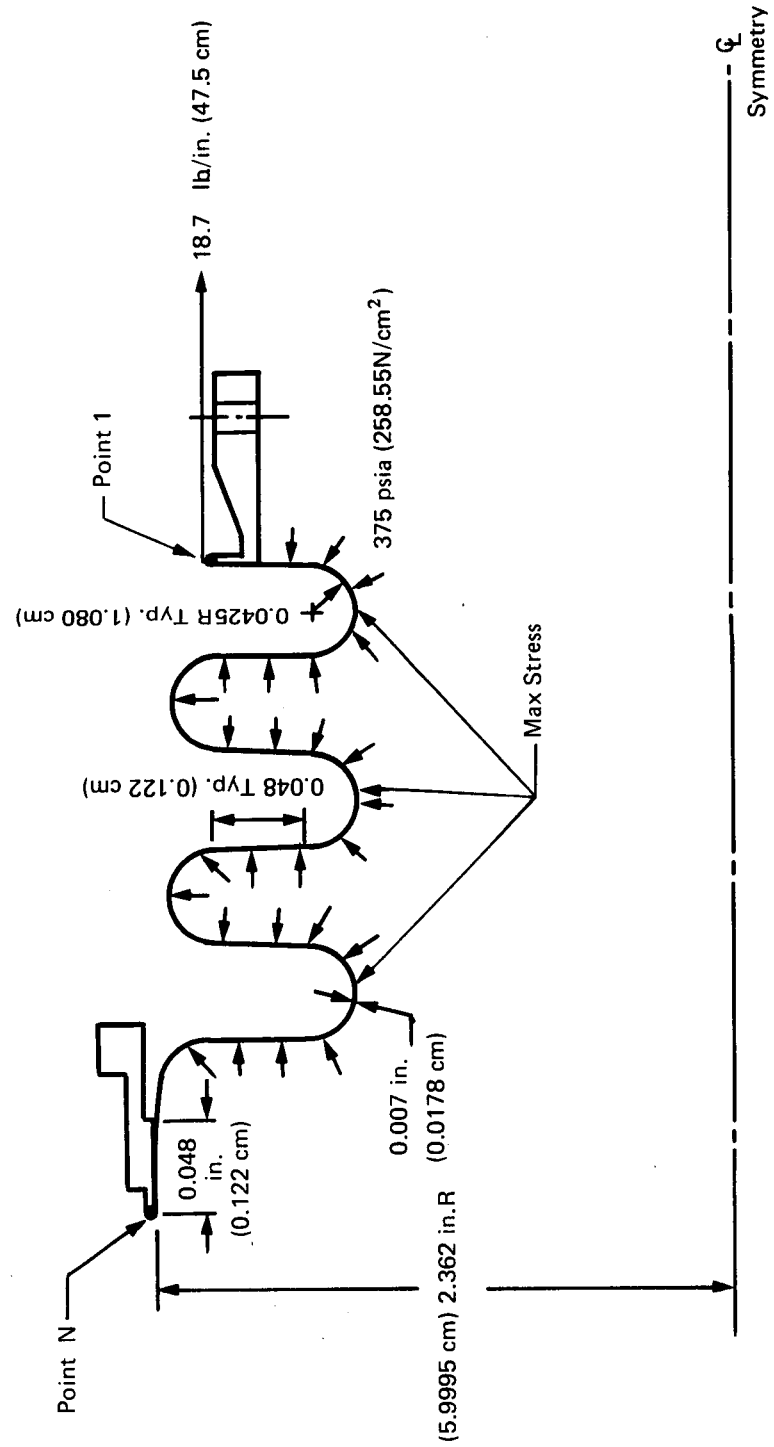

Figure 149. Bellows Expansion Joint

The stress deflection characteristics of the bellows shown in Figure 149 were obtained with the BAC Nonlinear Symmetric Shell Analysis Computer Program. When subjected to an internal pressure of 375 psi (258.55 N/cm^2) and an axial extension of 0.020 (0.051 cm) inches in the worst condition, the bellows would have a maximum combined stress of 133,800 psi (92,250 N/cm^2) on the outer surface of the convolution roots. A force of 18.7 lb/in. (12.89 N/cm^2) is required at point 1, as shown in Figure 149, to produce this condition. For the assumption that the bellows is at its free length at installation, each chamber operation to steady-state temperatures would produce one stress cycle from zero to 133,800 psi (92,250 N/cm^2).

Evaluation of the fatigue life for any material under 133,800 psi (92,250 N/cm^2) stress cycle requires a Goodman type diagram for the operating temperature. Such a diagram can be constructed from a conventional reverse bending fatigue curve and the appropriate ultimate tensile stress. This method, outlined in Ref. 23 produces cycle life values that are somewhat conservative. Based on values in published data for A286 material at 250°R (139°K), a stress cycle of zero to 134,000 psi (92,400 N/cm^2) will sustain at least 100,000 cycles, at maximum extension, when temperatures are at steady state and considerably more for pulse type operations. Considering the expected cycle life together with the small end force on the bellows, the design concept was shown to be feasible. In addition, the stresses at the welds at points 1 and N of Figure 149 are much less than the maximum values at the roots. This fact would allow adjustment of the radial location of point 1 to reduce the end force required for a 0.020-in. (0.051 cm) deflection thus virtually eliminating thermally induced compression on the inner nozzle wall.

Liner fatigue calculations were conducted to explore the suitability of integral liner designs which would require less provision for longitudinal growth than free-standing configurations. Various nickel liners were included as part of the effort to define a liner which could be exposed to a reentry heating environment. An integral copper liner with a zirconium hot wall and a regenerative passage root thickness of 0.070 inches (0.178 cm) plus an electrodeposited copper cooling passage closure indicated a pulse mode capability of 9×10^6 cycles, 4.9×10^5 steady-state cycles and a creep life much greater than 50 hours of accumulated operation. Therefore, the integral copper configuration would exceed the contract design goals. Figures 150 and 151 show the calculated steady-state firing fatigue life capabilities of various nickel liners and integral cooling passage closures. The figures indicate that the liners would not be capable of achieving the 100,000 steady-state firing goal based on the method of fatigue-life calculations employed. A more rigorous analysis of the platic deformations of the nickel liners would undoubtedly show an increase of fatigue life.

b. Nozzle Section – Restricted Axial Growth

A second design approach consisted of using the flexibility of the inlet manifold, included as an integral part of the outer shell, to absorb the differential expansion of the nozzle liner. A sketch of this concept is shown in Figure 152. The inner and outer shells are connected only at points A and C so that an exact determination of stresses and deflections requires consideration of both shells as a unit. Since such a procedure is lengthy and costly, a conservative method was employed first to determine feasibility and approximate design parameters. The outer shell was assumed to absorb a differential expansion of 0.020 inch (0.051 cm) (maximum thermal expansion of free-standing liners) while supporting an internal pressure of 375 psi (258.55 N/cm^2) with the ends fixed against radial motion and rotation. The nonlinear symmetric shell computer program was again employed to determine the deformed state of the shell from point A to point C under the combined action of end forces at A and C and the 375 psi (258.55 N/cm^2) internal pressure. The thickness from A to B was assumed as 0.050 inch (0.127 cm), while three different

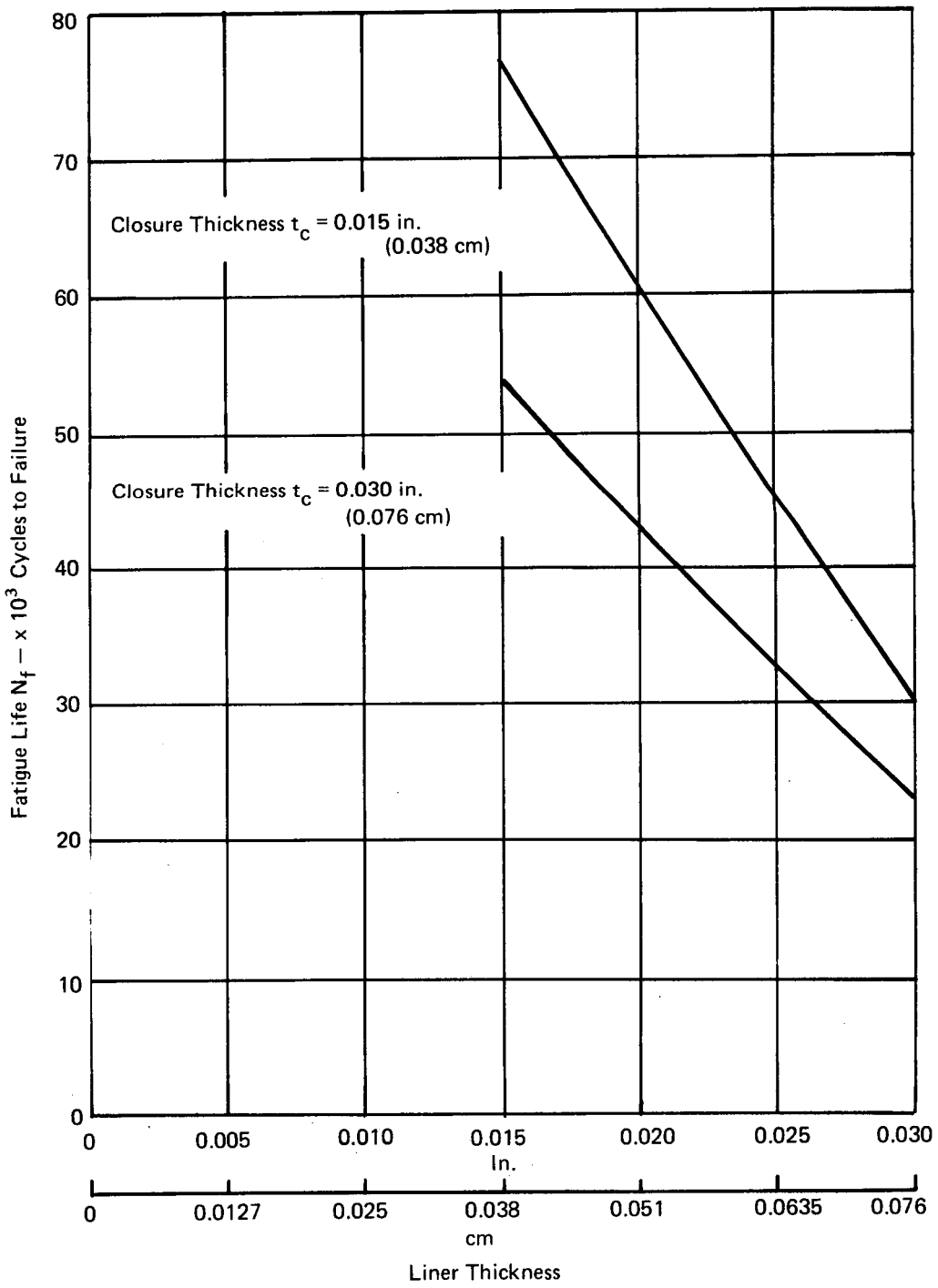

Figure 150. Design Fatigue Capability versus Liner Thickness, Integral Nickel Construction (T.D. Nickel Liner - E.D. Nickel Closure)

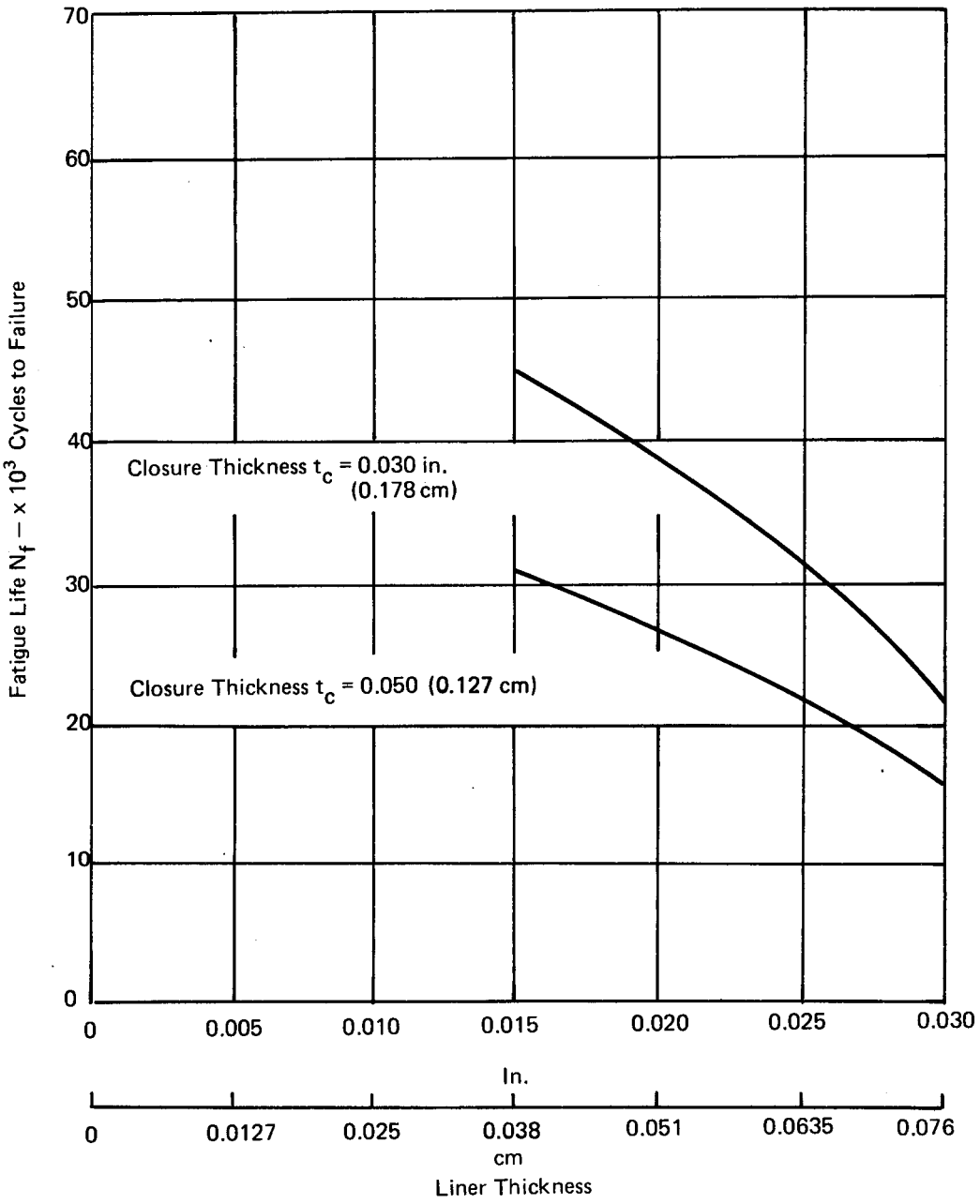

Figure 151. Design Fatigue Capability versus Liner Thickness, Integral Nickel - Copper Construction (T.D. Nickel Liner - E.D. Copper Closure)

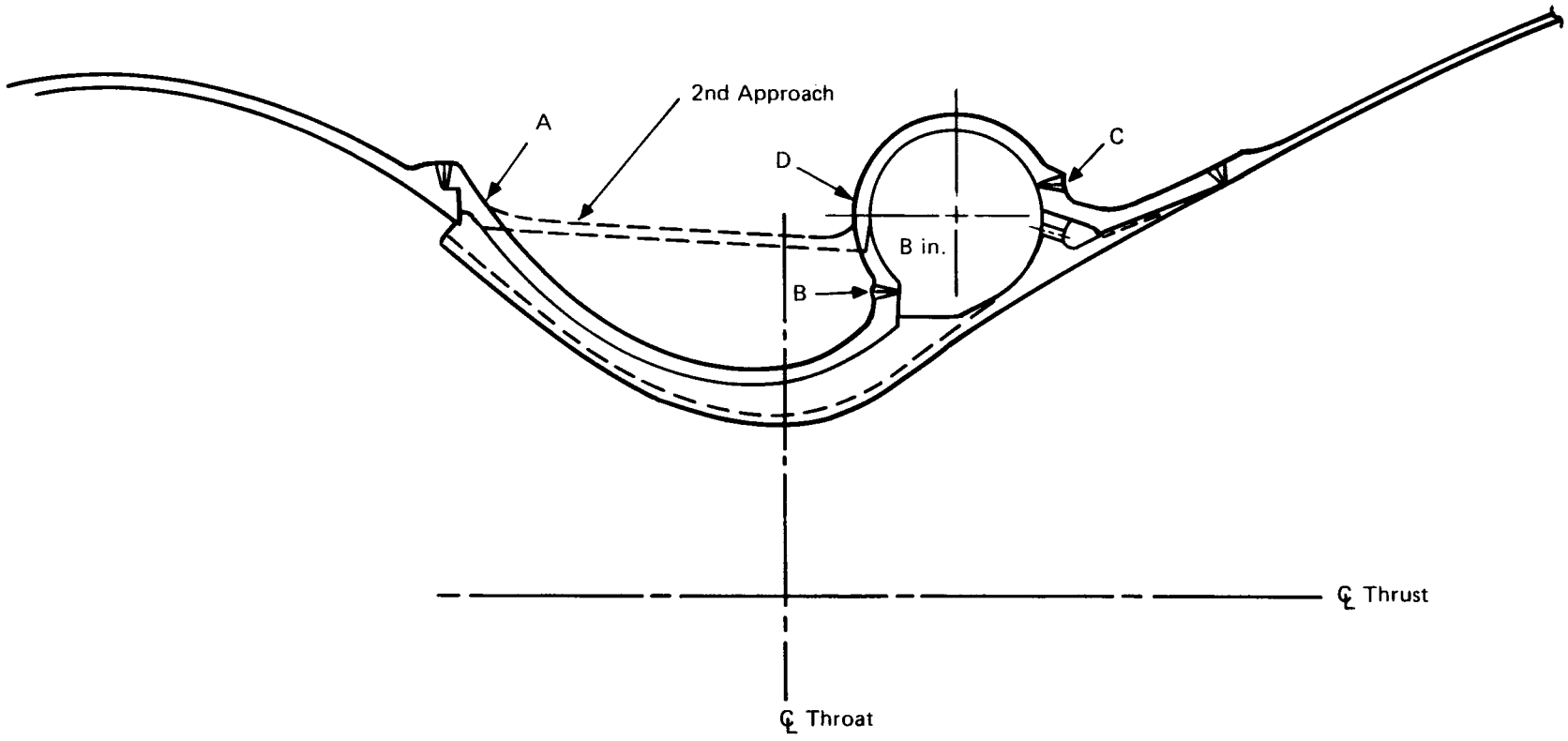

Figure 152. Nozzle/Liner Jacket Configuration

values of 0.015, 0.030 and 0.050 inch (0.038, 0.076, 0.127 cm) were assumed for the B to C connection. In all three cases the internal pressure causes a net contraction of C toward A. This was objectionable because such a contraction adds to the 0.020 inch (0.051 cm) relative expansion which the shell must absorb by action of the attachment forces at A and C. Thus the shell stresses and the attachment forces are prohibitively large.

An alternate concept was examined which provided an attachment between A and B of Figure 152. Preliminary evaluation of this design was made using the computer results of the previous design but considering only the stresses and deflections from points C to D. With a constant 0.050 inch (0.127 cm) thickness stainless steel manifold the maximum combined stress under the action of 375 psi (258.55 N/cm^2) and a deflection of 0.020 inch (0.051 cm) was found to be 67,000 psi (46,200 N/cm^2). For a 100,000 cycle life 347 steel can be cycled from zero to 70,000 psi (48,260 N/cm^2). Thus, the configuration is shown to be feasible. Additional detailed calculations were required because the manifold design was considerably stiffer than that using a bellows. The attachment force on the liner was 175 lb/in. (307 N/cm) or about 10 times that found in the bellows design.

The more detailed calculations of the second approach of the nozzle liner/jacket configuration of Figure 152 were carried out to include the effect of low H_2 feed temperature on stainless steel jacket. The calculations were based on a liner extending to a divergent nozzle area ratio of 6. The lower area ratio was attractive for reduced thrust chamber weight and represented a minor deviation from the contract test hardware. The test hardware nozzle area ratio and the station of H_2 dump cooling for the nozzle extension was approximately 10:1. The reduction of the dump coolant station to 6:1 in the flight configuration represents a minor design change in view of the demonstrated effectiveness of the dump cooling with the H_2 injection pressure designed to match the local static pressure of the core gases. Little change in the nozzle extension temperature profile would be anticipated for dump coolant from an area ratio of 6 rather than 10:1.

The more detailed calculations included three cases of liners with the stainless steel jacket configuration of a shell parallel to the thrust chamber centerline and a semitoroidal section to reduce axial constraint. The three liner configurations were free-standing nickel, free-standing copper and integral copper. The jacket material was 316 or 347 stainless steel. The calculations included consideration of each configuration operating with 540 and 250°R (300 and 139°K) H_2 fuel temperature. Stainless steel jacket thickness was optimized for each configuration. The results of the calculations are presented in Table LIX.

The data of Table LIX shows that the steady-state cycle capability of 100,000 firings was exceeded by all the configurations and that the element with the lowest fatigue capability was the liner and not the stainless steel jacket. The superiority of the free-standing AMZIRC liner over an integral AMZIRC/Electrodeposited copper liner is also indicated.

The calculated cycle life capability of the cylindrical jacket, torous expansion shell, its simplicity and lower weight relative to the bellows approach led to the selection of that configuration for the preliminary flight weight engine design, Figure 153. The figure assumes adequate material joining techniques for TD nickel to stainless steel or zirconium copper to stainless steel.

3. Joining Techniques

The definition of a thrust chamber nozzle section without mechanical joints required joining techniques for the systems of TD nickel to stainless steel and zirconium copper to stainless

TABLE LIX
NOZZLE SECTION CALCULATIONS

Liner Configuration	SS Jacket Thickness inches (cm)	No. of Steady-State Cycles ①	Controlling Element
Free-Standing Amzirc	0.050 (0.127)	490,000	Outer Surface of Liner Land
Integral Copper	0.085 (0.216)	180,000	ED Copper Closeout
Free-Standing TD Nickel	0.075 (0.191)	180,000	Outer Surface of Liner Land

① 250°R (139°K) H_2 Feed Temperature

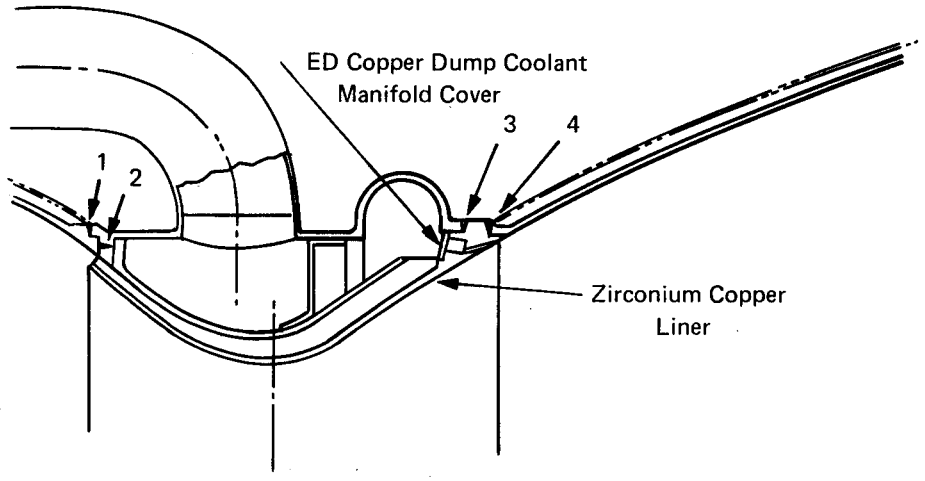

Figure 153. 1,2,3,4 - Joints Zirconium Copper to Stainless Steel

steel, Figure 153. Welding of TD nickel to stainless steel had been demonstrated on other programs at BAC, but joining of copper and stainless steel had not been accomplished. Therefore, a limited effort program was initiated to establish the best approach to joining those materials. The feasibility of brazed joints appeared to be substantiated. A literature review indicated that direct EB welding was also possible. EB weld samples were prepared and tested. The data from those tests, described below, showed that EB welding of stainless steel and zirconium copper could be incorporated in the flight weight thrust chamber design.

Four EB weld samples of Amzirc copper alloy to A151 347 stainless steel were prepared by the BAC Manufacturing Engineering Department and were submitted to the Metallurgical Laboratories for the determination of tensile and bend properties. Load-deflection curves were constructed from bend data obtained by using a three-point loading fixture on a 0.8T bend radius. The resulting curves are shown in Figure 154. The data are consistent for both samples. The majority of the deformation occurred in the Amzirc side of the weld, and good ductility was obtained. Post-test photographs of the samples are presented in Figure 155. Tensile curves for the two tensile tests are given in Figure 156. One specimen broke close to the weld but maintained an elongation value of 3%. This value compares to a 15% elongation noted when failure occurred on the Amzirc side of the weld. Most importantly, the 0.2% offset yield strength values were in close agreement showing satisfactory joining for design purposes. Figure 157 is a post-test photograph of the tensile test specimen.

4. Combustion Chamber and Nozzle Extensions

The combustion chamber of the baseline TCA and the final preliminary design TCA are identical. The internal contour of the combustion chamber is also identical to the 1500-pound (6667 N) thrust hardware tested. A wall thickness of 0.050 inch (0.127 cm) was calculated as adequate for 1×10^6 cycles to a maximum temperature of 1650°F (1172°K). The peak operating temperature observed for tests at 540°R (300°K) feed temperature, an O/F of 4:1 and a chamber pressure of 300 psia (206.8 N/cm^2) was below 1300°F (978°K).

The nozzle extensions included in the flight weight engines would be fabricated from Haynes 25 alloy or columbium. The columbium extension would require a flanged attachment to the chamber nozzle section. The columbium extension would be required for chambers exposed to reentry heating. The Haynes 25 extension would be attached by a weld joint and would require an increased amount of H_2 dump coolant compared to columbium extension which can operate at a higher temperature. Both nozzle extensions could be designed to minimum gage thickness, 0.020 inches (0.051 cm).

5. Weight Breakdown

The predicted thrust chamber weight for the flight configuration engine was established for the preliminary design as depicted by Figure 147 and amplified by Figure 153. The weight breakdown is given in Table LX based on nominal material thicknesses.

Weight reduction below that of Table LX is undoubtedly feasible by modification of the throat liner. The selected cooling passage geometry of the liner was not optimized for weight. Further study is required to trade-off the rectangular passage width and the land height. The overall effect of increased width and decreased height would be to reduce the land volume and thereby reduce the overall liner weight. The effort associated with the flight weight TCA definition was concluded before the liner optimization was completed.

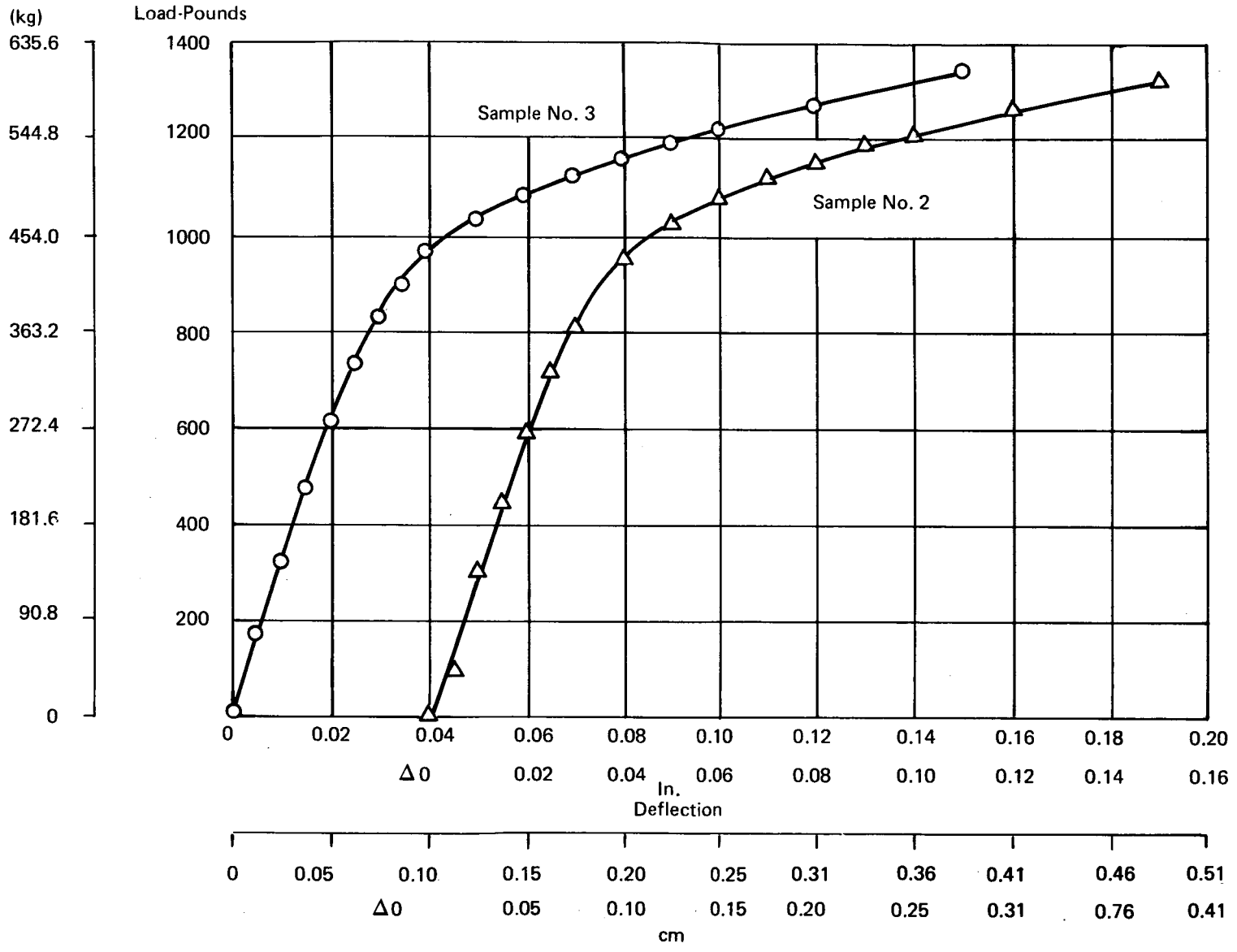

Figure 154. Bend Test Data for E.B. Weldments of Amzirc to AISI 347 Stainless Steel
Bend Radius ≈ 0.8T

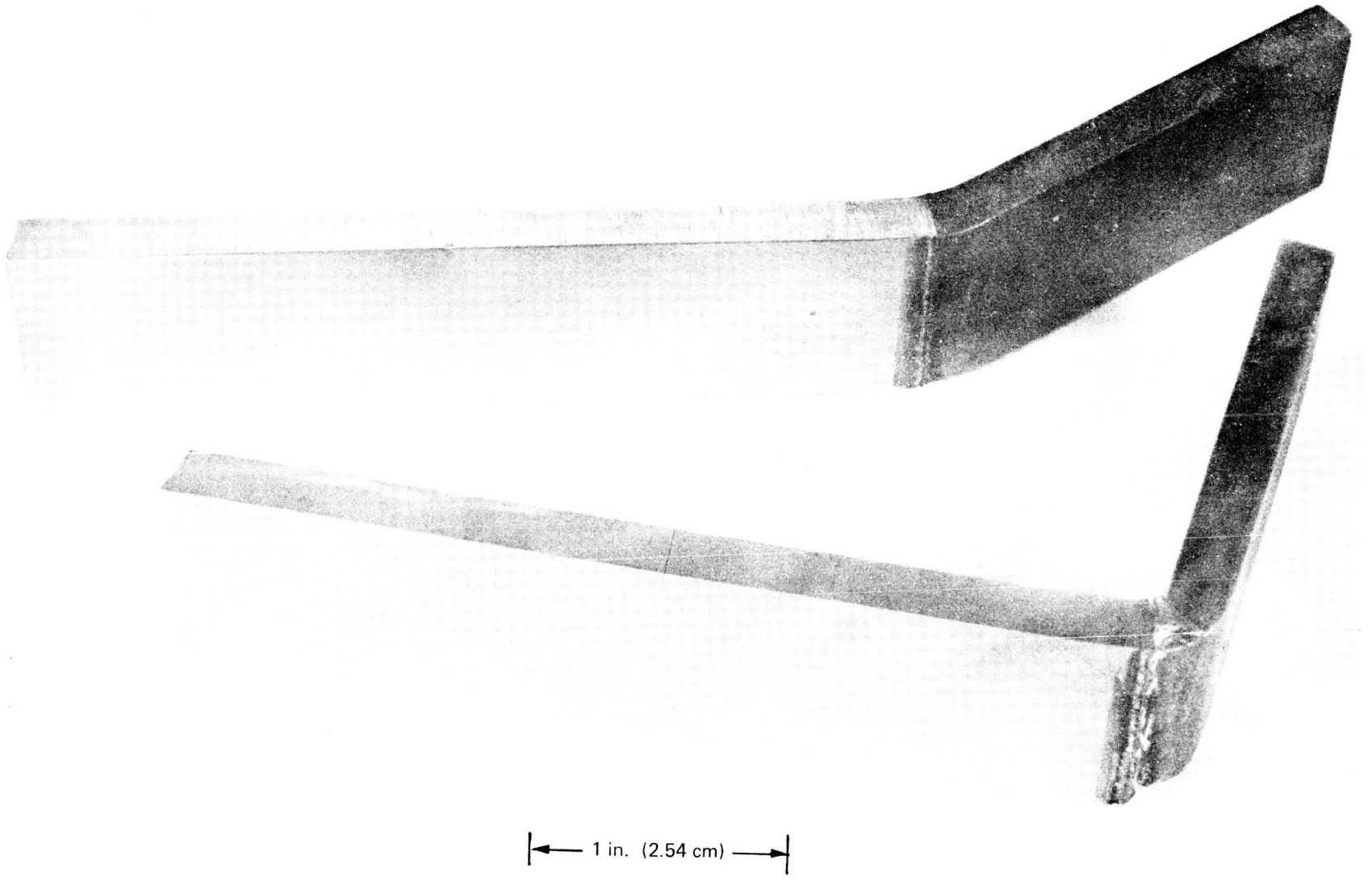

Figure 155. Bend Test Specimens 347 SS and Amzirc

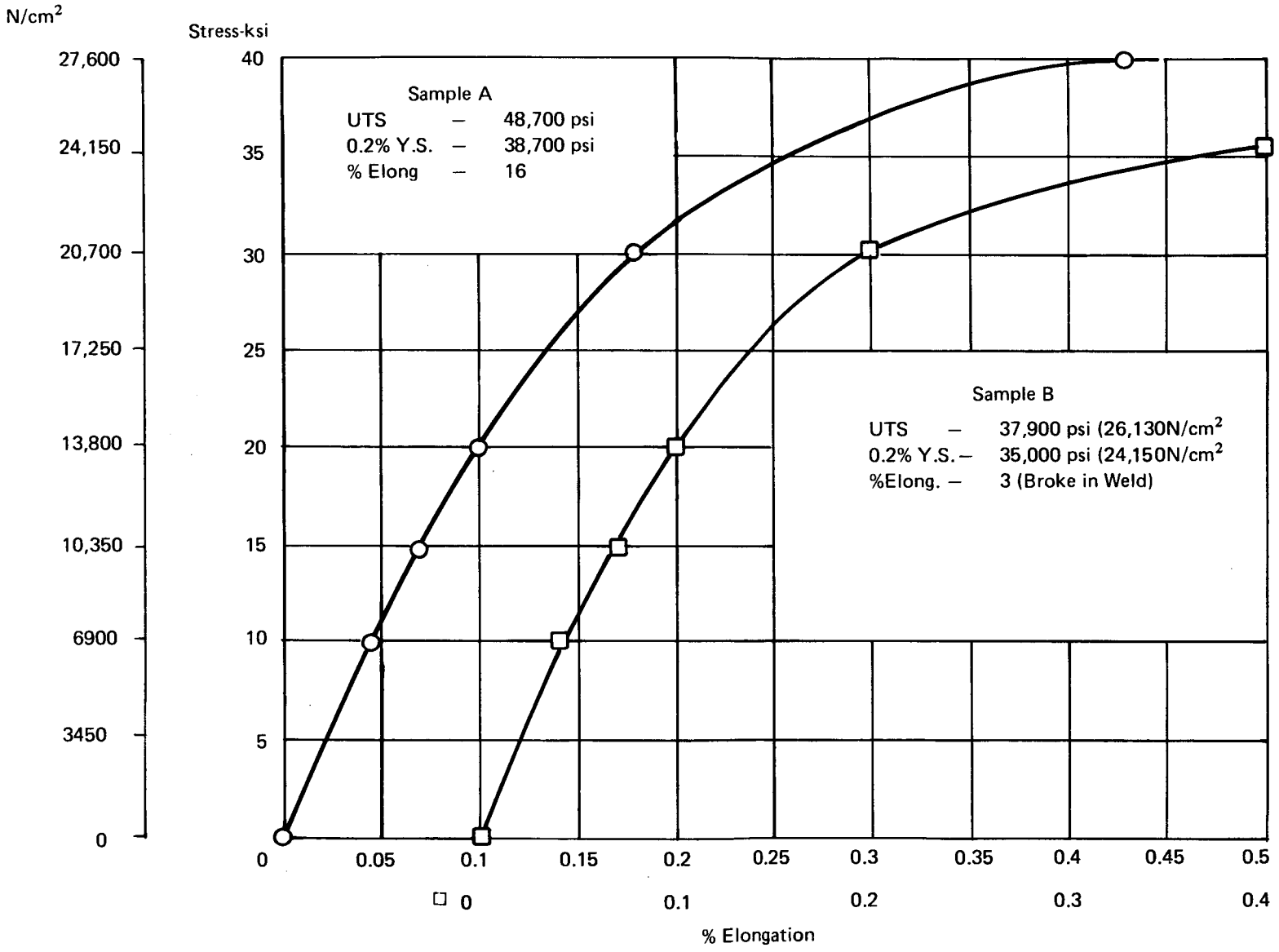

Figure 156. Tensile Data for E.B. Weldments of Amzirc to AISI 347 Stainless Steel

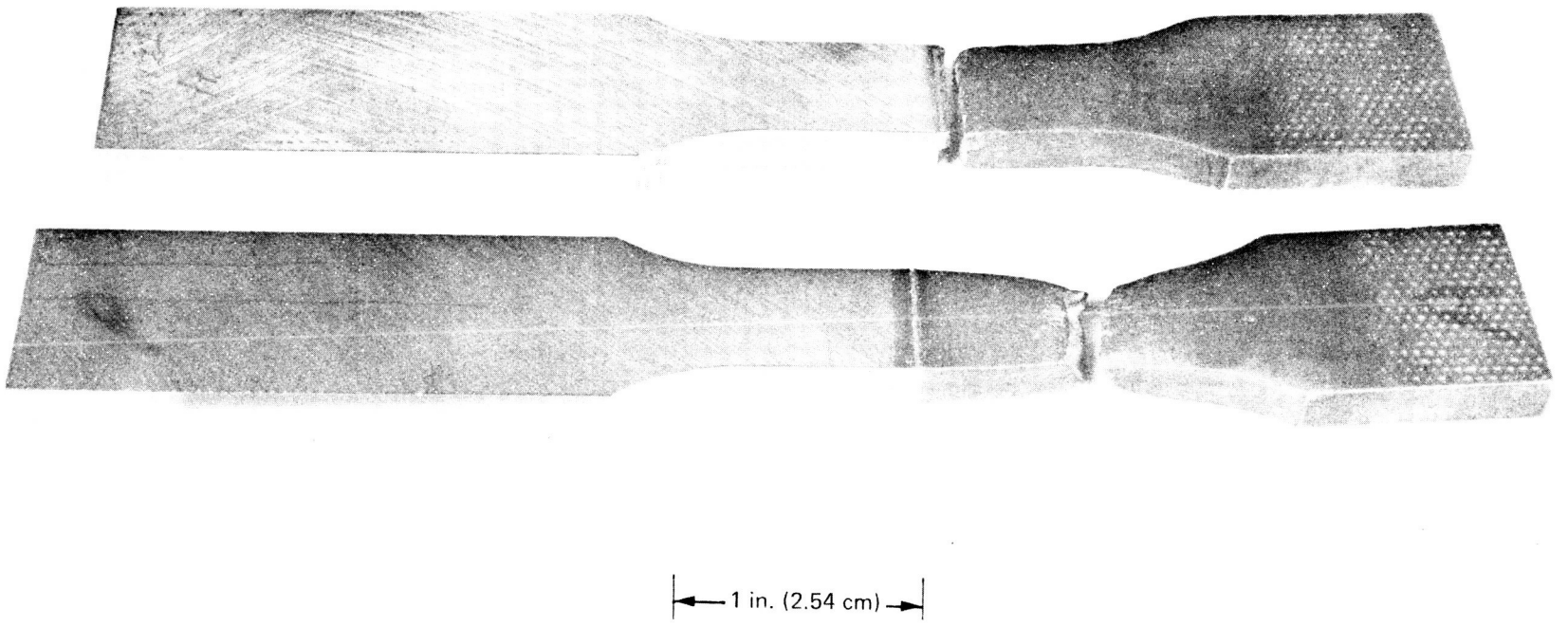

Figure 157. Tensile Test Specimens 347 SS and Amzirc

TABLE LX

TCA WEIGHT BREAKDOWN

	lb	Kg
Thrust Chamber		
O_2 Inlet and Injector Assembly	1.49	0.676
Chamber Shell	1.27	0.577
Spark Plug Part	0.16	0.074
Nozzle Section SS Jacket	1.00	0.454
Nozzle Section Liner	4.10	1.860
Divergent Nozzle Extension	2.10	0.954
	10.12	4.595
Thrust Chamber Assembly		
O_2 Augmentation Line	0.02	0.009
H_2 Feed Line Valve to Nozzle Section	0.50	0.227
Lugs and Bolts for Exciter	0.22	0.100
Engine Mount Bosses	0.31	0.141
Total, TCA	11.17	5.072

C. BIPROPELLANT VALVE

Early versions of the flight weight reverse flow engine incorporated a ball type bipropellant valve sized for the nominal 1500 lbf (6672 N) operating conditions and low propellant feed temperatures. The valve technology effort under contracts NAS3-14349 and NAS3-14350 demonstrated the capability of poppet valve seats for the application. The ball valve approach was dropped in favor of the demonstrated capability of the poppet valve seats. Preliminary designs of a poppet type bipropellant valve were prepared. A preliminary valve specification was sent to the valve technology contractors for additional inputs. A review of the in-house designs and the data forwarded by the valve technology contractors lead to the selection of the Marquardt bipropellant valve configuration.

The principal requirements of the preliminary valve specification requirements are summarized in Table LXI.

The Marquardt valve is a mechanically linked bipropellant valve operated by H_2 gas at engine feed pressure through a three-way solenoid pilot valve. The main valve opens when the solenoid valve is cycled to the vent position. The valve fails safe (closes) for either low propellant feed pressure or interruption of the electrical power to the pilot valve. The bipropellant valve incorporates polymide seats. The three-way pilot valve features a ball poppet which is shuttled back and forth between two all metal seats to alternately open the common port to the vent line and the pressure supply port. The mixing of O_2 and H_2 gas in the event of a single malfunction is

TABLE LXI

PROPELLANT VALVE DESIGN REQUIREMENTS
(Sheet 1 of 2)

PROPELLANTS & TEMP RANGE	
(a) Fuel	(a) Hydrogen gas at 200°R (111°K) to 800°R (444°K)
(b) Oxidizer	(b) Oxygen gas at 250°R to (139°K) to 800°R (444°K)
OPERATING TEMP. RANGE	The unit shall meet all design requirements while being subjected to operating temps of 200°R (111°K) to 850°R (472°K)
PRESSURES	
(a) Nominal Feed	(a) 400 ± 10 psia (275.8 ± 6.9 N/cm^2)
(b) Proof	(b) 600 ± 15 psia (413.7 ± 10.3 N/cm^2)
(c) Burst	(c) 800 ± 20 psia (551.6 ± 13.8 N/cm^2)
DESIGN FLOW RATE	
(a) Fuel	(a) 0.69 lb/sec Hydrogen Gas (0.313 kg/sec)
(b) Oxidizer	(b) 2.76 lb/sec Oxygen Gas (1.25 kg/sec)
PRESSURE DROP	
(a) Fuel	(a) 17.5 ± 2.5 psi (12.07 ± 1.72 N/cm^2) at rated flow & 200°R (111°K)
(b) Oxidizer	(b) 17.5 ± 2.5 psi (12.07 ± 1.72 N/cm^2) at rated flow & 300°R (167°K)
RESPONSE TIME	
(a) Opening	(a) 0.030 seconds maximum (0.015 sec max for electrical at 28.0 VDC and 0.015 sec max for mechanical)
(b) Closing	(b) 0.030 seconds maximum (0.015 sec max for electrical at 28.0 VDC and 0.015 sec max for mechanical)
LEAKAGE	
(a) Internal (maximum)	(a) 100 scc/HR He Gas-5 to 600 psia (3.45 to 413.7 N/cm^2)
(b) External (maximum)	(b) 1 x 10^{-6} scc/sec He gas-5 to 400 psia (3.45 to 275.8 N/cm^2)

TABLE LXI

PROPELLANT VALVE DESIGN REQUIREMENTS
(Sheet 2 of 2)

OPERATING CYCLE LIFE	
(a) Required (minimum)	(a) 100,000 cycles
(b) Design Goal	(b) 1,000,000 cycles
DESIGN SERVICE LIFE (Minimum)	10 Years
MAINTENANCE	The units shall require no maintenance during its design life.
ELECTRICAL CHARACTERISTICS	
(a) Power Requirements	(a) 42 Watts maximum at 28 VDC at 70°F (294°K)
(b) Insulation Resistance	(b) 5K megohms minimum at 500 VDC
(c) Dielectric Strength	(c) With 1000 volts RMS (60 Hz) applied, leakage shall not exceed 1.0 milliamperes between circuit and case.
POSITION INDICATION	Opened and closed valve position indication shall be provided by means of switches or potentiometers.
EMI REQUIREMENTS	The requirements of MIL-STD-826 - Electromagnetic Interference Test Requirements and Test Methods - shall be followed.
VIBRATION - SINUSOIDAL & RANDOM	To be determined.
Shock Acceleration	

precluded by the bipropellant valve design. The proposed valve configuration was described as capable of meeting all the requirements of Table LXI at a weight of 3.75 pounds (1.70 kg) with the three-way solenoid valve contributing another 1.25 pounds (0.567 Kg).

Cycle-life testing of formed bellows was carried out in support of the bipropellant valve definition. The use of bellows in the valve actuator would eliminate the use of sliding seals with a potential improvement of valve assembly reliability. The definition of suitable bellows for a 1×10^6 cycle life application had not been demonstrated to BAC's knowledge. The bellows testing was also desired to check the extensive analytic design techniques which were evolved at BAC as part of the Minuteman III bellows tank development. The Minuteman program also includes a pressure regulator with a bellows of applicable size.

The bellows test definition started with the physical definition of the regulator bellows, Figure 158, and the prediction of its cycle life as a function of its total stroke or deflection. The calculated stroke was 0.075 inches (0.191 cm) for 1×10^6 cycles at a peak actuation pressure of 245 psig (178.9 N/cm^2). A test setup was prepared that provided controlled bellows operation and suitable monitoring to ensure a complete stroke for each cycle (Refer to Figure 159). The first bellows was exercised for a 0.0740-inch (0.188-cm) stroke at approximately 3 cycles/second and progressed to over 500,000 cycles. Failure occurred in the form of a minute circumferential crack approximately 0.18 inch (0.457 cm) in length on the crease of the 3rd convolution from the bottom. A second bellows was tested at the same cyclic rate with the stroke reduced to 0.0715 inches (0.816 cm). The second bellows was tested without failure to 1,532,000 cycles. Prior to the cycle testing both bellows had been subjected to acceptance testing which included 52 minutes of 70 to 450 Hz vibration at 30 second g peak in each axis and 10,000 cycles of operation.

The cycle tests verified the adequacy of the analytical model for bellows design to high cycle life.

D. IGNITION SYSTEMS

Quotations were received from three manufacturers for the exciter, cable and spark plug envelopes consistent with Figure 147. Additional preliminary igniter specification data is given in in Table LXII.

The flight weight engine includes O_2 augmentation at the spark plug and plug cooling with the O_2 augmentation flow identical to the test hardware configuration fired for 500 seconds.

E. ENGINE ASSEMBLY

Based on the preceding discussions the complete layout of the flight configuration engine required one additional definition; the positioning of the valve relative to the TCA. The complete engine weight required a further description of the external insulation thickness.

The engine assembly definition does not include a rigorous analysis of assembly interactions for vibration, shock and acceleration loads due to the absence of definition of those loads. The applicability of the engine mounting arrangement and the interface of the nozzle extension and vehicle skin also require further definition of vehicle requirements and/or restraints.

Side mounted and head mounted valves were considered and the former selected for two reasons:

Dimension	S/N-1190		S/N-1221	
	in.	cm	in.	cm
X (I.D.)	1.110	2.819	1.109	2.807
Y (O.D.)	1.6075	4.083	1.621	4.117
Z (Free Length)	0.9975	2.534	0.9945	2.411
Z (Installed)	0.9605	2.440	0.9605	2.440
Z (Compressed)	0.8865	2.252	0.889	2.258
Stroke	0.074	0.188	0.0715	0.182
Total Deflection	0.111	0.282	0.1055	0.268

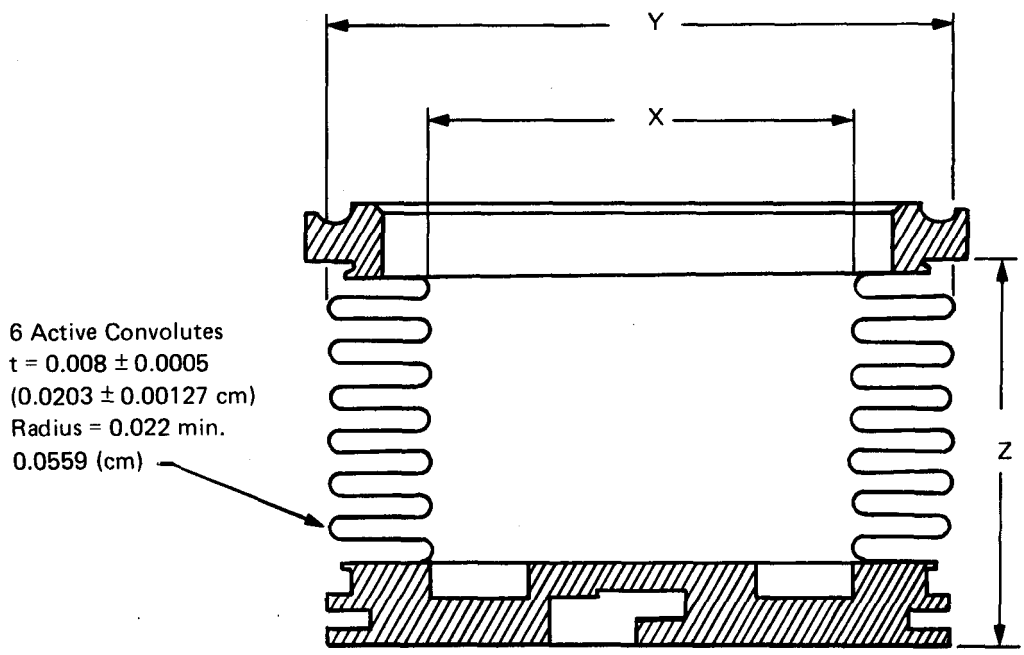

Figure 158. Regulator Bellows

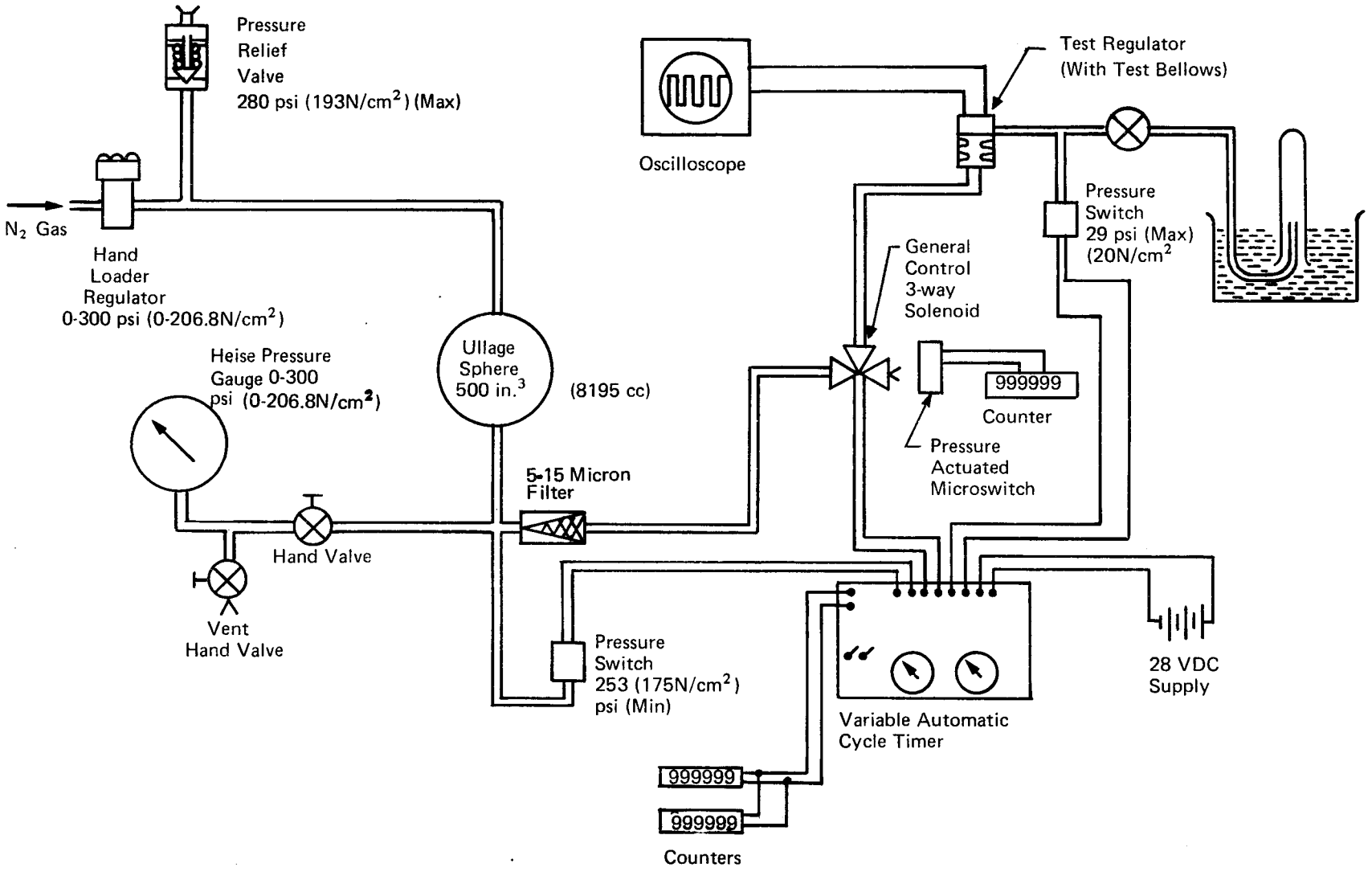

Figure 159. Test Setup for Bellow Cycle Test

TABLE LXII

IGNITION SYSTEM REQUIREMENTS

System Requirements	
Altitude	Sea level to Vacuum
Temperature	
Spark plug	200 to 2000°R (111 to 1111°K), tip (694°K) 1250°R max at mounting flange
Exciter & Cable	200 to 710°R (111 to 394°K)
Vibration	Rising input 5 to 200 Hz 5g, 200 to 2000 Hz.
Acceleration	±3g
EMI	To specification MIL-STD-461A
Life	1,000,000 operations of 0.050 sec. dur.
Spark Timing Repeatab.	±0.5 ms
Envelope	Per BAC Sketch.
Weight, Exciter	To Be Determined
Cable	To Be Determined
Spark plug	To Be Determined
Component Requirements	
Exciter	
Type	Capacitive Discharge
Voltage Input	20 to 30 volts, DC
Spark Rate	150 SPS @ 20 VDC 300 SPS @ 30 VDC
Stored Energy	Define
Output Voltage	10-25 KV
Timer	Exciter "OFF" 0.050 sec. from "ON" signal
Minimum Time Between Cycles	0.050 sec.
Spark Plug	
Type	Surface Gap
Gap Dimension	0.050 inch (0.127 cm)
Breakdown Voltage	4-5 KV at sea level
Spark Energy	10 millijoules @ 28 VDC
Leakage	Zero internal leakage @ 500 psi (344.7 N/cm^2) N_2 pressure at max. temperature

1. The shorter axial length of the reverse-flow TCA relative to conventional designs including the head-end-mounted igniter of the conventional approaches.

2. The reduction of the problem of combustion chamber axial growth during firing and the loads which could be introduced into a side-mounted valve. A single bellows expansion joint in the H_2 feed line eliminates the problem with a head-end-mounted valve.

The insulation thickness depicted in Figure 147 was based on the engine definition for space operation only and an external surface temperature of 800°F (700°K) maximum. That engine would incorporate a zirconium copper nozzle section liner and a Haynes 25 nozzle extension with approximately 9% H_2 dump cooling of the nozzle extension. That coolant flow would give a maximum insulated extension temperature of 2100°F (1423°K) based on the firing test results. The alternate engine designed to withstand reentry heating would incorporate a TD nickel nozzle section liner and a bolt-on columbium nozzle extension. That extension definition would be identical to the test hardware; C103 columbium alloy with Sylcor R512A oxidation resistant coating. The higher operating temperature capability of the columbium extension would result in less dump cooling than the Haynes 25 extension with a corresponding increase in I_{sp}. The colubmium extension would be designed for 2600°F (1700°K) peak operating temperature (insulated) which would require 6% dump cooling based on test data. The higher temperature would result in an increased insulation thickness.

The weight breakdown and performance of the alternate versions of the flight-weight engine are presented in Table LXIII.

TABLE LXIII

WEIGHT BREAKDOWN AND SPECIFIC IMPULSE

Space Operation Engine

Weight Breakdown		lb.	Kg
TCA (with mount)		11.17	5.0711
Insulation Chamber		0.07	0.0318
Insulation Extension		0.56	0.2552
Bipropellant Valve		3.75	1.7025
Solenoid Pilot Valve		1.25	0.5675
Exciter, Cable, Sparkplug		2.50	1.1350
	Total	19.30	8.7631
	$I_{sp\infty}$ *	431 seconds	

Reentry Heating Engine

Weight Breakdown			
TCA (flanged Cb Extension)		11.92	5.4117
Insulation Chamber		0.07	0.0318
Insulation Extension		0.84	0.3814
Bipropellant Valve		3.75	1.7025
Solenoid Pilot Valve		1.25	0.5675
Exciter Cable, Spark plug		2.50	1.1350
	Total	20.33	9.2299
	$I_{sp\infty}$ *	428 seconds (4197 N sec/Kg)	

*Area ratio 40:1, 75% bell nozzle, 375°R (208°K) O_2, 250°R (139°K) H_2 feed temp.

XVI. RECOMMENDED FOLLOW-ON TECHNOLOGY

The results of the reverse flow engine demonstration program were sufficiently successful to demonstrate the usefulness of the concept and the direct applicability of the 1500-pound (6672 N) thrust engine. However, several features need further identification. For the reverse flow engine the two areas requiring effort appear to be the demonstration of flight hardware and demonstration of ignition at the desired propellant temperatures.

The flight-weight demonstration program would be valuable in obtaining information as it relates to the lighter weight hardware. Fabrication of such a unit would also produce real estimates of future problem areas and cost breakdowns. The demonstration of the lighter weight hardware would remove all latent concern about heat transfer confirmation and eliminate any concern that may be related to heat dissipation factors and other operating parameters.

An altitude ignition program is also recommended on the basis that no torch igniter has been evaluated for use with this type of engine configuration. The sequencing of propellants, the valve timing, and the igniter operating parameter data base was considered encouraging but not confirming. It is further recommended that additional testing be conducted with a simplified ignition system providing for optimum valve timing and propellant sequencing. Testing with the simplified system after the background experience of the present program should suffice to prove the capability of producing reliable, reproducible starts.

APPENDIX A

TEST FACILITIES DESCRIPTION

A. TEST FACILITIES

The space shuttle engine test firings were performed at the Bell Test Center Facility. Test cell 1AW was used for all sea-level tests and test cell 1BN was used for all altitude tests. The following sections describe these facilities.

1. Test Facility 1AW

The test facility in which the program injector tests were performed is designed for sea-level tests only and is designated 1AW. A block diagram of the feed system for the heat-sink engine is shown in Figure 160. The propellants used for the program are gaseous O_2, Spec MIL-P-25508A, and gaseous H_2, Spec MIL-P-27201. The O_2 was provided by a trailer which was originally at 2400 psi (1655 N/cm^2). The H_2 was supplied from a 1400-psi (966 N/cm^2) cascade of 48 bottles, with 9.6 ft^3 (2.9 m^3) of gas per bottle. The helium actuation pressure was provided from bottles at 2400 psia, (1655 N/cm^2) with the N_2 supplied from a cascade at over 1000 psia, (690 N/cm^2). Each propellant was fed into the system through a 100-micron filter, then a regulator, which controlled the pressure to the engine. The oxygen flowed through a 2-inch (5.08 cm) diameter swirlmeter and the hydrogen through a 4-inch (10.16 cm) diameter swirlmeter to measure flow rates. The swirlmeters have pressure and temperature sensors to provide the required information to convert volumetric flow rate to mass flow rate. Downstream of the swirlmeters, the propellants pass through a stand valve, then to the engine valves which are monopropellant Flowdyne ball valves. The engine valves have a bleedline tap located just upstream of the valves, allowing the propellants to be bled to the valve inlet prior to firing. The engine has purges downstream of the valves to clear the manifolds of propellants after shutdown, and to allow the hardware to be cooled more rapidly after each test.

The cell is built with a louvered roof to allow dispersion of any hydrogen which might be present.

2. Test Facility 1BN

The altitude simulation system for the thrust chamber cooling tests is located in the test facility identified as 1BN.

The 1BN Facility was constructed for use in the development of the LM Ascent Engine for the Apollo Program (Figure 161). The altitude simulation system includes a 9-1/2-foot (2.9 m) diameter by 24-foot (73.2 m) long chamber (Figure 162) a water-cooled diffuser duct, a water-spray chamber, a 6-foot (1.83 m) diameter vacuum isolation valve, a steam generator and two-stage non-condensing steam ejector (Figure 163). A mechanical vacuum pump is connected to this system for initial pumping down and calibrations prior to firing. The steam source for the ejector system is a gas generator which burns 19.3 lb/sec (8.77 Kg/sec) of alcohol, and 34.6 lb/sec (15.7 Kg/sec) of liquid oxygen which is quenched with 102 lb/sec (46.3 Kg/sec) of water to produce 155 lb/sec (70.4 Kg/sec) of steam at 300 psig (206.8 N/cm^2).

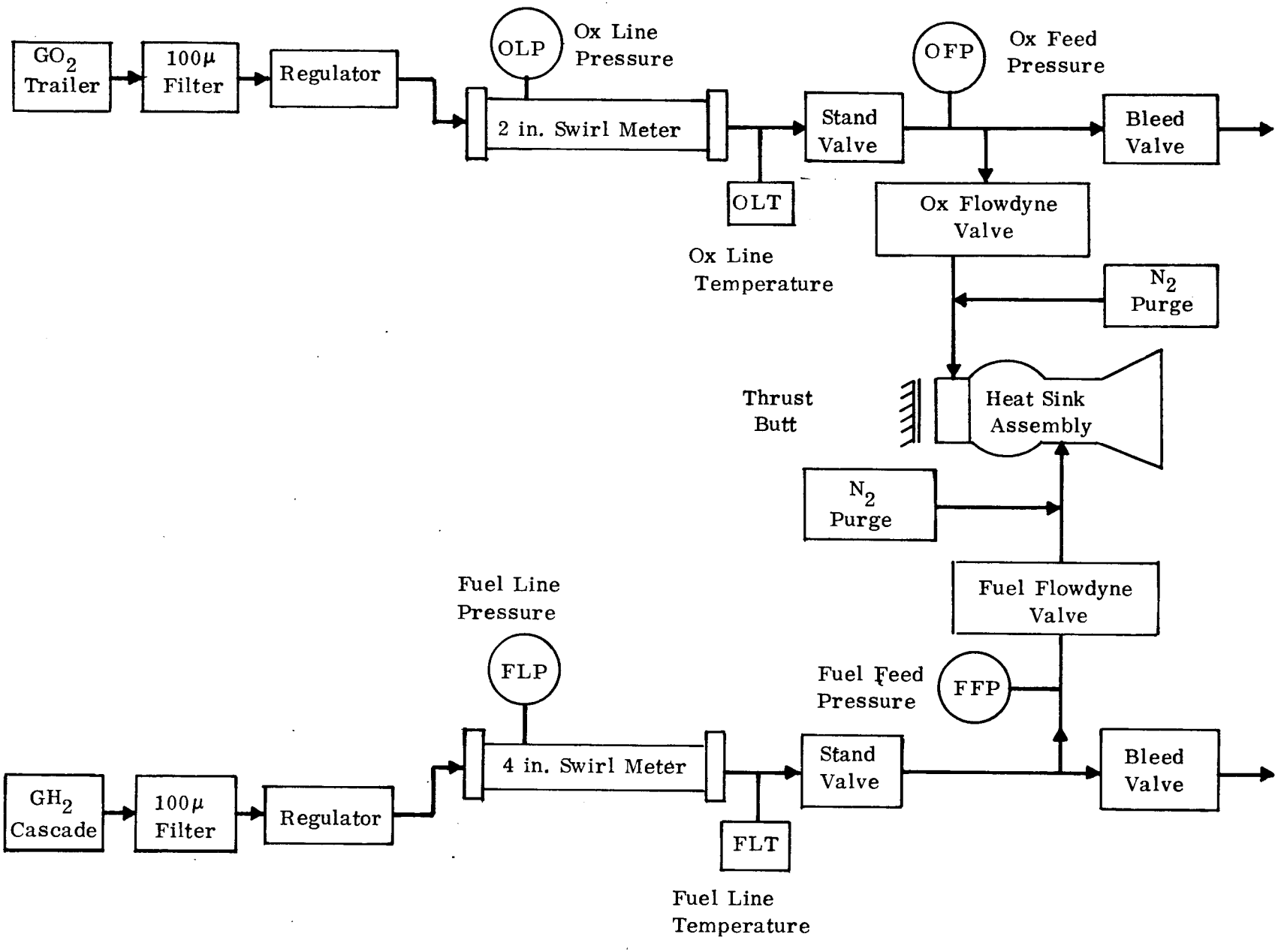

Figure 160. Schematic O_2/H_2 Test Stand Propellant Feed System

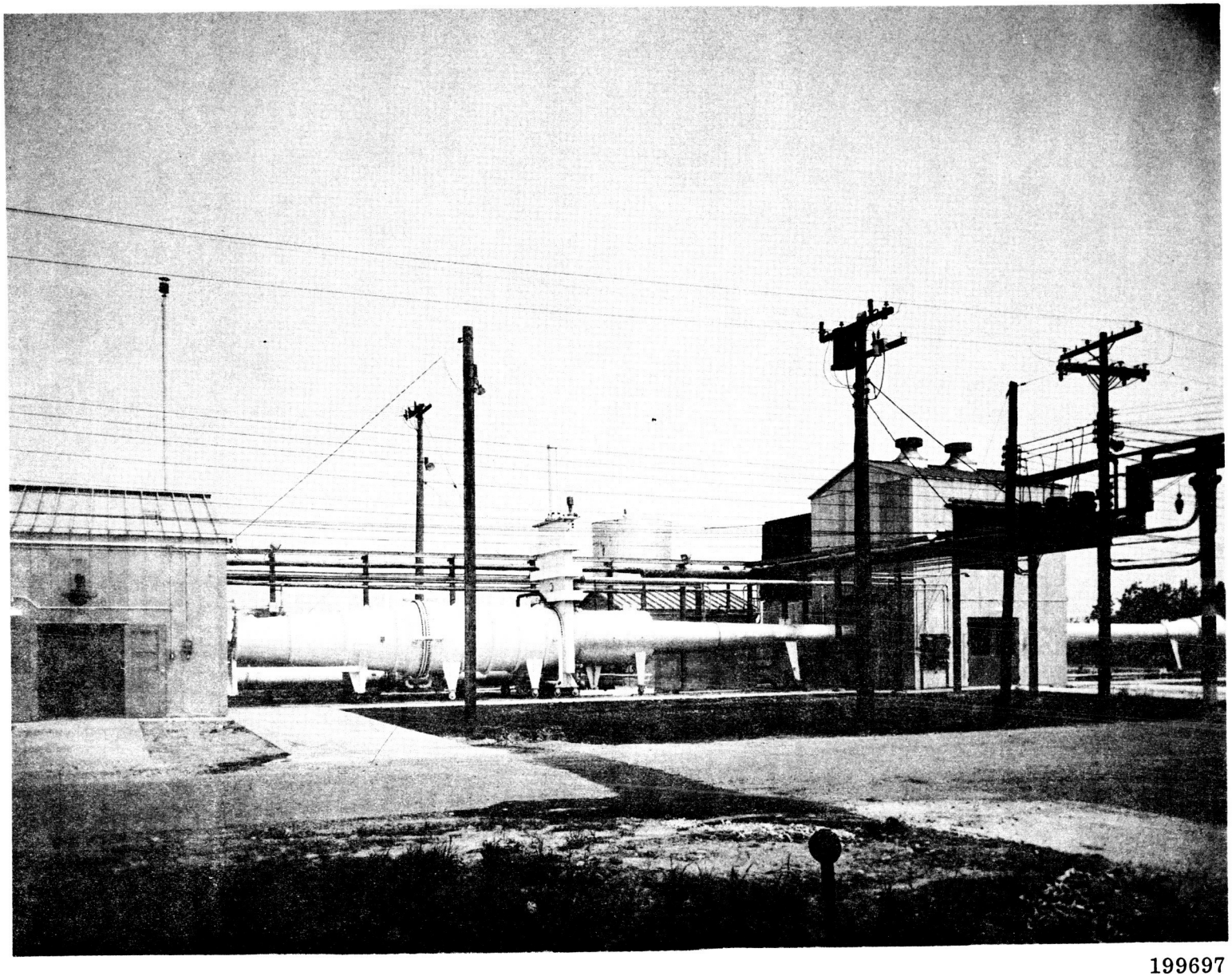

199697

Figure 161. Altitude Facility 1BN

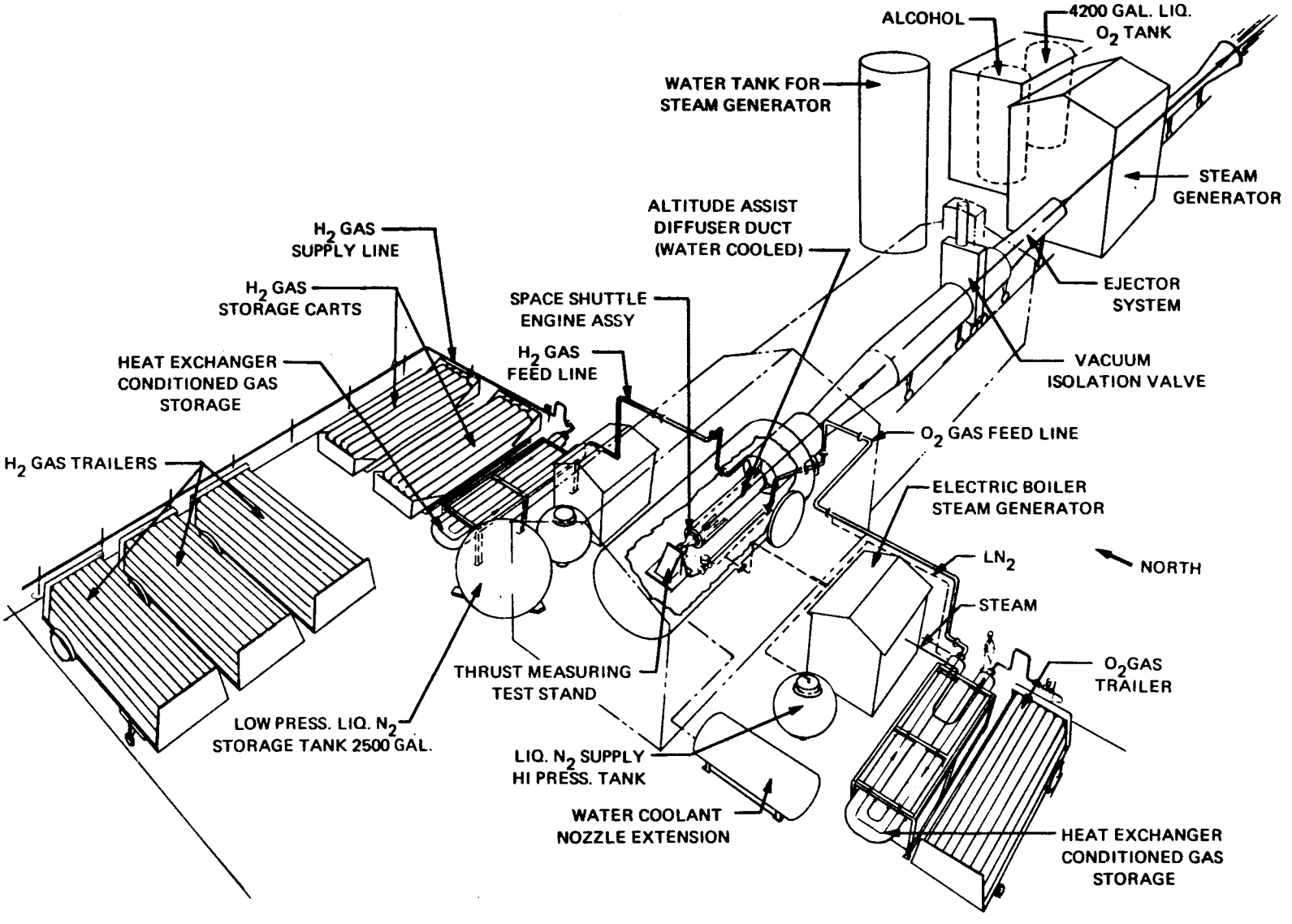

Figure 162. 1BN Facility - Space Shuttle Program

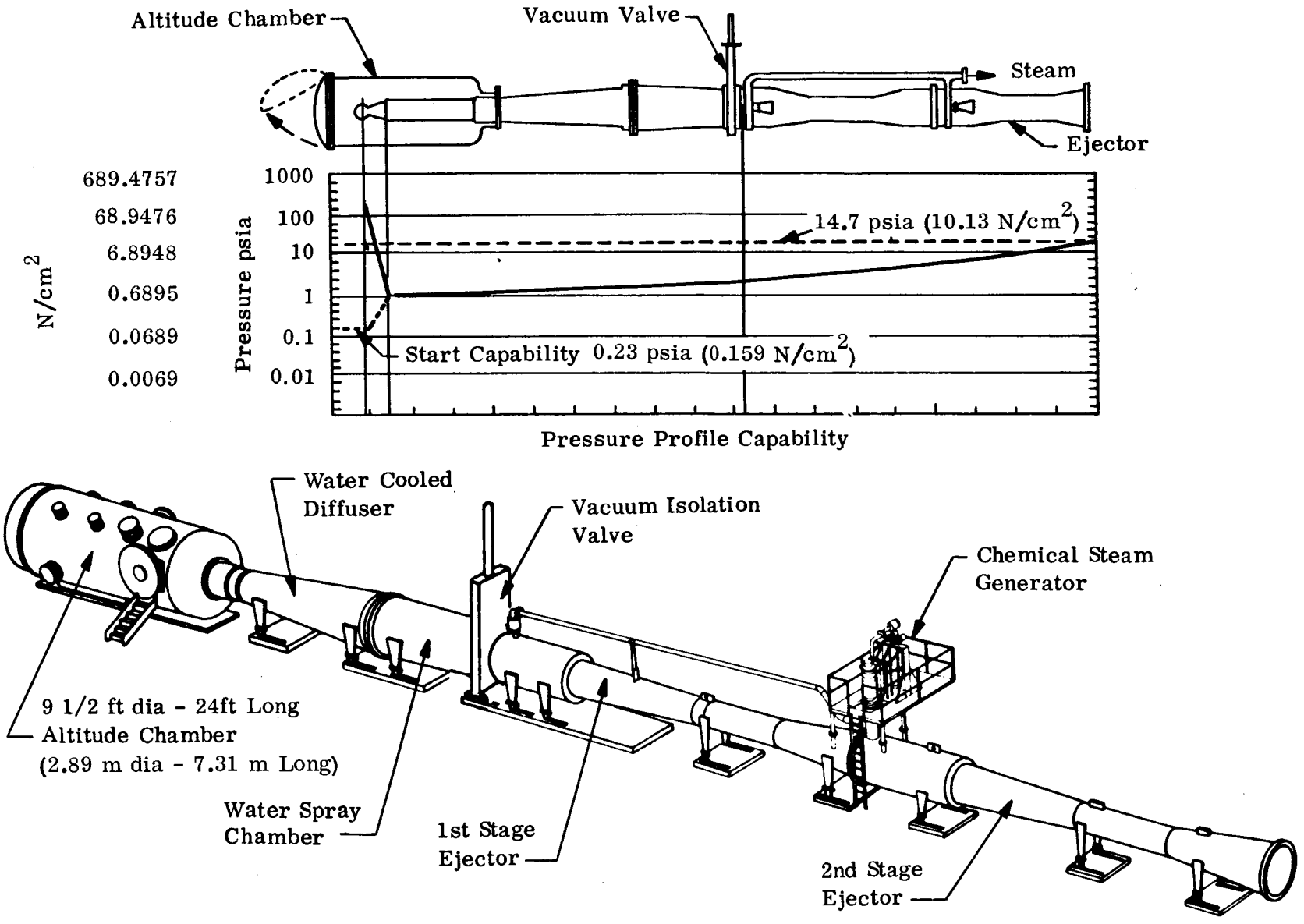

Figure 163. Altitude Facility 1BN Schematic Diagram

This system as originally designed uses a center body diffuser to maintain a cell pressure of 90,000 feet (27,432 m) equivalent altitude while hot-firing the 3500-pound (15,569 N) thrust LM Ascent Engine for 600 seconds. The thermal load imposed by the engine exhaust is cooled to 1000°F (811°K) in the water-spray chamber by injecting water directly in the gas stream. Thermal expansion of the system is achieved without restraint by permitting all components to roll on tracked casters. Provision is made to retract the entire system approximately two feet by an hydraulic cylinder to faciliate service on test stand inside the altitude chamber.

This facility was used, with some modifications and additions, for testing the Space Shuttle engine. A new cylindrical straight diffuser was designed, fabricated and installed to insure that the engine nozzle extension would flow full and maintain simulated altitude. The altitude system is capable of providing a start pressure of 0.15 psia (0.1034 N/cm^2) as demonstrated during the Space Shuttle Engine firings. During pulse mode firings of a maximum of 1.0 sec on and a minimum of 1.0 sec off, the system is capable of maintaining a minimum pressure of 0.5 psia (0.3447 N/cm^2). An updated pressure profile of the altitude system during steady-state test firings of the Space Shuttle Engine is shown in Figure 163.

A schematic of the O_2/H_2 feed system for steady-state testing is shown in Figure 164 and an aerial view of the facility is shown in Figure 165.

Firing Control Console

The firing control console provides separate control of the ignition exciter and the fuel and oxidizer stand valves through solid-state driver circuits with individual regulated power supplies for fast response.

Continuous duty or pulsed firing is possible and shutdown can be made automatically at the end of preset time or preset pulse count or manual shutdown may be made. Pulse width can be varied from 1 millisecond to 10 seconds, fuel and oxidizer start and stop times can be varied from one to 16 milliseconds and ignition exciter duration can be varied from 20 to 200 milliseconds.

A safety interlock system prevents applying power to the control console unless all switches are in the off position and also coordinates firing with the vacuum chamber system to prevent mutual interaction or malfunction of the two systems.

Remote control of propellant tank functions, engine nozzle coolant, and chamber vacuum relief and exhaust functions is provided, and chamber environment is continuously monitored for dangerous concentrations of fuel vapors.

Propellant Conditioning System

The propellant conditioning system consists of a jacketed heat exchanger with a propellant line volume of 26.72 ft^3 (0.7564 m^3) H_2 and 26.76 ft^3 (0.7575 m^3) O_2 at 540°R (300°K).

The heat exchanger has a supply of LN_2 which enters the jacketed heat exchanger at the bottom and is allowed to boil off out of the top port. This method gives the capability to maintain a propellant temperature of 200°R (111°K) on the H_2 side and 275°R (153°K) on the O_2 side. These temperatures are monitored by 24 temperature probes throughout the system. The possible firing duration of the heat exchanger is 45.0 sec O_2 and 13.1 sec H_2 at a cold temperature condition.

The propellant conditioning system also consists of the jacketed propellant feed line with a propellant volume of 5.393 ft^3 (0.1527 m^3) H_2 and 1.838 ft^3 (0.05205 m^3) O_2 at 540°R (300°K).

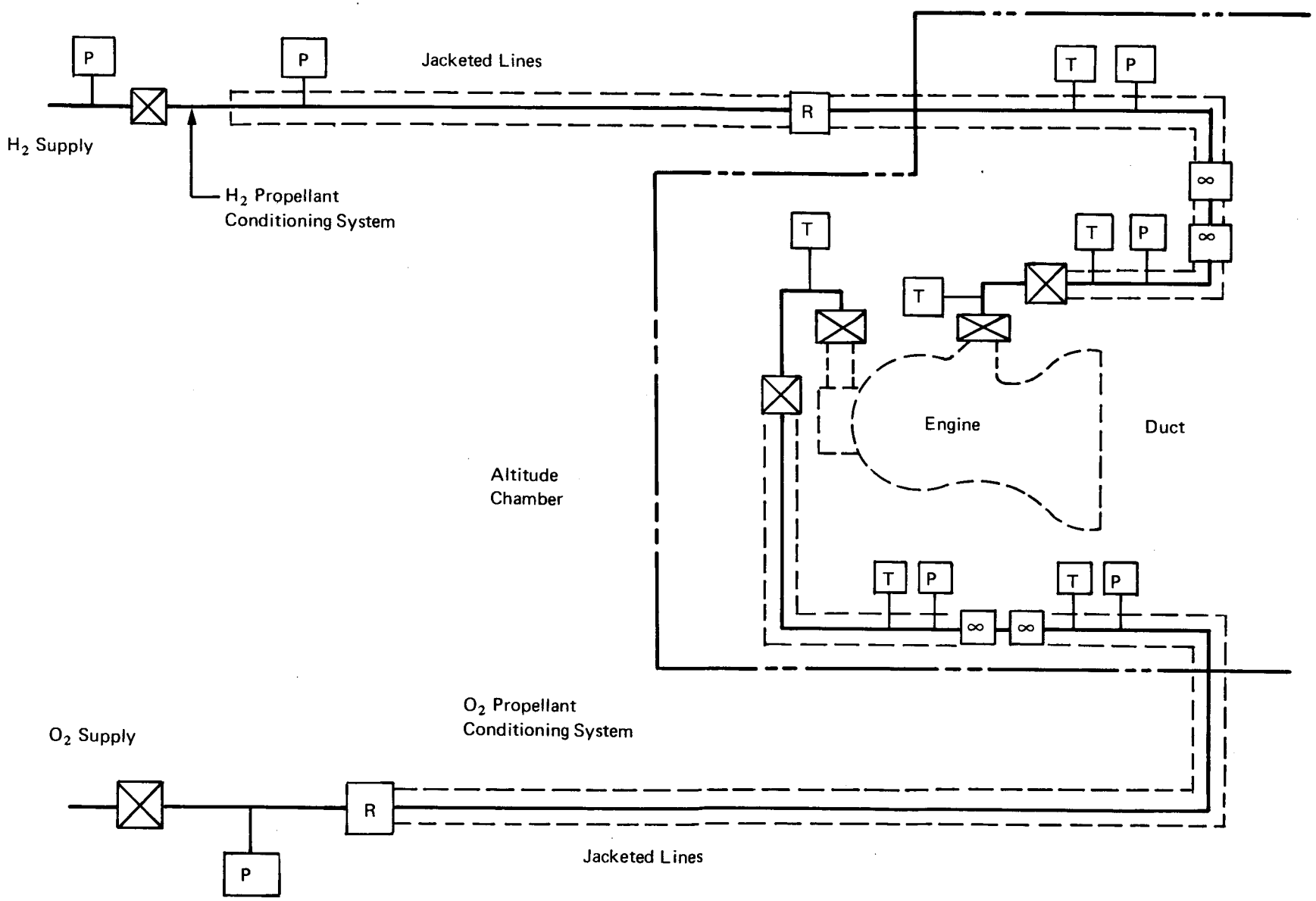

Figure 164. Engine Feed System Schematic

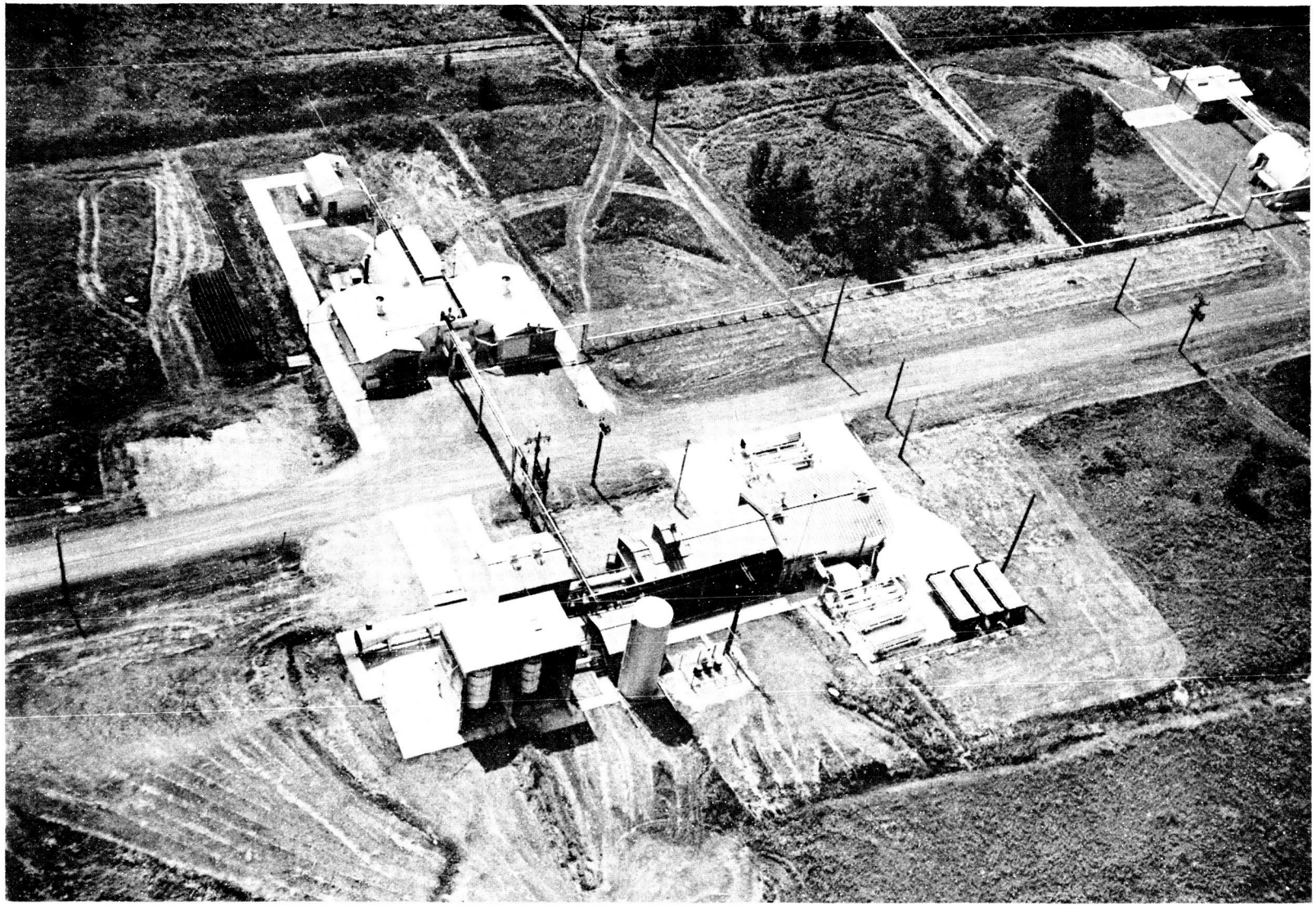

Figure 165. Feed System Testing Facility

The jacketed propellant feed line is supplied by LN_2 in the same manner as the heat exchanger. This provides an additional possible firing duration of 2.2 sec O_2 and 2.9 sec H_2 at a cold temperature condition.

The same jacket line configuration also has an electric steam boiler system which supplies steam at 125 psia (86.18 N/cm^2). This system was used to provide heat for tests having propellant temperature to 800° R (444° K).

Blow-Down System

The blow-down system on the O_2 system consists of a propellant volume of 28.597 ft^3 (0.8099 m^3).

These blow-down line volumes were used as tanks and were charged, isolated and allowed to stabilize for 30 minutes prior to each test. After the tests, the 30-minute stabilization was also followed, allowing temperatures and pressure to come to equilibrium and provide the basis for a total mass flow calculation.

B. INSTRUMENTATION AND DATA ACQUISITION

The following sections describe the instrumentation and data acquisition systems for this program.

1. Instrumentation

In order to obtain the thermal and performance data, standard instruments were used. Parameters were measured to define the starting response, ignition delays, combustion performance, heat flux at the chamber walls and on the nozzle and the system pressure drops. Table LXIV lists the data required, the parameters measured and the type of instruments used. Table LXV lists the instrumentation used and nominal values. Figure 166 shows the heat-sink engine with the instrumentation labeled.

a. Thrust Measurement

For the steady-state tests, a strain gage load cell was used for measuring thrust. The load cell was calibrated with normal feed pressures in the system. The installation in 1BN included the capability for remote cell calibration at altitude.

b. Ambient Pressure

The test cell ambient pressure for 1AW was measured with a mercury monometer and for 1BN was determined by three CEC strain gage transducers.

c. Feed Pressures

Taber strain gage transducers were used for measuring propellant feed system pressures and engine feed pressures.

d. Chamber Pressure

Two types of pickups were employed to measure chamber pressure. One type was a minimum volume Taber transducer with low frequency response and the other was a high frequency response Kistler transducer. The engine normally contained two low frequency transducers and a single high frequency transducer.

TABLE LXIV
ENGINE OPERATING CHARACTERISTICS MEASUREMENT

Engine Characteristics Investigated	Parameters Measured	Instruments Used
1. Heat Rejection	Chamber skin temps. and Nozzle wall temps.	Chromel-alumel thermocouples
2. Injector and Chamber Materials Compatibility and Durability	Wall temps. and visual inspection	Chromel-alumel thermocouples
3. Steady-state performance I_{sp} and c*	Flow rate, thrust and chamber pressures	Swirlmeters, strain gauge load cells and stathem transducers
4. Start response	Rise time from valve start to open to 90% steady-state thrust	Strain gauge load cells and timers
5. System Pressure Drop	Feed, manifold and injector pressures.	Stathem transducers

TABLE LXV
INJECTOR TEST INSTRUMENTATION

Parameter	Nominal Value	Quantity
1. Fuel Flow Rate	0.69 lb/sec (0.313 kg/sec	1
2. Ox Flow Rate	2.80 lb/sec (1.27 kg/sec	1
3. Line Temp	540°R (300°K)	4
4. Line Pressure	600 psia (413.6 N/cm^2)	4
5. Chamber Pressure	300 psia (206.8 N/cm^2)	2
6. Thrust	1145 lb (5093N)	1
7. Feed Pressure	400 psia (275.8 N/cm^2)	2
8. Manifold Pressure	375 psia (258.6 N/cm^2)	2
9. Injector Inlet Pres.	360 psia (248.2 N/cm^2)	2
10. Manifold Temps	70°F (294°K)	2
11. Injector Inlet Temp	70°F (294°K)	1
12. Skin Temp	1000°F (811°K)	12
13. Nozzle Temp	1000°F (811°K)	7
14. Valve Temp	100°F (311°K)	2
15. Valve Voltage		
16. Valve Current		
17. Switch Pip		

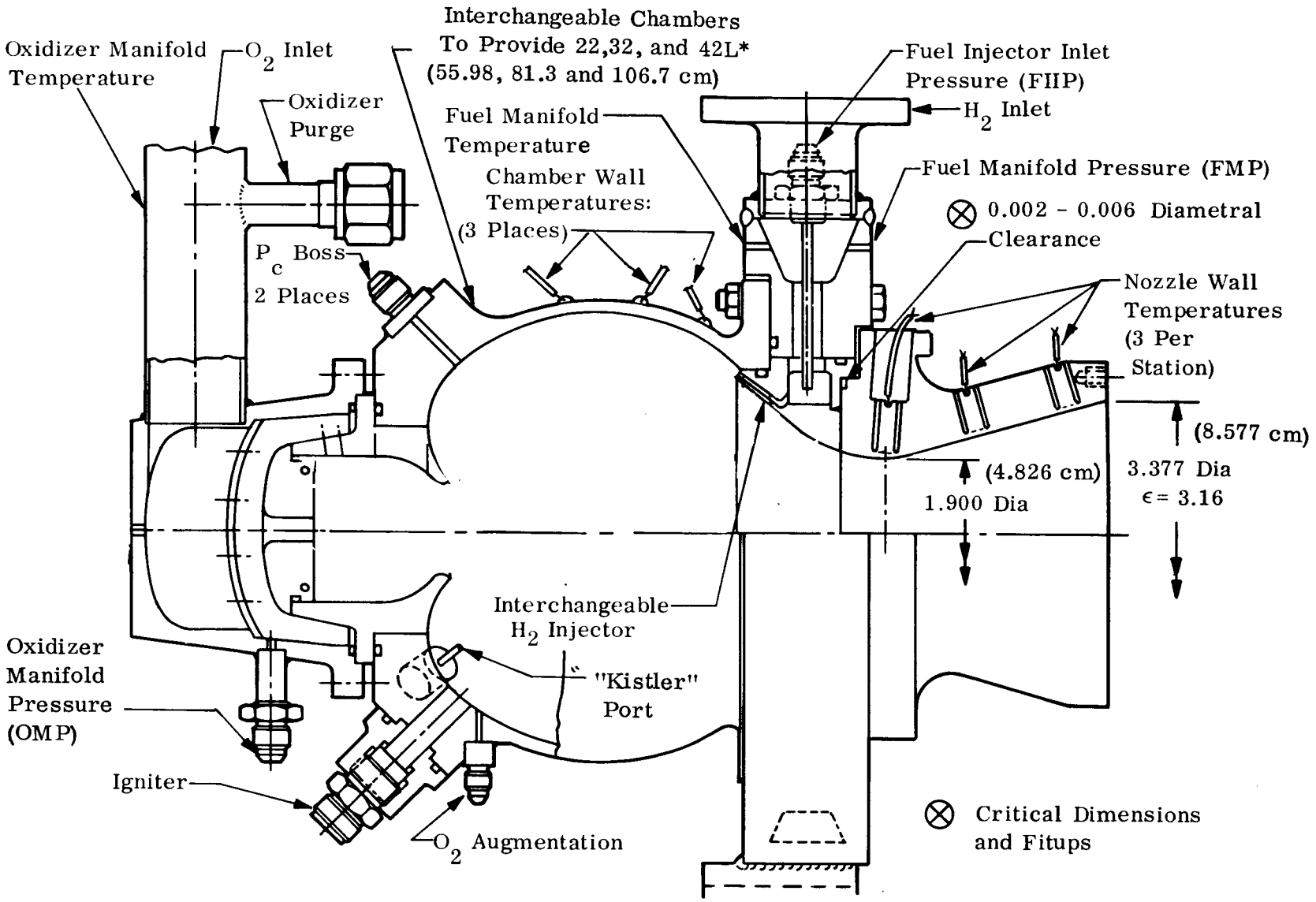

Figure 166. Heat Sink Thrust Chamber Assembly

e. Temperatures

Temperature data were acquired with the following types of thermocouples:

(1) Chromel Alumel - chamber outside wall temperature, nozzle liner temperatures, regenerative nozzle extension temperatures, propellant feed temperatures.

(2) Platinum-Platinum/Rhodium - Columbium nozzle extension outside surface temperatures.

Chromel-alumel thermocouples were spot-welded onto the stainless steel chambers to measure circumferential and axial distribution of the heat flux. The temperatures measured by this arrangement are indicative of those obtained at the oxidizer and fuel injector stations. The temperatures in the copper nozzle section were determined by machining discrete plateaus in the copper nozzle, providing locations at which all the heat transferred is only because of axial conduction. Figure 166 shows this type of configuration. The chromel-alumel open tip thermocouple was joined to the copper at this station by drilling a shallow hole, putting the thermocouple tips in, then peening it over. The temperature readings obtained are directly related to the axial heat transfer in that location.

f. Propellant Flow Measurement Transducer Selection and Description

Fischer and Porter Company series 10/1000 two-and four-inch (5.08 and 10.16 cm) diameter swirlmeters were selected as primary instruments to measure oxygen and hydrogen gas propellant flow, respectively. This choice was originally made on the basis that the swirlmeter has no moving parts, and that the only part susceptible to damage is a thermistor sensor which can be readily replaced. Previous ambient temperature gas flow experience had been very encouraging and, hence, the use for this program.

The swirlmeter generates a precessing vortex at its inlet by vanes of the swirler. As the vortex passes the thermistor probe which is heated by a constant current power supply, the probe resistance and consequently voltage varies. The frequency of variation is proportional to volumetric flow. The vortex is deswirled by straightening vanes at the meter exit and a port is provided in the meter body to pick up static pressure. Propellant total temperature was sensed three diameters downstream of the meter.

ITT Barton Series 7400 two- and three-inch (5.08 and 7.62 cm) diameter gas turbine meters were selected as backup instruments to measure oxygen and hydrogen flow, respectively. These meters employ nonlubricated ball bearings and a free-moving suspended multibladed rotor. Gas flowing through the meter causes the rotor to turn at an angular velocity proportional to volumetric flow rate. A hermetically sealed pickup coil is located on the meter housing in the plane of the rotor. As each rotor blade passes the pickup, a sinusoidal pulse is generated. Inlet and outlet guide vane assemblies are provided which also serve as bearing housings. The turbine meter static pressure was measured two diameters upstream of the meter and the total temperature was measured three diameters downstream.

Signal conditioners were required for both swirlmeters and turbine meters before inputing to a Beckman Type 210 digital data acquisition system. In addition, the swirlmeters required constant current power supplies and variable bandpass filters. The swirlmeter and turbine meter recording systems are shown in block diagrams in Figures 167 and 168.

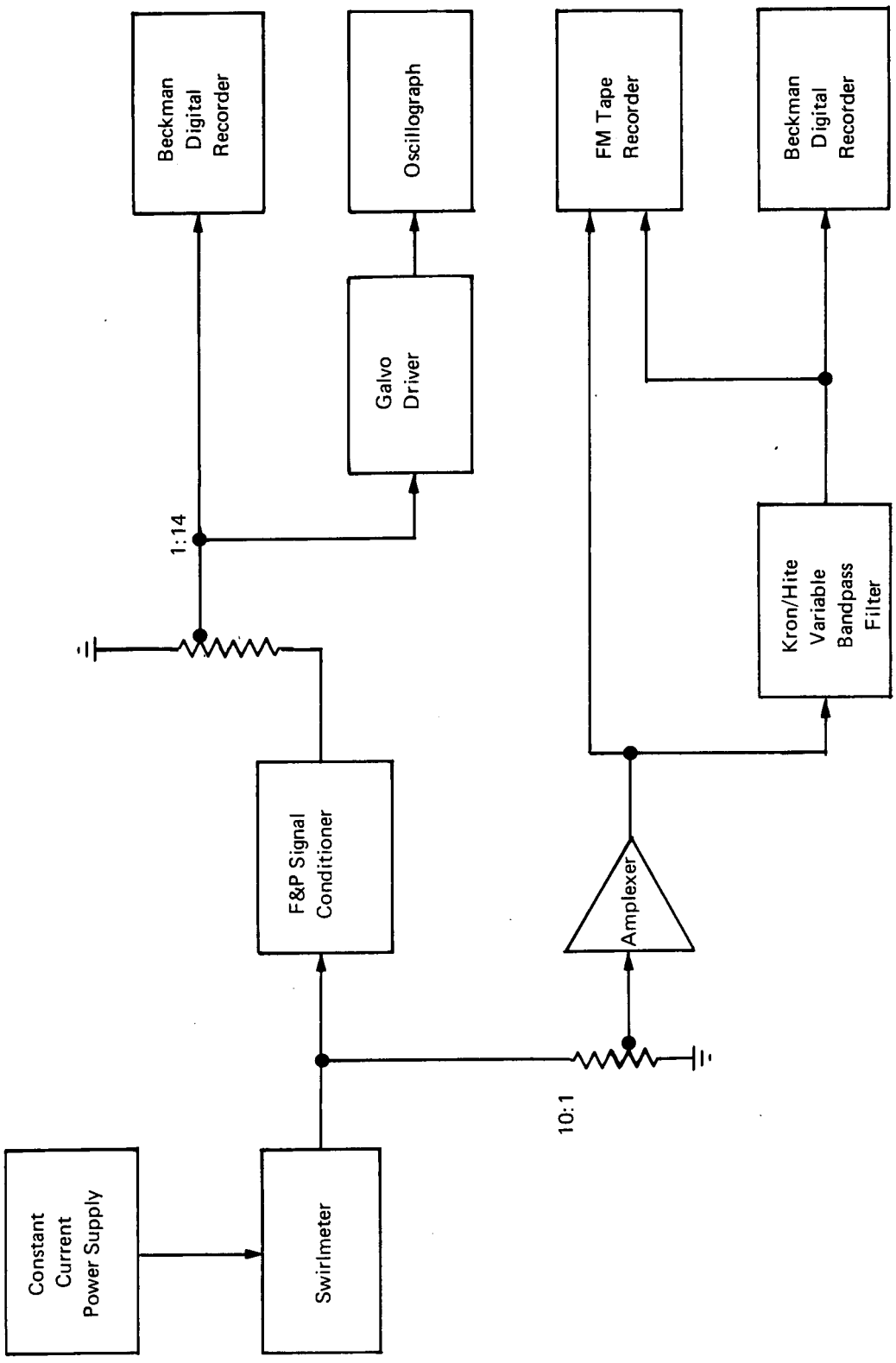

Figure 167. Space Shuttle Swirl Meter Recording System

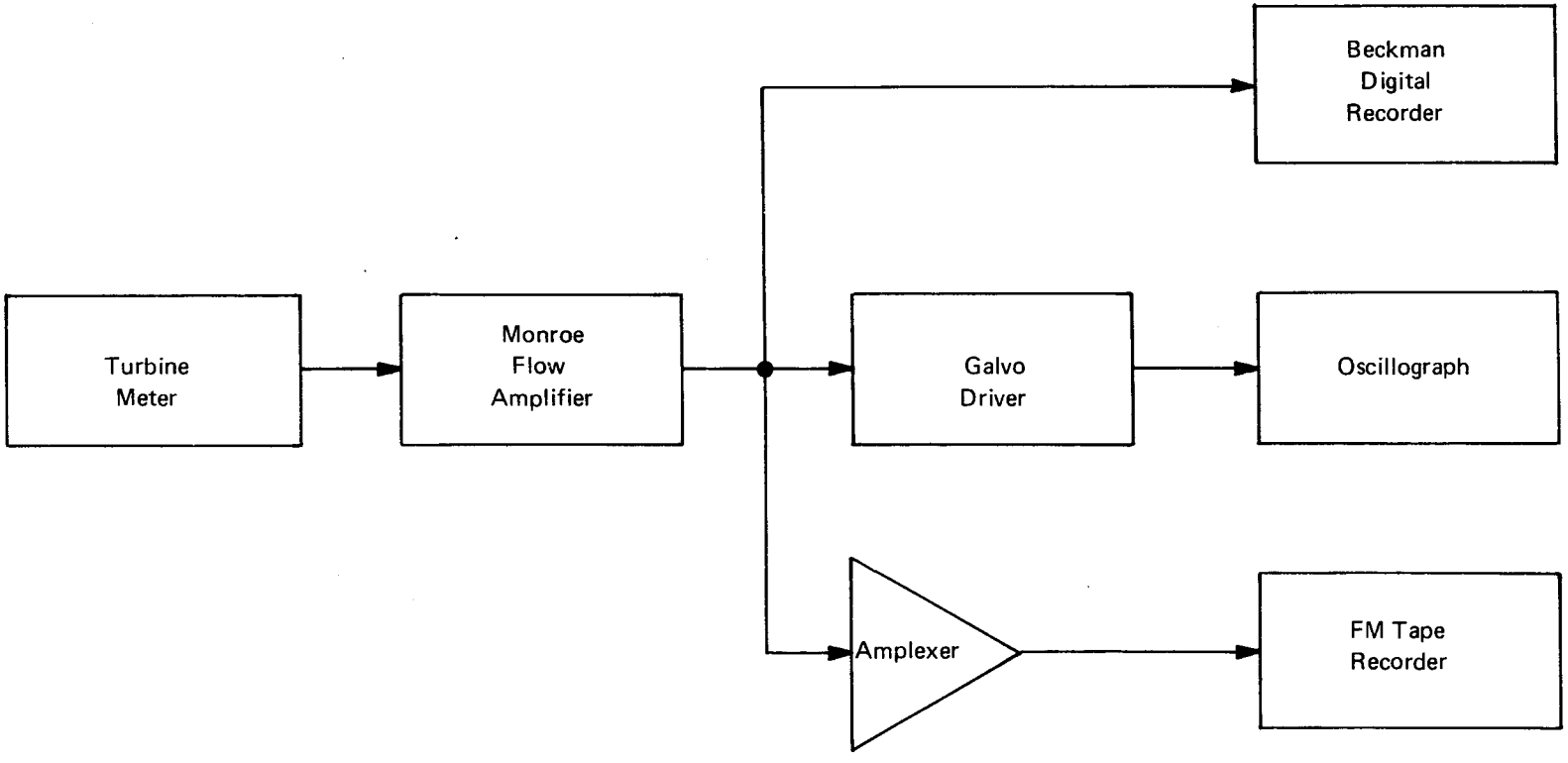

Figure 168. Space Shuttle Turbine Meter Recording System

Ancillary Transducers

Since both types of flowmeters are volumetric devices, it was necessary to measure pressures and temperatures at the meters to compute mass flow rates.

Taber Instrument Corporation series 187 Teledyne absolute pressure transducers were used to measure pressure. The sensing element of these transducers is a one piece Ni-Span C beam to which are bonded four precision strain gages in a Wheatstone Bridge configuration. The bridge is powered by a precision constant current power supply with a series shunt calibrate resistor, thus eliminating cable length errors. Force on the measuring element produces an output voltage proportional to the applied pressure. The sensing element and compensation network are hermetically sealed and isolated from the propellants by a stainless steel diaphragm. The pressure transducers were calibrated against a Gilmore Industries Inc. Model 289 automatic primary pressure standard.

To measure gas temperatures, Conax Corporation type SS6 0.062-in. (0.157 cm) diameter, sheathed, 30-gauge, chromel-alumel thermocouple probes with velocity heads added to minimize velocity error were employed. The oxygen probes had bare wire junctions and the hydrogen probes were swaged down to 0.042-in. (0.1067 cm) diameter since chromel-alumel bare thermocouples are not recommended for application in a reducing atmosphere. The thermocouples were used with a Pace Engineering Company series BRJ 150°F (339°K) reference junction and calibrated against a Hewlett Packard Model 2801A quartz thermometer.

Data Acquisition

All propellant flow parameters are recorded by a high-speed data acquisition system. The millivolt analog inputs from the pressure transducers and thermocouples probes are sampled at a rate of either 200 or ten samples per second. The frequencies are sampled ten times per second.

Analog inputs are amplified and commutated through a buffer amplifier to a sample and hold amplifier where the analog signal is digitized by a four-digit binary-coded decimal (BCD) bipolar analog/digital converter and recorded on magnetic tape.

Each flow frequency is inserted into a counter. The first flow pulse following a start pulse gates a 100-kHz clock into a second counter. After 50 milliseconds, a stop pulse is generated and the first flow pulse following the stop pulse closes the gates of both. Thus, the clock counter contains a precise measure of time required to accumulate an integer of flow counts in the flow counter. The outputs of both counters are recorded on magnetic tape in BCD.

Test Results

The instrumentation used on this program was considered standard with the exception of the gaseous propellant flow meters. The assumption of standard instrumentation for temperature pressure and thrust measurements was borne out in test, and no apparent difficulties existed in these measurements at either ambient or extreme temperature conditions.

The evaluation of the flow meters was a little less positive with all indications of excellent ambient results and some discrepancies apparent at both hot and cold conditions.

The initial ambient tests were conducted with Fisher and Porter swirlmeters. During testing the pressure drop across the flow system was checked against changes in flow and excellent correlation was maintained. When operating cold, however, the thermistor of the swirlmeter was never operated satisfactorily and the collection of flow data was relegated to the ITT Barton turbine meters.

The turbine flow meters worked quite well until the fuel temperature was dropped to less than 250°R (139°K). At the very cold temperature, the data check against system ΔP deviated substantially with the flow meter indicating a lesser flow. Since no cold temperature calibrations were made with these meters, it is difficult to project which parameter is erroneous; however, it is suggested that the ΔP is probably more correct and that the flow meter slowed due to internal binding or some related variance. Admittedly, calibration will be required before the data can be verified. Calibration at both high and low temperatures is a relatively expensive and time consuming task, and was not attempted within the scope of this program.

Operation of the flow meters at high temperature also appears doubtful from the recorded data; however, no direct parameter variation has been found that would relate to a specific piece of doubtful information. The reason the data appeared in error is the extremely high performance recorded at the 750°R (417°K) + propellant temperatures. The differential pressure correlation with flow was again attempted with no error of note being identified.

In summation, the performance data recorded at ambient temperatures appeared to be very representative. The cold temperature data was also considered valid down to approximately 250°R (139°K). At higher temperatures ($>$ 600°R) ($>$ 333°K) and at lower temperatures ($<$ 250°R) ($<$139°K) further calibration is warranted.

2. Data Acquistion

a. The Data Acquisition system used at Bell Aerospace for the Space Shuttle APS engine consists of the following hardware items:

(1) Beckman 210 Data Acquisition System,

(2) IBM 2400 Series Magnetic Tape Recorders,

(3) IBM 360 Digital Computer System, and

(4) IBM 1403 Printing System.

Note:

(1) The Beckman 210 Systems SPACE converts the analog (dc) or frequency output of the transducers to a digital signal and writes this information on magnetic tape. The Beckman System has 30 channels for high-speed recording (200 samples/sec) and 72 channels for low speed recording (10 samples/sec) plus 18 frequency channels.

(2) The IBM Digital Computer system uses a preprocesses program written specifically for this computer system. The preprocesses program converts the incoming digitized signal of the transducers to basic data by using the transducer transfer functions (sensitivities derived in the calibration of the transducer). The basic data, i.e., temperature, pressure, thrust, etc. are written on magnetic tape and

are also printed out for review and analysis. A computer program, written specifically for the Space Shuttle effort, uses the basic data written on tape and computes the steady-state basic engine performance parameters.

b. Basic engine performance parameters are calculated according to instructions contained in the software program. Among the more important of these parameters are:

1. Propellant flow rate – this parameter is composed of the following elements:

   (a) the frequency output of the turbine or swirlmeter,

   (b) a transfer function (cycles/ft^3) for the meter, defined as a function of Reynolds Number, derived in calibration (with test lines and in actual propellants) against a nozzle calibrated against secondary standards at the Colorado Engineering Experimental Station Inc., and

   (c) a calculation of specific weight, as a function of propellant temperature and pressure, by means of interpolation of tables derived from NBS Technical Note 384 for oxidizer and NBS Nomograph 94 for fuel.

2. The parameter, thrust at inifinity, is a calculated value and is composed of the following elements:

   (a) a transfer function for the individual load cells, derived from in-place load cell (BAC secondary standards) calibrations at altitude with feed line pressure at rated value,

   (b) the output of a dual bridge load cell, and

   (c) an extrapolation from the simulated altitude of the test to vacuum conditions.

3. Vacuum Specific Impulse is a calculated parameter composed of the quotient of vacuum thrust and total propellant flow.

4. Pressures are calculated using

   (a) the transducer transfer function (PSI/MV) derived in calibration against a BAC secondary standard dead-weight calibration stand, and

   (b) the output of the transducer in millivolts.

5. Temperature is measured by:

   (a) chromal-alumual thermocouples Ref. 150°F (339°K) used and reduced from standard tables (NBS Circular 561), and

   (b) an optical scanning pyrometer used for large surface area temperatures $>1500°F$ ($>1089°K$); calibrated against a standard calibrated by NBS.

6. Impulse measurement is accomplished by a separate software program in which thrust is directly integrated as a function of time. Flow measurement during pulse mode operation (a pulse train) was accomplished by the pre- and post-pulse train measurement of total weight of propellant in tanks and lines of known volume. The specific weight was calculated from previously referenced tables based on measured propellant temperatures and pressures. The differences in weight, pre-to-post-run calculations, was the amount of propellant consumed in firing the pulse train.

APPENDIX B
SUPPLEMENTARY THERMAL ANALYSES

A. REGENERATIVE COOLING HEAT TRANSFER AND PRESSURE DROP

The steady-state heat transfer analysis is accomplished by axially segmenting the nozzle and performing heat balances on each segment. The heat balance is calculated by a series resistance comprised of the gas-film boundary layer, the thermal resistance of the physical wall of known thickness and the coolant boundary layer. The heat balance is usually made with a one-dimensional flow of heat where the area exposed to both boundary layers is equal. The basic heat transfer equations, the justification for use of specific boundary layer equations, and the calculation of the transport properties of the combustion gas mixtures are presented. The methods employed for coolant passage pressure drop conclude the discussion.

The one-dimensional heat balance equation is

$$\dot{q} = \frac{T_r - T_{wg}}{\frac{1}{h_g}} = \frac{T_{wg} - T_{w\ell}}{\frac{t}{k}} = \frac{T_{w\ell} - T_\ell}{\frac{1}{h_l}} = \frac{\dot{w}_l C_{p_l}}{A_s} \left[\left[T_{\ell_o} - T_{\ell_i} \right] - \left[\frac{\dot{w}_\ell}{A_{\ell_1} + A_{\ell_2}} \right] \left[\frac{V_i^2 - V_o^2}{2gJ} \right] \right]$$

The equation includes the change of kinetic energy of the coolant.

with

$\dot{q}$ = local heat flux rate, BTU/in.^{2} sec

T = temperature, °R

$\dot{w}$ = mass flow rate, lb/sec

h = heat transfer coefficient, BTU/in.^{2} sec° R

C_p = specific heat, BTU/lb° R

t = wall thickness, inches

k = thermal conductivity°, $\frac{\text{BTU in.}}{\text{ft}^2 \text{ hr}^\circ \text{ R}}$

A = exposed area, in.^{2}

V = coolant velocity, ft/sec

g = gravitational constant, ft/sec^2

J = mechanical equivalent of heat, 778 ft lb/BTU

subscripts

r	=	recovery	o	=	outlet
w	=	wall	i	=	inlet
g	=	gas	s	=	surface facing driving temperature
ℓ	=	coolant			

The "Reference Enthalpy" method of Eckert (Reference 24) is used to define the heat transfer coefficient of the high-speed exhaust gas to the wall where a large temperature differential exists. This method considers compressibility effects, recombination of highly dissociated gas species and variable transport properties in the boundary layers. At any axial station the flow properties may be found, using compressible flow relations so that the proper local densities and velocities can be specified. Definition of the state of the combustion gas is obtained from the three-dimensional flow through the nozzle determined by methods of characteristic computer solutions.

In Reference 24, Eckert recommends that the transport properties appearing in the correlation equations be evaluated at a temperature corresponding to a reference enthalpy given by the equation:

$$H^* = 0.5\,(H_s + H_w) + 0.22\,(Pr^*)^{1/3}\,(H_{tot}-H_s) \qquad \text{(B-1)}$$

with

H = enthalpy, BTU/lb

Pr = Prandtl number

Subscript

s = static

w = wall

tot = total

Superscript

* = reference

The equilibrium transport properties used for the O_2/H_2 reverse-flow engine thermal analysis are listed on accompanying tables.

In Reference 12, test data for an oxygen-hydrogen engine were examined and compared with predicted values based on the turbulent pipe flow equation using Eckert's reference enthalpy giving,

$$St^* Pr^{*\,0.7} = C\,Re^{*\,-0.2}$$

For fully developed turbulent pipe flow the value of C is 0.026. It was found that in order to correlate with the test data from the hydrogen-oxygen thrust chamber firings the value of C had to be varied with the area ratio, being a minimum at the throat as shown (from Reference 12):

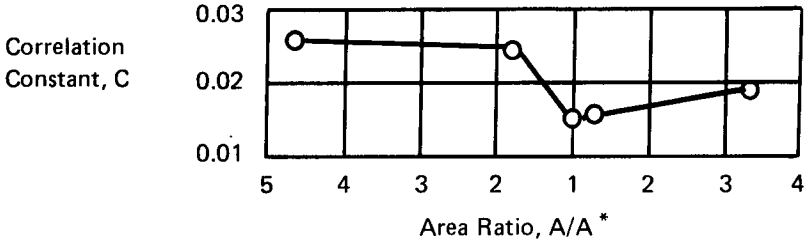

The correlation constant used at BAC was extended to larger area ratios and is shown on Figure 169.

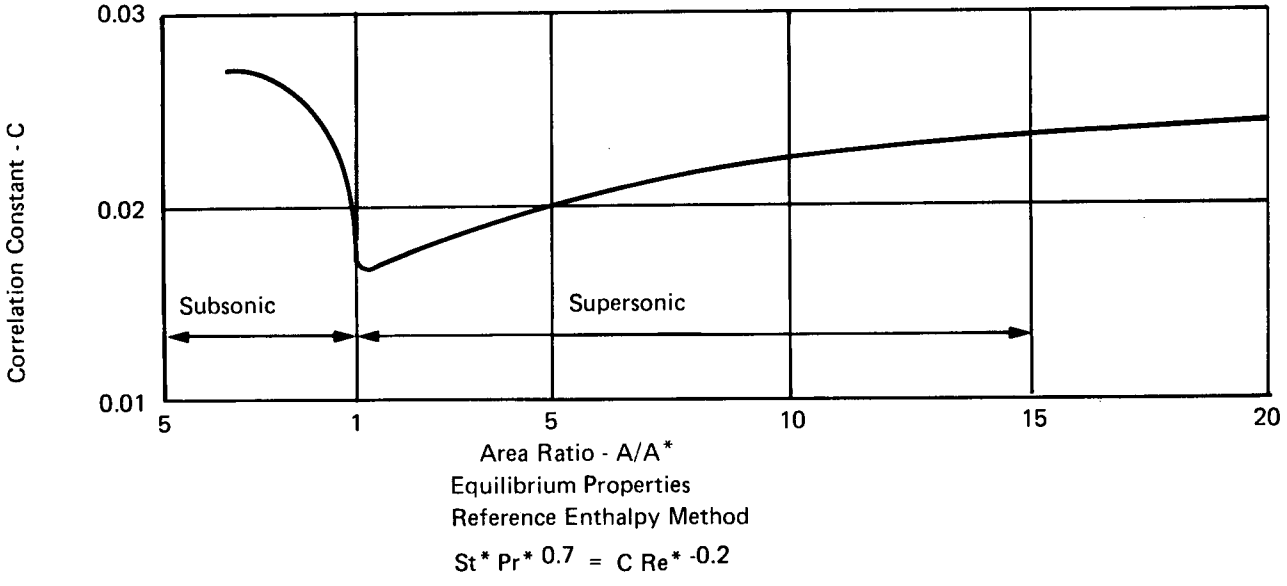

Figure 169. Distribution of Gas-Side Heat Transfer Correlation Constant

The transport properties of the exhaust gas used in the equation are for equilibrium composition gases at the mixture ratio of the gases adjacent to the wall. The properties on accompanying tables, were calculated by Bell Aerospace following methods outlined in Reference 25. A sample of the data generated is given by Table LXVI.

Coolant flowing inside the passages absorbs heat rejected by the combustion gas on the driving side. The coolant, hydrogen gas, is similar to the combustion gas inasmuch as a large temperature differential exists between the bulk temperature of the fluid and the higher temperature of the wall. This factor causes large variations in transport properties within the gas.

The McCarthy-Wolf correlation, as reported in Reference 13, is considered most applicable for hydrogen above 380° R (211°K) at large bulk-to-wall temperature ratios and has been used in the heat transfer analysis of the Space Shuttle thrusters.

The modified equation of McCarthy and Wolf, for supercritical hydrogen for cooling within tubes is expressed in terms of the local mass velocity, hydrogen transport properties evaluated at local temperature and pressure and includes a term from boundary layer density.

$$h_\ell = 0.024 \left[\frac{\dot{w}}{A_\ell}\right]^{0.8} \left[\frac{C_p{}^{0.4}\, k^{0.6}}{0.4}\right]_1 \left[\frac{T_\ell}{T_{w\ell}}\right]^{0.55} \frac{(EFHL)}{D^{0.2}} \qquad \text{(B-2)}$$

with

C_p = specific heat, BTU/lb° F

k = thermal conductivity, $\frac{\text{BTU}}{\text{in. sec° F}}$

μ = viscosity, $\frac{\text{lb}}{\text{in. sec}}$

The McCarthy-Wolf correlation is based on straight heated tube tests. If the coolant passage is curved sufficiently, as in the vicinity of the throat, there is flow rotation inside the passage which will increase the cooling heat transfer coefficient at the large radius facing the combustion gas and reduces the wall temperature for a given applied heat flux. An enhancement factor (EFHL) is for additional cooling of outside walls of passages with curvatures, which has been found to persist downstream of the curved section. An enhancement factor of 1.0 is for a straight tube. Experimental evidence of cooling enhancement within tubes due to rotation is described in Reference 14.

The pressure drop of the compressible gas in the coolant passage is calculated concurrently with the heat transfer analysis. Pressure changes result from heat input, friction and coolant passage area changes over the axial incremental sections. Equations solved are:

$$\Delta P_m = 2 \frac{\dot{w}}{A_o + A_i} \frac{[V_o - V_i]}{g} \qquad \text{(B-3)}$$

$$\Delta P_f = f \frac{(V_o + V_i)^2}{2} \frac{\Delta L}{D} \qquad \text{(B-4)}$$

TABLE LXVI
TRANSPORT PROPERTY DATA - ISENTROPIC EXPANSION

MIXTURE RATIO = 4/1

P atm/N/cm^2	18.7126	189.605	10.6445	107.856	3.7425	37.929	1.8713	18.961	1.2475	12.640
T °R/°K	5462.1	3034.5	5066.2	2814.5	4326.3	2292.4	3837.7	2132.0	3559.8	1977.7
MW lbm/Kgm)	9.885	4.483	9.959	4.517	10.045	4.558	10.069	4.567	10.075	4.570
S BTU/lb-°F/ joule/Kg °C	5.461	23.603 x 10^3	5.461	23.603 x 10^3	5.461	23.603 x 10^3	5.461	23.603 x 10^3	5.461	23.603 x 10^3

P atm/N/cm^2	1.0000	10.1325	0.9356	9.480	0.3743	3.793	0.1871	1.896
T °R/°K	3412.4	1895.8	3368.8	1871.5	2803.4	1557.4	2420.9	1344.9
MW lbm/Kgm	10.077	4.571	10.078	4.5713	10.080	4.5725	10.080	4.5725
S BTU/lb-°F/ joule/Kg °C	5.461	23.603 x 10^3	5.461	23.603 x 10^3	5.461	23.603 x 10^3	5.461	23.603 x 10^3

Specie	Mole Fractions								
H_2	0.47797	0.48381	0.49191	0.49461	0.49536	0.49560	0.49566	0.49597	0.49599
H_2O	0.48391	0.49240	0.50113	0.50320	0.50368	0.50381	0.50384	0.50399	0.50400
H	0.02791	0.01828	0.00584	0.00194	0.00087	0.00054	0.00046	0.00004	0.00000
O	0.00035	0.00013	0.00001	0.00000	0.00000	0.00000	0.00000	0.00000	0.00000
CH	0.00973	0.00533	0.00110	0.00025	0.00008	0.00004	0.00004	0.00000	0.00000
O_2	0.00014	0.00005	0.00000	0.00000	0.00000	0.00000	0.00000	0.00000	0.00000

P atm	Press. (N/cm^2)	T °R	T °K	AE/AT	RHO lb/ft^3	RHO Kg/m^3	Mu lb/ft-sec	Mu Kg/m-sec	CP-EQ BTU/lb-deg joule/Kg °C	
18.7126	189.605	5462.1	3034.5		4.638E-02	0.742936	5.214E-05	7.75942 x 10^{-5}	1.8658	7806.51
10.6445	107.856	5066.2	2814.5	1.0000	2.866E-02	0.459089	4.956E-05	7.37546 x 10^{-5}	1.6191	6774.32
3.7425	37.929	4326.3	2292.4	1.4823	1.190E-02	0.19062	4.442E-05	6.61054 x 10^{-5}	1.2544	5428.41
1.8713	18.961	3837.7	2132.0	2.2529	6.724E-03	0.107708	4.076E-05	6.05191 x 10^{-5}	1.1048	4622.48
1.2475	12.640	3559.8	1977.7	2.9354	4.835E-03	0.0774493	3.859E-05	5.74292 x 10^{-5}	1.0485	4386.93
1.0000	10.1325	3412.4	1895.8	3.4046	4.044E-03	0.0647787	3.740E-05	5.56583 x 10^{-5}	1.0255	4290.69
0.9356	9.480	3368.8	1871.5	3.5617	3.833E-03	0.0613988	3.705E-05	5.51374 x 10^{-5}	1.0197	4266.425
0.3743	3.793	2803.4	1557.4	6.7271	1.843E-03	0.0295220	3.225E-03	4.79941 x 10^{-5}	0.9528	3986.516
0.1871	1.896	2420.9	1344.9	11.0196	1.067E-03	0.0170917	2.876E-05	4.28003 x 10^{-5}	0.9122	3816.65

CP-FR BTU/lb-deg joule/Kg °C		K-EQ BTU/ft-sec-deg joule/m-sec - °K		K-FR BTU/ft-sec-deg joule/m-sec-°K		PR-EQ Prandtl No. Equilibrium		PR-EQ Prandtl No. Frozen		H BTU/lb joules/Kg	
1.1047	4622.07	2.171E-04	-0.4175	1.041E-04	0.2002	0.4480	These no.	0.5532	These no.	-124.5	-289.4 x 10^3
1.0901	4560.98	1.763E-04	0.3390	9.751E-05	0.1875	0.4551	are dim-	0.5541	are dim-	-719.3	-1672.2 x 10^3
1.0570	4422.49	1.138E-04	0.2188	8.470E-05	0.1629	0.4894	ensionless;	0.5543	ensionless;	-1694.2	-3938.1 x 10^3
1.0288	4304.50	8.675E-05	0.1668	7.581E-05	0.1458	0.5191	hence,no	0.5531	hence,no	-2252.9	-5236.7 x 10^3
1.0110	4230.02	7.599E-05	0.1461	7.068E-05	0.1359	0.5325	conver-	0.5520	conver-	-2548.9	-5924.8 x 10^3
1.0009	4187.77	7.137E-05	0.1372	6.795E-05	0.1306	0.5374	sion	0.5511	sion	-2700.8	-6277.9 x 10^3
0.9978	4174.795	7.011E-05	0.1348	6.711E-05	0.1290	0.5388	needed.	0.5508	needed.	-2745.2	-6381.06 x 10^3
0.9504	3976.47	5.655E-05	0.1087	5.624E-05	0.1081	0.5434		0.5451		-3301.7	-7674.6 x 10^3
0.9119	3815.39	4.872E-05	0.0937	4.867E-05	0.0936	0.5385		0.5388		-3653.2	-8503.3 x 10^3

where

f = friction factor

ΔL = length increment of tube

D = average hydraulic diameter of tube

and after Von Karman

$$\frac{1}{\sqrt{f}} = 4.0 \log (R_e \sqrt{f}) - 0.40 \qquad \text{(B-5)}$$

These equations were coded into the heat transfer digital computer programs. A required outlet pressure of the coolant is stipulated and the equations solved iteratively by estimating initial coolant pressures until the calculated outlet pressure and stipulated outlet pressure converge. The thermodynamic and transport properties of equilibrium hydrogen are taken from References 26, 27 and 28. The properties are kept as a function of pressure and temperature within pressures of 14.6 to 3000 psia (10.06 to 2068 N/cm^2) and within temperatures of 60-3000° R (33.3 - 1666.7° K).

Losses in total pressure at turns, during sudden contractions and expansions were calculated from empirical data. The losses are calculated in terms of the upstream dynamic pressure for each explicit geometric case. The SAE report (Reference 29) used for this analysis was especially valuable as it included loss coefficients for branch configurations and mitered duct turns not found elsewhere. A more thorough and up-to-date document is Reference 30.

B. CORRELATION OF REGENERATIVE COOLING ANALYSIS WITH 1K (4448N) CHAMBER DATA

1. General

The test data obtained previously on the company-sponsored 1000-lbf (4448N) reverse-flow engine were correlated with heat transfer and pressure drop analyses early in the NAS3-14353 program. These tests were conducted on two types of regeneratively cooled, reverse-flow chambers, one incorporating a drilled copper nozzle section, the other an EDM'd, channeled TD nickel nozzle section. Drawing 8612-478005, Figure 170 shows the thruster assembly.

The correlation of test data and analyses was made for the following:

(1) Coolant (H_2) temperature rise through the drilled copper nozzle section versus mixture ratio.
(2) Hot-wall temperature of the TD nickel-channeled nozzle section versus mixture ratio.
(3) Pressure drop of the TD nickel-channeled nozzle section versus mixture ratio.

The following parameters and assumptions were used for the pressure drop and heat transfer analysis.

Chamber pressure	250 psia (173.3 N/cm^2)
Throat diameter	1.70 in. (4.32 cm)
Mixture ratio	3, 4, 5
Combustion Efficiency	94%, 100%

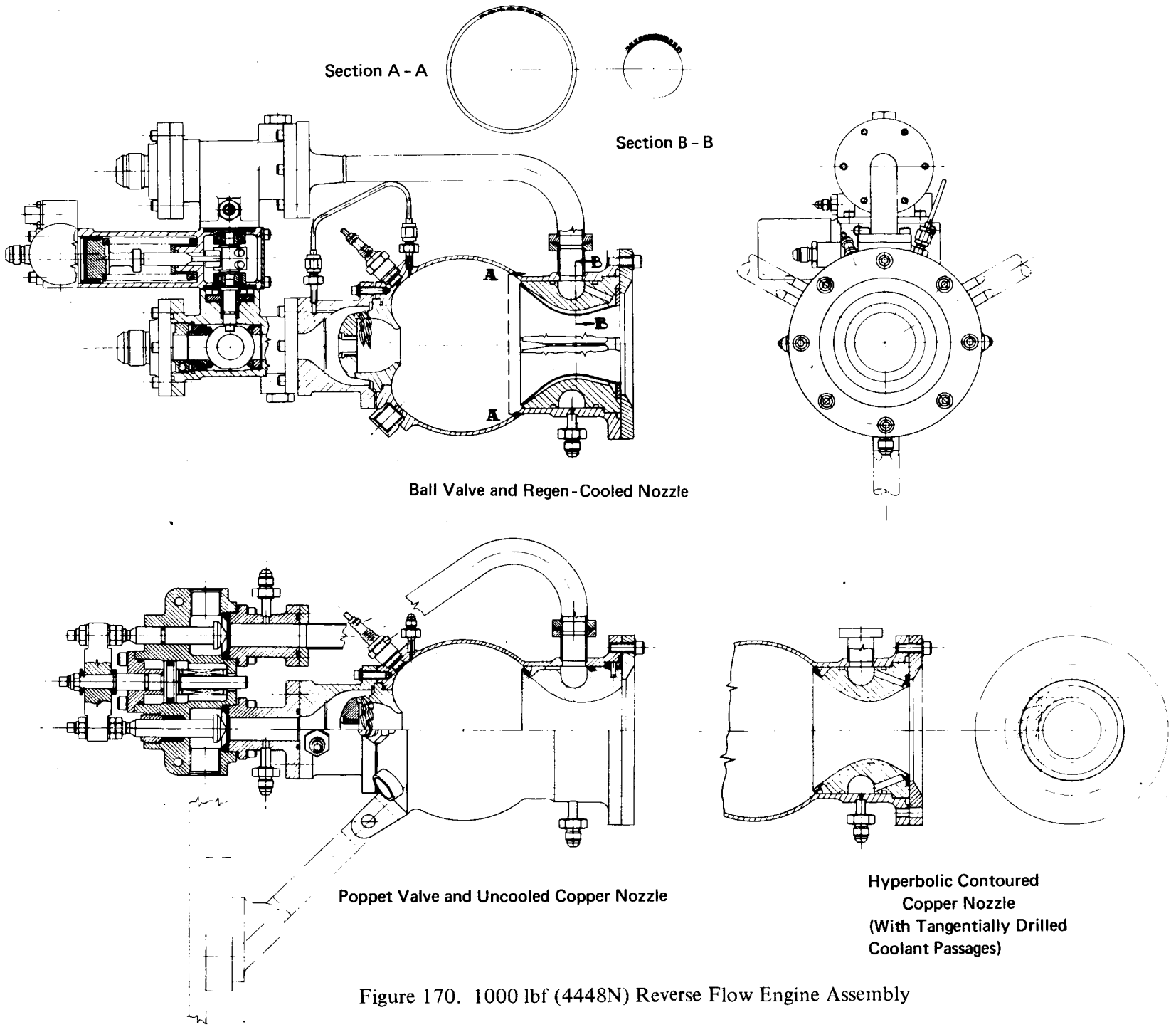

Figure 170. 1000 lbf (4448N) Reverse Flow Engine Assembly

The analysis was based on one-dimensional flow-no film or barrier cooling in the nozzle. An enhancement factor of 50% was assumed for the coolant film coefficient in passing through the curved, channeled TD nickel passages. Details of the equations and techniques used for these analyses were presented in paragraph B of this appendix.

2. Results of Analysis

The total heat rejected to the coolant was compared to theory for the drilled nozzle configuration only. It was not possible to measure fuel outlet temperature on the channeled nozzle, because the plenum upstream of the injection orifices was not accessible to a thermocouple. Figure 171 shows a comparison of theoretical and test coolant temperature rise as a function of mixture ratio for the drilled nozzle. In contrast to the theoretical curves plotted for 94%, and 100% c* efficiency, which peak at a mixture ratio of approximately 4.6, the test data indicate a steady increase of coolant temperature rise between mixture ratios of 2.8 and 5.2. The test data are consistently higher than the calculated value for η c* = 0.94. The average difference is about 15%, but reaches a minimum of 10% at MR = 4.0.

The explanation for the discrepancy of calculated and measured heat rejection is not clear. However, since the hot gas film constitutes the major thermal resistance, the most probable source of error is underestimation of the film coefficient h_g. Thus the observed film coefficient in the nozzle is higher than the average film coefficients reported in Reference 12. Adjustments in h_g were made in the thermal analysis model.

Two wall thermocouples were installed in the channeled nozzle 180 degrees apart at a station 0.837 in. (2.126 cm) forward of the throat to establish wall temperatures. The thermocouple wells were drilled on land centerlines to within 0.009 in. (0.0229 cm) of the inside surface of the nozzle. The chromel-alumel thermocouple wires were fused into these holes, but the precise depth location of the junctions was not known. Therefore, the absolute magnitude of the observed temperatures is of questionable significance. However, the variation of temperature with mixture ratio is an indication of the corresponding variation in heat flux.

A finite element method was used to calculate theoretical wall temperatures. As shown in Figure 172, a half-channel and a half land were divided into 41 nodal elements. The calculated wall temperatures in the thermocouple well for a mixture ratio of 4.0 and a combustion efficiency of 94% are shown. The variation of calculated and observed wall temperatures versus mixture ratio are shown in Figure 173. The calculated wall temperatures tend to be overpredicted at low mixture ratios and underpredicted at high mixture ratios. The trend of the test data corroborates the coolant rise data obtained with the drilled copper nozzle.

Pressure drops were calculated for the channeled nozzle at mixture ratios of 3, 4, and 5, with hydrogen flow rates compatible with a chamber pressure of 250 psia (172:1 N/cm^2) and a combustion efficiency of 94%. A comparison of calculated and measured pressure drop for the channel nozzle is shown in Figure 174. Instrumentation limitations prevented separation of the measured ΔP into the cooling passage and injector segments. The total measured pressure loss is about 11% higher than calculated, mainly due to underestimation of the dynamic head losses at changes in the flow areas between the drilled split shroud and nozzle liner. This emphasized the importance of designing for low hydrogen velocity in inlet lines and distribution holes, and of avoiding abrupt changes in flow area and direction.

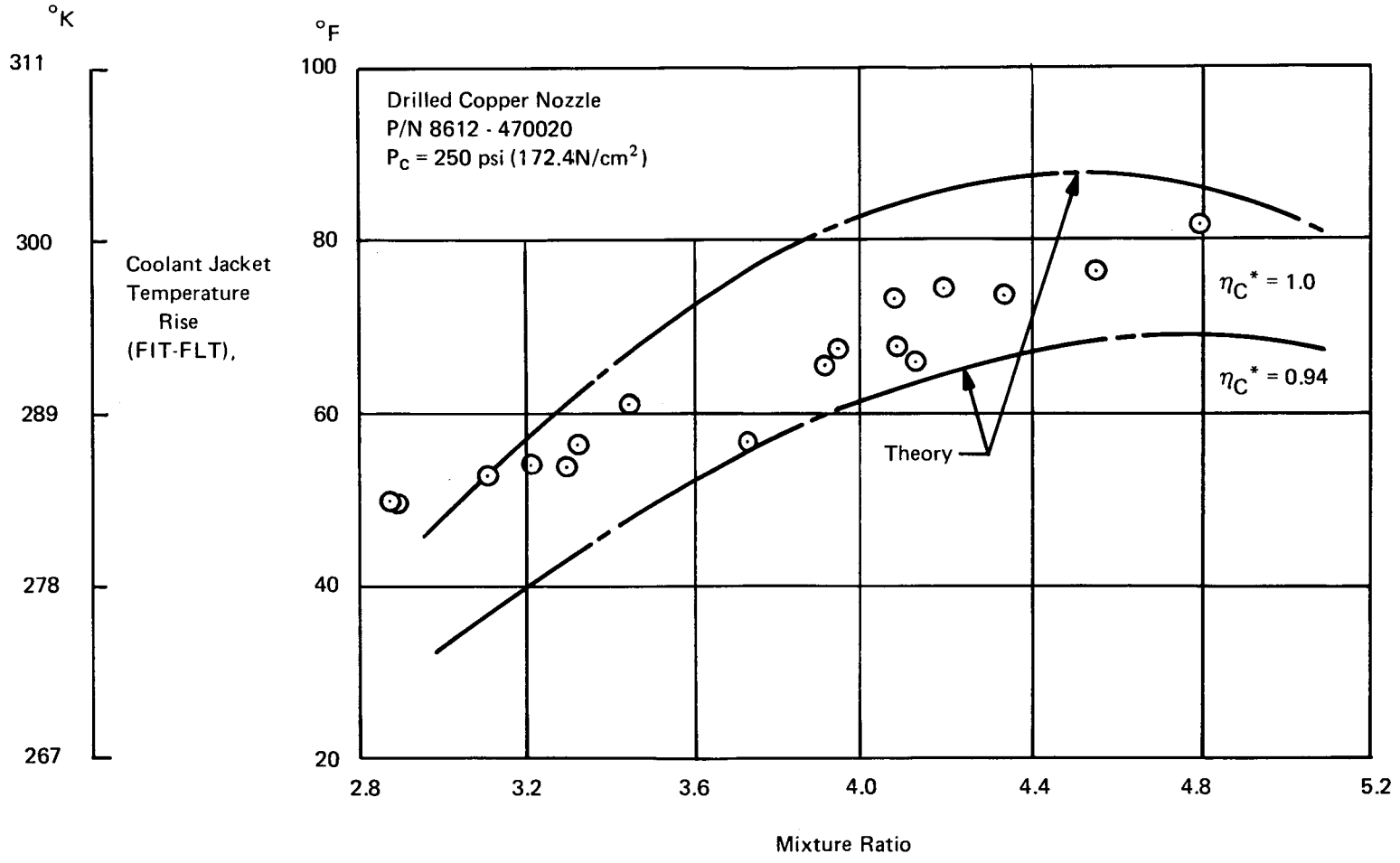

Figure 171. Coolant Temperature Rise

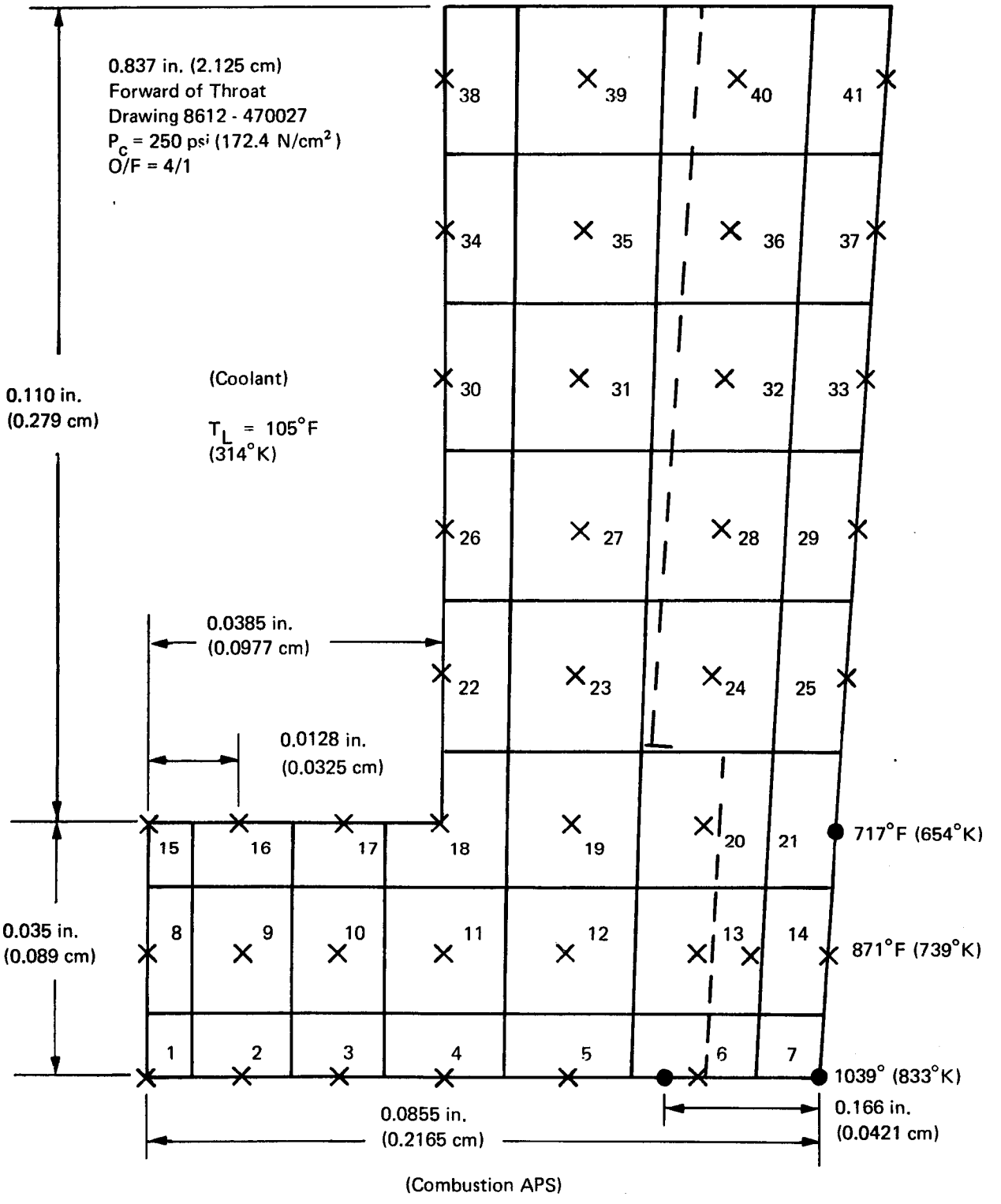

Figure 172. Wall-Temperature Measurement Section

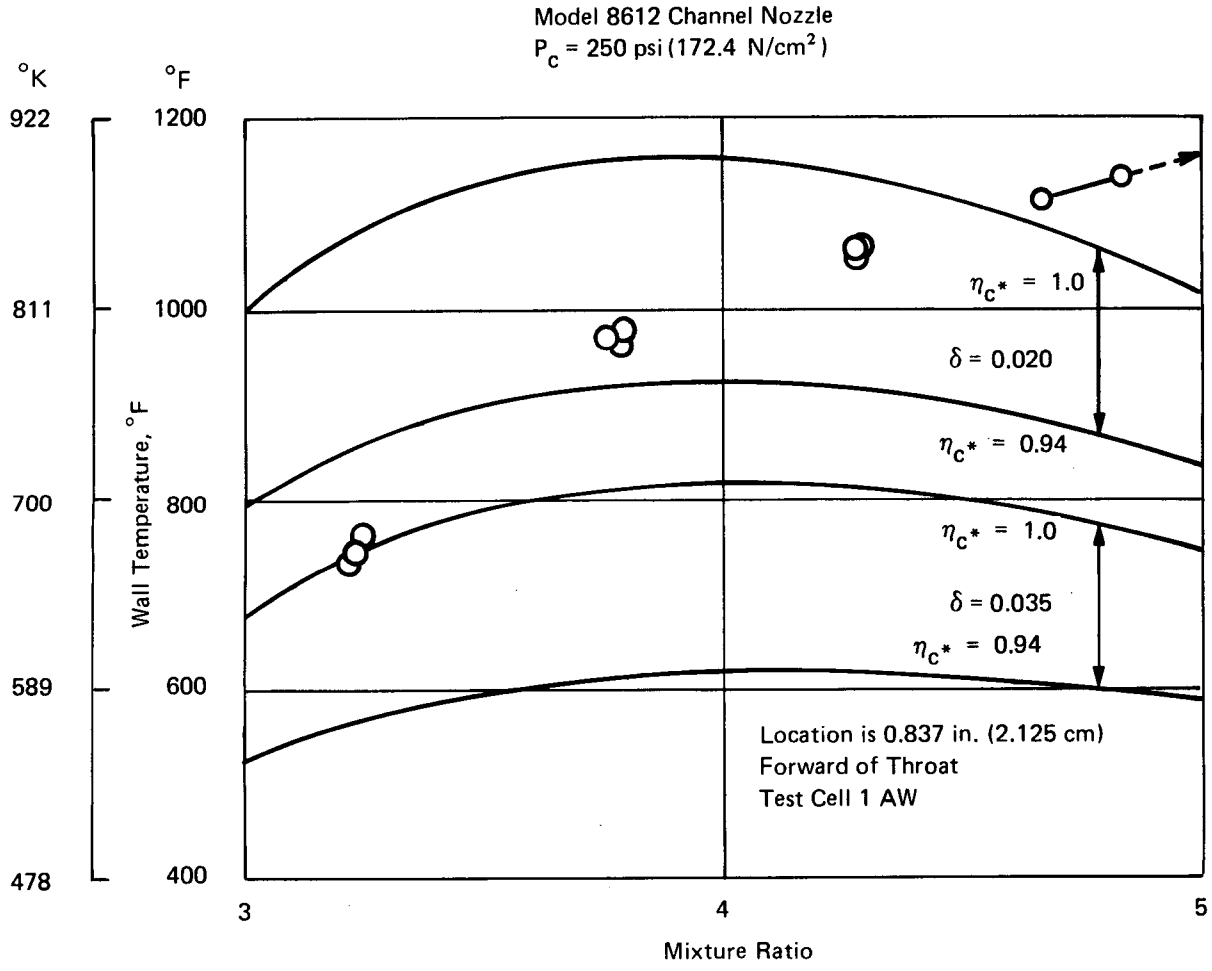

Figure 173. Wall Temperature versus Mixture Ratio

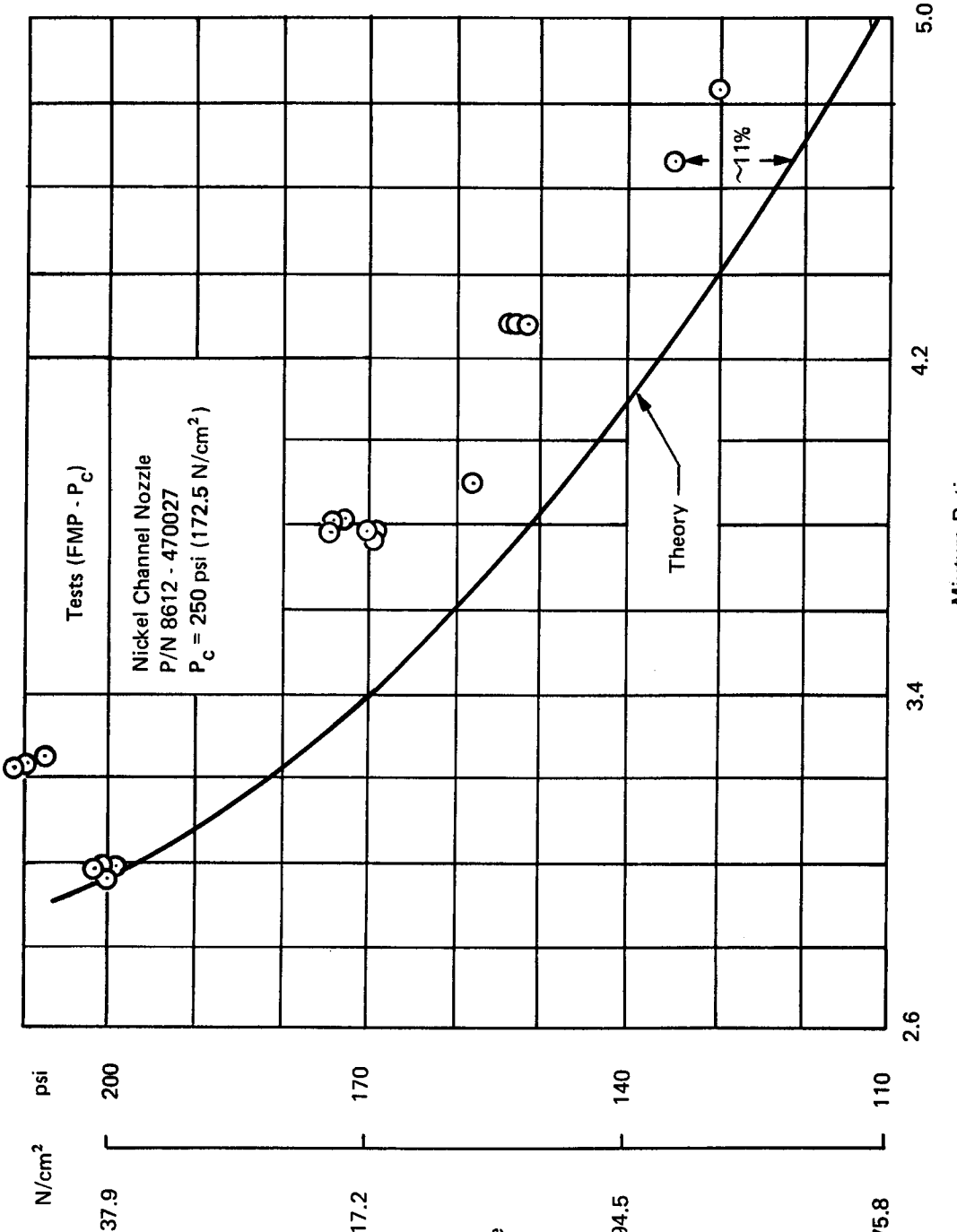

Figure 174. Hydrogen Coolant Pressure Drop

C. METHOD OF REDUCING TRANSIENT HEAT FLUX DATA FROM COPPER HEAT SINK NOZZLES

The transient temperature histories recorded at the throat station and at two points downstream of the throat were employed to determine an average heat flux for each of the injector combinations tested. The configuration of the nozzle and thermocouple installation is shown in Figures 175 and 176. Subsequent paragraphs describe the method of data reduction. Experimental heat fluxes, so determined, are compared with calculated values of heat fluxes based on theory.

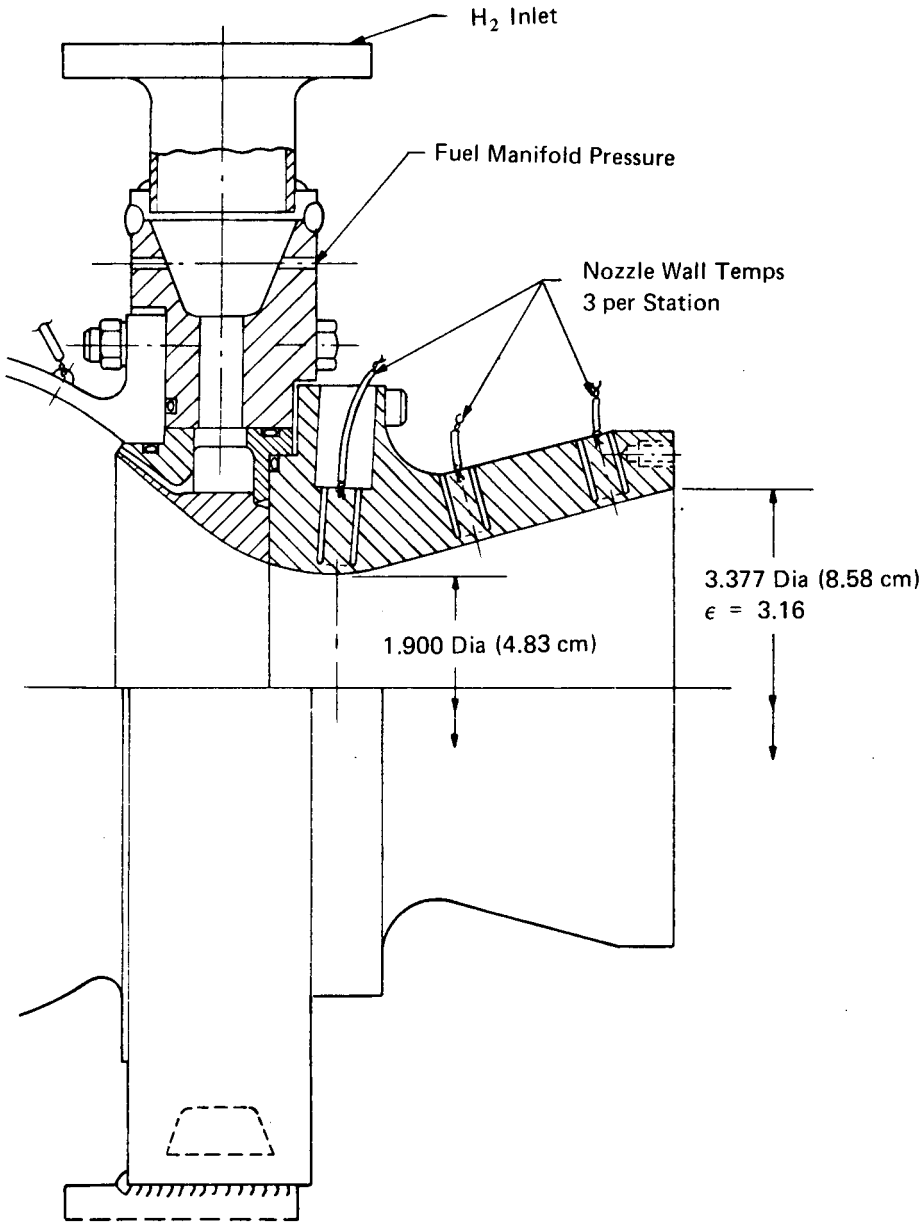

Figure 175. Heat Sink Thrust Chamber Assembly

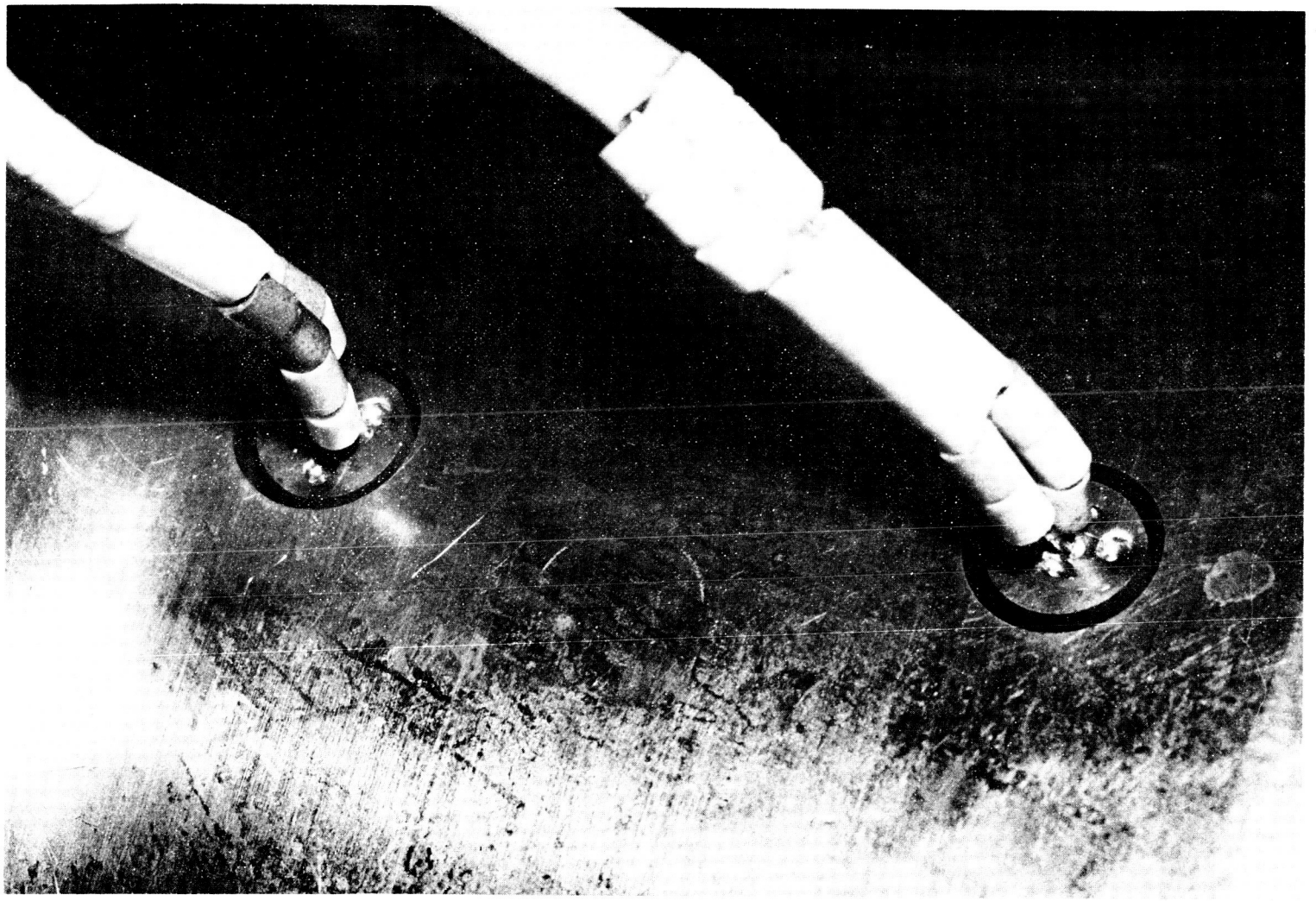

Figure 176. Nozzle Thermocouple Installation

The technique of deriving the average heat flux includes solution of the one-dimensional, nonsteady heat flow equation:

$$\frac{\partial T}{\partial \theta} = \alpha \frac{\partial^2 T}{\partial x^2} \tag{B-6}$$

where

T	=	temperature	x	=	distance from the outer surface
θ	=	time	α	=	thermal diffusivity

Since only the outer surface temperature is known from the thermocouple data, it is necessary to predict the inner surface temperature and heat flux to the inner surface. First, it is assumed that the temperature equation has the form:

$$T = a\theta^2 + b\theta + c \tag{B-7}$$

where a, b, and c are functions of the distance from the outer surface, x. Substituting equation (B-7) into equation (B-6) and setting the coefficient of powers of time equal to zero results in the following equations:

$$\frac{d^2 a}{dx^2} = 0 \qquad \frac{d^2 b}{dx^2} = 2a \qquad \frac{d^2 c}{dx^2} = b \tag{B-8}$$

At the outer surface from the thermocouple data at three times, $\theta_1, \theta_2, \theta_3$ the temperature can be approximated by the equation

$$T = A\theta^2 + B\theta + C \tag{B-9}$$

where A, B, and C are constant.

Therefore at $x = 0$

$$a = A \qquad b = B \qquad c = C \tag{B-10}$$

Assuming, no heat loss from the outer surface,

$$\frac{\partial T}{\partial x} = a'\theta^2 + b'\theta + c' = 0 \text{ at } x = 0$$

therefore at $x = 0$

$$a' = 0 \qquad b' = 0 \qquad c' = 0 \tag{B-11}$$

Solving equation (B-8) with the boundary conditon of equations (B-10) and (B-11) yields the following equations for the inner wall temperature (T_{wg}) and the heat flux ($\dot{q}$):

$$T_{wg} = A\theta^2 + \left(B + \frac{A\tau^2}{\alpha}\right)\theta + C + \frac{A\tau^4}{12\alpha^2} + \frac{B\tau^2}{2\alpha} \tag{B-12}$$

$$\dot{q} = K\left(\frac{2A\tau}{\alpha}\theta + \frac{A\tau^3}{3\alpha^2} + \frac{B\tau}{\alpha}\right) \tag{B-13}$$

where

τ = thickness

K = thermal conductivity

This solution has been programmed for the IBM 360/50 computer. The method of solution is to find the heat flux and inner surface temperature at a given time, θ_1, using the thermocouple data at that time and the times θ_{i-1} and θ_{i+1}, prior to and after the given time, find A, B, and C from equation (B-9). Using these values in equations (B-12) and (B-13), the inner surface temperature and heat flux can be determined at the given time, θ_i. This procedure is repeated at the next time, etc., until the end of the data, yielding a time history of the inner wall temperature and heat flux.

There is a constantly diminishing heat flux with increasing time and wall temperature. A local recovery temperature is used as input at each station considering:

Theoretical gas temperature

Combustion efficiency

Effect or recovery factor and nozzle Mach number

The heat transfer coefficient for the data points in the time history is found from the several heat fluxes at the given time:

$$h_{G,i} = \frac{\dot{q}_i}{T_R - T_{wg,i}} \qquad \text{(B-14)}$$

An average heat transfer coefficient is calculated from the instantaneous heat transfer coefficients. The heat flux to a wall of arbitrary temperature of 1000°F (811°K) is then calculated from the average heat transfer coefficient;

$$\dot{q} = h_G\,(T_R - 1000) = h_G\,(T_K - 811) \qquad \text{(B-15)}$$

D. HEAT TRANSFER STUDIES OF IGNITER CONFIGURATIONS

1. Summary

The purpose of the analyses was to determine the steady-state temperature of the adapter and spark plug outer sheath in the immediate vicinity of the spark plug seating gasket for the basic reverse-flow engine igniter configuration. Calculations were also made for a torch igniter mounted in the combustion chamber wall. Evaluation of the temperatures near the spark plug seal is required to assure that nonmetallic seal parts attaching the electrical harness to the top of the igniter does not overheat. Period low wall temperatures on the torch igniter are necessary for flow control and structural integrity.

For the cooled spark plug configurations the calculations showed that:

(a) Approximately 2% flow of either propellant around the igniter was satisfactory for cooling.

(b) The compressible coolant, within the passages, would be in the low subsonic range.

(c) Thermal barriers, in the form of adapter/chamber spacers, were also beneficial.

The torch igniter analyses indicated that a mixture ratio of 6/1 torch can be made with coolant passages of a reasonable dimension.

The calculations were made on the basis of nominal operation at 1500 lbf (6672 N), a chamber pressure of 300 psia (206.8 N/cm^2) and a mixture ratio of 4. The O_2 and H_2 mass flow rates were 2.76 and 0.69 lb/sec (1.25 and 0.313 kg/sec) respectively. The heating rates were based on the spherical combustion chamber surface temperatures of 1200°F (922°K).

2. Oxidizer Augmentation Cooled

The coolant requirements, compared with the total oxidizer flow, were calculated for three different spacer and seal configurations and a given spark plug. The basic configuration is per Figure 177 for which, in lieu of making nodal mathematic mode, a simple series/parallel resistance flow circuit was made as per Figure 178. The major proportion of the heat flows through the chamber wall and across the spacer joint into the coolant wall machined in the adapter. Coolant flow requirements are found by determining the heat flow rates ($\dot{Q}$) for various spacers and temperature differentials ($1200 - T_{wL}$) or ($810.9 - T_{wL}$ (K). The coolant flow rate is found from the coolant heat transfer coefficient (h_L) determined from the heat flow rate and the temperature differential between coolant wall (T_{wL}) and bulk temperature (T_L);

$$\dot{Q} = \left[\frac{1}{R_1 + \frac{1}{\frac{1}{R_2} + \frac{1}{R_3}}} + \frac{1}{R_4}\right]\left[1200 - T_{wL}\right] = h_L A_S \left[T_{wL} - T_L\right]$$

where the coolant surface area (A_S) is the total surface area of the annular groove.

The oxygen coolant flow rate required to maintain the wall temperature was found from the following form of Nusselt-number equation:

$$N_L = 0.023\left[\frac{\dot{W}}{A}\right]^{0.8} \frac{1}{D^{0.2}}\left[\frac{C_p^{0.4}\, K^{0.6}}{N^{0.4}}\right]_L \left[\frac{T_L}{T_{wL}}\right]^{0.34}$$

Coolant requirements for three adapter seal configurations appear on Figure 179. A narrow-faced spacer identified as 8636-470118 is more effective in blocking heat than are full width seals or no spacer, similar to the 8636-470024 adapter which is bolted directly on the chamber.

Figure 180 is the detailed nodal model of the selected design configuration. It differs from the preceding analysis in that a copper ring is compressed between adapter, chamber wall and igniter sheath to prevent coolant flow from the annular coolant passage down the igniter sheath into the chamber, bypassing the oxidizer augmentation function. The copper ring forms a thermal short across the chamber/igniter/adapter interface resulting in a complex heat flow path. A high (3000 BTU/ft² hr°F) (3.0 joule/meter sec °K) joint conduction was used for the compression ring because of the wedging nature of the seal surfaces.

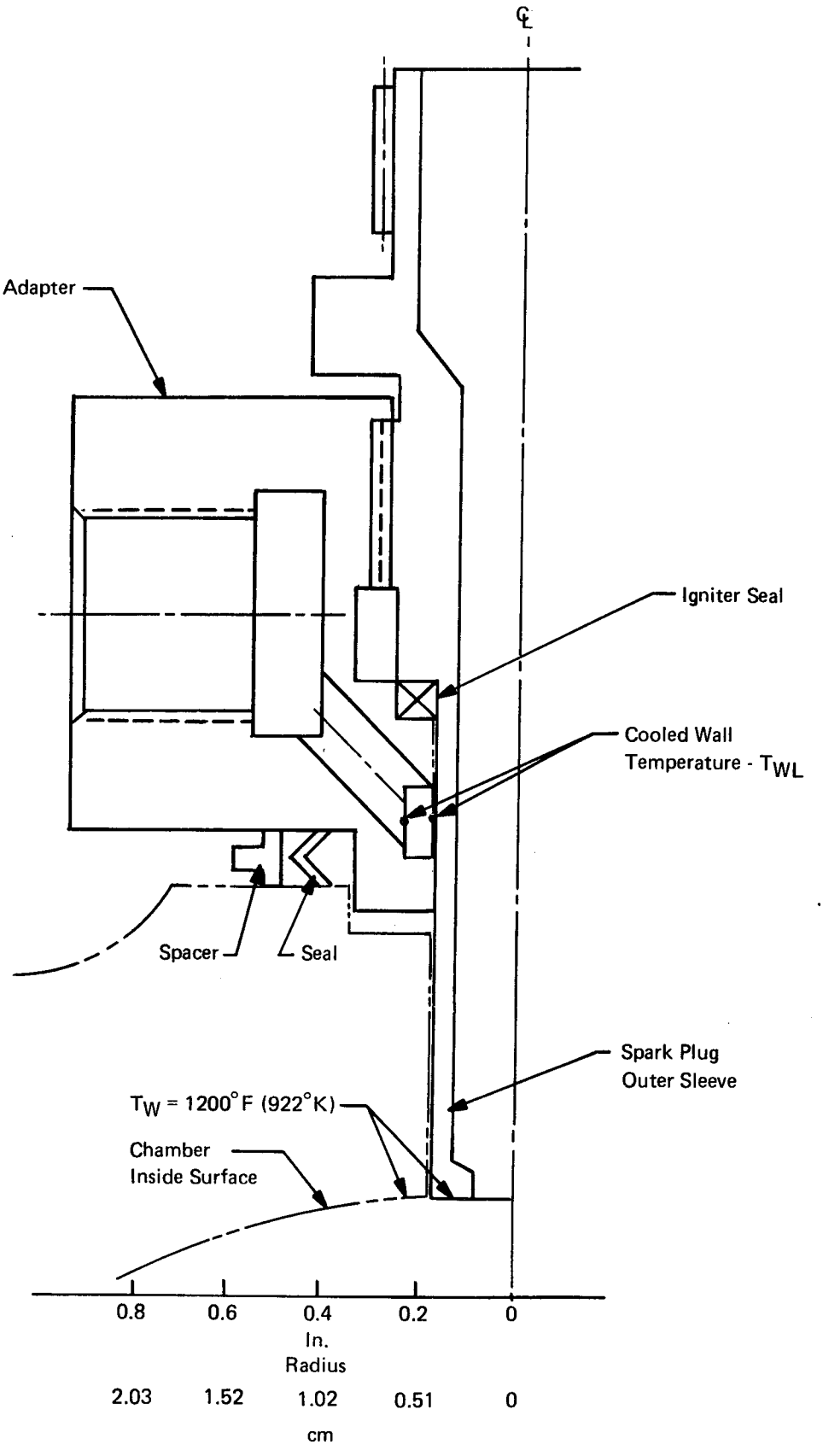

Figure 177. Oxidizer Augmentation Cooled Assembly Spark Plug

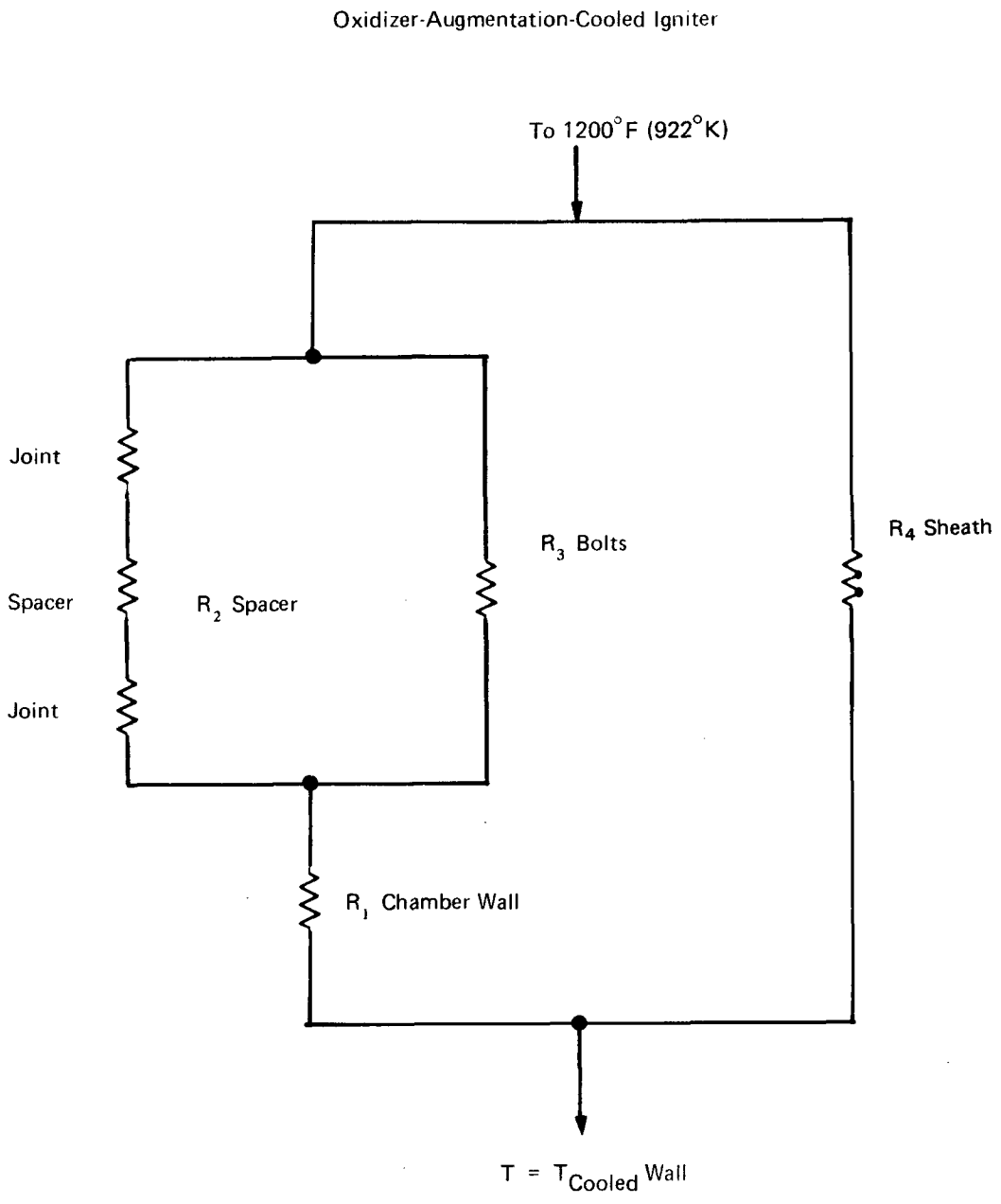

Figure 178. Simplified Igniter Heat Flow Network

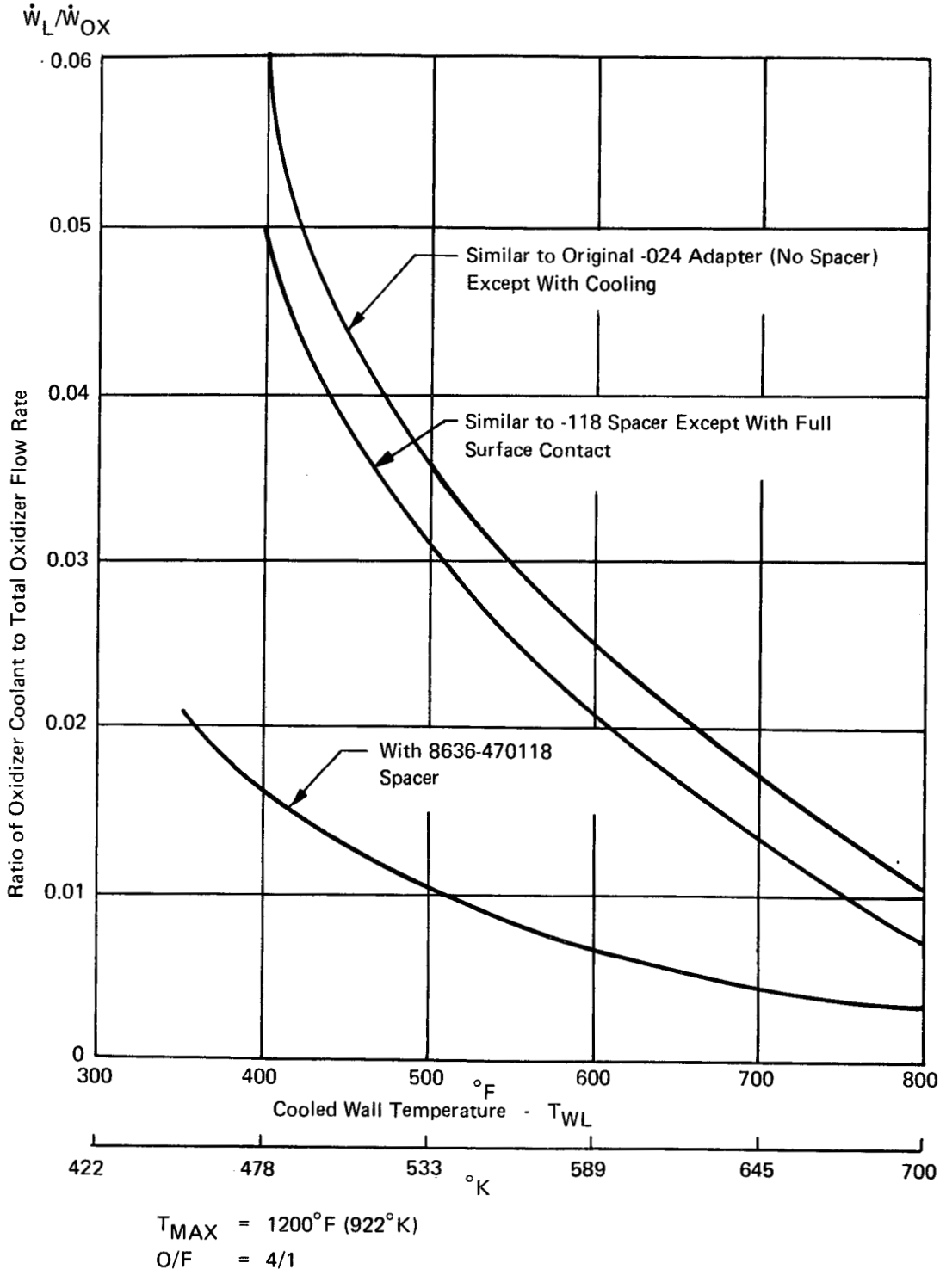

Figure 179. Oxidizer Augmentation Cooling

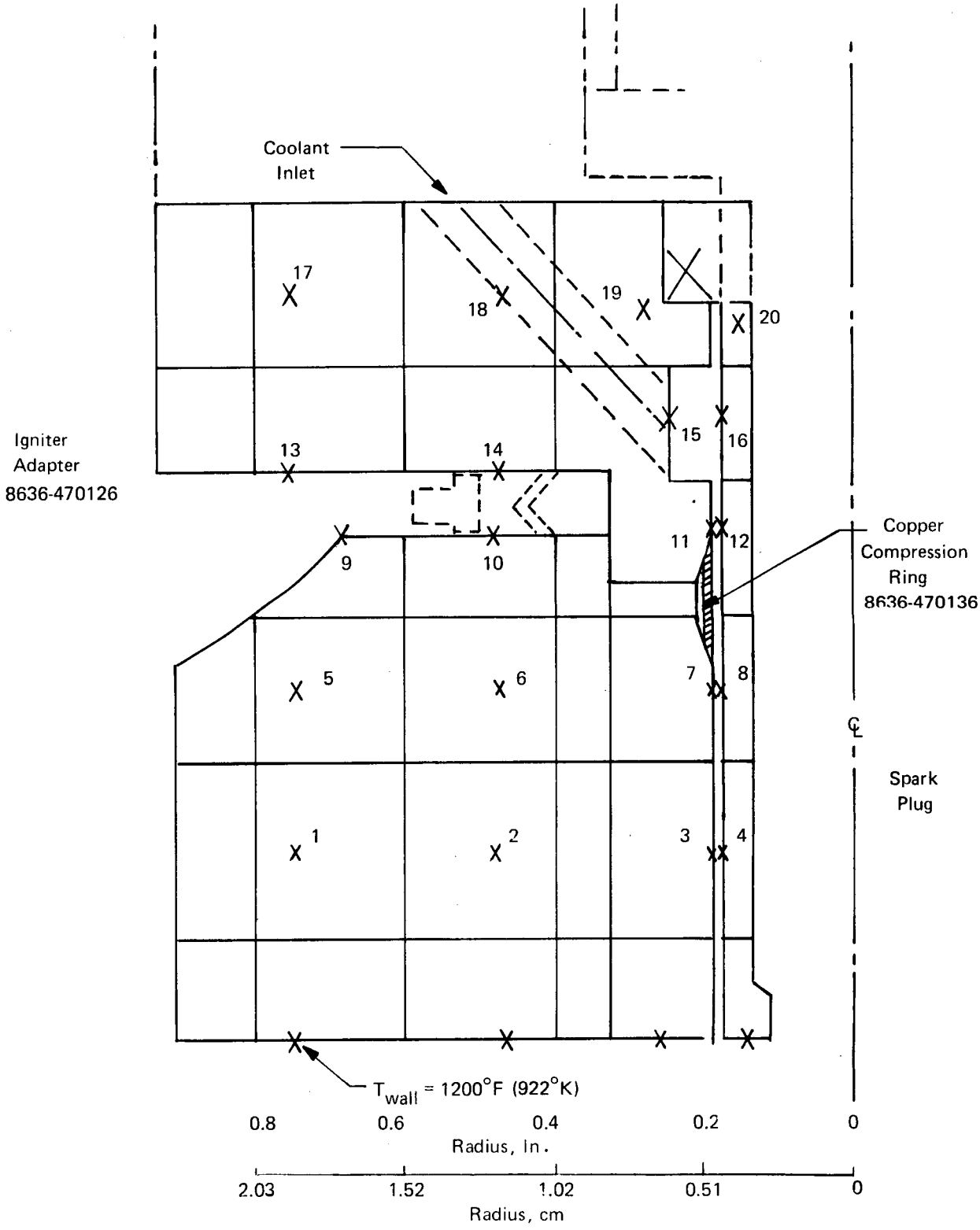

Figure 180. Oxidizer Augmentation Cooled Bendix/Champion Igniter

Temperatures in the adapter and sleeve adjacent to the igniter seal are shown on Figure 181 as a function of percent of total oxidizer flow rate. Inclusion of the compression seal allows heat to flow into the adapter coolant passage area at a rate sufficient to raise the adapter and sleeve temperatures 89°F (305°K) and 63°F (291°K) respectively, with 2% of the oxidizer used as coolant.

3. Coaxially Cooled Spark Plug Arrangement

Figure 182 is the igniter/adapter/chamber configuration where either propellant can enter the annular coolant passage in the adapter and flow around the exterior of the igniter sleeve into the combustion chamber. The ability to cool is a strong function of the annular gap mass velocity ($\dot{W}/A$). The analysis was made with a variable coolant passage Mach number at the exit of the sleeve/chamber gap by stipulation of 2% of the flow rates through an annular gap. Results are presented on Figure 183. The design radial spark plug gap of 0.020 inch (0.051 cm) would result in coolant Mach numbers of 0.17 and 0.19 for oxidizer and fuel, respectively. Temperatures of adapter and sleeve may be read for these Mach numbers.

If temperatures resulting from a coolant flow rate of other than 2% and at some specified radial gap dimension are of interest, a correction factor can be calculated to reevaluate the independent variable (Mach number) and read the computed temperatures at the corrected Mach number ($M^1{}_L$). The correction factor would be:

$$\frac{M^1{}_L}{M_L} = \left[\frac{\dot{W}^1}{0.02}\right]^{0.8}$$

The sleeve temperatures (T_W) near the seal are cooler than the oxidizer-augmentation-cooled designs because of the cooling provided all along the length of the igniter sleeve to the 1200°F (922°K) end exposed to combustion.

4. Torch Igniter

A torch configuration including the General Laboratory Associates (G.L.A.) igniter features a center flow combustion at a mixture ratio of 45/1 inside a nickel tube and flowing sonically through a 0.25-in. (0.635 cm) diameter throat. Surrounding the tube, 0.050-in. (0.127 cm) wall thickness, is a hydrogen flow of 0.0094 lb/sec (0.00425 kg/sec). A thermal analysis was conducted to determine the throat maximum wall temperature with cooling that can be obtained with this coolant flow. The coolant heat transfer coefficient is strongly affected by the mass velocity and hence increases with diminishing radial gap.

Figure 184 is the result of varying the radial gap around the 0.403-in. (1.024 cm) diameter sleeve. The analysis included the radial growth of the conduction flow outward through the 0.05-in. (0.127 cm) thick wall and the combustion efficiency of 97% for the core mixture ratio. A coolant exit velocity was calculated in terms of the radial gap to aid in making a selection based on fuel momentum, as well as predicted maximum wall temperature. This also is shown on Figure 184.

The core velocity was calculated to be 2656 fps (809.5 m/sec) based on a combustion efficiency of 97% and theoretical c* = 4000 fps (1219 m/sec) at a mixture ratio = 45/1.

The choice of a design gap was not made, but 0.015-in. (0.038 cm) appears to be a reasonable value.

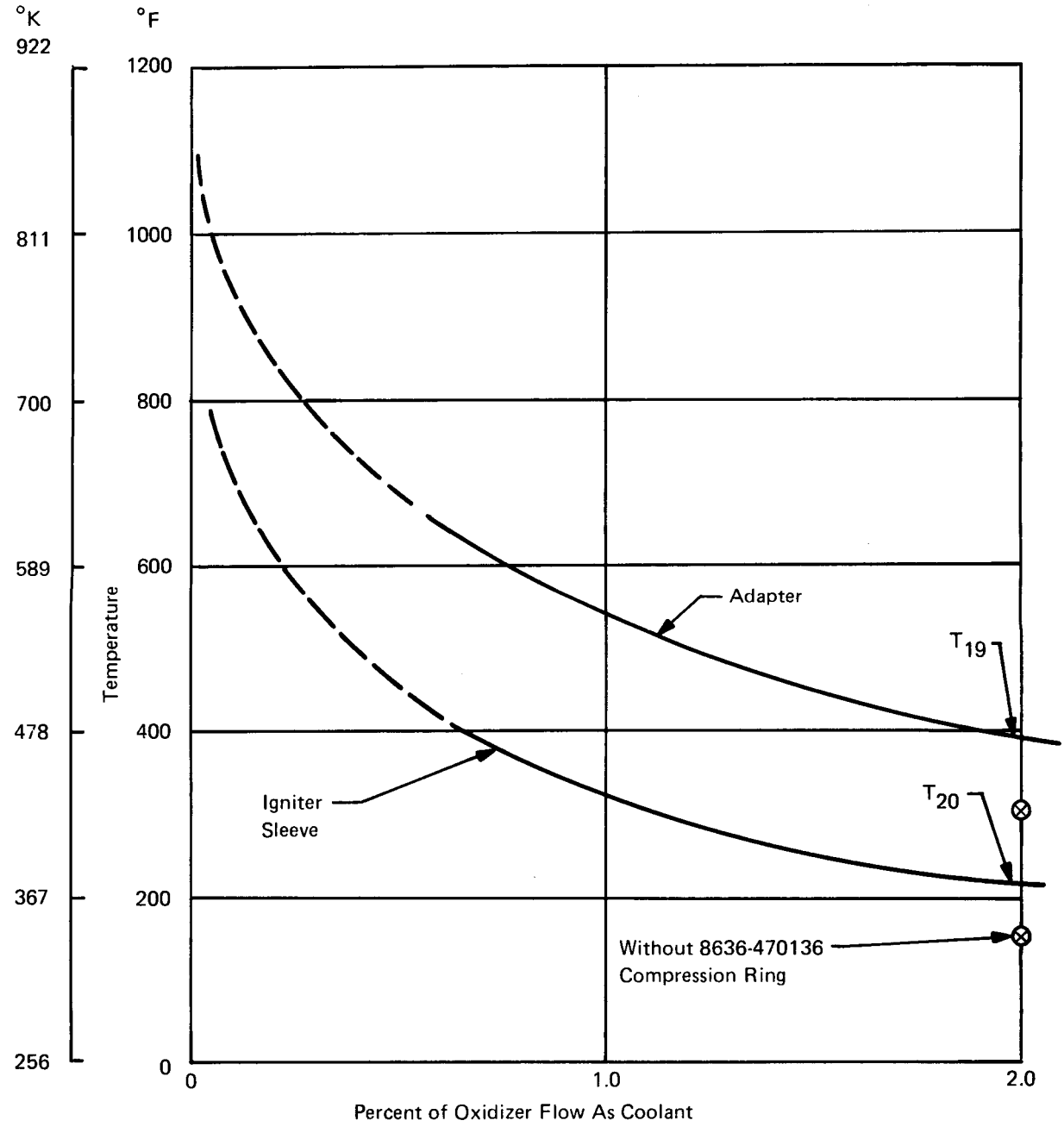

Figure 181. Temperature versus Percent Oxidizer Coolant

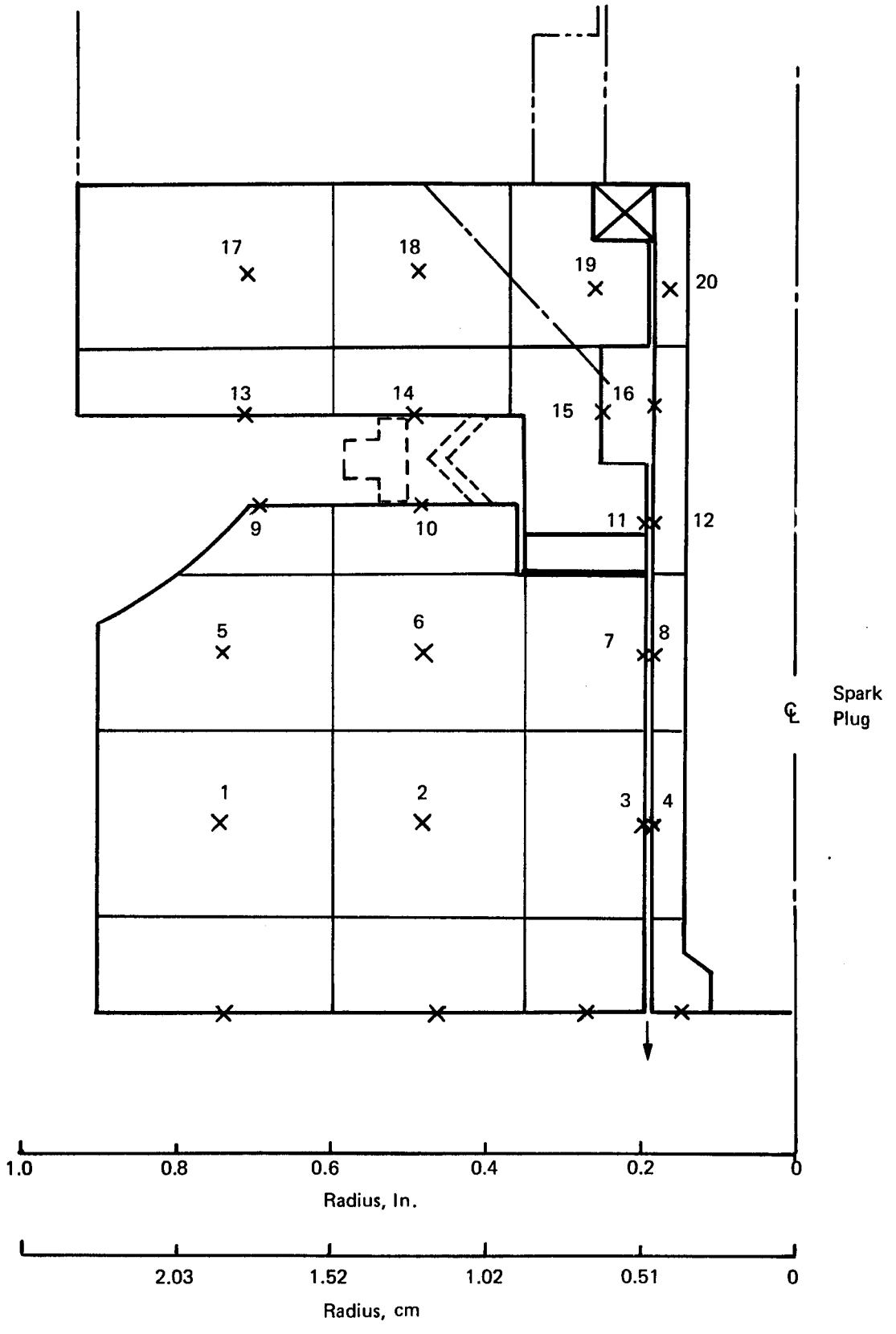

Figure 182. Co-Axially Cooled Bendix/Champion Igniter

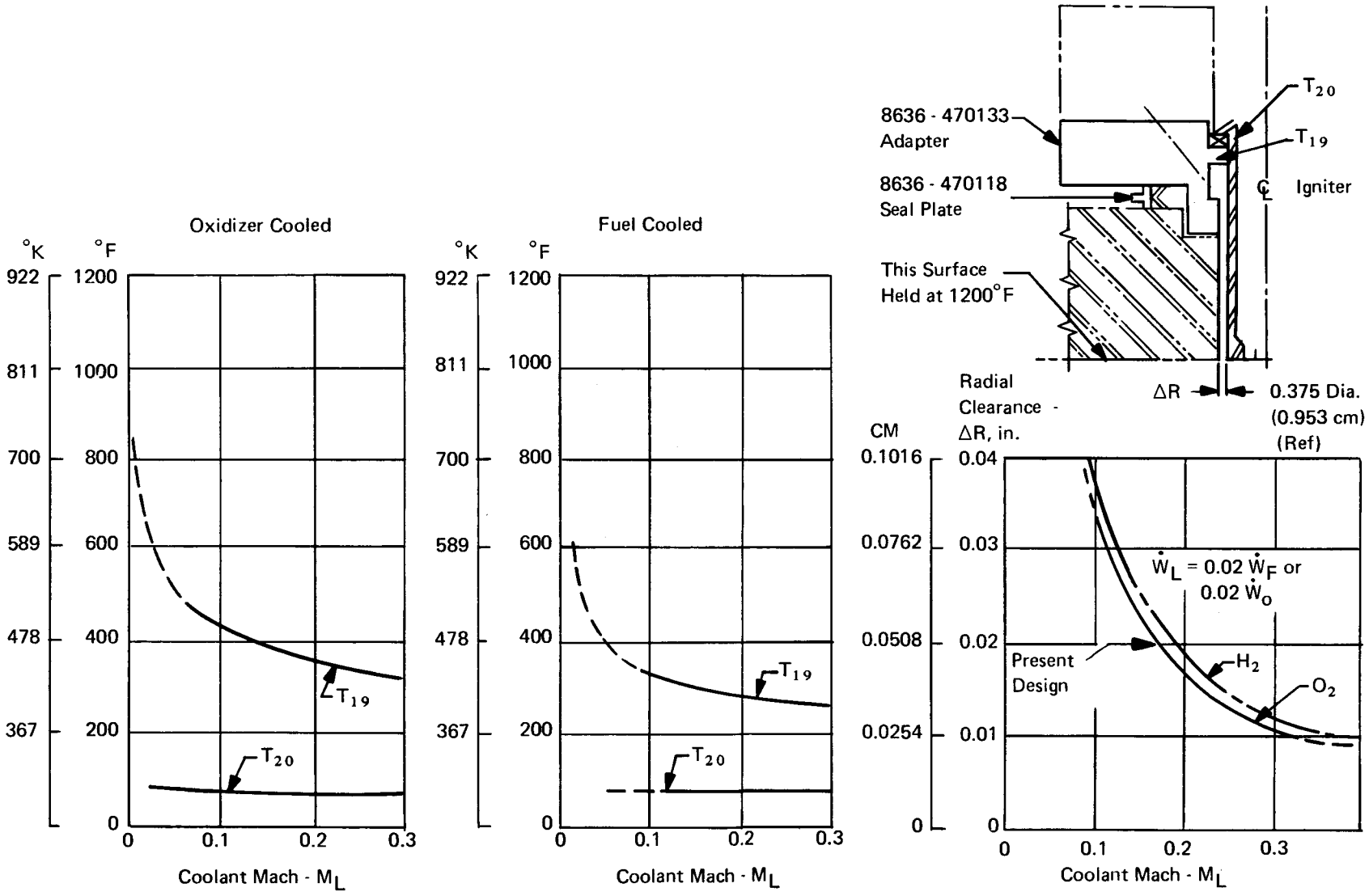

Figure 183. Co-Axially Cooled Bendix/Champion Igniter Temperature versus Coolant Mach Number

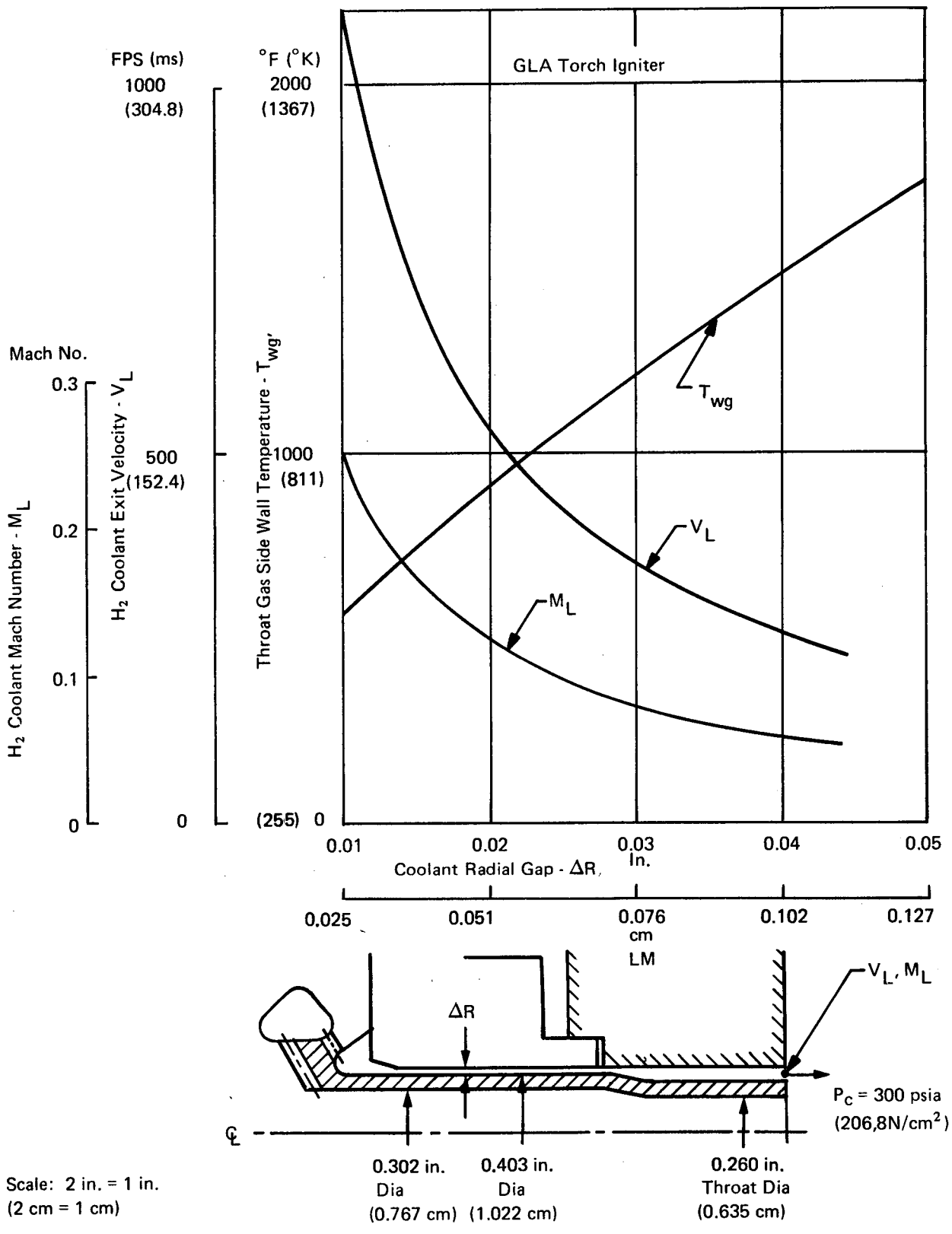

Figure 184. Wall Temperature and Exit Velocity versus Coolant Radial Gap

APPENDIX C
SUPPLEMENTARY FLOW ANALYSES

A. NOZZLE CONTOUR DESIGN

1. Introduction

Performance and cooling optimizations conducted early in the program included the selection of a specific convergent/divergent nozzle contour. That contour was maintained in the design of all altitude test hardware. The following material describes the rationale in designing a conventional bell nozzle and the performance gains feasible if the nozzle length or area ratio is changed.

Optimization of a rocket engine usually considers the delivery of maximum specific impulse as a function of engine overall diameter and length. This involves tradeoffs in the length of chamber and divergent nozzle. Basically, the combustion efficiency for a combustion device employing a well designed, high-performance injector is relatively constant above a threshold characteristic length. Below that value, it begins to decay substantially. The highest performance at minimum chamber length occurs at or near this threshold length. The remaining length within a given envelope is then available for the divergent nozzle. For this given length, it has been shown that the highest performance is obtained by increasing the area ratio to an optimized size. Figure 185 shows this tradeoff of performance with length and area ratio. The family of nozzle exit lengths at constant area ratio is joined by a dashed line connecting optimum expansion nozzles expanding to vacuum.

However, if the envelope limit is on diameter, then higher performance could be achieved with a longer nozzle at a given area ratio corresponding to that diameter. For the Space Shuttle APS engines, length and diameter constraints have not been defined. Inasmuch as the contract required only an area ratio of 40/1, the nozzle contour was designed to a length comensurate with good performance.

2. Theory

The aerodynamic thrust of a supersonic nozzle primarily depends on the nozzle exit area ratio and the mass flow of the rocket. Maximum thrust for a given nozzle area ratio is obtained with a parallel flow (ideal) nozzle where the nozzle flow is uniform and parallel at the exit. This type of nozzle is not used for a propulsion system as the designer can produce more thrust within the same length by increasing the exit area ratio. The nozzle contour for a given area ratio may be selected arbitrarily (conical or truncated ideal nozzles) or calculated explicitly to some optimum area ratio and profile. Such a mathematical technique is developed by G. V. Rao in Reference 31. It describes Rao's derivation of equations which apply to defining the stream through a three-dimensional axisymmetric nozzle.

Rao used the method of variational calculus to prescribe the conditions for maximum thrust on a nozzle, assuming a constant nozzle length and flow rate. He examined the variation of the nozzle thrust in terms of conditions on a control surface between a point F and E (Figure 186) and allowed a variation of all flow conditions on the control surface as well as a radial variation of the point E. As a result, he was able to specify that the control surface under examination must be

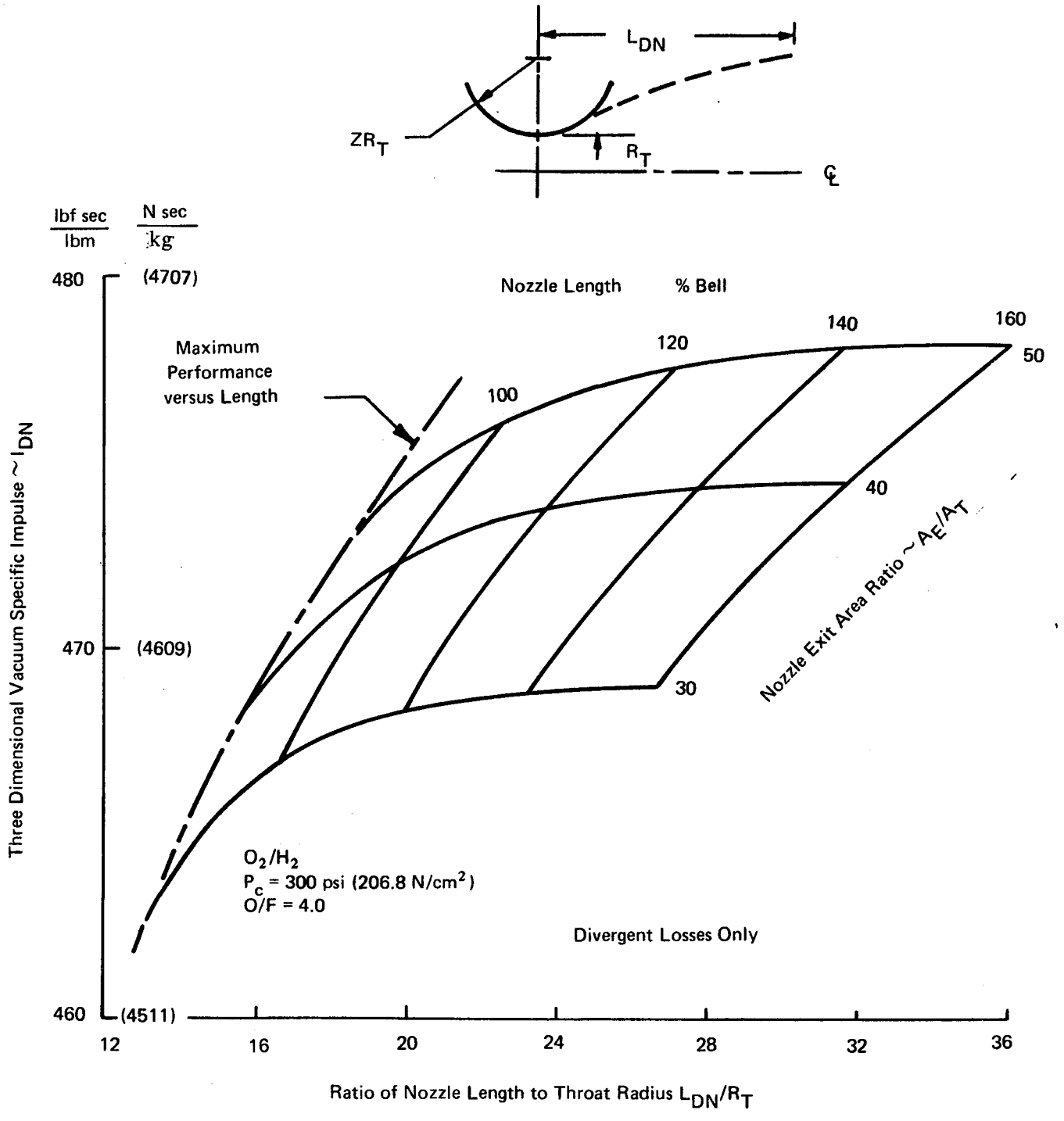

Figure 185. Divergent Nozzle Performance versus Length

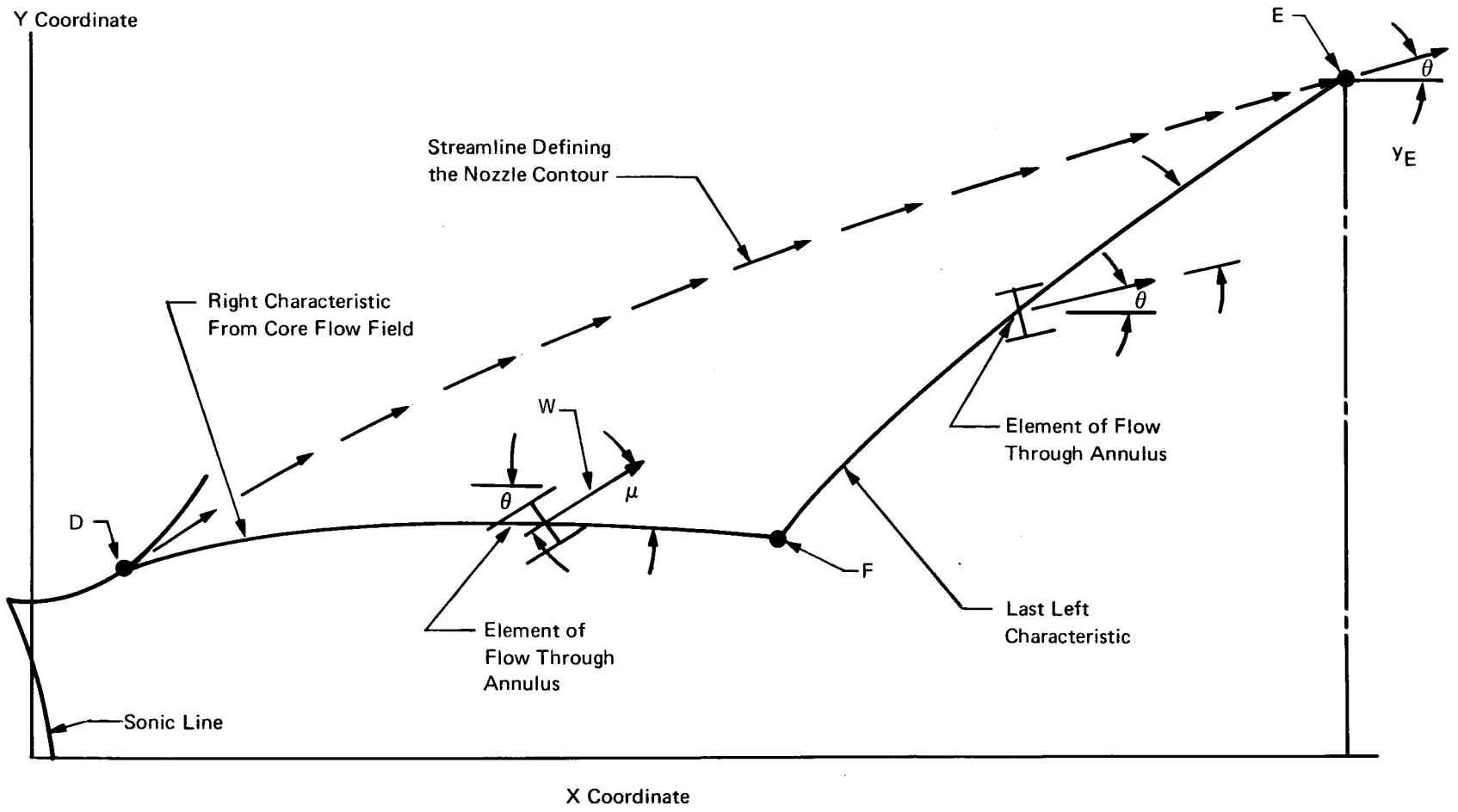

Figure 186. Control Surfaces for Rao's Optimum Nozzle

a characteristic and that the flow conditions along this characteristic are specified by the following relations:

$$\frac{W \cos(\theta - \mu)}{\cos} = -\lambda_1 \tag{C-1}$$

$$Y W^2 \rho \sin^2 \theta \tan \mu = -\lambda_2 \tag{C-2}$$

He found that the conditions at E are:

$$\sin 2\theta_E = \frac{(P_E - P_a) \cot \mu_E}{(1/2) P_E W_E^2} \tag{C-3}$$

Since it was shown that the control surface is a characteristic, either equation (C-1) or (C-2) can be replaced by the differential equation for a characteristic in an axisymmetric flow. The following form is equivalent to that presented in Reference 32.

$$\frac{dY}{Y} = \left[-d\theta + \frac{dM \sqrt{M^2 - 1}}{M\left(1 - \frac{1}{2}M^2\right)}\right]\left(\sqrt{M^2 - 1} + \cot \theta\right) \tag{C-4}$$

The flow crossing (FE) and the axial length of (FE) are assumed constant in the derivation; therefore, it is intrinsic in the method that the location of (F) fixes the overall length of the nozzle in that (DF) fixes the flow across (FE). This immediately suggests that a nozzle design for a given length cannot be obtained without a number of trial solutions in which the point (F) is varied.

It is worthwhile at this point to inspect the equations to establish the effect of the various parameters, as well as to get a physical picture of the method.

Nozzle length of a stated area ratio is a minimum if $P_a = 0$; θ will be maximum in equation (C-3). Increasing P_a as an independent variable will allow the nozzle to lengthen and form families of relative lengths (% bell) for given area ratios.

Once the equation for the conditions at the lip is established, Rao also postulates that the mass flow along the last left-running characteristic to the exit be equated to that through the nozzle conforming with the law of continuity.

A physical conception of Rao's method may be derived by inspection of the equation presented. Consider a nozzle of a given length and assume that the flow at the exit is uniform and will increase and the flow will become slightly divergent. With the increase in Mach number, the thrust is increased, but the flow divergence reduces the effectiveness of this thrust improvement. As the area is increased further, at some point the thrust improvement with area increase will be exactly balanced by the thrust loss due to the flow divergence. This corresponds to the maximum-thrust nozzle defined by Rao's method when ($P_a = 0$). If (P_a) is not zero, an increase in exit area of the uniform flow nozzle results again in a thrust increase due to the increased Mach number, but the thrust decrement is now due not only to divergence, but also to the pressure force ($-P_a A_{ex}$) acting on the nozzle. Obviously, the optimum thrust nozzle for this situation will have a smaller exit area than that for ($P_a = 0$). In the limit, if ($P_a = P_e$) for the uniform parallel-flow nozzle, any change in the exit area will result in a thrust loss.

The important conclusion to be drawn from Figure 185 is that a large area ratio nozzle can produce more thrust than a more aerodynamically efficient, smaller-area-ratio nozzle of the same length.

The losses due to three-dimensional effects may be included with losses due to combustion efficiency, combustion kinetics and viscous drag to predict the overall efficiency of the thruster.

3. Computational Method

The determination of the nozzle profile and the Mach number distribution within the nozzle is accomplished by applying the following steps:

1. The throat diameter and transonic wall radius are selected.

2. The throat flow field is computed by Sauer's method described in Reference 32.

3. The "core" flow field, defined by the throat contours, is computed.

4. The last left-running characteristic is evaluated by Rao's equations.

5. A point in the "core" flow field is found where the local Mach number and flow direction is identical to that defined by the equations of the left-running characteristic. This point (F of Figure 186) is also restricted in that the flow crossing the right characteristic (DF) is equal exactly to the flow crossing the left-running characteristic (FE).

6. The "backward," or optimized flow field, is then computed, using the right and left characteristics as input. A streamline is selected which originates at the point on the throat contour indicated by (D) in Figure 186. This streamline is the optimum nozzle contour.

The computer program for calculating the nozzle profiles proceeds from a line of constant Mach number near the throat through a characteristics net to the exit area and ambient pressure specified. The method of characteristics is a computational technique where the partial differential equations of supersonic compressible flow are expressed in incremental form in terms of space (X, Y), flow direction (θ) and Mach number. Four difference equations are solved simultaneously step-wise through the flow field. The gas flow is assumed to be inviscid, irrotational, isentropic and axisymmetric. The equations are coded for the computer program with the ability to accept variable thermodynamic properties of the exhaust gas. Properties are determined at every computed point on the nozzle contour and every point within the supersonic flow field. Since the flow is assumed isentropic, any other property, may be expressed as a function of only one additional property; namely pressure in this case. The other properties as dependent variables are its enthalpy, temperature, molecular weight and ratio of specific heats. As many as 50 sets may be used as four tables of data, with pressure used as the argument in each case.

The initial boundary of the calculations is composed of spatial points at a constant Mach number which is located in the transonic vicinity of the throat. Reference 32 describes Sauer's series, solutions and development of equations by which the spatial coordinates and flow angles are found. A Mach number distribution is calculated in terms of a radius of curvature of the wall which is frequently dictated by the method of fabrication or configuring of cooling passages. Simple circular arcs of hyperbolae are used. Application of the method of Sauer indicates negligible entrance losses ($<0.2\%$) for circular arcs describing the wall larger than 2.0 times the throat radius.

Output of the computer program includes:

(a) for each mesh (or field) point: coordinate location, flow angle, pressure and ratio of temperature to molecular weight

(b) for each wall point: same as for mesh point plus Mach number, ratio of specific heats, velocity and accumulative surface area

(c) for each nozzle exit: same as wall point plus atmospheric pressure and vacuum specific impulse.

4. Application

The nozzle profile presented in this section was assumed to be aerodynamically optimized for maximum performance at a specified length. This nozzle contour (79.9% bell) may not be optimum for a diameter envelope limited constraint where a relatively long nozzle can be employed (~ 160% bell) which has essentially zero divergence losses. Preliminary examination of thruster requirements for both boost and orbiter Space Shuttle vehicles indicate both length and diameter envelope restrictions and a final choice must be left for future vehicle studies. A long nozzle can be designed using the same methods as in the short one illustrated in Figure 187.

A wall radius symmetric about the throat was selected to cover all types of cooling schemes including the regeneratively cooled nozzle with straight drilled passages. This approach logically leads to the downstream radius held to a large radius (as is the subsonic upstream wall radius) which will tend to minimize kinetic losses at the mixture ratio and area ratio specified in the RFP.

Nomenclature

W	–	flow velocity (scalar)
θ	–	angle between flow direction and nozzle axis
μ	–	Mach angle
Y	–	coordinate in the radial direction
ρ	–	density
λ_1, λ_2	–	Lagrangian multipliers
P_E	–	pressure at E of Figure 186
P_a	–	ambient pressure
M	–	Mach number
A_{ex}	–	exit area of the nozzle

Subscripts

E	–	conditions at point E
a	–	ambient conditions

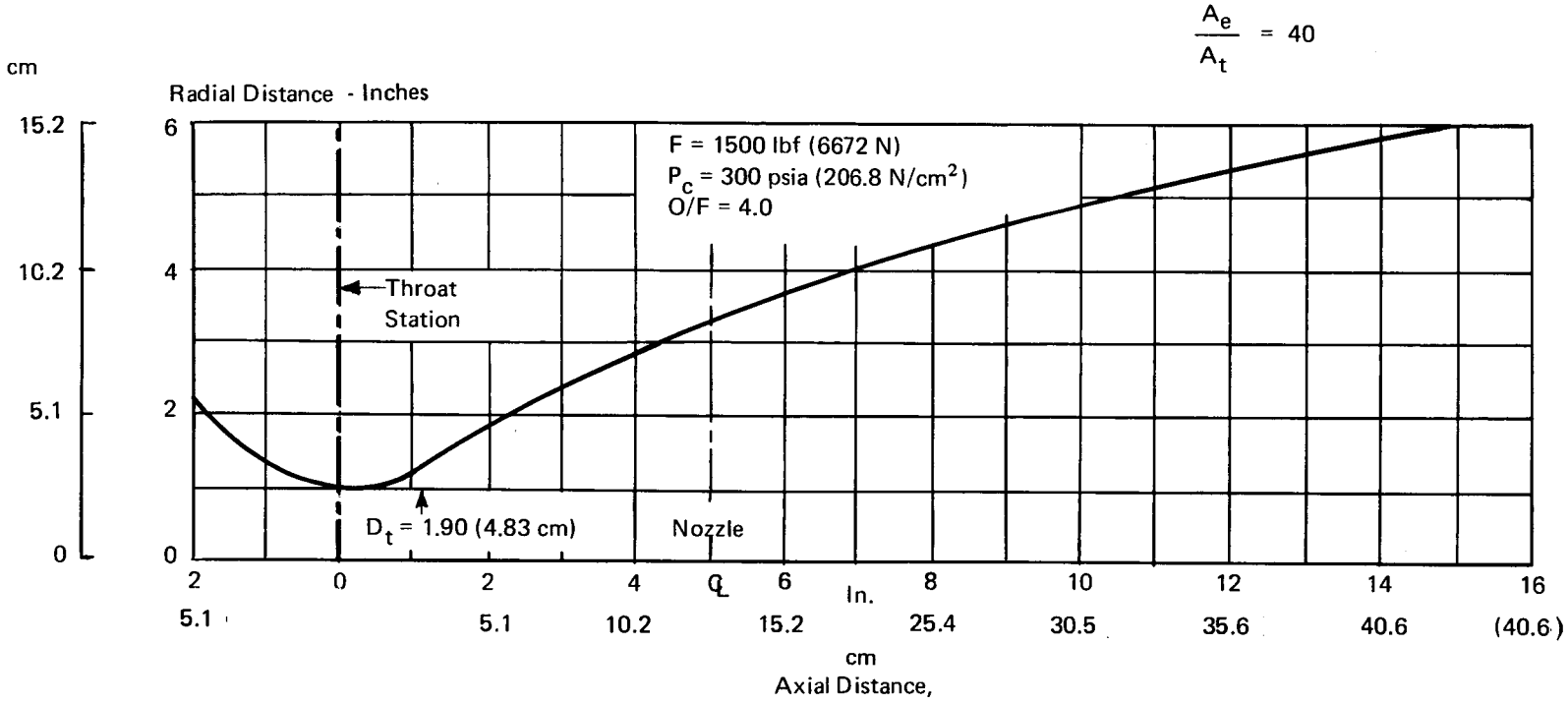

Figure 187. Nozzle Profile

B. MACH NUMBER, P_o CALCULATIONS – REGENERATIVE COOLING PASSAGES

A linear increment of a passage flowing an ideal compressible fluid having a known dimension and change of total temperature such as found in a hydrogen cooled wall was analyzed by calculation of the change in Mach number over its length by use of influence coefficients derived by Shapiro (Ref. 33).

$$dM^2 = F_A \frac{dA}{A} + F_{T_o} \frac{dT_o}{T_o} + F_f \frac{4fdx}{D_H}$$

where:

M = Mach number
f = friction factor
D_H = passage perimeter

The influence coefficients are given as:

$$F_A = \frac{-2M^2 \left(1 + \frac{\gamma - 1}{2} M^2\right)}{1 - M^2} \qquad F_{T_o} = \frac{(1 + \gamma M^2)\left(1 + \frac{\gamma - 1}{2} M^2\right)}{1 - M^2}$$

$$F_f = \frac{\gamma M^4 \left(1 + \frac{\gamma - 1}{2} M^2\right)}{1 - M^2}$$

where γ = the ratio of specific heats

The ratio of the surface finish (e) to the passage diameter (D_H) is a variable from which the friction coefficient (f) is calculated by the Von Karman-Nikuradse equation from NASA TN D-3798 (Ref. 34).

$$\frac{1}{\sqrt{f}} = -4.0 \log_{10} \left[\frac{e}{3.7 D_H} + \frac{1.255}{Re \sqrt{f}} \right]$$

The Reynolds number (Re) is computed from the mass flow rate, local passage flow area hydraulic diameter and viscosity of hydrogen.

After the change in Mach number through the element of passage length, the change in total pressure is found using the equation,

$$\frac{dP_o}{P_o} = -\frac{\gamma M^2}{2} \frac{dT_o}{T_o} - \frac{\gamma M^2}{2} 4f \frac{dx}{D_H}$$

C. SCARFED NOZZLE CHARACTERISTICS

1. Introduction

The normal axis of many of the attitude control system engines to be installed in the Space Shuttle Vehicles, will not be perpendicular to the vehicle skin. Aerodynamic cleanliness requires the nozzle to be scarfed. The exhaust nozzle will become unsymmetrical due to the scarfing of the nozzle and the thrust line will no longer act along the thruster axis. The following information is presented to illustrate the thrust line deviation characteristics of scarfed nozzles applied to the oxygen/hydrogen Reverse Flow engine.

Analytic results, using methods which have proven valid in Minuteman III PSRE experience, are offered along with comments on body forces on the vehicle. Prediction of the magnitude and location of the body forces are beyond the scope of this program but the calculation techniques for determining them will be reviewed.

2. Method of Analysis

One side of a scarfed divergent nozzle is expanded to a larger area ratio than its opposite wall. Such a configuration is illustrated on Figure 188. The gases continue to expand out to the outer lip. An accumulative radial and axial thrust is built up in this scarfed portion which, when added vectorially to the thrust of the nozzle upstream of the scarf, will result in a total thrust at an angle to the geometric axis. The net effective thrust must pass through a known centerline and point in space. It is assumed for the Reverse Flow engine that a simple conical section is added to a contoured high performance nozzle.

The wall angle of the conical section will be that of the exit lip of the contoured nozzle. In this manner, a nearly infinite number of scarfed nozzles can be built by simple changes to a basic engine. Axial and radial pressure forces within the scarf are integrated into the single vector (F_S) comprised of axial and radial forces and added to the axisymmetric thrust (F_O) as in Figure 189. The absence of the cut away opposite wall will not affect the nozzle flow field (within limits to be described later) because of the supersonic nature of the flow.

3. Application to Reverse Flow

The pressure distribution within the conical section attached to the initial contoured section is calculated first using the method of characteristics computer program for calculations of the flow field within supersonic nozzles of arbitrary contour, described in Reference 35. The four variables in the difference equations used in the method of characteristics are the coordinate spacial coordinates (X, Y), the flow angle (θ) and local Mach number (M). The three-dimensional pressure distribution within the contoured nozzle with conical section attached appears on Figure 190. The three-dimensional pressure at the wall is larger than the one-dimensional pressure but, after leaving the initial $A/A^* = 40$ axisymmetric contoured nozzle, it then approaches the one-dimensional pressure as no further compression due to wall curvature occurs.

The semidivergent cone angle (α) is 9.91° for the 75% bell nozzle. Previous analyses have indicated the exit lip (and hence cone angle) to be nearly constant for nozzles of various exit area ratio when longer than aerodynamically length optimized nozzles are used.

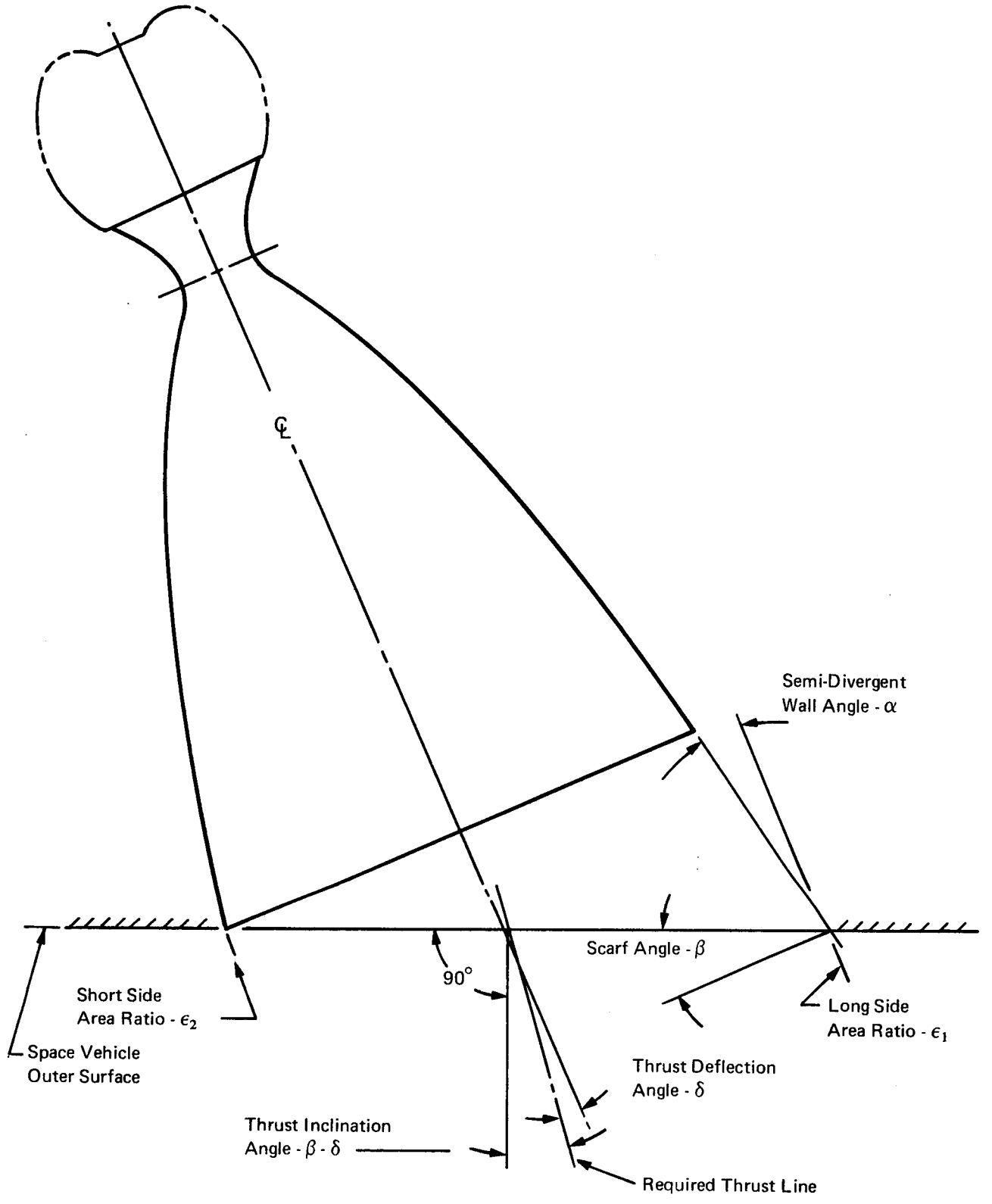

Figure 188. Scarf Nozzle Nomenclature

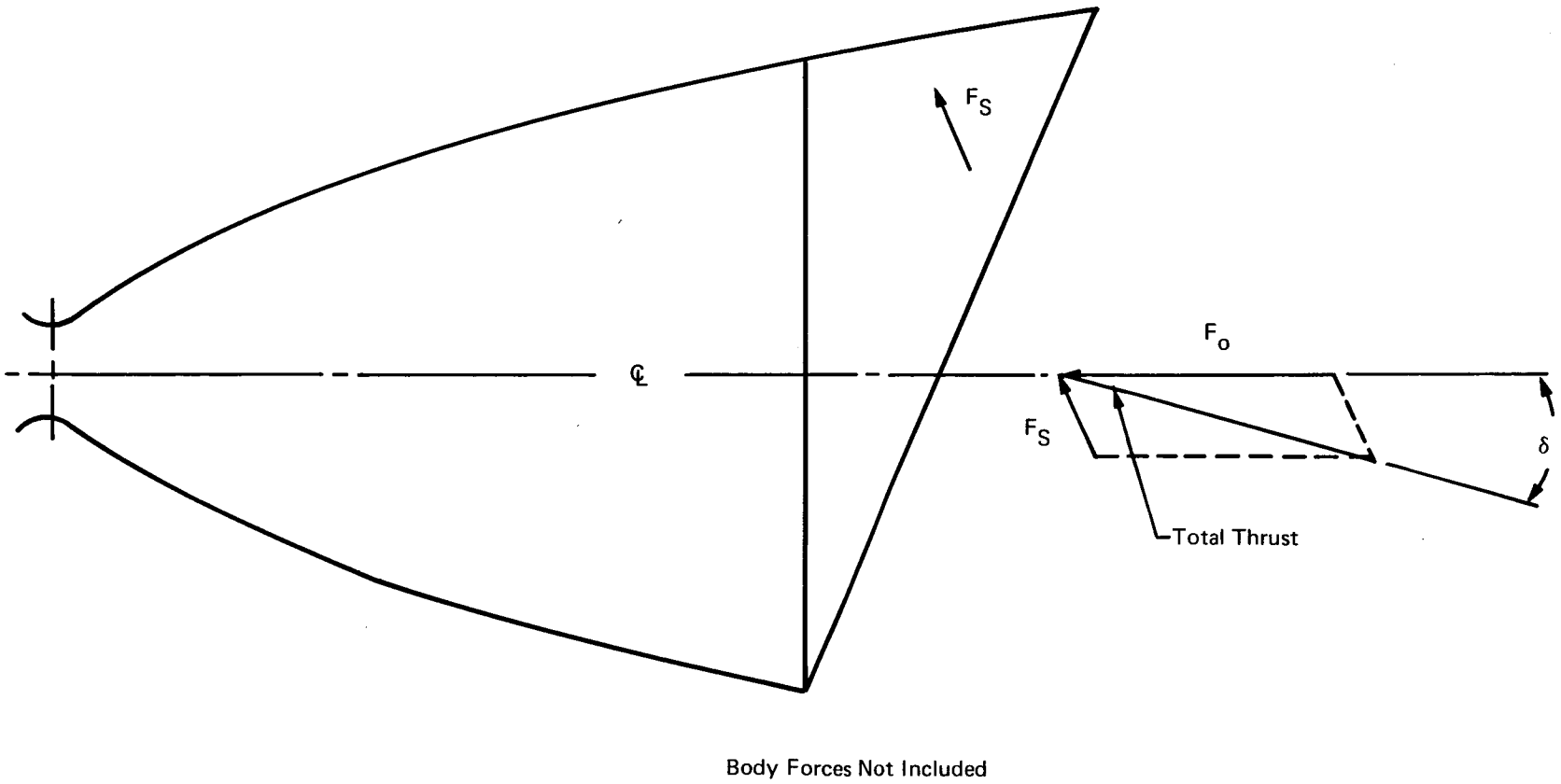

Figure 189. Scarf Nozzle Thrust Diagram

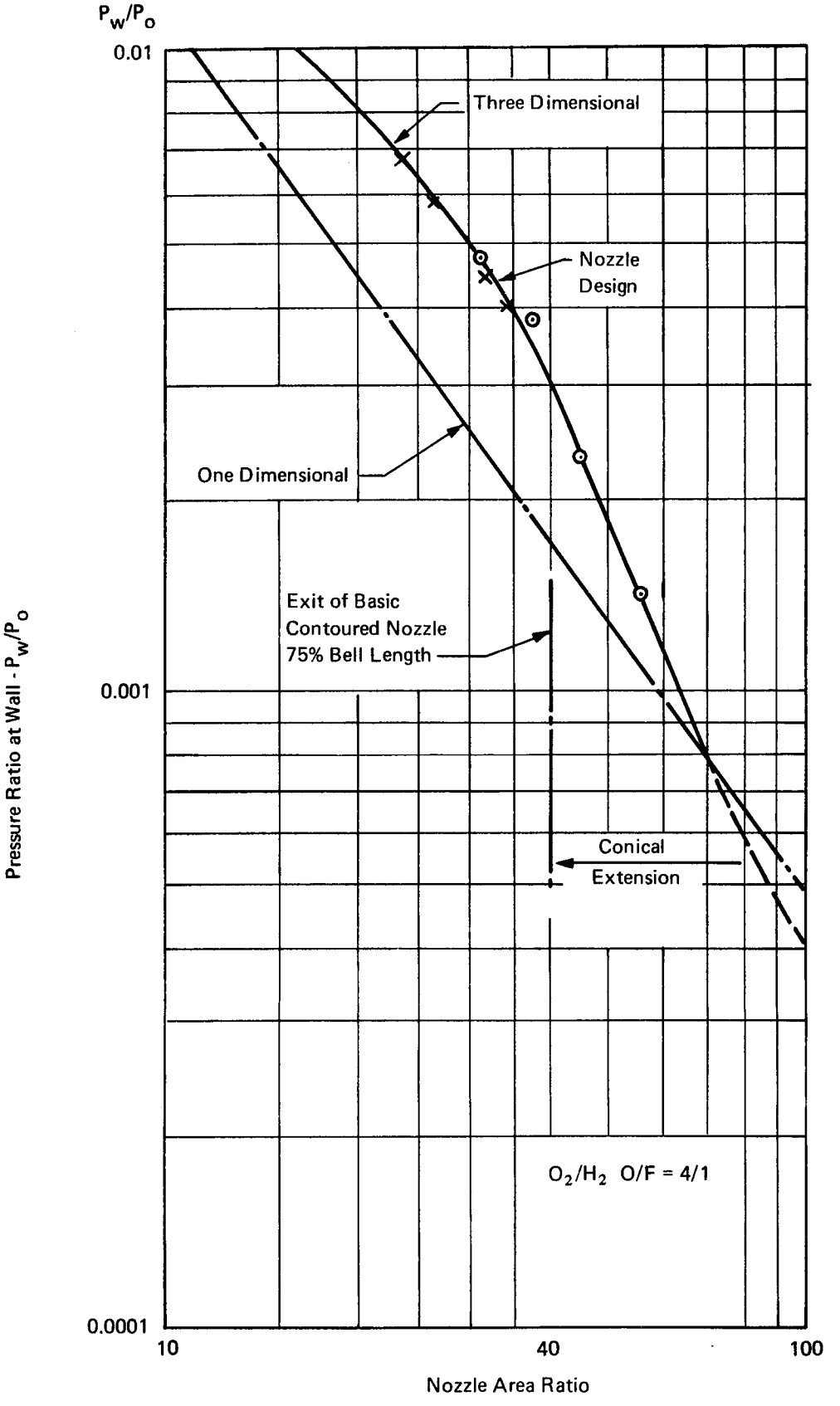

Figure 190. Pressure Ratio versus Area Ratio

Thrust inclination angles from the vertical (β-δ) as a function of scarf angle and initial axisymmetric area ratio are shown in Figure 191. From this figure, the space vehicle designer can determine the proper angle of scarf for a basic engine to suit his particular application. Scarf angles up to 70° are permitted before the absence of the missing scarfed wall will affect the wall pressure and thrust vector.

The validity of the use of this method was verified in cold flow tests at FluiDyne Engineering, Minneapolis, on scarfed nozzles with various scarf angles. The side thrust and axial thrusts were measured and compared with calculations. This work is summarized in Reference 36 and the data are presented for comparison on Table 1 of that reference. Tests were shown to agree well with predictions.

As surface is added to the nozzle with scarfing, the total thrust, neglecting body forces, will vary as on Figure 192. The data base is the Model 8636 unscarfed nozzle of area ratio = 40/1 which develops 1500 lbf (6672 N) in vacuum. With the same throat size and nozzle total pressure, the vacuum thrust will vary from 1500 lbf (6672 N), depending on the initial area ratio and scarf angle. This applies to a throat diameter = 1.90 inches (4.83 cm) at a mixture ratio of 4/1 and a chamber pressure of 300 psia (206.8 N/cm^2).

If the scarfed nozzle exits at a flat plane surface, the opening will be an ellipse with a long-side area ratio (ϵ_1) increasing with the scarf angle (β). The variation of long-side (maximum) area ratio is presented on Figure 193. It is from and around this long-side lip that the exhaust gas will continue to expand into a vacuum developing a pressure "foot pad" on the downstream adjacent surface. This integrated pressure field adds a small force vector to be added to the axisymmetric thrust and scarf thrust as previously mentioned. The size of the opening, that is the maximum dimension of the ellipse, increases with scarf angle as on Figure 194.

Boraas and Ashby, in Reference 36, made a detailed study of the pressure field around this nozzle opening in the vehicle skin and concluded that the pressure on the vehicle skin can be predicted by calculations of the Newtonian pressure or conservation of mass method on the surfaces in the rocket plume, depending on how much the plume is distorted by the presence of the plane in the plume. The authors recommended that the body force can be calculated from the measured pressures on incremental surface areas rather than measuring the body force with load cells directly.

Figure 195 shows the shape of the pressure distribution (Isobars) and illustrates the method of calculation of the body force and centroid from test pressure data of a Minuteman III scarfed nozzle with an area ratio nozzle of 1.35/1. Pressure taps are located along the lines A-A, B-B and C-C. The pressures are integrated on the grid areas in a manner shown on the figure.

A report of the test program at AEDC is found as Reference 37 which highlights the fact that a very sophisticated experimental facility is required to make the pressure measurements.

Although no numerical results of the body forces for the Space Shuttle application can be offered at this time, it is hoped the previous explanation defines the method of approach. The installed thrust angle compared with the thrust angle without body forces will not be larger than the 0.25° based on the Minuteman III PSRE experience.

D. DETERMINATION OF THE DISCHARGE COEFFICIENT FOR FILMCOOLING

Proper sizing of the film cooling slots was recognized as a critical design area because of the effect on performance of variations in the amount of film coolant employed. Before proper sizing

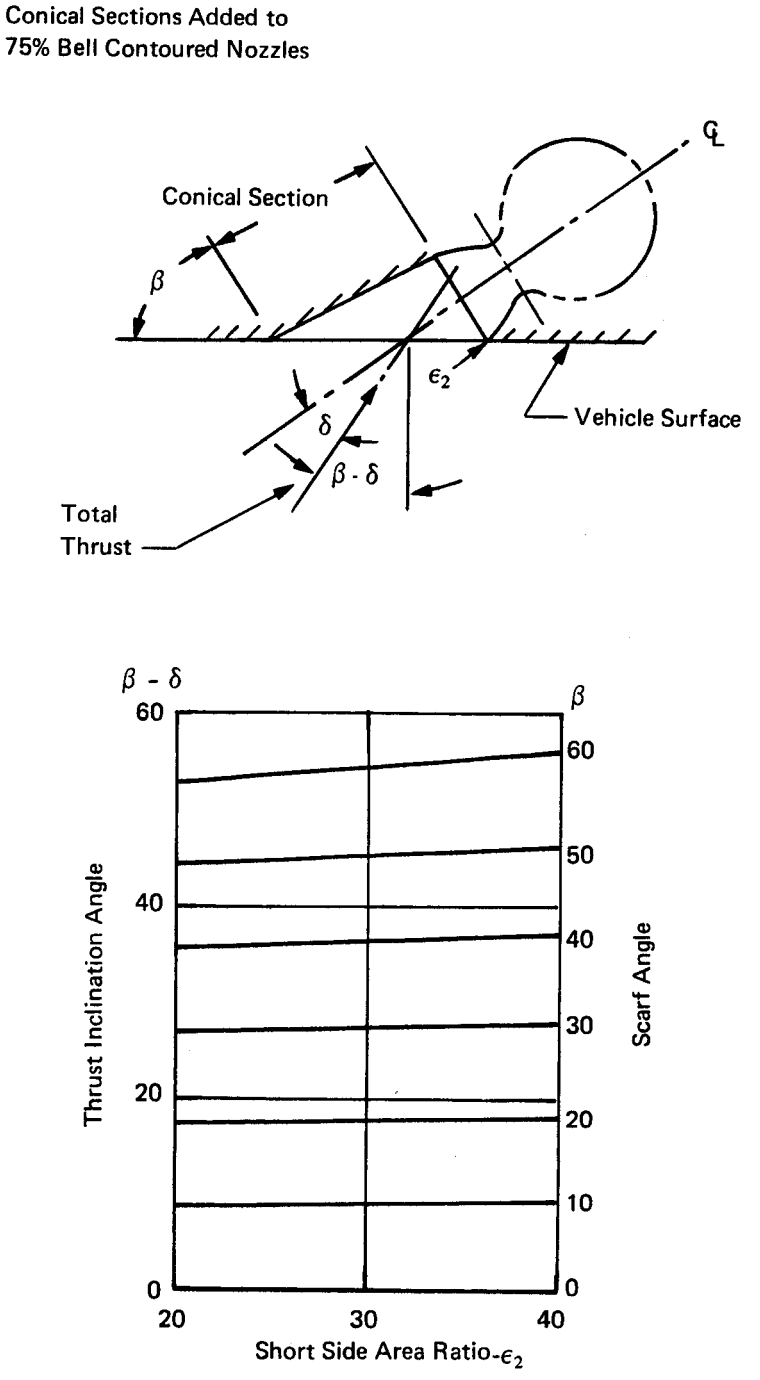

Figure 191. Thrust Inclination Angle as a Function of Scarf Angle and Area Ratio

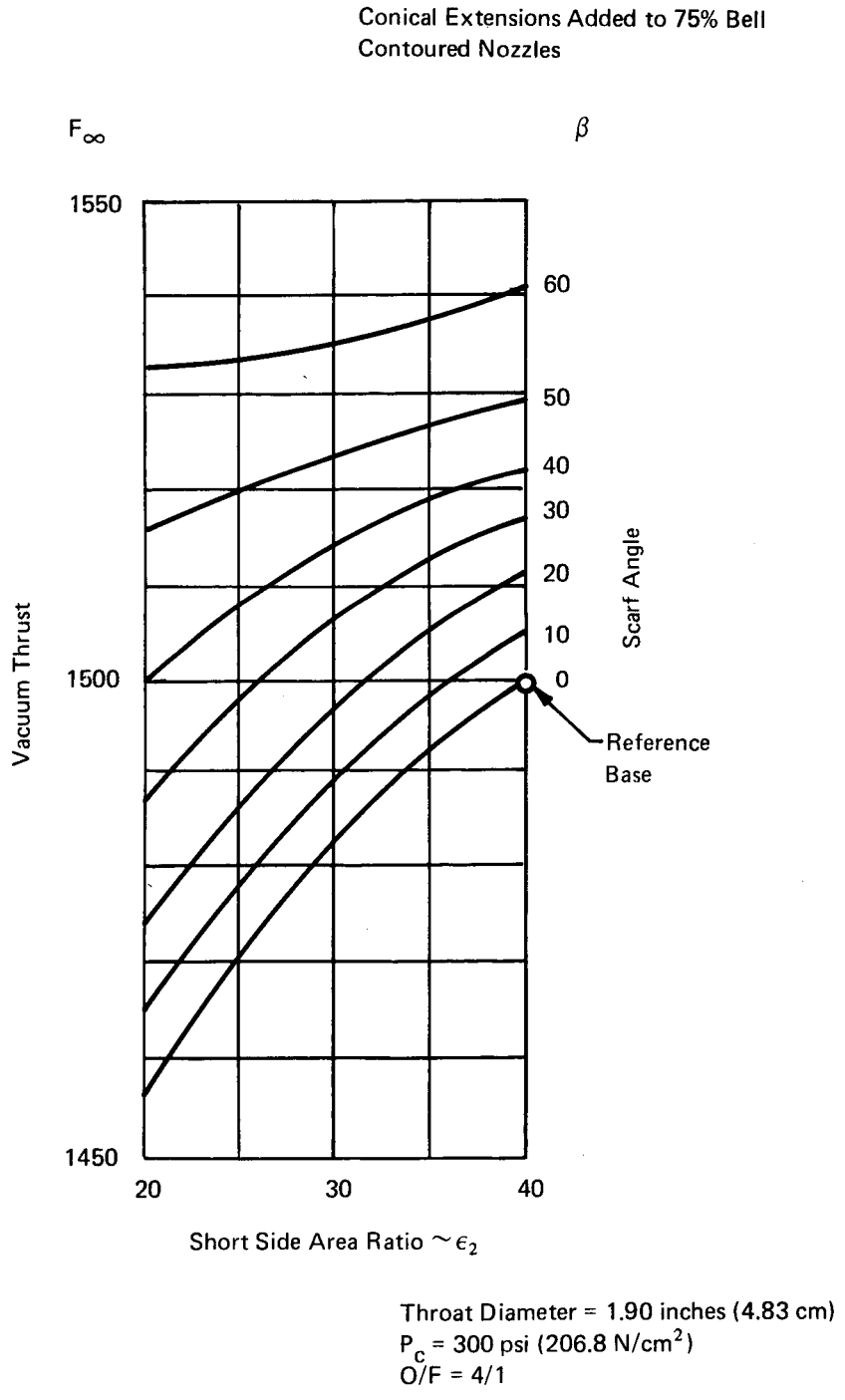

Figure 192. Vacuum Thrust as a Function of Scarf Angle and Area Ratio

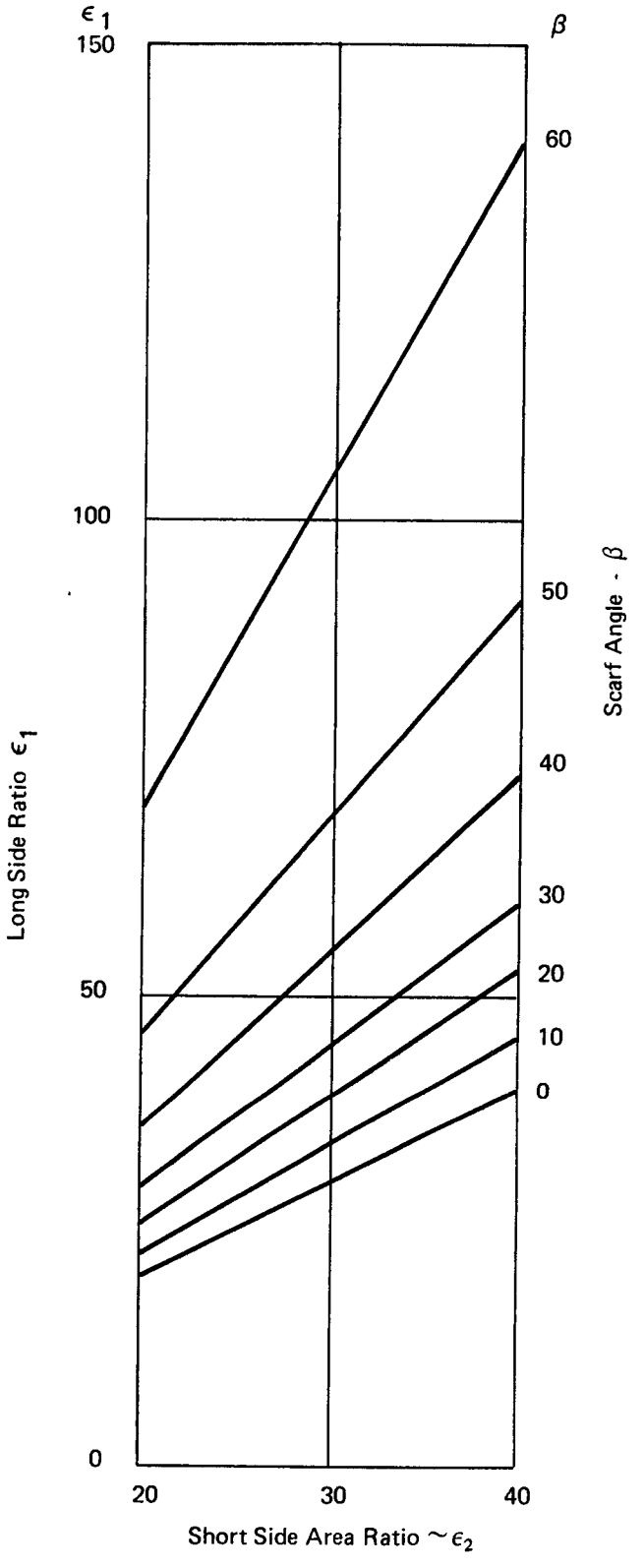

Figure 193. Long Side Area Ratio as a Function of Scarf Angle and Area Ratio

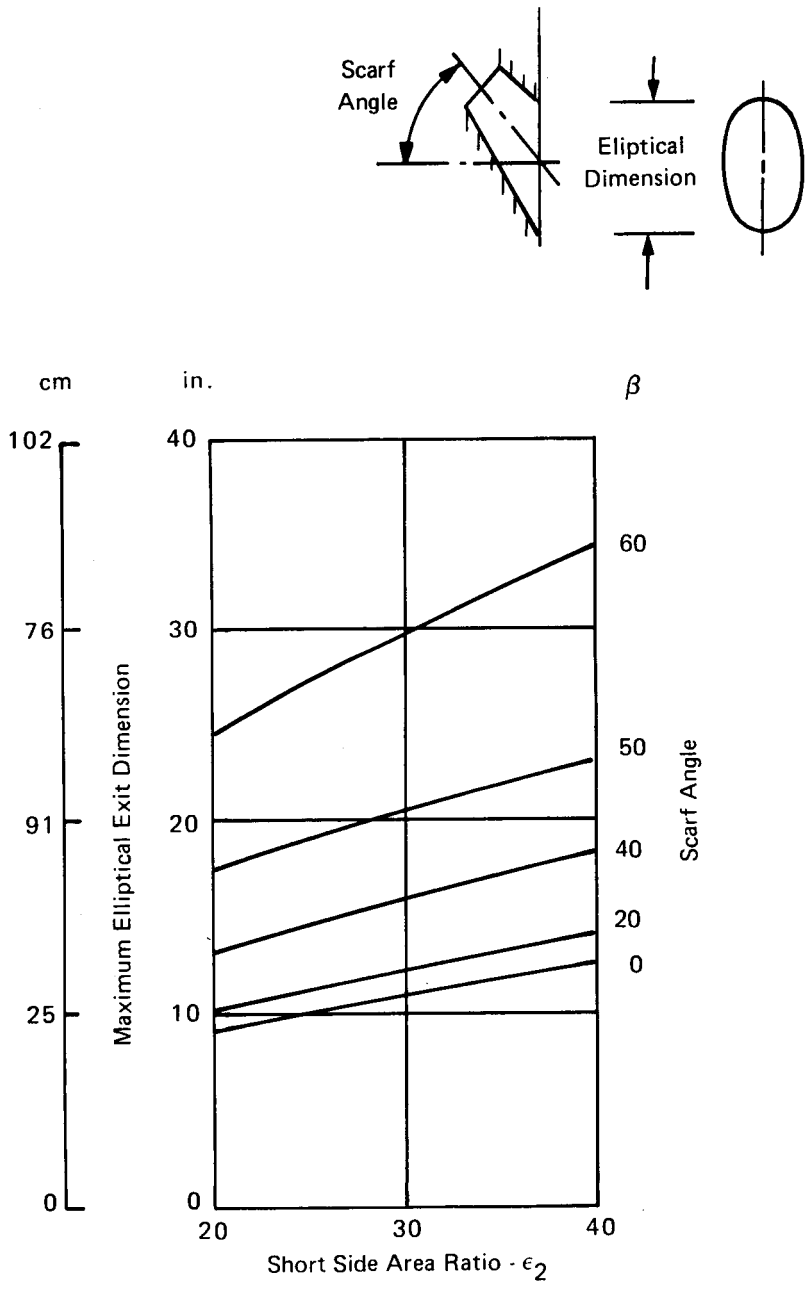

Throat Diameter = 1.90 inches (4.83 cm)

Figure 194. Maximum Elliptical Exit Dimension as a Function of Scarf Angle and Area Ratio

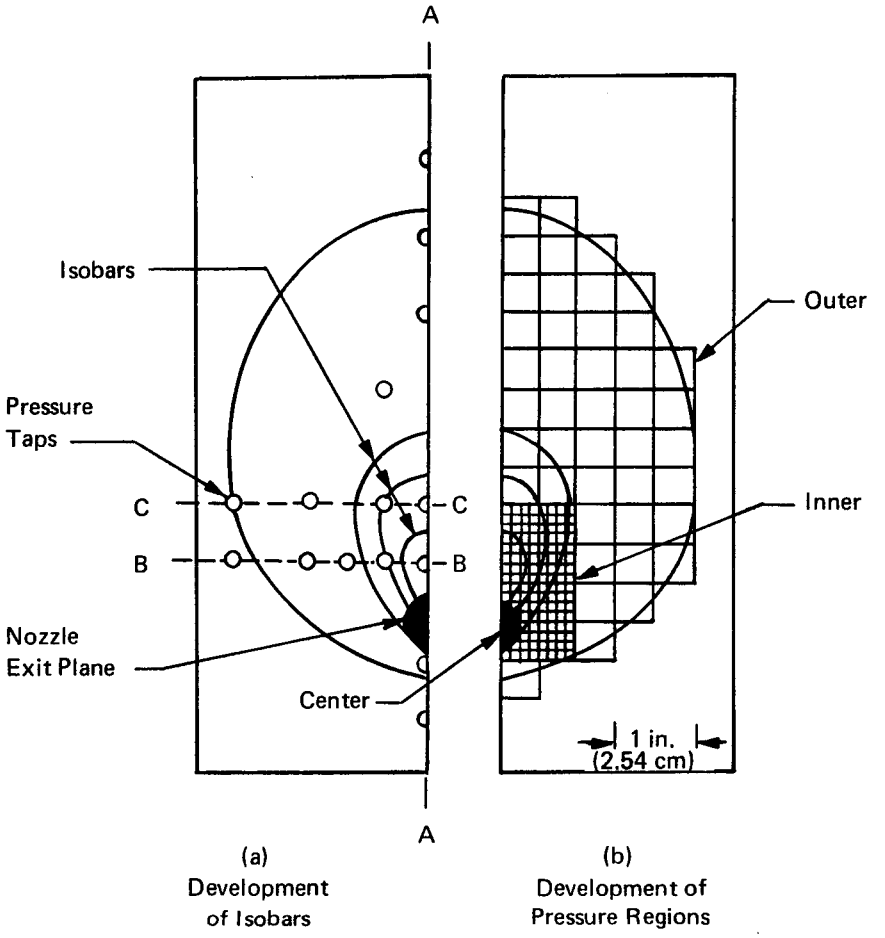

Figure 195. Body Force Determination AEDC Tests

of the slots could be accomplished, an accurate determination of the discharge coefficient was required. The configuration of the suggested slot, used to bleed film cooling gas from the channels is shown in Figure 196. This is a unique configuration upon which no discharge coefficient data are currently available in the literature. Therefore, a flow model was fabricated and tested to determine the following effects on discharge coefficient:

1. Slot thickness
2. ΔP across slot
3. Main duct Mach number
4. Slot entrance conditions

The following ground rules were established for the slot based upon film coolant injection considerations, and the contour of the throat section regenerative cooling passages;

1. A slot inclination of 35° to the regen channel
2. A slot length of 0.130 in. (0.330 cm)
3. A slot width of 0.220 in. (0.559 cm)

A schematic of the flow model and test rig used is shown in Figures 196 and 197.

The flow tests were conducted at a constant outlet pressure to simulate local static pressure in the chamber, but with varying inlet pressures (flow rate variations) and varying ΔP's between the injector slot exit and film coolant slot exit. The latter simulates variations in the location of the film coolant slot in the convergent nozzle section.

The Mach number of the efflux gases in the collection circuit was found from the measured static pressure, flow rate, total temperature, and cross sectional area using the continuity equation for compressible flow

$$M = \frac{\dot{w}\, RT_S}{P_S A \sqrt{\gamma\, g\, RT_S}} = \frac{\dot{w}}{P_S A}\sqrt{\frac{RT_O}{g\,\gamma}} \Bigg/ \sqrt{\left(1 + \frac{\gamma - 1}{2} M^2\right)} \qquad \text{(C-5)}$$

which is solved by an iterative process. The total gas pressure is then computed from the isentropic relation:

$$P_T = P_S \left\{ 1 + \left(\frac{\gamma - 1}{2}\right) M^2 \right\}^{\gamma/\gamma-1} \qquad \text{(C-6)}$$

Once the total pressure of the gas at the orifice exit is determined, the efflux Mach number can be computed from equation (C-5) where (C-6) is employed for the unknown local static pressure. An iterative solution yields efflux Mach number which can then be used in conjunction with equation (C-6) to determine the static pressure of the gas at the slot exit.

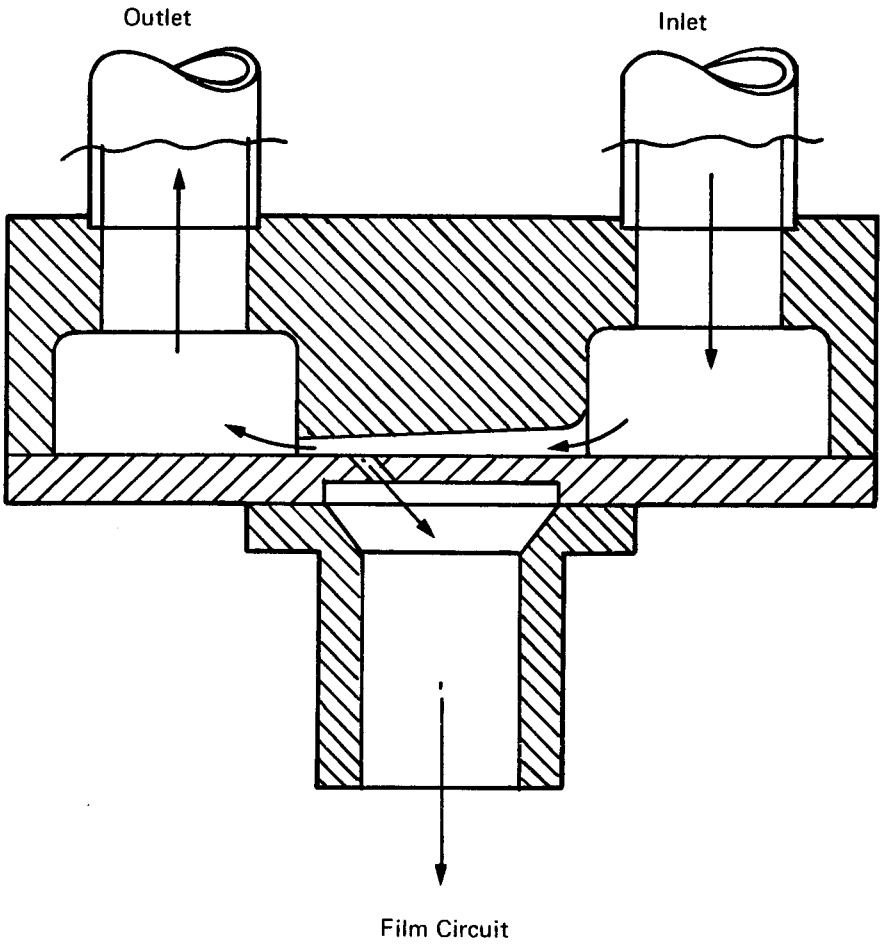

Figure 196. Flow Model

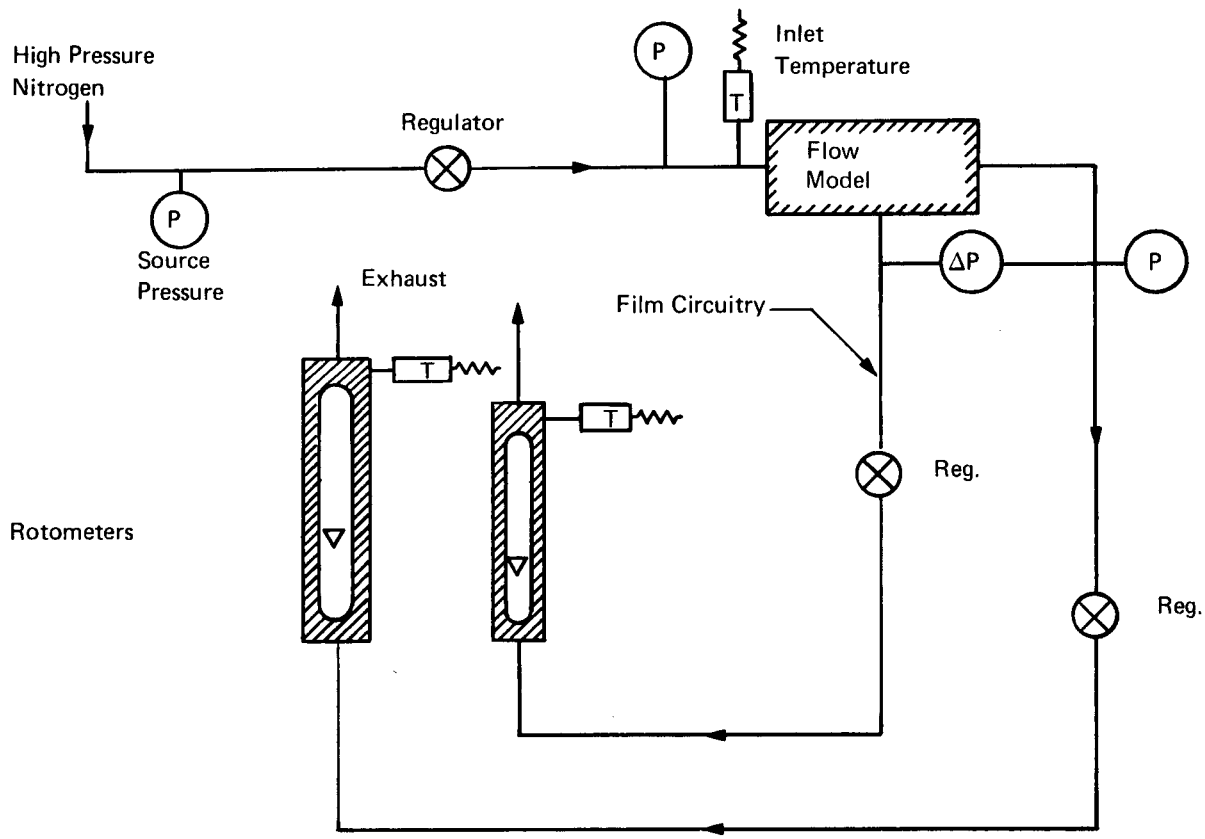

Figure 197. Test Schematic

The results of these tests for three different slot thicknesses is shown in Figure 198. The ordinate of the graph is the percent of the total flow which exits through the film coolant slot. The abscissa is the difference in static outlet pressures between the injector and film coolant slots. It is seen that the percent film coolant is essentially independent of Mach number for static pressure differences between 0 and +5 psi (0 and 3.45 N/cm^2). This is significant since it means that the % film coolant will be insensitive to flow rate (mixture ratio) and propellant temperature variations in this regime. At larger pressure differences the expected trend of less flow with increasing Mach number is evident.

A coefficient of discharge was computed for each slot configuration at zero static pressure difference by assuming the flow is divided according to the effective area of the flow circuits. It is logical to assume a discharge coefficient of unity for the main injection orifice because of geometry. The C_D for the film coolant slot can then be computed from the relationship:

$$C_D = \frac{A_I}{A_C} \left(\frac{Per}{100 - Per} \right)$$

where

A_I = Geometric area of main injection slot
A_C = Geometric area of film coolant slot
Per = Percent film coolant

The coefficient of discharge for the four slot configurations tested is shown in Figure 199 for a static pressure difference of 0 psi (0 N/cm^2). An increase in the C_D is seen as both the slot thickness is decreased, and as the entrance is rounded. The first effect is due to a reduction in the main duct disturbance as the slot area decreases. The second effect is due to a larger radius of curvature for the streamlines entering the coolant slot.

A 6% film cooling flow was selected on the basis of heat transfer analyses. The sharp edge entrance slot was chosen for ease of fabrication. The final selected dimensions of a slot height of 0.007 inch (0.018 cm) and a width of 0.160 inch (0.406 cm) were based on a compromise of EDM fabricability and the desire to maximize the circumferential uniformity (minimum spacing between slots) of the film coolant flow. The design was incorporated into the film-cooled nozzle where 40 of the identified film cooling slots (one per channel) were used.

E. SIZING OF SUPERSONIC DUMP COOLANT ORIFICES

The design of the dump-cooled (supersonic injection) orifices included the following criteria:

(1) Sonic flow through manifold distribution orifices and dump slots for six percent flow.
(2) Supersonic injection into divergent nozzle.
(3) A matching of local static pressure for the coolant and core gases.
(4) Maximum coverage reasonably obtainable.

The following equations were derived for the dump coolant slots of constant height and varying width:

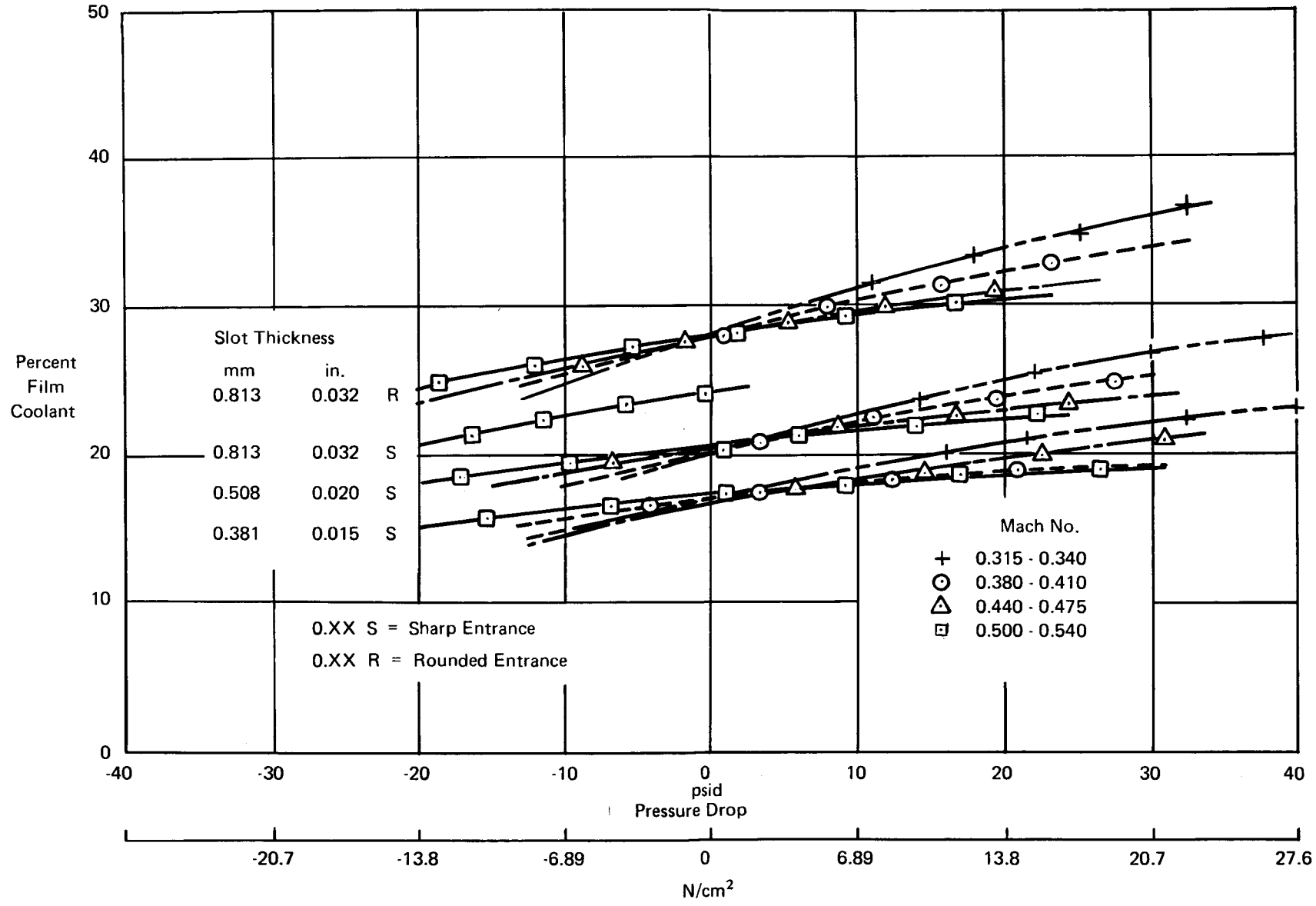

Figure 198. Percent Film Flow versus Static Pressure Difference

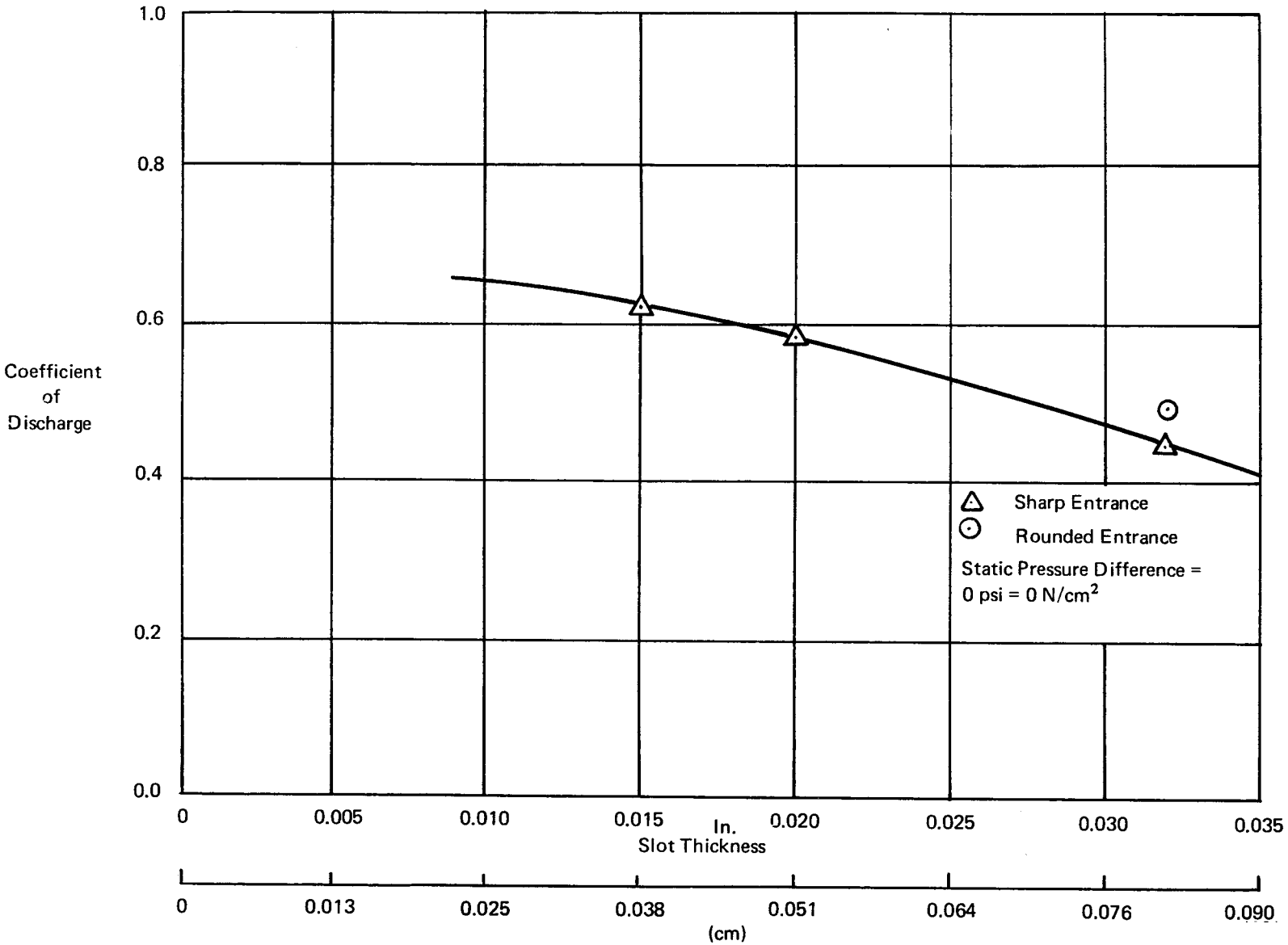

Figure 199. Coefficient of Discharge versus Slot Thickness

(a) Slot Exit Width, ℓ

$$\ell = \frac{(\%)\,(P)}{100\ N_s}$$

$\%$ = Percent Coverage

P = Perimeter at injection station = 18.57 inches (47.17 cm)

N_s = Number of slots

(b) Area Ratio and Total Pressure

The total pressure $P'_{o_{(2)}}$ at the slot throat and slot area ratio are related through the graph in Figure 200. This graph was defined to maintain a constant static exit pressure of 4.12 psia (2.84 N/cm^2) for 6% dump cooling.

The area ratio is given by:

$A_r = \ell / C_D m$

m = Slot entrance width

C_D = Slot discharge coefficient ≈ 0.7.

(c) Slot Height

Slot height is given by the relation:

$$h = \frac{16565.38 \times W \times A_r}{\% \times P \times P'_{o_{(2)}}}$$

$\dot{W}$ = (0.06) (0.6896) = Flow Rate

A_r = Area ratio

$\%$ = Percent coverage

P = Perimeter

$P'_{o_{(2)}}$ = Slot total pressure

The results of the analysis led to the following design point:

6% Dump Coolant Slot Design Summary

Gas Temperature	540°R (300°K)
Slot Height	0.0205 inch (0.0521 cm)
Slot Width	
Entrance	0.1326 inch (0.3368 cm)
Exit	0.1857 inch (0.4717 cm)
Area Ratio	2.0 at C_D = 0.7
Injection Velocity	6,750 ft/sec (2,057 m/sec)
Static Pressure	4.116 psia (2.833 N/cm^2)
% Coverage	80%
Number of Slots	80
Land Width	0.0464 inch (0.1179 cm)

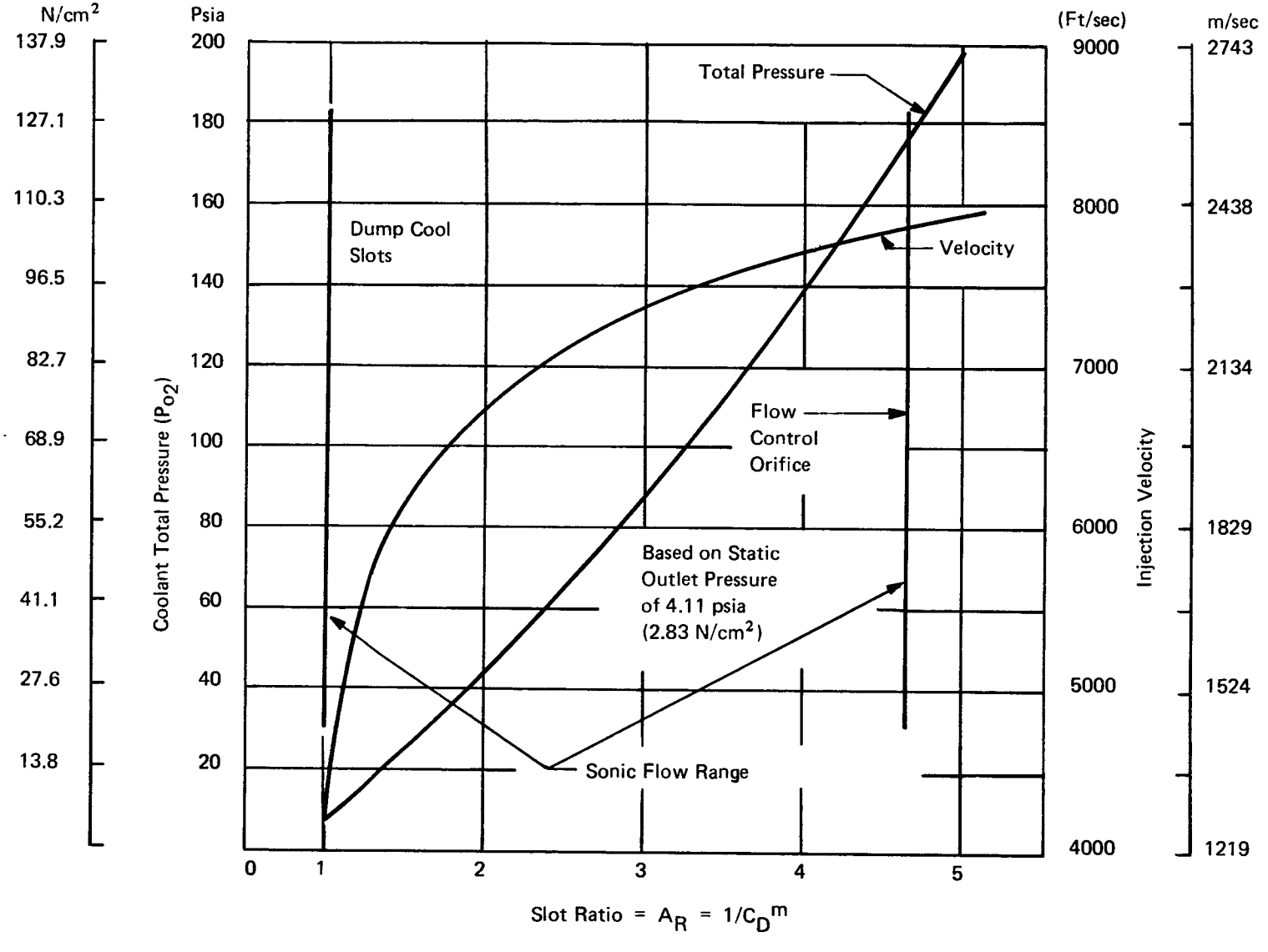

Figure 200. Total Pressure versus Area Ratio

(d) Distribution Orifices

Sizing of the flow control distribution orifices is dependent upon injector feed pressure. Analysis of the flow indicated a pressure of 375 psia (258.5 N/cm^2) is reasonable which establishes P_c in the formula:

$$A = \frac{\dot{w}}{C_D P_o} \sqrt{\frac{R\,To}{\gamma g} \left(\frac{2}{\gamma + 1}\right)^{\frac{\gamma + 1}{1 - \gamma}}}$$

Using:

C_D = 0.85
P_o = 375.0 psia (258.5 N/cm^2)
γ = 1.4
To = 540°R (300°K)
g = 32.174 ft/sec^2 (9.8066 m/sec^2)
$\dot{w}$ = (0.06) (0.6896) lbm/sec (0.3128 Kg/sec)

A is computed to be:

A = 0.021495 square inch (0.138677 sq cm).

This yields the following hole sizes (for 6% dump flow):

No. of Holes	Diameter - inches
6	0.0523 (0.1328 cm)
12	0.0478 (0.1214 cm)
18	0.0390 (0.0991 cm)
20	0.0370 (0.0940 cm)
24	0.0338 (0.0859 cm)

Twenty holes were selected as the design point.

F. PERFORMANCE LOSS DUE TO FUEL FILM AND DUMP COOLING

1. Types of Cooling and Definitions

Performance degradation with supplementary cooling was calculated for three separate types of cooling. Types of cooling and methods for calculation of performance loss to be described are:

(a) Film cooling with subsonic hydrogen injection.

(b) Open tube or external dump cooling; supersonic nozzle coolant flow exit at nozzle exit plane.

(c) Internal dump cooling with hydrogen injected in the supersonic nozzle.

In all cases, fuel diverted from the combustion process which is to be expanded adjacent to the wall results in losses from the following phenomena:

(a) Fuel so diverted forces the core from a mixture ratio of 4/1 to increased mixture ratios and decreased kinetic performance as on Figure 201.

(b) Sensible heat is removed from the hot core to the cooler fuel flowing adjacent to the wall.

Losses for all types of cooling to be described were based on computation of a cooling efficiency (η_C) which is the ratio of the sum of coolant and core thrusts to the thrust at the overall mixture ratio of 4/1. Thrusts of coolant and core, in turn, were calculated by products of their weight flows and impulses:

$$\eta_C = \frac{\dot{w}_1 I_1 + \dot{w}_2 I_2}{[\dot{w}_1 + \dot{w}_2] I_O}$$

where

$\dot{w}_1$ = coolant flow rate
$\dot{w}_2$ = core flow rate
I_1 = specific impulse of coolant with heat gain
I_2 = specific impulse of core with heat loss
I_O = kinetic specific impulse at O/F = 4/1

Cooling efficiencies for the three types were governed by:

(a) The amount of fuel as coolant

(b) The rate at which heat is transferred from core to coolant

(c) Particular ground rules for the expansion process

2. Open Tube Dump Cooling

The heat absorbed by coolant inside was calculated by convective heat balance to the coolant passages based on assumed values of the maximum wall temperature. The assumption was made that the coolant exit was sized for sonic flow. The function is:

$$\frac{\Delta M^2}{M^2} = \left[\frac{(1+\gamma M^2)(1+\frac{\gamma-1}{2} M^2)}{1-M^2}\right] \frac{\Delta T_O}{T_O} - \frac{2(1+\frac{\gamma-1}{2} M^2)}{1-M^2} \frac{\Delta A}{A}$$

The numerical integration is accomplished by iteration using a digital computer (BAC IBM Program XY 5239).

Coolant and core specific impulses were calculated in terms of the exit Mach number and exit total temperatures.

$$I_1 = 9.0369 \sqrt{T_{O_1 E}} \quad ; \quad M_1 = 1$$

$$I_2 = \frac{P_{2E} A_{2E}}{\dot{w}_2} + \frac{M_{2E}}{g} \left[\frac{\gamma g R T_{O_2,E}}{\frac{\gamma-1}{2} M^2_{2E}}\right]^{1/2}$$

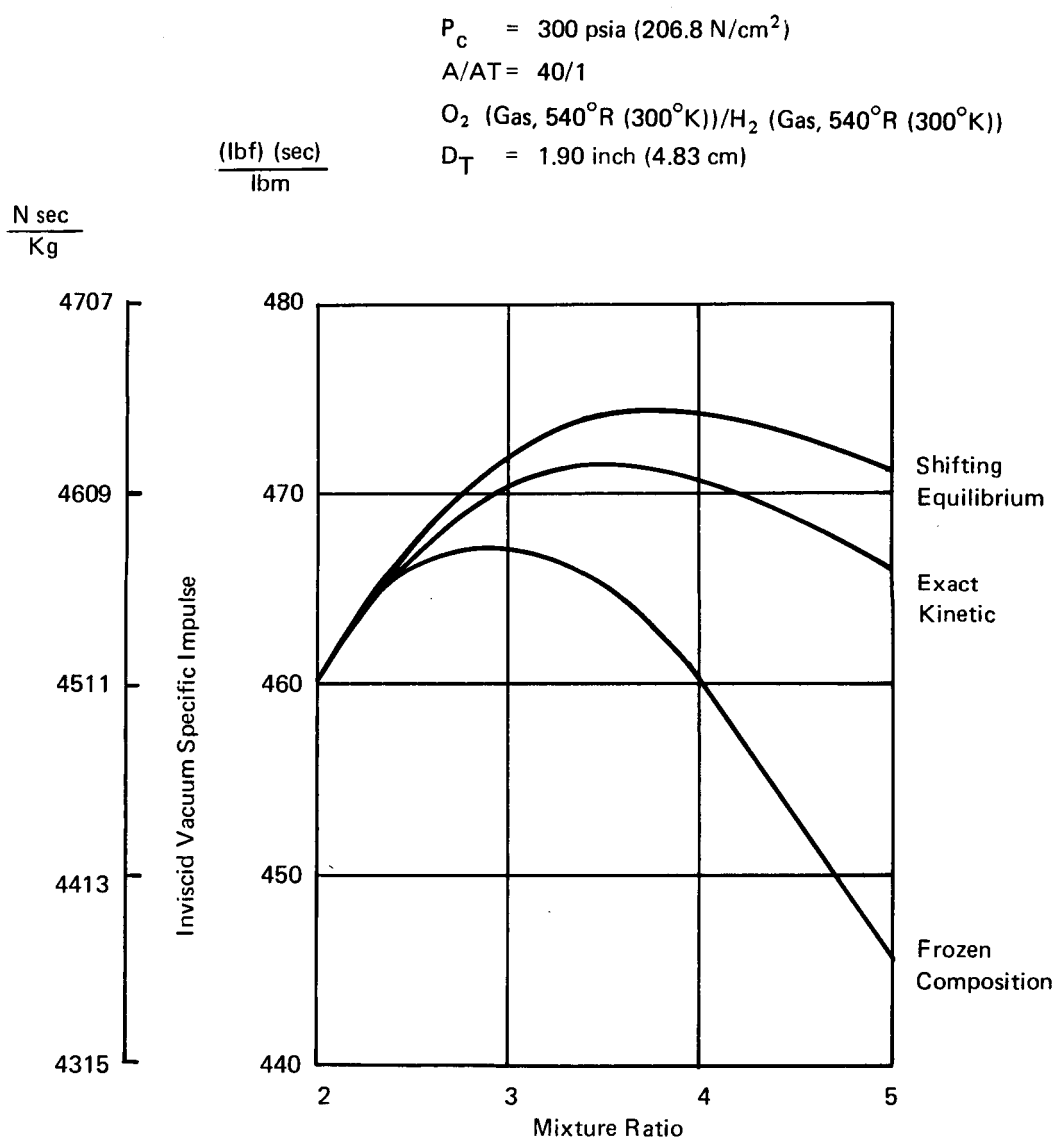

Figure 201. Theoretical Vacuum Specific Impulse versus Mixture Ratio

T_O = Total temperature
M = Mach number
P = Pressure
A = Area

Subscripts

E = Exit

3. Internal Dump Cooling

Coolant flow injected in the supersonic nozzle absorbs heat from core as an adiabatic temperature at the wall. The adiabatic temperature was calculated by the method of Zakkay previously described. His expression is:

$$\left(\frac{T_O - T_{aw}}{T_O - T_c}\right) = 15.8 \left[\left(\frac{x}{S}\right)\left(\frac{\rho_c V_c}{\rho_g V_g}\right)^{-0.8}\right]^{-0.55}$$

where

T_O = total temperature of gas
T_{aw} = adiabatic wall temperature
T_c = coolant total temperature
x = distance from injection
S = coolant slot height
$\rho_c V_c$ = mass velocity of coolant
$\rho_g V_g$ = mass velocity of gas

There are at least three ways to describe expansion of coolant gas:

(1) Assume Mach number of the coolant gas is constant and equal to 1.0.
(2) Calculate final Mach number at exit with coolant static pressure equal to core static pressure at their interface.
(3) Calculate final coolant Mach number at exit with coolant and core of equal velocity at their interface.

The core flow performance was calculated on the basis of the heat extraction and expansion less than the nozzle geometric area ratio. The core flow at the nozzle exit is displaced from the physical wall by the coolant flow.

4. Film Cooling

The heat absorbed by the coolant is again characterized by adiabatic film temperature as calculated by Hatch and Papell film cooling correlation for subsonic flow. Their expression is:

$$\log_e \left[\frac{T_{ad} - T_w}{T_{ad} - T_c} \right] = - \left[\left(\frac{h_g L x - 0.04}{(\dot{w} C_p)_c} \right) \left(\frac{S' V_g}{\alpha_c} \right)^{0.125} f\left(\frac{V_g}{V_c} \right) \right]$$

$$+ \log_e \cos (0.8 i_{eff})$$

where

T_{ad}	=	adiabatic recovery temperature
T_w	=	static gas temperature at wall
T_c	=	static coolant temperature
h_g	=	convective heat transfer coefficient
L	=	width of adiabatic wall
x	=	distance along wall from injection
S'	=	effective coolant slot height
α_c	=	thermal diffusivity of coolant
V_c	=	coolant velocity
V_g	=	gas velocity
$f(V_g/V_c)$	=	function dependent upon the ratio of gas to coolant velocity
i_{eff}	=	effective coolant injection angle relative to surface to be cooled

Coolant gas can expand in three ways, similar to internal dump cooling. The calculations carried out were limited to the one case of a constant Mach number equal to 1. Core performance is calculated based on the heat extracted and expansion to an area ratio consistent with the annular displacement of the core flow by the coolant flow.

5. Results and Comments

Most of the analytic effort was devoted to the prediction of thrust loss with internal dump cooling. The only useful set of impulse loss as a function of coolant flow rate was calculated with the assumption of sonic exit of hydrogen and full area ratio flow of the core. The use of this assumption, for coolant flows of low percentages ($< \approx 5\%$), is deemed feasible by Quan and Melde, Ref. (38).

Calculations for the performance loss with dump cooling and the assumption of a coolant Mach number = 1.0 resulted in a linear variation in specific impulse of 2.67 seconds with 10% fuel as coolant. The second assumption of equal static pressures throughout the nozzle was coded for the IBM 360/50 computer but the numerical results were unsatisfactory because of a lack of definition of the mixing between the two streams.

Future work with turbulent mixing of coaxial streams might be slanted toward use of a mixing zone and total pressure loss investigated by researchers such as Chow and Addy, Ref. (39). Their interest lies in supersonic ejector systems which shares a great similarity with supersonic dump cooling in rocket nozzles.

APPENDIX D
COMPUTATIONAL TECHNIQUE FOR COMBUSTOR MODELING

Recent analytical efforts performed at the Bell Aerospace Company have been directed toward combustion modeling using as a reference, the work of Professor D. Spalding. These efforts have mainly included conventional combustor configurations, the effort being reported in Reference 40. Interest in the reverse-flow engine prompted a modeling effort for this type of combustor, the results of this effort are reported in this appendix. They are considered to be preliminary in nature and have been included in this report to illustrate the current progress of the technique.

In a recent book (Reference 41) Prof. D. Spalding and associates at the Imperial College of Science and Technology, outlined a numerical procedure for the solution of the flow and energy equations which allows for the existence of recirculation, reacting gases (combustion), eddy mixing and compressibility. The only major restriction is the assumption that the flow field be two-dimensional or axisymmetrical. The uniqueness of the Spalding approach lies in the transformation of the separate conservation equations --mass, stream function (line), vorticity and energy --into one standard format, a nonlinear, elliptic, partial differential equation. This is solved by a finite difference, successive substitution procedure, using the Gauss-Seidel iterative technique.

In Reference 41, a sample case was presented for a single coaxial element, injecting, at equal velocities, low energy release propellants [combustion temperature = 2500° R (1389° K)] of constant density into a cylindrical combustion chamber. Our efforts have been directed toward adapting these numerical techniques to the solution of the hydrogen-oxygen reverse flow combustor problem.

Before discussing these Bell Aerospace efforts, a brief description of the computer program input and forms of output is in order. Full geometric boundary definitions are required; specifically: the chamber and throat radius, the chamber and throat length, and the inside and outside radii of each orifice. The fluid flow boundary conditions include the flow rates and velocity (including swirl components at each orifice), the chamber pressure, respective propellant temperatures, density and molecular weight, the heat release and stoichiometric mixture ratio and an exit and wall boundary condition. The output is in three separate forms. First the flow variables (that is, axial and radial velocity components, density, vorticity, stream function, temperature, viscosity and mixture fraction) are printed out at every nodal point in the system. Then, for the independent variables (vorticity, stream function, mixture fraction and temperature) a map is printed out, showing the value of each of these variables at each node in the chamber. The final output form is an on-line computer graphical representation of lines of constant stream function, vorticity and temperature.

Two major problems were worked on in solving for the flow field within the reverse-flow motor. The first was to add the capability of handling high combustion temperature dissimilar density gases, such as 6500° F (3867° K) temperature products from GH_2/GO_2 (density ratio = 16). This work was accomplished in 1970, and presented to the 8th JANNAF Liquid Propellant Combustion Instability Meeting in October 1971 (Reference 40). The second job was to adapt the modified Spalding computational technique, which handled boundaries that were parallel to the coordinate system (vertical and horizontal) to the noncoordinate reverse-flow geometry. This problem too was eventually resolved.

The 1500-lb (6672N) thrust reverse-flow engine was then analytically modeled both with and without swirling oxidizer flow. The oxidizer was injected with an axial velocity of 400 fps (121.9 m/sec)[and, when used, a tangential velocity of 400 fps (121.9 m/sec)] and the fuel at 2400 fps (731.5 m/sec). The resultant flow field, for the swirling oxidizer case, using the off-line Cal-Comp

plotter, is shown in Figures 202, 203, 204 and 205. Figure 201 maps the stream lines. Lines of constant stream lines indicate the path a particle would take in traversing the chamber. Figure 203 shows the local temperature within the chamber. These numbers are high near the wall, an inaccuracy probably due to a poor approximation of the eddy viscosity mixing model near the wall. Figure 204 shows local values of the swirl velocity. It is interesting to note that the swirl component of velocity dampens quite rapidly as the oxidizer enters the chamber. Figure 205 shows the local value of mixture fraction, f, related to mixture ratio by the expression

$$MR = \frac{1 - f}{f}$$

Therefore, values of f below 0.111 are oxidizer rich, and regions above 0.111 are fuel rich.

Engine performance was computed by weight averaging the local values of characteristic velocity and dividing by the value of c* that would be obtained if perfect mixing had occurred. The local values of c* were obtained from the computed local values of mixture ratio and the known relationship between c* and MR.

Although the values of the computed performance compared quite well, (94% versus measured values of 95%), the effect of correct eddy viscosity mixing models becomes quite obvious when studying effects directly involving mixing, such as swirl. Analytically, swirling the oxidizer added about 1% to c* efficiency, considerably less than the experimentally realized gain in ηc^* due to swirl. Therefore, some additional analytical work is required to improve the mixing model, so as to provide closer correlations on wall temperature and swirl velocity effects.

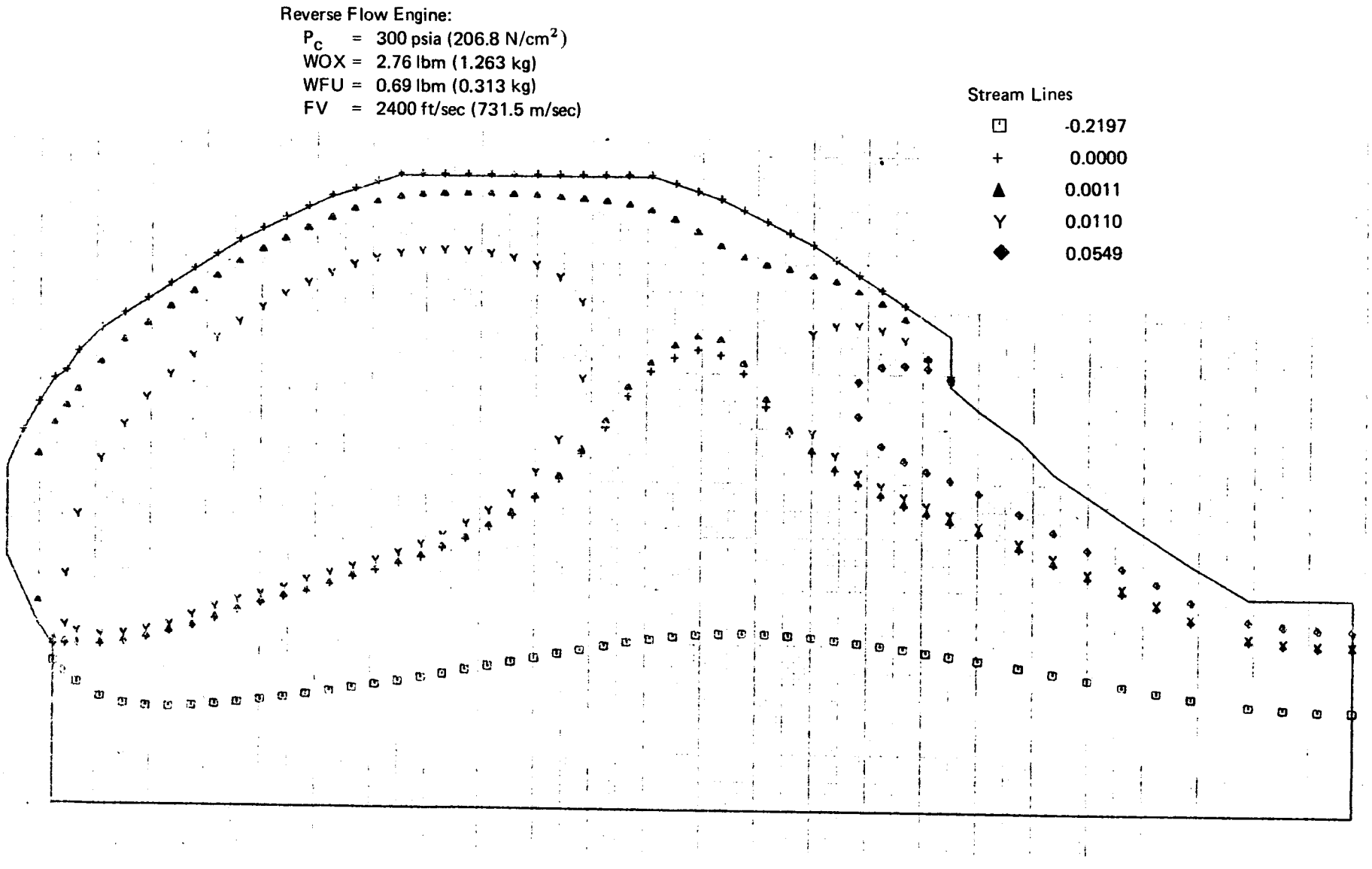

Figure 202. 1500 lb (6672 N) H_2O_2 Reverse Flow Engine Contour Plot for Stream Lines

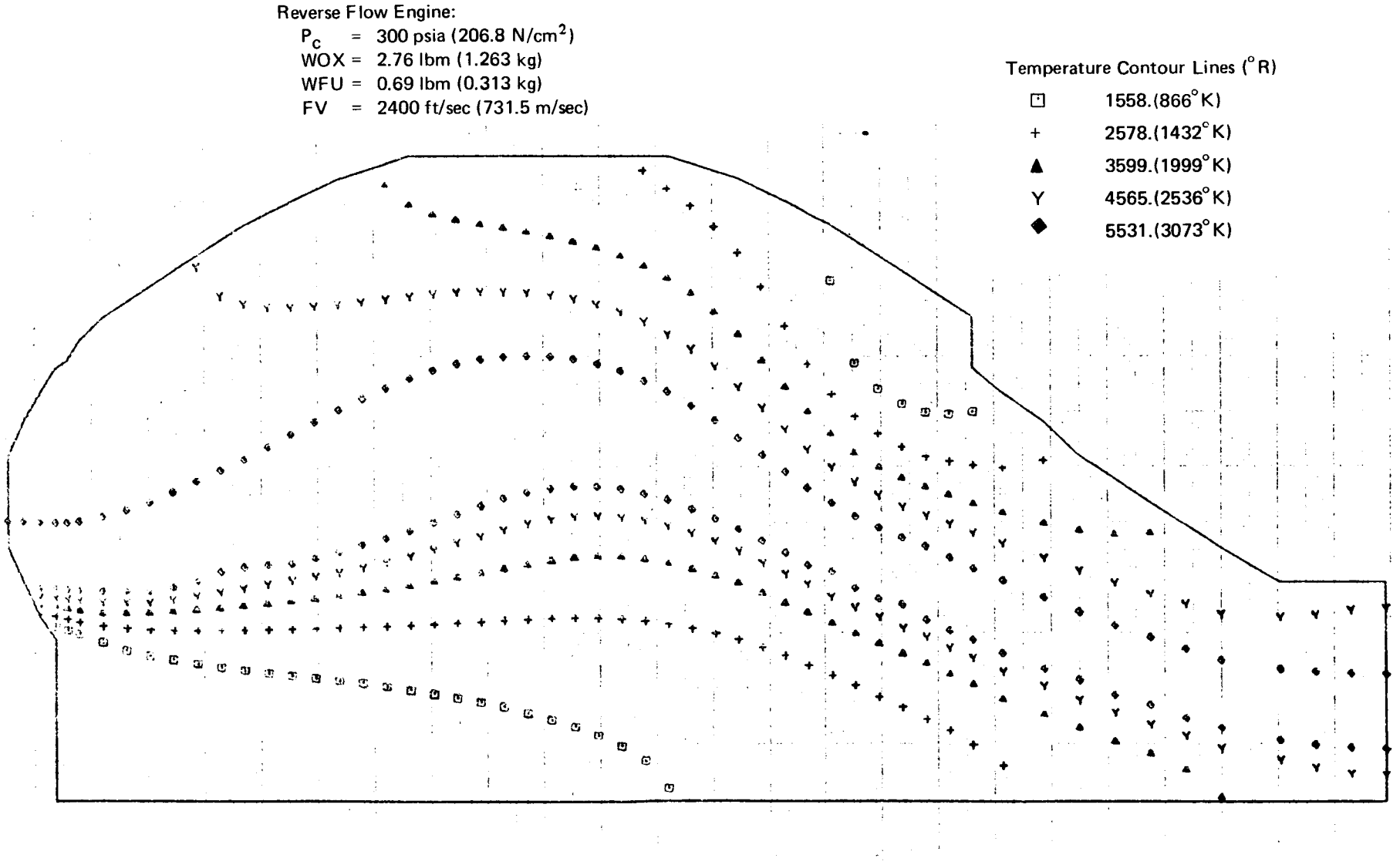

Figure 203. 1500 lb (6672 N) H_2O_2 Reverse Flow Engine Contour Plot for Temperature

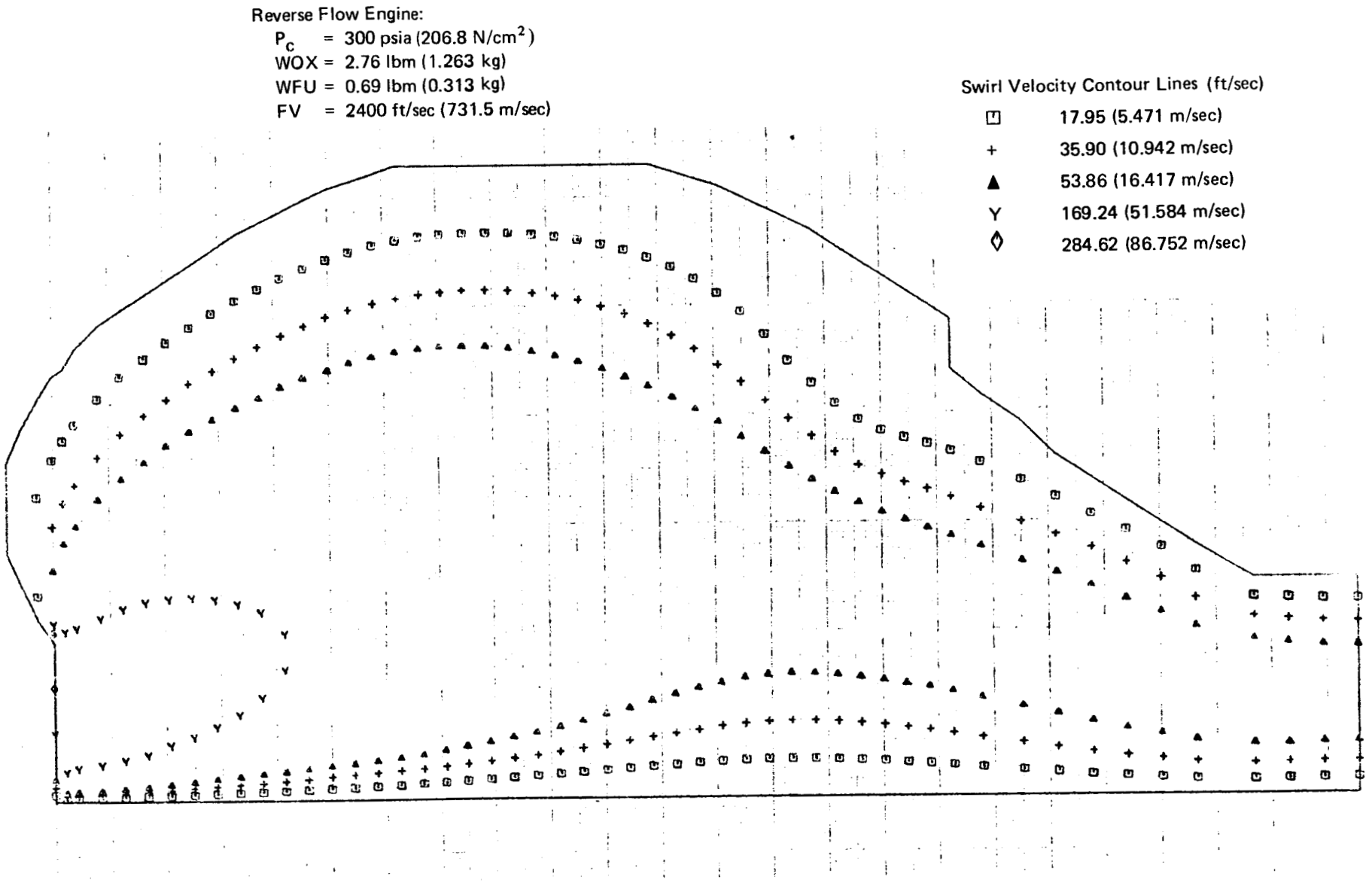

Figure 204. 1500 lb (6672 N) H_2O_2 Reverse Flow Engine Contour Plot for Swirl Velocity

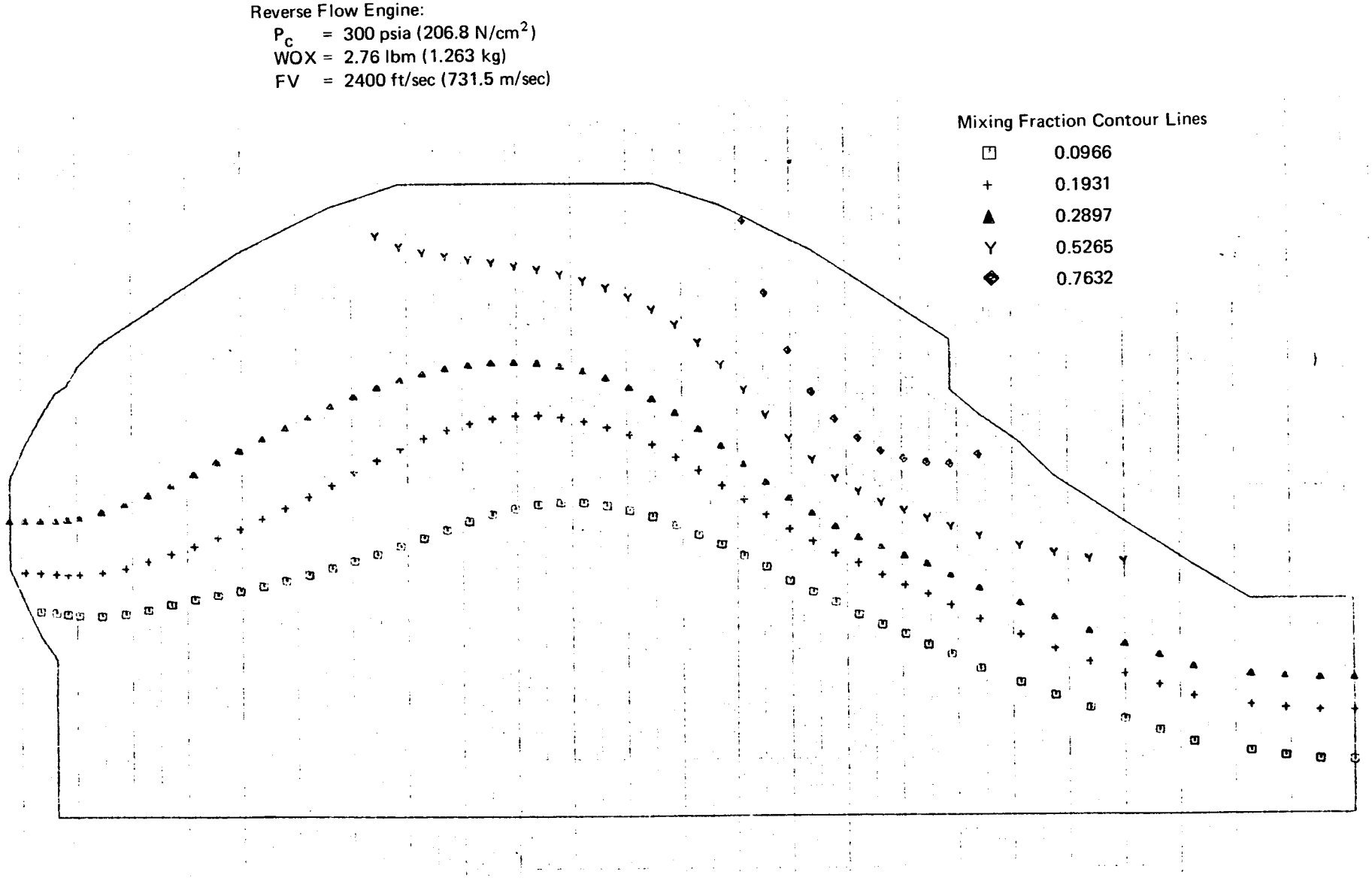

Figure 205. 1500 lb (6772 N) H_2O_2 Reverse Flow Engine Contour Plot for Mixture Fraction

REFERENCES

1. Vaughan, J. C., "Effect of Chamber Pressure on the Performance of a Small Reverse-Flow Rocket Engine," MS Thesis, AF Institute of Technology, WPAFB, Ohio (1964).

2. Guarino, N. J., "An Experimental Study of Airflow Injected Tangentially into a 2-Dimentional Chamber of Circular Shape," MS Thesis, AF Institute of Technology, WPAFB, Ohio (1958).

3. Nolan, L. S., "An Interferometer Study of Reverse-Flow in a 2-Dimensional Chamber," MS Thesis, AF Institute of Technology, WPAFB, Ohio (1960).

4. Morton, L.C., "The Design and Testing of a Small Rocket Motor of 50 Pounds Thrust, Utilizing Reversed-Flow Cooling with Gaseous Hydrogen and Oxygen as Propellant Combination," MS Thesis, AF Institute of Technology, WPAFB, Ohio (1959).

5. James, R. N., "An Evaluation of a Reverse-Flow Film-cooled Rocket Engine," MS Thesis, AF Institute of Technology, WPAFB, Ohio (1960).

6. Tsongas, G. A., "Reverse-Flow Film Cooling of a Small Rocket Engine Chamber," J. Spacecraft Vol. 3, No. 3. p 444, AF Institute of Technology, WPAFB, Ohio.

7. CPIA Publication No. 201, Vol. I p. 479, October 1970.

8. Drexhage, M., "Reverse Flow Thrust Chamber Development," Report No. AFRPL-TR-71-42 (1971).

9. Malina, F. J., "Characteristics of the Rocket Motor Based on the Theory of Perfect Gases," Journal of the Franklin Institute, Vol. 230, 1940.

10. Pieper, J. L., "ICRPG Liquid Propellant Thrust Chamber Performance Evaluation Manual," Chemical Propulsion Information Agency (JHU/APL) Publication No. CPIA 178, September 1968.

11. Eckert, E. R. G., and Drake, R. M., "Heat and Mass Transfer," McGraw-Hill, 1959.

12. Schact, Ralph L., Quentmeyer, Richard J., and Jones, William I., "Experimental Investigation of Hot-Gas Heat Transfer Rates for a Hydrogen-Oxygen Rocket," NASA TND-2832, 1965.

13. McCarthy, J. R. and Wolf, H., "Forced Convection Heat Transfer to Gaseous Hydrogen at High Heat Flux and High Pressure in a Smooth, Round, Electrically Heated Tube," ARS Journal, p. 423, April 1960.

14. Miller, W. S., "Heat Transfer to Hydrogen Flowing Turbulently in Tubes," AIAA Paper 66-580, 1966.

15. Hatch, J. and Papell, S. S., "Use of a Theoretical Flow Model to Correlate Data for Film Cooling or Heating an Adiabatic Wall by Tangential Injection of Gases of Different Fluid Properties," NASA TND-130, November 1959.

16. Lucas, J. G. and Golladay, R. L., "Gaseous Film Cooling of a Rocket Motor with Injection Near the Throat," NASA TND-3836, 1967.

17. Zakkay, V., Sakell, L. and Parthasarathy, K., "An Experimental Investigation of Supersonic Slot Cooling," Proceedings of Heat Transfer and Fluid Mechanics Institute, pp. 88-013, 1970.

18. Anon., "AMZIRC Technical Data," American Metal Climax Inc., Publication O/F 66-2791.

19. Anon., "Aerospace Insulation Selector," Johns-Manville Corp., Form No. IN-728A, 11/66.

20. Rolinski, Edmund J., "Investigation of Radiation and Conduction Heat Transfer in Fibrous High Temperature Insulations," Air Force Materials Laboratory Technical Report AFML-TR-67-251, December 1967.

21. "RL10 Torch Ignition Systems," Pratt and Whitney, PWA FR303.

22. Litchfield, E. L., "Spark Ignition," Bureau of Mines, AFAL-TR-68-290.

23. Manson, S. S., "Thermal Stress and Low-Cycle Fatigue," McGraw-Hill Book Co., N.Y.C., Copyright 1966.

24. Eckert, E. R. G., and Drake, Robert M. Jr., "Heat and Mass Transfer," McGraw-Hill Book Co., 1950.

25. Svehla, R. A., "Thermodynamics of Transport Properties for the Hydrogen-Oxygen System," NASA SP-3011, 1964.

26. Rogers, J. D., Ziegler, R. K., and McWilliams, P., "Hydrogen Transport Properties Calculation," LASL Report LA-2529, 29 May 1961.

27. Rogers, J. D., Ziegler, R. K., and McWilliams, P., "Hydrogen Transport Correlations," LASL Report LA-2719, 17 September 1962.

28. Shaffer, A., and Rosseam, J., "Thermodynamic Properties of 20.4°R Equilibrium Hydrogen," Air Research Mfg. Co., ASD Tech, Report 61-360, October 1961.

29. Anon., "Airplane Heating and Ventilating Equipment Engineering Data," SAE Aeronautical Information Report No. 2, January 1943.

30. Kelnhofer, W. J., Smith, R. A., "Testing of Gas Turbine, High-Velocity Duct Systems," Catholic University of America Final Report, Contract No. 92176 submitted to Naval Ship Engineering Center, 31 August 1966.

31. Rao, G. V. R., "Exhaust Nozzle Contour for Optimum Thrust," Jet Propulsion, Volume 28, June 1958, pp. 377-382.

32. Sauer, R., "General Characteristics of the Flow Through Nozzles at Near Critical Speeds," NASA TN 1147, 1947.

33. Shapiro, A., "The Dynamics and Thermodynamics of Compressible Fluid Flow," Vol. 1, pp. 226-31.

34. Rohde, J. E., Duscha, R. A., and Derderian, G., "Digital Codes for Design and Evaluation of Convectively Cooled Rocket Nozzle With Application to Nuclear-Type Rockets," NASA TND-3798.

35. Thompson, D. et. al., "A Fortran Program to Calculate the Flow Field and Performance of an Axially Symmetri DeLaval Nozzle," NASA TND-2579, January 1965.

36. Boraas, S. and Ashby, R., "Installed Thrust Vector for Scarfed Nozzles," Journal of Spacecraft and Rockets, Vol. 6, No. 12, December 1969.

37. Miller, H., "Minuteman Propulsion System Test," AEDC Ret. AEDC TR-67-69 (Revised).

38. Quan, V. et. al., "Kinetic Performance of Barrier-Cooled Rocket Nozzles," J. Spacecraft and Rockets, Vol. 5, No. 10, October 1968.

39. Chow, W. L. and Addy, A. L., "Interaction Between Primary and Secondary Streams of Supersonic Ejector Systems and Their Performance," AIAA Journal, Vol. 2, No. 4, April 1964.

40. Schorr, C. J., Berman, K. and Worner, G., "Modeling of High Energy Gaseous Combustion for Performance Prediction," Presented at the 8th JANNAF Liquid Propellant Combustion Instability Meeting, October 1971.

41. Gosman, A. D., "Heat and Mass Transfer in Recirculating Flow," Academic Press, London, 1969.

42. Moffat, Robert J., "Gas Temperature Measurement," "Temperature, Its Measurement and Control in Science and Industry," Vol. 3, Part 2, Reinhold Publishing.

DISTRIBUTION LIST FOR FINAL REPORT

NAS3-14353 Bell CR 120881

REPORT COPIES R	D	RECIPIENT	DESIGNEE
		National Aeronautics & Space Administration Lewis Research Center 21000 Brookpark Road Cleveland, Ohio 44135	
1		Attn: Contracting Officer, MS 500-313	
5		E.A. Bourke, MS 500-203	
1		Technical Report Control Office, MS 5-5	
1		Technology Utilization Office, MS 3-16	
2		AFSC Liaison Office, 501-3	
2		Library	
1		Office of Reliability & Quality Assurance, MS 500-111	
1		J.W. Gregory Chief, MS 500-203	
3		S.M. Cohen Project Manager, MS 500-202	
1			
1			
1			
1		Director, Shuttle Technology Office, RS Office of Aeronautics & Space Technology NASA Headquarters Washington, D. C. 20546	
2		Director Space Propulsion and Power, RP Office of Aeronautics & Space Technology NASA Headquarters Washington, D. C. 20546	
1		Director, Launch Vehicles & Propulsion, SV Office of Space Science & NASA Headquarters Washington, D. C. 20546	
1		Director, Materials & Structures Division, RW Office of Aeronautics & Space Technology NASA Headquarters Washington, D. C. 20546	
1		Director, Advanced Manned Missions, MT Office of Manned Space Flight NASA Headquarters Washington, D. C. 20546	

REPORT COPIES R	D	RECEIPIENT	DESIGNEE
12		National Technical Information Service Springfield, Virginia 22151	
1		National Aeronautics & Space Administration Ames Research Center Moffett Field, California 94035 Attn. Library	Hans M. Mark Mission Analysis Division
1		National Aeronautics & Space Administration Flight Research Center P.O. Box 273 Edwards, California 93523 Attn: Library	
1		Director, Technology Utilization Division Office of Technology Utilization NASA Headquarters Washington, D. C. 20546	
1		Office of the Director of Defense Research & Engineering Washington, D. C. 20301 Attn: Office of Asst. Dir. (Chem Technology)	
2		NASA Scientific and Technical Information Facility P.O. Box 33 College Park, Maryland 20740 Attn: NASA Representative	
1		National Aeronautics & Space Administration Goddard Space Flight Center Greenbelt, Maryland 20771 Attn: Library	Merland L. Moseson, Code 620
1		National Aeronautics & Space Administration John F. Kennedy Space Center Cocoa Beach, Florida 32931 Attn: Library	Dr. Kurt H. Debus
1		National Aeronautics & Space Administration Langley Research Center Langley Station Hampton, Virginia 23365 Attn: Library	E. Cortwright Director

REPORT COPIES R	D	RECIPIENT	DESIGNEE
1		National Aeronautics & Space Administration Manned Spacecraft Center Houston, Texas 77001 Attn: Library	J.G. Thiobodaux, Jr. Chief, Propulsion & Power Division
1		National Aeronautics & Space Administration George C. Marshall Space Flight Center Huntsville, Alabama 35912 Attn: Library	Hans G. Paul I. G. Yates Leon J. Hastings Clyde Nevins James Thomas J. Blumrich Dale Burrows
1		Jet Propulsion Laboratory 4800 Oak Grove Drive Pasadena, California 91103 Attn: Library	Henry Burlage, Jr. Duane Dipprey
1		Defense Documentation Center Cameron Station Building 5 5010 Duke Street Alexandria, Virginia 22314 Attn: TISIA	
1		RTD (RTNP) Bolling Air Force Base Washington, D. C. 20332	
1		Arnold Engineering Development Center Air Force Systems Command Tullahoma, Tennessee 37389 Attn: Library	Dr. H.K. Doetsch
1		Advanced Research Projects Agency Washington, D.C. 20525 Attn: Library	
1		Aeronautical Systems Division Air Force Systems Command Wright-Patterson Air Force Base, Dayton, Ohio Attn: Library	D.L. Schmidt Code ARSCNC-2
1		Air Force Missile Test Center Patrick Air Force Base, Florida Attn: Library	L.J. Ullian

REPORT COPIES R	D	RECIPIENT	DESIGNEE
1		Air Force Systems Command Andrews Air Force Base Washington, D. C. 20332 Attn: Library	Capt. S.W. Bowen SCLT
1		Air Force Rocket Propulsion Laboratory (RPR) Edwards, California 93523 Attn: Library	
1		Air Force Rocket Propulsion Laboratory (RPM) Edwards, California 93523 Attn: Library	
1		Air Force FTC (FTAT-2) Edwards Air Force Base, California 93523 Attn: Library	Donald Ross
1		Air Force Office of Scientific Research Washington, D. C. 20333 Attn: Library	SREP, Dr. J.F. Masi
1		Space & Missile Systems Organization Air Force Unit Post Office Los Angeles, California 90045 Attn: Technical Data Center	
1		Office of Research Analyses (QAR) Holloman Air Force Base, New Mexico 88330 Attn: Library RRRD	
1		U. S. Air Force Washington, D. C. Attn: Library	Col. C.K. Stambaugh, Code AFRST
1		Commanding Officer U. S. Army Research Office (Durham) Box CM, Duke Station Durham, North Carolina 27706 Attn: Library	
1		U. S. Army Missile Command Redstone Scientific Information Center Redstone Arsenal, Alabama 35808 Attn: Document Section	Dr. W. Wharton

REPORT COPIES R	D	RECIPIENT	DESIGNEE
1		Bureau of Naval Weapons Department of the Navy Washington, D. C. Attn: Library	J. Kay, Code RTMS-41
1		Commander U. S. Naval Missile Center Point Mugu, California 93041 Attn: Technical Library	
1		Commander U. S. Naval Weapons Center China Lake, California 93557 Attn: Library	
1		Commanding Officer Naval Research Branch Office 1030 E. Green Street Pasadena, California 91101 Attn: Library	
1		Director (Code 6180) U. S. Naval Research Laboratory Washington, D. C. 20390 Attn: Library	H.W. Carhart J.M. Krafft
1		Picatinny Arsenal Dover, New Jersey 07801 Attn: Library	I. Forsten
1		Air Force Aero Propulsion Laboratory Research & Technology Division Air Force Systems Command United States Air Force Wright-Patterson AFB, Ohio 45433 Attn: APRP (Library)	R. Quigley C. M. Donaldson
1		Electronics Division Aerojet-General Corporation P.O. Box 296 Azusa, California 91703 Attn: Library	W. L. Rogers

REPORT COPIES R	D	RECIPIENT	DESIGNEE
1		Space Division Aerojet-General Corporation 9200 East Flair Drive El Monte, California 91734 Attn: Library	S. Machlawski
1		Aerojet Ordance and Manufacturing Aerojet-General Corporation 11711 South Woodruff Avenue Fullerton, California 90241 Attn: Library	
1		Aerojet Liquid Rocket Company P.O. Box 15847 Sacramento, California 95813 Attn: Technical Library 2482-2015A	R. Stiff
1		Aeronutronic Division of Philco Ford Corp. Ford Road Newport Beach, California 92663 Attn: Technical Information Department	Dr. L.H. Linder
1		Aerospace Corporation 2400 E. El Segundo Blvd. Los Angeles, California 90045 Attn: Library-Documents	J.G. Wilder
1		Arthur D. Little, Inc. 20 Acorn Park Cambridge, Massachusetts 02140 Attn: Library	A.C. Tobey
1		Astropower Laboratory McDonnell-Douglas Aircraft Company 2121 Paularino Newport Beach, California 92163 Attn: Library	

REPORT COPIES R	D	RECIPIENT	DESIGNEE
1		ARO, Incorporated Arnold Engineering Development Center Arnold AF Station, Tennessee 37389 Attn: Library	
1		Susquehanna Corporation Atlantic Research Division Shirley Highway & Edsall Road Alexandria, Virginia 22314 Attn: Library	
1		Beech Aircraft Corporation Boulder Facility Box 631 Boulder, Colorado Attn: Library	Douglas Pope
1		Bell Aerospace Co. Box 1 Buffalo, New York 14240 Attn: Library	
1		Instruments & Life Support Division Bendix Corporation P.O. Box 4508 Davenport, Iowa 52808 Attn: Library	W. M. Carlson
1		Bellcomm 955 L'Enfant Plaza, S. W. Washington, D. C. Attn: Library	H.S. London
1		Boeing Company Space Division P.O. Box 868 Seattle, Washington 98124 Attn: Library	J.D. Alexander C.F. Tiffany
1		Boeing Company 1625 K Street, N. W. Washington, D. C. 20006	
1		Boeing Company P.O. Box 1680 Huntsville, Alabama 35801	Ted Snow

REPORT COPIES R	D	RECIPIENT	DESIGNEE
1		Curtiss-Wright Corporation Wright Aeronautical Division Woodridge, New Jersey Attn: Library	G. Kelley
1		University of Denver Denver Research Institute P. O. Box 10127 Denver, Colorado 80210 Attn: Security Office	
1		Fairchild Stratos Corporation Aircraft Missiles Division Hagerstown, Maryland Attention: Library	
1		Research Center Fairchild Hiller Corporation Germantown, Maryland Attn: Library	Ralph Hall
1		Republic Aviation Fairchild Hiller Corporation Farmington, Long Island New York	
1		General Dynamics/Convair P. O. Box 1128 San Diego, California 92112 Attn: Library	Frank Dore
1		Missiles and Space Systems Center General Electric Company Valley Forge Space Technology Center P. O. Box 8555 Philadelphia, Pennsylvania 19101 Attn: Library	A. Cohen F. Schultz
1		General Electric Company Flight Propulsion Lab. Department Cincinnati, Ohio Attn: Library	D. Suichu Leroy Smith

REPORT COPIES R	D	RECIPIENT	DESIGNEE
1		Chemical Propulsion Information Agency Applied Physics Laboratory 8621 Georgia Avenue Silver Spring, Maryland 20910	Tom Reedy
1		Chrysler Corporation Missile Division P.O. Box 2628 Detroit, Michigan Attn: Library	John Gates
1		Chrysler Corporation Space Division P.O. Box 29200 New Orleans, Louisiana 70129 Attn: Librarian	
1		Grumman Aircraft Engineering Corporation Bethpage, Long Island, New York Attn: Library	Joseph Gavin
1		Hercules Powder Company Allegheny Ballistics Laboratory P.O. Box 210 Cumberland, Maryland 21501 Attn: Library	
1		Honeywell Inc. Aerospace Division 2600 Ridgeway Road Minneapolis, Minnesota Attn: Library	
1		IIT Research Institute Technology Center Chicago, Illinois 60616 Attn: Library	C.K. Hersh
1		Kidde Aer-Space Division Walter Kidde & Company, Inc. 367 Main Street Belleville, N. J.	R.J. Hanville
1		Ling-Temco-Vought Corporation P.O. Box 5907 Dallas, Texas 75222 Attn: Library	

REPORT COPIES R	D	RECIPIENT	DESIGNEE
1		Lockheed Missiles and Space Company P.O. Box 504 Sunnyvale, California 94087 Attn: Library	
1		Lockheed Propulsion Company P.O. Box 111 Redlands, California 92374 Attn: Library, Thackwell	H.L. Thackwell
1		Marquardt Corporation 16555 Saticoy Street Box 2013 - South Annex Van Nuys, California 91409	L.R. Bell, Jr.
1		Martin-Marietta Corporation (Baltimore Division) Baltimore, Maryland 21203 Attn: Library	
1		Denver Division Martin-Marietta Corporation P.O. Box 179 Denver, Colorado 80201 Attn: Library	Dr. Morganthaler F.R. Schwartzberg
1		Orlando Division Martin-Marietta Corporation Box 5827 Orlando, Florida Attn: Library	J. Fern
1		Western Division McDonnell Douglas Astronautics 5301 Bolsa Avenue Huntington Beach, California 92647 Attn: Library	R.W. Hallet G.W. Burge P. Klevatt
1		McDonnell Douglas Aircraft Corporation P.O. Box 516 Lambert Field, Missouri 63166 Attn: Library	R.A. Herzmark

REPORT COPIES R	D	RECIPIENT	DESIGNEE
1		Rocketdyne Division North American Rockwell Inc. 6633 Canoga Avenue Canoga Park, California 91304 Attn: Library, Department 596-306	Dr. R. J. Thompson S. F. Iacobellis
1		Space & Information Systems Division North American Rockwell 12214 Lakewood Blvd. Downey, California Attn: Library	
1		Northrop Space Laboratories 3401 West Broadway Hawthorne, California Attn: Library	Dr. William Howard
1		Purdue University Lafayette, Indiana 47907 Attn: Library (Technical)	Dr. Bruce Reese
1		Radio Corporation of America Astro-Electronics Products Princeton, New Jersey Attn: Library	
1		Rocket Research Corporation Willow Road At 116th Street Redmond, Washington 98052 Attn: Library	F. McCullough, Jr.
1		Stanford Research Institute 333 Ravenswood Avenue Menlo Park, California 94025 Attn: Library	Dr. Gerald Marksman
1		Thiokol Chemical Corporation Redstone Division Huntsville, Alabama Attn: Library	John Goodloe
1		TRW Systems Inc. 1 Space Park Redondo Beach, California 90278 Attn: Tech. Lib. Doc. Acquisitions	D. H. Lee

REPORT COPIES R	D	RECIPIENT	DESIGNEE
1		TRW TAPCO Division 23555 Euclid Avenue Cleveland, Ohio 441117	P. T. Angell
1		United Aircraft Corporation Corporation Library 400 Main Street East Hartford, Connecticut 06108 Attn: Library	Dr. David Rix Erle Martin Frank Owen Wm. E. Taylor
1		United Aircraft Corporation Pratt & Whitney Division Florida Research & Development Center P.O. Box 2691 West Palm Beach, Florida 33402 Attn: Library	R. J. Coar Dr. Schmitke
1		United Aircraft Corporation United Technology Center P.O. Box 358 Sunnyvale California 94038 Attn: Library	Dr. David Altman
1		Vickers Incorporated Box 302 Troy, Michigan	
1		Vought Astronautics Box 5907 Dallas, Texas Attn: Library	

REPORT COPIES R	D	RECIPIENT	DESIGNEE
1		Wright-Patterson Air Force Base, Ohio 45433 Attn: AFML (MAAE)	
1		Wright-Patterson Air Force Base, Ohio 45433 Attn: AFML (MAAM)	R. E. Headrick (Code Mame)
1		Commanding Officer Ballistic Research Laboratories Aberdeen Proving Ground Maryland 21005 Attn: AMXBR-L	
1		Department of the Army U.S. Army Material Command Washington, D.C. 20315 Attn: AMCRD-RC	
1		Commander U.S. Naval Ordnance Laboratory White Oak Silver Spring, Maryland 20910 Attn: Library	
1		B.F. Goodrich Company Aerospace & Defense Products 500 South Main Street Akron, Ohio 44311	
1		Thiokol Chemical Corporation Elkton Division Elkton, Maryland 21921 Attn: Librarian	
1		Thiokol Chemical Corporation Rocket Operations Center P.O. Box 1640 Ogden, Utah 84401 Attn: Library	
1		Westinghouse Research Laboratories Beulah Road, Churchill Boro Pittsburgh, Pennsylvania 15235 Attn: Library	G. O. Sankey J. H. Bitler

REPORT COPIES R	D	RECIPIENT	DESIGNEE
1		Frankford Arsenal Philadelphia, Pennsylvania 19137 Attn: 1320, Library	Carl Carman
1		Director Special Projects Office Department of the Navy Washington, D.C. 20360	
1		General Dynamics P.O. Box 748 Fort Worth, Texas 76101 Attn: Library	D. E. Westerneide
1		General Electric Company Apollo Support Department P.O. Box 2500 Daytona Beach, Florida 32015 Attn: Library	C. Day
1		Institute for Defense Analyses 400 Army-Navy Drive Arlington, Virginia 22202 Attn: Classified Library	
1		AEC-NASA Space Nuclear Propulsion Office, NPO NASA Headquarters Germantown, Maryland	F. C. Schwenk N. J. Gerstein
1		National Science Foundation Engineering Division 1800 G. Street N.W. Washington, D.C. 20540 Attn: Library	
1		Sandia Corporation P.O. Box 969 Livermore, California 94550 Attn: Technical Library	H. Lucas
1		Sandia Corporation Sandia Base Albuquerque, New Mexico 87115 Attn: Library	John L. Leaman W. Herrmann W. K. Cox H. E. Montgomery

REPORT COPIES R	D	RECIPIENT	DESIGNEE
1		Battelle Memorial Institute Columbus Laboratories 505 King Avenue Columbus, Ohio 43201 Attn: Library	C. M. Allen
1		California Institute of Technology Pasadena, California Attn: Library (Technical)	Dr. A. Acosta
1		Massachusetts Institute of Technology Cambridge, Massachusetts Attn: Library	Dr. R. W. Mann
1		Case Western Reserve University 100900 Euclid Avenue Cleveland, Ohio 44115 Attn: Technical Library	Dr. E. Reshotke
1		Franklin Institute Research Labs Benjamin Franklin Parkway Philadelphia, Pennsylvania 19103 Attn: Library	J. Ramerberger